Non-unitary conformal field theories for geometrical problems : a lattice approach

Linnea Grans-Samuelsson

université PARIS-SACLAY

Non-Unitary Conformal Field Theories for Geometrical Problems: a Lattice Approach

Théories Conformes Non Unitaires et Problèmes Géométriques: Approche par le Réseau

Thèse de doctorat de l'université Paris-Saclay

École doctorale n° 564, physique en Île-de-France (PIF)
Spécialité de doctorat: Physique
Graduate School : Physique, Référent : Faculté des sciences d'Orsay

Thèse préparée dans l'unité de recherche **IPhT (Université Paris-Saclay, CNRS, CEA)** sous la direction de **Hubert SALEUR**, directeur de recherche et la co-direction de **Jesper JACOBSEN**, professeur des universités.

Thèse soutenue à Paris-Saclay, le 13 Septembre 2022, par

Linnea GRANS-SAMUELSSON

Composition du jury

Paul FENDLEY Professeur, University of Oxford	Président & Rapporteur
Zhenghan WANG Professeur, UCSB	Rapporteur & Examinateur
Didina SERBAN Directrice de recherche, IPhT Saclay	Examinatrice
Jean-Michel MAILLET Directeur de recherche, ENS de Lyon	Examinateur
Hubert SALEUR Directeur de recherche, IPhT Saclay	Directeur de thèse

THESE DE DOCTORAT
NNT : 2022UPASP077

université PARIS-SACLAY | ÉCOLE DOCTORALE Physique en Île-de-France (PIF)

Titre: Théories conformes non unitaires et problèmes géométriques: approche par le réseau
Mots clés: CFT, modèles sur réseau, invariance conforme

Résumé:

Dans cette thèse, nous étudions les théories conformes des champs non unitaires à deux dimensions qui apparaissent dans la limite continue de certains modèles critiques sur réseau, y compris les modèles de Potts et O(n). Ces modèles ont des applications à des problèmes géométriques tels que la percolation et les marches auto-évitantes (polymères). Pour traiter les difficultés techniques causées par la non-unitarité, nous considérons une approche par le réseau, qui inclut des techniques telles que l'ansatz de Bethe, la théorie des représentations de l'algèbre affine de Temperley-Lieb et l'utilisation d'une discrétisation de l'algèbre de Virasoro (les générateurs de Koo-Saleur).

Nous fournissons une formulation graphique des fonctions de corrélation dans les modèles minimaux RSOS et les comparons à des quantités similaires dans le modèle de Potts. Cela nous permet d'expliquer pourquoi une conjecture antérieure pour les fonctions à quatre points de Potts, bien qu'incorrecte, ait donné des résultats en bon accord avec les simulations numériques. Nous détaillons les connexions entre les modèles RSOS et les systèmes anyoniques, en montrant que le calcul des fonctions de corrélation se réduit à l'évaluation de certains diagrammes de fusion anyoniques.

La partie principale de la thèse est consacrée à l'étude des modules de Virasoro présents dans le modèle à six vertex et dans les modèles de Potts et de boucles à charge centrale générique (irrationnelle). Ceci est fait principalement en utilisant les générateurs de Koo-Saleur. Nous trouvons dans le modèle à six vertex à la fois des modules de Verma et des modules co-Verma, tandis que dans les modèles de Potts et de boucles, la principale découverte est la présence de modules logarithmiques correspondants à des cellules de Jordan de rang deux. Ces cellules de Jordan ne sont pas présentes à taille finie, mais apparaissent seulement dans la limite continue. Nous montrons également la convergence des générateurs de Koo-Saleur vers les générateurs de Virasoro dans une procédure à double limite appelée limite d'échelle, où l'ordre des limites est crucial.

Enfin, l'information sur les modules logarithmiques est utilisée dans le bootstrap du modèle O(n) pour des valeurs complexes génériques de n, en utilisant des blocs conformes logarithmiques dans les équations de croisement. Nous calculons numériquement les fonctions à quatre points impliquant les opérateurs les plus simples et constatons que le nombre de solutions aux équations de croisement est compatible avec la théorie des représentations de O(n).

Title: Non-unitary conformal field theories for geometrical problems: a lattice approach
Keywords: CFT, lattice models, conformal symmetry

Abstract:

In this thesis we study non-unitary two-dimensional bulk conformal field theories that appear in the continuum limit of certain critical lattice models, including the Potts and O(n) models. These models have applications to geometrical problems such as percolation and self-avoiding walks (polymers). To handle the technical difficulties caused by the non-unitarity we consider a lattice approach, which includes techniques such as the Bethe ansatz, representation theory of the affine Temperley-Lieb algebra and the usage of a discretization of the Virasoro algebra (the Koo-Saleur generators).

We provide a graphical formulation of correlation functions in RSOS minimal models and compare to similar quantities in the Potts model. This allows us explain why an earlier conjecture for the Potts four-point functions, although incorrect, gave results in good agreement with numerical simulations. We detail the connections between RSOS models and anyonic systems, showing that the computation of correlation functions reduce to the evaluation of certain anyonic fusion diagrams.

The main part of the thesis is dedicated to investigating what Virasoro modules are present in the six-vertex model, Potts and loop models at generic (irrational) central charge. This is mainly done using the Koo-Saleur generators. We find in the six-vertex model both Verma and co-Verma modules, while in the Potts and loop models the main finding is the presence of logarithmic modules corresponding to rank-two Jordan cells. These Jordan cells are not present at finite size, but appear only in the continuum limit. We also show the convergence of the Koo-Saleur generators to the Virasoro generators in a double limit procedure called the scaling limit, where the order of the two limits is crucial.

Finally, knowledge of the logarithmic modules is used to bootstrap the O(n) model at generic complex values of n, using logarithmic conformal blocks in the crossing equations. We numerically compute four-point functions involving the simplest operators, and find that the number of solutions to the crossing equations is consistent with O(n) representation theory.

Acknowledgements

I first want to thank my supervisor, Hubert Saleur, and my co-supervisor, Jesper Jacobsen. Working with and learning from you both has been an invaluable experience.

Many thanks to the other members of the jury: Zhenghan Wang, Paul Fendley, Didina Serban and Jean-Michel Maillet. Special thanks to Zhenghan and Paul for agreeing to be referees, and for your feedback on this manuscript.

I want to thank the members of our research group – Jonathan, Thiago, Yifei, Michal, Romain, Etienne, Niall, Lawrence – both for great scientific discussions and good company. Jonathan in particular: your helpful explanations and answers to my many questions have been invaluable. I also want to thank our collaborators, Sylvain and Rongvoram, for an enjoyable time working together.

Nick and Lisa, it has been wonderful to get to know you, and I hope we will have the occasion to spend time again in the future. Until then, give Nellie and Einstein many hugs from me.

Other friends and colleagues in the Paris area: you have all made my years as a PhD student more enjoyable, and I hope our paths cross in the future. There are too many names to list them all without running the risk of forgetting one, but a few that stand out are Ingrid, Sebastian, Elba, Natanael, Giulia, Källan, Konie and Manuel.

The support and encouragement of my family has meant a lot. My father, Kjell: you not only set me on the track of becoming a physicist from an early age, you were also the one who sent me an article on conformal field theory that opened my eyes to this particular field. My mother, Ulrika: the way you reinvented your life while I was growing up has been an immense inspiration, showing that with hard work and ambition you can aim for the stars and land in a castle (or a few). Håkan, Madeleine, Melinda, Signe, Robin: I am incredibly happy to have you all in my life.

Finally, and most importantly, to my partner Elie: there is no way I can put into words how amazing you are, nor how much it has meant to have you by my side during these past years. All I can say is that I hope I will have you by my side for the rest of my life as well!

CONTENTS

“ There is an order to the Universe we live in. Roughly speaking, little things affect big things. Not the other way round. ”

– David Tong, lecture notes on statistical field theory

CHAPTER

1

INTRODUCTION

Since its beginnings in the early 20th century, quantum field theory has become a corner stone of theoretical physics. Within the context of particle physics, quantum electrodynamics is arguably the most successful theory in any field of science when it comes to the accuracy of its predictions, as measured by number significant digits confirmed by experiment. More broadly, many interesting problems in physics and beyond involve a large number of degrees of freedom and are effectively modelled by a field theory of some sort.

Quantum field theories that are invariant under conformal (angle-preserving) transformations – conformal field theories, or CFTs – sit at unique spots in the space of all quantum field theories as fixed points of the renormalization group flow. At these points the field theories become massless, the correlation length diverges and the correlation functions decay as power laws rather than exponentially. In fact, the conformal symmetry strongly constrains the form of n-point functions, so that it suffices to know a certain set of data for the CFT of interest to construct all of them. This is the basis for the conformal bootstrap approach.

While CFTs show up in many contexts, the context of interest in this thesis is that of two-dimensional lattice models at criticality. Figure 1.1 shows the quintessential example: the Ising model at its critical point. Other examples include the Q-state Potts model, which in the limit $Q \to 1$ describes bond percolation [1], and the $O(n)$ model, which in the limit $n \to 0$ describes self-avoiding walks (polymers) [2]. A single CFT can describe the long-distance properties of several critical systems that on the microscopical scale look wildly different, as long as they fall in the same universality class. For this reason, the exact same power laws can crop up in seemingly unrelated fields of science. It is often the case that at least one model within a given universality class is *integrable*, possessing an infinite number of conserved quantities allowing for an exact solution of the model. As such, integrable lattice models at criticality are especially useful to study. In particular each minimal model – a class of particularly well-behaved CFTs – admits an integrable lattice realization [3].

In general dimensions D the conformal symmetry is finite – governed by the conformal group generated by dilation, rotation, translation and the special conformal transformation. However, the story is radically different in $D = 2$. We know from complex analysis that any

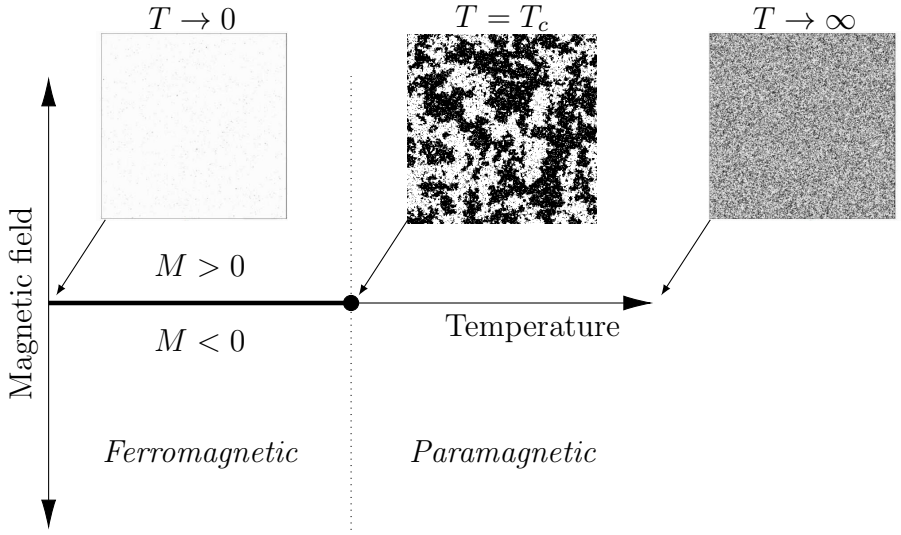

Figure 1.1: The ferromagnetic Ising model. At zero temperature, the spins will align either up or down (spontaneous symmetry breaking); there is perfect correlation. At infinite temperature, each spin will be independent of its neighbours; there is no correlation. At finite temperature other than the critical point, the spin-spin correlation function decays exponentially. At the critical point $T = T_c$, the correlation function decays as a power law, and clusters of all sizes are present – there is scale invariance.

holomorphic function yields a conformal map, so that the symmetry algebra of local conformal transformations in two dimensions becomes infinite. More precisely, the symmetry algebra of a two-dimensional conformal field theory is the unique central extension of the Witt algebra, the *Virasoro algebra*, generated by $L_n, n \in \mathbf{Z}$ under the relation

$$[L_m, L_n] \;=\; (m-n)L_{m+n} + \frac{c}{12} m(m^2-1)\delta_{m+n,0} \tag{1.0.1}$$

where c is the central charge.

The study of two-dimensional conformal field theories thus relies on the study of representations of the Virasoro algebra. The CFTs that correspond a direct sum of finitely many irreducible Virasoro representations have been fully classified and solved (by which we mean that we can compute their correlation functions). These are the minimal models mentioned above, which provide the most famous example of rational CFTs, defined as CFTs with a finite number of primary fields (fields annihilated by $L_n, n > 0$). Meanwhile, CFTs with a more complicated representation theory are far less well understood, and a main theme of this thesis will be ways of dealing with them – from lattice approaches to the conformal bootstrap.

Let us briefly review precisely how the conformal symmetry constrains the form of the correlation functions in two dimensions. This material can be found in any standard reference, such as [4]. We will in this thesis exclusively deal with bulk CFTs, whose symmetry algebra consists of two copies of the Virasoro algebra: $\mathrm{Vir} \otimes \overline{\mathrm{Vir}}$. We consider fields that are covariant under conformal transformation, so-called quasi-primary fields. They are eigenstates of L_0 and $\bar{L}_0$[1], and are characterized by their eigenvalues $h, \bar{h}$, the conformal weights. We call $h + \bar{h}$ the conformal dimension, and $h - \bar{h}$ the conformal spin.

Ignoring for the moment the possibility of certain limits in which the conformal weights of different fields become the same, which can lead to logarithmic corrections as discussed in

[1]Or generalized eigenstates, in case $L_0, \bar{L}_0$ are not diagonalizable – see Section 3.5

Section 3.5, their 2-point functions are fixed by conformal invariance to be of the form

$$\langle \phi_1(z_1,\bar{z}_1)\phi(2)(z_2,\bar{z}_2)\rangle = \frac{C_{12}}{z_{12}^{2h_1}\bar{z}_{12}^{2\bar{h}_1}}\delta_{h_1,h_2}\delta_{\bar{h}_1,\bar{h}_2}\,, \tag{1.0.2}$$

where $z_{ij} = z_i - z_j$, and the 3-point functions are fixed to be of the form

$$\langle \phi_1(z_1,\bar{z}_1)\phi_2(z_2,\bar{z}_2)\phi_3(z_3,\bar{z}_3)\rangle = \frac{C_{123}}{\prod_{i<j} z_{ij}^{2h_i+2h_j-h}\bar{z}_{ij}^{2\bar{h}_i+2\bar{h}_j-\bar{h}}} \tag{1.0.3}$$

with $h = \sum_i h_i$ and $\bar{h} = \sum_i \bar{h}_j$.

While the two-point constants C_{12} can be removed by a redefinition of the fields, which we shall do from now on unless otherwise specified, the structure constants C_{123} are part of the data that defines a conformal field theory together with the conformal weights themselves.

The form of the 3-point function follows from a stronger statement: the existence of the operator product expansion (OPE) in which any two fields that are close enough (by which we mean that they can be separated from all other field insertions by a circle) can be expanded as

$$\phi_1(z_1,\bar{z}_1)\times\phi_2(z_2,\bar{z}_2) = \sum_p \frac{C_{12p}}{z_{12}^{h_1+h_2-h_p}\bar{z}_{12}^{\bar{h}_1+\bar{h}_2-\bar{h}_p}}\phi_p(z_2,\bar{z}_2)\,, \tag{1.0.4}$$

where $h = h_1 + h_2 + h_p$. Combining this with (1.0.2), and keeping in mind that z_1 and z_2 are close enough with respect to z_3 that we can substitute one for the other, we immediately obtain (1.0.3).

For $n \geq 4$, the form of the n-point functions is not completely determined, as it is now possible to construct $n(n-3)/2$ independent conformal invariants of the positions, so-called *cross ratios*. In the case of four points, we find the cross-ratio $z = z_{12}z_{34}/z_{13}z_{24}$ and similarly for $\bar{z}$, and conformal invariance fixes the 4-point function to be of the general form

$$\langle\prod_{i=1}^{4}\phi_i(z_i,\bar{z}_i)\rangle = \frac{f(z,\bar{z})}{\prod_{i<j} z_{ij}^{h_i+h_j-h/3}\bar{z}_{ij}^{\bar{h}_i\bar{h}_j-\bar{h}/3}}. \tag{1.0.5}$$

However, from the structure of the Virasoro representations involved, the 4-point function can be further fixed to be an expansion in terms of a set functions called the *conformal blocks* [5]. In the case of the most typical Virasoro representations, the Verma modules, the conformal blocks are well-known. In terms of these blocks, which we denote by $\mathscr{F}, \bar{\mathscr{F}}$, we can write

$$f(z,\bar{z}) = \sum_p C_{12p}C_{34p}\mathscr{F}_p^{(s)}(z)\bar{\mathscr{F}}_p^{(s)}(\bar{z}) \tag{1.0.6}$$

where we have used the OPE to make a s-channel expansion of the 4-point function, and each block can be represented pictorially as:

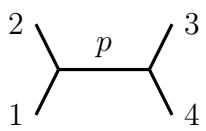

(1.0.7)

The computations of 4-point functions (as well as n-point functions for higher n) thus reduce to determining the same conformal data that shows up in the 2-point and 3-point functions:

the conformal weights and the structure constants, with the addition of the determination of what Virasoro representations are involved, which fixes the form of the conformal blocks.

Even lacking some of the data, such as the structure constants, imposing crossing symmetry – that the s, t, u-channel expansions all agree – places constraints so strong that the missing data can typically be deduced. The goal is therefore to find part of the data: the conformal weights – that is, the spectrum of L_0 and $\bar{L}_0$ – and the structure of the Virasoro representations. For the latter, the situation is made more complicated in theories that are *non-unitary*. While unitarity is a natural feature to demand in particle physics, many problems of physical interest in condensed matter physics are described by non-unitary CFTs at criticality. This includes geometrical problems such as polymers and percolation, which lack locality, and systems where one has to average over disorder.

Removing the constraint of unitarity means that the Virasoro representations may no longer be fully reducible; the representation theory becomes "wild" in the technical sense. We shall in particular see the appearance of logarithmic conformal blocks, corresponding to logarithmic Virasoro modules. The expressions for these blocks were first found in [6] by considering limits of non-logarithmic CFTs.

The general roadmap that we shall follow is:

1. To gain information about the spectrum and relevant Virasoro representations that describe the CFT of a lattice model

2. To use this information in the bootstrap to compute correlation functions

The majority of this thesis will be dedicated to the first step, while an the second step is treated in Chapter 8.

Several recent works (see [7–10] and references therein for a few illustrative examples) have made great progress in the boundary case, whose symmetry algebra consists of only one copy of the Virasoro algebra. The bulk case has proven more challenging, motivating the present thesis. Apart from making fundamental progress in our understanding of geometrical problems, this work is also more generally relevant to the understanding and solution of non-unitary conformal field theories, such as those occurring in the description of critical points in different universality classes of topological insulators (like the plateau transition in the integer quantum Hall effect) [11].

One of the main tools utilized in this thesis is a lattice discretization of the Virasoro algebra, introduced by Koo and Saleur in the early nineties [12], where the discretized Virasoro generators are written in terms of a lattice algebra called the affine Temperley-Lieb algebra. Two of the main chapters, 6 and 7, will be focused on using this tool to deduce the structure of Virasoro representations in different models. In the former we shall also give results about the convergence of the discretization in the continuum limit.

Other than providing us with vital information about the structure of the Virasoro representations directly from the lattice, the discretization of the Virasoro algebra is of importance in quantum computing for the construction of quantum computers and algorithms able to simulate quantum field theories [13, 14]. Additionally, any study of quantum field theory based on lattice discretizations is of high interest to mathematicians, since quantum fields and path integrals prove so difficult to define rigorously.

Plan of the thesis and chapter summaries

Chapters 2–3 cover prerequisites, while Chapters 4–8 cover original work, most of which can be found in references [15–18].[2]

In Chapter 2 we define the lattice models that will appear in this thesis: the six vertex model, the Restricted Solid-On-Solid model, the Q-state Potts model and the $O(n)$ model. We show how they are each related to a loop model, and discuss some general features of loop models, such as their continuum description in terms of the Coulomb Gas formalism and the origin of non-unitarity in the continuum limit CFTs.

Chapter 3 covers the algebraic and representation-theoretic prerequisites. We define the lattice affine Temperley-Lieb algebra and the affine Temperley-Lieb representations that will be relevant in the later chapters. We also introduce the Schur-Weyl dual of the Temperley-Lieb algebra, the quantum group $U_{\mathfrak{q}}sl(2)$, and some features of its representation theory. We then describe the relevant features of the Virasoro representation theory, in particular in non-unitary CFTs including logarithmic CFTs. Finally we present the Koo-Saleur generators.

In Chapter 4, which is based on [15], we provide a geometrical interpretation of the four-point functions built in a paper by Picco et al. [19]. The bootstrap determination of the geometrical correlation functions proposed in [19] was later shown in [20] to be incorrect, the actual spectrum of the Potts model being considerably more complex than initially conjectured. We explain why the results obtained by these authors, albeit incorrect, appeared so close to those of their numerical simulations of the Potts model. Our strategy is based on a cluster expansion of correlation functions in RSOS minimal models, and a subsequent numerical and algebraic analysis of the corresponding s-channel spectrum, in full analogy with early work on the Potts model [20]. Remarkable properties of the lattice amplitudes are uncovered, which explain in particular the truncation of the spectrum of [20] to the much simpler one of the RSOS models, and which lays the groundwork for the determination of the geometric four-point functions of the Potts model itself.

Chapter 5 is a short interlude, detailing the connections between RSOS models and anyonic systems. While Section 5.2 appears in reference [15], the rest of the material is added to this thesis. We show that the computation of correlation functions of the order operators in the A_n RSOS model corresponds to evaluations of certain $su(2)_k$ anyonic fusion diagrams, with $k = n - 1$, and that the anisotropic limit of the A_n RSOS model yields the $su(2)_k$ anyon chain. We also make the connection to topological defects in CFTs.

In Chapter 6, which is based on [16], we investigate the action the Koo-Saleur generators in the critical XXZ quantum spin chain. We explore the structure of the continuum-limit Virasoro modules at generic central charge for the six-vertex model. We find indecomposable modules, but not logarithmic ones. The limit of the Temperley-Lieb modules $\mathscr{W}_{j,1}$ for $j \neq 0$ contains pairs of "conjugate states" with conformal weights $(h_{r,s}, h_{r,-s})$ and $(h_{r,-s}, h_{r,s})$ that give rise to dual structures: Verma or co-Verma modules. The limit of $\mathscr{W}_{0,\mathfrak{q}^{\pm 2}}$ contains diagonal fields $(h_{r,1}, h_{r,1})$ and gives rise to either only Verma or only co-Verma modules, depending on the sign of the exponent in $\mathfrak{q}^{\pm 2}$. In order to obtain matrix elements of Koo-Saleur generators at large system size N we use Bethe ansatz and Quantum Inverse Scattering methods, computing the form factors for relevant combinations of three neighbouring spin operators. Relations between form factors ensure that the above duality exists already at the lattice level. We also study in which sense Koo-Saleur generators converge to Virasoro generators. We consider convergence in the weak sense, investigating whether the commutator of limits is the same as the limit of

[2] Some of the material from these references has been omitted for the sake of brevity, and some of the material in Chapter 5 does not appear in them.

the commutator? We find that it coincides only up to the central term. As a side result we compute the ground-state expectation value of two neighbouring Temperley-Lieb generators in the XXZ spin chain.

In Chapter 7, which is based on [17], we explore the structure of the continuum-limit Virasoro modules at generic central charge for the loop model. This is achieved by a mixture of different techniques: a careful study of the Koo-Saleur generators, combined with measurements of four-point amplitudes, on the numerical side, and OPEs and the four-point amplitudes recently determined using the "interchiral conformal bootstrap" in [21] on the analytical side. We find that null-descendants of diagonal fields having weights $(h_{r,1}, h_{r,1})$ (with $r \in \mathbb{N}^*$) are truly zero, so these fields come with simple Vir $\otimes$ $\overline{\text{Vir}}$ ("Kac") modules. Meanwhile, fields with weights $(h_{r,s}, h_{r,-s})$ and $(h_{r,-s}, h_{r,s})$ (with $r, s \in \mathbb{N}^*$) come in indecomposable but not fully reducible representations mixing four simple Vir $\otimes$ $\overline{\text{Vir}}$ modules with a familiar "diamond" shape. The "top" and "bottom" fields in these diamonds have weights $(h_{r,-s}, h_{r,-s})$, and form a two-dimensional Jordan cell for L_0 and $\bar{L}_0$. This establishes, among other things, that the Potts-model CFT is logarithmic for Q generic. Unlike the case of non-generic (root of unity) values of Q, these indecomposable structures are not present in finite size, but we can nevertheless show from the numerical study of the lattice model how the rank-two Jordan cells build up in the infinite-size limit.

In Chapter 8, which is based on [18], we define the two-dimensional $O(n)$ conformal field theory as a theory that includes the critical dilute and dense $O(n)$ models as special cases, and depends analytically on the central charge. For generic values of $n \in \mathbb{C}$, we write a conjecture for the decomposition of the spectrum into irreducible representations of $O(n)$. We then explain how to numerically bootstrap arbitrary four-point functions of primary fields in the presence of the global $O(n)$ symmetry. We determine the needed conformal blocks, including logarithmic blocks, including in singular cases. We argue that $O(n)$ representation theory provides upper bounds on the number of solutions of crossing symmetry for any given four-point function. We study some of the simplest correlation functions in detail, and determine a few fusion rules. We count the solutions of crossing symmetry for the 30 simplest four-point functions, and find that the number of solutions varies from 2 to 6, saturating the bound from $O(n)$ representation theory in 21 out of 30 cases.

Finally Chapter 9 concludes the thesis, discussing the main results and outlining some future directions.

CHAPTER

2

FOUR LATTICE MODELS

And I looked, and behold a lattice model...

In this chapter we introduce the four lattice models that will appear in this thesis: the six-vertex model, the Restricted Solid-On-Solid (RSOS) model, the Q-state Potts model and the $O(n)$ model. This introduction is kept very brief, with a focus on the features that will be relevant for later chapters. For more in-depth analysis and exposition there are numerous references such as [22].

This chapter is structured as follows: In Section 2.1 we give a brief introduction to integrability and define the four lattice models. These models can all be described in terms of loop models, which we treat in Section 2.2. Here we describe several features including geometrically defined operators, the continuum description in terms of the Coulomb Gas formalism, and the origins of non-unitarity in loop models. Finally in Section 2.3 we show in detail a map between the Q-state Potts model and the RSOS model.

2.1 Defining the models

We shall here consider the models on a a planar lattice, where the degrees of freedom can be situated on edges, vertices and faces. The partition functions will take the general form

$$Z = \sum_{c \in \mathscr{C}} W(c) \tag{2.1.1}$$

where $\mathscr{C}$ are all possible configurations and $W(c)$ the Boltzmann weight of a given configuration. The boundary conditions will be either periodic or twisted periodic.

We will mainly focus on the square lattice, which is the most natural setting for transfer matrix formalism and integrability. Written in terms of a transfer matrix $\mathbf{T}$ with which we build the lattice row-by-row,

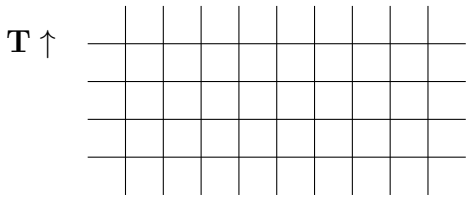

we find $Z = \operatorname{tr} \mathbf{T}^M$ with M the height of the lattice. The transfer matrix is parametrized by a parameter u called the spectral parameter, $\mathbf{T} = \mathbf{T}(u)$, that controls the anisotropy of the system. It is further rewritten as $\mathbf{T}(u) = \operatorname{Tr}_a \left(R_{a,N}(u) R_{a,N-1}(u) ... R_{a,1}(u)\right)$, with N the width of the lattice, a labelling the auxiliary space (horizontal line) and the second index labelling the quantum space (vertical line). The R-matrix $R_{a,j}(u)$ is pictorially represented by two lines crossing, $\perp\!\!\!\perp$. The condition for integrability is that the R-matrix must fulfil the Yang-Baxter relation

$$R_{12}(u_1 - u_2) R_{13}(u_1 - u_3) R_{23}(u_2 - u_3) = R_{23}(u_2 - u_3) R_{13}(u_1 - u_3) R_{12}(u_1 - u_2)\,, \qquad (2.1.2)$$

pictorially represented as

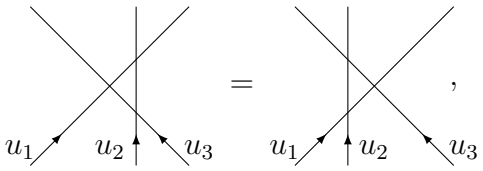

(2.1.3)

as well as the inversion relation $R_{12}(u_1 - u_2) R_{12}(u_2 - u_1) \propto \mathbf{1}$ [22]. As a consequence of these relations $[\mathbf{T}(u), \mathbf{T}(v)] = 0\ \forall u, v$ in an integrable system, forming an infinite family of conserved charges. From this we also see that the spectral parameter u only changes the eigenvalues (spectrum) and not the eigenstates, motivating its name. The models below are either integrable as defined, and can be solved through the Bethe ansatz, or – in the case of the $O(n)$ model – can be related to an integrable model. Historically, the $O(n)$ model at criticality was first solved through the Bethe ansatz by Baxter via a mapping to a zero-temperature antiferromagnetic Potts model on the triangular lattice [23].

Starting from an isotropic lattice model on the square lattice, it is well known that the corresponding universality class generally extends to a critical manifold with properly related horizontal and vertical couplings. The case of an infinitely large vertical coupling (we take the vertical direction as imaginary time) leads to the Hamiltonian limit where the model dynamics is described by a Hamiltonian instead of a transfer matrix: a 1+1D quantum system instead of a 2D classical system. This is the limit, which will correspond to $u \to 0$ and which is also called the anisotropic limit, that will be of most interest in the later chapters, in order to match as closely as possible the lattice model to the formalism of radial quantization of the continuum CFT. Instead considering different finite values of the spectral parameter, which generally leads to a family of non-local conserved charges, one can construct a family of *local* commuting charges from the nth derivatives of $\log \mathbf{T}(u)$ taken at $u = 0$, the first two being the translation operator and the Hamiltonian. At the critical point these conserved charges give the conformal spin (n even) and conformal dimension (n odd) in the corresponding CFT, a fact that is central to the Koo-Saleur construction [12, 24].

The other type of planar lattice we shall encounter in this thesis is the hexagonal lattice. We note that models on the hexagonal lattice can be directly obtained from models on the square lattice in the case of particular choices of Boltzmann weights, obtained by choosing a particular finite value of u (see [25] where this is done in the $O(n)$ model for a concrete example), such that they factorize and each square vertex can be "pulled apart":

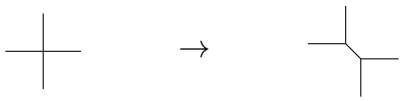

We now give the relevant Boltzmann weights for the different models. For the square lattice $G = (V, E)$ we shall denote by V is the set of vertices and by E the set of edges. For the hexagonal lattice $H = (X, I)$ we shall denote by X the set of vertices and by I the set of edges.

The six-vertex model

Consider a square lattice with each edge $e \in E$ given an orientation, in such a way that the only allowed vertices are those with two ingoing and two outgoing edges. To each type of vertex is associated a Boltzmann weight W_v:

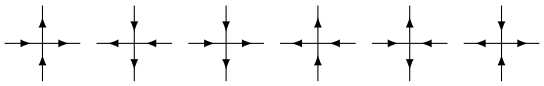

$W_1 \quad W_2 \quad W_3 \quad W_4 \quad W_5 \quad W_6$ (2.1.4)

The partition function is given by

$$Z = \sum_{c \in \mathscr{C}} \prod_{v=1}^{6} W_v^{n_v} \tag{2.1.5}$$

with $\mathscr{C}$ the set of allowed configurations of edge orientations and n_v the number of vertices of type v.

Historically, this model was introduced as a simplified way of understanding residual entropy in ice, by placing oxygen atoms on the vertices and hydrogen atoms on the edges. The arrows indicate which oxygen atom a given hydrogen is closest to, with the requirement that each oxygen atom has two close hydrogen atoms. The model also goes under the name of ice-type model. In the context of computing residual entropy of ice, all Boltzmann weights W_v are set to one. The model was first solved by Lieb in the sixties [26]. The more general eight-vertex model was solved a few years later by by Baxter [27].

The model is integrable when the weights are invariant under a global reversal of arrows, up to a gauge freedom where W_5, W_6 may be varied as long as $W_5 W_6$ is kept fixed.) Denoting $W_1 = W_2 = a, W_3 = W_4 = b, \sqrt{W_5 W_6} = c$, and defining the anisotropy parameter

$$\Delta = \frac{a^2 + b^2 - c^2}{2ab}\,, \tag{2.1.6}$$

the model is critical when $-1 \leq \Delta \leq 1$. [26, 28].

We shall parametrize the weights of the integrable and critical model on the following form:

$$\begin{aligned} W_1 &= W_2 = \sin(\gamma - u) \\ W_3 &= W_4 = \sin u \\ W_5 &= e^{-iu} \sin\gamma \\ W_6 &= e^{iu} \sin\gamma \end{aligned} \tag{2.1.7}$$

with u being the spectral parameter.

Interpreting the edge orientation as spins, the R-matrix is easily seen to be expressible in terms of Pauli matrices, and in the anisotropic limit we recover the Hamiltonian of the XXZ Heisenberg spin chain

$$\mathscr{H} = \frac{\gamma}{2\pi \sin\gamma} \sum_{j=1}^{N} \left[\sigma_j^x \sigma_{j+1}^x + \sigma_j^y \sigma_{j+1}^y + \Delta(\sigma_j^z \sigma_{j+1}^z - 1) + 2e_\infty\right] \tag{2.1.8}$$

with anisotropy parameter

$$\Delta = \cos\gamma\,. \tag{2.1.9}$$

(e_∞ is a constant energy density added to cancel out extensive contributions to the ground state energy, whose value will be given in (3.2.3).)

The six-vertex model can be turned into a height model, which also goes by the name Solid-On-Solid model, by assigning a height σ to each face. The height increases by one when traversing an edge if the arrow on the edge points to the left with respect to the direction in which it is traversed, and decreases by one if the arrow points to the right:

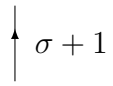

It suffices then to fix the height of an arbitrary face in order to fix the height on all other faces. The height model can in turn be mapped to a loop model by considering clusters of equal heights, and surrounding these clusters by loops.

The Restricted Solid-On-Solid model

The Restricted Solid-On-Solid (RSOS) model, also called the Interaction-Round-a-Face (IRF) model, is a modification of the Solid-On-Solid (SOS) model mentioned above. In the SOS model, each vertex $i \in V$ is assigned an integer height, with the heights of neighbouring vertices differing by at most one.

As a simple restriction, one can impose that heights may only take integer values between 1 and n, with neighbouring heights differing by exactly one. More generally, consider a connected graph $\mathscr{G} = (\mathscr{V}, \mathscr{E})$, and let the vertices $i \in V$ of the square lattice take values ("heights") σ_i among $\mathscr{V}$ in such a way that neighbouring vertices $\langle i, j\rangle$ have heights that are connected by edges in $\mathscr{E}$ – in other words, we consider a graph homomorphism from $\mathscr{G}$ to G. Together with the Boltzmann weights given below, this defines an RSOS model [29, 30]. Considering heights between 1 and n with neighbouring heights differing by exactly one is equivalent to choosing the Dynkin diagram A_n for the graph $\mathscr{G}$.

The Boltzmann weights consist of both vertex weights W_i and face weights W_F. They are given in terms of the adjacency matrix $\mathscr{A}$ of $\mathscr{G}$. Let $S = (S_\sigma)_{\sigma\in X}$ be an eigenvector of $\mathscr{A}$ with no zero elements. A natural choice is the Perron-Frobenius vector, in which case the model is unitary. The other choices lead to a non-unitary model. The vertex weights are given by

$$W_i(\sigma_i) \;=\; S_{\sigma_i}\,. \tag{2.1.10}$$

Labelling the weights around a face as

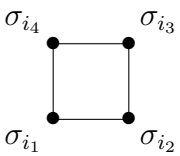

(2.1.11)

the face weights are given by

$$W_F(\sigma_{i_1},\sigma_{i_2},\sigma_{i_3},\sigma_{i_4}) \;=\; a_e\, S^{-1}_{\sigma_{i_1}}\delta(\sigma_{i_1},\sigma_{i_3}) \;+\; b_e\, S^{-1}_{\sigma_{i_2}}\delta(\sigma_{i_2},\sigma_{i_4})\,. \tag{2.1.12}$$

We can represent the face weights symbolically by $W_F = \boxslash + \boxbslash$, with the vertices connected by diagonal lines having the same heights.

The partition function is given by

$$Z = \sum_{c\in\mathscr{C}} \prod_{i\in\mathscr{V}} W_i(\sigma_i) \prod_{F\in\mathscr{F}} W_F(\sigma_F) \tag{2.1.13}$$

with $\mathscr{C}$ the set of height configurations allowed by the graph homomorphism. Here σ_F denotes the collection of variables σ_i for sites i lying on the boundary of the face F, and $\mathscr{F}$ denotes the set of all faces. As discussed in the above section, we can further turn this (now restricted) height model into a loop model by drawing loops on the medial graph around clusters of equal heights. In this representation the face weights $W_F = \boxslash + \boxbslash$ are drawn with loops bouncing off of the diagonal lines.

Choosing any Dynkin diagram of type ADE (simply laced) for the graph $\mathscr{G}$ will yield an RSOS model that is both integrable and critical, as found by Pasquier [29]. For any other choice of $\mathscr{G}$ one can associate a model that is still integrable, but not critical [31–33].

The Q-state Potts model

In the Q-state Potts model on the square lattice, each vertex $i \in V$ is assigned a spin $\sigma_i = 1, 2, ...Q$. For each edge the Boltzmann weight depends on the two corresponding vertices i, j:

$$W_e = e^{K\delta_{\sigma_i,\sigma_j}} \,. \tag{2.1.14}$$

That is, we assign an energy $-K$ whenever two neighbouring spins are aligned.

The partition function is given by

$$Z = \sum_{c\in\mathscr{C}} \prod_{e\in E} W_e \tag{2.1.15}$$

with $\mathscr{C}$ the set of all spin configurations. We recognize the Ising model as the 2-state Potts model.

While this initial formulation requires $Q \in \mathbb{N}^*$, it is easy to rewrite Z more generically in terms of the cluster formulation due to Fortuin and Kasteleyn (FK). Setting $v = e^K - 1$, we note that $e^{K\delta_{\sigma_i,\sigma_j}} = 1 + v\delta_{\sigma_i,\sigma_j}$. We then make a high-temperature (small K) expansion where we for each configuration rewrite the product $\prod_{e\in E}(1 + v\delta_{\sigma_i,\sigma_j})$ in terms of the subset of edges $A \subseteq E$ for which we have taken the term $v\delta_{\sigma_i,\sigma_j}$. The partition function then takes the form

$$Z = \sum_{A\subseteq E} Q^{k(A)} v^{|A|} \,, \tag{2.1.16}$$

where the sum runs over all possible subsets A of the set of edges E, $|A|$ is the number of edges in a given subset and $k(A)$ is the number of connected components in the graph $G_A = (V, A)$. We note that despite the name "high-temperature expansion", this rewriting is exact.

Using the Euler relation one has equivalently

$$Z = Q^{|V|/2} \sum_{A\subseteq E} \left(\frac{v}{\sqrt{Q}}\right)^{|A|} Q^{\ell(A)/2} \,, \tag{2.1.17}$$

where the sum is now over loops on the medial lattice—another square lattice, rotated through 45 degrees, with vertices being the midpoints of the edges E. These loops bounce off of the edges in A and cut through those in the complement $E \setminus A$. Configurations in these two formulations are completely equivalent: given a cluster configuration, the loops surround each

connected component as well as its inner cycles; and conversely each loop touches a cluster on its inside and a dual cluster on its outside, or vice versa. In this way, the loops separate the FK clusters and their dual clusters. (See figures 4.1a and 4.1b in Chapter 4 for an example.) For this reason, we henceforth refer to either of these formulations as the *loop/cluster formulation*. As a loop model, the loop weight is $\sqrt{Q}$.

For any $0 \leq Q \leq 4$ there is a critical value [34, 35]

$$v_c(Q) = \sqrt{Q}\,. \tag{2.1.18}$$

The partition function (2.1.17) is then simplified, losing the dependence on $|A|$.

The $O(n)$ model

The $O(n)$, also called the n-vector model, is most conveniently discussed on the hexagonal lattice. Each vertex $x \in X$ is assigned a variable $\phi(x)$ with n components, subject to the quadratic constraint $\phi(x)\cdot\phi(x) = 1$, and transforming in the vector representation of the group $O(n)$ [36, 37]. Each edge $e \in I$ is given a Boltzmann weigh that depends on the value of ϕ two adjacent vertices x, y as

$$W_e = 1 + K\phi(x)\cdot\phi(y)\,. \tag{2.1.19}$$

The above expression can be compared to the more common definition of the $O(n)$ model, in which one considers an interaction energy $J\phi(x)\cdot\phi(y)$. The truncation of the exponential was introduced in [36], and it was not *a priori* clear that this would not change the universality class. See further discussion in [38].

As the degrees of freedom are now continuous, the partition function is given by an integral

$$Z = \int_{c\in\mathscr{C}} \prod_{e\in I} W_e\,, \tag{2.1.20}$$

where $\int_{c\in\mathscr{C}}$ is shorthand for $\prod_{x\in X}\int \mathrm{d}\phi(x)$.

As for the Q-state Potts model we can make a high-temperature (small K) expansion, where an edge belongs to the subset $A \in E$ if we have taken the term $K\phi(x)\cdot\phi(y)$ in (2.1.19). We note that for the scalar product $\phi(x)\cdot\phi(y) = \sum_{i=1}^{n}\phi(x)^i\phi(y)^i$, we have $\int \mathrm{d}\phi\,\phi(x)^i\phi(x)^j = 0, i \neq j$, forcing one given label i to propagate along each loop in the loop formulation. The contribution of a configuration comes with a factor K for each occupied edge, and a factor n for each closed loop. In this formulation, the model is called a dilute loop gas, and we are allowed to consider non-integer values of n.

For any $-2 \leq n \leq 2$, there is a critical value [37]

$$K_c(n) = \frac{1}{\sqrt{2+\sqrt{2-n}}}\,. \tag{2.1.21}$$

(For $n = 0$, this formula has been proved rigorously [39].) In Chapter 8 we shall furthermore consider complex values of n. Note that it is a priori not obvious that taking this does not destroy criticality; the analytic continuation in n was recently discussed in [40].

2.2 Loop models, Coulomb Gases, non-unitarity

While the four models of the previous section may initially look rather different, we have seen above that they can all be expressed in terms of a lattice loop gas, or loop model. The last

model discussed above, the $O(n)$ model, gives rise to the most general loop model description out of the four: the dilute loop model, where the loops do not have to cover all edges of the lattice.

Consider a configuration of non-intersecting loops on a lattice. On the square lattice, a vertex may be of one of the following types

(2.2.1)

On the hexagonal lattice, a vertex may be of one of the following types

(2.2.2)

where it is understood that each of the vertices in (2.2.2) must be be rotated by 0°, 120° or 240° to match the orientation of the surrounding edges at a given position.

The partition function is written as

$$Z = \sum_{c \in \mathscr{C}} n^{l(c)} \prod_i W(i) \tag{2.2.3}$$

with $i \in V$ or $i \in X$ depending on the lattice, and where $\mathscr{C}$ is the set of all loop configurations, n is the loop weight, $l(c)$ is the number of loops in a configuration c and W are local weights that depend on the vertices. For loop weights $-2 \leq n \leq 2$, these models have a universal critical behaviour that varies continuously with n and does generally not depend on the local weights [41]. Note that setting the vertex weight to zero for the first seven vertex types in (2.2.1), or the first vertex type in (2.2.2), forces the loops to cover all edges.

In the four lattice models of the previous section we have specified the partition functions, but have so far not introduced any specific operators. This is because the types of operators that we shall be mainly dealing with are most naturally introduced in the context of the loop model formulations. Note that some "typical" operators such as, say, measuring the spin at a given site in the Q-state Potts model, are only valid for certain values of the parameters – here, only as long as Q is integer. Here, we instead focus on geometrically defined operators. A natural first example is an operator that marks a point on a loop. n-point functions of such an operator give the probability of n given points all lying on the same loop, which can be used for instance to find the fractal dimension of the loops by marking two points [42].

Locally, this operator would look like a point inserting two lines, but the computation of an n-point function is a *non-local* problem – for instance, the two-point function must involve another point absorbing the *same* two lines:

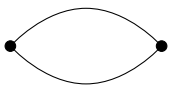

(2.2.4)

More generally we can define operators that insert k lines. These are called k-leg watermelon operators. [2, 42]

In the case where the loop model is interpreted as separating clusters from dual clusters, as in the FK formulation of the Q-state Potts model, another natural operator to define instead marks a point in a cluster. The n-point function then gives the probability of n given points all belonging to the same cluster.

It is also natural to define operators that change the weights of any surrounding loops from n to $n_{\mathcal{O}}$:

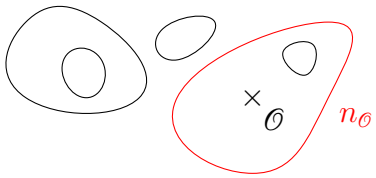

(2.2.5)

We shall see in Chapter 5 how the order parameters in the RSOS models, which in their original definition change the vertex weights at the points where they are inserted, take this form in the loop formulation.

Coulomb Gas formalism

Already before the advent of modern-day methods for 2D CFT, starting with the BPZ paper, it was known that the continuum limit of many 2D critical lattice models could be described by a Gaussian free field theory with specific boundary conditions, in what is called the Coulomb Gas (CG) formalism [4, 43, 44].

The loop model formulation and its equivalent height model formulation provide a particularly useful language for making the link between lattice models and the Coulomb gases. The height field will play the role of the free scalar field ϕ. A standard argument [45] shows that starting from a specific loop configuration, a series of local changes can take $\phi \to \phi \pm 2$ while returning to that same loop configuration, so that the field ϕ must be compactified on a circle.

We consider initially the action

$$\mathcal{A} = \frac{g}{4\pi} \int |\nabla\phi|^2 \mathrm{d}^2\mathbf{x}\,, \tag{2.2.6}$$

although to capture all properties of the loop model two more terms must be added (the reader is referred to [4, 46] for details).

The basic operators of the theory are vertex operators $\mathcal{O}_e = e^{ie\phi}$ (spin waves) and their dual operators $\mathcal{O}_m$ (screw dislocations), whose two-point function corresponds to a line of discontinuity of $2m\pi$ in the height field between the insertion points. Here e is called an electric charge, and m is called a magnetic charge. More general operators $\mathcal{O}_{em}$ are built by combining electric and magnetic charges. They have conformal dimension and spin

$$\begin{aligned} h + \bar{h} &= \frac{e^2}{2g} + \frac{gm^2}{2}\,, \\ h - \bar{h} &= em\,. \end{aligned} \tag{2.2.7}$$

While the CG formalism in its original formulation describes a $c = 1$ theory, a $c < 1$ theory can be constructed by inserting charges $\pm e_0$ at infinity, changing the central charge to $c - 6e_0^2/g$. The conformal weight of a vertex operator is changed from $e^2/2g$ to $e(e - 2e_0)/2g$, which can be thought of as the charge e being screened by a floating charge $2e_0$ originating from the charges at infinity [43]. Finally the coupling constant can be related to this charge at infinity as $g = 1 - e_0$.

Going back to the geometrically defined operators in the previous section, the operators that change the weight of the surrounding loops are electric operators, $e = e_{\mathcal{O}}, m = 0$, such that $n_{\mathcal{O}} = 2\cos(\pi e_{\mathcal{O}})$. Meanwhile, the k-leg watermelon operators are related to screw dislocations, $m = k/2$, with a vertex operator contribution $e = e_0$ to cancel out phase factors that would otherwise arise whenever the lines wind around the insertion points [47]. More general operators

insert k lines, with the rule that any line winding around the insertion point picks up a phase e_φ. This is discussed further in Section 8.4.2 in the context of the $O(n)$ model.

Non-unitarity

Since the Boltzmann weights depend on non-local objects – the loops – the loop models are non-local. It is however possible to trade this non-locality for *non-unitarity*: we can rewrite the Boltzmann weights so that they only depend on local objects, for the price of turning them complex. This is most easily described on the hexagonal lattice. Consider the following example configuration:

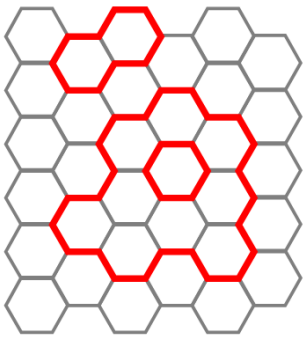

(2.2.8)

Instead of assigning a weight n per loop, we can follow the red curve in a chosen direction and an assign a *local* weight e^{iv} (e^{-iv}) for each right (left) turn. Letting n_r (n_l) be the number of right (left) turns, we find $n_l - n_r \equiv 0 \mod 6$ for a closed loop, and by summing over both orientations we recover $d = 2\cos 6v$, but with *complex* local Boltzmann weights. This leads to the expectation that the continuum limit of the loop model is a non-unitary CFT. This is true even if n is integer. For example, the $O(1)$ model coincides with the Ising model, whose local observables are described by a unitary minimal model. However, the loop model allows us to define non-local observables, whose critical limits do not belong to the minimal model but to a larger, non-unitary CFT.

2.3 Potts-RSOS partition function identity

In the above, we have seen examples of relations between the different lattice models. We finish this chapter by giving a detailed derivation of a map between the Potts model and the RSOS model that will play an important role in Chapter 4. In this section we adopt a more mathematical style. Note: this section appeared in [15] and was adapted from an unpublished work by A.D. Sokal and J.L. Jacobsen [48].

We consider the Potts model on a connected plane graph $G = (V, E, F)$ (with vertices V, edges E and faces F) and write the partition function in the Fortuin-Kasteleyn representation as

$$Z_G(Q, \mathbf{v}) \;=\; \sum_{A \subseteq E} Q^{\kappa(A)} \prod_{e \in A} v_e \;, \tag{2.3.1}$$

where $\kappa(A)$ denotes the number of connected components in the subgraph (V, A). Note that we here we consider the formulation in its most general form. Setting $v_e = v$, $\forall e \in A$ reduces to (2.1.16).

The related RSOS model is defined on the connected plane quadrangulation $\Gamma = (\mathscr{V}, \mathscr{E}, \mathscr{F})$, where $\mathscr{V} = V \cup V^*$ and each face $f = \langle i_1 i_2 i_3 i_4 \rangle \in \mathscr{F}$ has $i_1, i_3 \in V$ and $i_2, i_4 \in V^*$ with diagonals $i_1 i_3 \in E$ and $i_2 i_4 \in E^*$. It takes values in another finite graph $H = (X, \mathbf{E})$ with adjacency

matrix $\mathscr{A} = (\mathscr{A}_{\sigma,\sigma'})_{\sigma,\sigma' \in X}$. In most of this thesis we focus on the case where H is a Dynkin diagram $\mathscr{D}$ of type A or D, while we here consider the generic formulation. We write the RSOS partition function as

$$Z_\Gamma^{\mathrm{RSOS}} \;=\; \sum_{\sigma\colon\, \mathscr{V}\to X} \left(\prod_{(ij)\in\mathscr{E}} \mathscr{A}_{\sigma(i)\sigma(j)} \right) W(\sigma)\;, \tag{2.3.2}$$

where the sum runs over all maps $\sigma\colon \mathscr{V} \to X$ but the adjacency matrix restricts them to be graph homomorphisms (neighbours map to neighbours).

We recall that the weight function W is a product of local contributions from vertices and faces:

$$W(\sigma) \;=\; \left(\prod_{i\in\mathscr{V}} W_i(\sigma_i) \right) \left(\prod_{F\in\mathscr{F}} W_F(\sigma_F) \right)\;, \tag{2.3.3}$$

where the weights W_i, W_F are given by (2.1.10),(2.1.12).

In the following, we shall also need topological identity

$$\kappa(A) \;=\; |V| \,-\, |A| \,+\, c(A) \tag{2.3.4}$$

where $c(A)$ is the cyclomatic number (i.e., number of linearly independent cycles) of the graph (V, A). Having defined our models, we now state the relation between them:

Potts-RSOS equivalence for the partition function

$$Z_\Gamma^{\mathrm{RSOS}}(\mathbf{a},\mathbf{b}) \;=\; \left(\sum_{\sigma\in X} S_\sigma^2 \right) \lambda^{-|V|} \left(\prod_{e\in E} b_e \right) Z_G(\lambda^2, \lambda\mathbf{a}/\mathbf{b})\;. \tag{2.3.5}$$

Proof. Insert (2.1.10)/(2.1.12) into (2.3.3) and expand out the product over faces F of Γ, which are in one-to-one correspondence with edges $e \in E$. Each term in this expansion can be associated to a subset $A \subseteq E$ and the complementary subset A^* as follows:

- If the term contains the factor a_e, then $e \in A$ and hence $e^* \notin A^*$.
- If the term contains the factor b_e, then $e \notin A$ and hence $e^* \in A^*$.

This gives a formulation of the partition function in terms of cluster configurations. On each connected component (cluster) $\mathscr{C}$ of the graph $(V \cup V^*, A \cup A^*)$, the σ value must be constant (let us call it simply $\sigma_{\mathscr{C}}$). Such a configuration then gets a weight

$$\left(\prod_{i\in V\cup V^*} S_{\sigma_i} \right) \left(\prod_{e\in A} a_e \right) \left(\prod_{e^*\in A^*} b_e \right) \left(\prod_{\text{components } \mathscr{C}} S_{\sigma_{\mathscr{C}}}^{-|\mathrm{edges}(\mathscr{C})|} \right) \tag{2.3.6a}$$

$$= \left(\prod_{e\in A} a_e \right) \left(\prod_{e^*\in A^*} b_e \right) \left(\prod_{\text{components } \mathscr{C}} S_{\sigma_{\mathscr{C}}}^{|\mathrm{vertices}(\mathscr{C})|-|\mathrm{edges}(\mathscr{C})|} \right) \tag{2.3.6b}$$

$$= \left(\prod_{e\in A} a_e \right) \left(\prod_{e^*\in A^*} b_e \right) \left(\prod_{\text{components } \mathscr{C}} S_{\sigma_{\mathscr{C}}}^{1-c(\mathscr{C})} \right)\;, \tag{2.3.6c}$$

where the last equality used (2.3.4) with $k(\mathscr{C}) = 1$ per component, and $c(\mathscr{C})$ here denotes the cyclomatic number of the chosen component $\mathscr{C}$.

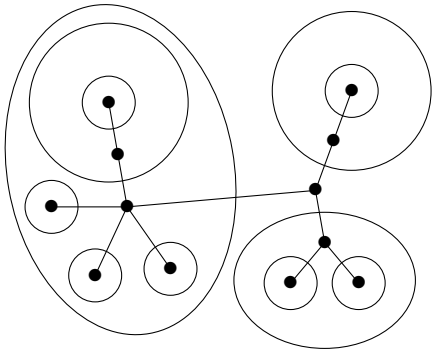

Figure 2.1: The tree T associated to a cluster configuration on the sphere. Each vertex in the tree corresponds to a cluster, each edge corresponds to a loop separating two clusters.

Now form the graph $\mathsf{T} = (\mathsf{V}, \mathsf{E})$ whose vertices are the connected components $\mathscr{C}$ of $(V \cup V^*, A \cup A^*)$ and which puts an edge between $\mathscr{C}_1$ and $\mathscr{C}_2$ whenever at least one vertex of $\mathscr{C}_1$ is adjacent in Γ to at least one vertex of $\mathscr{C}_2$. One observes that T is a tree, and that a component $\mathscr{C}$ of cyclomatic number c is adjacent in T to exactly $c+1$ other components (namely its exterior and c cycles on the interior). Therefore, $S_{\sigma_\mathscr{C}}^{1-c(\mathscr{C})} = S_{\sigma_\mathscr{C}}^{2-\mathrm{d}_\mathsf{T}(\mathscr{C})}$ where $\mathrm{d}_\mathsf{T}(\mathscr{C})$ is the degree of $\mathscr{C}$ in T. An example of a tree T associated to a cluster configuration is shown in Figure 2.1.

To proceed we need the following lemma:

Lemma 2.3.1. *Let $\mathsf{T} = (\mathsf{V}, \vec{\mathsf{E}})$ be a rooted tree whose edges are directed towards the root vertex $\rho \in \mathsf{V}$. For each $i \in \mathsf{V}$, let $\mathrm{d}_{\mathrm{in}}(i)$ (resp. $\mathrm{d}_{\mathrm{out}}(i)$) denote the in-degree (resp. out-degree) of i in T. (Thus, $\mathrm{d}_{\mathrm{out}}(i) = 1$ for all $i \neq \rho$, and $\mathrm{d}_{\mathrm{out}}(\rho) = 0$.) Let M be a matrix indexed by a finite set X, and let S be an eigenvector of M with eigenvalue λ. Then, for each $\tilde{\sigma} \in X$, we have*

$$\sum_{\substack{\sigma\colon \mathsf{V} \to X \\ \sigma_\rho = \tilde{\sigma}}} \left(\prod_{(ij) \in \vec{\mathsf{E}}} M_{\sigma_j, \sigma_i} \right) \left(\prod_{i \in \mathsf{V}} S_{\sigma_i}^{\mathrm{d}_{\mathrm{out}}(i) - \mathrm{d}_{\mathrm{in}}(i)} \right) \;=\; \lambda^{|\mathsf{V}|-1} \,. \tag{2.3.7}$$

Proof. The proof of (2.3.7) is by induction on the cardinality of V. If $|\mathsf{V}| = 1$ (i.e., T consists of the root vertex and no edges), then (2.3.7) is trivial. If $|\mathsf{V}| > 1$, then T contains at least one leaf vertex $i \neq \rho$, for which $\mathrm{d}_{\mathrm{out}}(i) = 1$ and $\mathrm{d}_{\mathrm{in}}(i) = 0$. Letting j be the parent of i we can perform the sum over σ_i using $MS = \lambda S$, yielding λS_{σ_j}. This extra factor of S_{σ_j} is exactly what we need to apply the inductive hypothesis to the tree $\mathsf{T} \setminus i$, in which j has in-degree one lower than it does in T. □

In particular, if M is a symmetric matrix, as is the case for our adjacency matrix, we can ignore the orientations of the edges. We then have

$$\sum_{\substack{\sigma\colon \mathsf{V} \to X \\ \sigma_\rho = \tilde{\sigma}}} \left(\prod_{(ij) \in \mathsf{E}} M_{\sigma_i, \sigma_j} \right) \left(\prod_{i \in \mathsf{V}} S_{\sigma_i}^{2-d(i)} \right) \;=\; S_{\tilde{\sigma}}^2 \lambda^{|\mathsf{V}|-1} \tag{2.3.8}$$

where $d(i)$ is the total degree of the vertex i; the result is independent of the choice of the root vertex ρ. This result follows immediately from Lemma 2.3.1, since $\mathrm{d}_{\mathrm{out}}(i) = 1$ for all $i \neq \rho$ and $\mathrm{d}_{\mathrm{out}}(\rho) = 0$.

We now resume the proof of the main result (2.3.5). Using (2.3.8) to sum over RSOS configurations satisfying $\sigma_\rho = \tilde{\sigma}$ we obtain

$$S_{\tilde{\sigma}}^2 \, \lambda^{\kappa(A)+\kappa(A^*)-1} \left(\prod_{e \in A} a_e \right) \left(\prod_{e^* \in A^*} b_e \right) \ . \tag{2.3.9}$$

But by (2.3.4) we have

$$\kappa(A) + \kappa(A^*) - 1 \ = \ \kappa(A) + c(A) \ = \ 2\kappa(A) + |A| - |V| \ , \tag{2.3.10}$$

which proves (2.3.5) by summing over $\tilde{\sigma} \in X$. $\square$

CHAPTER

3

TEMPERLEY-LIEB, VIRASORO, KOO-SALEUR

In this chapter we give the algebraic and representation-theoretic prerequisites for the later chapters. We shall take a physicist's point of view, using terms such as "module" and "representation" interchangeably.

On the lattice, the algebra of interest is the affine Temperley-Lieb algebra T_N^a. For the three of the models described in Chapter 2 that correspond to loop models with loops covering all edges of the lattice – the six-vertex model, the RSOS model and the Potts model – the R-matrix of the lattice model and the corresponding Hamiltonian in the anisotropic limit are written in terms of generators of this algebra. For the $O(n)$-model the relevant algebra is rather the dilute Temperley-Lieb algebra. We shall not discuss it in this thesis; the interested reader is referred to [49, 50].

As discussed further below, we think of models based on the affine Temperley-Lieb algebra as providing some lattice analogue of the Virasoro algebra—or more precisely, since we study systems with closed (i.e., periodic or twisted periodic) boundary conditions, the product of the left and the right Virasoro algebras, $\mathrm{Vir} \otimes \overline{\mathrm{Vir}}$—at central charge $c \leq 1$. Other types of models could be considered in the same fashion. For instance models based on the Birman-Wenzl-Murakami algebra would naturally lead to a lattice analog of the $N = 1$ super-Virasoro algebra [51], while models involving higher-rank quantum groups (e.g., $U_\mathfrak{q} sl(3)$, as compared to $U_\mathfrak{q} sl(2)$ for models based on the Temperley-Lieb algebra) would lead to lattice analogs of W-algebras [52].[1]

This chapter is structured as follows: After defining the affine Temperley-Lieb algebra and representations relevant for this thesis in Sections 3.1, 3.2 and 3.3, and giving a short introduction to the quantum group $U_\mathfrak{q} sl(2)$ in Section 3.4, we shall turn our attention to the Virasoro algebra that was introduced in Chapter 1. We describe relevant features of its representation theory in Sections 3.5 and how the torus partition function gives information about its characters in Section 3.6. Finally in Section 3.7 we show the construction of discretized Virasoro

[1] We note in this respect that a lattice regularization of a W-algebra at $c = -2$ was proposed in [53].

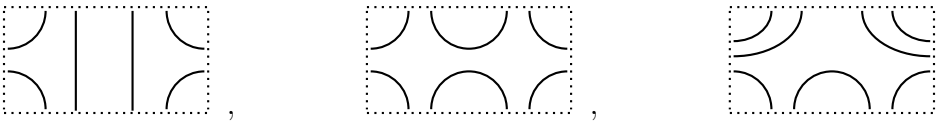

Figure 3.1: Three examples of affine diagrams for $N = 4$, with the left and right sides of the framing rectangle identified. The first diagram represents e_4, the second e_2e_4, and expressing the last one is left as an exercise.

generators in terms of Temperley-Lieb generators introduced by Koo and Saleur in [12].

3.1 The Temperley-Lieb algebra in the periodic case

3.1.1 The algebra $\mathsf{T}_N^a(\mathfrak{m})$

A basis for affine Temperley-Lieb algebra T_N^a is provided by particular diagrams, called *affine diagrams*, drawn on an annulus with N sites on the inner and N on the outer boundary (we henceforth assume N even), such that the sites are pairwise connected by simple curves inside the annulus that do not cross. Some examples of affine diagrams are shown in Fig. 3.1; for convenience we have here cut the annulus and transformed it into a rectangle, which we call *framing*, with the sites labeled from left to right and periodic boundary conditions across.

We define a *through-line* as a simple curve connecting a site on the inner and a site on the outer boundary of the annulus. Let the number of through-lines be $2j$, and call the $2j$ sites on the inner boundary attached to a through-line *free* or *non-contractible*. The inner (resp. outer) boundary of the annulus corresponds to the bottom (resp. top) side of the framing rectangle.

The multiplication of two affine diagrams, a and b, is defined by joining the inner boundary of the annulus containing a to the outer boundary of the annulus containing b, and removing the interior sites. In other words, the product ab is obtained by joining the bottom side of a's framing rectangle to the top side of b's framing rectangle, and removing the corresponding joined sites. Any closed contractible loop formed in this process is replaced by its corresponding weight $\mathfrak{m}$.

In abstract terms, the algebra T_N^a is generated by the e_j's together with the identity, subject to the well-known Temperley-Lieb relations [54]

$$e_j^2 = \mathfrak{m} e_j \,, \tag{3.1.1a}$$

$$e_j e_{j\pm1} e_j = e_j \,, \tag{3.1.1b}$$

$$e_j e_k = e_k e_j \qquad (\text{for } j \neq k,\ k \pm 1) \,, \tag{3.1.1c}$$

where $j = 1, \ldots, N$ and the indices are interpreted modulo N. In addition, T_N^a contains the elements u and u^{-1} generating translations by one site to the right and to the left, respectively. They obey the following additional defining relations

$$u e_j u^{-1} = e_{j+1} \,, \tag{3.1.2a}$$

$$u^2 e_{N-1} = e_1 \cdots e_{N-1} \,, \tag{3.1.2b}$$

and we note that $u^{\pm N}$ is a central element. The *affine* Temperley–Lieb algebra T_N^a is then defined abstractly as the algebra generated by the e_i and $u^{\pm1}$ together with these relations.

We shall parametrize the loop weight as $\mathfrak{m} = \mathfrak{q} + \mathfrak{q}^{-1}$, with $\mathfrak{q}$ the deformation parameter of the quantum group $U_\mathfrak{q} sl(2)$. $U_\mathfrak{q} sl(2)$ that will be introduced in Section 3.4.

3.1.2 Standard modules

It is readily checked that for any finite N, the algebra $\mathsf{T}_N^a(\mathfrak{m})$ obeying the defining relations (3.1.1)–(3.1.2) is in fact infinite-dimensional. We wish however to focus on lattice models having a finite number of degrees of freedom per site. Their proper description involves certain finite-dimensional representations of T_N^a, the so-called *standard modules* $\mathscr{W}_{j,e^{i\phi}}$, which depend on two parameters. Diagrammatically, the first parameter defines the number of through-lines $2j$, with $j = 0, 1, \ldots, \frac{N}{2}$. In addition to the action of the algebra described in the previous subsection, we now require that the result of this action be zero in the standard modules whenever the affine diagrams obtained have a number of through-lines strictly less than $2j$, i.e., whenever two or more free sites are contracted. Moreover, for any $j > 0$ the algebra action can cyclically permute the free sites. Such cyclic permutations give rise to a *pseudomomentum*, which we parametrize by ϕ and define as follows: Whenever $2j$ through-lines wind counterclockwise around the annulus l times, we can unwind them at the price of a factor $e^{ijl\phi}$; and similarly, for clockwise winding, the phase is $e^{-ijl\phi}$ [55,56]. In other words, there is a phase $e^{\pm i\phi/2}$ attributed to each winding through-line.

To define the representation $\mathscr{W}_{j,e^{i\phi}}$ in more convenient diagrammatic terms, we now make the following remark. As free sites cannot be contracted, the pairwise connections between non-free sites on the inner boundary is unchanged under the algebra action. This part of the diagrammatic information is thus irrelevant and can be omitted. Therefore, it is enough to concentrate on the upper halves of the affine diagrams, obtained by cutting a diagram into two parts across its $2j$ through-lines. Each upper half diagram is then called a *link state*. We still call through-lines the cut "upper half" through-lines attached to the free sites on the outer boundary (or, equivalently, top side of the framing rectangle). A phase $e^{i\phi/2}$ (resp. $e^{-i\phi/2}$) is attributed as before, namely each time one of these through-lines moves through the periodic boundary condition of the framing rectangle in the rightward (resp. leftward) direction. It is not difficult to see that the Temperley-Lieb algebra action obtained by stacking the affine diagrams on top of the link states produces exactly the same representations $\mathscr{W}_{j,e^{i\phi}}$ as defined above.

To identify the dimensions of these modules $\mathscr{W}_{j,e^{i\phi}}$ over $\mathsf{T}_N^a(m)$ we simply need to count the link states. The result is

$$\hat{d}_j = \binom{N}{\frac{N}{2}+j} \tag{3.1.3}$$

for the $j > 0$ case, and we shall return to the $j = 0$ case below. Notice that these dimensions are independent of ϕ (although representations with different $e^{i\phi}$ are not isomorphic). The standard modules $\mathscr{W}_{j,e^{i\phi}}$ are also called *cell* $\mathsf{T}_N^a(\mathfrak{m})$-modules [57].

Let us parametrize $\mathfrak{m} = \mathfrak{q}+\mathfrak{q}^{-1}$. For generic values of $\mathfrak{q}$ and ϕ the standard modules $\mathscr{W}_{j,e^{i\phi}}$ are irreducible, but degeneracies appear when the following *resonance criterion* is satisfied [56,57]: [2]

$$e^{i\phi} \;=\; \mathfrak{q}^{2j+2k}, \qquad \text{for } k > 0 \text{ integer}\,. \tag{3.1.4}$$

The representation $\mathscr{W}_{j,\mathfrak{q}^{2j+2k}}$ then becomes reducible, and contains a submodule isomorphic to $\mathscr{W}_{j+k,\mathfrak{q}^{2j}}$. The quotient of those two is generically irreducible, with dimension

$$\bar{d}_j := \hat{d}_j - \hat{d}_{j+k}\,, \qquad \text{for } j > 0\,. \tag{3.1.5}$$

[2] In [57] a slightly different criterion is given, involving some extra liberty in the form of certain $\pm$ signs. We shall however not need these signs here.

For $\mathfrak{q}$ a root of unity, there are infinitely many solutions to (3.1.4), leading to a complex pattern of degeneracies whose discussion we defer for now.

As already mentioned, the case $j = 0$ is a bit different. There is no pseudomomentum in this case, but representations are still characterized by a parameter other than j, specifying now the weight of non-contractible loops. (For obvious topological reasons, non-contractible loops are not possible for $j > 0$.) Upon parametrizing this weight as $z + z^{-1}$, the corresponding standard module of $\mathsf{T}_N^a(\mathfrak{m})$ is denoted $\mathscr{W}_{0,z^2}$. Note that this module is isomorphic to $\mathscr{W}_{0,z^{-2}}$. With the identification $z = e^{i\phi/2}$, the resonance criterion (3.1.4) still applies to the case $j = 0$.

It is physically well-motivated to require that $z + z^{-1} = \mathfrak{m}$, meaning that contractible and non-contractible loops get the same weight. Imposing this leads to the module $\mathscr{W}_{0,\mathfrak{q}^2}$. Notice that this is reducible even for generic $\mathfrak{q}$, as (3.1.4) is satisfied with $j = 0$, $k = 1$. Therefore $\mathscr{W}_{0,\mathfrak{q}^2}$ contains a submodule isomorphic to $\mathscr{W}_{1,1}$, and taking the quotient $\mathscr{W}_{0,\mathfrak{q}^2}/\mathscr{W}_{1,1}$ leads to a simple module for generic $\mathfrak{q}$ which we denote by $\overline{\mathscr{W}}_{0,\mathfrak{q}^2}$. This module is isomorphic to $\overline{\mathscr{W}}_{0,\mathfrak{q}^{-2}}$. Its dimension is

$$\bar{d}_0 = \binom{N}{\frac{N}{2}} - \binom{N}{\frac{N}{2}+1}, \tag{3.1.6}$$

which coincides with the general formula (3.1.5) for $k = 1$.

There is a geometrical significance of the difference between $\mathscr{W}_{0,\mathfrak{q}^2}$ and $\overline{\mathscr{W}}_{0,\mathfrak{q}^2}$. In the latter case, we only register which sites are connected to which in the diagrams, while in the former one also keeps information of how the connectivities wind around the periodic direction of the annulus (this ambiguity does not arise when there are through-lines propagating). The corresponding formal result is the existence of a surjection ψ between different quotients of the T_N^a algebra:

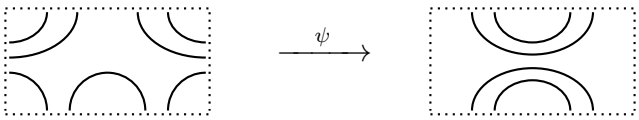

(3.1.7)

The previous definition of link states as the upper halves of the affine diagrams is also meaningful for $j = 0$. As before, the representation $\mathscr{W}_{0,\mathfrak{q}^2}$ requires keeping track of whether each pairwise connection between the sites on the outer boundary (or top side of the framing rectangle) goes through the periodic boundary condition, whereas the quotient module $\overline{\mathscr{W}}_{0,\mathfrak{q}^2}$ omits this information. In either case, it is easy to see that the number of link states coincides with the dimension $\hat{d}_0$ or $\bar{d}_0$, respectively.

3.2 Physical systems and the Temperley-Lieb Hamiltonian

When the R-matrix introduced in Chapter 2 is of the form

$$R_j(u) = \sin(\gamma - u)\left[\mathbf{1} + \frac{\sin(u)}{\sin(\gamma - u)} e_j\right], \tag{3.2.1}$$

the Hamiltonian $\mathscr{H} = \mathbf{T}(0)^{-1}\frac{\partial}{\partial u}\mathbf{T}|_{u=0}$ of the anisotropic limit is (up to changes in the prefactor and constant term) given by

$$\mathscr{H} = -\frac{\gamma}{\pi \sin\gamma} \sum_{j=1}^{N} (e_j - e_\infty). \tag{3.2.2}$$

Here, the prefactor is chosen to ensure relativistic invariance at low energy, and $\gamma \in [0, \pi]$ is defined through $\mathfrak{q} = e^{i\gamma}$, so $\mathfrak{m} \in [-2, 2]$. e_∞ is a constant energy density added to cancel out

extensive contributions to the ground state. Its value is given by

$$e_\infty = \sin\gamma\, I_0, \tag{3.2.3}$$

with I_0 being given by the integral

$$I_0 = \int_{-\infty}^{\infty} \frac{\sinh(\pi-\gamma)t}{\sinh(\pi t)\cosh(\gamma t)}\mathrm{d}t. \tag{3.2.4}$$

In (3.2.2), the e_j can be taken to act in different representations of the $\mathsf{T}_N^a(\mathfrak{m})$ algebra.

For dense loop models, the relevant representation is the *loop representation*, which is simply the representation in terms of affine diagrams introduced in Section 3.1, or equivalently in terms of the corresponding link states. This loop representation is useful for describing geometrical problems such as percolation or dense polymers. It is also strictly equivalent to the cluster representation familiar from the study of the Q-state Potts model with $Q = \mathfrak{m}^2$ [20]. The RSOS model representation is introduced in Chapter 4.2, see (4.2.4). Finally for the six-vertex model, where the degrees of freedom are spins, we must consider the XXZ spin chain representation. In the rest of this section we will discuss this latter representation in more detail, and compare it to the loop representation in the case where the modules are indecomposable. Other representations are possible—such as the one involving alternating $3, \bar{3}$ representations of $sl(2|1)$ discussed in [58] to study percolation. These will not be discussed in the present thesis.

In the XXZ representation the e_j act on $\mathbb{C}^{2N}$ with

$$e_j = -\sigma_j^-\sigma_{j+1}^+ - \sigma_j^+\sigma_{j+1}^- - \frac{\cos\gamma}{2}\sigma_j^z\sigma_{j+1}^z - \frac{i\sin\gamma}{2}(\sigma_j^z - \sigma_{j+1}^z) + \frac{\cos\gamma}{2}\,, \tag{3.2.5}$$

where the σ_j are the usual Pauli matrices, so the Hamiltonian is the familiar XXZ spin chain Hamiltonian (2.1.8), repeated here for convenience:

$$\mathscr{H} = \frac{\gamma}{2\pi\sin\gamma}\sum_{j=1}^{N}\left[\sigma_j^x\sigma_{j+1}^x + \sigma_j^y\sigma_{j+1}^y + \Delta(\sigma_j^z\sigma_{j+1}^z - 1) + 2e_\infty\right]. \tag{3.2.6}$$

In the usual basis where $\left[\begin{smallmatrix}1\\0\end{smallmatrix}\right]$ corresponds to spin up in the z-direction at a given site, the Temperley-Lieb generator e_j acts on spins $j, j+1$ (with periodic boundary conditions) as

$$e_j = \cdots \otimes \mathbf{1} \otimes \begin{pmatrix} 0 & 0 & 0 & 0 \\ 0 & \mathfrak{q}^{-1} & -1 & 0 \\ 0 & -1 & \mathfrak{q} & 0 \\ 0 & 0 & 0 & 0 \end{pmatrix} \otimes \mathbf{1} \otimes \cdots . \tag{3.2.7}$$

It is also possible to introduce a twist in the spin chain without changing the expression (3.2.2), by modifying the expression of the Temperley-Lieb generator acting between first and last spin with a twist parametrized by ϕ. In terms of the Pauli matrices, this twist imposes the boundary conditions $\sigma_{N+1}^z = \sigma_1^z$ and $\sigma_{N+1}^\pm = e^{\mp i\phi}\sigma_1^\pm$. For technical reasons, we will later on "smear out" the twist by taking ϕ/N for *each* Temperley Lieb generator:

$$e_j = \cdots \otimes \mathbf{1} \otimes \begin{pmatrix} 0 & 0 & 0 & 0 \\ 0 & \mathfrak{q}^{-1} & -e^{i\phi/N} & 0 \\ 0 & -e^{-i\phi/N} & \mathfrak{q} & 0 \\ 0 & 0 & 0 & 0 \end{pmatrix} \otimes \mathbf{1} \otimes \cdots . \tag{3.2.8}$$

This is equivalent, and is done in order to preserve invariance under the usual translation operator, which will be useful later on. Note that the value of the energy density e_∞ is independent of ϕ and remains given by (3.2.3). In the generic case, the XXZ model with magnetization $S_z = j$ and twist $e^{i\phi}$ provides a representation of the module $\mathscr{W}_{j,e^{i\phi}}$. This is not true in the non-generic case—see below.

There are many common features of the XXZ and the loop representations. In particular, they have the same ground-state energy and the same "velocity of sound" determining the correct multiplicative normalization of the Hamiltonian in (3.2.2). This reason is that the ground state is found in the same module $\mathscr{W}_{j,e^{i\phi}}$ for both models, or in closely related modules for which the extensive part of the ground-state energy (and hence the constant e_∞) is identical. However, the XXZ and loop representations generally involve mostly *different modules*. The modules appearing in the XXZ chain depend on the twist angle ϕ, while for the loop model the modules depend on the rules one wishes to adopt to treat non-contractible loops, or lines winding around the system. For a generic and non-degenerate situation, studying the physics in each irreducible module $\mathscr{W}_{j,e^{i\phi}}$ would suffice to answer all questions about all $\mathsf{T}_N^a(\mathfrak{m})$ models as well as the related Virasoro modules obtained in the scaling limit. But it turns out, importantly, that degenerate cases are always of relevance to the problems at hand. In such cases, a crucial issue that we will be interested in is how the modules "break up" or "get glued". This issue is highly model-dependent, and is central to the understanding of logarithmic CFT in particular.

The XXZ spin chain representation is studied in Chapter 6, and the loop representation in Chapter7. One main goal of these chapters will be to establish the continuum limit of standard modules, which will turn out different in the two representations. An important point to keep in mind for these chapters is that the difference between the loop and XXZ spin chain representations is manifest already at the smallest possible finite size. To see this, we next give a detailed discussion of the module $\mathscr{W}_{0,\mathfrak{q}^{\pm 2}}$ at $N = 2$ sites.

3.3 Indecomposable Temperley-Lieb modules

Consider the standard module $\mathscr{W}_{0,\mathfrak{q}^{\pm 2}}$ for $N = 2$, i.e., the loop model for two sites, in the sector with no through-lines and with non-contractible loops given the same weight $\mathfrak{m} = \mathfrak{q} + \mathfrak{q}^{-1}$ as contractible ones. We emphasize that since $\mathfrak{q}$ only enters in the combination $\mathfrak{q} + \mathfrak{q}^{-1}$, the sign of the exponent ($\mathfrak{q}^2$ versus $\mathfrak{q}^{-2}$) does not matter, motivating the notation $\mathscr{W}_{0,\mathfrak{q}^{\pm 2}}$.

In order to illustrate the differences between the XXZ and loop representations, let us first write the two elements of the Temperley-Lieb algebra in the basis of the two link states  and :

$$e_1 = \begin{pmatrix} \mathfrak{q}+\mathfrak{q}^{-1} & \mathfrak{q}+\mathfrak{q}^{-1} \\ 0 & 0 \end{pmatrix}, \qquad e_2 = \begin{pmatrix} 0 & 0 \\ \mathfrak{q}+\mathfrak{q}^{-1} & \mathfrak{q}+\mathfrak{q}^{-1} \end{pmatrix}. \tag{3.3.1}$$

It is apparent that $e_1($  $-$  $) = e_2($ $-$ $) = 0$. Meanwhile, the action of e_1 and e_2 on the single state  in $\mathscr{W}_{1,1}$ vanishes by definition of the standard module, since the number of through-lines would decrease. By comparison we see that $\mathscr{W}_{0,\mathfrak{q}^{\pm 2}}$ admits a submodule, generated by ($-$), that is isomorphic to $\mathscr{W}_{1,1}$. In pictorial terms we thus have

$\mathscr{W}_{0,\mathfrak{q}^{\pm 2}}$:  , (3.3.2)

where $\bullet$ denotes the submodule and $\circ$ the quotient module. The meaning of the arrow is that within the standard module $\mathscr{W}_{0,\mathfrak{q}^{\pm 2}}$ a state in $\mathscr{W}_{1,1}$ can be reached from a state in the complement $\overline{\mathscr{W}}_{0,\mathfrak{q}^{\pm 2}}$ through the action of the Temperley-Lieb algebra, whereas the opposite is impossible. (3.3.2) is an example of a *Loewy diagram*. Loewy diagrams are used to represent the structure of indecomposable modules.

We next consider instead the XXZ representation with $S_z = 0$ and twisted boundary conditions $e^{i\phi} = \mathfrak{q}^{-2}$, here without "smearing" of the twist. We chose the basis of this sector as $u = |\uparrow\downarrow\rangle$ and $v = |\downarrow\uparrow\rangle$. We have then

$$e_1 = \begin{pmatrix} \mathfrak{q}^{-1} & -1 \\ -1 & \mathfrak{q} \end{pmatrix}, \; e_2 = \begin{pmatrix} \mathfrak{q} & -\mathfrak{q}^2 \\ -\mathfrak{q}^{-2} & \mathfrak{q}^{-1} \end{pmatrix}. \tag{3.3.3}$$

We find that $e_1(u + \mathfrak{q}^{-1}v) = e_2(u + \mathfrak{q}^{-1}v) = 0$ while $e_1(u - \mathfrak{q}v) = (\mathfrak{q} + \mathfrak{q}^{-1})(u - \mathfrak{q}v)$ and $e_2(u - \mathfrak{q}v) = (\mathfrak{q} + \mathfrak{q}^{-1})(u - \mathfrak{q}v) + (\mathfrak{q}^3 - \mathfrak{q}^{-1})(u + \mathfrak{q}^{-1}v)$. Considering instead the module $\mathscr{W}_{1,1}$, which is the spin $S_z = 1$ sector with no twist and where $e_1 = e_2 = 0$, we see that $(u + \mathfrak{q}^{-1}v)$ generates a module isomorphic to $\mathscr{W}_{1,1}$. Meanwhile, $u - \mathfrak{q}v$ does not generate a submodule, since e_2 acting on this vector yields a component along $u + \mathfrak{q}^{-1}v$. However, if we quotient by $u + \mathfrak{q}^{-1}v$, we obtain a one-dimensional module where e_1 and e_2 act as $\mathfrak{q} + \mathfrak{q}^{-1}$, which is precisely the module $\overline{\mathscr{W}}_{0,\mathfrak{q}^{\pm 2}}$. We thus obtain the same result as for the loop model, i.e., the structure (3.3.2) of the standard module.

Considering instead $e^{i\phi} = \mathfrak{q}^2$, we have

$$e_1 = \begin{pmatrix} \mathfrak{q}^{-1} & -1 \\ -1 & \mathfrak{q} \end{pmatrix}, \; e_2 = \begin{pmatrix} \mathfrak{q} & -\mathfrak{q}^{-2} \\ -\mathfrak{q}^{2} & \mathfrak{q}^{-1} \end{pmatrix}. \tag{3.3.4}$$

We see that $e_1(u - \mathfrak{q}v) = e_2(u - \mathfrak{q}v) = (\mathfrak{q} + \mathfrak{q}^{-1})(u - \mathfrak{q}v)$, while $e_1(u + \mathfrak{q}^{-1}v) = 0$ and $e_2(u + \mathfrak{q}^{-1}v) = (\mathfrak{q} - \mathfrak{q}^{-3})(u - \mathfrak{q}v)$. Hence this time we get a proper $\overline{\mathscr{W}}_{0,\mathfrak{q}^{\pm 2}}$ module, while we only get $\mathscr{W}_{1,1}$ as a quotient module. The corresponding structure can be represented as

$\widetilde{\mathscr{W}}_{0,\mathfrak{q}^{\pm 2}}$: $\overline{\mathscr{W}}_{0,\mathfrak{q}^{\pm 2}}$ $\bullet$ $\uparrow$ $\circ$ $\mathscr{W}_{1,1}$. (3.3.5)

Observe that the shapes in (3.3.3) and 3.3.5) are related by inverting the (unique in this case) arrows; the module in (3.3.5) is referred to as "co-standard", and we indicate this dual nature by placing a tilde on top of the usual $\mathscr{W}_{0,\mathfrak{q}^{\pm 2}}$ notation for the standard module.

To emphasize that in the XXZ chain the standard module $\mathscr{W}_{0,\mathfrak{q}^{\pm 2}}$ corresponds to the twisted boundary condition $e^{i\phi} = \mathfrak{q}^{-2}$, while the co-standard module $\widetilde{\mathscr{W}}_{0,\mathfrak{q}^{\pm 2}}$ corresponds to the twisted boundary condition $e^{i\phi} = \mathfrak{q}^2$, we introduce the notations $\mathscr{W}_{0,\mathfrak{q}^{-2}} \equiv \mathscr{W}_{0,\mathfrak{q}^{\pm 2}}$ and $\mathscr{W}_{0,\mathfrak{q}^{2}} \equiv \widetilde{\mathscr{W}}_{0,\mathfrak{q}^{\pm 2}}$. Later on, we shall write diagrams of the type above as

$\mathscr{W}_{0,\mathfrak{q}^{-2}}$: $[0,\mathfrak{q}^{-2}]$ $\downarrow$ $[1,1]$, $\mathscr{W}_{0,\mathfrak{q}^{2}}$: $[0,\mathfrak{q}^{2}]$ $\uparrow$ $[1,1]$, (3.3.6)

where it is implicit that any relevant quotients have been taken.

In summary, from this short exercise we see that while in the generic case the loop and spin representations are isomorphic, this equivalence breaks down in the non-generic case, where ϕ is such that the resonance criterion (3.1.4) is met. Only standard modules are encountered in the loop model [3] while in the XXZ spin chain both standard and co-standard are encountered. This feature extends to larger N, according to a pattern we will discuss later. We will also see what this means in the continuum limit when comparing the XXZ spin chain results to the results in the loop representation. We note that in the case where $\mathfrak{q}$ is also a root of unity, the distinction between the two representations becomes even more pronounced: in this case the modules in the XXZ chain are no longer isomorphic to standard *or* co-standard modules. This will be further explored in a future work [59].

3.4 The quantum group $U_\mathfrak{q} sl(2)$

The choice to parametrize the loop weight as $\mathfrak{m} = \mathfrak{q} + \mathfrak{q}^{-1}$ is motivated by the close connection between the Temperley-Lieb algebra and the quantum group $U_\mathfrak{q} sl(2)$, which is a $\mathfrak{q}$-deformation of the enveloping algebra of $sl(2)$ generated by $S^+, S^-, \mathfrak{q}^{\pm S^z}$ under the relations

$$\mathfrak{q}^{S^z} S^\pm \mathfrak{q}^{S^z} = \mathfrak{q}^{\pm 1} S^\pm \,, \quad [S^+, S^-] = \frac{\mathfrak{q}^{2S^z} - \mathfrak{q}^{-2S^z}}{\mathfrak{q} - \mathfrak{q}^{-1}} \,. \tag{3.4.1}$$

These relations reduce to the usual $su(2)$ commutation relations in the limit $\mathfrak{q} \to 1$. Adding some further structure such as a co-product and an antipode turns $U_\mathfrak{q} sl(2)$ into a Hopf algebra [60,61]. $U_\mathfrak{q} sl(2)$ is most naturally introduced in the context of the open XXZ spin chain, which with the appropriate boundary conditions has a $U_\mathfrak{q} sl(2)$ symmetry just as the XXX spin chain has an $su(2)$ symmetry. This is a consequence of $U_\mathfrak{q} sl(2)$ being the Schur-Weyl dual of the Temperley-Lieb algebra on $(\mathbf{C}^2)^{\otimes N}$ [7, 62], and of the Hamiltonian being an element of the Temperley-Lieb algebra. In the periodic case, the situation is considerably more complicated, and a full understanding thereof forms the basis of ongoing work [7, 49, 63].

When $\mathfrak{q}$ is generic, as it will be for most of this thesis, the Hilbert space will decompose into irreducible representations labelled by spin $j = 0, \frac{1}{2}, ...$ that are in a one-to-one correspondence to $su(2)$ representations, with the basis-vectors being $\mathfrak{q}$-deformed. We shall however also need $\mathfrak{q}$ root of unity in Chapter 5. [64] provides a self-contained discussion of the fusion rules for representations in the $\mathfrak{q}$ root of unity case; the matter is also discussed in detail in [65]. Let $\mathfrak{q}^n = \pm 1$. The Hilbert space splits into two types of representations: "type I" representations are indecomposable, while "type II" representations have the same structure as for $\mathfrak{q}$ generic. The spin labels for type II representations are restricted to $0 \leq j \leq (n-2)/2$. In the height model formulation of the six-vertex model, truncating the Hilbert space to include only type II representations (which can be accomplished by inserting $\mathfrak{q}^{2S^z}$ into the trace of the transfer matrix) leads to the restriction on heights appearing in the A_n RSOS models.

There are many parallels between the representation theory of $U_\mathfrak{q} sl(2)$ as restricted to type II representations, and that of the $\widehat{su(2)}$ Kac-Moody algebra at level $k = n - 2$. For the latter, the unitary representations are precisely labelled by $0 \leq j \leq k/2$. In both cases the fusion rules for the representations are truncated as compared to the $su(2)$ fusion rules, and we will see these fusion rules appear in Chapter 5 as the fusion rules for $su(2)_k$ anyons. While the name of these anyons only makes reference to the Kac-Moody algebra, it is natural to describe them

[3] Of course, the co-standard module would be formally obtained by reversing the arrows, which corresponds formally to propagating "towards the past", or acting with the transpose of the transfer matrix to build partition and correlation functions. It is not clear what this means physically.

in the context of $\mathfrak{q}$-deformation, with $\mathfrak{q} = e^{\pi r i/(k+2)}$ – this language makes their connection to RSOS models especially clear.

3.5 Virasoro modules in unitary and non-unitary CFTs

We now turn to the symmetry algebra of the continuum theory, and its representation theory. Useful references include [4, 66]. At the critical point the long-range behaviour of the lattice models in Chapter 2, taken with periodic boundary conditions, is described by bulk conformal field theories, whose symmetry algebra is given by two copies of the Virasoro algebra (1.0.1): $\mathrm{Vir} \otimes \overline{\mathrm{Vir}}$. The Hilbert space decomposes into representations of this symmetry algebra.

The conserved current corresponding to the conformal symmetry is the stress-energy tensor $T_{\alpha\beta}$. In complex coordinates $T_{z\bar{z}} = T_{\bar{z}z} = 0$ and $\bar{\partial} T_{zz} = \partial T_{\bar{z}\bar{z}} = 0$, and we write $T(z) \equiv T_{zz}(z)$, $\bar{T}(\bar{z}) \equiv T_{\bar{z}\bar{z}}(\bar{z})$. The modes of T and $\bar{T}$ generate the Virasoro algebra: on the plane,

$$T(z) = \sum_{n=-\infty}^{\infty} \frac{L_n}{z^{n+2}} \tag{3.5.1a}$$

$$\bar{T}(\bar{z}) = \sum_{n=-\infty}^{\infty} \frac{\bar{L}_n}{\bar{z}^{n+2}}\,, \tag{3.5.1b}$$

and on the cylinder,

$$T(w) = -\sum_{n=-\infty}^{\infty} e^{inw} L_n + \frac{c}{24} \tag{3.5.2a}$$

$$\bar{T}(\bar{w}) = -\sum_{n=-\infty}^{\infty} e^{-in\bar{w}} \bar{L}_n + \frac{\bar{c}}{24}\,, \tag{3.5.2b}$$

where the cylinder is related to the plane through the conformal map $z = e^{-iw}$. We will in the following always have $c = \bar{c}$.

When $L_0, \bar{L}_0$ are diagonalizable, we call their eigenvalues $h, \bar{h}$ the chiral and antichiral conformal weights. We shall parametrize the weights by r, s:

$$h_{r,s} = \frac{[(x+1)r - xs]^2 - 1}{4x(x+1)}\,, \tag{3.5.3}$$

where x is related to the central charge as

$$c = 1 - \frac{6}{x(x+1)}\,. \tag{3.5.4}$$

We call r, s the Kac labels, but note that they will not necessarily be integer.

The most typical example of representations we shall encounter is *Verma modules*. These are highest weight representations generated by a primary field (a field that is annihilated by all raising operators $L_n, \bar{L}_n, n > 0$) of conformal weights $h, \bar{h}$ by the action of lowering operators $L_n, \bar{L}_n, n < 0$. They are infinite-dimensional. Showing schematically the action of the chiral lowering operators only, the Verma module $\mathsf{V}_{r,s}$ generated by a primary field $\phi_{r,s}$ with a chiral conformal weight $h_{r,s}$ takes the following form, with each level having fields with weights as

listed on the right:

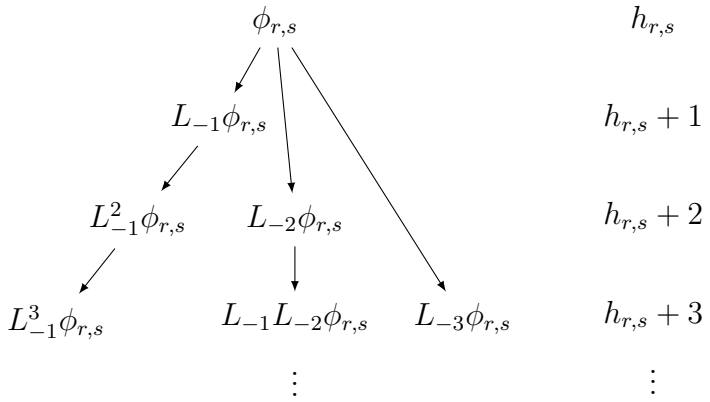

(3.5.5)

When r, s are not both positive integers, the Verma module is irreducible and is denoted $\mathsf{V}_{r,s}$. When both r, s are positive integers, one of the descendant states on level rs, with conformal weight $h_{r,-s} = h_{r,s} + rs$, will itself be a primary state – a *null state* – and it generates a submodule $\mathsf{V}_{r,-s}$.[4] Whether or not its complement $\mathsf{X}_{r,s}$ is constrained to also be a submodule, so that the Verma module is completely reducible, depends on whether or not the theory is unitary. We first give some more details on unitarity, before focusing on the indecomposable modules that will show up in the non-unitary setting of this thesis.

Unitarity and complete reducibility

In radial quantization, an "in-state" is created by the action of an operator $\mathcal{O}$ at a position $(z, \bar{z})$ inside the unit circle, and a conjugate "out-state" is created by an operator $\mathcal{O}$ at inverse position $(\bar{z}^{-1}, z^{-1})$ outside the unit circle. Let $\mathcal{O}$ have conformal weights $h, \bar{h}$. For a unitary theory, a Hermitian operator satisfies

$$\mathcal{O}(z,\bar{z})^\dagger = \bar{z}^{-2h} z^{-2\bar{h}} \mathcal{O}(\bar{z}^{-1}, z^{-1}) \,, \tag{3.5.6}$$

where the pre-factor takes care of the normalization of

$$\langle h, \bar{h} | h, \bar{h} \rangle = \bar{z}^{-2h} z^{-2\bar{h}} \langle 0 | \lim_{z\to 0} \mathcal{O}(\bar{z}^{-1}, z^{-1}) \mathcal{O}(z,\bar{z}) | 0 \rangle \tag{3.5.7}$$

in which we must compensate for the factor

$$\lim_{z\to 0} \frac{C_{\mathcal{O}\mathcal{O}}}{(\bar{z}^{-1} - z)^{2h} (z^{-1} - \bar{z})^{2\bar{h}}} = C_{\mathcal{O}\mathcal{O}} \bar{z}^{2h} z^{2\bar{h}} \,. \tag{3.5.8}$$

Applying (3.5.6) to $T, \bar{T}$ and using its mode decomposition (3.5.1) gives

$$L_n^\dagger = L_{-n} \,, \quad \bar{L}_n^\dagger = \bar{L}_{-n} \,. \tag{3.5.9}$$

If (3.5.9) is not fulfilled in a given Virasoro representation, this representation must be non-unitary.

The unitary representations are completely reducible, as the following reasoning shows. Consider a Verma module, that we here denote $\hat{\mathsf{V}}_{r,s}^{(\mathrm{d})}$ (d for degenerate), with r, s positive integers such that $\hat{\mathsf{V}}_{r,s}^{(\mathrm{d})}$ has a submodule $\mathsf{V}_{r,-s}$. We now want to show that the complement $\mathsf{X}_{r,s}$

[4] Note: at c rational there can be several null states, leading to more complicated modules. We here consider c generic.

of the submodule in $\hat{\mathsf{V}}^{(\mathrm{d})}_{r,s}$ is itself closed under the action of the Virasoro algebra. Let $|u\rangle$ be a state in $\mathsf{X}_{r,s}$ and $|v\rangle$ a state in $\mathsf{V}_{r,-s}$, By (3.5.9), we have for any Virasoro generator L_n

$$\langle v|L_n|u\rangle = \left(\left(\langle v|L_n|u\rangle\right)^\dagger\right)^* = \left(\langle u|L_{-n}|v\rangle\right)^* = 0\,, \tag{3.5.10}$$

and same for any matrix elements between one state in the complement, one state in the submodule. This means that we cannot have the situation that was depicted in the Loewy diagrams (3.3.2); it is impossible to reach the submodule from the complement and the representation is completely reducible. The corresponding Loewy diagram is

$$\hat{\mathsf{V}}^{(\mathrm{d})}_{r,s}\colon \quad \begin{array}{c} \mathsf{X}_{r,s} \\ \bullet \\ \\ \bullet \\ \mathsf{V}_{r,-s} \end{array} \,. \tag{3.5.11}$$

Non-unitarity and indecomposable representations

Lifting the constraint of unitarity means that the representations are no longer constrained to be completely reducible. When the complement $\mathsf{X}_{r,s}$ is not a submodule we denote the now indecomposable Verma module $\mathsf{V}^{(\mathrm{d})}_{r,s}$. We call the corresponding quotient module a *Kac module*, also denoted by $\mathsf{X}_{r,s}$. The Loewy diagram describing $\mathsf{V}^{(\mathrm{d})}_{r,s}$ has the same structure as (3.3.2):

$$\mathsf{V}^{(\mathrm{d})}_{r,s}\colon \quad \begin{array}{c} \mathsf{X}_{r,s} \\ \circ \\ \downarrow \\ \bullet \\ \mathsf{V}_{r,-s} \end{array} \,, \tag{3.5.12}$$

We call the dual of (3.5.12) a *co-Verma* module, denoted by $\widetilde{\mathsf{V}}^{(\mathrm{d})}_{r,s}$. It has the same structure as (3.3.5)

$$\widetilde{\mathsf{V}}^{(\mathrm{d})}_{r,s}\colon \quad \begin{array}{c} \mathsf{X}_{r,s} \\ \bullet \\ \uparrow \\ \circ \\ \mathsf{V}_{r,-s} \end{array} \tag{3.5.13}$$

Furthermore, in a non-unitary theory $L_0, \bar{L}_0$ may not be diagonalizable at all. We consider then instead the generalized eigenvalues, defined as the elements on the diagonal when $L_0, \bar{L}_0$ are written in Jordan normal form. In particular we shall encounter Virasoro modules that take a diamond form, as in the following example:

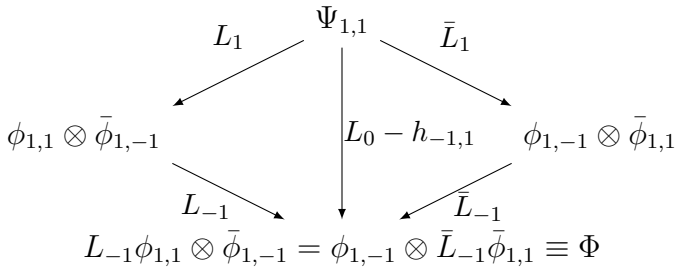

(3.5.14)

Such modules lead to Jordan cells of rank two: here $L_0 = \begin{pmatrix} h_{-1,1} & 1 \\ 0 & h_{-1,1} \end{pmatrix}$ in the basis $(\Phi, \Psi_{1,1})$. Correlation functions involving the fields connected by such Jordan blocks obtain logarithmic corrections [67, 68] – in the rank-two example, they take the form

$$\begin{aligned} \langle \Phi(0)\Phi(z\bar{z})\rangle &= 0 \\ \langle \Phi(0)\Psi_{1,1}(z,\bar{z})\rangle &= \frac{b}{(z\bar{z})^{2h_{-1,1}}} \\ \langle \Psi_{1,1}(0)\Psi_{1,1}(z,\bar{z})\rangle &= \frac{-2b\log(z\bar{z})+a}{(z\bar{z})^{2h_{-1,1}}}\,. \end{aligned} \tag{3.5.15}$$

For this reason, such modules are called *logarithmic* Virasoro modules, and $\Psi_{1,1}$ in the above example is called the logarithmic partner of Φ.

When c is rational, the indecomposable modules can be more complicated still, leading to Jordan cells of higher rank. In this thesis, we restrict to generic (non-rational) values of c.

3.5.1 Jordan cells and logarithms from limits of ordinary CFTs

Jordan cells can appear when the conformal weights of two or more fields collide. Let us consider an illustrative example, taken from [69]. In this example we consider two fields $\phi, \tilde{\phi}$ such that

$$\begin{aligned} \langle \phi(r)\phi(0)\rangle &= \frac{A(n)}{n-n_c}\, r^{-2x(n)}\,, \\ \langle \tilde{\phi}(r)\tilde{\phi}(0)\rangle &= -\frac{\widetilde{A}(n)}{n-n_c}\, r^{-2\tilde{x}(n)}\,, \\ \langle \phi(r)\tilde{\phi}(0)\rangle &= 0\,, \end{aligned} \tag{3.5.16}$$

with colliding weights $x(n) \to \tilde{x}(n)$ as $n \to n_c$, $A(n)$ and $\widetilde{A}(n)$ having the same finite limits as $n \to n_c$, and with $x(n), \tilde{x}(n)$ differentiable at n_c. In this limit, the correlation functions of the fields

$$D \equiv \phi - \tilde{\phi}\,, \qquad C \equiv \big(x(n) - \tilde{x}(n)\big)\phi\,, \tag{3.5.17}$$

then take the form

$$\begin{aligned} \langle D(r)D(0)\rangle &= \frac{A(n)}{n-n_c}\frac{1}{r^{2x(n)}} - \frac{\widetilde{A}(n)}{n-n_c}\frac{1}{r^{2\tilde{x}(n)}} \to -\frac{2\alpha\big(\log r + O(1)\big)}{r^{2x(n_c)}}\,, \\ \langle C(r)D(0)\rangle &= \frac{A(n)(x(n)-\tilde{x}(n))}{n-n_c}\frac{1}{r^{2x(n)}} \to \frac{\alpha}{r^{2x(n_c)}}\,, \\ \langle C(r)C(0)\rangle &= \frac{A(n)(x(n)-\tilde{x}(n))^2}{n-n_c}\frac{1}{r^{2x(n)}} \to 0\,, \end{aligned} \tag{3.5.18}$$

where α is a rescaling of A: $\alpha = \big(x'(n_c) - \tilde{x}'(n_c)\big)A(n_c)$. We have recovered the form of correlation functions in (3.5.15). The fields C, D form a logarithmic pair and span a Jordan cell of rank two. Higher rank Jordan cells can appear when the conformal weights of more than two fields collide.

Finding features of logarithmic conformal field theories by considering limits of ordinary conformal field theories is also the principle behind the derivation of logarithmic conformal *blocks* in the bootstrap approach [6].

3.6 From lattice to CFT: the torus partition function

Some information about the Virasoro representations in the continuum theory can be inferred from the partition function on a torus. We first consider periodic boundary conditions in space, and denote by $\mathscr{H}$ and $\mathscr{P}$ the Hamiltonian and lattice momentum on the resulting cylinder. We then close the cylinder into a torus by imposing as well periodic boundary conditions in time, possibly after twisting the cylinder. More precisely, we consider a torus with modular parameter τ:

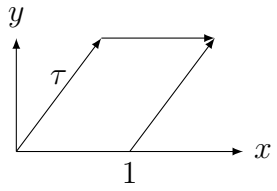

The partition function on this torus is[5]

$$Z(\tau) = \operatorname{Tr} e^{-2\pi(\operatorname{Im}\tau)\mathscr{H}} e^{-2\pi i(\operatorname{Re}\tau)\mathscr{P}} . \tag{3.6.1}$$

In the continuum limit, we rewrite it using

$$\begin{aligned} \mathscr{H} &= L_0 + \bar{L}_0 - \frac{c}{12} \\ \mathscr{P} &= L_0 - \bar{L}_0 . \end{aligned} \tag{3.6.2}$$

(We here assume Vir and $\overline{\text{Vir}}$ to have the same central charge.) Setting $q = e^{2i\pi\tau}, \bar{q} = e^{-2i\pi\bar{\tau}}$ we recover the character χ of $\text{Vir} \otimes \overline{\text{Vir}}$:

$$Z(\tau) = \operatorname{Tr} q^{L_0 - c/24} \bar{q}^{\bar{L}_0 - c/24} = \chi(q) . \tag{3.6.3}$$

As a representation of $\text{Vir} \otimes \overline{\text{Vir}}$ the Hilbert space decomposes as a sum over irreducible or indecomposable representations $\mathscr{R}$, so that

$$Z(q) = \chi(q) = \sum_{\mathscr{R}} D_{\mathscr{R}}\, \chi_{\mathscr{R}}(q) , \tag{3.6.4}$$

with "multiplicities" $D_{\mathscr{R}}$ that may, in general, be non-integer.

We will encounter two types of irreducible representations: Verma modules when r, s are not both positive integers, and Kac modules when they are. In the simplest example, an irreducible Verma module (r, s not both positive integers), the character is given by [4]

$$\chi_{\mathsf{V}_{r,s}}(q) = \frac{q^{h_{r,s} - c/24}}{\prod_{n=1}^{\infty}(1 - q^n)} \tag{3.6.5}$$

on the chiral side, and same on the anti-chiral side.

Additionally we will encounter indecomposable representations of various kinds: Verma and co-Verma modules when r, s are both integers, which both contain a submodule that is not quotiented out, as well as logarithmic modules of the type seen above.

The decomposition provides us with valuable information about the continuum limit, such as the conformal weights of its operators. However, being defined by a trace, the torus partition function contains no information about off-diagonal elements – that is, about the presence of the Jordan cells of L_0 and $\bar{L}_0$ that appear in logarithmic conformal field theories. To obtain the detailed structure of the representations needed to detect Jordan cells, we can use lattice methods such as the Koo-Salur generators that are the subject of the next section.

[5] We shall later instead use the notation β_R and β_I in the torus partition function, following the correspondence between periodic time and inverse temperature.

3.7 Discrete Virasoro algebra: the Koo-Saleur generators

In [12], Koo and Saleur introduced a lattice discretization of the Virasoro algebra, in which the Virasoro generators are written in terms of Temperley-Lieb generators. In this original derivation, the authors used lattice Ward identities to derive an expression for the discrete stress-energy tensor, and the expression of the discrete Virasoro generators then follows immediately from the Fourier mode expansion on a cylinder (3.5.2).

We here present the discrete stress-energy tensor in terms of the energy density and momentum density, following [24]. By (3.2.2) we define the Hamiltonian density as $\hbar_j = -\frac{\gamma}{\pi \sin\gamma} e_j$, from which we may construct a lattice momentum density $\wp_j = i[\hbar_j, \hbar_{j-1}] = -i\big(\frac{\gamma}{\pi \sin\gamma}\big)^2 [e_{j-1}, e_j]$ by using energy conservation. We define the corresponding momentum operator $\mathscr{P}$ as

$$\mathscr{P} = -i \left(\frac{\gamma}{\pi \sin\gamma} \right)^2 \sum_{j=1}^{N} [e_j, e_{j+1}]. \tag{3.7.1}$$

From the densities $\hbar_j$ and $\wp_j$ we may build components of a discretized stress tensor as

$$\mathscr{T}_j = \frac{1}{2}(\hbar_j + \wp_j)\,, \tag{3.7.2a}$$

$$\bar{\mathscr{T}}_j = \frac{1}{2}(\hbar_j - \wp_j)\,. \tag{3.7.2b}$$

Using (3.7.2) together with (3.5.2) leads to the Koo-Saleur generators[6]

$$\mathscr{L}_n[N] = \frac{N}{4\pi} \left[-\frac{\gamma}{\pi \sin\gamma} \sum_{j=1}^{N} e^{inj2\pi/N} \left(e_j - e_\infty + \frac{i\gamma}{\pi \sin\gamma} [e_j, e_{j+1}] \right) \right] + \frac{c}{24} \delta_{n,0}\,, \tag{3.7.3a}$$

$$\bar{\mathscr{L}}_n[N] = \frac{N}{4\pi} \left[-\frac{\gamma}{\pi \sin\gamma} \sum_{j=1}^{N} e^{-inj2\pi/N} \left(e_j - e_\infty - \frac{i\gamma}{\pi \sin\gamma} [e_j, e_{j+1}] \right) \right] + \frac{c}{24} \delta_{n,0}\,. \tag{3.7.3b}$$

The crucial additional ingredient in these formulae is the central charge, given as in (3.5.4) by $c = 1 - \frac{6}{x(x+1)}$ related to γ through the parametrization

$$\gamma = \frac{\pi}{x+1}\,. \tag{3.7.4}$$

This choice (3.5.4) is known to apply to models with Hamiltonian (3.2.2), such as the ferromagnetic Q-state Potts model with $Q = \mathfrak{m}^2$. Note, however, that the identification (3.5.4) is actually a rather subtle question, since it may be affected by boundary conditions. We discuss this aspect in details in Chapter 6; further discussion can be found in Appendix G of [16].

[6] We here use calligraphic fonts for the lattice analogs of some key quantities: the Hamiltonian $\mathscr{H}$, the momentum $\mathscr{P}$—with their corresponding densities $\hbar_j$ and $\wp_j$—, the Virasoro generators $\mathscr{L}_n$, $\bar{\mathscr{L}}_n$ and the stress-energy tensor $\mathscr{T}$, $\bar{\mathscr{T}}$. We denote the corresponding continuum quantities by Roman fonts: H, P and L_n, $\bar{L}_n$, as well as T, $\bar{T}$. One of the paramount questions is of course whether we have the convergence $\mathscr{L}_n, \bar{\mathscr{L}}_n \mapsto L_n, \bar{L}_n$ in the continuum limit $N \to \infty$—and if we do, what precisely is the nature of this convergence.

CHAPTER

4

CORRELATION FUNCTIONS IN THE POTTS AND RSOS MODELS

In the pioneering work [19], a simple crossing symmetric spectrum was proposed to describe some of the four-point functions of the order operator in the Potts model; in terms of clusters, these correspond to probabilities of having four points connected in different ways, as we shall discuss below. The proposal was checked using Monte-Carlo simulation, and reasonable agreement was found. A later work [20] based on a combination of algebraic and numerical techniques however showed that the speculated spectrum cannot be the true spectrum for the Potts model: it misses an infinite number of states which, despite having small amplitudes, are essential to cancel the unwanted singularities in Q appearing in the four-point function of [19]. To this day, the full four-point functions remain therefore unknown. [1]

Interestingly, it was found afterwards in [71] that the spectrum of [19] could be obtained from a certain limit of minimal models when the central charge is taken to be an irrational number (see Section 4.1.4 below). The corresponding CFT was further elucidated analytically in [72,73]. The main question however remains: what statistical physics model does the spectrum in [19] actually describe, if it is not the Potts model, and why does it give results apparently so close numerically [74] to those of the Potts model? The goal of the present chapter is to answer this question. Remarkably, we shall also obtain results of considerable importance for the solution of the Potts problem itself [21].

We will focus on the geometrical interpretation of correlation functions in restricted solid-on-solid (RSOS) models, following and extending the early work of, in particular, V. Pasquier [29, 75, 76] and I. Kostov [30]. We shall find that the lattice correlation functions of certain operators in these models have graphical expansions that are very similar to—albeit slightly different from—those occurring in the Potts model. The main difference between the two models is, perhaps not surprisingly, the weight given to clusters with non-trivial topologies. The fine structure of these weights allows for intricate cancellations of the Potts spectrum given in [20], leading to the spectrum of (unitary or non-unitary) minimal models in the corresponding limits.

[1] See also [70] for some recent study of the four-spin correlations using the Coulomb Gas approach.

By following the logic in [71], and taking appropriate limits of the lattice model, we are then able to provide a geometrical interpretation of the correlation functions proposed in [19], and explain why—and by how much—they differ from the true Potts model ones.

The chapter is organized as follows. In the next section, we briefly review the geometrical correlations in the Potts model, and provide further motivations to study the relation with minimal models. In Section 4.2, we describe the general strategy for comparing the Potts and RSOS correlations, and we state in particular the main results about the RSOS lattice model relevant for establishing its connection with the Potts model. These will be used in the following section to study in detail the geometrical formulation of four-point functions in minimal models of type A and D. There, we define the relevant geometrical quantities—the "pseudo-probabilities" in the RSOS minimal models, which are to be compared with the true probabilities in the Potts model. In Section 4.4, we turn to the s-channel spectra involved in these two quantities, which we exhibit in terms of the affine Temperley-Lieb algebra as studied in [20]. The properties of the spectra in the two cases are characterised by several striking facts about the ratios between certain amplitudes entering the s-channel expressions of the probabilities. The amplitude ratios are exact expressions (ratios of integer-coefficient polynomials in Q), which we obtain here conjecturally based on numerical observations, deferring the task of proving them to a future publication. These facts are then used in Section 4.5 to recover the minimal models spectra. In Section 4.6, we discuss the limit when the central charge goes to an irrational number and compare with the CFT results. The last section contains our conclusions.

To focus on the comparison with the Potts model, we only state relevant results on the RSOS model in this chapter, but also provide a more systematic formulation elsewhere. In particular, in Section 2.3 we give a proof of the identity of the RSOS and Potts partition functions.In Section 5.2, we state the rules for computing the RSOS N-point functions. Finally Appendix A gives the results on 3-point couplings in the type A and D RSOS model which are used in the main text for the geometrical formulation of the minimal models four-point functions. The reader is referred to Appendix D of [15] for details on the numerical methods (beyond those already described extensively in the appendices of [20]) used for extracting the exact amplitude ratios.

4.1 Correlation functions in the Potts model

4.1.1 Lattice model

We consider the lattice Q-state Potts model [34] on a graph $G = (V, E)$ with vertices V and edges E, with the partition function (2.1.16). We take G to be the two-dimensional square lattice and the temperature parameter to be its critical value $v_c = \sqrt{Q}$ [34,35] such that in the continuum limit the model is conformally invariant. In this limit, we consider the geometry of the infinite plane, so that boundary effects are immaterial.

In Chapter 2 we saw that the partition function can be formulated in terms of a loop model. Let us recall and slightly rewrite the partition function (2.1.17) as

$$Z = Q^{|V|/2} \sum_{A \subseteq E} \left(\frac{v}{n}\right)^{|A|} n^{\ell(A)} , \tag{4.1.1}$$

using the loop weight n. It is given by

$$n = \sqrt{Q} = \mathfrak{q} + \mathfrak{q}^{-1} , \tag{4.1.2}$$

where $\mathfrak{q}$ is the deformation parameter of the quantum group introduced in Section 3.4. Notice that on a square lattice, we have simply $\frac{v_c}{n} = 1$, i.e., at the critical point, (4.1.1) depends only on $\ell(A)$.

4.1.2 Correlation functions on the lattice

On the lattice, it is natural to consider the correlation functions of the order parameter (spin) operator

$$\mathcal{O}_a(\sigma_i) \equiv Q\delta_{\sigma_i,a} - 1. \tag{4.1.3}$$

One can however define more general correlation functions of a geometrical type by switching to the cluster or loop formulations, as described in Chapter 2. We are mainly interested in the geometrical correlation functions defined in terms of the FK clusters as following. Consider a number of distinct marked vertices $i_1, i_2, \ldots, i_N \in V$, and let $\mathscr{P}$ be a partition of a set of N elements. One can then define the probabilities

$$P_{\mathscr{P}} = \frac{1}{Z} \sum_{A \subseteq E} v^{|A|} Q^{\kappa(A)} \mathcal{I}_{\mathscr{P}}(i_1, i_2, \ldots, i_N | A)\,, \tag{4.1.4}$$

where Z is given in terms of FK clusters by (2.1.16), and $\mathcal{I}_{\mathscr{P}}(i_1, i_2, \ldots, i_N|A)$ is the indicator function that, $\forall k, l \in \{1, \ldots, N\}$ belong to the same block of the partition $\mathscr{P}$ if and only if vertices i_k and i_l belong to the same connected component in A. We will denote $\mathscr{P}$ by an ordered list of N symbols $(a, b, c, \ldots)$ where identical symbols refer to the same block. Taking $N = 2$ for instance, P_{aa} is the probability that vertices i_1, i_2 belong to the same FK cluster, whereas $P_{ab} = 1 - P_{aa}$ is the probability that i_1, i_2 belong to two distinct FK clusters.

The probabilities $P_{\mathscr{P}}$ can be related to the correlation functions of the spin operator

$$G_{a_1,a_2,\ldots,a_N} = \langle \mathcal{O}_{a_1}(\sigma_{i_1}) \mathcal{O}_{a_2}(\sigma_{i_2}) \cdots \mathcal{O}_{a_N}(\sigma_{i_N}) \rangle\,, \tag{4.1.5}$$

where the expectation value is defined with respect to the normalization Z. Here $a_1, a_2, \ldots, a_N$ is a list of (identical or different) symbols defining a partition $\mathscr{P}$. To evaluate the expectation value of a product of Kronecker deltas, one initially supposes that Q is integer, and uses that spins on the same FK cluster are equal, while spins on different clusters are statistically independent. This leads to Q-dependent relations, which can be analytically continued to real values of Q. In the case of $N = 2$, one finds that

$$G_{a_1,a_2} = (Q\delta_{a_1,a_2} - 1)\, P_{aa}, \tag{4.1.6}$$

i.e., the two-point function of the spin operator is proportional to the probability that the two points belong to the same FK cluster. Therefore $\mathcal{O}_a(\sigma_i)$ effectively "inserts" an FK cluster at $i \in V$ and ensures its propagation until it is "taken out" by another spin operator.

In the context of four-point functions, there are 15 probabilities $P_{aaaa}, P_{aabb}, \ldots, P_{abcd}$ whose combinatorial properties were discussed in [77]. We will focus on the same subset of four-point functions as studied in [19] which are the probabilities of the four points belonging to one or two clusters, namely: P_{aaaa}, P_{aabb}, P_{abba} and P_{abab}. The relation with the corresponding $G_{\mathscr{P}}$ reads [77]

$$\begin{aligned}
G_{aaaa} &= (Q-1)(Q^2-3Q+3)P_{aaaa} + (Q-1)^2(P_{aabb} + P_{abba} + P_{abab})\,, && \text{(4.1.7a)}\\
G_{aabb} &= (2Q-3)P_{aaaa} + (Q-1)^2 P_{aabb} + P_{abba} + P_{abab}\,, && \text{(4.1.7b)}\\
G_{abba} &= (2Q-3)P_{aaaa} + P_{aabb} + (Q-1)^2 P_{abba} + P_{abab}\,, && \text{(4.1.7c)}\\
G_{abab} &= (2Q-3)P_{aaaa} + P_{aabb} + P_{abba} + (Q-1)^2 P_{abab}\,. && \text{(4.1.7d)}
\end{aligned}$$

As stated before, for arbitrary real values of Q, the left-hand sides of these equations are only formally defined: it is in fact the right-hand sides that give them a meaning. Notice that the linear system has determinant $Q^4(Q-1)(Q-2)^3(Q-3)$ and therefore cannot be fully inverted for $Q = 0, 1, 2, 3$.

4.1.3 Continuum limit

In the continuum limit, and at the critical point, the Potts model is conformally invariant for $0 \leq Q \leq 4$. One then expects that the correlation functions (4.1.7) are given by the spin correlation functions in the corresponding CFT. We parametrize

$$\sqrt{Q} = 2\cos\left(\frac{\pi}{x+1}\right), \text{ with } x \in [1, \infty], \tag{4.1.8}$$

with x related to the central charge as in (3.5.4). Note that the quantum-group related parameter $\mathfrak{q} = \mathrm{e}^{\frac{i\pi}{x+1}}$ is not a root of unit in this generic case, i.e., we do *not* restrict x to be integer, as would be the case for the minimal models. We also use the Kac table parametrization (3.5.3) of conformal weights.[2] Usually, the Kac labels (r, s) are positive integers, but—like for the parameter x—we shall here allow them to take more general values. Of course, when (r, s) are not integer, the corresponding conformal weight is not degenerate. It is well known in particular that the order parameter operator has conformal weight $h_{1/2,0}$ [47, 78]. Part of the challenge since the early days of CFT has been to understand what such weight exactly means—in particular, what are the OPEs of the field with itself, and how they control the four-point functions.

4.1.4 A potential relationship with minimal models

It so happens that when

$$x = \frac{q}{p-q}, \text{ with } p > q \text{ and } p \wedge q = 1, \tag{4.1.9}$$

for p even and q odd, the conformal weight $h_{1/2,0}$ belongs to the Kac table

$$h_{m,n} = \frac{(pm - qn)^2 - (p-q)^2}{4pq} \tag{4.1.10}$$

of the minimal models $\mathscr{M}(p, q)$ with central charge

$$\mathscr{M}(p,q): \; c = 1 - 6\frac{(p-q)^2}{pq}, \tag{4.1.11}$$

where the cases $p-q = 1$ correspond to unitary minimal models, and $p-q > 1$ are non-unitary. Using the parametrization

$$p = 2n, \quad q = 2m+1, \tag{4.1.12}$$

with non-negative integers $n > m$ (and $n - m = 1$ corresponding to unitary cases), it is easy to see from (4.1.10) that indeed $h_{1/2,0} = h_{m,n}$ (since $p/2 = n$, while $pm - qn = -n$). The

[2] To compare with [19] one must identify $\beta^2 = \frac{x}{x+1}$ (so that $\frac{1}{2} \leq \beta^2 \leq 1$). Moreover, the conventions used in their paper for the exponents are switched with respect to ours: they call Δ_{sr} what we call h_{rs}.

question then arises, as to whether (some of) the geometrical correlations of interest for the corresponding value of Q with

$$\sqrt{Q} = 2\cos\frac{\pi(p-q)}{p} \tag{4.1.13}$$

could conceivably be obtained from the four-point functions of the field with $h = h_{m,n}$, for positive integer Kac labels m, n, in a minimal model[3] CFT with the same central charge.

In [19], the authors first conjectured CFT four-point functions describing the Potts probabilities:

$$\underline{\text{Conjecture in [19]:}}$$
$$\langle V^D V^N V^D V^N\rangle \propto P_{aaaa} + \mu P_{abab} \tag{4.1.14}$$

where μ is a constant, and similarly for P_{abba} and P_{aabb} with the left hand side replaced by $\langle V^D V^N V^N V^D\rangle$ and $\langle V^D V^D V^N V^N\rangle$. The V^D and V^N here have conformal dimension $h_{1/2,0} = \bar{h}_{1/2,0}$ and were later found in [72] to originate from the diagonal and non-diagonal sectors respectively of the type D minimal models. While the central charge in the minimal models is rational, the following limit of the minimal models spectrum was taken [72] to provide an extension to the irrational cases:[4]

$$p, q \to \infty, \quad \frac{q}{p-q} \to x\,, \tag{4.1.15}$$

where x is a finite number. In such a limit, it was argued in [71, 73] that the levels of the null vectors, which are removed in irreducible modules of minimal models, go to infinity, and one obtains Verma modules with the same conformal dimensions: the non-diagonal sector contains fields with conformal dimensions $(h_{r,s}, h_{r,-s})$ where $r \in \mathbb{Z} + \frac{1}{2}, s \in 2\mathbb{Z}$, and the spectrum in the diagonal sector becomes continuous. The limit spectrum was then used in a conformal block expansion for the numerical bootstrap of the four-point function (4.1.14), and the results obtained were found to be in reasonable agreement with Monte-Carlo simulations [74]. The corresponding structure constants were later obtained and shown to match [72] with a non-diagonal generalization [79] of the Liouville DOZZ formula [80].

This elegant and tempting procedure does not, however, give the true Potts probabilities. In particular, the latter are expected to be smooth functions in Q (as already argued in [20]), while there are poles in the four-point functions (4.1.14) at rational values of x when [71]:

$$p \equiv 0 \bmod 4\,, \tag{4.1.16}$$

corresponding to the values of Q:

$$Q = 4\cos^2\left(\frac{\pi}{4}\right),\ 4\cos^2\left(\frac{\pi}{8}\right),\ 4\cos^2\left(\frac{3\pi}{8}\right),\ \ldots\,. \tag{4.1.17}$$

The authors of [19] then further conjectured the following relation in [74] (hence, proposing an formula for their μ parameter, which was initially adjusted numerically):

$$\underline{\text{Conjecture in [74]:}}$$
$$\langle V^D V^N V^D V^N\rangle \propto\!\!\!\!\!\approx P_{aaaa} + \frac{2}{Q-2} P_{abab}. \tag{4.1.18}$$

[3] *A* rather than *the* minimal model, as there might be several modular invariants.

[4] With the identification of the parameters as explained in footnote 2, the p, q in [71] is also switched with respect to ours and the limit (4.1.15) correspond to the limit $\frac{p}{q} \to \beta^2$ in [71].

This expression accommodates the first pole of (4.1.17) at $Q = 2$ in the four-point function, and was observed using Monte-Carlo simulations [74] to be approximately correct. It also becomes exact for $Q = 0, 3, 4$. *A priori*, there is no reason why such a combination of the geometric quantities should enter the four-point function in the CFT. In addition, it is unclear how the other poles in Q given by (4.1.17)—which were truncated out in the conformal block expansion in [74]—could be accounted for in the four-point function (4.1.18) in terms of the geometric quantities.

Despite these issues, it is fascinating to see that the four-point functions of minimal models (and their irrational limits) do indeed seem to provide some insights on the geometrical problem of the Potts model. The question is why, and whether this is useful.

An important motivation for this chapter is to clarify this matter, and to establish in particular that the geometrical four-point functions (4.1.4) cannot be obtained by analytic continuation of the minimal models results in this way. It will turn out that the difference between the two types of correlation functions is numerically small, and probably indiscernible by Monte-Carlo methods [74], although they are certainly detectable by the transfer matrix techniques developed in [20] and used in the present work. The quantities defined and studied in [19, 71–74] will prove to be skewed versions of the true correlation functions (4.1.4), as we shall explain in detail in Section 4.6.

To make progress, we shall follow a direct approach, and study the geometrical correlation functions of minimal models on the lattice. Setting aside the CFT aspects for a moment, let us recall that minimal models can in fact be obtained as a continuum limit of well-defined RSOS lattice models associated with Dynkin diagrams of the ADE type [29, 75, 81]. In this formalism, the correlation functions of the order parameters on the lattice become, in the continuum limit, (some of) the correlation functions of minimal models. In particular, certain order parameter(s) in the RSOS lattice model give rise to the field with conformal weight $h_{m,n}$ in the Kac table and thus coincide with the Potts order parameter at the same central charge—recall the relation (4.1.12). On the other hand, the RSOS lattice model has a natural formulation in terms of clusters and loops [29, 30, 75, 76], somewhat similar to the one in the Potts model, and therefore the correlation functions acquire a geometrical interpretation which can be compared with that of the Potts model. In the following sections, we will study the RSOS four-point functions and their geometrical content, with focus on the operator whose conformal weight coincides with the one of the Potts order parameter, in order to understand the relation and differences with geometrically defined correlation functions of the Potts model. We will use the main results of RSOS correlations functions without detailed proofs, which we leave to Chapter 5.

4.2 Comparing Potts and RSOS correlations: general strategy

Let us take a more detailed look at the formulation of the Potts model in terms of clusters and loops. Consider a Potts cluster configuration given by the subgraph $G_A = (V, A)$, where the loops are formulated in the usual way as described in Chapter 2. Taking the centers of each plaquette (i.e., lattice face), and defining them as the vertices V^* of another lattice, we obtain the dual Potts model on the graph $G^* = (V^*, E^*)$. The previous loop configuration in fact predetermines the clusters on the dual lattice given by subgraph $G^*_{A^*} = (V^*, A^*)$, where the A^* are all the edges in E^* which do not cross the loops. There is thus a one-to-one map between the Potts cluster configurations G_A and its dual $G^*_{A^*}$. As shown in figures 4.1a and 4.1b, we

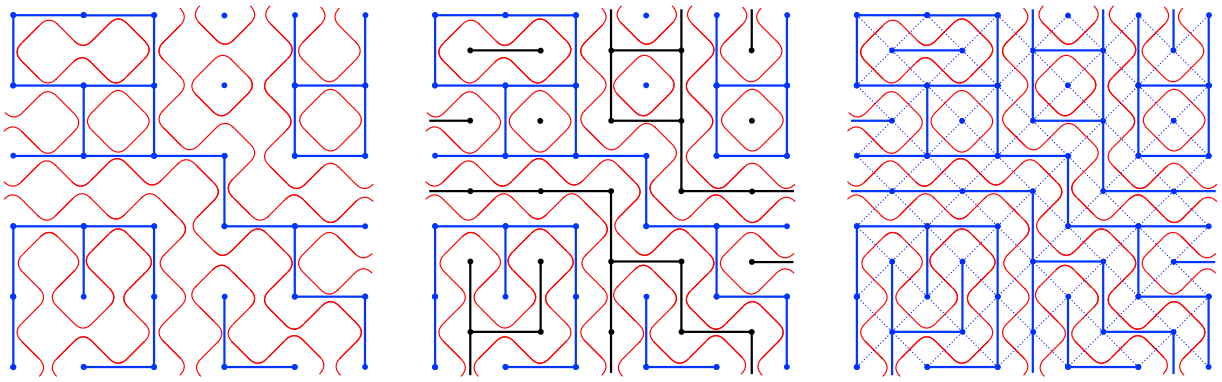

(a) (b) (c)

Figure 4.1: In 4.1a, we show a cluster configurations on the Potts lattice (blue) and the corresponding loops (red). The clusters are separated by an even number of loops. From here, one can draw the clusters on the dual lattice (black) as shown in 4.1b. An RSOS clusters/loops configuration 4.1c is equivalent to this Potts clusters/loops configuration. The links forming the clusters are on the diagonals of the plaquettes, the latter being indicated with dashed lines. The loop configuration is the same as in the Potts case; however, the weights of the loops are different.

see that when put together, the loops separate the Potts clusters from their dual clusters. A consequence of this mapping, which will turn out particularly important in the following, is that going from one Potts cluster to another one requires traversing an *even* number $k = 2l$ of loops, with $l \geq 1$ integer. Namely, when the first Potts cluster is separated from the second one by $l - 1$ distinct surrounding clusters, there will also be l surrounding dual clusters, and since clusters and dual clusters alternate each time we traverse a loop, the number of surrounding loops will be $2l$ indeed. In this chapter we are only interested in correlation functions in which all the marked clusters reside on the direct (not dual) lattice.

The RSOS model, on the other hand, is defined through a map from the lattice to a finite graph H, see Chapter 2 and [3, 82]. The nodes on H are taken as the possible values of a "height" variable σ_i associated with site i, while neighbouring sites are constrained to have heights which are neighbours on H. As a result, the clusters on the RSOS lattice are formed by linking the diagonals of the plaquettes, and each plaquette takes one of the diagonal links:

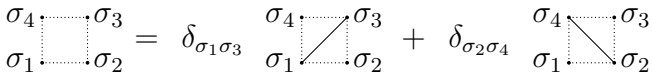

(4.2.1)

where the choice of the local weights multiplying each term is given in (2.1.10)(2.1.12) and will be recalled in the next paragraph. It is straightforward to see that there is an equivalence between the RSOS clusters/loops configurations and the ones in the Potts model, as shown in Figure 4.1b and 4.1c. This is discussed in more details in Chapter 2.3, where we also give a proof of the equivalence between the partition functions of the two models. Notice, however, that two distinct clusters on the RSOS lattice are mapped to Potts clusters only when separated by an even number of loops (otherwise one is mapped to a Potts cluster and the other one to a dual Potts cluster). This will play a role when we consider the geometric four-point functions of the two models.

Taking the graph H to be a Dynkin diagram $\mathscr{D}$ of the ADE type with Coxeter number p

and introducing its adjacency matrix $\mathscr{A}$, the eigenvalues $\lambda_{(r)}$ take the form

$$\lambda_{(r)} = 2\cos\frac{r\pi}{p}\,, \tag{4.2.2}$$

and the normalized eigenvectors are denoted $S^{\sigma_i}_{(r)}$, where r takes values in the set $\mathscr{D}^*$ of exponents of the algebra. (See Figure 4.3 for the diagrams $\mathscr{D}$ and their corresponding exponents $\mathscr{D}^*$ to be considered in this chapter.) They enter the definition of the Boltzmann weight of a certain configuration, as we discuss in details in Sections 2.3 and 5.2. Choosing a special eigenvector

$$S_{\sigma_i} \equiv S^{\sigma_i}_{(p-q)}, \tag{4.2.3}$$

where $p > q$ and $p \wedge q = 1$ as in (4.1.9), a representation of the Temperley-Lieb (TL) algebra [54] is defined by the basic action of the generator e on a face:[5]

$$e_i := e(\sigma_{i-1}\sigma_i\sigma_{i+1}|\sigma_{i-1}\sigma'_i\sigma_{i+1}) = \sigma_{i-1}$$

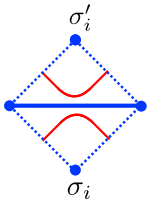

$$\sigma_{i+1} = \delta_{\sigma_{i-1},\sigma_{i+1}}\frac{\left(S_{\sigma_i}S_{\sigma'_i}\right)^{1/2}}{S_{\sigma_{i-1}}}\,. \tag{4.2.4}$$

Here the label i refers to the spatial position of the face. These generators satisfy the relations

$$e_i^2 = \lambda_{(p-q)}e_i\,, \tag{4.2.5a}$$

$$e_ie_{i\pm1}e_i = e_i\,, \tag{4.2.5b}$$

$$e_ie_j = e_je_i\,,\ \text{when } |i-j| \geq 2 \tag{4.2.5c}$$

defining the TL algebra. The continuum limit of the RSOS model thus defined is known to be given by the ADE minimal models with central charge (4.1.11) [83, 84].

Like for the Potts model, the torus partition function of the RSOS model can be expanded into configurations of clusters/loops [29,30,75,76]. For each configuration, the contractible loops get the weight $\lambda_{(p-q)}$, while the situation for the non-contractible loops is more complicated: one must sum over terms for $r \in \mathscr{D}^*$ [85], in each of which the non-contractible loops get the weight $\lambda_{(r)}$. This is in contrast with the Potts model [86] where one sums over only two terms: one where non-contractible loops get the same weight as contractible ones, and one where they get the weight zero (this last term comes formally with multiplicity $Q-1$). As a result, the operator content of the two models is profoundly different: the minimal models are rational, while the Potts model is irrational.

In general, the operators whose two-point function is defined by assigning to non-contractible loops (on the twice punctured sphere) the weight $\lambda_{(r)}$ have conformal weight

$$h_r = \bar{h}_r = \frac{r^2-(p-q)^2}{4pq}\,. \tag{4.2.6}$$

(While not explicitly appearing in the literature as far as we know, this equation follows the mapping of the non-unitary minimal models onto a Coulomb gas – see e.g. [85] and the discussion on geometrically defined operators in Section 2.2.) The difference between the minimal models and Potts spectra thus becomes particularly important in the non-unitary case, $p-q > 1$.

[5] Since we shall consider non-unitary cases in which some of the components S_σ are non-positive, we stress that one should use the determination of the square root satisfying always $(S_\sigma S_\sigma)^{1/2} = S_\sigma$.

In this case, the minimal models always contain an operator of negative conformal weight associated with the term for which non-contractible loops get the weight $\lambda_{(1)}$. This operator leads thus to an effective central charge $c_{\text{eff}} = c - 24h_1 = 1 - \frac{6}{pq}$. Meanwhile, in the Potts model, all conformal weights are positive, and $c_{\text{eff}} = c$. The only potential origin of non-positive conformal weights is the sector where non-contractible loops have vanishing weight. But since $\sqrt{Q} > 0$,[6] we have necessarily $p - q < \frac{p}{2}$, and thus the dimension of the order parameter $h_{1/2,0} > 0$.

To study the correlation functions, we consider the RSOS order parameters originally obtained in [29, 75]:

$$\phi_r(i) = \frac{S^{\sigma_i}_{(r)}}{S_{\sigma_i}}\,, \tag{4.2.7}$$

with the conformal weights given in (4.2.6). We therefore see that if p is even, $p = 2n$, we have $h_{p/2} = h_{1/2,0}$, i.e., the conformal weight of the operator $\phi_{p/2}$ coincides with the conformal weight of the Potts order parameter. In the case of type D, there are two such operators which we will denote as $\phi_{p/2}$ and $\phi_{\bar{p}/2}$. Therefore we will be mainly interested in the four-point functions of the operators $\phi_{p/2}$ and $\phi_{\bar{p}/2}$ in the RSOS model and their cluster interpretation, for the purpose of comparing with the geometric correlations in the Potts model. Notice that with our special eigenvector (4.2.3), the contractible loop weight is

$$\lambda_{(p-q)} = 2\cos\frac{\pi(p-q)}{p} = \sqrt{Q}\,, \tag{4.2.8}$$

the same as in the Potts model. Since $h_{p-q} = 0$ by (4.2.6), this corresponds to the identity field.

4.2.1 RSOS four-point functions

Consider now the four-point function $\langle\phi_{r_1}(i_1)\phi_{r_2}(i_2)\phi_{r_3}(i_3)\phi_{r_4}(i_4)\rangle$ on the sphere where the operators are inserted at the special sites i_1, i_2, i_3, i_4. Similar to the torus partition function, the four-point function can be expanded in terms of clusters/loops configurations [30]. A detailed study of the RSOS weights (see Section 5.2) reveals that the weight of any loop is unchanged when it is turned inside out, i.e., wrapping around the "point at infinity" on the sphere punctured at the positions of the operator insertions. In particular, the loops surrounding all four insertion points are in fact contractible on the sphere, and hence they receive the usual weight $\lambda_{(p-q)} = \sqrt{Q}$ as in the Potts model. We will from now on refer to the contractible/non-contractible loops in this sense of the four-times punctured sphere.

For non-contractible loops, their weights in a certain configuration are given by simple rules of which we provide the detailed formulation in Section 5.2 and give a brief summary here. As illustrated in Figure 4.2, one starts by representing the domains between loops (namely, the clusters) as vertices on a graph, and loops separating the domains as legs connecting these vertices. The graph thus obtained can be evaluated by giving the legs and vertices the factors as shown in the figure. Notice that one needs to sum over $r \in \mathscr{D}^*$ for the internal legs.

In the special cases where there are no non-contractible loops involved, i.e., all four points belong to the same big cluster, one still represents the cluster by a vertex and associate it with a four-leg vertex. As studied in Section 5.2 (see (5.2.30) and (5.2.31)), the four-leg vertex can be decomposed into three-leg vertices [30] as indicated in the last diagram in the box of Figure 4.2. This results in the diagram's acquiring a non-trivial multiplicity, of which we will see an explicit example in the next section.[7]

[6] We are restricting here to the "physical part" of the self-dual Potts model [87].

[7] Here there is no factor associated with the internal leg, since it does not represent any loops.

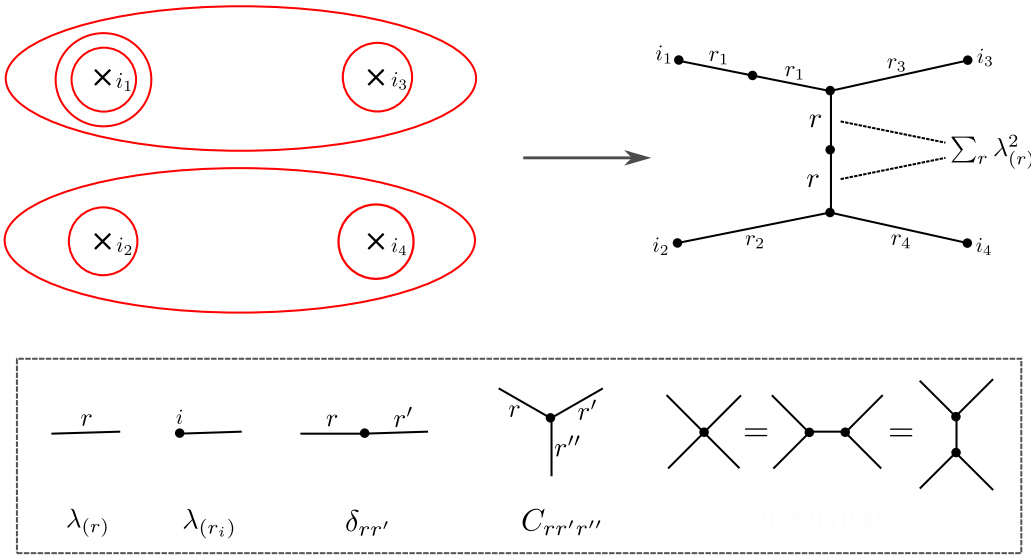

Figure 4.2: Determination of the weights of non-contractible loops in the four-point function $\langle\phi_{r_1}(i_1)\phi_{r_2}(i_2)\phi_{r_3}(i_3)\phi_{r_4}(i_4)\rangle$. In this example, the loop encircling points $1,3$ is represented by a three-leg vertex fusing r_1, r_3, and the one encircling points $2,4$ by a vertex fusing r_2, r_4. The weight of these two loops must be equal since they are connected by a topologically trivial domain as indicated by the two-leg vertex in the graph, and one needs to sum the loop weight $\lambda_{(r)}$ over $r \in \mathscr{D}^*$. We give in the box the general rule for assigning factors to the vertices and legs. The last diagram in the box is relevant for the configurations where all four points are within the same cluster. The derivation is given in Section 5.2.

In the example of Figure 4.2, we have the contribution of the diagram:

$$\lambda^2_{(r_1)}\lambda_{(r_2)}\lambda_{(r_3)}\lambda_{(r_4)}\sum_r C_{r_1r_3r}C_{rr_2r_4}\lambda^2_{(r)}\,, \tag{4.2.9}$$

as well as extra factors for the contractible loops (not shown). The three-point coupling $C_{rr'r''}$ can be calculated as we discuss in detail in Section 5.2, and we also give the explicit expressions for type A and type D in Appendix A, which will be used in the next section. There, we will see that things simplify drastically for the four-point functions of $\phi_{p/2}$ (and $\phi_{\bar{p}/2}$ in type D) we are interested in, where we can make direct contact with the Potts correlation functions.

Note: In our notations we shall henceforth in this chapter not differentiate between the lattice correlation functions and their continuum limit, with the latter interpreted as the minimal-models correlation functions.

4.3 Geometrical interpretation of four-point functions in minimal models

Since we are mainly interested in the comparison with the Potts model, in this section, we focus on the RSOS four-point functions $\langle\phi_r\phi_r\phi_r\phi_r\rangle$ where ϕ_r coincides with the Potts order parameter, i.e., $h_r = h_{1/2,0}$. This involves the operator $\phi_{p/2}$ in type A (with p even) and $\phi_{p/2}, \phi_{\bar{p}/2}$ in type D (with $p = 2 \bmod 4$). In Figure 4.3, we list the Dynkin diagrams $\mathscr{D}$ involved and the relevant conventions, which are used in Appendix A for obtaining the three-point couplings C_{r_1,r_2,r_3}.

algebra	diagram $\mathcal{D}$	Coxeter number	exponents $r \in \mathcal{D}^*$
A_{p-1}	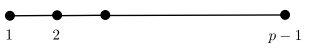	p	$r = 1, 2, ..., p-1$
D_N	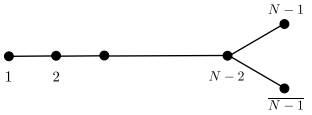	$p = 2(N-1)$	$r = 1, 3, ..., p-1$, odd

Figure 4.3: The type A and type D Dynkin diagrams $\mathscr{D}$ we are studying, where p is even. In the case of type D we have N even, i.e., $p \equiv 2 \bmod 4$, and the exponents $r = 1, 3, ..., p-1$, odd. In the following, we will often denote D_N as $D_{1+\frac{p}{2}}$.

As it turns out, the four-point functions we are interested in can be expanded in terms of clusters/loops configurations exactly like in the Potts model, but the geometric interpretation is different.

4.3.1 Type A_{p-1}

In the case of type A, we consider the four-point function $\langle \phi_{p/2}\phi_{p/2}\phi_{p/2}\phi_{p/2} \rangle$. Since $\lambda_{p/2} = 2\cos(\pi/2) = 0$, any diagram with a loop encircling a single special site has weight 0 and does not contribute. The four-point function then involves four types of diagrams as shown in Figure 4.4. We denote them using the notations D_{abcd} with the same convention as the Potts probabilities P_{abcd}. For example, the first type of diagrams D_{aaaa} involves configurations where the four points are all within the same cluster, and the other three—$D_{aabb}, D_{abab}, D_{abba}$—involve two distinct clusters for the four points with D_{abab}, for instance, denoting the set of diagrams where 1 and 3 are within the same cluster, while 2 and 4 belong to another cluster.

The three-point couplings in this case are given in (A.0.2) and with $r_i = p/2$ are simply:[8]

$$C_{p/2,p/2,r} = \begin{cases} (-1)^{\mathsf{b}},\ 1 \le r \le p-1 \text{ and } r \text{ odd},\ r + \mathsf{b}p = \mathsf{a}(p-q) \\ 0,\ \text{otherwise.} \end{cases} \tag{4.3.1}$$

In the following, we will consider the weight of a diagram where all loops get the factor $\sqrt{Q}$ as its "basic weight" for the obvious reason to relate to the Potts model, and refer to the ratio of the weight in the graphical expansion with respect to this basic weight as the "multiplicity". According to the rules summarized in Section 4.2.1 (see the last diagram in the box in Figure 4.2), we obtain that the multiplicities in D_{aaaa} are equal to

$$M_{aaaa}^{A_{p-1}} = \sum_r (C_{p/2,p/2,r})^2 = \sum_{r=1 \text{ odd}}^{p-1} 1 = \frac{p}{2}. \tag{4.3.2}$$

The other three types of diagrams have the special sites encircled pairwise by one or more big loops respectively and connected by a topologically trivial domain where, in the case of type A_{p-1}, one should sum over $r = 1, 2, \ldots, p-1$ for the weight $\lambda_{(r)}$ of the non-contractible

[8] As discussed in Appendix A, the expression of the three-point coupling involves integers a, b from solving a Diophantine equation $r + \mathsf{b}p = \mathsf{a}(p-q)$ for given r, p, q. This can be done easily using the function `FindInstance` in MATHEMATICA.

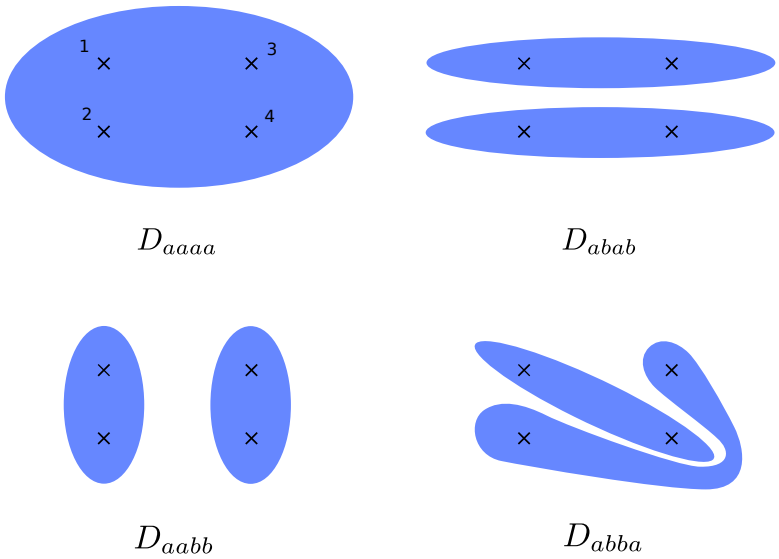

Figure 4.4: Four types of diagrams contributing to the four-point function $\langle \phi_{p/2}\phi_{p/2}\phi_{p/2}\phi_{p/2}\rangle$. Here we only draw the basic clusters while there can be extra contractible and non-contractible clusters surrounding them.

loops. However, thanks to the simplicity of the three-point coupling (4.3.1) for the four-point function we are considering, one in fact only needs to sum over $r = 1, 3, \ldots, p-1$, odd. Denoting the number of non-contractible loops as k, we therefore see a significant simplification of the diagrammatic expansion involved: since

$$\sum_{r=1 \text{ odd}}^{p-1} \lambda_{(r)}^k = \sum_{r=1 \text{ odd}}^{p-1} \left(2\cos\frac{r\pi}{p}\right)^k = 0, \text{ for } k \text{ odd}, \tag{4.3.3}$$

any diagram with the two clusters separated by odd number of loops has weight zero in the four-point function $\langle \phi_{p/2}\phi_{p/2}\phi_{p/2}\phi_{p/2}\rangle$. Recalling that two RSOS clusters are mapped to Potts clusters only when they are separated by even number of loops, here we see that for the four-point function we are interested in, these are exactly the types of configurations that contribute. For this reason we henceforth suppose k even and set

$$k = 2l\,. \tag{4.3.4}$$

From the remarks made at the beginning of Section 4.2 this is equivalent to supposing that all clusters marked in the correlation functions that we shall consider are of the Potts (and not dual) type.

In the next section, we will consider the s-channel spectrum involved in the RSOS four-point functions using the techniques developed in [20] for the Potts model, where we take the four points to be on a cylinder as depicted in Figure 4.7 below. If we now consider the contribution from the third type of diagrams D_{aabb} in Figure 4.4 we see that, after mapping to the cylinder, this will give rise to diagrams just like for the calculation of P_{aabb} in the Potts case, **but** there is the important difference that in the sum over sectors, loops encircling the cylinder between points $1, 2$ and $3, 4$ have weight $\lambda_{(r)}$. The appearance of $\lambda_{(1)}$ is crucial. In the non-unitary case, it does not correspond to the identity field, but rather to the field with dimension

$$h_1 = \frac{1-(p-q)^2}{4pq} < 0\,. \tag{4.3.5}$$

As mentioned before, this is in fact the field of most negative dimension in the theory, responsible for the value of the effective central charge $c_{\text{eff}} = 1 - \frac{6}{pq}$. In the case of the Potts model, however, as discussed in [20], only states with positive conformal weights propagate along the cylinder and no effective central charge appears despite the non-unitarity of the CFT.

The full diagrammatic expansion of the four-point function with $\langle \phi_{p/2}\phi_{p/2}\phi_{p/2}\phi_{p/2}\rangle$ is summarized in Figure 4.5. Note that in $D_{aabb}, D_{abab}, D_{abba}$, there are always two basic clusters connecting a to a and b to b respectively, plus extra clusters encircling the basic pair, and non-contractible on the sphere. Instead of clusters we can count their boundaries:[9] the basic pair gives rise to two boundaries, and every surrounding cluster contributes an extra pair. The total number of boundaries—namely, the number of non-contractible loops—k (even) give rise to the multiplicity of the configurations

$$\begin{aligned} M^{A_{p-1}}(k) &\equiv \frac{1}{\sqrt{Q}^k} \sum_{r=1 \text{ odd}}^{p-1} \lambda_{(r)}^k \\ &= \frac{1}{\sqrt{Q}^k} \sum_{\mathsf{a}=1 \text{ odd}}^{p-1} (\mathfrak{q}^{\mathsf{a}} + \mathfrak{q}^{-\mathsf{a}})^k \,, \end{aligned} \tag{4.3.6}$$

where $\mathfrak{q} = e^{i\pi\frac{p-q}{p}}$, and a is given in (4.3.1). It is not hard to find a general formula for these multiplicities:

$$M^{A_{p-1}}(k) = \frac{p}{2\sqrt{Q}^k} \begin{pmatrix} k \\ k/2 \end{pmatrix} + \frac{p}{\sqrt{Q}^k} \sum_{n\in\mathbb{N}^*}^{\lfloor \frac{k}{p} \rfloor} \begin{pmatrix} k \\ \frac{k-np}{2} \end{pmatrix} (-1)^n. \tag{4.3.7}$$

Notice when $p > k$, $\lfloor \frac{k}{p} \rfloor = 0$ and (4.3.7) reduces to

$$M^{A_{p-1}}(k) = \frac{p}{2\sqrt{Q}^k} \begin{pmatrix} k \\ k/2 \end{pmatrix}. \tag{4.3.8}$$

In particular we have in this case $M^{A_{p-1}}(2) = p/Q$, $M^{A_{p-1}}(4) = 3p/Q^2$, etc. The multiplicity $p/2$ in the D_{aaaa} diagram (eq. (4.3.2)) where all loops are contractible is independent of Q. Note that this formally coincides with $M^{A_{p-1}}(0)$ as it should.

We then introduce "pseudo-probabilities", such as

$$\tilde{P}_{abab}^{A_{p-1}} = \frac{1}{Z_{\text{Potts}}} \sum_{D\in D_{abab}} W_{\text{Potts}}(D) M^{A_{p-1}}(k)\,, \tag{4.3.9}$$

where k is the number of boundaries of the diagram D. We similarly define the pseudo-probabilities $\tilde{P}_{aabb}$ and $\tilde{P}_{abba}$ for the other cases of interest. Notice that in this notation, we have the true Potts probability given by

$$P_{abab} = \frac{1}{Z_{\text{Potts}}} \sum_{D\in D_{abab}} W_{\text{Potts}}(D). \tag{4.3.10}$$

We can then reexpress the four point-function in a more compact form

$$\langle \phi_{p/2}\phi_{p/2}\phi_{p/2}\phi_{p/2}\rangle \propto \frac{p}{2} P_{aaaa} + \tilde{P}_{abab}^{A_{p-1}} + \tilde{P}_{aabb}^{A_{p-1}} + \tilde{P}_{abba}^{A_{p-1}}. \tag{4.3.11}$$

[9] Although we have used so far mostly the language of loops, the mapping on the cluster formulation is obvious, simply by taking loops as cluster boundaries.

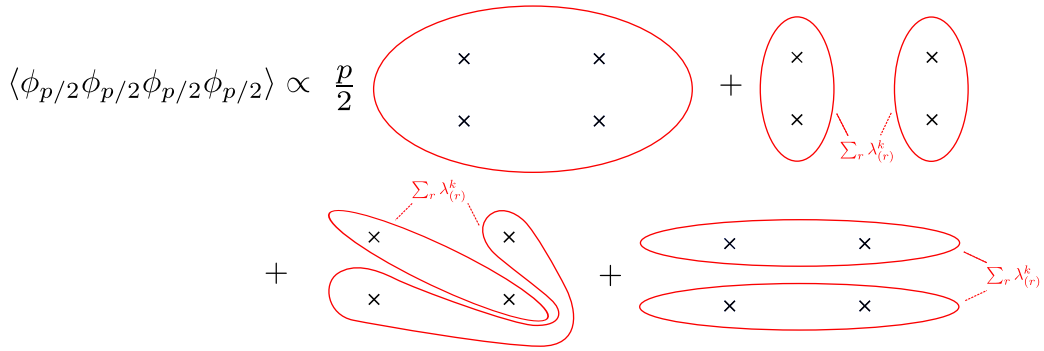

Figure 4.5: The diagrammatic expansion of four-point function $\langle\phi_{p/2}\phi_{p/2}\phi_{p/2}\phi_{p/2}\rangle$. The first type of diagram where all four sites are in one big loop comes with a multiplicity $\frac{p}{2}$. In the last three types of diagrams, one needs to sum over $\lambda^k_{(r)}$, $r = 1, 3, ..., p-1$ for even k – number of non-contractible loops encircling two of the special sites.

Note that, while we use the notation P for the last three terms, the sum of pseudo-probabilities is not equal to unity anymore.

Let us as an application consider the Ising model with $p = 4$, $q = 3$, corresponding to $\sqrt{Q} = 2\cos\frac{\pi}{4} = \lambda_{(1)}$. In the expansion, the D_{aaaa} diagrams get multiplicity $p/2 = 2$, corresponding to the two fusion channels

$$\sigma \times \sigma = \mathbb{I} + \epsilon\,, \tag{4.3.12}$$

where σ and ϵ denote the order parameter and energy operators, and we have used the usual simplified notation for operator product expansions (OPE). Meanwhile, the other geometries also get multiplicity two, because $\lambda^k_{(1)} = \lambda^k_{(3)} = \sqrt{Q}^k$: in other words $\tilde{P}^{A_3} = 2P$. Hence, in this case we find

$$\langle\phi_{p/2}\phi_{p/2}\phi_{p/2}\phi_{p/2}\rangle \propto P_{aaaa} + P_{aabb} + P_{abba} + P_{abab}\,, \tag{4.3.13}$$

which is a well known result as can be seen directly from (4.1.7a).

Consider now the case $p = 6$, $q = 5$, corresponding to $\sqrt{Q} = 2\cos\frac{\pi}{6} = \lambda_{(1)}$. Diagrams D_{aaaa} now get multiplicity $p/2 = 3$, or since there are three fusion channels:

$$\sigma \times \sigma = \mathbb{I} + \sigma + \epsilon. \tag{4.3.14}$$

The other diagrams still get multiplicity two since $\lambda^k_{(1)} = \lambda^k_{(5)} = \sqrt{Q}^k$ while $\lambda^k_{(3)} = 0$. Hence in this case, we have

$$\langle\phi_{p/2}\phi_{p/2}\phi_{p/2}\phi_{p/2}\rangle \propto 3P_{aaaa} + 2(P_{aabb} + P_{abba} + P_{abab}). \tag{4.3.15}$$

Meanwhile, since there is only one field with conformal weight $h_{1/2,0} = h_{33} = \frac{1}{15}$, this four-point function should be the same as the four-point function of the spin operator in the three-state Potts model, in agreement with (4.1.7a).

The $\phi_{p/2}$ four-point function will cease being expressed entirely in terms of the probabilities P for other minimal models. Consider for instance the case $p = 8$, $q = 7$, corresponding to $\sqrt{Q} = 2\cos\frac{\pi}{8} = \lambda_{(1)}$. In this case we have $\lambda^k_{(1)} = \lambda^k_{(7)} = (2+\sqrt{2})^{k/2} = \sqrt{Q}^k$, whilst $\lambda^k_{(3)} = \lambda^k_{(5)} = (2-\sqrt{2})^{k/2} \neq \sqrt{Q}^k$. So for instance, a diagram in D_{abab} with one loop encircling each pair of points gets a weight $2(\lambda^2_{(1)} + \lambda^2_{(3)})$, while a diagram with two loops encircling each

pair of points gets a weight $2(\lambda_{(1)}^4 + \lambda_{(3)}^4)$, etc. As soon as $\lambda_{(1)}^2 \neq \lambda_{(3)}^2$, this skews the statistics compared with the pure probability/Potts problem: the $\tilde{P}$'s are *not proportional* to the P's.

Note that in weighing the diagrams, p and q play quite different roles. The weight of topologically trivial loops is $\sqrt{Q} = 2\cos\pi\frac{p-q}{p}$, while the weight of configurations with non-contractible loops depends only on p, since it involves a sum over all the eigenvalues of the adjacency matrix.

4.3.2 Type $D_{1+\frac{p}{2}}$

The above results can be easily extended to the type D models by considering the corresponding Dynkin diagram D_N where $p = 2(N-1)$, as shown in Figure 4.3. This is particularly interesting when $p \equiv 2 \bmod 4$, corresponding to the case N even. In this case, it is known that the modular invariant partition function contains *two* primary fields with dimension $h_{1/2,0} = h_{m,n}$, where we recall that m and n are defined in (4.1.12). Associated to these two fields are in fact two order parameters which we denote $\phi_{p/2}$ and $\phi_{\bar{p}/2}$. The existence of these two fields is related to the symmetry of the D_N diagram under the exchange of the two fork nodes traditionally labeled as $N-1$ and $\overline{N-1}$, as can be seen from Figure 4.3. Their lattice version can still be obtained using equation (4.2.7).

Since $\lambda_{p/2} = \lambda_{\bar{p}/2} = 0$, the two operators cannot be distinguished by their two-point function which, in both cases, are obtained by giving a vanishing weight to non-contractible loops on the twice punctured sphere. Four-point functions are much more interesting, and can be obtained by the same construction as for the type A models. It is easy to see that in this case the result (4.3.3) still holds. Also, the same four types of diagrams (Figure 4.4) with even number of non-contractible loops $k = 2l$ participate and can be directly related to the Potts model. To expand the four-point functions in terms of diagrams, one needs the three-point couplings (A.0.8) for $r_i = p/2, \bar{p}/2$ given by:

$$C_{p/2,p/2,r} = (-1)^{\frac{\mathsf{a}-1}{2}},\ r + \mathsf{b}p = \mathsf{a}(p-q) \tag{4.3.16a}$$
$$C_{\bar{p}/2,\bar{p}/2,r} = 1\,, \tag{4.3.16b}$$
$$C_{p/2,p/2,\bar{p}/2} = C_{\bar{p}/2,\bar{p}/2,\bar{p}/2} = 0\,, \tag{4.3.16c}$$

with $1 \leq r \leq p-1$ and r odd, and one has $\sum_r = \sum_{\mathsf{a}}$.[10] Note that the vanishing of $C_{p/2,p/2,\bar{p}/2}$ follows from invariance of the D_N diagram under exchange of the two fork nodes. We see that the fields of interest obey the OPEs

$$\phi_{p/2}\phi_{p/2} \sim \phi_{p/2}\,, \tag{4.3.17a}$$
$$\phi_{\bar{p}/2}\phi_{\bar{p}/2} \sim \phi_{p/2}\,, \tag{4.3.17b}$$
$$\phi_{p/2}\phi_{\bar{p}/2} \sim \phi_{\bar{p}/2}\,. \tag{4.3.17c}$$

These OPEs are similar to those of the fields V^D, V^N from [71], as mentioned below eq. (4.1.14). Since there are only two fields with the correct dimensions in the CFT, we will in what follows make the identifications

$$\phi_{p/2} \leftrightarrow V^D, \quad \phi_{\bar{p}/2} \leftrightarrow V^N. \tag{4.3.18}$$

[10] This comes from the fact that a is simply a rearrangement of r with a shift $(p-q-1)/2$ and a cyclic spacing $p-q$, which results from normalizing with the $S^{\sigma}_{(p-q)}$. Taking $p = 10, q = 7$ for instance, $r = 1, 3, 5, 7, 9$ and $\mathsf{a} = 7, 1, 5, 9, 3$ where the position of 1 is shifted by $(p-q-1)/2 = 1$ and the spacing of consecutive odd integers is $p - q = 3$. It is of course essential here that $p \wedge q = 1$, as we have supposed in (4.1.9).

Among the four-point functions involving $\phi_{p/2}$, $\phi_{\bar{p}/2}$, only the ones with even numbers of $\phi_{\bar{p}/2}$ are non-vanishing, as can been seen by directly carrying out the cluster expansions. This is similar to what happens for the four-point functions of V^D, V^N in [71]. On the other hand, the cluster expansions of the four-point functions $\langle\phi_{p/2}\phi_{p/2}\phi_{p/2}\phi_{p/2}\rangle$ and $\langle\phi_{\bar{p}/2}\phi_{\bar{p}/2}\phi_{\bar{p}/2}\phi_{\bar{p}/2}\rangle$ in this case are exactly the same as the four-point function $\langle\phi_{p/2}\phi_{p/2}\phi_{p/2}\phi_{p/2}\rangle$ in the type A models. This is easily seen by recognizing that the calculation of the multiplicities in the cluster expansion of these four-point functions involves the factors

$$C^2_{p/2,p/2,r} = C^2_{\bar{p}/2,\bar{p}/2,r} = 1\,, \tag{4.3.19}$$

so the situation reduces to the case of type A. Namely, the non-trivial sign difference in the three-point couplings (4.3.16a), (4.3.16b) and (4.3.1) between type D and type A does not manifest itself in the four-point functions $\langle\phi_{p/2}\phi_{p/2}\phi_{p/2}\phi_{p/2}\rangle$ and $\langle\phi_{\bar{p}/2}\phi_{\bar{p}/2}\phi_{\bar{p}/2}\phi_{\bar{p}/2}\rangle$.

A particularly interesting case here is to consider the four-point function

$$\langle\phi_{p/2}\phi_{\bar{p}/2}\phi_{p/2}\phi_{\bar{p}/2}\rangle \propto \langle V^D V^N V^D V^N\rangle\,, \tag{4.3.20}$$

which is in fact the four-point function (4.1.14), (4.1.18) studied in details in [19, 71–74]. In this case, since the only three-point coupling involving $\phi_{p/2}$ and $\phi_{\bar{p}/2}$ is $C_{p/2,\bar{p}/2,\bar{p}/2}$, and since $\lambda_{\bar{p}/2} = 0$, considerable simplification occurs in the cluster expansion of this correlator: diagrams where $\phi_{p/2}$ and $\phi_{\bar{p}/2}$ are in the same cluster with no other insertions are given a vanishing weight and thus disappear. Regarding (4.3.20) we are thus left with diagrams of type D_{abab} and D_{aaaa} only.

Diagrams of type D_{aaaa} come with multiplicity

$$M^{D_{1+\frac{p}{2}}}_{aaaa} = \sum_{r=1 \text{ odd}}^{p-1} (-1)^{\frac{\mathsf{a}-1}{2}} = \sum_{\mathsf{a}=1 \text{ odd}}^{p-1} (-1)^{\frac{\mathsf{a}-1}{2}} = 1\,. \tag{4.3.21}$$

For the other three types of diagrams, we can again define the multiplicities

$$\begin{aligned} M^{D_{1+\frac{p}{2}}}(k) &\equiv \frac{1}{\sqrt{Q}^k} \sum_{r=1 \text{ odd}}^{p-1} (-1)^{\frac{\mathsf{a}-1}{2}} \lambda^k_{(r)}, \text{ with } k \text{ even} \\ &= \frac{1}{\sqrt{Q}^k} \sum_{\mathsf{a}=1 \text{ odd}}^{p-1} (-1)^{\frac{\mathsf{a}-1}{2}} (\mathfrak{q}^{\mathsf{a}} + \mathfrak{q}^{-\mathsf{a}})^k\,, \end{aligned} \tag{4.3.22}$$

where again $\mathfrak{q} = e^{i\pi\frac{p-q}{p}}$. It is easy to transform this expression into one that depends only on $\mathfrak{q}$ and not on p (provided $p \equiv 2 \bmod 4$). One finds

$$M^{D_{1+\frac{p}{2}}}(k = 2l) = \frac{2}{Q^l} \sum_{\mathsf{m}=-l}^{l} \begin{pmatrix} 2l \\ l+\mathsf{m} \end{pmatrix} \frac{1}{\mathfrak{q}^{2\mathsf{m}} + \mathfrak{q}^{-2\mathsf{m}}}\,. \tag{4.3.23}$$

Using $\sqrt{Q} = \mathfrak{q} + \mathfrak{q}^{-1}$, we can express these in terms of Q. This is most easily done by noticing that

$$\mathfrak{q}^{\mathsf{j}} + \mathfrak{q}^{-\mathsf{j}} = 2T_{\mathsf{j}}\left(\frac{\sqrt{Q}}{2}\right)\,, \tag{4.3.24}$$

where $T_{\mathsf{j}}(x)$ denotes the j'th order Chebyshev polynomial of the first kind. We obtain the explicit expressions

$$M^{D_{1+\frac{p}{2}}}(k=2) = \frac{2}{Q-2}, \tag{4.3.25a}$$

$$M^{D_{1+\frac{p}{2}}}(k=4) = \frac{2(3Q-10)}{(Q-2)(Q^2-4Q+2)}, \tag{4.3.25b}$$

$$M^{D_{1+\frac{p}{2}}}(k=6) = \frac{4(5Q^2-35Q+61)}{(Q-2)(Q^2-4Q+2)(Q^2-4Q+1)}. \tag{4.3.25c}$$

A number of special cases of these will be discussed in Section 4.6. Note that the multiplicities in the D case can be expressed only in terms of Q, while in the A case, an extra factor of p remains (see equation (4.3.8)). We see that the multiplicity $M^{D_{1+\frac{p}{2}}}(k)$ has poles at $\mathsf{q} = e^{i\pi(2\mathsf{n}+1)/4\mathsf{m}}$, for any $\mathsf{m} = -l, \ldots, l$, corresponding to

$$\sqrt{Q} = 2\cos\left(\frac{\pi(2\mathsf{n}+1)}{4\mathsf{m}}\right). \tag{4.3.26}$$

The pseudo-probabilities can then be defined as usual, for example

$$\tilde{P}^{D_{1+\frac{p}{2}}}_{abab} = \frac{1}{Z_{\text{Potts}}} \sum_{D \in D_{abab}} W_{\text{Potts}}(D) M^{D_{1+\frac{p}{2}}}(k), \tag{4.3.27}$$

and it follows that

$$\langle \phi_{p/2}\phi_{\bar{p}/2}\phi_{p/2}\phi_{\bar{p}/2}\rangle \propto P_{aaaa} + \tilde{P}^{D_{1+\frac{p}{2}}}_{abab}. \tag{4.3.28a}$$

Other correlations with two $\phi_{p/2}$ and two $\phi_{\bar{p}/2}$ follow by braiding:

$$\langle \phi_{p/2}\phi_{p/2}\phi_{\bar{p}/2}\phi_{\bar{p}/2}\rangle \propto P_{aaaa} + \tilde{P}^{D_{1+\frac{p}{2}}}_{aabb}, \tag{4.3.28b}$$

$$\langle \phi_{p/2}\phi_{\bar{p}/2}\phi_{\bar{p}/2}\phi_{p/2}\rangle \propto P_{aaaa} + \tilde{P}^{D_{1+\frac{p}{2}}}_{abba}. \tag{4.3.28c}$$

Three-state Potts model

The simplest of all cases for the D_N models of interest is with $p = 6$, $q = 5$, corresponding to the D_4 unitary CFT which is in fact the same as the $Q = 3$ state Potts model [88,89]. Notice that the D_4 Dynkin diagram is a three-star graph having the same S_3 symmetry as the permutations of the three Potts spins. In this case, r takes values $r = 1, 3, 5$ and the multiplicity (4.3.22) becomes simply 2, due to the symmetry $\lambda^k_{(1)} = \lambda^k_{(5)} = \sqrt{Q}^k$; note also that $\lambda_{(3)} = 0$. In other words, $\tilde{P}^{D_4}_{abab} = 2P_{abab}$, $\tilde{P}^{D_4}_{abba} = 2P_{abba}$ and $\tilde{P}^{D_4}_{aabb} = 2P_{aabb}$. We conclude that, for $Q = 3$,

$$\langle \phi_{p/2}\phi_{\bar{p}/2}\phi_{p/2}\phi_{\bar{p}/2}\rangle \propto P_{aaaa} + 2P_{abab}. \tag{4.3.29}$$

Consider now the antisymmetric combination

$$\langle \phi_{p/2}\phi_{\bar{p}/2}\phi_{p/2}\phi_{\bar{p}/2}\rangle - \langle \phi_{p/2}\phi_{\bar{p}/2}\phi_{\bar{p}/2}\phi_{p/2}\rangle \propto \tilde{P}^{D_{1+\frac{p}{2}}}_{abab} - \tilde{P}^{D_{1+\frac{p}{2}}}_{abba} \tag{4.3.30}$$

which, for the $Q = 3$ state Potts model becomes simply

$$\tilde{P}^{D_4}_{abab} - \tilde{P}^{D_4}_{abba} \propto P_{abab} - P_{abba}. \tag{4.3.31}$$

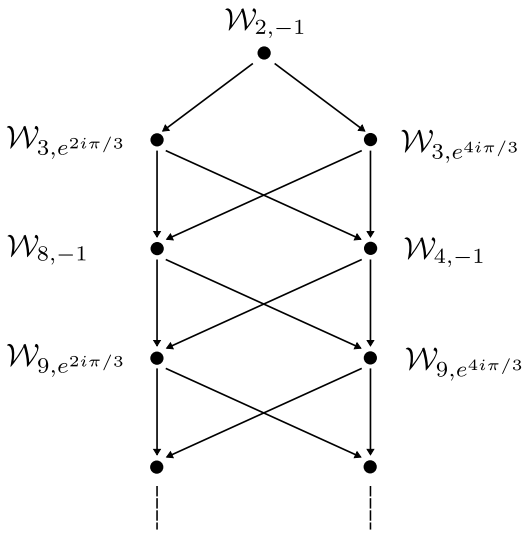

Figure 4.6: When $\mathfrak{q} = e^{i\pi/6}$, the generically irreducible affine Temperley-Lieb module $\mathscr{W}_{2,-1}$ (which contributes in its entirety to the Potts correlations for $\mathfrak{q}$ generic) becomes reducible, and admits a decomposition in terms of submodules as represented in this figure. Only the "top" contributes to the $Q = 3$ correlations, leading to the disappearance of a large number of states in the s-channel.

In general, at $Q = 3$, we expect that combinations such as (4.3.29) or the antisymmetric combination (4.3.31) simplifies considerably. This, we believe, is in sharp contrast with the P_{abcd} themselves, whose expressions remain as complicated for $Q = 3$ as in the generic case. This is confirmed by concrete numerical evidence (eigenvalue cancellations) on finite-size cylinders.

This expectation is of course also in agreement with general results from representation theory of affine Temperley-Lieb algebras. Indeed, as we will discuss in more details in the following sections, from the set of all possible affine Temperley-Lieb modules $\mathscr{W}_{j,z^2}$ appearing generically in the Q-state Potts model, only the simple tops $\mathscr{X}$ of $\mathscr{W}_{0,\mathfrak{q}^2}, \mathscr{W}_{0,-1}, \mathscr{W}_{2,-1}$ (with $\mathfrak{q} = e^{i\pi/6}$) are relevant for the D_4 RSOS model [90]. The continuum limit of these modules is

$$\mathscr{X}_{0,\mathfrak{q}^2} \;\mapsto\; \sum_{r=1}^{4} |\chi_{r,1}|^2 = \sum_{r=1}^{4} |\chi_{r,5}|^2 \,, \tag{4.3.32a}$$

$$\mathscr{X}_{2,-1} \;\mapsto\; \sum_{r=1}^{4} \chi_{r,1}\overline{\chi}_{r,5} = \sum_{r=1}^{4} \overline{\chi}_{r,1}\chi_{r,5} \,, \tag{4.3.32b}$$

$$\mathscr{X}_{0,-1} \;\mapsto\; \sum_{r=1}^{4} |\chi_{r,3}|^2 \,. \tag{4.3.32c}$$

The structure of the $\mathscr{W}_{2,-1}$ module is shown for example in Figure 4.6.

Note that the particular combinations (4.3.29) and (4.3.31) at $Q = 3$ could in fact be obtained from the general relationship (4.1.7) between spin correlation functions in the Potts model G_{abcd} and geometrical objects P_{abcd}. Setting $Q = 3$ in these relations gives

$$4G_{abab} - G_{aaaa} \;=\; 6(P_{aaaa} + 2P_{abab}) \,, \tag{4.3.33a}$$

$$G_{abab} - G_{abba} \;=\; 3(P_{abab} - P_{abba}) \,. \tag{4.3.33b}$$

Since the left hand sides can be expressed strictly within the $Q = 3$ Potts model, this means the same holds for the right-hand side, as we have directly established in eqs. (4.3.29) and (4.3.31).

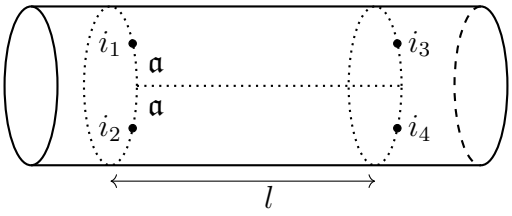

Figure 4.7: Four-point functions in the cylinder geometry. The distance between the two operator insertions on each time slice is denoted $2\mathfrak{a}$.

4.4 Pseudo-probabilities and affine Temperley-Lieb algebra

4.4.1 General setup

To proceed, we first recall the general framework discussed in [20]. In the scaling limit, the Potts model correlation functions (4.1.7) as well as the geometrical correlations P_{abcd} admit an s-channel expansion

$$\begin{aligned} \mathrm{G}(z,\bar{z}) &= \sum_{\Delta,\bar{\Delta}\in\mathcal{S}} C_{\Phi_1\Phi_2\Phi_{\Delta\bar{\Delta}}} C_{\Phi_{\Delta\bar{\Delta}}\Phi_3\Phi_4} \mathscr{F}^{(s)}_{\Delta}(z)\overline{\mathscr{F}}^{(s)}_{\bar{\Delta}}(\bar{z}) \\ &= \sum_{\Delta,\bar{\Delta}\in\mathcal{S}} A_{\Phi_{\Delta\bar{\Delta}}} \mathscr{F}^{(s)}_{\Delta}(z)\overline{\mathscr{F}}^{(s)}_{\bar{\Delta}}(\bar{z})\,, \end{aligned} \tag{4.4.1}$$

where $A_{\Phi_{\Delta\bar{\Delta}}}$ denotes the amplitude of the field $\Phi_{\Delta,\bar{\Delta}}$ and the conformal blocks themselves can be expanded in (integer) powers of z. This full z expansion is analogous to the expansion of lattice correlation functions on a cylinder in powers of eigenvalues of the geometrical transfer matrix discussed in [20], where the s-channel geometry as shown in Figure 4.7 corresponds to taking the two points i_1, i_2 to reside on one time slice and i_3, i_4 on another. The two expansions can be matched exactly in the limit where all lattice parameters (the width of the cylinder L as well as the separation between points) are much larger than 1,[11] using the usual logarithmic mapping. We shall occasionally in the following also need to discuss the other two channels. For future reference, the definition of the channels is

$$s\text{-channel} \;:\; i_1 \sim i_2 \text{ and } i_3 \sim i_4\,, \tag{4.4.2a}$$
$$t\text{-channel} \;:\; i_1 \sim i_4 \text{ and } i_2 \sim i_3\,, \tag{4.4.2b}$$
$$u\text{-channel} \;:\; i_1 \sim i_3 \text{ and } i_2 \sim i_4\,, \tag{4.4.2c}$$

where the t and u-channels can just be obtained from the s-channel by relabelling the points.

A key aspect of the geometrical transfer matrix is that it can be expressed in terms of the affine Temperley-Lieb (ATL) algebra introduced in Chapter 3. The eigenvalues can therefore be classified in terms of (generically irreducible) representations of this algebra. The representations of interest in the case of the Potts model are of two types: $\mathscr{W}_{j,z^2=e^{2i\pi \mathrm{p}/\mathrm{M}}}$ and $\overline{\mathscr{W}}_{0,z^2=\mathfrak{q}^2}$, which respectively indicate conformal weights $(h_{\mathbb{Z}+\frac{\mathrm{p}}{\mathrm{M}},j}, h_{\mathbb{Z}+\frac{\mathrm{p}}{\mathrm{M}},-j})$ and $(h_{\mathbb{Z},1}, h_{\mathbb{Z},1})$. Their contributions to the correlation functions P_{abcd} in the s-channel have been established in [20] and are

[11] All measured in units of the lattice spacing.

summarized in the table[12]:

	s-channel	Parities
P_{aaaa}	$\mathscr{W}_{0,-1} \cup \mathscr{W}_{j,e^{2i\pi \mathrm{p}/\mathrm{M}}}$	$j \in 2\mathbb{N}^*$, $j\mathrm{p}/\mathrm{M}$ even
P_{aabb}	$\mathscr{W}_{0,-1} \cup \overline{\mathscr{W}}_{0,\mathfrak{q}^2} \cup \mathscr{W}_{j,e^{2i\pi \mathrm{p}/\mathrm{M}}}$	$j \in 2\mathbb{N}^*$, $j\mathrm{p}/\mathrm{M}$ even
$P_{abab/abba}$	$\mathscr{W}_{j,e^{2i\pi \mathrm{p}/\mathrm{M}}}$	$j \in 2\mathbb{N}^*$, $j\mathrm{p}/\mathrm{M}$ integer

(4.4.3)

We will often consider the symmetric and anti-symmetric contributions:

$$P_S = P_{abab} + P_{abba}\,, \tag{4.4.4a}$$
$$P_A = P_{abab} - P_{abba}\,. \tag{4.4.4b}$$

Their spectra select $j\mathrm{p}/\mathrm{M}$ even and odd respectively.

The ATL representations $\mathscr{W}_{j,z^2}$ are discussed in details in Chapter 3, and we recall some features here. They are standard modules of the algebra acting on so-called link patterns that encode the necessary information about the state of the loop model to the left of a given timeslice of the cylinder (recall Figure 4.7), namely the pairwise connectivities between loop ends intersecting the time slice, as well as the position of certain defect lines. More precisely, the number j corresponds to the number of clusters propagating along the cylinder: this number is half the number of cluster boundaries, often referred to as "through lines" in the literature. When $j = 0$, modules $\mathscr{W}_{0,z^2}$ correspond to giving to non-contractible loops wrapping around the axis of the cylinder the weight $z + z^{-1}$, and we shall need in particular the module with $z+z^{-1} = 0$ that imposes the propagation of one cluster (although no through lines are present). When $j \neq 0$, the parameter z encodes the phases gathered by through lines as they wrap around the cylinder: there is a weight z (resp. z^{-1}) for a through line that goes through the periodic direction in one directon (resp. the opposite direction). To account for these factors of z, it is in general necessary to keep track of whether a pairwise connectivity between loop ends straddles the periodic direction or not. However, when no cluster is propagating, the latter information is nugatory, and we shall need only the smaller quotient representation $\overline{\mathscr{W}}_{0,z^2}$ that is devoid of this information.

For the ease of comparison with the appendices of [20], we recall that this reference also used the following simpler notation:

- V_0 is the sector with no through-lines, and non-contractible loops have weight $\sqrt{Q}$: $V_0 = \overline{\mathscr{W}}_{0,z^2=\mathfrak{q}^2}$,
- V_1 is the sector with no through-lines, and non-contractible loops have weight zero: $V_1 = \mathscr{W}_{0,z^2=-1}$,
- $V_{\ell,k}$ is the sector with $j = \ell \geq 2$ *pairs* of through-lines and phases $z^2 = e^{2i\pi k/j}$: $V_{\ell,k} = \mathscr{W}_{j,z^2=e^{2i\pi k/j}}$.

The basic fact we want to explain now is how the complicated spectra for the P_{abcd} found in [20] can reduce to the much simpler s-channel spectra of minimal models where, instead of the genuine probabilities, we consider the proper combinations of pseudo-probabilities $\tilde{P}^{A,D}$ that appear in the geometrical reformulation of the four-point functions of order operators in minimal models. Note that this reduction should occur in finite size as well.

[12] We take this opportunity to correct a few misprints in [20]: in Remark 3 of this reference, $\mathscr{W}_{j,z}$ (resp. $\mathscr{W}_{j,z'}$) should read $\mathscr{W}_{j,z^2}$ (resp. $\mathscr{W}_{j,z'^2}$).

Recall that after the logarithmic conformal mapping, the s-channal corresponds to the cylinder geometry shown in Figure 4.7. This can be studied in finite size by performing transfer matrix computations on an $L \times M$ lattice strip, with periodic boundary conditions in the L-direction, and in the semi-infinite limit $M \gg L$. The representations acted on by the transfer matrix are those of the corresponding affine Temperley-Lieb (ATL) algebra. Using the numerical methods described in Appendix D of [15] – and with further technical details being given in the appendices of [20]—we can extract, for each correlation function P_{a_1,a_2,a_3,a_4} of interest, the finite-size amplitude $A_i := A(\lambda_i)$ of each participating transfer matrix eigenvalue λ_i; see eq. D.1. of [15]. These A_i are the finite-size precursors of the conformal amplitudes $A_{\Phi_{\Delta\bar{\Delta}}}$ appearing in (4.4.1).

We have made a number of striking obversations about ratios of the amplitudes A_i, which, crucially, turn out to be independent of L and hence should carry over directly to their conformal counterparts, after the usual identification of representations. Although we do not presently have complete analytical derivations of these amplitude-ratio results in the lattice model, we wish to stress that the numerical procedures by which the observations were made and thoroughly checked leaves no doubt that they are exact results. For the lack of a better word, we shall therefore simply refer to them as **facts** in the following.

In full analogy with the occurence of minimal model representations of the Virasoro algebra in the continuum limit, it is well known indeed that only a small set of "minimal" representations of the affine Temperley-Lieb algebra appears in the correlation functions of minimal RSOS models on the lattice [29, 62, 75]. The reduction to the spectra of minimal models is made possible by virtue of the facts which we have observed.

We will now list these facts, and use them in our discussion of minimal models in the next section.

4.4.2 Facts of type 1

Whenever the same ATL module contributes to different P_{abcd}, the ratios of the corresponding amplitudes in these different P_{abcd}, depend only on the module, and are independent of the eigenvalues within this module. They also do not depend on the size L.

To make this more explicit, consider for instance the modules $\mathscr{W}_{j,e^{2i\pi \mathrm{p}/\mathrm{M}}}$ with $j\mathrm{p}/\mathrm{M}$ even that contribute to P_{aaaa}, P_{aabb} and P_S, where we recall (4.4.4). For such a module, consider in a certain size L the eigenvalues λ_i of the transfer matrix. The powers of these eigenvalues contribute to different probabilities with different amplitudes $A_{aaaa}(\lambda_i), A_{aabb}(\lambda_i)$ and $A_S(\lambda_i)$. Our claim is that the ratios $A_{aabb}(\lambda_i)/A_{aaaa}(\lambda_i)$ and $A_S(\lambda_i)/A_{aaaa}(\lambda_i)$:

- are the same for all eigenvalues λ_i in a given module, and thus only depend on the module;
- are independent of the size L of the system (provided it is big enough to allow the corresponding value of j

The same claim holds for eigenvalues within $\mathscr{W}_{0,z^2=-1}$ for A_{aaaa}/A_{aabb}.

We were able, by numerical fitting, to determine some of these ratios in closed form. Defining first

$$\alpha_{j,z^2} \equiv \frac{A_{aabb}}{A_{aaaa}}(\mathscr{W}_{j,z^2})\,, \tag{4.4.5}$$

we have then

$$\alpha_{0,-1} = -1\,, \tag{4.4.6a}$$
$$\alpha_{2,1} = \frac{1}{1-Q}\,, \tag{4.4.6b}$$
$$\alpha_{4,1} = -\frac{Q^5-7Q^4+15Q^3-10Q^2+4Q-2}{2(Q^2-3Q+1)}\,, \tag{4.4.6c}$$
$$\alpha_{4,-1} = \frac{2-Q}{2}\,. \tag{4.4.6d}$$

Similarly defining

$$\overline{\alpha}_{j,z^2} \equiv \frac{A_S}{A_{aaaa}}(\mathscr{W}_{j,z^2})\,, \tag{4.4.7}$$

we have then

$$\overline{\alpha}_{2,1} = 2-Q \tag{4.4.8a}$$
$$\overline{\alpha}_{4,1} = -\frac{(Q^2-4Q+2)(Q^2-3Q-2)}{2} \tag{4.4.8b}$$
$$\overline{\alpha}_{4,-1} = \frac{(Q-1)(Q-4)}{2}\,. \tag{4.4.8c}$$

We now turn to the question of weighing differently non-contractible loops. This must be done in two quite different cases. For diagrams of type D_{aabb}, we can have a large number of such loops separating our two pairs of points in the s-channel cylinder geometry in Figure 4.7. For diagrams D_{abab} and D_{abba} on the contrary, this number of loops—which is at least equal to two by definition—remains finite and bounded by $L/2$, and cannot increase during imaginary time propagation. Accordingly, we have two different sets of facts.

4.4.3 Facts of type 2

We focus now on the Potts probabilities involving long clusters: P_{abab} and P_{abba}. A suitable modification of the code in [20]—details of which are provided in Appendix D.2 of [15]—allows us to determine, for a given eigenvalue λ_i from $\mathscr{W}_{j,z^2}$, the refined amplitudes corresponding to imposing a fixed number k (even) of non-contractible loops. These refined amplitudes will allow us to reweigh the non-contractible loops and hence relate the pseudo-probabilities $\tilde{P}$ to the true probabilities P.

We first claim that the two pseudo-probabilities, $\tilde{P}_{abab}$ and $\tilde{P}_{abba}$ involve the same ATL modules exactly as their siblings P_{abab} and P_{abba}: the only effect of the modified weights $M(k)$ is to modify the amplitudes. To be more precise, let us consider the amplitude $A(\lambda_i)$ of some eigenvalue λ_i occurring in the s-channel of the diagram of the type D_{abab} or D_{abba} in finite size (for simplicity we do not indicate which type of diagram in the amplitudes). In the Potts case, this amplitude comes from summing over configurations where all loops, contractible or not, are given the same weight $\sqrt{Q}$. We now split this amplitude into sub-amplitudes corresponding to configurations with a fixed number k (even) of non-contractible loops occurring in the diagrams. Note that $k \geq 2$ since we have a least two loops each surrounding one cluster. The case $k = 4$, for instance, corresponds to having, on top of these two basic clusters, an extra "surrounding cluster", i.e., an extra pair of loops as shown in Figure 4.8. Denoting by $A(\lambda_i)$ the total

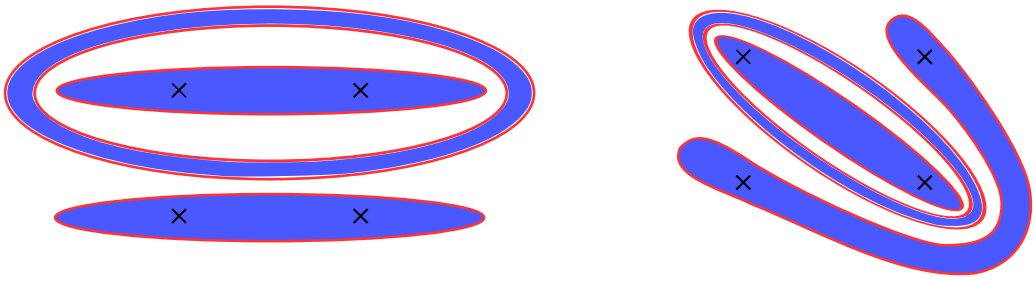

Figure 4.8: Diagrams of the types D_{abab} and D_{abba} with an extra cluster surrounding the basic clusters, i.e., the number of non-contractible loops is $k = 4$.

amplitude—that is, the one occurring in the Potts model, where no distinction is made between different values of k, as discussed in [20]—we have

$$A(\lambda_i) = \sum_{k=2 \text{ even}} A^{(k)}(\lambda_i) \tag{4.4.9}$$

We now state our facts of type 2:

For the eigenvalues in $\mathscr{W}_{j,e^{2i\pi \mathrm{p/M}}}$, the ratios of their amplitudes contributing to configurations with precisely k non-contractible loops, depend only on the module and on k, and are independent of the eigenvalues within this module. They also do not depend on the size L.

We define

$$\beta^{(k)}_{j,z^2} \equiv \frac{A^{(k)}_{abab}}{A^{(2)}_{abab}}(\mathscr{W}_{j,z^2}). \tag{4.4.10}$$

Note that, since the amplitudes for the symmetric combination P_S involve only $j\mathrm{p/M}$ even, the amplitudes for $j\mathrm{p/M}$ odd are necessarily equal and opposite in P_{abab} and P_{abba}. Similarly, since the amplitudes for P_A involve only $j\mathrm{p/M}$ odd, the amplitudes for $j\mathrm{p/M}$ even are the same for P_{abab} and P_{abba}. The ratios $\beta^{(k)}_{j,z^2}$ are thus the same for both cases.

Numerical determination leads to the following results (by definition, $\beta^{(2)} = 1$):

$$\beta^{(4)}_{4,1} = -\frac{Q^2}{3Q+2}, \tag{4.4.11a}$$

$$\beta^{(4)}_{4,-1} = -\frac{Q(Q-2)}{3Q-4}, \tag{4.4.11b}$$

$$\beta^{(4)}_{4,i} = -\frac{Q^2-4Q+2}{3Q-10}. \tag{4.4.11c}$$

We finally turn to the case of P_{aabb}, which as we will see must be handled a bit differently.

4.4.4 Facts of type 3

We now consider calculating statistical sum with D_{aabb} geometries. Unlike the previous cases, the non-contractible loops are now those that wrap around the axis of the cylinder. For a finite separation l of the points along the cylinder axis (recall Figure 4.7) there can be up to $2l$ such loops. As $l \to \infty$, it is known that the average number of such loops in the Potts model grows

like $\ln l$ [91]. In this case, the natural thing to do is not to focus on fixing the number of such loops, but rather in modifying their fugacity, i.e., giving them a modified weight

$$n_{\mathsf{a}} \equiv \mathfrak{q}^{\mathsf{a}} + \mathfrak{q}^{-\mathsf{a}} \,. \tag{4.4.12}$$

We denote such sums by $\tilde{P}^{(\mathsf{a})}_{aabb}$. The probability P_{aabb} in the Potts model corresponds to $\mathsf{a} = 1$ and involves modules $\overline{\mathscr{W}}_{0,\mathfrak{q}^2}, \mathscr{W}_{0,-1}$, and $\mathscr{W}_{j,e^{2i\pi \mathrm{p}/\mathrm{M}}}$ with $j \in \mathbb{N}^*$, $j\mathrm{p}/\mathrm{M}$ even. The sums in $\tilde{P}^{(\mathsf{a})}_{aabb}$ involve the same modules, except for $\overline{\mathscr{W}}_{0,\mathfrak{q}^2}$ which is replaced by $\mathscr{W}_{0,\mathfrak{q}^{2\mathsf{a}}}$. This is expected, since such modules precisely correspond to giving to non-contractible loops the weight n_{a}.

For different values of a (including $\mathsf{a} = 1$, i.e., the case of Potts), the $\tilde{P}^{(\mathsf{a})}_{aabb}$ involve eigenvalues from different modules. Among these are of course the modules $\mathscr{W}_{0,\mathfrak{q}^{2\mathsf{a}}}$ for which, since they themselves depend on a, there is not much point comparing amplitudes. However, the modules $\mathscr{W}_{0,-1}$ and $\mathscr{W}_{j,e^{2i\pi \mathrm{p}/\mathrm{M}}}$ also contribute to the $\tilde{P}^{(\mathsf{a})}_{aabb}$. For these, we can indeed compare the amplitudes of their eigenvalues contributions. Like before, another type of remarkable facts is then observed:

The ratios of the amplitudes of eigenvalues from $\mathscr{W}_{0,-1}$, and $\mathscr{W}_{j,e^{2i\pi \mathrm{p}/\mathrm{M}}}$ that contribute to the $\tilde{P}^{(\mathsf{a})}_{aabb}$ depend only on the module and on a, and are independent of the eigenvalues within this module. They also do not depend on the size L.

Now define

$$\gamma^{(\mathsf{a})}_{j,z^2} \equiv \frac{A^{(\mathsf{a})}_{aabb}}{A_{aabb}}(\mathscr{W}_{j,z^2}) \,, \tag{4.4.13}$$

where $A^{(\mathsf{a})}$ is the amplitude in $\tilde{P}^{(\mathsf{a})}_{aabb}$, and A the amplitude in $P_{aabb} = \tilde{P}^{(1)}_{aabb}$. Denoting $Q_{\mathsf{a}} = n^2_{\mathsf{a}}$ such that we have $Q = n^2$ as usual, we have determined the following:

$$\gamma^{(\mathsf{a})}_{0,-1} = 1 \,, \tag{4.4.14a}$$

$$\gamma^{(\mathsf{a})}_{2,1} = \frac{(Q_2 - Q_1)Q_{\mathsf{a}}}{(Q_2 - Q_{\mathsf{a}})Q_1} \,, \tag{4.4.14b}$$

$$\gamma^{(\mathsf{a})}_{4,1} = \frac{(c_1 + Q_{\mathsf{a}})Q_{\mathsf{a}}(Q_4 - Q_1)}{c_2(Q_4 - Q_{\mathsf{a}})} \,, \tag{4.4.14c}$$

$$\gamma^{(\mathsf{a})}_{4,-1} = \frac{Q_{\mathsf{a}}}{Q_1} \,. \tag{4.4.14d}$$

The expression for $\gamma^{(\mathsf{a})}_{4,1}$ involves two quantities, c_1 and c_2, which are independent of a, but which have a complicated Q-dependence. They are given by the following expressions:

$$c_1 = \frac{8 - 26Q + 60Q^2 - 110Q^3 + 112Q^4 - 54Q^5 + 12Q^6 - Q^7}{Q(2 - 4Q + Q^2)} \,, \tag{4.4.15a}$$

$$c_2 = \frac{(Q-4)(Q-1)(2 - 4Q + 10Q^2 - 15Q^3 + 7Q^4 - Q^5)}{2 - 4Q + Q^2} \,. \tag{4.4.15b}$$

The fact that the ratios (4.4.5), (4.4.7), (4.4.10) and (7.5.6) exist and are independent of the size of the system suggests strongly that they have a simple, algebraic origin—e.g., occurring as recoupling coefficients in quantum group representation theory. We hope to discuss this more in a forthcoming paper. For now, we use these facts (which, strictly speaking, must be considered as conjectures, since we have only checked them for a finite number of values of L—see Appendix D of [15] for details) to discuss correlation functions in the RSOS models.

We also note that when a is an integer, the representation theory of ATL is not generic: the modules $\mathscr{W}_{0,\mathfrak{q}^{2\mathsf{a}}}$ are reducible, and contain a sub-module isomorphic to $\mathscr{W}_{\mathsf{a},1}$. This does not affect the coefficients in (4.4.14): more details can be found in Appendix D of [15].

4.5 Recovering minimal model four-point functions

Recovering the s-channel spectrum of the minimal model transfer matrix is a subtle process. It involves not only "throwing away" many modules $\mathscr{W}_{j,z^2}$, but also restricting to the irreducible tops of those which are kept. More precisely, in the continuum limit, the representation of the ATL algebra relevant for the A_{p-1} RSOS minimal model is [90, 92]:

$$\rho_{\text{per}} \simeq \bigoplus_{n=1}^{p-1} \mathscr{X}_{0,\mathfrak{q}^{2n}} \ , \tag{4.5.1}$$

with $\mathfrak{q} = e^{i\pi\frac{p-q}{p}}$. Here, each module $\mathscr{X}_{0,\mathfrak{q}^{2n}}$ is the irreducible top of the modules $\mathscr{W}_{0,\mathfrak{q}^{2n}}$, which become reducible when $\mathfrak{q}$ is a root of unity. The structure of the some of these modules is given in Figure 4.9.

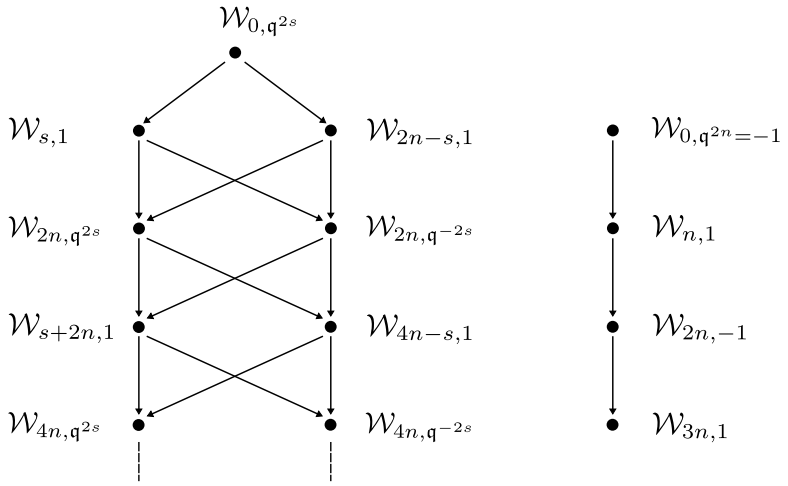

Figure 4.9: The structure of the standard modules involved in the RSOS model for $\mathfrak{q} = e^{i\pi/2n}$ corresponding to $p = 2n, q = 2n-1$. The RSOS model is obtained by restricting to the simple tops.

In addition, different affine Temperley-Lieb modules $\mathscr{W}_{j,z^2}$ may get glued in the loop model representation relevant for the Potts correlation functions. The full analysis of what happens is not our concern here, however, and will be discussed elsewhere. In this chapter, we simply wish to illustrate the mechanism by which *unwanted eigenvalues disappear* from the s-channel spectrum in finite size. This turns out to be in one-to-one correspondence with the simplification of the spectrum in the continuum limit, since we have [90]:

$$\mathscr{X}_{0,\mathfrak{q}^{2n}} \mapsto \sum_{r=1}^{q-1} |\chi_{rn}|^2 \tag{4.5.2}$$

Note in particular that this only involves diagonal fields.

4.5.1 The case of A_{p-1}

Consider the A_{p-1} models for which we have seen in (4.3.11) that

$$\langle \phi_{p/2}\phi_{p/2}\phi_{p/2}\phi_{p/2}\rangle \propto \frac{p}{2} P_{aaaa} + \tilde{P}^{A_{p-1}}_{aabb} + \tilde{P}^{A_{p-1}}_{abba} + \tilde{P}^{A_{p-1}}_{abab} \, . \tag{4.5.3}$$

Let us now examine, for instance, the module $\mathscr{W}_{4,-1}$ corresponding to $j = 4$ and $z^2 = e^{2i\pi \mathrm{p}/\mathrm{M}} = -1$ with $\mathrm{p}/\mathrm{M} = 1/2$. Using that $\mathfrak{q} = e^{i\pi/2n}$, we can write $z^2 = \mathfrak{q}^{2s}$ with $s = n$. For $p > 4$, it is clear that the module $\mathscr{W}_{4,-1}$ does not appear in any of the "ladders" (such as the ones in Figure 4.9) associated with the simple modules describing the minimal model. Barring spurious degeneracies,[13] this means the total amplitude for the corresponding eigenvalues in (4.5.3) should vanish. Let us now see how each term in (4.5.3) contributes to this amplitude.

While the first term in (4.5.3) involves P_{aaaa}, all other terms involve modified weights. The total amplitude can thus be written as:

$$\tilde{A}(\mathscr{W}_{4,-1}) = \frac{p}{2} A_{aaaa}(\mathscr{W}_{4,-1}) + \tilde{A}_{aabb}(\mathscr{W}_{4,-1}) + \tilde{A}_{abba}(\mathscr{W}_{4,-1}) + \tilde{A}_{abab}(\mathscr{W}_{4,-1})\,. \tag{4.5.4}$$

Here we have introduced modified amplitudes $\tilde{A}$, determined by the modified weights given to non-contractible loops in the RSOS correlation functions, when compared to the Potts model ones. For notational simplicity, we ignore the superscript A_{p-1} for $\tilde{A}$ here—and similarly we shall omit in the next subsection the superscripts for modified amplitudes of type D—, while one should keep in mind that the modified amplitudes depend on the algebra in consideration due to the difference in the three-point couplings (4.3.1) and (4.3.16). We have in general

$$\tilde{A}(\lambda_i) = \sum_{k=2 \text{ even}}^{j} A^{(k)}(\lambda_i) M(k)\,, \tag{4.5.5}$$

where A denotes the Potts amplitudes in (4.4.9). The sum in (4.5.5) is truncated to the maximum value j since for an eigenvalue λ_i in $\mathscr{W}_{j,z^2}$, we have at most $k = j$, as is clear from the geometrical interpretation of the ATL modules in Section 4.4.1. Using our facts of type 2—see eq. (4.4.10)—we can therefore write

$$\left.\frac{\tilde{A}_{abab}}{A_{abab}}\right|_{\mathscr{W}_{j,z^2}} = \frac{\sum_{k=2 \text{ even}}^{j} \beta^{(k)}_{j,z^2} M(k)}{\sum_{k=2 \text{ even}}^{j} \beta^{(k)}_{j,z^2}}\,. \tag{4.5.6}$$

The same holds for A_{abba}, since, for $\mathscr{W}_{4,-1}$, the amplitudes for the two sectors A_{abab} and A_{abba} are identical. We therefore write

$$\tilde{A}_{abab}(\mathscr{W}_{4,-1}) = A_{abab}(\mathscr{W}_{4,-1}) \frac{M^{A_{p-1}}(2) + \beta^{(4)}_{4,-1} M^{A_{p-1}}(4)}{1 + \beta^{(4)}_{4,-1}}\,. \tag{4.5.7}$$

Now use that $\beta^{(4)}_{4,-1} = -\frac{Q(Q-2)}{3Q-4}$ from (4.4.11b), together with $M^{A_{p-1}}(2) = \frac{p}{Q}$ and $M^{A_{p-1}}(4) = \frac{3p}{Q^2}$ from (4.3.8). Hence

$$\tilde{A}_{abab}(\mathscr{W}_{4,-1}) = -\frac{2p}{Q(Q-1)(Q-4)} A_{abab}(\mathscr{W}_{4,-1})\,, \tag{4.5.8}$$

and the same for $\tilde{A}_{abba}$.

Next, we have

$$\begin{aligned} \tilde{A}_{aabb}(\mathscr{W}_{4,-1}) =& A_{aabb}(\mathscr{W}_{4,-1}) \sum_{\mathsf{a}=1 \text{ odd}}^{p-1} \frac{A^{(\mathsf{a})}_{aabb}}{A_{aabb}}(\mathscr{W}_{4,-1}) \\ =& A_{aabb}(\mathscr{W}_{4,-1}) \sum_{\mathsf{a}=1 \text{ odd}}^{p-1} \gamma^{(\mathsf{a})}_{4,-1} \\ =& \frac{p}{Q} A_{aabb}(\mathscr{W}_{4,-1})\,, \end{aligned} \tag{4.5.9}$$

[13] Since we study a specific Hamiltonian or transfer matrix, such degeneracies cannot be excluded *a priori*, though they are not observed in our numerical analysis.

where we used that $\gamma_{4,-1}^{(\mathsf{a})} = \frac{Q_\mathsf{a}}{Q_1}$ from (4.4.14d), together with the identity

$$\sum_{\mathsf{a}=1 \text{ odd}}^{p-1} (\mathfrak{q}^\mathsf{a} + \mathfrak{q}^{-\mathsf{a}})^2 = p\,, \tag{4.5.10}$$

valid when p is even, as we have supposed in (4.1.12).

We therefore see that (4.5.4) becomes

$$\begin{aligned}\tilde{A}(\mathscr{W}_{4,-1}) &= \frac{p}{2} A_{aaaa}(\mathscr{W}_{4,-1}) + \frac{p}{Q} A_{aabb}(\mathscr{W}_{4,-1}) - \frac{2p}{Q(Q-1)(Q-4)} \left(A_{abba} + A_{abab}\right)(\mathscr{W}_{4,-1}) \\ &= p A_{aaaa}(\mathscr{W}_{4,-1}) \left(\frac{1}{2} + \frac{\alpha_{4,-1}}{Q} - \frac{2}{Q(Q-1)(Q-4)} \overline{\alpha}_{4,-1}\right),\end{aligned} \tag{4.5.11}$$

where in the last line we have used (4.4.5) and (4.4.7). Recall that $\overline{\alpha}_{4,-1} = \frac{(Q-1)(Q-4)}{2}$ and $\alpha_{4,-1} = \frac{2-Q}{2}$. We arrive at

$$\left(\frac{1}{2} + \frac{\alpha_{4,-1}}{Q} - \frac{2}{Q(Q-1)(Q-4)} \overline{\alpha}_{4,-1}\right) = 0. \tag{4.5.12}$$

We have thus established that the amplitude of eigenvalues coming from $\mathscr{W}_{4,-1}$ all vanish in the four-point function (4.5.3).

In fact, since the s-channel of the four-point function (4.5.3) involves only diagonal fields in the type A minimal models, the amplitudes of eigenvalues from all modules $\mathscr{W}_{j,z^2}$ should vanish in (4.5.3) since they correspond to non-diagonal fields in the continuum limit, leaving only the diagonal fields from $\overline{\mathscr{W}}_{0,\mathfrak{q}^2}$. We therefore expect, from the vanishing of the $\mathscr{W}_{j,z^2}$ contributions, to have the following relation:

$$\frac{p}{2} + \alpha_{j,z^2} \sum_{\mathsf{a}=1 \text{ odd}}^{p-1} \gamma_{j,z^2}^{(\mathsf{a})} + \bar{\alpha}_{j,z^2} \frac{\sum_{k=2 \text{ even}}^{j} \beta_{j,z^2}^{(k)} M^{A_{p-1}}(k)}{\sum_{k=2 \text{ even}}^{j} \beta_{j,z^2}^{(k)}} = 0. \tag{4.5.13}$$

While this can be checked numerically for $\mathscr{W}_{0,-1}$, $\mathscr{W}_{2,1}$ and $\mathscr{W}_{4,1}$ using the α, $\bar{\alpha}$, β and γ we provided in the previous section, we do not have, for the moment, closed-form expressions for all the coefficients involved. Note that here $\mathscr{W}_{2,1}$ and $\mathscr{W}_{4,1}$ appear as submodules of some other modules when $\mathfrak{q}$ is the relevant root of unity, so one might have feared that the overall cancellation of its contributions might involve also some of the coefficients of these other modules—this is, however, not the case.

4.5.2 The case of $D_{1+\frac{p}{2}}$

We next consider amplitudes in the $D_{1+\frac{p}{2}}$ case. Let us study the case of $\mathscr{W}_{2,1}$, for example. Recall from (4.3.28a) that

$$\langle \phi_{p/2} \phi_{p/2} \phi_{\bar{p}/2} \phi_{\bar{p}/2} \rangle = P_{aaaa} + \tilde{P}_{aabb}^{D_{1+\frac{p}{2}}}. \tag{4.5.14}$$

Because of (4.3.21) the amplitude in the first term does not depend on the modification of the weights M, so we have

$$\tilde{A}(\mathscr{W}_{2,1}) = A_{aaaa}(\mathscr{W}_{2,1}) + \tilde{A}_{aabb}(\mathscr{W}_{2,1}), \tag{4.5.15}$$

and

$$\begin{aligned}\tilde{A}_{aabb}(\mathscr{W}_{2,1}) =& A_{aaaa}(\mathscr{W}_{2,1})\frac{A_{aabb}(\mathscr{W}_{2,1})}{A_{aaaa}(\mathscr{W}_{2,1})}\sum_{\mathsf{a}=1\ \text{odd}}^{p-1}(-1)^{\frac{\mathsf{a}-1}{2}}\frac{A^{(\mathsf{a})}_{aabb}(\mathscr{W}_{2,1})}{A_{aabb}(\mathscr{W}_{2,1})}\\ =& A_{aaaa}(\mathscr{W}_{2,1})\left(\alpha_{2,1}\sum_{\mathsf{a}=1\ \text{odd}}^{p-1}(-1)^{\frac{\mathsf{a}-1}{2}}\gamma^{(\mathsf{a})}_{2,1}\right),\end{aligned} \tag{4.5.16}$$

where we have used (4.3.16) (from which the $(-1)^{\frac{\mathsf{a}-1}{2}}$ occurs) and (7.5.6). Recall $\alpha_{2,1}=\frac{1}{1-Q}$, and $\gamma^{(\mathsf{a})}_{2,1}$ is given in (4.4.14), so we have

$$\tilde{A}(\mathscr{W}_{2,1}) = A_{aaaa}(\mathscr{W}_{2,1})\left(1+\frac{Q_2-Q}{Q(1-Q)}\sum_{\mathsf{a}=1\ \text{odd}}^{p-1}(-1)^{\frac{\mathsf{a}-1}{2}}\frac{Q_{\mathsf{a}}}{Q_2-Q_{\mathsf{a}}}\right)=0\,, \tag{4.5.17}$$

which can be checked to vanish using MATHEMATICA.

In general, from the identification of (4.3.18), the s-channel spectrum of (4.5.14) involves only diagonal fields as argued in [71] and therefore we should have the following identity for modules $\mathscr{W}_{j,z^2}$:

$$1+\alpha_{j,z^2}\sum_{\mathsf{a}=1\ \text{odd}}^{p-1}(-1)^{\frac{\mathsf{a}-1}{2}}\gamma^{(\mathsf{a})}_{j,z^2}=0. \tag{4.5.18}$$

This can be checked to be true for $\mathscr{W}_{0,-1}$, $\mathscr{W}_{4,-1}$, $\mathscr{W}_{4,1}$ using (4.4.6) and (4.4.14).

Finally let us look at $\mathscr{W}_{4,i}$. Its amplitude in $\langle\phi_{p/2}\phi_{\bar{p}/2}\phi_{p/2}\phi_{\bar{p}/2}\rangle$ comes entirely from the term $\tilde{P}_{abab}^{D_{1+\frac{p}{2}}}$, since by (4.4.3) P_{aaaa} has no contribution from $\mathscr{W}_{4,i}$. By the result analogous to (4.5.7) we then have

$$\tilde{A}_{abab}(\mathscr{W}_{4,i}) = A_{abab}(\mathscr{W}_{4,i})\frac{M^{D_{1+\frac{p}{2}}}(2)+\beta^{(4)}_{4,i}M^{D_{1+\frac{p}{2}}}(4)}{1+\beta^{(4)}_{4,i}}\,. \tag{4.5.19}$$

Inserting now $\beta^{(4)}_{4,i}$ from (4.4.11) we find

$$\frac{M^{D_{1+\frac{p}{2}}}(4)}{M^{D_{1+\frac{p}{2}}}(2)}=\frac{3Q-10}{Q^2-4Q+2}=-\frac{1}{\beta^{(4)}_{4,i}}\,, \tag{4.5.20}$$

so indeed (4.5.19) vanishes exactly.

4.6 Comparison with the results of [19, 71–74]

We now wish to return to the thread left behind in Section 4.1.4, namely the comparison between our approach and the one advocated in [19,71–74]. One of the principal ideas promoted originally in [19,72] is to obtain the geometrical correlation functions in the generic Q-state Potts model by suitable analytic continuations from correlations in the type D minimal models. It has been argued in subsequent work [20, 71, 74] that such procedure is inaccurate and could at best provide an approximate description of the Potts geometrical correlations. Here we have provided an explanation of this issue, in particular why the geometrical correlation functions in the Potts model *cannot* be obtained this way, by explicitly reformulating the correlation functions of minimal models (i.e., their RSOS lattice realizations) to give them a geometric interpretation, and then directly comparing with the geometric correlations in the Potts model. We have seen

in sections 4.4 and 4.5 that many of the ATL representations $\mathscr{W}_{j,z^2}$ which were found in [20] to provide contributions to the s-channel spectrum of the Potts geometrical correlations have, in fact, zero net amplitude in the RSOS models and therefore in the continuum limit disappear from the minimal models spectra. Moreover, since the discussion so far have been formulated in a way that depends only on Q, the results apply to the spectrum first proposed in [19], which is an analytic continuation of the spectrum of minimal models obtained by taking the limit (4.1.15):

$$\mathscr{M}(p,q): \quad p,q\to\infty,\ \frac{q}{p-q}\to x, \tag{4.6.1}$$

where x is a finite number and the central charge (4.1.11) becomes (3.5.4). In this section we aim at further elucidating the nature of this limit, via the RSOS models of type D, for the purpose of making a direct comparison with results in [19, 71–74].

In the case of $D_{1+\frac{p}{2}}$ models, the multiplicity $M^{D_{1+\frac{p}{2}}}(k)$ in (4.3.23) is well defined in the limit (4.6.1)—as witnessed by its rewriting (4.3.24) as polynomials in Q—and we will denote it as $M^{D_\infty}(k)$. The diagrammatic expansions of P_{aaaa}, $\tilde{P}^{D_{1+\frac{p}{2}}}_{abab}$, $\tilde{P}^{D_{1+\frac{p}{2}}}_{abba}$ in the s-channel (4.4.2a) are also well defined. By taking the corresponding limit of (4.3.28a) and (4.3.28c) it follows that

$$\operatorname*{Lim}_{p\to\infty}\langle\phi_{p/2}\phi_{\bar{p}/2}\phi_{\bar{p}/2}\phi_{p/2}\rangle \ \propto\ P_{aaaa}+\tilde{P}^{D_\infty}_{abba}\,, \tag{4.6.2a}$$

$$\operatorname*{Lim}_{p\to\infty}\langle\phi_{p/2}\phi_{\bar{p}/2}\phi_{p/2}\phi_{\bar{p}/2}\rangle \ \propto\ P_{aaaa}+\tilde{P}^{D_\infty}_{abab}\,, \tag{4.6.2b}$$

where on the right-hand side, the pseudo-probabilities are defined by using (4.3.23) and (4.3.27) with multiplicity M^{D_∞}. They depend only on Q, so we have in (4.6.2) two quantities that ressemble similar combinations in the Potts model. There is however an important difference with the Potts model: while the probabilities (and thus their combinations) in the Potts model are expected to be smooth functions of Q, the combinations in (4.6.2) have infinitely many poles at the values of Q given by (4.3.26) which originate from the multiplicities $M^{D_\infty}(k)$. Due to (4.3.20), we will in the following make the identifications

$$\operatorname*{Lim}_{p\to\infty}\langle\phi_{p/2}\phi_{\bar{p}/2}\phi_{\bar{p}/2}\phi_{p/2}\rangle \ \leftrightarrow\ \langle V^D V^N V^N V^D\rangle\,, \tag{4.6.3a}$$

$$\operatorname*{Lim}_{p\to\infty}\langle\phi_{p/2}\phi_{\bar{p}/2}\phi_{p/2}\phi_{\bar{p}/2}\rangle \ \leftrightarrow\ \langle V^D V^N V^D V^N\rangle\,, \tag{4.6.3b}$$

where the right-hand side now represent the four-point functions after taking the limit (4.6.1), so as to extend (4.3.20) to generic central charges. We see then that the poles (4.3.26) in (4.6.2) obtained from direct lattice calculations exactly recover the poles (4.1.16) and (4.1.17) from the CFT analysis in [71]. As was already argued in [20], on the basis of examples, the richer s-channel spectrum (4.4.3) for the Potts model has indeed the effect of cancelling these poles.

Now recall the conjecture (4.1.18) inferred from Monte-Carlo simulations in [74]. To be more specific, it was observed there that the four-point functions were given approximately by the combination of Potts probabilities

Conjecture in [74]:

$$\operatorname*{Lim}_{p\to\infty}\langle\phi_{p/2}\phi_{\bar{p}/2}\phi_{\bar{p}/2}\phi_{p/2}\rangle \ \approx\ \frac{1}{2}\left(P_{aaaa}+\frac{2}{Q-2}P_{abba}\right), \tag{4.6.4a}$$

$$\operatorname*{Lim}_{p\to\infty}\langle\phi_{p/2}\phi_{\bar{p}/2}\phi_{p/2}\phi_{\bar{p}/2}\rangle \ \approx\ \frac{1}{2}\left(P_{aaaa}+\frac{2}{Q-2}P_{abab}\right) \tag{4.6.4b}$$

and that these become exact at $Q = 0, 3, 4$. In particular, near $Q = 2$, the authors of [74] conjectured:

Eqs. (3.34), (3.36) in [74]:

$$\operatorname*{Lim}_{p\to\infty}\langle\phi_{p/2}\phi_{\bar{p}/2}\phi_{\bar{p}/2}\phi_{p/2}\rangle \overset{Q\to 2}{=} \frac{1}{Q-2}P_{abba} + O(1)\,, \tag{4.6.5a}$$

$$\operatorname*{Lim}_{p\to\infty}\langle\phi_{p/2}\phi_{\bar{p}/2}\phi_{p/2}\phi_{\bar{p}/2}\rangle \overset{Q\to 2}{=} \frac{1}{Q-2}P_{abab} + O(1)\,, \tag{4.6.5b}$$

We now fix the coefficients in (4.6.2) to be $\frac{1}{2}$ —same as (4.6.4)— for the purpose of comparing our results with their claims.

For $Q = 3$ we have

$$T_{2\mathsf{m}}\left(\frac{\sqrt{3}}{2}\right) = \cos\left(\frac{\mathsf{m}\pi}{3}\right) \tag{4.6.6}$$

in (4.3.24), and using the identity

$$\sum_{\mathsf{m}=-l}^{l}\binom{2l}{l+\mathsf{m}}\cos^{-1}\left(\frac{\mathsf{m}\pi}{3}\right) = 2\times 3^l \tag{4.6.7}$$

the multiplitiy (4.3.23) becomes independent of k:

$$M^{D_4}(k) = 2 = \frac{2}{Q-2}\,. \tag{4.6.8}$$

Therefore, for $Q = 3$, (4.6.2) reduces to (4.6.4) exactly. Meanwhile, for $Q = 4$, we have $T_{2\mathsf{m}}(1) = 1$, so that (4.3.23) becomes simply:

$$M^{D_\infty}(k = 2l) = \frac{1}{4^l}\sum_{\mathsf{m}=-l}^{l}\binom{2l}{l+\mathsf{m}} = 1 = \frac{2}{Q-2}\,, \tag{4.6.9}$$

and again one identifies (4.6.2) with (4.6.4).

The situation with $Q \to 0$ is more subtle, since the Potts model partition function (2.1.16) itself vanishes in this case. As discussed in [20], one should renormalize the partition function by a factor of Q to redefine it as the number of spanning trees. In the $Q \to 0$ limit, extra clusters disappear by the factors of Q they carry, and therefore the only configuration contributing to P_{aaaa} is a single spanning tree. The only configurations contributing to P_{abab} and P_{abba} are thus diagrams with $k = 2$. Therefore, (4.6.2) is written explicitly as

$$\operatorname*{Lim}_{p\to\infty}\langle\phi_{p/2}\phi_{\bar{p}/2}\phi_{\bar{p}/2}\phi_{p/2}\rangle \overset{Q\to 0}{=} \frac{1}{2}\left(P_{aaaa} + \frac{2}{Q-2}\sum_{D_{abba}} W_{\text{Potts}}(k=2)\right), \tag{4.6.10a}$$

$$\operatorname*{Lim}_{p\to\infty}\langle\phi_{p/2}\phi_{\bar{p}/2}\phi_{p/2}\phi_{\bar{p}/2}\rangle \overset{Q\to 0}{=} \frac{1}{2}\left(P_{aaaa} + \frac{2}{Q-2}\sum_{D_{abab}} W_{\text{Potts}}(k=2)\right), \tag{4.6.10b}$$

which agrees with (4.6.4).

Near $Q = 2$, we see from (4.3.25), (4.3.27) and (4.6.2) that we have, for instance:

$$\operatorname*{Lim}_{p\to\infty}\langle\phi_{p/2}\phi_{\bar{p}/2}\phi_{p/2}\phi_{\bar{p}/2}\rangle \overset{Q\to 2}{=} \frac{1}{Q-2}\frac{1}{Z_{\text{Potts}}}\left(\sum_{D_{abab}} W_{\text{Potts}}(k=2) + 2\sum_{D_{abab}} W_{\text{Potts}}(k=4) + \dots\right) + O(1)\,. \tag{4.6.11}$$

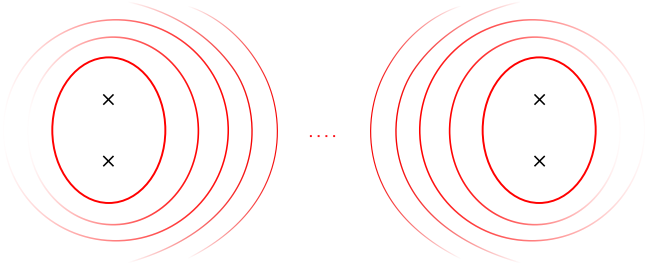

Figure 4.10: There are a large number of non-contractible loops surrounding the basic clusters when the distance separating them is large. Here we show this picture for s-channel of $\tilde{P}_{aabb}$.

On the other hand, (4.6.5) reduces to:

Diagrammatic expansion of eqs. (3.34), (3.36) in [74]:

$$\lim_{p\to\infty}\langle\phi_{p/2}\phi_{\bar{p}/2}\phi_{p/2}\phi_{\bar{p}/2}\rangle \overset{Q\to 2}{=} \frac{1}{Q-2}\frac{1}{Z_{\text{Potts}}}\left(\sum_{D_{abab}} W_{\text{Potts}}(k=2)+\sum_{D_{abab}} W_{\text{Potts}}(k=4)+\dots\right)+O(1). \tag{4.6.12}$$

The difference is

$$\frac{1}{Q-2}\frac{1}{Z_{\text{Potts}}}\left(\sum_{D_{abab}} W_{\text{Potts}}(k=4)+\dots\right)+O(1), \tag{4.6.13}$$

still of order $\frac{1}{Q-2}$, but this is dominated by configurations with $k\geq 4$, whose probabilities are small and are numerically challenging to properly sample.

Let us now turn to the third combination (4.3.28b), which reads

$$\lim_{p\to\infty}\langle\phi_{p/2}\phi_{p/2}\phi_{\bar{p}/2}\phi_{\bar{p}/2}\rangle \propto P_{aaaa}+\tilde{P}^{D_\infty}_{aabb}\,. \tag{4.6.14}$$

While this four-point function is related to (4.6.2) by crossing, here we focus on the s-channel which now involves a large number of non-contractible loops separating the basic clusters in the diagrammatic expansion of $\tilde{P}_{aabb}$, as depicted in Figure 4.10. From (4.5.18), we have seen that only diagonal fields—i.e., the modules $\mathscr{W}_{0,\mathsf{q}^{2\mathsf{a}}}$—remain in the s-channel of this four-point function. It was claimed in [71] that in the limit (4.6.1), the spectrum becomes continuous. Here, in terms of the ATL representations, we can formally write

$$\bigoplus_{\mathsf{a}=1}^{p-1}\mathscr{W}_{0,\mathsf{q}^{2\mathsf{a}}}\simeq\int_0^\pi \mathscr{W}_{0,e^{2i\pi\theta}}\,\mathrm{d}\theta\,, \tag{4.6.15}$$

where the sum is replaced by an integral over a compact variable θ for generic x:

$$\theta=\frac{\mathsf{a}\pi}{x+1}. \tag{4.6.16}$$

Geometrically, this corresponds to integrating over non-contractible loop weights

$$n_z=z+z^{-1},\quad z=e^{i\theta}. \tag{4.6.17}$$

The same picture also applies for the four-point functions

$$\lim_{p\to\infty}\langle\phi_{p/2}\phi_{p/2}\phi_{p/2}\phi_{p/2}\rangle=\lim_{p\to\infty}\langle\phi_{\bar{p}/2}\phi_{\bar{p}/2}\phi_{\bar{p}/2}\phi_{\bar{p}/2}\rangle\propto\frac{p}{2}P_{aaaa}+\tilde{P}^{A_\infty}_{abab}+\tilde{P}^{A_\infty}_{aabb}+\tilde{P}^{A_\infty}_{abba}\,, \tag{4.6.18}$$

where all three channels give rise to the geometric picture of Figure 4.10, with the s, t and u-channels corresponding respectively to the diagrammatic expansions of $\tilde{P}_{aabb}$, $\tilde{P}_{abba}$ and $\tilde{P}_{abab}$. In the CFT, one obtains continuous spectra in all three channels. See [93] for a related discussion.

This section concludes Chapter 4.

CHAPTER

5

RSOS MODELS AND ANYONS

This chapter provides a short interlude, in which we show the correspondence between RSOS models and anyonic systems. In particular, we shall detail the computation of n-point functions in RSOS models and show how, in the case of A_n RSOS models, this computation reduces to evaluating certain fusion diagrams of $su(2)_k$ anyons, where $k = n - 1$.

$su(2)_k$ anyons are an example of non-abelian anyons, which have attracted much interest as a possible basis for topological quantum computing, which is inherently fault-tolerant [94–96]. Initially such quantum computation was proposed to be carried out through braiding, but a measurement-only implementation was described in [97] some years later. Some notable examples of $su(2)_k$ anyons are $su(2)_2$ anyons, also called Ising anyons, and $su(2)_3$ anyons, which are closely related to Fibonacci anyons. These are unitary examples, meaning in particular that the F-symbols (to be defined below) are unitary in a properly chosen basis. There are also closely related non-unitary examples such as the Yang-Lee anyons. We shall focus on the unitary theories, making only a brief comment about how the non-unitary theories are obtained from the unitary ones.

The $su(2)_k$ anyons can be considered a deformation of $SU(2)$ spins with deformation parameter $\mathfrak{q} = e^{\pi ri/(k+2)}$, following the convention common in RSOS literature [98] that a $\mathfrak{q}$-deformed number is given by

$$[n]_{\mathfrak{q}} = \frac{\mathfrak{q}^n - \mathfrak{q}^{-n}}{\mathfrak{q} - \mathfrak{q}^{-1}}\,. \tag{5.0.1}$$

Note that it is common in anyonic literature to instead define

$$[n]_q = \frac{q^{n/2} - q^{-n/2}}{q^{1/2} - q^{-1/2}} \tag{5.0.2}$$

such that the deformation parameter is the r'th root of unity $q = e^{2\pi ri/(k+2)}$. The deformation parameter modifies the usual $SU(2)$ $6j$ symbols as shown in [98] and [99] using RSOS conventions and anyonic conventions, respectively. In unitary theories $r = 1$, while in non-unitary theories $r > 1$. The process of increasing r is referred to as Galois conjugation [100]. The deformation parameter $\mathfrak{q}$ is the same as the $U_{\mathfrak{q}}sl(2)$ deformation parameter appearing in

the loop weight of the affine Temperley-Lieb algebra: applying (4.2.2) to an A_n RSOS model, which has Coxeter number $n+1 = k+2$, the loop weight is $\lambda_{(r)} = 2\cos\frac{\pi}{k+2}$, i.e. $\mathfrak{q} = e^{\pi r i/(k+2)}$ with $r = p - q$. As noted in Section 3.4 the fusion rules of the $su(2)_k$ anyons show up in the representation theory for both the quantum group $U_\mathfrak{q} sl(2)$ and the affine Kac Moody $\widehat{su(2)}$ at level k, and while the name of the anyons only makes reference to the latter, the connection to $U_\mathfrak{q} sl(2)$ is more natural in the present context.

5.1 $su(2)_k$ anyons: a brief introduction

We begin by recalling some relevant features of $su(2)_k$ anyons, and setting the notation. For general introductions, see [96, 99]. For a given level k, we label the $su(2)_k$ anyons by their "spins" $j = 0, \frac{1}{2}, 1, \ldots \frac{k}{2}$. They obey the fusion rules

$$j \times j' = \sum_j N_{j,j'}^{j''} = \sum_{j''=|j-j'|}^{\min(j+j', k-j-j')} j\,. \tag{5.1.1}$$

These fusion rules reduce to those of $SU(2)$ in the limit $k \to \infty$. We call the matrices N_j, with entries $N_{j,j'}^{j''}$, the *fusion matrices*. We call $j = \frac{1}{2}$ the *generating anyon*, since all other anyons can be obtained by its repeated fusion. We define the quantum dimension of an anyon labelled by j as $d_j = [2j+1]_\mathfrak{q}$. It governs the asymptotic growth of the fusion space of N anyons of label j as $d \sim d_j^N$ at large N. In the limit $\mathfrak{q} \to 1$ the quantum dimensions become integers, and we recover for instance $d_{\frac{1}{2}} = 2, d = 2^N$ for $j = \frac{1}{2}$. Imposing $d_j > 0$ is equivalent truncating the allowed spins to $j \le \frac{k}{2}$.

We note that by (5.1.1) each $su(2)_k$ anyon is its own anti-particle. For this reason, we shall not give the lines an orientation, writing diagrams such as creation and annihilation as cups and caps,

(5.1.2)

with time flowing upwards.

Based on these fusion rules we can draw *fusion diagrams*, in which the edges have labels among the anyon "spins" and each vertex connects three edges j, j', j'', with the requirement that $N_{j,j'}^{j''}$ is non-zero. When drawing these diagrams we shall typically draw as dashed or even omit any line carrying the label $j = 0$. An example of a simple fusion diagram is

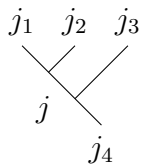

(5.1.3)

The above diagram is also an example of a fusion *tree*.

We need a few more rules in order to evaluate fusion diagrams. The first fundamental transformation is to move internal lines through the F-transformation:

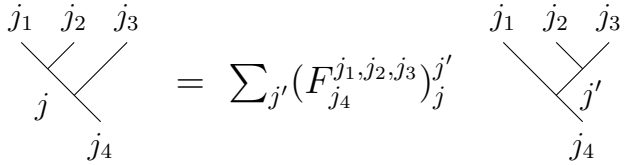

(5.1.4)

The second fundamental transformation is braiding:

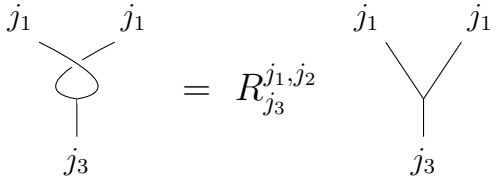

(5.1.5)

Together with the anyon species, the F-symbols and R-symbols fully specify the anyon model. For consistency, they are required to obey the Pentagon and Hexagon equations [101]. The following relations are consequences of (5.1.4) and (5.1.5) together with these consistency conditions.

We can remove loops around any line using

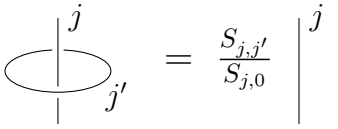

(5.1.6)

where $S_{j,j'}$ is the modular S-matrix, which is defined from the R-symbols and which for $su(2)_k$ anyons is given by

$$S_{j,j'} = \sqrt{\frac{2}{k+2}} \sin\left(\frac{\pi(2j+1)(2j'+1)}{k+2}\right) . \tag{5.1.7}$$

As a special case, when the label of the line going through the loop is $j = 0$, we find the weight of an isolated anyon loop, the quantum dimension $d_j = \frac{S_{1j}}{S_{11}}$.

Meanwhile, "bubbles" are removed by

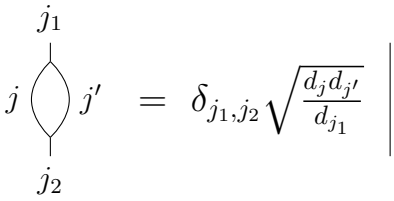

(5.1.8)

Finally we wish to bend and straighten lines. Any horizontal bends, such that they do not involve annihilation or creation, can be trivially created and removed. Meanwhile, by the rules above, vertical bends introduce the Frobenius-Schur indicator $\kappa_j = d_j (F_j^{jjj})_0^0$:

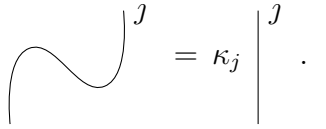

(5.1.9)

This is seen by using an F-transformation to "take a short cut" across one of the bends and removing the resulting loop. For self-dual anyons, the Frobenius-Schur indicator $\kappa_j = \pm 1$. For a pedagogical description of a common prescription, in which flags are introduced to keep track of pairings of cups and caps in order to impose isotopy invariance on the fusion diagrams, see [99]. In what follows, we shall not need to worry about it. We call (5.1.9) the "zig-zag' identity.

The fusion matrices are diagonalized by the modular S-matrix S, a fact that can be expressed through the Verlinde formula

$$N_{j,j'}^{j''} = \sum_l \frac{S_{j,l} S_{j',l} S_{l,j''}^*}{S_{0,l}} \tag{5.1.10}$$

with S^* the conjugate of S. (In the case of $su(2)_k$, $S_{j,j'}$ is real and symmetric, which will be relevant in the expressions below.)

In Section 5.2 of this chapter we shall forget for a minute about anyons, and detail the computation of N-point functions of the order operator (4.2.7) in the RSOS models, considered in the loop model formulation. The reader is however encouraged to keep in mind that it is not a coincidence that we choose to denote by $S^{\sigma}_{(r)}$ the eigenvectors of the adjacency matrix – in the case where we consider the Dynkin diagram A_n, the matrix formed by these eigenvectors is precisely the modular S-matrix discussed above. In Section 5.3 we shall specialize to A_n-type RSOS models and and draw the $su(2)_k$ fusion diagrams corresponding to the computation of the N-point functions. We shall also briefly discuss how the A_n RSOS model in the anisotropic limit turns into the $su(2)_k$ anyon chain (Section 5.4), and how the 2-point function of the order operator relates to the topological defects, or "hoop operators", Y and $\bar{Y}$ (Section 5.5).

5.2 RSOS N-point functions

In this section we shall focus on the equivalence between the RSOS model and the loop model defined on the medial graph $\mathscr{M}(G) = \Gamma^*$, i.e. the dual of the plane quandrangulation. The loops are shown in Figure 2.1 together with the tree $\mathsf{T} = (\mathsf{V}, \mathsf{E})$, which shall play an important role in the following. In terms of loops and trees, the essential part of the result (2.3.5) is that

- The expansion of the local weights in the RSOS model followed by the summation over heights, subject to the constraints imposed by the adjacency matrix $\mathscr{A}$, leads to a corresponding formulation in terms of clusters on G, or equivalently to a completely packed loop model on $\mathscr{M}(G)$.
- Each loop gets a weight λ equal to the eigenvalue of the chosen eigenvector S of the adjacency matrix $\mathscr{A}$. These weights are due to the recurrence relation on the tree T that serves to eliminate it starting from the leaves.
- There is an extra factor $\sum_{\sigma\in X} S_\sigma^2$ coming from the summation over the root vertex. Henceforth we choose to normalize all eigenvectors of $\mathscr{A}$, so that this factor is 1.

We label the different eigenvectors and eigenvalues of $\mathscr{A}$ as $S^{\sigma}_{(r)}$ and $\lambda_{(r)}$, with $r = 1, 2, \ldots, \dim \mathscr{A}$. Below, we shall also refer to the $S_{(r)}$ as states, calling $S \equiv S_{(r_{\rm id})}$ the identity state.[1] $\mathscr{A}$ is real and symmetric, so the matrix $\mathscr{O}$ formed by its normalized eigenvectors is orthogonal. Both the rows and columns of $\mathscr{O}$ provide an orthonormal basis of $\mathbb{R}^{\dim \mathscr{A}}$:

$$\sum_{\sigma} S^{\sigma}_{(r_1)} S^{\sigma}_{(r_2)} = \delta_{r_1,r_2} \tag{5.2.1}$$

and

$$\sum_{r} S^{\sigma_1}_{(r)} S^{\sigma_2}_{(r)} = \delta_{\sigma_1,\sigma_2}\,. \tag{5.2.2}$$

The definition of order parameters from the normalized eigenvectors extends that of [29, 75] (in which $S_{(r_{\rm id})}$ is the Perron-Frobenius vector) to any $r_{\rm id}$ such that $S_\sigma := S^{\sigma}_{(r_{\rm id})} \neq 0$:

$$\phi_r(i) = \frac{S^{\sigma_i}_{(r)}}{S_{\sigma_i}}\,. \tag{5.2.3}$$

[1] In the RSOS lattice formulation of minimal models $\mathscr{M}(p,q)$, we have $r_{\rm id} = p - q$ (see Section 4.2).

We mark N vertices $i \in V$ by a label $r_i \in \{1, 2, \ldots, \dim \mathscr{A}\}$. The corresponding N-point correlation functions are given by insertions of $\phi_{r_i}(i)$, which amounts to replacing the vertex weights S_{σ_i} of (2.1.10) by $S^{\sigma_i}_{(r_i)}$ at each marked vertex. The corresponding weights in the loop model will depend on how the marked vertices are situated in the tree T. In particular, in the edge subset expansion, it will be possible for a given vertex in V to be marked several times, if the corresponding marked vertices in V are situated in the same cluster.

In Section 5.2.1 below we shall revisit the inductive argument on T, first for the partition function, and then generalising it to all N-point correlation functions in the RSOS model with $N \leq 3$. We shall then describe the case of $N > 3$ from a slightly different perspective in Section 5.2.2.

5.2.1 Explicit computation on T up to $N = 3$

A common feature of the proofs in this section is that we have the liberty to chose the root of $\mathsf{T} = (\mathsf{V}, \mathsf{E})$ at any vertex in V. Certain calculations can be done in different ways, depending on the choice of the root, but the result will of course be independent of that choice. This independence is guaranteed by certain identities that we shall establish along the way.

Partition function

Chose any $\rho \in \mathsf{V}$ as the root of T. To sum out a leaf $i \in \mathsf{V}$, let j denote its (unique) parent. The leaf has degree $\mathrm{d}_i = 1$, and let d_j denote the degree of the parent vertex before the summation. The inductive argument made in Lemma 2.3.1 then hinges on the eigenvalue identity for the adjacency matrix $\mathscr{A}$

$$\sum_{\sigma_i} \mathscr{A}_{\sigma_j,\sigma_i} S_{\sigma_i} S^{2-\mathrm{d}_j}_{\sigma_j} = \lambda S^{2-(\mathrm{d}_j-1)}_{\sigma_j} , \tag{5.2.4}$$

where $\mathrm{d}_j - 1$ is now the degree of j after the leaf has been summed out. This produces a weight λ per loop. After summing out inductively all the leaves, only the root vertex ρ will remain. Since $\mathrm{d}_\rho = 0$ the corresponding sum produces

$$\sum_{\sigma_\rho} S^2_{\sigma_\rho} = 1 , \tag{5.2.5}$$

where we have used the normalisation of the eigenvectors.

One-point function

Take the marked point $i_1 := \rho \in \mathsf{V}$ as the root of T, and let r_1 denote the corresponding label of $S_{(r_1)}$. The argument for the leaves can be taken over from the computation of the partition function, producing again a factor $\lambda^{|\mathsf{V}|}$. At the root we get an extra factor

$$\sum_{\sigma_\rho} S^2_{\sigma_\rho} \phi_{r_1}(i_1) = \sum_{\sigma_\rho} S_{\sigma_\rho} S^{\sigma_\rho}_{(r_1)} = \delta_{r_1, r_{\mathrm{id}}} , \tag{5.2.6}$$

where we have used the definition (5.2.3) of the order parameters, followed by the orthogonality (5.2.1) of the eigenvectors. (Recall $S \equiv S_{(r_{\mathrm{id}})}$.)

Two-point function

With more than one point, the regrouping of marked vertices in V into connected components in $(V \cup V^*, A \cup A^*)$ will induce a set partition of the marked vertices. Specifically, with $N = 2$ marked vertices, we shall denote by $\{12\}$ the situation in which the two marked vertices $i_1, i_2 \in V$ correspond to the same vertex of the tree T , and by $\{1\}\{2\}$ the situation in which they correspond to two distinct vertices. In either case, the corresponding labels of the eigenvectors are denoted r_1 and r_2.

We first treat the case of the partition $\{12\}$. We take the marked points to be at the root, a choice that we write for short as $\rho = \{12\}$. As before we get a factor $\lambda^{|\mathsf{V}|}$ from the summation over the leaves, while at the root we obtain

$$\sum_{\sigma_\rho} S^2_{\sigma_\rho} \phi_{r_1}(i_1)\phi_{r_2}(i_2) = \sum_{\sigma_\rho} S^{\sigma_\rho}_{(r_1)} S^{\sigma_\rho}_{(r_2)} = \delta_{r_1,r_2}\,. \tag{5.2.7}$$

In the case of the partition $\{1\}\{2\}$ we take $i_2 := \rho \in \mathsf{V}$ to be the root of T. The other marked point i_1 corresponds to a different vertex in V. Since T is a tree, there is a unique path P from i_1 to i_2. We denote by ℓ the number of edges in P. All the vertices not in P can be summed out using (5.2.4), giving rise to a total factor of $\lambda^{|\mathsf{V}|-|\mathsf{P}|}$. Once this has been done, we must sum over the vertices remaining in P. We start by summing over i_1. Let j denote its parent in T, of degree d_j. We get that (5.2.4) must be replaced by

$$\begin{aligned}
\sum_{\sigma_{i_1}} \mathscr{A}_{\sigma_j,\sigma_{i_1}} S_{\sigma_{i_1}} S^{2-\mathrm{d}_j}_{\sigma_j} \phi_{r_1}(i_1) &= \sum_{\sigma_1} \mathscr{A}_{\sigma_j,\sigma_1} S^{\sigma_1}_{(r_1)} S^{2-\mathrm{d}_j}_{\sigma_j} \\
&= \lambda_{(r_1)} \left(S^{\sigma_j}_{(r_1)} / S_{\sigma_j} \right) S^{2-(\mathrm{d}_j-1)}_{\sigma_j} \\
&= \lambda_{(r_1)} \phi_{r_1}(j) S^{2-(\mathrm{d}_j-1)}_{\sigma_j}\,.
\end{aligned} \tag{5.2.8}$$

This has the effect of producing a factor $\lambda_{(r_1)}$ corresponding to the summed-out vertex $i \in \mathsf{P}$, and moving the marked weight to the parent vertex j. Therefore the inductive argument can be continued until we have reduced P to the root vertex $\rho = i_2$, and summing over this provides the same factor (5.2.7) as before. In total we obtain

$$\lambda^{|\mathsf{V}|-\ell} \lambda^\ell_{(r_1)} \delta_{r_1,r_2}\,. \tag{5.2.9}$$

We could divide by the partition function Z to write the correlation function as

$$\left(\frac{\lambda_{(r_1)}}{\lambda} \right)^\ell \delta_{r_1,r_2}\,; \tag{5.2.10}$$

however, in what follows we prefer to keep the correlation functions un-normalised as in (5.2.9).

The result in (5.2.9) can be summarised by saying that any loop that separates the two marked vertices $i_1, i_2 \in V$ has its weight modified from λ to $\lambda_{(r_1)}$. In addition there is a factor δ_{r_1,r_2}, so it is equivalent to say that the weight is modified to $\lambda_{(r_2)}$. This equivalence agrees naturally with the possibility to turn a loop inside out on the Riemann sphere. We also notice that the case of the partition $\{12\}$ emerges as a particular case of the $\{1\}\{2\}$ computation; it suffices to set $\ell = 0$ in (5.2.9). This is a general observation that will carry over to appropriate N-point functions with $N > 2$.

Three-point functions

We begin by considering the case of the partition $\{123\}$. Take the root $\rho = \{123\}$. We get the factor $\lambda^{|V|}$ as usual, meaning the all loop weights are unchanged. At the root we obtain the factor

$$\sum_{\sigma_\rho} S^{\sigma_\rho}_{(r_1)} S^{\sigma_\rho}_{(r_2)} S^{\sigma_\rho}_{(r_3)} S^{-1}_{\sigma_\rho} =: C_{r_1,r_2,r_3} \,. \tag{5.2.11}$$

By definition the structure constant C_{r_1,r_2,r_3} is symmetric in all three indices. Note also that (5.2.11) correctly contains the two-point function as a special case, since

$$C_{r_1,r_2,r_{\mathrm{id}}} = \sum_{\sigma_\rho} S^{\sigma_\rho}_{(r_1)} S^{\sigma_\rho}_{(r_2)} = \delta_{r_1,r_2} \,, \tag{5.2.12}$$

where we have used (5.2.1).

Next consider the partition $\{12\}\{3\}$. The easiest way to compute this correlation function is to take $\rho = \{12\}$ and $i = \{3\}$. We strip off the leaves of T as usual, ending up with the path graph P with ℓ edges and extremities i and r. To perform the sum over σ_i, we can take over the inductive argument (5.2.8) from the computation of the two-point function to get a factor $\lambda^\ell_{(r_3)}$ by undoing P. Finally at the root we get C_{r_1,r_2,r_3} by the same calculation as above.

We can redo this computation the other way around by taking the root $\rho = \{3\}$ and $i = \{12\}$. We shall use the following lemma:

Lemma 5.2.1. *Let $\mathscr{A}$ be a real and symmetric matrix, $S_{(r)}$ (with $r = 1, 2, \ldots, \dim \mathscr{A}$) its normalized eigenvectors with corresponding eigenvalues $\lambda_{(r)}$, and S a distinguished eigenvector whose entries are all non-zero. For C_{r_1,r_2,r_3} as defined by* (5.2.11) *we have*

$$\sum_{\sigma_i} \mathscr{A}_{\sigma_j,\sigma_i} S^{\sigma_i}_{(r_1)} S^{\sigma_i}_{(r_2)} S^{-1}_{\sigma_i} = \sum_r \lambda_{(r)} C_{r_1,r_2,r} S^{\sigma_j}_{(r)} \,. \tag{5.2.13}$$

Proof. Since the eigenvectors $S_{(\tilde{r})}$ form a basis of $\mathbb{R}^{\dim \mathscr{A}}$, this identity can be proven by showing the the left-hand and right-hand sides have the same projections on each of these vectors. First consider the left-hand side:

$$\sum_{\sigma_j} S^{\sigma_j}_{(\tilde{r})} [\text{l.h.s.}] = \lambda_{(\tilde{r})} \sum_{\sigma_i} S^{\sigma_i}_{(\tilde{r})} S^{\sigma_i}_{(r_1)} S^{\sigma_i}_{(r_2)} S^{-1}_{\sigma_i} = \lambda_{(\tilde{r})} C_{r_1,r_2,\tilde{r}} \,, \tag{5.2.14}$$

where the first equality uses the symmetry of $\mathscr{A}$. Similarly, the projection of the right-hand side reads:

$$\sum_{\sigma_j} S^{\sigma_j}_{(\tilde{r})} [\text{r.h.s.}] = \sum_r \lambda_{(r)} C_{r_1,r_2,r} \sum_{\sigma_j} S^{\sigma_j}_{(r)} S^{\sigma_j}_{(\tilde{r})} = \sum_r \lambda_{(r)} C_{r_1,r_2,r} \delta_{r,\tilde{r}} = \lambda_{(\tilde{r})} C_{r_1,r_2,\tilde{r}} \,, \tag{5.2.15}$$

proving (5.2.13). □

Lemma 5.2.1 is exactly what is needed in the inductive proof in order to replace the marking $\{12\}$ from vertex i by a marking (r) of the parent vertex j. At the same time we obtain a sum over all r, a structure constant $C_{r_1,r_2,r}$, and a factor $\lambda_{(r)}$. This can be physically interpreted as the fusion of the two states $S_{(r_1)}$ and $S_{(r_2)}$ into the superposition of all intermediate channels $S_{(r)}$, as will be discussed further in Section 5.2.2.

Undoing successive vertices of P we get more factors of $\lambda_{(r)}$, and at the root we end up with

$$\sum_r \lambda^{\ell}_{(r)} C_{r_1,r_2,r} \sum_{\sigma_\rho} S^{\sigma_\rho}_{(r)} S^{\sigma_\rho}_{(r_3)} = \sum_r \lambda^{\ell}_{(r)} C_{r_1,r_2,r} \delta_{r,r_3} = \lambda^{\ell}_{(r_3)} C_{r_1,r_2,r_3} \,, \tag{5.2.16}$$

which is the same result as obtained by the first, easy computation. We shall need Lemma 5.2.1 further below.

We finally consider the partition $\{1\}\{2\}\{3\}$. The three marked points can be positioned in various ways on the tree T. Once all unmarked leaves have been undone (giving rise to factors of λ), all arrangements are special cases of the situation where T has been reduced to a three-star graph $\mathsf{S}_{\ell_1,\ell_2,\ell_3}$

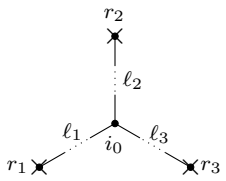

(5.2.17)

with marked points $\{1\}$, $\{2\}$ and $\{3\}$ positioned at each extremity of the branches which have respective lengths ℓ_1, ℓ_2 and ℓ_3 as indicated in (5.2.17). The three branches meat at a central vertex i_0 that we take as the root, $\rho := i_0$. In this configuration, it is simple to undo the branches, giving rise to a factor $\lambda^{\ell_1}_{(r_1)}\lambda^{\ell_2}_{(r_2)}\lambda^{\ell_3}_{(r_3)}$. At the end, we sum over the root, which reduces to the computation (5.2.11) done for the $\{123\}$ partition, and leads to a contribution C_{r_1,r_2,r_3}.

We see that all cases of three-point functions are special cases of the $\mathsf{S}_{\ell_1,\ell_2,\ell_3}$ arrangement, provided we allow some or all of the branch lengths to be zero. The general result for the three-point function can be summarised as

$$\lambda^{\ell_1}_{(r_1)}\lambda^{\ell_2}_{(r_2)}\lambda^{\ell_3}_{(r_3)} C_{r_1,r_2,r_3} \,. \tag{5.2.18}$$

In other words, apart from the structure constant, there is a factor $\lambda_{(r_j)}$ for each loop that separates point $j \in \{1,2,3\}$ from the other two points. Each loop that surrounds none or all of the points meanwhile gets the usual weight λ. This is very similar to the setup in [102] for the non-unitary loop model with generic loop weights. We note once again that for any given loop on the Riemann sphere, we may freely choose which of the two regions separated by the loop to consider as the inside.

5.2.2 Higher N-point functions and Feynman rules for the trees

To consider general N-point functions it is convenient to shift perspective, making links with the formulation in [30] in terms of "Feynman rules" for the relevant trees. To obtain these rules, consider weight of a single cluster in the cluster expansion of the partition function. One important feature of the arguments below can be summarized as follows: As seen in (2.3.6), any cluster $\mathscr{C}$ comes with a weight that depends on its cyclomatic number $c(\mathscr{C})$ as $W_{\mathscr{C}} = S^{1-c(\mathscr{C})}$. An n-vertex—i.e., a vertex $i \in \mathsf{T}$ with $\mathrm{d}_i = n$—corresponds to a cluster that is adjacent to n other clusters: the cluster surrounding it and $c(\mathscr{C}) = n-1$ cycles on the interior. We shall call the latter circuits in the following. When considering the tree corresponding to a given cluster configuration, we can decompose an n-vertex ($n > 3$) into $S^{2-n} = S^{-1} \times S^{-1} \times ... \times S^{-1}$, where each of the $(n-2)$ factor S^{-1} corresponds to a 3-vertex. We will represent this decomposition with "identity loops", as shown below. Such loops are also used to handle other situations, such as when several marked points are in the same cluster. After taking care of these details, any tree for any value of N will be computed from the Feynman rules stated in List 1, which

generalize those in Figure 5 of [30] to the case with marked points where order parameters $S_{(r)}/S$ are inserted.

Position space:

- each edge corresponds to a propagator $\mathscr{A}_{\sigma,\sigma'}$
- each 1-vertex (leaf) gives
  1. $S^{\sigma}_{(r_{\rm id})}$ if it has no marked points
  2. $S^{\sigma}_{(r)}$ if it has one marked point corresponding to the state $S_{(r)}$
  3. if there are several marked points we first fuse the states
- each 2-vertex gives 1
- each 3-vertex gives S_σ^{-1}
- we sum over any internal lines
- any marked point that is not on a leaf will get fused into the tree

Momentum space:

- each edge carries a label r' and corresponds to a propagator $\lambda_{(r')}$
- each 1-vertex (leaf) gives
  1. $\delta_{r',r_{\rm id}}$ if it has no marked points
  2. $\delta_{r',r}$ if it has one marked point corresponding to the state $S_{(r)}$
  3. if there are several marked points we first fuse the states
- each 2-vertex gives $\delta_{r,r'}$
- each 3-vertex gives C_{r_1,r_2,r_3}
- we sum over any internal lines
- any marked point that is not on a leaf will get fused into the tree

List 1: Feynman rules for RSOS models

Fusion of states

Consider a cluster configuration on a sphere where we take N marked vertices, some of these possibly belonging to the same cluster. We first establish a convenient pictorial reformulation of some results already seen in the sections above. We have seen that (5.2.8) lets us recursively sum out clusters, starting at the leaves and gaining a factor $\lambda_{(r)}$ any time we cross a loop. We repeat this equation here for convenience:

$$\sum_{\sigma'} \mathscr{A}_{\sigma,\sigma'} S^{\sigma'}_{(r)} S_\sigma^{2-\mathrm{d}} = \lambda_{(r)} \left(S^{\sigma}_{(r)}/S_\sigma \right) S_\sigma^{2-(\mathrm{d}-1)} . \tag{5.2.19}$$

Within any given cluster of $1-\tilde{c}$ circuits, that includes any number m of marked points, we can use the similar looking but trivial identity

$$\sum_{\sigma'} \delta_{\sigma,\sigma'} \prod_{i=1}^{k} \left(S^{\sigma'}_{(r_i)}/S_{\sigma'} \right) S_{\sigma'}^{c_1} \prod_{j=k+1}^{m} \left(S^{\sigma}_{(r_j)}/S_{\sigma} \right) S_{\sigma}^{c_2} = \prod_{i=1}^{m} \left(S^{\sigma}_{(r_k)}/S_{\sigma} \right) S_\sigma^{\tilde{c}} \tag{5.2.20}$$

to formally split this cluster into two, one inside the other, such that $c_1 + c_2 = \tilde{c}$. Comparing the two expressions above, we represent the latter pictorially as inserting an "identity loop" where instead of a factor $\mathscr{A}_{\sigma,\sigma'}$ at the boundary, we have a factor $\delta_{\sigma,\sigma'}$, and where we do not get a weight $\lambda_{(r)}$ when removing the loop. We draw this identity loop as a dashed line, as in the following example of a leaf with one marked point $\times$:

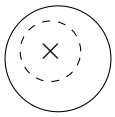

(5.2.21)

Now insert such loops around two marked points sitting in the same cluster with respective RSOS variables $\sigma', \sigma'' \in X$:

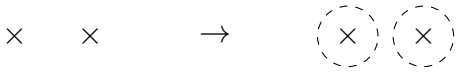

(5.2.22)

If we consider the *surrounding* cluster, it contributes a weight of $S_\sigma^{1-c} = S_\sigma^{-1}$ due to its two circuits, while the two identity loops will insert a factor of $\delta_{\sigma,\sigma'}\delta_{\sigma,\sigma''}$. With some rewriting of (5.2.11) using (5.2.2) this gives

$$\delta_{\sigma,\sigma'}\delta_{\sigma,\sigma''}S_\sigma^{-1} = \sum_r \sum_{r'} \sum_{r''} C_{r,r',r''} S^\sigma_{(r)} S^{\sigma'}_{(r')} S^{\sigma''}_{(r'')}. \tag{5.2.23}$$

We can now express the fusion of the two states $S_{(r_1)}$ and $S_{(r_2)}$, by which we mean that each of the marked points in (5.2.22) carries an additional factor $S^{\sigma'}_{(r_1)}$ or $S^{\sigma''}_{(r_2)}$, respectively. Using now (5.2.1), this simplifies as

$$\sum_{\sigma'} \sum_{\sigma''} \sum_r \sum_{r'} \sum_{r''} C_{r,r',r''} S^\sigma_{(r)} S^{\sigma'}_{(r')} S^{\sigma''}_{(r'')} S^{\sigma'}_{(r_1)} S^{\sigma''}_{(r_2)} = \sum_r C_{r,r_1,r_2} S^\sigma_{(r)}. \tag{5.2.24}$$

That is: any time we have two marked points of labels r_1, r_2 within the same cluster, we can replace them by a sum over the possible fusion products. To recover the 3-point function discussed above we introduce a third marked vertex, with a corresponding $\sum_\sigma S^\sigma_{(r_3)}$, which will take care of the last sum and single out C_{r_1,r_2,r_3} as the only surviving term. With only two marked vertices, we must use $C_{r_1,r_2,r_{\rm id}} = \delta_{r_1,r_2}$, as in (5.2.12). We then recover the 2-point function. Similarly if two of the vertices are unmarked we use $C_{r_1,r_{\rm id},r_{\rm id}} = \delta_{r_1,r_{\rm id}}$ to recover the 1-point function.

When we encounter a marked point that is not on a leaf, we can use an identity loop to treat if as if it were, constructing a 3-vertex and fusing it into the tree. We have seen a similar idea already in the general three-point result of (5.2.18), where we could allow branch lengths to be zero. We note that fusing any state $S_{(r)}$ with the identity state $S_{(r_{\rm id})}$ will give back $S_{(r)}$ as the only output. Here is a sample Figure (with the loop weights indicated on the r.h.s.):

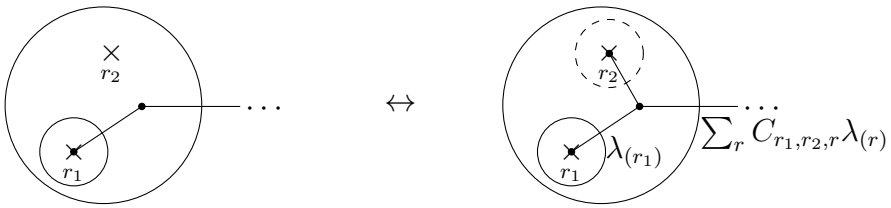

(5.2.25)

n-vertices, $n > 3$

An n-vertex corresponds to a cluster with $n-1$ circuits, giving a weight $S_\sigma^{1-c} = S_\sigma^{2-n}$ in position space. With the results established above, the aforementioned idea of factorising vertices as $S^{2-n} = S^{-1} \times S^{-1} \times ... \times S^{-1}$ is made rigorous. Consider for instance $n = 4$, as in e.g.:

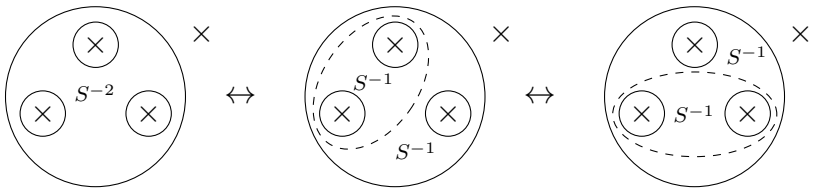

(5.2.26)

In terms of trees, the above figures correspond to:

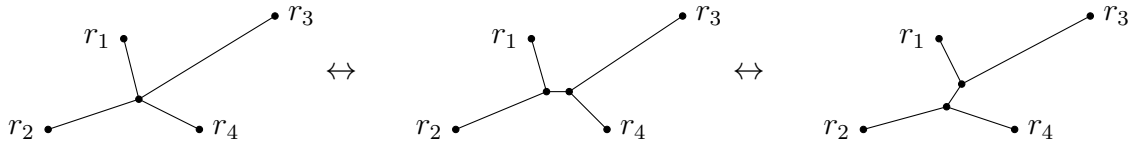

(5.2.27)

In the two trees on the right, (5.2.24) applies at the new 3-vertices such that we have one sum $\sum_r$ along the internal line, which we can interpret as an s/t-channel. The result must be the same, showing the notion of crossing symmetry mentioned in [30].

It is clear that we can follow the same scheme for any vertex with $n > 3$, as well as for any case of several marked points sitting in the same cluster. Any states $S_{(r)}$ that are "close" (by which we that they would sit in the same cluster after taking away any loop surrounding only one state) can be fused with each other, and crossing symmetry makes the result independent of in which order we perform the fusion. Having established this final result, we see that we can write all N-point functions in terms of the Feynman rules stated before.

Expressions for the N-point functions

For the 4-point function, we can consider a H-shaped tree $\mathsf{H}_{\ell_1,\ell_2;\ell;\ell_3,\ell_4}$

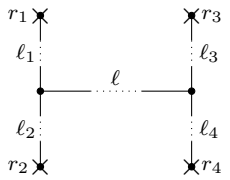

(5.2.28)

where upper left, lower left, upper right and lower right vertical branches have respective lengths $\ell_1, \ell_2, \ell_3, \ell_4$, while the connecting horizontal branch has length ℓ. Up to factors of $\lambda_{(r_{\mathrm{id}})}$ from summing out the loops not separating the marked points, we get the weight

$$\left(\prod_{j=1}^{4} \lambda_{(r_j)}^{\ell_j}\right) C^{(\ell)}_{r_1,r_2,r_3,r_4} \,, \tag{5.2.29}$$

with

$$C^{(\ell)}_{r_1,r_2,r_3,r_4} := \sum_r C_{r_1,r_2,r} \lambda_{(r)}^{\ell} C_{r,r_3,r_4} \,. \tag{5.2.30}$$

That is, each loop separating one of the points points $j \in \{1,2,3,4\}$ from the other three points provides a factor $\lambda_{(r_j)}$, whereas the ℓ loops that separate the fused group $\{12\}$ from the other block $\{34\}$ of the set partition provide a total contribution of $C^{(\ell)}_{r_1,r_2,r_3,r_4}$. Allowing for some of the ℓ_j and/or ℓ to be zero, any other type of tree contributing to the 4-point function leads to a special case of this result. Taking the positions of the marked points into account we note that there are three possible configurations when all $\ell, \ell_j > 0$: the s, t and u-channel trees.[2] The diagram in (5.2.28) illustrates the s-channel.

When $\ell = 0$, the s, t and u-channels coincide. We therefore have

$$\sum_r C_{r_1,r_2,r} C_{r,r_3,r_4} = \sum_r C_{r_1,r_3,r} C_{r,r_2,r_4} = \sum_r C_{r_1,r_4,r} C_{r,r_2,r_3} \,, \tag{5.2.31}$$

[2]If we consider $\ell = 0$ to be a separate case, we can compare the resulting four types of trees to the four diagrams in Figure 4.4.

a statement referred to as crossing symmetry in [30]. An equivalent statement is that $C^{(0)}_{r_1,r_2,r_3,r_4}$, defined by (5.2.30), is symmetric in all its four indices.

Let us briefly remark on higher-point correlation functions. For the 5-point function, we can consider a tree

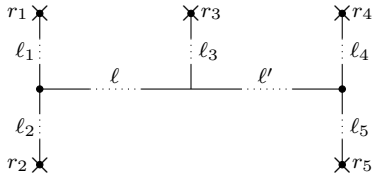

(5.2.32)

Let ℓ, ℓ' be the lengths of the horizontal branches, and let $\ell_j,\ j = 1, \ldots, 5$ be the lengths of the vertical branches, as shown. Up to factors of $\lambda_{(r_{\rm id})}$ from summing out the loops not separating the marked points, we get the weight

$$\left(\prod_{j=1}^{5} \lambda^{\ell_j}_{(r_j)}\right) C^{(\ell,\ell')}_{r_1,r_2,r_3,r_4,r_5}\,, \tag{5.2.33}$$

with

$$C^{(\ell,\ell')}_{r_1,r_2,r_3,r_4,r_5} := \sum_{r,r'} C_{r_1,r_2,r} \lambda^{\ell}_{(r)} C_{r,r_3,r'} \lambda^{\ell'}_{(r')} C_{r',r_4,r_5}\,. \tag{5.2.34}$$

As in the cases of $N \leq 4$ we recover all possible shapes of trees when we allow some or all of ℓ, ℓ', ℓ_j to be zero. Taking the positions of the marked points into account we need to consider 4×3 possible configurations; starting from any of the three 4-point trees (s, t or u-channel), we can let any of the four branches $j = 1, \ldots, 4$ split into two branches j and 5.

The recursive method of finding all N-trees by splitting branches of the $(N-1)$-trees extends to $N > 5$. As before we consider trees with 3-vertices only, seeing the other trees as special cases with some branch lengths set to zero. It is important to keep in mind that different trees with the same number of internal lines may be non-isomorphic, for instance at $N = 6$:

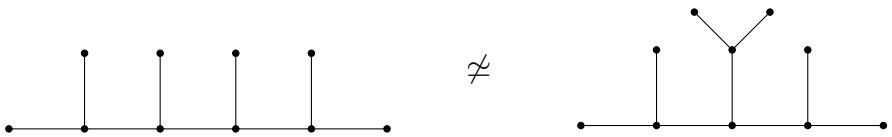

(5.2.35)

For any given tree, the corresponding weight will follow the general pattern seen in (5.2.9), (5.2.18), (5.2.29), (5.2.33), encoded in the Feynman rules of List 1.

5.3 A_n RSOS models and $su(2)_k$ anyons

Having carefully established the rules for evaluating the RSOS partition function (in Section 2.3) and n-point functions (in the section above), we now make the link to the $su(2)_k$ anyonic fusion diagrams introduced in the beginning of this chapter. We focus on the unitary theories. Non-unitary theories are obtained through the process of Galois conjugation, in which another column of S takes the place of the Perron-Frobenius vector in such a way that the fusion matrices as computed via the Verlinde formula (5.1.10) still have positive integer elements. In practice this generally involves not only moving the new column to the left, but also rearranging the other columns and multiplying some by a sign – none of which changes the RSOS interpretation of S as a matrix of eigenvectors of $\mathscr{A}$. As an example, non-unitary Yang-Lee anyons are obtained from unitary Fibonacci anyons through Galois conjugation [100].

The eigenvectors for the adjacency matrix $\mathscr{A}$ of the A_n Dynkin diagram are given by

$$S^{\sigma}_{(r)} = \sqrt{\frac{2}{n+1}} \sin\left(\frac{\pi r \sigma}{n+1}\right) . \tag{5.3.1}$$

Comparing notation, we see that when taking $k = n-1$ and $r, \sigma = 2j+1$, these eigenvectors form the modular S-matrix (5.1.7), and the expression for the structure constants $C_{r,r',r''}$ (5.2.11) is nothing but the Verlinde formula for the fusion matrices $N^{j''}_{j,j'}$. The weight of contractible loops is given by the quantum dimension of the generating anyon, $d_{1/2}$. For non-contractible loops due to the insertion of order operators, the loop weight is given by replacing the eigenvalue λ of $\mathscr{A}$ with the eigenvalue $\lambda_{(r)}$, which is nothing else than the factor obtained by removing a loop of the generating anyon $j = \frac{1}{2}$ that encircles a line carrying $j_r = (r-1)/2$. Labelling the anyons by the corresponding heights and considering the unitary theory, we have

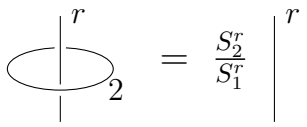

(5.3.2)

with

$$\frac{S^r_2}{S^r_1} = \frac{\sin(2r\pi/(n+1))}{\sin(r\pi/(n+1))} = 2\cos\left(\frac{r\pi}{n+1}\right) = \lambda_{(r)}. \tag{5.3.3}$$

The correspondence is thus as follows. The partition function is computed by considering fusion diagrams that are made up of loops of the generating anyon $j = \frac{1}{2}$, which has $d_j = \lambda$, that densely cover the lattice. N-point functions of order operators $\phi_{r_1}(i_i), \phi_{r_2}(i_2), ...$ are obtained by inserting the corresponding anyons $j_1, j_2, ...$ at the same positions, and fusing them "above" the loops, as in the following example with three order operator insertions:

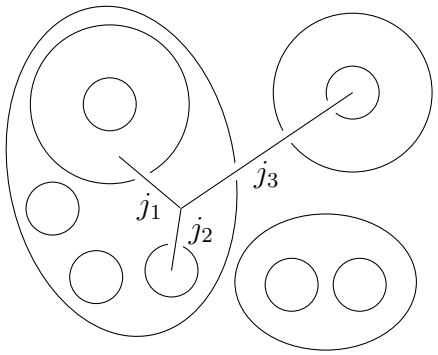

(5.3.4)

As just seen, having these anyons passing through modifies the weight of the surrounding loops precisely as required by the rules listed in List 1, and the structure constants ensure the proper fusion vertices. (For a more direct comparison with Diagram (5.3.2), consider the lines carrying j_1, j_2, j_3 continuing outwards below the loops.) Any internal lines are summed over.

In the language of $su(2)_k$ anyons, the expectation values of A_n RSOS order parameters correspond to anyon condensate fractions, as described in [103].

5.4 Anyon chains – the anisotropic limit of RSOS models

Similar to how the six-vertex model in the anisotropic limit gives rise to the Heisenberg XXZ spin chain, the A_n RSOS model in the anisotropic limit gives rise to an $SU(2)_k$ anyon chain.

In fact, taking $k \to \infty$ we do recover precisely the $SU(2)$ spin-1/2 chain (the XXX spin chain), and we have seen in Chapter 2 that the six-vertex model can be mapped to a height model without restrictions on the height ($n \to \infty$).

We first show that the Hilbert spaces are equivalent, before considering the Hamiltonian. Consider the periodic RSOS model on a square lattice tilted by 45°. A state is a row with a configuration of integer heights between 1 and n such that $|\sigma_i - \sigma_{i+1}| = 1$, where we impose $\sigma_0 = \sigma_{N+1}$:

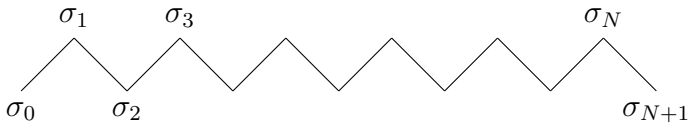

. (5.4.1)

This is equivalent to an $N+1$-step walk on the A_n Dynkin diagram

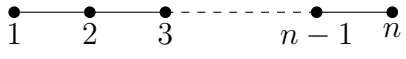

(5.4.2)

that returns to its origin.

Consider now an anyon chain in which we repeatedly fuse in the generating anyon $j = \frac{1}{2}$ and impose $j_0 = j_{N+1}$, obtaining the fusion diagram

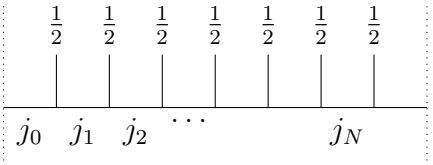

. (5.4.3)

The dotted lines represent the periodic boundary conditions. The Hilbert space consists of all such states, which are denoted by $|j_0, j_1, ..., j_N\rangle$.

We can map the internal labels to heights $\sigma_i = 2j_i + 1$ to obtain a height state $|\sigma_0, \sigma_1, ..., \sigma_N\rangle$, and we see that the fusion rules (5.1.1) enforce the condition that neighbouring heights vary by one.

The Hamiltonian will follow from the logarithmic derivative of the transfer matrix, and will as usual be built out of Temperley-Lieb generators e_i. Considering that the quantum dimension of the generating anyon is precisely the weight of contractible loops in the RSOS model, it is natural to interpret e_i diagrammatically as

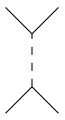

(5.4.4)

where the dashed line has label 0 and the solid lines have label $\frac{1}{2}$. We can interpret this diagram as the annihilation and creation of a pair of generating anyons. We then immediately recover the relation $e_i^2 = d_{1/2} e_i$ by stacking one diagram on top of the other and removing the resulting loop, while the relation $e_i e_{i\pm1} e_i = e_i$ follows by "straightening the line":

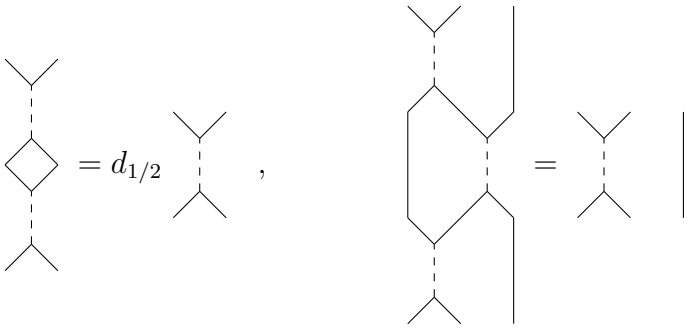

(5.4.5)

Note that when straightening the line we employ the "zig-zag"-identity twice, so that even with a Frobenius-Schur indicator of -1 the final result acquires no sign.

In the basis of states $|j_0, j_1, ..., j_N\rangle$ the matrix element of this Hamiltonian density is [104]

$$\langle ...j'_{i-1}j'_ij'_{i+1}...|e_i|...j_{i-1}j_ij_{i+1}...\rangle = ...\delta_{j'_{i-1},j_{i-1}} \left(\delta_{j_{i-1},j_{i+1}} \frac{\left(S^0_{j_i}S^0_{j'_i}\right)^{1/2}}{S^0_{j_{i-1}}} \right) \delta_{j'_{i+1},j_{i+1}}... \tag{5.4.6}$$

Translated to heights, this yields precisely the RSOS representation of the Temperley-Lieb generators as given in (4.2.4).

5.5 Connection to topological defects

Consider the computation of n-point functions, interpreted as the evaluation of fusion diagrams in which additional anyons are braided across the diagram. We restrict our attention to the 2-point function, and draw the anyon j across the anyon chain:

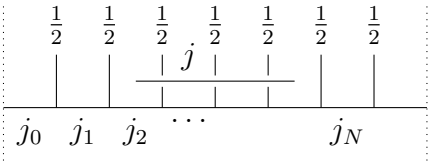

. (5.5.1)

Now, let j cross not only a part of the anyon chain, but form a loop around the entire chain:

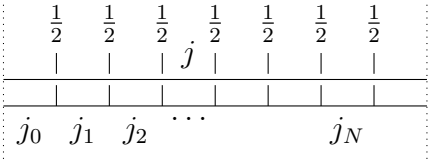

. (5.5.2)

Considered as an operator acting on the chain, this loop is called a *hoop operator* and is denoted Y_j [105]. A second hoop operator is constructed by considering a loop on the inside of the chain,

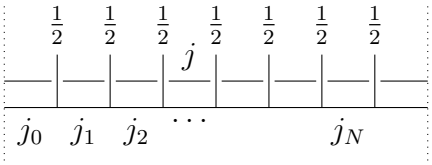

. (5.5.3)

It is denoted $\bar{Y}_j$.

Take the encircling anyon to be the generating anyon $j = \frac{1}{2}$. In the language of Temperley-Lieb generators, the hoop operators can then be written in terms of the braid generators

$$\begin{aligned} g_i &= (-\mathfrak{q})^{1/2}\mathbf{1} + (-\mathfrak{q})^{-1/2}e_i \;=\; \\ g_i^{-1} &= (-\mathfrak{q})^{-1/2}\mathbf{1} + (-\mathfrak{q})^{1/2}e_i \;=\; \end{aligned} \tag{5.5.4}$$

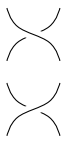

as

$$\begin{aligned} Y_{1/2} &= -i\mathfrak{q}^{-1/2}g_1^{-1}...g_{N-1}^{-1}u^{-1} + i\mathfrak{q}^{1/2}ug_{N-1}...g_1\,, \\ \bar{Y}_{1/2} &= -i\mathfrak{q}^{-1/2}ug_{N-1}^{-1}...g_1^{-1} + i\mathfrak{q}^{1/2}g_1...g_{N-1}u^{-1}\,. \end{aligned} \tag{5.5.5}$$

Hoop operators with $j > 1/2$ are obtained from $Y_{1/2}, \bar{Y}_{1/2}$ through fusion. $Y_{1/2}$ and $\bar{Y}_{1/2}$ generate the center of the affine Temperley-Lieb algebra, which thus contains all hoop operators [105].In particular, all hoop operators commute with the Koo-Saleur generators. In the continuum limit this implies that $Y_j, \bar{Y}_j$ can be freely moved across the stress-energy tensor, earning them the name *topological defects* or *purely-transmissive defects*. More specifically, they describe topological defects of type $(1, s)$, with $Y_{1/2}, \bar{Y}_{1/2}$ describing type $(1, 2)$; a lattice expression for defects of type $(r, 1)$ has also recently been proposed [106].

Topological defects are interesting objects that have long been studied. As they follow the same fusion rules as anyons, they make a connection between 1+1D CFTs and 2+1D topological quantum field theories. The latter describe a novel kind of order occurring in two-dimensional quantum matter. Topological defects often come in conjunction with zero-energy modes, which lead to a deviation from the usual logarithmic scaling of entanglement entropy characteristic of conformal field theories [107, 108].

CHAPTER

6

VIRASORO REPRESENTATIONS IN THE SIX-VERTEX MODEL

In this chapter we consider the anisotropic limit of the six-vertex model – the XXZ spin chain – for generic values of $\mathfrak{q}$ (not a root of unity). The purpose of this chapter is twofold. The first is to revisit the construction of Koo-Saleur generators in [12] by carrying out much more sophisticated numerics than was possible at the time. This involves in particular the techniques of *lattice form factors*, thanks to which matrix elements of the discrete Virasoro generators can be expressed in closed form using Bethe-ansatz roots. By contrast, in [12], only eigenstates were obtained with the Bethe ansatz, while matrix elements were calculated by brute-force numerics. The quantitative improvement is substantial. While in [12] only chains up to length ten or so were studied, we are here easily able to tackle lengths up to 80 on a standard laptop. Our results fully confirm the validity of the proposal in [12], and shed some extra light on the nature of the scaling limit, and the convergence of the lattice Virasoro algebra to $\mathrm{Vir} \otimes \overline{\mathrm{Vir}}$.

The second purpose of this chapter is to find out specifically what kind of Virasoro modules occur in the XXZ chain when the Virasoro representations are degenerate—that is, (some) fields belong to the extended Kac table. We will do this straightforwardly, by exploring the action of the lattice Virasoro generators, and checking directly whether the relevant combinations vanish or not—in technical parlance, whether "null states" or "singular vectors" are zero indeed. This is of course of utmost importance in practice, as this criterion determines the applicability of the BPZ formalism [5] to the determination of correlation functions, such as the four-point functions currently under investigation (Chapter 4, [20, 21]). We shall find some unexpected results, that we hope to complete in a future paper [59] by studying the cases when the central charge is rational (e.g., the case $c = 0$ with applications to percolation).

A similar investigation in the cognate link-pattern representation of the XXZ chain (relevant for the corresponding loop model) will appear in Chapter 7. We will remark on the important differences between the two representations throughout the present chapter.

The chapter is organized as follows. In Section 6.1 we recall the Hamiltonian of the XXZ spin chain and discuss expected features of the continuum limit, based in part on the Dotsenko-

Fateev or Feigin-Fuchs free-boson construction. We also discuss partly the issue of scalar products—with more remarks on this topic being given in Appendix B. In Section 6.2 we recall several aspects of the Bethe-ansatz solution of the XXZ chain, in particular those concerning the form-factor calculations and the definition of scaling states. Relations between the form factors show that duality relations between certain expected continuum modules are already present at finite size. In Section 6.3 we discuss the continuum limit of the Koo-Saleur generators in the *non-degenerate case*, where none of the conjectured conformal weights belong to the extended Kac table. Following this, Section 6.4 discusses their continuum limit in the *degenerate cases* where the conjectured conformal weights take on values in the extended Kac table. Finally, Section 6.5 discusses the nature of the convergence of the Koo-Saleur generators to their Virasoro-algebra continuum limit.

Several technical aspects are addressed in the appendices. In Appendix B we briefly remind the reader of the physical meaning of the "conformal scalar product" for which $L_n^\ddagger = L_{-n}$ (we reserve the notation † for another scalar product). In Appendix C we discuss the form factors for the Koo-Saleur generators. In Appendix D more details about numerical results for the action of the Koo-Saleur generators are provided. A proof of (6.5.21), an expression involving the ground-state expectation of two neighbouring Temperley-Lieb generators that we initially conjectured based on our numerical results, is provided in Appendix E. In Appendix F we discuss in further detail the continuum limit of commutators of Koo-Saleur generators. Finally, details about a particular commutation relation—which we call the chiral-antichiral commutator—are given in Appendix G.

Main results: Our main results for relations between form factors and lattice duality are given in equations (6.2.9) and (6.2.20). Our main results for the nature of the modules arising in the continuum limit are given in equations (6.4.4) and (6.4.7). Our main results for the nature of the convergence of the Koo-Saleur generators are given in (6.5.12), (6.5.21),(6.5.22) and (6.5.23).

6.1 Some features of the continuum limit

We recall the Temperley-Lieb Hamiltonian (3.2.2)

$$\mathscr{H} = -\frac{\gamma}{\pi \sin\gamma} \sum_{j=1}^{N} (e_j - e_\infty), \tag{6.1.1}$$

which in the XXZ spin chain representation takes the familiar form of (2.1.8), repeated here for convenience:

$$\mathscr{H} = \frac{\gamma}{2\pi \sin\gamma} \sum_{j=1}^{N} \left[\sigma_j^x \sigma_{j+1}^x + \sigma_j^y \sigma_{j+1}^y + \Delta(\sigma_j^z \sigma_{j+1}^z - 1) + 2e_\infty\right] . \tag{6.1.2}$$

In the generic case where $\mathfrak{q}$ is not a root of unity, the relevant Temperley-Lieb modules will be irreducible standard modules $\mathscr{W}_{j,1}$ and indecomposable standard and co-standard modules on the form seen in (3.3.6), repeated here for convenience:

$$\mathscr{W}_{0,\mathfrak{q}^{-2}}: \begin{array}{c} [0,\mathfrak{q}^{-2}] \\ \downarrow \\ [1,1] \end{array} , \qquad \mathscr{W}_{0,\mathfrak{q}^{2}}: \begin{array}{c} [0,\mathfrak{q}^{2}] \\ \uparrow \\ [1,1] \end{array} . \tag{6.1.3}$$

For a standard module $\mathscr{W}_{j,e^{i\phi}}$, whenever ϕ is such that the resonance criterion (3.1.4) is not met we say that ϕ is *generic*; and when (3.1.4) is satisfied ϕ is referred to as *non-generic*.

6.1.1 Modules in the continuum

Choosing $S_z = j$ the XXZ representation for generic $\mathfrak{q}$ and ϕ provides a faithful representation of the modules $\mathscr{W}_{j,e^{i\phi}}$. The Hamiltonian acting on this module has a CFT low-energy spectrum, encoding conformal weights $h, \bar{h}$. These weights are known from a variety of techniques like the Bethe-ansatz or Coulomb-gas mappings, combined with extensive numerical studies [62, 109]. It is convenient to encode their values by using the trace

$$\operatorname{Tr} e^{-\beta_R \mathscr{H}} e^{-i\beta_I \mathscr{P}}\,, \tag{6.1.4}$$

where β_R and β_I are real, and $\beta_R > 0$. Introducing the (modular) parameters

$$q = \exp\left[-\frac{2\pi}{N}(\beta_R + i\beta_I)\right], \tag{6.1.5a}$$

$$\bar{q} = \exp\left[-\frac{2\pi}{N}(\beta_R - i\beta_I)\right] \tag{6.1.5b}$$

and recalling the Kac-table parametrization of conformal weights

$$h_{r,s} = \frac{[(x+1)r - xs]^2 - 1}{4x(x+1)} \tag{6.1.6}$$

we have, in the limit where $N \to \infty$, with $\beta_R, \beta_I \to \infty$ so that q and $\bar{q}$ remain finite,

$$\operatorname{Tr}_{\mathscr{W}_{j,e^{i\phi}}} e^{-\beta_R \mathscr{H}} e^{-i\beta_I \mathscr{P}} \xrightarrow{N\to\infty} F_{j,e^{i\phi}}\,, \tag{6.1.7}$$

where [58]

$$F_{j,e^{i\phi}} = \frac{q^{-c/24}\bar{q}^{-c/24}}{P(q)P(\bar{q})} \sum_{e\in\mathbb{Z}} q^{h_{(e-e_\phi),-j}} \bar{q}^{h_{(e-e_\phi),j}} \tag{6.1.8}$$

and

$$P(q) = \prod_{n=1}^{\infty}(1-q^n) = q^{-1/24}\eta(q)\,, \tag{6.1.9}$$

where $\eta(q)$ is the Dedekind eta function and $e_\phi = \phi/2\pi$.

Since $\mathfrak{q}$ is generic throughout, both c and its parametrization x from (3.5.4) takes generic, irrational values. The conformal weights may be degenerate or not, depending on the lattice parameters. In the non-degenerate case, which corresponds to generic lattice parameters (the opposite does not always hold) it is natural to expect that the Temperley-Lieb module decomposes accordingly into a direct sum of Verma modules,

$$\mathscr{W}_{j,e^{i\phi}} \mapsto \bigoplus_{e\in\mathbb{Z}} \mathsf{V}_{e-e_\phi,-j} \otimes \mathsf{V}_{e-e_\phi,j}\,. \tag{6.1.10}$$

The symbol $\mapsto$ means that the action of the lattice Virasoro generators *restricted to scaling states* on $\mathscr{W}_{j,e^{i\phi}}$ corresponds to the decomposition on the right-hand side when $N \to \infty$. We will try to make this more precise below. Note that to make notation lighter, we are not indicating explicitly that in $\mathsf{V}\otimes\mathsf{V}$ the right tensorand is for the $\overline{\text{Vir}}$ algebra: this should always be obvious from the context.

Recall that a Verma module is a highest-weight representation of the Virasoro algebra (1.0.1) generated by a highest-weight vector $|h\rangle$ satisfying $L_n|h\rangle = 0, n > 0$, and for which all the descendants

$$L_{-n_1}\ldots L_{-n_k}|h\rangle\,,\ \text{with } 0 < n_1 \le n_2 \le \cdots \le n_k \text{ and } k > 0 \tag{6.1.11}$$

are considered as independent, subject only to the commutation relations (1.0.1). In the non-degenerate case where the Verma module is irreducible, it is the only kind of module that can occur, motivating the identification in (6.1.10).

Meanwhile, in the degenerate cases the conformal weights may take degenerate values $h = h_{r,s}$ with $r, s \in \mathbb{N}^*$, in which case a singular vector appears in the Verma module. By definition, a singular vector is a vector that is both a descendent and a highest-weight state. For instance, starting with $|h_{1,1} = 0\rangle$ we see, by using the commutation relations (1.0.1), that

$$L_1(L_{-1}|h_{1,1}\rangle) = 2L_0|h_{1,1}\rangle = 0\,, \tag{6.1.12}$$

while of course $L_n|h = h_{1,1}\rangle = 0$ for $n > 1$. Hence $L_{-1}|h = h_{1,1}\rangle$ is a singular vector. The action of the Virasoro algebra on this vector generates a sub-module. For $\mathfrak{q}$ generic, this sub-module is irreducible, and thus we have the decomposition

$$\mathsf{V}^{(\mathrm{d})}_{1,1}: \quad \begin{array}{c} \mathsf{X}_{1,1} \\ \circ \\ \downarrow \\ \bullet \\ \mathsf{V}_{1,-1} \end{array}\,, \tag{6.1.13}$$

where we recall the notation $\mathsf{V}^{(\mathrm{d})}$ to denote the degenerate Verma module, and we denote by $\mathsf{X}_{r,s}$ the irreducible Virasoro module (in this case, technically a "Kac module"), with generating function of levels

$$K_{r,s} = q^{h_{rs}-c/24}\,\frac{1-q^{rs}}{P(q)}\,. \tag{6.1.14}$$

The subtraction of the singular vector at level rs gives rise to a quotient module, and corresponds to the use of an open circle in the diagram (6.1.13).

We stress that in cases of degenerate conformal weights there is more than one possible module that could appear, and the identification in (6.1.10) may no longer hold. Furthermore the identification is different in the XXZ spin-chain representation of the Temperley-Lieb generators, as compared to the loop-model representation, since these are no longer isomorphic. In later sections we will discuss which identifications hold for the XXZ spin chain representation. For this purpose we recall the notation $\widetilde{\mathsf{V}}^{(\mathrm{d})}_{r,s}$ for the dual of the (degenerate) Verma modules, or "co-Verma" modules. As an example, the dual of (6.1.13) is

$$\widetilde{\mathsf{V}}^{(\mathrm{d})}_{1,1}: \quad \begin{array}{c} \mathsf{X}_{1,1} \\ \bullet \\ \uparrow \\ \circ \\ \mathsf{V}_{1,-1} \end{array} \tag{6.1.15}$$

6.1.2 Bosonization and expected results

Many algebraic aspects of the continuum limit of Temperley-Lieb based models can be understood using bosonization of the underlying XXZ spin chain and its relation with the free-field (Dotsenko-Fateev) description [44] of $c < 1$ CFTs, see further the Coulomb Gas discussion in Section 2.2. This construction will involve the screening charges $\alpha_+ = \sqrt{(x+1)/x}$ and $\alpha_- = -\sqrt{x/(x+1)}$ (recalling the parametrization of c in terms of x (3.5.4)) as well as the background charge

$$\alpha_0 = \frac{\alpha_+ + \alpha_-}{2} = \frac{1}{2\sqrt{x(x+1)}}\,. \tag{6.1.16}$$

(Note that the background charge was instead denoted by e_0 in Section 2.2.) We start with some basic results here, concerning in particular the identification of the stress-energy tensor and its "twisted" version, the role of vertex operators, and the nature of corrections to scaling. These results will be useful later to formulate conjectures about the continuum limit of modules.

The free field (FF) representation starts with a pair of (chiral and anti-chiral) bosonic fields $\varphi, \bar{\varphi}$ with the stress-energy tensors

$$T_{\mathrm{FF}} = -\frac{1}{4} :(\partial\varphi)^2: , \tag{6.1.17a}$$

$$\bar{T}_{\mathrm{FF}} = -\frac{1}{4} :(\bar{\partial}\bar{\varphi})^2: , \tag{6.1.17b}$$

where $:-:$ denotes normal order. The Hamiltonian is

$$H_{\mathrm{FF}} = -\int \frac{d\sigma}{2\pi} (T_{\mathrm{FF}} + \bar{T}_{\mathrm{FF}}) , \tag{6.1.18}$$

and the propagators are

$$\langle \varphi(z)\varphi(z') \rangle = -2\ln(z - z') , \tag{6.1.19a}$$

$$\langle \bar{\varphi}(\bar{z})\bar{\varphi}(\bar{z}') \rangle = -2\ln(\bar{z} - \bar{z}') . \tag{6.1.19b}$$

Here $z = \sigma + i\tau$, where σ is the space coordinate and τ the imaginary time coordinate.

To further analyse this free-field problem we define the vertex operators

$$V_{\alpha(e,m),\bar{\alpha}(e,m)} = :\exp\Big(i\frac{e}{2}\alpha_+ \Phi - i\frac{m}{2}\alpha_- \Theta \Big): , \tag{6.1.20}$$

expressed here in terms of the non-chiral components

$$\Phi \equiv \varphi + \bar{\varphi} , \tag{6.1.21a}$$

$$\Theta \equiv \varphi - \bar{\varphi} . \tag{6.1.21b}$$

The integers $e, m \in \mathbb{Z}$ can be interpreted as electric and magnetic charges in the Coulomb gas formalism [43, 110], and in terms of those we have

$$\alpha(e,m) = \frac{1}{2}\left(e\alpha_+ - m\alpha_- \right) , \tag{6.1.22a}$$

$$\bar{\alpha}(e,m) = \frac{1}{2}\left(e\alpha_+ + m\alpha_- \right) , \tag{6.1.22b}$$

where $\alpha_\pm$ are coupling constants related to the compactification radius of the boson. The conformal weights of the vertex operators (6.1.20) are then

$$h_{\mathrm{FF}} = [\alpha(e,m)]^2 , \tag{6.1.23a}$$

$$\bar{h}_{\mathrm{FF}} = [\bar{\alpha}(e,m)]^2 . \tag{6.1.23b}$$

We consider specifically low-energy excitations over the ground state of the antiferromagnetic Hamiltonian (2.1.8), which are described by (6.1.18), with

$$\alpha_+ \equiv \sqrt{\frac{x+1}{x}} , \tag{6.1.24a}$$

$$\alpha_- \equiv -\sqrt{\frac{x}{x+1}} \tag{6.1.24b}$$

in the parametrization $\gamma = \frac{\pi}{x+1}$.

Defining

$$f_j = -\sigma_j^- \sigma_{j+1}^+ - \sigma_j^+ \sigma_{j+1}^- - \frac{\cos\gamma}{2}\sigma_j^z\sigma_{j+1}^z + \frac{\cos\gamma}{2} \tag{6.1.25}$$

we note that we can equivalently write the Hamiltonian (2.1.8) as

$$\mathscr{H} = -\frac{\gamma}{\pi\sin\gamma}\sum_{j=1}^{N}(f_j - f_\infty)\,, \tag{6.1.26}$$

where $f_\infty = e_\infty$. Let us now consider the scaling limit of each individual term. We use the basic formulae from the literature (see, e.g., [111])

$$\sigma_j^z = a\frac{\alpha_+}{2\pi}\frac{\mathrm{d}\Phi}{\mathrm{d}\sigma} + (-1)^j C_1^z a^{d_{1,0}}\sin\frac{\alpha_+\Phi}{2}(\sigma) + \dots\,, \tag{6.1.27a}$$

$$\sigma_j^\pm = \exp\left(\pm\frac{i\alpha_-}{2}\Theta\right)(\sigma)\left[a^{d_{0,1}}C_0^\pm + a^{d_{1,1}}C_1^\pm(-1)^j\cos\frac{\alpha_+\Phi}{2}(\sigma) + \dots\right], \tag{6.1.27b}$$

where a is the cutoff (lattice spacing) and the physical coordinate $\sigma = ja$. The $C_1^z, C_0^\pm, C_1^\pm$ are (known) constants that depend only on x. The numbers $d_{e,m}$ are the physical dimensions of the operators (6.1.20), namely $d_{e,m} \equiv h_{\mathrm{FF}} + \bar{h}_{\mathrm{FF}}$.

Using these formulae, one can write a similar expansion for the elementary Hamiltonians [111]

$$f_j - f_\infty = a^2\frac{\sin\gamma}{2\gamma}(T_{\mathrm{FF}} + \bar{T}_{\mathrm{FF}})(\sigma) + C_1(-1)^j a^{d_{1,0}}\cos\frac{\alpha_+\Phi}{2}(\sigma) + \dots\,. \tag{6.1.28}$$

The important quantity is the dimension

$$d_{1,0} = \frac{\alpha_+^2}{2} = \frac{x+1}{2x}\,. \tag{6.1.29}$$

In the regime we are interested in, $\gamma \in [0,\pi]$, whence $x \in [0,\infty)$. The leading contribution to (6.1.28) comes from the first term only when $d_{1,0} > 2$, that is $1 - \frac{\gamma}{\pi} < \frac{1}{4}$, or $\gamma \in]\frac{3}{4},\pi]$. Equivalently, the anisotropy parameter $\Delta \in [-1, -\frac{\sqrt{2}}{2}]$ from (2.1.9), or the conformal parameter $x < \frac{1}{3}$ from $\gamma = \frac{\pi}{x+1}$. For values inside this interval, we can thus safely write, as $a \to 0$:

$$-\frac{\gamma}{a^2\pi\sin\gamma}(f_j - f_\infty) \approx -\frac{1}{2\pi}(T_{\mathrm{FF}} + \bar{T}_{\mathrm{FF}})\,. \tag{6.1.30}$$

Outside this interval—i.e. for $x > \frac{1}{3}$ (including x integer)—the second term dominates. A very important fact however is that the second term comes with a $(-1)^j$ alternating prefactor, i.e., it only contributes to excitations at lattice momentum near π. As a result, for all Virasoro generators L_n at finite n—and thus at momentum of order $1/N$—the alternating term is effectively scaling with a dimension $d_{1,0}+2$. For instance, for L_0 we have

$$f_{j-1} + f_{j+1} + 2f_j = 4a^2\frac{\sin\gamma}{2\gamma}(T_{\mathrm{FF}} + \bar{T}_{\mathrm{FF}})(\sigma) + C_1(-1)^j a^{d_{1,0}+2}\frac{\mathrm{d}^2}{\mathrm{d}\sigma^2}\cos\frac{\alpha_+\Phi}{2}(\sigma) + \dots\,, \tag{6.1.31}$$

and we see that all corrections are irrelevant.

The same analysis can now be carried out for the Temperley-Lieb generators e_j. Comparing (6.1.25) and (3.2.5) we see that

$$e_j = f_j - i\frac{\sin\gamma}{2}\left(\sigma_j^z - \sigma_{j+1}^z\right)\,, \tag{6.1.32}$$

for which we get the continuum limit

$$-\frac{\gamma}{a^2\pi\sin\gamma}(e_j - e_\infty) = -\frac{1}{2\pi}(T_{\rm FF} + \bar{T}_{\rm FF})(\sigma) + i\frac{\gamma}{(2\pi)^2}\alpha_+\frac{\mathrm{d}^2\Phi}{\mathrm{d}\sigma^2}\,. \tag{6.1.33}$$

Since in the models we study, the Temperley-Lieb generators are the fundamental Hamiltonian densities, we must interpret the right-hand side of this equation as a modified or "improved" stress-energy tensor, which is the sum of its free field analog $T_{\rm FF}+\bar{T}_{\rm FF}$ and a new "deformation" term. In terms of the parameter x, the "twist term" multipliying the second derivative of Φ is

$$\frac{1}{2\pi}\times\frac{1}{2(x+1)}\sqrt{\frac{x+1}{x}} \equiv \frac{1}{2\pi}\alpha_0\,, \tag{6.1.34}$$

where we have introduced the *background charge* α_0, defined as in (6.1.16), familiar from the Coulomb-gas analysis (Section 2.2, [44]). Using that $\partial_\sigma^2\Phi = \partial^2\varphi + (\bar{\partial})^2\bar{\varphi}$, we finally get the expressions for the modified stress-energy tensor

$$T = -\frac{1}{4}\,{:}(\partial\varphi)^2{:} + i\alpha_0\partial^2\varphi\,, \tag{6.1.35a}$$

$$\bar{T} = -\frac{1}{4}\,{:}(\bar{\partial}\bar{\varphi})^2{:} + i\alpha_0\bar{\partial}^2\bar{\varphi}\,. \tag{6.1.35b}$$

This is the well known "twisted" stress-energy tensor studied in [44,112,113]. It is this modified stress-energy tensor—rather than the free-field version $T_{\rm FF}, \bar{T}_{\rm FF}$ of (6.1.17)—that is relevant for a lattice discretization based on the Temperley-Lieb algebra. We shall henceforth consider $T, \bar{T}$ throughout the chapter. In Appendix G of [16] we give an alternative construction based on the untwisted stress-energy tensor.

With respect to this stress-energy tensor, the vertex operators $V_{\alpha,\bar{\alpha}}$ get the modified conformal weights

$$h = \alpha^2 - 2\alpha\alpha_0\,, \tag{6.1.36a}$$

$$\bar{h} = \bar{\alpha}^2 - 2\bar{\alpha}\alpha_0\,, \tag{6.1.36b}$$

to be compared to the previous free-field expressions (6.1.22).

The eigenvalues of $\mathscr{H}$ and $\mathscr{P}$ only allow one to determine the conformal weights, not the value of the charges. For a given conformal weight, two values are possible in general, α and $2\alpha_0 - \alpha$. Using the notation

$$\alpha_{r,s} = \frac{1-r}{2}\alpha_+ + \frac{1-s}{2}\alpha_-\,. \tag{6.1.37}$$

we now state the result, first shown in [12], which we will justify in detail below:

In the XXZ spin chain with twisted boundary conditions parametrized by $\phi = 2\pi e_\phi$, the scaling states in the sector of magnetization S_z correspond in the scaling limit to primary states $V_{\alpha,\bar{\alpha}}$ with charges on the form

$$\alpha = \alpha_{-(e-e_\phi),S_z} = \frac{1}{2}(e-e_\phi)\alpha_+ + \alpha_0 - \frac{1}{2}S_z\alpha_- \tag{6.1.38a}$$

$$\bar{\alpha} = \alpha_{-(e-e_\phi),-S_z} = \frac{1}{2}(e-e_\phi)\alpha_+ + \alpha_0 + \frac{1}{2}S_z\alpha_-, \tag{6.1.38b}$$

where e is an integer, and their descendants. The conformal weights are given by (6.1.36).

The precise correspondence, including the proper identification of the integers e, will be discussed in Section 6.2, as well as the exact meaning of the words *scaling states* and *scaling limit*.

We conclude this section by some remarks about corrections to scaling. The leading corrections to e_j look a bit different from (6.1.28). We have

$$(e_j - e_\infty) = a^2 \frac{\sin\gamma}{2\gamma}(T+\bar{T})(\sigma) - i\alpha_+ a^2 \frac{\sin\gamma}{4\pi}\frac{\mathrm{d}^2\Phi}{\mathrm{d}\sigma^2} + (-1)^j a^{d_{1,0}} \left(C_1^z \sin\frac{\alpha_+\Phi}{2}(\sigma) + 2iC_1 \cos\frac{\alpha_+\Phi}{2}(\sigma) \right) + \dots . \quad (6.1.39)$$

Meanwhile, it is expected that the leading correction should now be given by the operator $\Phi_{2,1}$ with conformal weights $h = \bar{h} = h_{2,1} = \frac{x+3}{4x}$ in the twisted theory. Under twisting, we expect in general the field

$$:\exp(ni\alpha\Phi): \text{ with } \alpha = \frac{\alpha_+}{2} \quad (6.1.40)$$

to get the weight

$$h = \alpha^2 - 2\alpha\alpha_0 = h_{1-n,1}\,. \quad (6.1.41)$$

This means the term $\exp(i\alpha_+\Phi/2)$ should disappear from the combination in (6.1.39), leading to a relationship between the two constants

$$C_1^z = 2C_1\,. \quad (6.1.42)$$

While (6.1.42) can be checked to hold in some cases using results in [114,115], we are not aware of a general proof: more investigation of this question would be very interesting, but is outside the scope of this thesis.

6.1.3 The choices of metric

We have just recovered the well-known result that the continuum limit of the XXZ spin chain is made up of sectors of a twisted free-boson theory. The space of states in the continuum limit can be built out of vertex-operator states $V_\alpha = :e^{i\alpha\varphi}:$ (in this section we shall only consider the chiral part for notational brevity) and derivatives $\partial\varphi, \partial^2\varphi, (\partial\varphi)^2, \dots$.

From the free-boson current $J(z) = \frac{1}{4}\partial_z\varphi$, we define a_n as its modes, such that we have the Heisenberg algebra

$$[a_n, a_m] = n\delta_{n+m,0}. \quad (6.1.43)$$

We can then equivalently consider the state space to be built from states of the form

$$(a_{-n_1})^{N_1} \cdots (a_{-n_k})^{N_k} V_\alpha\,. \quad (6.1.44)$$

The vertex operator V_α is a highest-weight state for the Heisenberg algebra, with

$$a_n V_\alpha = 0\,, \quad \forall n > 0\,, \quad (6.1.45a)$$
$$a_0 V_\alpha = \sqrt{2}(\alpha - \alpha_0)V_\alpha\,. \quad (6.1.45b)$$

In terms of a_n we have for the twisted boson theory

$$L_n = \sum_{k=0}^{\infty} a_{n-k}a_k - \sqrt{2}\alpha_0 n a_n\,, \quad \text{for } n \neq 0\,, \quad (6.1.46a)$$

$$L_0 = \sum_{k=1}^{\infty} a_{-k}a_k + \frac{1}{2}a_0^2 - \alpha_0^2 \quad (6.1.46b)$$

for which the Virasoro algebra relations (1.0.1) are readily shown to be satisfied with

$$c = 1 - 24\alpha_0^2 \,. \tag{6.1.47}$$

Two possible scalar products can be introduced in the CFT. The one for which $a_n^\dagger = a_{-n}$, denoted in what follows by $\langle -, - \rangle$, is positive definite and corresponds to the usual positive definite scalar product for the spin chain, where the conjugation sending a ket to a bra is anti-linear. A crucial observation is that for this scalar product $L_n^\dagger \neq L_{-n}$. This means that norm squares of descendants cannot be obtained using Virasoro algebra commutation relations. Also, this scalar product must be used with great care when calculating correlation functions; this point is discussed more in Appendix B. Instead of using the Virasoro relations directly we shall use the Heisenberg relations (6.1.43).

We shall in the following sections, especially when comparing to the numerical results, refer to the *conjectured* values of various norms. What we refer to is then the value we obtain by considering the states to be given as V_α with α as in (6.1.38), writing any Virasoro generator in terms of a_n using (6.1.46), using the Heisenberg commutation relations (6.1.43) to move a_n with $n > 0$ to the right and finally applying the highest-weight relation (6.1.45).

The second scalar product is denoted $(-, -)$ and corresponds to the conjugation $\ddagger$. Compared to the conjugation $\dagger$, where we write L_n in terms of a_n as in (6.1.46) and use $a_n^\dagger = a_{-n}$ to define the conjugate $L_n^\dagger$, we instead define the conjugate $L_n^\ddagger$ as simply $L_n^\ddagger = L_{-n}$. This "conformal scalar product" $(-, -)$ is known to correspond [9, 10, 116], on the lattice, to the "loop scalar product" defined through the Markov trace, or to a modified scalar product in the XXZ spin chain where $\mathfrak{q}$ is treated as a formal, self-conjugate parameter [117]. It is not a positive definite scalar product, and we will not use it much here, as our main goal is to establish whether various quantities are zero or not.

Of course, the relationship between the two scalar products is a question of great interest: for some recent results about this, see [118].

6.1.4 Feigin-Fuchs modules and conjugate states

When the lattice parameters are such that the corresponding twisted free boson only involves non-degenerate cases, the Verma modules are irreducible and coincide with the Fock spaces of the bosonic theory. We now consider what happens in the degenerate case. As a module over the Heisenberg algebra, the Fock space is irreducible. If we instead wish to consider it as a module over the Virasoro algebra, it will be a Feigin-Fuchs module, which is only irreducible (and then, a Verma module) if $\alpha \neq \alpha_{r,s}$ for any $r, s \in \mathbb{N}^*$, with $\alpha_{r,s}$ defined as in (6.1.37).

To see how Feigin-Fuchs modules differ from Verma modules, it is helpful to introduce the notion of conjugate states: we call states with the same conformal weight h but different charges α conjugates of each other. From (6.1.36) we see that a state V_α with charge α has a conjugate state V_{α^c} with charge α^c defined as

$$\alpha^c \equiv 2\alpha_0 - \alpha \,. \tag{6.1.48}$$

Note that this conjugation is an involution: $(\alpha^c)^c = \alpha$.

While the conformal weights of a pair of conjugate states are the same, we shall see that their behaviour under the action of the Virasoro algebra is in a sense dual. We illustrate the precise meaning of this statement with the case of the identity state, which has $\alpha = 0$, and its conjugate state with $\alpha = 2\alpha_0$. We obtain $L_{-1}V_\alpha = \partial_z V_\alpha = \sqrt{2}\alpha a_{-1}V_\alpha$, which is zero for $\alpha = 0$. Conversely, the action of L_1 on $a_{-1}V_\alpha$ (recall our state space (6.1.44)), yields $L_1 a_{-1}V_\alpha = \sqrt{2}(\alpha - 2\alpha_0)V_\alpha$, which is instead zero for the conjugate charge $\alpha^c = 2\alpha_0$. We thus obtain the following diagrams,

where crossed out arrows indicate that the state at the end of the arrow would have zero norm:

$$\begin{array}{cc} \mathbf{1} & V_{2\alpha_0} \\ L_{-1} \not\downarrow\uparrow L_1 & L_{-1} \downarrow\not\updownarrow L_1 \\ a_{-1}\mathbf{1} & a_{-1}V_{2\alpha_0} \\ h=1 & h=1 \end{array} . \tag{6.1.49}$$

We shall later on refrain from writing out such crossed-out arrows at all, using the same type of notation as already seen above for the standard modules. Since we restrict to the case where $\mathfrak{q}$ is not a root of unity, there are no other degeneracies in the modules, and we always get one of the two following diagrams:

 . (6.1.50)

We note that these can be seen as a co-Verma module and a Verma module. More details will be given in Section 6.4.

6.2 Bethe Ansatz picture

In the context of the XXZ spin chain the Bethe ansatz is a well-adapted tool to carry out the analysis [119]. We present the general picture, and refer the reader to Appendix C for more detail.

6.2.1 Bethe-ansatz and the identification of scaling states

When $\mathfrak{q}$ not a root of unity, and the resonance criterion (3.1.4) is not satisfied, the XXZ Hamiltonian can be fully diagonalized using a basis of orthonormal Bethe states (see [120, 121] and references therein). The corresponding Bethe equations are of the form

$$N\lambda_j = 2\pi I_j + \phi - \sum_{k\neq j} \Theta_{\mathrm{XXZ}}(\lambda_j, \lambda_k), \tag{6.2.1}$$

for $j = 1, 2, \ldots, \frac{N}{2} - S_z$, and are obtained (after some rewriting) by taking the logarithm of (C.1.3) as given in Appendix C; this defines the scattering kernel $\Theta_{\mathrm{XXZ}}(\lambda_j, \lambda_k)$. The Bethe integers I_j corresponding to a given solution shall play an important role in the discussion below. (Note: they are sometimes half-integers, despite their name.) The states have energies

$$\mathscr{E}(\{I_j\}) = -\frac{\gamma}{\pi \sin\gamma}\left[2\sum_j(\cos\gamma + \cos k_j) - Ne_\infty\right], \tag{6.2.2}$$

where k_j is related to the Bethe root λ_j by $\tan(\gamma/2)\tan(k_j/2) = \tanh(\lambda_j)$, and momenta

$$\mathscr{P}(\{I_j\}) = -\frac{2\pi}{N}\sum_j I_j + \frac{\phi}{N}\left(\frac{N}{2} - S_z\right). \tag{6.2.3}$$

For future convenience we also define the rescaled lattice momentum $\mathscr{p}$ as

$$\mathscr{p} = \frac{N}{2\pi}\mathscr{P} \tag{6.2.4}$$

such that when $\phi = 0$, $\mathscr{p}$ takes integer values $0, 1, \ldots, N-1$.

The ground state—i.e., the state of lowest energy—depends on the value of ϕ. It will be convenient in what follows to identify states by their corresponding set of Bethe integers, where the ground state is given by the symmetric, maximally packed set of integers [119]. The boundaries of this set of integers are referred to as "edges" (by analogy with the Fermi edge in solid state physics).

The third component S_z of the spin is conserved by the Hamiltonian (2.1.8), and we can split the problem of diagonalizing $\mathscr{H}$ into subsectors of fixed S_z. Within a given subsector, we identify states using the difference between their set of Bethe integers and the one of the lowest-energy state within the same subsector. As N increases, we focus only on *scaling states*, that is, states for which this difference *measured from the edge* remains fixed and finite. Representing the set of integers by filled circles, the edge simply refers to the boundary between filled and empty circles in the ground state configuration, as shown here marked by $\vdots$ for $N = 10$:

$$[-2, -1, 0, 1, 2] \quad \longleftrightarrow \quad \ldots \circ\circ\circ \vdots \bullet\bullet\bullet\bullet\bullet \vdots \circ\circ\circ \ldots$$

For a scaling state there can only be finitely many empty circles between the edges and only finitely many filled circles outside of the edges, and both must occur only at a finite distance from one of the edges. Examples of scaling states are provided by the "electric excitations" discussed below, where the set of integers from the ground state is shifted by a finite amount e.

Of course, the ground states of every finite-S_z sector are scaling states, since their integers coincide with those of the ground state but for S_z of them.[1] A non-scaling state would be, in contrast, a state whose magnetization increases with N, for instance the "ferromagnetic ground state" will all spins up, $S_z = \frac{N}{2}$. Another example of a non-scaling state is obtained if we make a hole for some finite integer which remains fixed as $N \to \infty$. In this case, the difference from the ground state configuration, measured from the edge, increases linearly with N.

We now wish to give a brief motivation for the conjecture (6.1.38) given above. To this purpose we first recall the Coulomb gas (CG) picture, where we consider a free field compactified on a circle (see Section 6.1.2). Our fundamental operators are vertex operators (exponentials of the field) and their duals (discontinuities in the field), with conformal weights parametrized by integers e, m called the electric and magnetic charges. The conformal weights corresponding to these electromagnetic excitations are shown in (6.1.6), with $-e, m$ corresponding to r, s as in (6.1.38).

In the context of the spin chain we can make a purely magnetic excitation by taking the lowest-energy state within a sector of non-zero total magnetization S_z. This means adding to or subtracting from the number of Bethe integers, while still keeping them symmetrical and maximally packed. An electric excitation can then be created within any sector of S_z by shifting all Bethe integers e steps from the symmetric configuration. Examples of such primary states are shown here. We mark the middle of each row of filled circles with a bar, which will intersect the middle circle if their number is odd. This will be helpful for the discussion of descendant

[1] Strictly speaking, changing the number of integers by an odd number means altering between I_j being integers or half-integers. We expand our definition of scaling states to take this into account.

states below.

$\ldots\circ\circ\circ\bullet\bullet\overset{\downarrow}{\bullet}\bullet\bullet\circ\circ\circ\ldots$ $\leftrightarrow$ ground state

$\ldots\circ\circ\circ\bullet\bullet|\bullet\bullet\circ\circ\circ\ldots$ $\leftrightarrow$ a magnetic excitation ($m=1$)

$\ldots\circ\circ\circ\circ\bullet\bullet\overset{\downarrow}{\bullet}\bullet\bullet\circ\circ\ldots$ $\leftrightarrow$ an electric excitation ($e=1$)

$\ldots\circ\circ\bullet\bullet\overset{\downarrow}{\bullet}\bullet\bullet\circ\circ\circ\circ\ldots$ $\leftrightarrow$ an electric excitation ($e=-1$)

$\ldots\circ\circ\circ\circ\bullet\bullet|\bullet\bullet\circ\circ\ldots$ $\leftrightarrow$ an electromagnetic excitation ($e=1, m=1$)

$\ldots\circ\circ\bullet\bullet|\bullet\bullet\circ\circ\circ\circ\ldots$ $\leftrightarrow$ an electromagnetic excitation ($e=-1, m=1$)

Note that the magnetic excitation changes the number of filled circles; this corresponds to alternating between having a set of integers or a set of half-integers.

From (6.2.3) we see that an electric excitation corresponds to a change in momentum. Here we also see that if we introduce twisted boundary conditions, $e_\phi = \phi/2\pi$ enters on the same footing as e. This mirrors how in the CG picture a twist can be implemented by inserting electric charges at infinity.[2] With the identification $e \leftrightarrow -(e - e_\phi)$ and $m \leftrightarrow S_z$ we claim that the scaling states corresponding to electromagnetic excitations in the spin chain can be written in the CG picture as vertex operators $V_{\alpha,\bar{\alpha}} = :e^{i\alpha\varphi + i\bar{\alpha}\bar{\varphi}}:$ of charges $\alpha, \bar{\alpha}$ as in (6.1.38). Indeed, we see that with these charges we reproduce the weights (6.1.6) for CG electromagnetic excitations.

From any primary state obtained in this fashion, we must make further excitations to reach its descendants. This is done by "creating holes" through shifting Bethe integers at the left edge (chiral excitations) or right edge (anti-chiral excitations) of the set. Knowing that the lattice momentum must shift in accordance with the change in conformal spin, we can easily read off which level we reach. If the level has more than one state, we obtain an orthonormal basis for these states. To better see which excitations are chiral and which are anti-chiral we compare to the bar inserted in the middle of the filled circles. We find the chiral level by first counting, for each filled circle on the left side of the bar, the number of empty circles separating it from the bar, and then adding up these numbers. We find the anti-chiral level in the same manner by considering the right side of the bar. Some examples of descendants:

$\ldots\circ\circ\bullet\circ\bullet\bullet|\bullet\bullet\bullet\circ\circ\circ\ldots$ $\leftrightarrow$ chiral level 1

$\ldots\circ\circ\circ\bullet\bullet\bullet|\bullet\bullet\circ\bullet\circ\circ\ldots$ $\leftrightarrow$ anti-chiral level 1

$\ldots\circ\circ\bullet\circ\bullet\bullet|\bullet\bullet\circ\bullet\circ\circ\ldots$ $\leftrightarrow$ chiral and anti-chiral level 1

$\left.\begin{array}{l}\ldots\circ\circ\bullet\bullet\circ\bullet|\bullet\bullet\bullet\circ\circ\circ\ldots\\ \ldots\circ\bullet\circ\circ\bullet\bullet|\bullet\bullet\bullet\circ\circ\circ\ldots\end{array}\right\}$ $\leftrightarrow$ chiral level 2

In practice, the Bethe integers may come in configurations where some integers coincide. We find (via the methods discussed in Appendix D.3) the sets of Bethe integers for all relevant scaling states based on the sets listed in [122], in which the possibility of coinciding integers is also briefly discussed. As a concrete example, take $N = 12, x = \pi, \phi = 0$ and consider the primary state that corresponds to the electromagnetic excitation $[-3, -2, -1, 0, 1]$. In this case, the level-one chiral excitation does not correspond to $[-4, -2, -1, 0, 1]$ but rather to $[-6, -1, 0, 0, 1]$, i.e., the integer 0 repeats. In such situations the simplified picture above fails to hold. The way to identify the states more generally will be to look at their energy together with the sum of their Bethe integers. A scaling state then corresponds to a state whose sum

[2]Note: *numerically*, our momentum only depends on e, since we have smeared out the twist. e_ϕ instead modifies the Hamiltonian itself.

of Bethe integers is equal to the sum of a "valid" configuration, and which is also one of the low-energy states within that sector of lattice momentum. The latter criterion can be quantified by demanding the state to be the kth excitation for some $k < k_0$. We only take $k_0 \to \infty$ after $N \to \infty$, a procedure that is called the double limit in [12]. We can see from the picture above the importance of taking $N \to \infty$ first: to accommodate the shifts in momentum that we get from creating the holes and shifts, we must keep N large enough.

Overlaps and mixing

Even when taking the possibility of repeating integers into account, the above picture of scaling states and their conjectured limits is neater than reality. An important example of a more complicated situation, which will be relevant for the numerical results below, is as follows.

Consider two scaling states on the lattice with the same $S_z \neq 0, \phi = 0$ but with opposite electric excitations $e, -e$ (with $e \neq 0$). By conjecture (6.1.38) these should correspond in the double limit to two primary states with the conformal weights switched with respect to one another, so that they both have the same energy. Following (6.2.3)-(6.2.4) and taking into account that lattice momentum is defined modulo the system size, the sectors of lattice momentum are only separated by $\Delta\mathscr{p} = 2eS_z$. Making holes to create the descendant states will shift $\mathscr{p}$ in integer steps, and it is clear that the momentum sectors of the left descendants of one state will start overlapping with those of the right descendants of the other state at level eS_z, no matter how large we take N.

By chiral/anti-chiral symmetry there is in such cases no way to distinguish from which primary a given state descends, and the symmetry may even force us to consider linear combinations of the scaling states as candidates for the descendant states in the limit. We then say that there is *mixing* of the scaling states. To make this issue more clear, let us specialize this example. Let V_1 be the primary state corresponding to $S_z = 1, e = -1$ and V_2 the primary state corresponding to $S_z = 1, e = 1$. Let W_1 be the level-1 chiral descendant of V_1, and let W_2 denote the level-1 anti-chiral descendant of V_2. The momentum sectors of W_1 and W_2 are the same. Within this sector, the lowest-energy state (whose energy comes with multiplicity one within this sector) can neither be identified with W_1 nor with W_2. The reason is that the energies of W_1, W_2 in the limit are the same, and "favouring" one over the other by assigning it a scaling state with lower energy would be incompatible with the symmetry of the system, which demands that chiral and anti-chiral quantities play equal roles. Instead, we must create W_1, W_2 out of linear combinations of more than one scaling state, such that each of them has the same contribution from the lowest-energy state. This phenomenon will be further discussed in Appendix D.1.

Since we wish to explore the indecomposable structure of the modules, the issue of mixing will be particularly important. The reason is that a primary state with a degenerate conformal weight given by the integers e and S_z, related to r, s as in (6.1.38), will have its null state precisely at level $|eS_z|$, in the sector of lattice momentum where mixing can occur.

6.2.2 Conjugate states and Bethe roots

In Section 6.1.4 we saw that in the degenerate case there are two possible diagrams for the structure of Virasoro modules, reproduced here for convenience (co-Verma module to the left, Verma module to the right):

(6.2.5)

Due to the sign in the conjecture (6.1.38), we see that degenerate chiral weights h (i.e., $h = h_{r,s}$ with $r, s \in \mathbb{N}^*$) are obtained by charges α corresponding to states where $(e - e_\phi)$ and S_z are of *opposite* signs, while degenerate anti-chiral weights $\bar{h}$ are obtained by charges $\bar{\alpha}$ corresponding to states where $(e-e_\phi)$ and S_z are of the same sign. With the sign conventions for magnetization and lattice momentum used in this chapter, we have found the co-Verma type for

$$\alpha = \alpha_{r,s} \quad \Leftrightarrow \quad (e - e_\phi) < 0 \text{ and } S_z > 0\,, \qquad \text{(chiral)} \tag{6.2.6a}$$
$$\bar{\alpha} = \alpha_{r,s} \quad \Leftrightarrow \quad (e - e_\phi) < 0 \text{ and } S_z < 0\,, \qquad \text{(anti-chiral)}\,, \tag{6.2.6b}$$

while the Verma type was found for the conjugate charges

$$\alpha = \alpha^{\mathrm{c}}_{r,s} \quad \Leftrightarrow \quad (e - e_\phi) > 0 \text{ and } S_z < 0\,, \qquad \text{(chiral)} \tag{6.2.7a}$$
$$\bar{\alpha} = \alpha^{\mathrm{c}}_{r,s} \quad \Leftrightarrow \quad (e - e_\phi) > 0 \text{ and } S_z > 0\,, \qquad \text{(anti-chiral)}\,, \tag{6.2.7b}$$

with $r, s \in \mathbb{N}^*$ as given in (6.1.38). As an example, $(e - e_\phi) = -1, S_z = 1 \Rightarrow \alpha = \alpha_{1,1} = 0$ while $(e - e_\phi) = 1, S_z = -1 \Rightarrow \alpha = \alpha^{\mathrm{c}}_{1,1} = 2\alpha_0$, which can be compared to (6.1.49). Of course the choice of conventions holds no deeper meaning, and the important takeaway is that *within each sector of S_z we expect to find pairs of conjugate primary states such that one has a chiral null state, the other an anti-chiral one, and the modules are of opposite types* (Verma or co-Verma).

We now show that such pairs of states, which differ by the sign of $(e - e_\phi)$, correspond to Bethe states that differ only by the sign of their Bethe integers and the sign of their Bethe roots. This can be seen directly from the shape of the Bethe equations (C.1.3) in Appendix C, reproduced here for convenience:

$$\frac{d(\lambda_j)}{a(\lambda_j)} \prod_{k \neq j} \frac{b(\lambda_k, \lambda_j)}{b(\lambda_j, \lambda_k)} = 1 \tag{6.2.8}$$

Leaving the definitions of the various terms to the Appendix, we here need only know that $b(-\lambda_k, -\lambda_j) = b(\lambda_j, \lambda_k)$, $a(\lambda) = 1$ and that for $\phi = 0$, $d(-\lambda) = (d(\lambda))^{-1}$ in the homogeneous limit (our case of interest). When $\phi \neq 0$, the only modification to the Bethe equations is $d(\lambda) \to e^{i\phi} d(\lambda)$, showing that one must take $e_\phi \to -e_\phi$ in order for the roots with opposite signs to be a solution.

That the Bethe roots for these pairs of states differ only by their sign will be important in Section 6.2.3, where we show that a strong duality of the corresponding modules can be seen directly on the lattice using Bethe ansatz techniques. To clarify the meaning of "strong", let us for comparison write out a weaker type of duality that is expected based only on the conjecture (6.1.38) as discussed above. We shall need a more precise notation for conjugate states than in Section 6.1.4. We write $V_{\bar{\alpha}^{\mathrm{c}}, \alpha^{\mathrm{c}}}$ for a state whose anti-chiral charge is the conjugate of the chiral charge of $V_{\alpha,\bar{\alpha}}$, and whose chiral charge is the conjugate of the anti-chiral charge of $V_{\alpha,\bar{\alpha}}$. In this notation, we have the following result:

Weak duality: *Whenever $V_{\alpha,\bar{\alpha}}$ has a degenerate chiral charge $\alpha = \alpha_{r,s}$ or $\alpha = \alpha^{\mathrm{c}}_{r,s}$ (with $r, s \in \mathbb{N}^*$) we expect that*

$$\langle W | A_{r,s} | V_{\alpha,\bar{\alpha}} \rangle = 0 \quad \Leftrightarrow \quad \langle V_{\bar{\alpha}^{\mathrm{c}}, \alpha^{\mathrm{c}}} | \bar{A}^{\ddagger}_{r,s} | W^{\mathrm{c}} \rangle = 0\,, \tag{6.2.9a}$$

where W, W^{c} are the corresponding null states at level rs, $A_{r,s}$ the relevant combination of lowering operators and $A^{\ddagger}_{r,s}$ the "conformal conjugate" for which $L^{\ddagger}_n = L_{-n}$. The same type of statements hold when $V_{\alpha,\bar{\alpha}}$ has a degenerate anti-chiral charge $\bar{\alpha} = \alpha_{r,s}$ or $\bar{\alpha} = \alpha^{\mathrm{c}}_{r,s}$:

$$\langle \overline{W} | \bar{A}_{r,s} | V_{\alpha,\bar{\alpha}} \rangle = 0 \quad \Leftrightarrow \quad \langle V_{\bar{\alpha}^{\mathrm{c}}, \alpha^{\mathrm{c}}} | A^{\ddagger}_{r,s} | \overline{W}^{\mathrm{c}} \rangle = 0\,. \tag{6.2.9b}$$

On the lattice, we expect that the corresponding matrix elements (with the Virasoro generators replaced by the Koo-Saleur generators, and primary/descendant states by their corresponding scaling states) will approach either zero or non-zero values in the limit according to this duality. Comparing to (6.2.9), the stronger duality that will be shown below is the statement that two matrix elements *have the same value* already on the lattice.

Before turning to the stronger duality we note that even without the Bethe ansatz we can, in fact, see the weaker duality already on the lattice for one particular case of interest: the modules $\mathscr{W}_{0,\mathfrak{q}^{-2}}$ and $\mathscr{W}_{0,\mathfrak{q}^2}$ as described in Section 3.3:

$$\mathscr{W}_{0,\mathfrak{q}^{-2}}: \begin{array}{c}[0,\mathfrak{q}^{-2}]\\ \downarrow \\ [1,1]\end{array}, \qquad \mathscr{W}_{0,\mathfrak{q}^{2}}: \begin{array}{c}[0,\mathfrak{q}^{2}]\\ \uparrow \\ [1,1]\end{array}. \tag{6.2.10}$$

Within these diagrams, the pair of states corresponding to $S_z = 0, |e| = 1$, $e_\varphi = \pm\alpha_-/\alpha_+$[3] can be found within $[0, \mathfrak{q}^{\pm 2}]$ while their corresponding level-1 null states can be found within $[1, 1]$. The duality under the action of the Koo-Saleur generators on the lattice then follows directly from the duality of the Temperley-Lieb modules, since the Koo-Saleur generators are built out of Temperley-Lieb generators.

6.2.3 Some results about form factors

In Appendix C we give a brief recapitulation of the Quantum Inverse Scattering Method, in which local operators such as σ_m^z are expressed in terms of entries of the monodromy matrix $\mathbf{T} = \left(\begin{smallmatrix} A & B \\ C & D \end{smallmatrix}\right)$. For a general overview of this method see [123]. The eigenstates of the XXZ Hamiltonian are given as $|\{\lambda\}\rangle = \prod_{k=1}^n B(\lambda_k)|0\rangle$ for a set of Bethe roots $\{\lambda\}$, their duals as $\langle\{\lambda\}| = \langle 0|\prod_{k=1}^n C(\lambda_k)$ and we wish to find matrix elements on the form $\langle\{\mu\}|\prod_i \sigma_{m_i}^{a_i}|\{\lambda\}\rangle$, where $a_i \in \{z, +, -\}$ and $m_i \neq m_j$ for $i \neq j$. The resulting expressions for these matrix elements in terms of functions of the Bethe roots are called form factors.

If we can find form factors for the Koo-Saleur generators $\mathscr{L}_n$, the work of looking at the action of the Virasoro algebra in the spin chain reduces to evaluating the expressions of these form factors, rather explicitly diagonalizing the finite Hamiltonian and then acting on the resulting eigenstates. For large system sizes N, this is a significant advantage: while the size of the Hamiltonian to be diagonalized grows exponentially in N, the time needed to evaluate form factors is only polynomial. A similar form-factor program has already been carried out in [124] for the case of the $SU(2)$-invariant six-vertex model and its descendants, which in the continuum correspond to $SU(2)_k$ WZW models. However, in this case the program was carried out for the current $J^a(z)$ rather than the Virasoro generators.

Finding form factors for $\mathscr{L}_n$ boils down to finding form factors for e_i and $[e_i, e_{i+1}]$. A priori this will involve form factors for all six permutations of three different neighbouring operators,

[3]Note that within (6.1.38), a charge with a twist of $e_\varphi = \pm\alpha_-/\alpha_+$ can be rewritten as a charge with $e_\varphi = 0$ where the magnetization S_z is shifted by one, which shows that these charges are on the form $\alpha_{r,s}$, $r, s \in \mathbf{Z}$ leading to degenerate conformal weights. In particular, with $|e| = 1$ we obtain the degenerate weight $h_{1,1}$.

namely

$$\sigma_m^z\sigma_{m+1}^-\sigma_{m+2}^+\,, \tag{6.2.11a}$$
$$\sigma_m^z\sigma_{m+1}^+\sigma_{m+2}^-\,, \tag{6.2.11b}$$
$$\sigma_m^+\sigma_{m+1}^-\sigma_{m+2}^z\,, \tag{6.2.11c}$$
$$\sigma_m^-\sigma_{m+1}^+\sigma_{m+2}^z \tag{6.2.11d}$$

and

$$\sigma_m^-\sigma_{m+1}^z\sigma_{m+2}^+\,, \tag{6.2.12a}$$
$$\sigma_m^+\sigma_{m+1}^z\sigma_{m+2}^-\,, \tag{6.2.12b}$$

as well as $\sigma_m^-\sigma_{m+1}^+, \sigma_m^+\sigma_{m+1}^-, \sigma_m^z\sigma_{m+1}^z$ and σ^z. Luckily we can reduce the number of form factors we need to compute by using various relations that follow from the Bethe ansatz. These relations also give us some general insight into how the lattice Virasoro generators $\mathscr{L}_n, \bar{\mathscr{L}}_n$ should act on Bethe states—in particular, we shall soon see how the duality for conjugate states appears already at finite size.

Properties under conjugation and parity, implications for the modules

The site dependence of the form factors does not depend on the choice of operators and can be factorized in the expressions. Following the notation in Appendix C we let $F_{\mathcal{O}_1\cdots\mathcal{O}_j}$ denote the site-independent part of the form factor for j neighboring operators $\mathcal{O}_1\cdots\mathcal{O}_j$. We wish to find relations between the site-independent part of the form factors of interest.

The first type of relations between the site-independent part of the form factors of interest is due to conjugation. The dual states of on-shell Bethe states are, up to a possible phase[4], their conjugates,

$$\langle\{\lambda\}| = (\text{phase})\big(|\{\lambda\}\rangle\big)^\dagger\,. \tag{6.2.13}$$

Combining this relation with

$$(\sigma^+)^\dagger = \sigma^-, \quad (\sigma^z)^\dagger = \sigma^z \tag{6.2.14}$$

we obtain

$$\langle\{\mu\}|\sigma_m^+\sigma_{m+1}^z\sigma_{m+2}^-|\{\lambda\}\rangle = (\text{phase})\Big(\langle\{\lambda\}|\sigma_m^-\sigma_{m+1}^z\sigma_{m+2}^+|\{\mu\}\rangle\Big)^*, \tag{6.2.15a}$$
$$\langle\{\mu\}|\sigma_m^z\sigma_{m+1}^+\sigma_{m+2}^-|\{\lambda\}\rangle = (\text{phase})\Big(\langle\{\lambda\}|\sigma_m^z\sigma_{m+1}^-\sigma_{m+2}^+|\{\mu\}\rangle\Big)^*, \tag{6.2.15b}$$

which relate $F_{\sigma^+\sigma^z\sigma^-}$ to $F_{\sigma^-\sigma^z\sigma^+}$ and $F_{\sigma^z\sigma^+\sigma^-}$ to $F_{\sigma^z\sigma^-\sigma^+}$ through the conjugation of each of the operators. Similarly we can relate $F_{\sigma^+\sigma^-}$ to $F_{\sigma^-\sigma^+}$.

The second type of relations between the site-independent part of the form factors of interest is due to parity. Following [125] we denote by Π the parity operator. It acts on a local operator X_m as

$$\Pi X_m\Pi^{-1} = X_{N+1-m} \tag{6.2.16}$$

and on the B-operators as

$$\Pi B(\lambda)\Pi^{-1} = (-1)^{N-1}B(-\lambda). \tag{6.2.17}$$

[4]In the numerics below, the phase is found for a given scaling state at small N, by explicitly comparing its dual with its conjugate, and stays the same as N is increased.

Thus, parity will act on Bethe states by taking $|\{\lambda\}\rangle$ into $|\{-\lambda\}\rangle$ (up to a possible sign) and act on j neighboring operators by reversing their order and the sites they act on. We obtain

$$\langle\{\mu\}|\sigma_m^-\sigma_{m+1}^+\sigma_{m+2}^z|\{\lambda\}\rangle = (\text{sign})\langle\{-\mu\}|\sigma_{N-m-1}^z\sigma_{N-m}^+\sigma_{N-m+1}^-|\{-\lambda\}\rangle\,, \quad (6.2.18a)$$

$$\langle\{\mu\}|\sigma_m^+\sigma_{m+1}^-\sigma_{m+2}^z|\{\lambda\}\rangle = (\text{sign})\langle\{-\mu\}|\sigma_{N-m-1}^z\sigma_{N-m}^-\sigma_{N-m+1}^+|\{-\lambda\}\rangle\,, \quad (6.2.18b)$$

which relate $F_{\sigma^-\sigma^+\sigma^z}$ to $F_{\sigma^z\sigma^+\sigma^-}$ and $F_{\sigma^+\sigma^-\sigma^z}$ to $F_{\sigma^z\sigma^-\sigma^+}$ through reversing the order of the operators. Altogether, the combined actions of conjugation and parity relate the four form factors (6.2.11) among themselves, and similarly for the remaining two (6.2.12). Thus, the only form factors involving three operators that we shall need to compute in Appendix C will be one of each group, here chosen to be $F_{\sigma^z\sigma^-\sigma^+}$ and $F_{\sigma^-\sigma^z\sigma^+}$.

Combining the expression for the Koo-Saleur generators (3.7.3) with the parity relations for the form factors yields relations for the matrix elements of $\mathscr{L}_n$ in the basis of Bethe states. In particular, we note that the term $[e_j, e_{j+1}]$ in (3.7.3) will pick up a sign when the order of all operators is reversed, changing $\mathscr{L}_n$ into $\bar{\mathscr{L}}_{-n}$. Thus we have

$$\langle\{\mu\}|\mathscr{L}_n|\{\lambda\}\rangle = \langle\{-\lambda\}|\bar{\mathscr{L}}_{-n}|\{-\mu\}\rangle. \quad (6.2.19)$$

Meanwhile, the pairs of conjugate states in a given sector of S_z are, as discussed in Section 6.2.2, related through a change of signs for all the Bethe roots, which is precisely the action of parity on states as seen in (6.2.17). Taken together, we find in particular that (6.2.9a) and (6.2.9b) can be turned into a much stronger statement:

Strong duality: *Let $V_{\alpha,\bar{\alpha}}, V_{\bar{\alpha}^c,\alpha^c}$ and W, W^c be a pair of conjugate primary states and their respective null states, as defined in connection to* (6.2.9a)–(6.2.9b)*, and $A_{r,s}$ the corresponding combination of Virasoro generators. We here denote the corresponding scaling states and lattice operators by calligraphic letters, e.g. $\mathscr{V}[N]_{\alpha,\bar{\alpha}}$. At each finite size N—large enough to accommodate the states of interest—we have the following equality of the matrix elements:*

$$\langle\mathscr{W}[N]|\mathscr{A}_{r,s}[N]|\mathscr{V}_{\alpha,\bar{\alpha}}[N]\rangle = (\text{phase})\langle\mathscr{V}_{\bar{\alpha}^c,\alpha^c}[N]|\bar{\mathscr{A}}_{r,s}^{\ddagger}[N]|\mathscr{W}^c[N]\rangle\,. \quad (6.2.20a)$$

The same type of duality holds when $V_{\alpha,\bar{\alpha}}$ has a degenerate anti-chiral charge $\bar{\alpha} = \alpha_{r,s}$ or $\bar{\alpha} = \alpha_{r,s}^c$:

$$\langle\overline{\mathscr{W}}[N]|\bar{\mathscr{A}}_{r,s}[N]|\mathscr{V}_{\alpha,\bar{\alpha}}[N]\rangle = (\text{phase})\langle\mathscr{V}_{\bar{\alpha}^c,\alpha^c}[N]|\mathscr{A}_{r,s}^{\ddagger}[N]|\overline{\mathscr{W}}^c[N]\rangle\,. \quad (6.2.20b)$$

Examples of this situation are seen in the numerical results, in Tables D.1 and D.8.

The considerations above hold for the matrix elements of single Temperley-Lieb generators as well, because of translational invariance (to be discussed in the next section):

$$\langle\{\mu\}|e_j|\{\lambda\}\rangle = (\text{phase})\langle\{-\lambda\}|e_j|\{-\mu\}\rangle. \quad (6.2.21)$$

This is in agreement with the result for the modules $\mathscr{W}_{0,\mathfrak{q}^{-2}}$ and $\mathscr{W}_{0,\mathfrak{q}^2}$ discussed in the end of Section 6.2.2. Of the previous examples mentioned, Table D.8 has exact results at finite size coming from the Temperley-Lieb structure.

6.3 Lattice Virasoro in the non-degenerate case

In this section we give a first example of the numerical results obtained in the XXZ spin-chain representation by the Bethe ansatz. We consider matrix elements of the Koo-Saleur generator

$\mathscr{L}_{-1}$ in the basis of Bethe states, in the non-degenerate case where neither α nor $\bar{\alpha}$ leads to a degenerate conformal weight $h_{r,s}$. We begin by some general considerations with regard to lattice momentum, which also carry over to the degenerate case.

6.3.1 Koo-Saleur generators and lattice momentum

Thanks to the smearing of the twist in (3.2.8) the Bethe states are invariant under the usual translation operator, and we can sort them by their (rescaled) lattice momentum $\mathscr{p} = 0, 1, \ldots, N-1$ defined in (6.2.4). We define the matrix $\boldsymbol{\mathscr{L}}_n[N]$ so that $(\boldsymbol{\mathscr{L}}_n[N])_{ab}$ is the matrix element $\langle a|\mathscr{L}_n[N]|b\rangle$ of the Koo-Saleur generator $\mathscr{L}_n[N]$ between two Bethe states at system size N. $\boldsymbol{\mathscr{L}}_n[N]$ can then be written as a block matrix, with the blocks indexed by values of $\mathscr{p}$. We now show how, thanks to the relations of the affine Temperley-Lieb algebra, only a few blocks of this matrix can have non-zero elements, namely the ones where the lattice momentum is shifted by precisely n between $|a\rangle$ and $|b\rangle$.

Recall that by (3.1.2) the generator of lattice translation u, fulfils $ue_ju^{-1} = e_{j+1}$. Meanwhile, when acting on a Bethe state $|v\rangle$ belonging to the sector of lattice momentum $\mathscr{p}$, the result is a phase $u|v\rangle = e^{i2\pi\mathscr{p}/N}|v\rangle$. Together these relations determine the behaviour of $\mathscr{L}_n|v\rangle$ under translation. Let us inspect the first part of the j'th term within the expression for $\mathscr{L}_n$ (3.7.3):

$$u\, e^{inj2\pi/N} e_j|v\rangle = e^{inj2\pi/N} e_{j+1} e^{i\mathscr{p}2\pi/N}|v\rangle = e^{i(\mathscr{p}-n)2\pi/N} e^{in(j+1)2\pi/N} e_{j+1}|v\rangle. \tag{6.3.1}$$

Up to a phase this is the corresponding part of the $(j+1)$'th term, which can be turned into the j'th by a relabelling of the indices within the sum. Applying the same procedure to the second part of the j'th term and summing over j yields in total

$$u\, \mathscr{L}_n|v\rangle = e^{i(\mathscr{p}-n)2\pi/N} \mathscr{L}_n|v\rangle, \tag{6.3.2}$$

i.e., we find that $\mathscr{L}_n|v\rangle$ is also a momentum eigenstate, and will therefore be orthogonal to any Bethe state with lattice momentum different than $\mathscr{p} - n$. In other words: already at finite size, the conformal spin must change by the proper integer value when we raise or lower a state using a Koo-Saleur generator.

The relations of the affine Temperley-Lieb algebra can also be used to speed up the numerics by computing only one term of the sum. Consider the blocks within which the matrix elements $(\boldsymbol{\mathscr{L}}_n[N])_{ab}$ may be non-zero, i.e., where the Bethe states fulfil $u|b\rangle = e^{i\mathscr{p}2\pi/N}|b\rangle$ and $u|a\rangle = e^{i(\mathscr{p}-n)2\pi/N}|a\rangle$, respectively. Let us write $\mathscr{L}_n[N]$ as $\sum_j f(e_j, e_{j+1})$. By (6.3.1) we can shift $f(e_j, e_{j+1})|b\rangle$ to $f(e_{j+1}, e_{j+2})|b\rangle$ by applying u, at the price of a phase. Considering the matrix element of a single term and inserting $\mathbf{1} = u^{-1}u$, we can let u^{-1} act to the left. The phases cancel:

$$\langle a|u^{-1}u\, f(e_j, e_{j+1})|b\rangle = e^{-i(\mathscr{p}-n)2\pi/N} e^{i(\mathscr{p}-n)2\pi/N} \langle a|f(e_{j+1}, e_{j+2})|b\rangle. \tag{6.3.3}$$

We thus see that all terms give the same contributions to the matrix elements within non-zero blocks of $\boldsymbol{\mathscr{L}}_n[N]$, and we can replace $\sum_j f(e_j, e_{j+1})$ by $N\, f(e_j, e_{j+1})$ in the numerical evaluations, gaining a factor N in speed.

6.3.2 Numerical results for $\mathscr{L}_{-1}$

We now show the first non-zero matrix elements of the matrix $\boldsymbol{\mathscr{L}}_{-1}[N]$ for increasingly large system size N and compare with the values we would expect from CFT computations. In this example we consider $S_z = 1, e = 0$ at $\phi = 1/10, x = \pi$. (Recall $\mathfrak{q} = e^{i\gamma} = e^{i\pi/(x+1)}$ and $e_\phi = \frac{\phi}{2\pi}$).

For non-zero matrix elements, the lattice momentum must shift by $p \to p - n = p + 1$ between the two Bethe states.

We shall consider the block between states in the momentum sectors $p = 0$ (denoted $|u_1\rangle, |u_2\rangle, \ldots$) and $p = 1$ (denoted $|v_1\rangle, |v_2\rangle, \ldots$). The set of Bethe integers for the lowest-energy state in the $p = 0$ sector, which we denote by $|u_1\rangle$, allows us to identify it with a primary state $V_{\alpha,\bar{\alpha}}$, which by (6.1.38) has a chiral charge $\alpha = -\frac{1}{40\pi}\alpha_+ + \alpha_0 - \frac{1}{2}\alpha_- = 0.56495148$. The other states we consider will be its descendants. At $N = 10$ we find the three lowest states in each sector, sorted by energy, for the following Bethe integers:[5]

$p = 0$:

$$\begin{aligned}
|u_1\rangle &\leftrightarrow \left\{-\frac{3}{2}, -\frac{1}{2}, \frac{1}{2}, \frac{3}{2}\right\} \leftrightarrow \circ\circ\bullet\bullet|\bullet\bullet\circ\circ \quad \leftrightarrow \quad \text{primary state } V_{\alpha,\bar{\alpha}} \\
|u_2\rangle &\leftrightarrow \left\{-\frac{5}{2}, -\frac{1}{2}, \frac{1}{2}, \frac{5}{2}\right\} \leftrightarrow \circ\bullet\circ\bullet|\bullet\circ\bullet\circ \quad \leftrightarrow \quad \text{chiral and anti-chiral level 1} \\
|u_3\rangle &\leftrightarrow \left\{-\frac{5}{2}, -\frac{3}{2}, \frac{3}{2}, \frac{5}{2}\right\} \leftrightarrow \circ\bullet\bullet\circ|\circ\bullet\bullet\circ \quad \leftrightarrow \quad \text{chiral and anti-chiral level 2}
\end{aligned} \tag{6.3.4}$$

$p = 1$:

$$\begin{aligned}
|v_1\rangle &\leftrightarrow \left\{-\frac{5}{2}, -\frac{1}{2}, \frac{1}{2}, \frac{3}{2}\right\} \leftrightarrow \circ\bullet\circ\bullet|\bullet\bullet\circ\circ \quad \leftrightarrow \quad \text{chiral level 1} \\
|v_2\rangle &\leftrightarrow \left\{-\frac{5}{2}, -\frac{3}{2}, \frac{1}{2}, \frac{5}{2}\right\} \leftrightarrow \circ\bullet\bullet\circ|\bullet\circ\bullet\circ \\
|v_3\rangle &\leftrightarrow \left\{-\frac{7}{2}, -\frac{1}{2}, \frac{1}{2}, \frac{5}{2}\right\} \leftrightarrow \bullet\circ\circ\bullet|\bullet\circ\bullet\circ
\end{aligned} \quad \leftrightarrow \quad \text{chiral level 2 and anti-chiral level 1} \tag{6.3.5}$$

These patterns extend to larger N by padding with filled circles in the middle. Taking the example of $|u_2\rangle$ we find $\circ\bullet\circ\bullet|\bullet\circ\bullet\circ \to \circ\bullet\circ\bullet\bullet|\bullet\bullet\circ\bullet\circ \to \circ\bullet\circ\bullet\bullet|\bullet\bullet\circ\bullet\circ \to \ldots$.

Recall the state space (6.1.44). Since there is only one state at level 1 we can immediately identify $|v_1\rangle$ with $a_{-1}V_{\alpha,\bar{\alpha}}$ and $|u_2\rangle$ with $a_{-1}\bar{a}_{-1}V_{\alpha,\bar{\alpha}}$. Meanwhile at level 2 there are two states, and the states $|v_2\rangle$ and $|v_3\rangle$ will correspond to an orthonormal basis for the two-dimensional vector space of $a_{-1}^2\bar{a}_{-1}V_{\alpha,\bar{\alpha}}$ and $a_{-2}\bar{a}_{-1}V_{\alpha,\bar{\alpha}}$. Finally $|u_3\rangle$ corresponds to one basis vector in an orthonormal basis for the four-dimensional vector space of states at chiral *and* anti-chiral level 2, the other three basis vectors being found by considering scaling states of higher energy.

Conjectures for the matrix elements:

- As in Section 6.1.4 we have $L_{-1}V_{\alpha,\bar{\alpha}} = \sqrt{2}\alpha a_{-1}V_{\alpha,\bar{\alpha}}$, leading to the conjectured value $\langle a_{-1}V_{\alpha,\bar{\alpha}}|L_{-1}|V_{\alpha,\bar{\alpha}}\rangle = \sqrt{2}\alpha = 0.79896205$ for the matrix element $(\mathscr{L}_{-1}[N])_{v_1,u_1}$ at $N \to \infty$. We can also find this value by considering the norm squared $\langle L_{-1}V_{\alpha,\bar{\alpha}}|L_{-1}V_{\alpha,\bar{\alpha}}\rangle = \langle V_{\alpha,\bar{\alpha}}|L_{-1}^\dagger L_{-1}V_{\alpha,\bar{\alpha}}\rangle$, where $L_{-1}^\dagger = L_1 + 2\sqrt{2}\alpha_0 a_1$ by (6.1.46). Using (6.1.43) and (6.1.45) we find $L_{-1}^\dagger L_{-1}V_{\alpha,\bar{\alpha}} = 2\alpha^2 V_{\alpha,\bar{\alpha}}$.[6]

[5] Here we see an example of half-integer "Bethe integers", since this is the maximally packed symmetric distribution around zero for four roots.

[6] In general, the calculations of this type that are seen in this chapter have been performed by adapting the Mathematica notebook "Virasoro" by M. Headrick, available at `http://people.brandeis.edu/~headrick/Mathematica/index.html`.

- The latter method carries over most easily to the next two matrix elements that we wish to consider: $(\mathscr{L}_{-1}[N])_{v_2,u_2}$ and $(\mathscr{L}_{-1}[N])_{v_3,u_2}$. We find the norm squared $\langle L_{-1}a_{-1}V_{\alpha,\bar{\alpha}}|L_{-1}a_{-1}V_{\alpha,\bar{\alpha}}\rangle = 2(1+2\alpha^2)$. Since $|v_2\rangle$ and $|v_3\rangle$ provide a basis, we expect to recover the full norm $\sqrt{2(1+2\alpha^2)} = 1.81016041$ by combining the projections on these states as $\sqrt{(\mathscr{L}_{-1}[N])^2_{v_2,u_2} + (\mathscr{L}_{-1}[N])^2_{v_3,u_2}}$ at $N \to \infty$.

- All other matrix elements among the states in (6.3.4) and (6.3.5) are conjectured to be zero in the limit, since the chiral levels do not match.

Using the form factors computed in Appendix C we can obtain the matrix elements $(\mathscr{L}_{-1}[N])_{v_iu_j}$ for increasingly large system size N. We then perform a polynomial extrapolation in $1/N$ to approximate the value at $N \to \infty$. This is shown in table 6.1 for $i = 1, j = 1$ and $i = 2, j = 1$.

N	$\langle v_1\|\mathscr{L}_{-1}\|u_1\rangle$	$\langle v_2\|\mathscr{L}_{-1}\|u_1\rangle$	⋮	⋮	⋮	⋮	⋮	⋮
10	0.73934396	0.01866525	36	0.79349714	0.00604396	62	0.79696357	0.00307821
12	0.75628984	0.0178073	38	0.79402136	0.00565977	64	0.79707638	0.00295725
14	0.76689996	0.01621625	40	0.79447152	0.00531584	66	0.79717949	0.00284442
16	0.77397144	0.01457925	42	0.79486106	0.00500654	68	0.79727401	0.00273896
18	0.77891781	0.01309015	44	0.79520048	0.0047272	70	0.79736087	0.00264022
20	0.78251286	0.01178876	46	0.79549811	0.0044739	72	0.79744089	0.0025476
22	0.78520823	0.01066614	48	0.79576061	0.00424336	74	0.79751479	0.00246056
24	0.7872816	0.00969992	50	0.79599334	0.00403281	76	0.79758317	0.00237865
26	0.78891124	0.00886622	52	0.7962007	0.00383989	78	0.79764659	0.00230144
28	0.79021581	0.00814359	54	0.79638628	0.00366257	80	0.79770552	0.00222856
30	0.79127676	0.0075138	56	0.79655307	0.00349914	p_{25}	0.79896913	$-4.846 \cdot 10^{-5}$
32	0.79215151	0.00696179	58	0.79670354	0.00334811	p_{30}	0.79896944	$-5.025 \cdot 10^{-5}$
34	0.79288148	0.00647521	60	0.79683979	0.00320817	p_{35}	0.79896858	$-4.558 \cdot 10^{-5}$
⋮	⋮	⋮	⋮	⋮	⋮	**conj**	0.79896205	0

Table 6.1: Matrix elements $(\mathscr{L}_{-1}[N])_{v_iu_j}$ for $i = 1, j = 1$ and $i = 2, j = 1$, where the scaling states $|u_j\rangle$ and $|v_i\rangle$ follow the patterns of Bethe integers shown in (6.3.4) and (6.3.5). The numerical values are given for the case of $S_z = 1, e = 0, x = \pi, \phi = 1/10$ for system size N up to 80, after which polynomial extrapolations $p_n(1/N)$ of degrees $n = 25, 30, 35$ to all the data points are made in order to approximate the value at $N \to \infty$.

The other seven matrix elements between the Bethe states listed above are found in the same fashion, and we do not write out the corresponding columns in Table 6.1. The results of the extrapolation p_{35} for all nine matrix elements are:

$$\mathscr{L}_{-1}[N] \xrightarrow[p_{35}]{N\to\infty} \begin{array}{c} \\ \\ \\ \\ \\ \end{array} \begin{array}{c} \text{𝓅} = 0 \\ \\ \\ \\ \\ \end{array} \begin{array}{c} \text{𝓅} = 1 \\ \\ \\ \\ \\ \end{array} \begin{array}{c} \dots \\ \\ \\ \\ \\ \end{array} \begin{pmatrix} 0 & 0 & \dots \\ \begin{bmatrix} 0.79896858 & -3.49 \cdot 10^{-6} & -5.407 \cdot 10^{-5} & \dots \\ -4.558 \cdot 10^{-5} & 1.80729191 & -2.66 \cdot 10^{-6} & \\ -1.722 \cdot 10^{-5} & 0.1039298 & 2 \cdot 10^{-8} & \\ \vdots & & & \ddots \end{bmatrix} & 0 & \\ \vdots & & \ddots \end{pmatrix} \begin{array}{l} \text{𝓅} = 0 \\ \\ \text{𝓅} = 1 \\ \\ \vdots \end{array} \tag{6.3.6}$$

We compare the extrapolation of $(\mathscr{L}_{-1})_{v_1,u_1}$ to the conjectured value of 0.79896205, and we compare the total contribution of the extrapolations of $(\mathscr{L}_{-1})_{v_2,u_2}$ and $(\mathscr{L}_{-1})_{v_3,u_2}$, which is $\sqrt{1.80729191^2 + 0.1039298^2} = 1.81027773$, to the conjectured value of 1.81016041. All other matrix elements are conjectured to be zero. We see that we overall obtain a precision of at least around 10^{-4} by considering system sizes up to $N = 80$.

We conclude this section with a note on the six matrix elements that are conjectured to be zero, whose values are small but non-zero at finite size. We shall call such matrix elements "parasitic couplings". They play an important role when considering products and commutators of Koo-Saleur generators. Consider a matrix element of the product of two Koo-Saleur generators, which can be decomposed into a sum over all Bethe states as $\langle a|\mathscr{L}_n\mathscr{L}_m|b\rangle = \sum_x \langle a|\mathscr{L}_n|x\rangle\langle x|\mathscr{L}_m|b\rangle$. Even if each parasitic coupling disappears in the limit $N \to \infty$, the *number* of parasitic couplings in the sum will grow rapidly, and may yield a finite contribution. Until this is further explored, one cannot assume that limits of products give the same results as products of limits. As a particular example, this non-interchangeability of limits applies when the products under consideration form a commutator of two generators. Indeed, the issue of limits and commutators was raised already in [12], where it was shown that the limit of commutators must sometimes differ from the commutators of limits. We shall return to this discussion in Section 6.5.

6.4 Lattice Virasoro in the degenerate case

In this section we turn to one of our main goals of this chapter: finding the precise nature of modules occurring in the XXZ spin chain representation in degenerate cases, possibly also with non-generic ϕ. Compared to the loop representation studied in Chapter 7 below, the XXZ spin chain representation allows for both standard and co-standard Temperley-Lieb modules at non-generic ϕ. The Virasoro modules in the limit may differ from those found in the loop representation both at generic and non-generic ϕ. Note that only the detailed structure of the representations is affected by the non-genericity and degeneracy: eigenvalues of the Hamiltonian and momentum —and thus values of the conformal weights—are perfectly regular at points where ϕ fulfils (3.1.4) or the conformal weights are degenerate (or, in fact, even when $\mathfrak{q}$ is a root of unity).

We here consider the modules where α (or $\bar{\alpha}$) is such that h (or $\bar{h}$) is degenerate. In this section we shall take $x = \pi$ as our type-example of $\mathfrak{q}$ generic, but we shall also show convergence of the central charge for a range of values $x \notin \mathbb{Q}$. Cases where $\mathfrak{q}$ is a root of unity will be considered in a future work [59].

We consider two types of situations where degenerate conformal weights appear: $j \neq 0$, $e^{i\phi} = 1$ and $j = 0$, $e^{i\phi} = \mathfrak{q}^{\pm 2}$. Note that for the latter, the resonance criterion $e^{i\phi} = \mathfrak{q}^{2j+2k}$—see (3.1.4)—is met, but not for the former.

6.4.1 Modules $\mathscr{W}_{j,1}$ for $j \neq 0$

While the modules $\mathscr{W}_{j,1}$ for $j \neq 0$ remain irreducible for generic $\mathfrak{q}$, the generating function of levels (see (6.1.8)) reads

$$F_{j,1} = \frac{q^{-c/24}\bar{q}^{-c/24}}{P(q)P(\bar{q})} \sum_{e\in\mathbb{Z}} q^{h_{e,-j}} \bar{q}^{h_{e,j}} \tag{6.4.1}$$

and involves degenerate values of the conformal weights. Let us first consider $S_z = j > 0$. As discussed in Section 6.2.2, the chiral weight h will be degenerate for $e < 0$, and the corresponding

module is conjectured to have the co-Verma structure

$$\widetilde{\mathsf{V}}^{(\mathrm{d})}_{e,-j}: \quad \begin{array}{c} \mathsf{X}_{e,-j} \\ \bullet \\ \uparrow \\ \circ \\ \mathsf{V}_{e,j} \end{array} . \tag{6.4.2}$$

Meanwhile the anti-chiral weight $\bar{h}$ will be degenerate for $e > 0$, and the corresponding module is conjectured to have the Verma structure

$$\mathsf{V}^{(\mathrm{d})}_{e,j}: \quad \begin{array}{c} \mathsf{X}_{e,j} \\ \circ \\ \downarrow \\ \bullet \\ \mathsf{V}_{e,-j} \end{array} . \tag{6.4.3}$$

For $S_z = -j < 0$ we find the same conjecture up to a switch of the chiral and anti-chiral sectors.

In Appendix D.1 we present the numerical results exploring the modules appearing in the scaling limit of $\mathscr{W}_{j,1}$ for $j = 1, 2$. The results are consistent with the conjectured correspondence between the charges in the Coulomb gas and the lattice parameters; see (6.1.38). Based on these results we claim that we have the general result:

XXZ spin-chain modules with non-zero magnetization: *For $j > 0$ we have the scaling limits*

$$S_z = j; \quad \mathscr{W}_{j,1} \mapsto \left(\bigoplus_{e>0} \mathsf{V}_{e,-j} \otimes \mathsf{V}^{(\mathrm{d})}_{e,j} \right) \oplus \left(\mathsf{V}_{0,-j} \otimes \mathsf{V}_{0,j} \right) \oplus \left(\bigoplus_{e<0} \widetilde{\mathsf{V}}^{(\mathrm{d})}_{e,-j} \otimes \mathsf{V}_{e,j} \right) , \tag{6.4.4a}$$

$$S_z = -j; \quad \mathscr{W}_{j,1} \mapsto \left(\bigoplus_{e>0} \mathsf{V}^{(\mathrm{d})}_{e,j} \otimes \mathsf{V}_{e,-j} \right) \oplus \left(\mathsf{V}_{0,j} \otimes \mathsf{V}_{0,-j} \right) \oplus \left(\bigoplus_{e<0} \mathsf{V}_{e,j} \otimes \widetilde{\mathsf{V}}^{(\mathrm{d})}_{e,-j} \right) . \tag{6.4.4b}$$

The concise notation means that, for $S_z = j > 0$, the states with conformal weights $(h_{e,-j}, h_{e,j})$ with $e < 0$ are annihilated by the combination of chiral Virasoro generators corresponding to the degenerate conformal weight $h_{e,j}$, while for $e > 0$ there appears a null state for the antichiral Virasoro algebra at level ej. Acting with the lowering operators $A_{e,-j}, \bar{A}_{e,j}$ on the primary state $V_{\alpha,\bar{\alpha}}(e, S_z)$ (with charges $\alpha(e, S_z), \bar{\alpha}(e, S_z)$ given by (6.1.38) for $e_\phi = 0$ and $S_z = \pm j$ as specified) we find

$$S_z = j > 0 \ : \ \begin{cases} \bar{A}_{e,j} V_{\alpha,\bar{\alpha}}(e, j) \neq 0 , & \text{for } e > 0 \quad (\bar{h} = h_{e,j}) , \\ A_{e,-j} V_{\alpha,\bar{\alpha}}(e, j) = 0 , & \text{for } e < 0 \quad (h = h_{e,-j} = h_{-e,j}) , \end{cases} \tag{6.4.5a}$$

while for negative S_z we have instead:

$$S_z = -j < 0 \ : \ \begin{cases} A_{e,j} V_{\alpha,\bar{\alpha}}(e, -j) \neq 0 , & \text{for } e > 0 \quad (h = h_{e,j}) , \\ \bar{A}_{e,-j} V_{\alpha,\bar{\alpha}}(e, -j) = 0 , & \text{for } e < 0 \quad (\bar{h} = h_{e,-j} = h_{-e,j}) . \end{cases} \tag{6.4.5b}$$

The converse holds when acting with the raising operators $A^\ddagger_{e,-j}, \bar{A}^\ddagger_{e,j}$ on the corresponding level $|ej|$ states, as in the example (6.1.49) shown in Section 6.1.4 for $|ej| = 1$.

We observe that $\mathscr{H}$ given by (2.1.8) is invariant under $\mathfrak{q} \to \mathfrak{q}^{-1}$ and $S_z \to -S_z$. It is also invariant under $\mathfrak{q} \to \mathfrak{q}^{-1}$ and parity $m \to N+1-m$ (where m denotes the lattice coordinate). Thus, we expect that the XXZ modules for S_z and $-S_z$ give rise to modules identical up to an exchange of the chiral and antichiral sectors, in agreement with this discussion.

6.4.2 Modules $\mathscr{W}_{0,\mathfrak{q}^{\pm 2}}$

We now switch to the modules $\mathscr{W}_{0,\mathfrak{q}^2}$ and $\mathscr{W}_{0,\mathfrak{q}^{-2}}$ as defined in (3.3.6). There will be several differences compared to the case of $\mathscr{W}_{j,1}$. First, the resonance criterion (3.1.4) is fulfilled. Second, due to having $S_z = 0$, the chiral and anti-chiral sectors will have same charges (6.1.38) and play the same role. Third, with $S_z = 0$ the lattice momentum (6.2.3) will change by $\Delta\mathscr{p} = \frac{N}{2}$ whenever the Bethe integers are shifted one step. Since the lattice momentum $\mathscr{p}$ is defined modulo the system size, as are the Bethe integers themselves, we cannot distinguish an electric excitation e from $-e$ and only the absolute value $|e|$ matters.

For the module $\mathscr{W}_{0,\mathfrak{q}^2}$ we have from (6.1.8)

$$\begin{aligned} F_{0,\mathfrak{q}^2} &= \frac{q^{-c/24}\bar{q}^{-c/24}}{P(q)P(\bar{q})} \sum_{n\in\mathbb{Z}} q^{h_{n+1/(x+1),0}} \bar{q}^{h_{n+1/(x+1),0}} \\ &= \frac{q^{-c/24}\bar{q}^{-c/24}}{P(q)P(\bar{q})} \sum_{n\in\mathbb{Z}} q^{h_{n,1}} \bar{q}^{h_{n,1}} \,. \end{aligned} \tag{6.4.6}$$

Note that the dual module $\mathscr{W}_{0,\mathfrak{q}^{-2}}$ leads to the same generating function of levels in the continuum limit. And yet, the nature of the Virasoro modules is profoundly different in both cases, in accordance with the discussion made in Section 6.2. We find the following result:

XXZ spin-chain modules with zero magnetization: *We have the scaling limits*

$$\mathscr{W}_{0,\mathfrak{q}^2} \mapsto \left(\bigoplus_{n>0} \widetilde{\mathsf{V}}^{(\mathrm{d})}_{n,1} \otimes \widetilde{\mathsf{V}}^{(\mathrm{d})}_{n,1} \right) \oplus \left(\mathsf{V}_{0,1} \otimes \mathsf{V}_{0,1} \right), \tag{6.4.7a}$$

$$\mathscr{W}_{0,\mathfrak{q}^{-2}} \mapsto \left(\bigoplus_{n>0} \mathsf{V}^{(\mathrm{d})}_{n,1} \otimes \mathsf{V}^{(\mathrm{d})}_{n,1} \right) \oplus \left(\mathsf{V}_{0,1} \otimes \mathsf{V}_{0,1} \right). \tag{6.4.7b}$$

Note that since we are in the $S_z = 0$ sector, we expect the problem to be symmetric under the exchange of chiral and antichiral sectors, in agreement with this conjecture.

We discuss numerical checks of this statement below, but it is (partly) a simple consequence of the structure of the Temperley-Lieb algebra modules themselves, since the $\mathscr{L}_n$ are made out of e_j. The numerical results in support of (6.4.7) are presented in Appendix D.2.

Having shown that the identity state $\mathbf{1}$ belongs to the module $\mathscr{W}_{0,\mathfrak{q}^2}$, we can also directly measure the central charge for various values of $x \notin \mathbb{Q}$, through a numerical study of the matrix element

$$\langle \mathbf{1} | \mathscr{L}_2 \mathscr{L}_{-2} | \mathbf{1} \rangle = \frac{c}{2} \,. \tag{6.4.8}$$

While the discussion has so far focussed on matrix elements of a single generator $\mathscr{L}_n$, we encounter here for the first time an example of matrix elements of a product of two generators. To follow up on the issue of "parasitic couplings"—briefly discussed at the end of Section 6.3.2—we employ two different methods to evaluate this matrix element. In the first (denoted "No

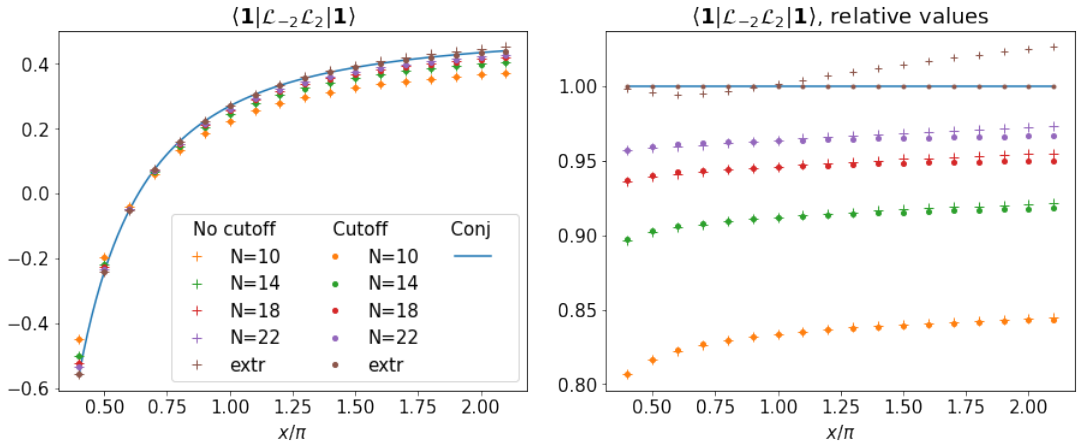

Figure 6.1: Finite-size estimates for the central charge c, obtained from (6.4.8) for various N, plotted against $\frac{x}{\pi}$. The left panel shows the actual estimates for c, and the right panel their ratio with respect to the CFT result ("Conj"). We display the results for $N = 10, 14, \ldots, 22$ obtained by two methods, "No cutoff" and "Cutoff", as explained in the main text. Also shown are extrapolations "extr" of the two data sets, obtained from a 7th-order polynomial fit to an extended set of sizes $N = 8, 10, \ldots, 22$.

cutoff" in the caption to Figure 6.1), we simply compute the total norm of (6.4.8), whereas in the second (denoted "Cutoff") we insert a projector onto a finite number of scaling states in-between the product of $\mathscr{L}_2$ and $\mathscr{L}_{-2}$ before computing the norm. We show in the left panel of Figure 6.1 how these finite-size estimates converge towards the conjectured CFT value $c = 1 - 24\alpha_0^2$, for x ranging from $4\pi/10$ to $21\pi/10$. We also display, in the right panel, the relative convergence, where we have divided through by the conjectured central charge. It is seen that although both methods give results close to the conjectured result, only the second one ("Cutoff") leads to full agreement over the whole range of x-values. The reason is that the first method ("No cutoff") suffers from parasitic couplings to non-scaling states. We defer the full discussion of this crucial phenomenon to Section 6.5.

6.5 Anomalies, and the convergence of the Koo-Saleur generators

The restriction to scaling states is crucial if one hopes to recover the Virasoro algebra relations (1.0.1) for the generators $\mathscr{L}_n$, obtained from the Temperley-Lieb algebra by the Koo-Saleur formulae (3.7.3). Otherwise—for instance—since the $\mathscr{L}_n$ act on a finite-dimensional Hilbert space for N finite, we would necessarily have that $\mathrm{Tr}\,[\mathscr{L}_n, \mathscr{L}_{-n}] = 0$ (by cyclicity of the trace), preventing the appearance of the central-charge "anomalous" term in (1.0.1). The procedure to correct this is well known [126] in free-field theory—e.g., for the Ising model or the free boson—and involves first restricting to excitations within a certain energy window, then calculating commutators, and finally taking the limit where the energy window goes to infinity.

In other words, the continuum limit of a commutator is not necessarily the commutator of the continuum limit. The difference between these two objects arises because of what we will call "parasitic couplings", that is, couplings that converge to zero as $N \to \infty$, but are non-zero at finite N. In computing, for instance, a matrix element such as (6.4.8) we encounter, in principle, an infinity of "unwanted terms" where L_{-2} acting on $|\mathbf{1}\rangle$ couples weakly to, in

particular, high-energy states, and L_2 in turn couples these states back to $\langle \mathbf{1}|$. While we expect each of these unwanted terms to vanish as $N \to \infty$, it is in principle possible that their sum builds up to a finite quantity [126, 127].

This phenomenon was already observed by Koo and Saleur (KS[7]) [12], whose observations are reproduced and generalized in Figure 6.1. We have already discussed the evaluation of the corresponding matrix element (6.4.8), by computing either full norms or projections (denoted "No cutoff" and "Cutoff" in the figure). Details about precisely how the projected results were obtained will be given below, in Section 6.5.1.

In KS (3.42) an analytical condition was given under which the central-charge term in (1.0.1) would be correctly produced for the $\mathscr{L}_n$ generators, despite of the possibility of parasitic couplings. This condition turns out to be satisfied precisely at the values $x = 1, 2, 3$, corresponding respectively to dense polymers, percolation and the Ising model. Close inspection of Figure 6.1 indeed reveals the perfect agreement between full norms and projections for $x = 1, 2, 3$ (note that $c = 0$ at $x = 2$)—however, the agreement is not exact in-between these integers, e.g., at $x = 2.5$.

Although the non-generic cases of x integer are not within the scope of the present thesis, we here make an exception to briefly comment on the fact that the exact results found in KS can be seen to match our knowledge about the affine TL modules $\overline{\mathscr{W}}_{0,\mathfrak{q}^{\pm 2}}$ at $x = 1, 2, 3$. For instance, at $x = 3$ we observe numerically that there is only one state V at the correct lattice momentum such that both $\langle V|e_i|\mathbf{1}\rangle$ and $\langle \mathbf{1}|e_i|V\rangle$ are non-zero, while at, e.g., $x = 4$ there are several. At x generic, the number of such states is observed to be equal to the dimension of the relevant momentum sector of $\overline{\mathscr{W}}_{0,\mathfrak{q}^{\pm 2}}$, as it should. A more clear-cut example occurs at $x = 2$ (i.e., $c = 0$), where the identity $|\mathbf{1}\rangle$ is the *only* state in the $[0, \mathfrak{q}^2]$ module (in that case, a simple Jones-Temperley-Lieb module of dimension 1), so there clearly is nothing at level 2 to couple to at all. As a consequence, the determination of c by the study of the matrix element (6.4.8) is exactly zero for any finite size N. Clearly there is much more to be said about these non-generic cases, and this will be the subject of a separate publication [59].

6.5.1 "Scaling-weak" convergence

The precise mathematical status of the convergence of the Koo-Saleur generators to the Virasoro generators is clearly a problem beyond the scope of this thesis. A very conservative statement, which we believe to hold true, is that 1) matrix elements of lattice Virasoro generators converge, when evaluated between scaling states, to their expected continuum limit and 2) matrix elements of *products* of lattice Virasoro generators converge, when evaluated between scaling states, to their expected continuum limit when the products are calculated using only such intermediate states which are scaling states, and using a double-limit procedure. While the meaning of statement 1) is obvious, the meaning of 2) will be explained in more detail below. We remind the reader that a sequence f_n in a Hilbert space is said to converge weakly to f, if the inner products $\langle f_n|g\rangle$ converge to $\langle f|g\rangle$ for all states g in the space. Accordingly we shall refer to the above phenomenon as **scaling-weak convergence**.[8] It is indeed a weak convergence, as the statement is only for matrix elements, but it is weaker than what is usually called weak convergence because of the restriction to scaling states, in particular in the intermediate states encountered when forming products of operators. In practice, this scaling-weak convergence can be implemented by the double limit procedure familiar to physicists, as discussed already in [12]. We can illustrate it more technically by writing some simple equations.

[7] We henceforth refer to equation (x.y) of Koo and Saleur [12] in the form KS (x.y).

[8] This is an example of what is sometimes called "conditioned weak convergence".

As we saw in Figure 6.1, computing $\langle \mathbf{1}|L_2L_{-2}|\mathbf{1}\rangle$ via the full norm ("No cutoff") of the matrix element does not quite give the conjectured result $\frac{c}{2}$. We can write

$$\langle \mathbf{1}|L_2L_{-2}|\mathbf{1}\rangle = \sum_{j=1}^{\mathcal{S}} \langle \mathbf{1}|L_2|v_{(j)}\rangle\langle v_{(j)}|L_{-2}|\mathbf{1}\rangle\,, \tag{6.5.1}$$

where $\mathcal{S}$ denotes the number of states (in the relevant momentum sector). We see that even if matrix elements of single Koo-Saleur generators converge towards those of the Virasoro generators, this does not guarantee weak convergence overall. As discussed at the end of Section 6.3.2, even if each parasitic matrix element $\langle v_{(j)}|L_{-2}|\mathbf{1}\rangle$ in (6.5.1) converges to zero as $N \to \infty$, the simultaneous rapid growth of $\mathcal{S}$ can destroy the convergence of the product of generators. To deal with this issue we can consider some fixed cutoff,

$$\sum_{j=1}^{\mathcal{S}_{\max}} \langle \mathbf{1}|L_2|v_{(j)}\rangle\langle v_{(j)}|L_{-2}|\mathbf{1}\rangle \tag{6.5.2}$$

(where the intermediate states are supposed to be conveniently ordered), sending the cutoff $\mathcal{S}_{\max} \to \infty$ *after* taking the scaling limit $N \to \infty$. The right-hand side of Figure 6.1 illustrates the most extreme cutoff, where we do not include any parasitic matrix elements at all, that is to say, "Cutoff" means that the intermediate states are just the $\mathcal{S}_{\max} = 2$ states existing at chiral level 2.

6.5.2 A closer look at limits and commutators

A priori, it looks like *any* product of Koo-Saleur generators might be strongly affected by parasitic couplings. We have, however, found serious evidence that only the central charge can come out wrong in calculations. In particular we shall in this section consider commutators, and our belief is that the scaling limit of Koo-Saleur commutators *is* the commutator of the scaling limit, *except for the anomalous central charge term*. This is probably expected on general grounds. After all, the Virasoro algebra is just a mode reformulation of the general stress-energy tensor OPE

$$T(z)T(w) = \frac{c}{2(z-w)^4} + \frac{2T(w)}{(z-w)^2} + \frac{\partial T}{z-w} + \text{reg.} \tag{6.5.3}$$

The second term is fixed by the dimension of $T(z)$, which—like for all conserved currents—is not renormalized, and the third one by consistency under the exchange $z \leftrightarrow w$. Only the first term is anomalous. Going back to the original paper by Koo and Saleur [12], there were some initial checks of how the limit of $[\mathscr{H}, \mathscr{P}]$ behaves. In this section we return to this question, exploring this kind of commutator in more detail. Our starting point is KS (3.30), which leads

to

$$\begin{aligned}[\mathscr{L}_{p+n}+\bar{\mathscr{L}}_{-p-n},\mathscr{L}_{-p}-\bar{\mathscr{L}}_{p}] &= 2\left(\frac{N}{2\pi}\right)^2\left(\frac{\gamma}{\pi\sin\gamma}\right)^3 \\ &\times\Bigg\{e^{2i\pi n/N}\sin\left(\frac{3\pi p+2\pi n}{N}\right)\sum_{j=1}^{N}e^{2i\pi nj/N}[e_j,[e_{j+1},e_{j+2}]] \\ &\quad+e^{2i\pi n(1/2)/N}\sin\left(\frac{\pi p+\pi n}{N}\right)\sum_{j=1}^{N}e^{2i\pi nj/N}\sqrt{Q}(e_je_{j+1}+e_{j+1}e_j) \\ &\quad-2\sin\left(\frac{\pi p}{N}\right)\sum_{j=1}^{N}e^{2i\pi nj/N}e_j\Bigg\}.\end{aligned} \tag{6.5.4}$$

If we could exchange freely limits and commutators, the fact that $\mathscr{L}_n \mapsto L_n$ (resp. $(\bar{\mathscr{L}}_n \mapsto \bar{L}_n$) would imply that the left-hand side of (6.5.4) converges to

$$\left[L_{p+n}+\bar{L}_{-p-n},L_{-p}-\bar{L}_p\right] = (2p+n)\left(L_n+\bar{L}_{-n}\right), \qquad \text{for } n\neq 0\,, \tag{6.5.5a}$$

$$\left[L_p+\bar{L}_{-p},L_{-p}-\bar{L}_p\right] = 2p\left(L_0+\bar{L}_0-\frac{c}{12}\right)+p^3\frac{c}{6}, \qquad \text{for } n=0\,. \tag{6.5.5b}$$

It is in fact known that (6.5.4) $\mapsto$ (6.5.5) when $x=1$ [128], or when $x=3$ if one restricts to the Ising subspace of the XXZ chain [12]. It is also known that (6.5.4) $\not\mapsto$ (6.5.5) for other values of x than these and the $x=2$ case (see KS (3.42)): our aim is to investigate in more detail what, exactly, fails.

General considerations

When studying the behaviour of (6.5.4) when acting on eigenstates of the lattice translation operator, it is convenient to first recall the discussion in Section 6.3.1, which yields two facts:

- Due to the relative phase $e^{2i\pi nj/N}$, matrix elements of (6.5.4) between two states are only non-zero when the lattice momentum $\not{p}$ of the states differs by precisely n.
- For such non-zero matrix elements, it suffices to evaluate a single summand, say at $j=0$; the matrix element corresponding to the entire sum is then obtained by multiplication with N.

We shall in the following use the word *term* to refer to the separate contributions for a single, fixed value of j. We note that any term that is constant will only contribute when considering matrix elements between a Bethe state and *itself*, since the Bethe states form an orthonormal basis. In particular, this means that whenever $n\neq 0$ we can omit any constant terms, which will allow us to drop normal ordering symbols in the next section.

We note that by the definition in (3.2.8) e_j will act on only two sites in the spin chain, and that the matrix elements are given by $\mathfrak{q}$ and $e^{i\phi/N}$—neither of which increases in norm as $N\to\infty$. As such, the matrix elements of a finite number of Temperley-Lieb generators can at most go towards a constant value as $N\to\infty$. We shall see that this occurs when matrix elements are between a state and itself—relevant for the $n=0$ case—while they otherwise decrease with N. The numerical results for matrix elements between various states will be shown for the generic example of $x=\pi$. Similar results were found for other generic and non-generic values of x. We shall consider matrix elements where the various operators act on either

the ground state or one of six low-energy scaling states of various types—electric excitation, magnetic excitation, creating a "hole", twisted boundary conditions, and combinations of these. (One of these six excited states is excluded from certain figures, where the matrix elements are exactly zero due to the indecomposability of $\mathscr{W}_{0,\mathfrak{q}^{\pm 2}}$.)

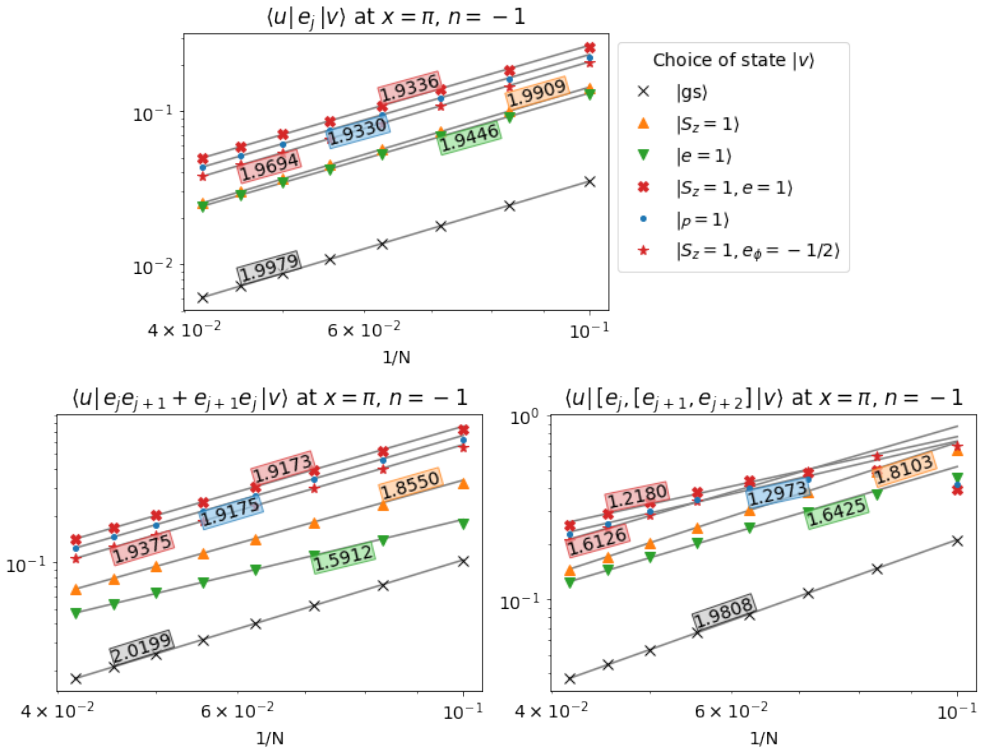

Figure 6.2: Absolute value of matrix elements, plotted with logarithmically scaled axes for sizes $N = 10, 12, \ldots, 24$. A linear fit is performed, excluding the lowest two sizes. The fit indicates that the matrix elements decay as $\mathcal{O}(1/N^r)$, where the estimated slope r is shown on each curve. The ground state $|\mathrm{gs}\rangle$ is given for the lattice parameters $S_z = e = e_\phi = \mathscr{p} = 0$. For the other choices of state $|v\rangle$ any non-zero lattice parameter is specified, with the others remaining zero. For each state $|v\rangle$ the state $|u\rangle$ corresponds to the same choice of lattice parameters up to a change in momentum sector, $\mathscr{p} \to \mathscr{p} + 1$. The lowest energy state for each choice of lattice parameters is used. The absolute values of the matrix elements are independent of j.

The case of $n \neq 0$

We now turn back to the comparison between (6.5.4) and (6.5.5). The first observation is that the right-hand-side of (6.5.4) contains trigonometric functions of $p/N, n/N$ while the right-hand side of (6.5.5) is linear in p, n. While this discrepancy could, by itself, explain why (6.5.4) $\not\mapsto$ (6.5.5), that is in fact not the case. Expanding the sinuses in powers of their arguments (at fixed p, n and with N large), it turns out that whenever $n \neq 0$ the terms in (6.5.4) that are subleading in the expansion fall off fast enough *separately* (this will not be the case at $n = 0$), compared to the leading term $(2p+n)\left\{2[e_j, [e_{j+1}, e_{j+2}]] + \sqrt{Q}(e_j e_{j+1} + e_{j+1} e_j)\right\}$. The leading term by itself goes as $\mathcal{O}(1/N^2)$ since the whole right-hand side of (6.5.4) is a term of $\mathcal{O}(1)$. Since the subleading terms come with prefactors $1/N^2, 1/N^4, \ldots$ relative to this leading term, it is enough that $[e_j, [e_{j+1}, e_{j+2}]]$, $(e_j e_{j+1} + e_{j+1} e_j)$ and e_j on their own have matrix elements that decay with N (i.e., being of order $\mathcal{O}(1/N^r)$ with $r > 0$). If they furthermore decay faster than $1/N$ ($r > 1$) we may also ignore the subleading terms in the expansion of

exponentials in n/N, so that we may put all phase factors on the same form. Numerical results indicate that this indeed holds: the case of $n = -1$ is shown in Figure 6.2, with slopes around $r = 2$, while the case of $n = -2$ is shown in Figure F.1 in Appendix F—here the finite size effects are larger, but the results still indicate $r > 1$. Keeping terms of leading order only, we have

$$[\mathscr{L}_{p+n} + \bar{\mathscr{L}}_{-p-n}, \mathscr{L}_{-p} - \bar{\mathscr{L}}_p] = \frac{N}{2\pi}\left(\frac{\gamma}{\pi \sin\gamma}\right)^3 \Bigg\{ (3p+2n) \sum_{j=1}^{N} e^{2i\pi n(j+1)/N} [e_j, [e_{j+1}, e_{j+2}]] + (p+n)\sqrt{Q} \sum_{j=1}^{2L} e^{2i\pi n(j+1)/N} (e_j e_{j+1} + e_{j+1} e_j) - 2p \sum_{j=1}^{N} e^{2i\pi n(j+1)/N} e_j \Bigg\} + \mathcal{O}\left(\frac{1}{N^{r-1}}\right). \tag{6.5.6}$$

We can now analyze the right-hand side by using a family of operators introduced in [12] as alternatives to the basic generators $\mathscr{L}, \bar{\mathscr{L}}$[9]. From the expression of what is denoted $\hat{h}^{(3)}$ in KS (2.54) and using the result KS (2.58)[10] we have that

$$\frac{N}{2\pi}\left(\frac{\gamma}{\pi \sin\gamma}\right)^3 \sum_{j=1}^{N} e^{2i\pi n(j+1)/N} \,{:}2[e_j, [e_{j+1}, e_{j+2}]] + \sqrt{Q}(e_j e_{j+1} + e_{j+1} e_j){:} \mapsto \left(L_n + \bar{L}_{-n} - \frac{c}{12}\delta_{n,0}\right), \tag{6.5.7}$$

where normal-order notation here means that the average in the ground state has been subtracted. As discussed at the beginning of this section, this normal ordering does not change the matrix elements when $n \neq 0$, and we shall use the left-hand side of (6.5.7) without normal ordering for the rest of this subsection.

Grouping by p and n and dividing through by $\frac{N}{2\pi}\left(\frac{\gamma}{\pi \sin\gamma}\right)^3$ we have from (6.5.6) the terms

$$2p\left[\frac{3}{2}\sum_{j=1}^{N} e^{2i\pi n(j+1)/N}[e_j, [e_{j+1}, e_{j+2}]] + \frac{\sqrt{Q}}{2}\sum_{j=1}^{N} e^{2i\pi n(j+1)/N} e_j e_{j+1} + e_{j+1} e_j - \sum_{j=1}^{N} e^{2i\pi n(j+1)/N} e_j\right] + n\left[2\sum_{j=1}^{N} e^{2i\pi n(j+1)/N}[e_j, [e_{j+1}, e_{j+2}]] + \sqrt{Q}\sum_{j=1}^{N} e^{2i\pi n(j+1)/N} e_j e_{j+1} + e_{j+1} e_j\right], \tag{6.5.8}$$

from which we subtract

$$2p\left[2\sum_{j=1}^{N} e^{2i\pi n(j+1)/N}[e_j, [e_{j+1}, e_{j+2}]] + \sqrt{Q}\sum_{j=1}^{N} e^{2i\pi n(j+1)/N} e_j e_{j+1} + e_{j+1} e_j\right] + n\left[2\sum_{j=1}^{N} e^{2i\pi n(j+1)/N}[e_j, [e_{j+1}, e_{j+2}]] + \sqrt{Q}\sum_{j=1}^{N} e^{2i\pi n(j+1)/N} e_j e_{j+1} + e_{j+1} e_j\right]. \tag{6.5.9}$$

[9] These alternatives were obtained by using the fact that all derivatives of the logarithm of the transfer matrix with respect to the spectral parameter u at $u = 0$ produce terms converging, in the weak-scaling sense, to the Hamiltonian and momentum of the associated CFT.

[10] Generalized to $n \neq 0$ in the same way as in KS (3.33).

We thus find, thanks to (6.5.7), that in the scaling limit $[\mathscr{L}_{p+n} + \bar{\mathscr{L}}_{-p-n}, \mathscr{L}_{-p} - \bar{\mathscr{L}}_{p}]$ behaves as $L_n + \bar{L}_{-n}$ (recall, $n \neq 0$ in this section) plus the following expression:

$$\frac{N}{2\pi}\left(\frac{\gamma}{\pi \sin\gamma}\right)^3 2p\Bigg[-\frac{1}{2}\sum_{j=1}^{N} e^{2i\pi n(j+1)/N}[e_j,[e_{j+1},e_{j+2}]] \\ -\frac{\sqrt{Q}}{2}\sum_{j=1}^{N} e^{2i\pi n(j+1)/N} e_j e_{j+1} + e_{j+1}e_j - \sum_{j=1}^{N} e^{2i\pi n(j+1)/N} e_j\Bigg]. \quad (6.5.10)$$

In order to have (6.5.4) $\mapsto$ (6.5.5) at $n \neq 0$, we need the matrix elements of (6.5.10) between any two relevant scaling states ($\Delta_{\mathscr{P}} = n$) to tend to zero with N. As discussed in the beginning of this section, it suffices to evaluate a single summand for a fixed value of j. For this reason we define the *remainder* $\mathscr{R}$ at $n \neq 0$ to be

$$\mathscr{R} = -[e_j,[e_{j+1},e_{j+2}]] - \sqrt{Q}(e_j e_{j+1} + e_{j+1}e_j) - 2e_j. \quad (6.5.11)$$

In order for the matrix elements of (6.5.10) between scaling states to tend to zero with N, we need that matrix elements of $\mathscr{R}$ be of $\mathcal{O}(1/N^r)$ for r strictly larger than 2. Results for $n = -1$ are shown in Figure 6.3, while results for $n = -2$ are shown in Figure F.2 in Appendix F. These two cases seem to have $r > 2$ indeed, which would indicate that the limit of the commutator is indeed the commutator of the limits for the states under consideration. Therefore, we have evidence for the following materialization of (6.5.5a):

Exchange of commutators and limits: *We have the conjecture*

$$[\mathscr{L}_{p+n} + \bar{\mathscr{L}}_{-p-n}, \mathscr{L}_{-p} - \bar{\mathscr{L}}_{p}] \mapsto (2p+n)(L_n + \bar{L}_{-n}), \quad \textit{for } n \neq 0. \quad (6.5.12)$$

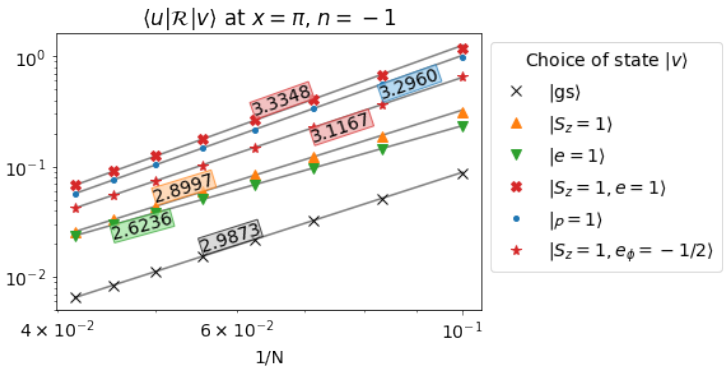

Figure 6.3: Absolute value of matrix elements of $\mathscr{R}$ as defined in (6.5.11), plotted using the same conventions as in Figure 6.2.

The case of $n = 0$

In the case of $n = 0$, however, we do *not* obtain the falloff for the individual terms seen in Figure 6.2. Indeed, to stand any chance of recovering the desired central-charge terms in (6.5.5b) we must have constant contributions. In Figure 6.4 we see that the matrix elements

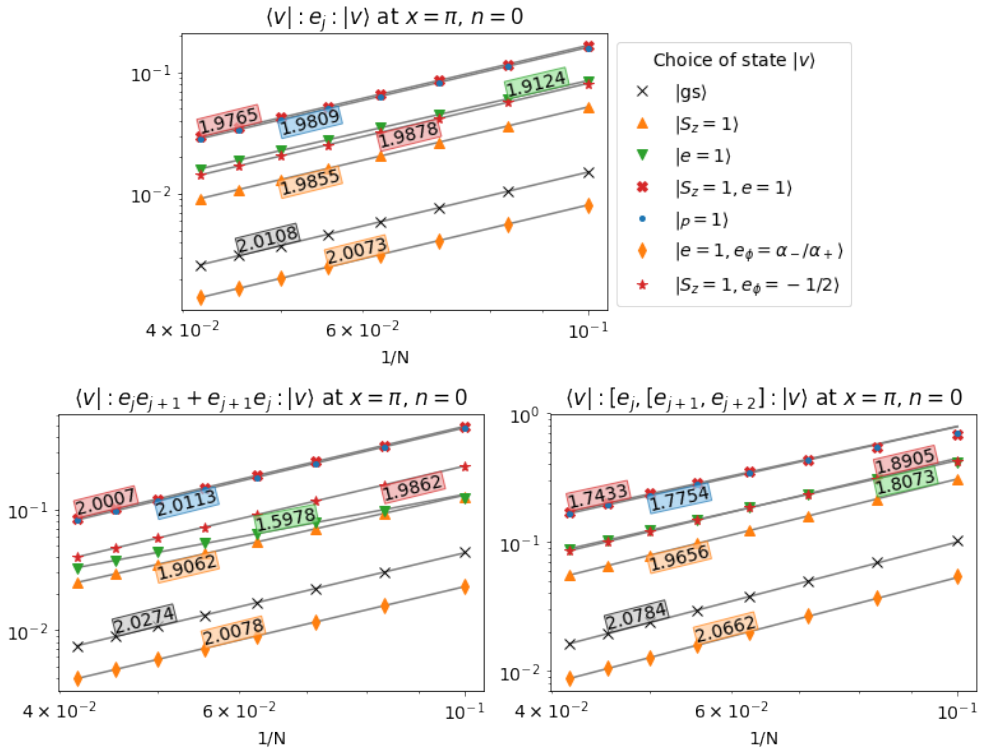

Figure 6.4: Absolute value of matrix elements, plotted using the same conventions as in Figure 6.2 but with the choice of $|u\rangle = |v\rangle$. The operators are here normal ordered: $:\mathcal{O}: \equiv O - O_\infty$ with O_∞ being the ground state expectation value as $N \to \infty$. This value is given for e_j in (3.2.3), and for $e_j e_{j+1} + e_{j+1} e_j$ and $[e_j, [e_{j+1}, e_{j+2}]]$ in (6.5.21).

of the individual terms between the ground state and itself indeed seem to stay constant as N increases, while they decrease as before between the ground state and the first excited state within the same momentum sector (see Figure F.3 in Appendix F).

While we must now consider both linear and cubic terms in the expansion of the sinuses, we can still ignore the quintic and higher terms. We also no longer need to expand any exponentials. This means that most of the derivation of $\mathscr{R}$ above is still valid, as long as we apply it to the *linear* term in n. There is only one modification we need to make, compared to (6.5.11): When $n = 0$ the normal ordering of (6.5.7) becomes important, and we need to subtract from $2[e_j, [e_{j+1}, e_{j+2}]] + \sqrt{Q}(e_j e_{j+1} + e_{j+1} e_j)$ its ground-state expectation value $4 \sin^3\gamma \, I_1$, where the constant I_1 follows from the Bethe ansatz [12]

$$I_1 = \int_{-\infty}^{\infty} t^2 \frac{\sinh(\pi - \gamma)t}{\sinh(\pi t)\cosh(\gamma t)} \, \mathrm{d}t \,. \tag{6.5.13}$$

Taking this into account we define the remainder at $n = 0$ as

$$\mathscr{R} = -[e_j, [e_{j+1}, e_{j+2}]] - \sqrt{Q}(e_j e_{j+1} + e_{j+1} e_j) - 2e_j + 8 \sin^3\gamma \, I_1 \,. \tag{6.5.14}$$

Including the cubic terms in the expansion of the trigonometric functions in (6.5.4) yields

$$\begin{aligned}[\mathscr{L}_p + \bar{\mathscr{L}}_{-p}, \mathscr{L}_{-p} - \bar{\mathscr{L}}_p] \\ = \frac{N}{2\pi}\left(\frac{\gamma}{\pi \sin\gamma}\right)^3 p \left\{3\sum_{j=1}^{N}[e_j,[e_{j+1},e_{j+2}]] + \sum_{j=1}^{N}\left(\sqrt{Q}(e_je_{j+1}+e_{j+1}e_j) - 2e_j\right)\right\} \\ - \frac{1}{12}\frac{\pi}{N}\left(\frac{\gamma}{\pi \sin\gamma}\right)^3 p^3 \left\{27\sum_{j=1}^{N}[e_j,[e_{j+1},e_{j+2}]] + \sum_{j=1}^{N}\left(\sqrt{Q}(e_je_{j+1}+e_{j+1}e_j) - 2e_j\right)\right\} \\ + \mathcal{O}\left(\frac{1}{N^2}\right).\end{aligned} \tag{6.5.15}$$

To see whether the term linear in p converges to the desired value we consider matrix elements of (6.5.14) numerically as shown in Figure 6.5, which indicates a falloff $\mathcal{O}(1/N^r)$ for $\langle gs|\mathscr{R}|gs\rangle$ with an exponent r around 4. We show similar figures for the first few excitations above the ground state in Appendix F. There the value of the slope r in the limit is more unclear due to larger finite-size effects, but the results still indicate $r > 2$ for these states.

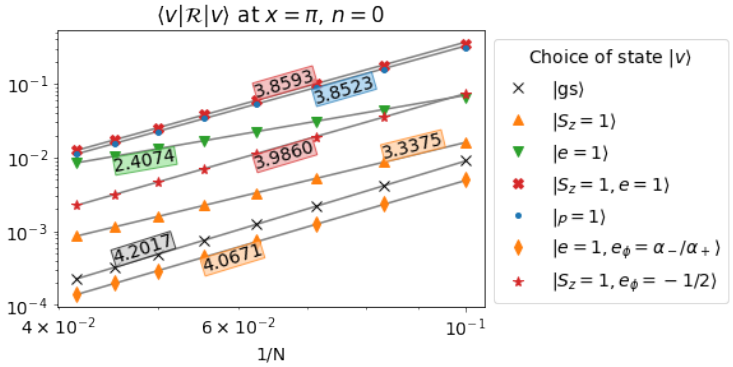

Figure 6.5: Absolute value of matrix elements of $\mathscr{R}$ as defined in (6.5.11), plotted using the same conventions as in Figure 6.2 but with the choice of $|u\rangle = |v\rangle$.

We now turn our attention to the term $\propto p^3$ in (6.5.15), which reads

$$-\frac{1}{12}\frac{\pi}{N}\left(\frac{\gamma}{\pi \sin\gamma}\right)^3 p^3 \left\{27\sum_{j=1}^{N}[e_j,[e_{j+1},e_{j+2}]] + \sum_{j=1}^{N}\left(\sqrt{Q}(e_je_{j+1}+e_{j+1}e_j) - 2e_j\right)\right\}, \tag{6.5.16}$$

and evaluate its average in the ground state. From our study of the $\propto p$ part of (6.5.15), we know already that the contribution from the terms $\mathscr{E}_p \equiv \langle gs|3[e_j,[e_{j+1},e_{j+2}]] + \sqrt{Q}(e_je_{j+1} + e_{j+1}e_j) - 2e_j|gs\rangle$ vanishes as $N \to \infty$. This leaves the contribution from $24[e_j,[e_{j+1},e_{j+2}]]$ in (6.5.16) and therefore, in order for (6.5.4 $\mapsto$ (6.5.5) also for $n = 0$, we would need the following miraculous identity to hold

$$\mathscr{E}_{p^3} \equiv [e_j,[e_{j+1},e_{j+2}]]_\infty + \frac{\pi^2 c}{12}\left(\frac{\sin\gamma}{\gamma}\right)^3 \stackrel{?}{=} 0\,, \tag{6.5.17a}$$

where we use the notation $[e_j,[e_{j+1},e_{j+2}]]_\infty = \lim_{N\to\infty}\langle gs|[e_j,[e_{j+1},e_{j+2}]]|gs\rangle$. Using results from the Bethe ansatz, it was shown in [12] (Section KS 3.3) that (6.5.17a) is equivalent to

$$c \stackrel{?}{=} c^*\,, \tag{6.5.17b}$$

where we have defined

$$c^* = -\frac{24\gamma^3 I_0}{\pi^2 \sin^2\gamma} + \frac{48\gamma^3}{\pi^2} I_1. \tag{6.5.18}$$

It was furthermore shown in [12] (Section KS 3.3) that (6.5.17) holds true indeed when $x = 1, 2, 3$, but not for general x. We conjecture that $\mathscr{E}_{p^3}$ will make up for the difference between the left- and right-hand side of criterion (6.5.17), that is precisely

$$\mathscr{E}_{p^3} = \frac{\pi^2}{12}\left(\frac{\sin\gamma}{\gamma}\right)^3 (c - c^*)\,. \tag{6.5.19}$$

The numerics indicate that this is true: the extrapolated values of $\mathscr{E}_{p^3}$ are shown for a range of x in Table 6.2. That is, the limit of (6.5.15) when applied to the ground state is incorrect only for the p^3 term, the one that contains the central charge.

$x = 1$:

N	$\mathscr{E}_{p^3}$
6	-0.09108037
8	-0.04173017
10	-0.02441356
12	-0.01616525
14	-0.01154442
16	-0.00867872
18	-0.00677235
20	-0.00543712
22	-0.00446415
24	-0.00373254
p_8	0.0000006
conj	0

$x = 1.5$:

N	$\mathscr{E}_{p^3}$
6	-0.18750921
8	-0.08790715
10	-0.05204436
12	-0.03471144
14	-0.0249148
16	-0.01880414
18	-0.01472315
20	-0.0118568
22	-0.00976384
24	-0.00818762
p_8	-0.00011095
conj	-0.00011266

$x = 2$:

N	$\mathscr{E}_{p^3}$
6	-0.26295146
8	-0.12396495
10	-0.07352658
12	-0.04905309
14	-0.03519046
16	-0.02653245
18	-0.02074547
20	-0.0166787
22	-0.01370811
24	-0.01147035
p_8	0.0000024
conj	0

$x = 2.5$:

N	$\mathscr{E}_{p^3}$
6	-0.3182588
8	-0.15047958
10	-0.08932876
12	-0.05959601
14	-0.04273623
16	-0.03220009
18	-0.0251554
20	-0.02020382
22	-0.01658653
24	-0.01386144
p_8	0.00010867
conj	0.00010568

$x = 3$:

N	$\mathscr{E}_{p^3}$
6	-0.3587194
8	-0.1700361
10	-0.10107585
12	-0.06750028
14	-0.04844759
16	-0.03653616
18	-0.02857005
20	-0.02297004
22	-0.01887873
24	-0.01579641
p_8	0.00000334
conj	0

$x = 4$:

N	$\mathscr{E}_{p^3}$
6	-0.41165366
8	-0.19603869
10	-0.11698482
12	-0.07843206
14	-0.05653502
16	-0.04283788
18	-0.03367441
20	-0.0272313
22	-0.02252338
24	-0.01897619
p_8	-0.00079389
conj	-0.00079737

$x = 6$:

N	$\mathscr{E}_{p^3}$
6	-0.46366442
8	-0.22244484
10	-0.13377148
12	-0.09046753
14	-0.06585191
16	-0.05044634
18	-0.04013642
20	-0.0328855
22	-0.02758643
24	-0.02359336
p_8	-0.00312128
conj	-0.00312477

$x = 10\pi$:

N	$\mathscr{E}_{p^3}$
6	-0.52432884
8	-0.25560287
10	-0.15658134
12	-0.10816223
14	-0.08061811
16	-0.06337137
18	-0.05182545
20	-0.04370333
22	-0.03776655
24	-0.03329234
p_8	-0.01034513
conj	-0.01034891

Table 6.2: Comparison of the numerical measures for $\mathscr{E}_{p^3}$, defined in (6.5.17a), and its conjectured value which is the right-hand side of (6.5.19). The agreement between the extrapolated values and the conjecture is seen to be excellent, with a precision of the order 10^{-6} for all values of x. The same conventions as in Table 6.1 are used for the extrapolated values p_8.

$\mathscr{E}_{p^3}$ satisfying the conjecture (6.5.19) is equivalent to the ground-state expectation value of

$[e_j, [e_{j+1}, e_{j+2}]]$ being equal to $2\sin\gamma I_0 - 4\sin^3\gamma I_1$. Combining this with the result KS (3.41)

$$[e_j, [e_{j+1}, e_{j+2}]]_\infty + \frac{\sqrt{Q}}{2}(e_j e_{j+1} + e_{j+1}e_j)_\infty = 2\sin^3\gamma\, I_1\,. \tag{6.5.20}$$

we can improve (6.5.20) by conjecturing the values of each of its terms separately:

Exchange of commutators and limits: *We have the results*

$$[e_j, [e_{j+1}, e_{j+2}]]_\infty = 2\sin\gamma\, I_0 - 4\sin^3\gamma\, I_1\,, \tag{6.5.21a}$$

$$(e_j e_{j+1} + e_{j+1}e_j)_\infty = \frac{6\sin^3\gamma\, I_1 - 2\sin\gamma\, I_0}{\cos\gamma}\,, \tag{6.5.21b}$$

where the integral I_0 is defined by (3.2.4) *and I_1 by* (6.5.13).

In Appendix E we prove these conjectures (so they are actually theorems), by using known ground state expectation values of spin operators in the XXZ spin chain [129]. In Appendix E.1 we consider the limit $\gamma \to 0$ corresponding to $x \to \infty$, showing that the integrals in (6.5.21) take the form of polylogarithms in agreement with the known results for ground state expectation values of spin operators in the XXX spin chain [130]. We note that the limit $\gamma \to 0$ is where the theory is the most interacting, and where the anomaly is the largest ($c = 1$). Solving the integrals within (6.5.19) numerically for increasingly large finite values of x indicates that $\mathscr{E}_{p^3}$ converges towards its limit of $\mathscr{E}_{p^3}(x)\big|_{x\to\infty} = -0.011\,114\,954\cdots$ from above, meaning that the magnitude of $\mathscr{E}_{p^3}$ is the largest in this limit. We also see that the effect of parasitic couplings in Figure 6.1 is the most pronounced at large x.

We next turn to the first few excited states. To have the same deviation for the central term we would need the matrix elements $\langle v|[e_j, [e_{j+1}, e_{j+2}]]|v\rangle$, for $|v\rangle$ any scaling state, to go towards the same value as for the ground state—that is, we need $\langle v|\ {:}[e_j, [e_{j+1}, e_{j+2}]]{:}\ |v\rangle$ to go to zero. This matrix element is shown in Figure 6.4, where the conjectured ground state expectation value in (6.5.21) is used for the normal ordering. We see that it indeed tends to zero as $N \to \infty$ for all scaling states under consideration, which indicates that the central term is wrong by a *constant* term, rather than by an operator. This constant deviation corresponds precisely to replacing c, as given by (3.5.4), by the slightly different value c^* given in (6.5.18) in the cubic term $\propto p^3$. Altogether we have:

Exchange of commutators and limits: *We have the conjecture*

$$[\mathscr{L}_p + \bar{\mathscr{L}}_{-p}, \mathscr{L}_{-p} - \bar{\mathscr{L}}_p] \mapsto 2p\left(L_0 + \bar{L}_0 - \frac{c}{12}\right) + p^3\frac{c^*}{6} \tag{6.5.22}$$

with c given by (3.5.4) *and c^* given by* (6.5.18).

Having shown by the combination of (6.5.12) and (6.5.22) that $[\mathscr{L}_{p+n} + \bar{\mathscr{L}}_{-p-n}, \mathscr{L}_{-p} - \bar{\mathscr{L}}_p]$ is conjectured to have the correct limit up to the central term, it is natural to ask if we can eliminate the chiral-antichiral "cross-terms" and write the relation for the limit of $[\mathscr{L}_{p+n}, \mathscr{L}_{-p}]$ on its own. In other words: is the limit of the chiral-antichiral commutator $[\mathscr{L}_{p+n}, \bar{\mathscr{L}}_p]$ zero? In Appendix G we explore this question using the same methodology as in this section, and show that numerical evidence indeed indicates that the chiral-antichiral commutator vanishes in the

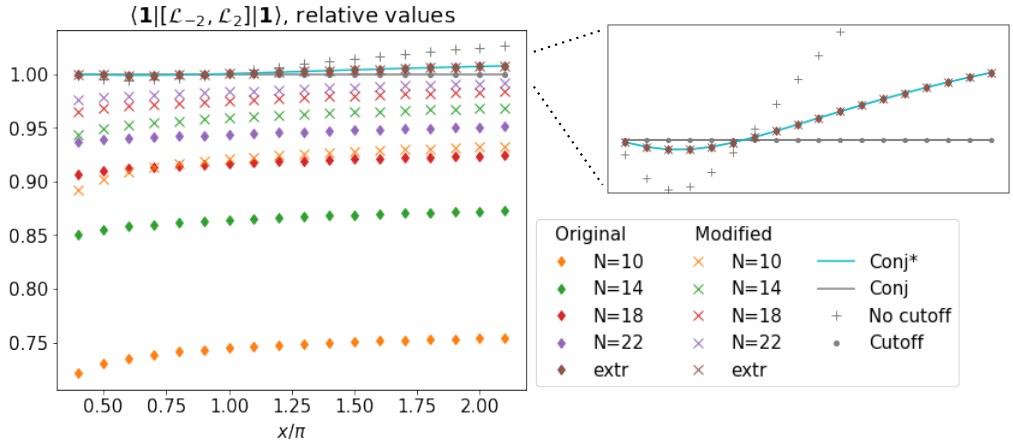

Figure 6.6: Remake of Figure 6.1. In this remake the commutator $[\mathscr{L}_{-2}, \mathscr{L}_2]$ is used, rather than the product $\mathscr{L}_{-2}\mathscr{L}_2$, and no cutoff is taken. This commutator is denoted "Original". We also show the result using a modified version of the Koo-Saleur generators given by (6.5.25), labelled "Modified". "Conj*" refers to the result found by applying (6.5.24), while "Conj" refers to the CFT result as in Figure 6.1. The same sizes N and method of extrapolation is used as in Figure 6.1, and the extrapolated values from Figure 6.1 are shown for comparison ("No cutoff" and "Cutoff").

limit:

Exchange of commutators and limits: *We have the conjecture*

$$[\mathscr{L}_{p+n}, \bar{\mathscr{L}}_p] \mapsto 0. \tag{6.5.23}$$

Combining the three conjectures (6.5.12), (6.5.22) and (6.5.23) we thus obtain in the scaling limit a modification of the Virasoro commutation relations (1.0.1) on the form

$$[\mathscr{L}_m, \mathscr{L}_n] = (m-n)\mathscr{L}_{m+n} + \delta_{m+n,0}\frac{1}{12}(m^3c^* - mc)\,. \tag{6.5.24}$$

We can remake Figure 6.1 using this new conjecture. This is done in Figure 6.6, where it is shown that the effect of the "parasitic couplings" is in agreement with (6.5.24). We stress that this conjecture applies for the *commutator* $[\mathscr{L}_2, \mathscr{L}_{-2}]$ and not for the product $\mathscr{L}_2\mathscr{L}_{-2}$ alone, as is seen in the figure. We conclude that the limit of commutators is the same as the commutator of limits up to a modification of the central term.

In Figure 6.6 we also show the modification recently suggested by Shokrian-Zini and Wang in [131] (Conjecture 5.5), which amounts to changing the phases within the Koo-Saleur generators (3.7.3) to

$$\begin{aligned}
\mathscr{L}_n[N] &= \frac{N}{4\pi}\left[-\frac{\gamma}{\pi\sin\gamma}\sum_{j=1}^{N} e^{in(j+1/2)2\pi/N}\,(e_j - e_\infty) + e^{in(j+1)2\pi/N}\frac{i\gamma}{\pi\sin\gamma}[e_j, e_{j+1}]\right] + \frac{c}{24}\delta_{n,0}\,,\\
\bar{\mathscr{L}}_n[N] &= \frac{N}{4\pi}\left[-\frac{\gamma}{\pi\sin\gamma}\sum_{j=1}^{N} e^{-in(j+1/2)2\pi/N}\,(e_j - e_\infty) - e^{-in(j+1)2\pi/N}\frac{i\gamma}{\pi\sin\gamma}[e_j, e_{j+1}]\right] + \frac{c}{24}\delta_{n,0}\,.
\end{aligned} \tag{6.5.25}$$

We find that while the numerical values show a faster convergence, the change of the central term is the same as with the original Koo-Saleur generators. That the central term must behave in the same way indeed follows directly from the calculations and numerical evidence above, where we in particular find that we may shift the phase by a finite amount without affecting the limit.

Although the relation in (6.5.24) is no longer the expected relation of the Virasoro algebra at central charge c, the Jacobi identity would nevertheless be satisfied:

$$\begin{aligned}
&[\mathscr{L}_m,[\mathscr{L}_n,\mathscr{L}_p]]+[\mathscr{L}_n,[\mathscr{L}_p,\mathscr{L}_m]]+[\mathscr{L}_p,[\mathscr{L}_m,\mathscr{L}_n]]\\
&\qquad=(n-p)[\mathscr{L}_m,\mathscr{L}_{n+p}]+(p-m)[\mathscr{L}_n,\mathscr{L}_{p+m}]+(m-n)[\mathscr{L}_p,\mathscr{L}_{m+n}]\\
&\qquad=\delta_{m+n+p,0}\frac{1}{12}\Big\{(n-p)(m^3c^*-mc)+(p-m)(n^3c^*-nc)+(m-n)(p^3c^*-pc)\Big\}\\
&\qquad=0\,.
\end{aligned}\tag{6.5.26}$$

Here, the first equality follows from the fact that all $\mathscr{L}_{m+n+p}$ terms cancel; the second equality is the application of (6.5.24); and to establish the third equality, note all terms proportional to c inside the parenthesis cancel out for any values of m,n,p, while those proportional to c^* cancel because of the constraint $p=-m-n$. We could indeed redefine the generators $\mathscr{L}_0,\bar{\mathscr{L}}_0$ to obtain from (6.5.24) the relation of the Virasoro algebra at central charge c^*. This would, however, not resolve the underlying difference between limits of commutators and commutators of limits.

This section concludes Chapter 6, in which we have explored Virasoro representations in the six-vertex model. We next turn to the Potts and loop models.

CHAPTER

7

VIRASORO REPRESENTATIONS IN POTTS AND LOOP MODELS

In this chapter, we turn our attention from the critical six-vertex model to the critical Q-state Potts model for Q generic (and its cousins, the critical and dense $O(n)$ models). The full solution of the continuum limit conformal field theory has long remained elusive.

While most critical exponents of interest were quickly determined (for some, even before the advent of CFT, using Coulomb-gas techniques) [47, 78, 132], the non-rationality of the theory (for Q generic) as well as its non-unitarity (inherited from the geometrical nature of the lattice model) made further progress using "top-down" approaches (such as the one used for minimal unitary models [133]) considerably more difficult. Several breakthroughs took place, however, in the last decade. First, many three-point functions were determined using connections with Liouville theory at $c < 1$ [102, 134, 135]. Second, a series of attempts using conformal bootstrap ideas (see Chapter 4 and [19–21, 74, 136]) led to the determination of some of the most fundamental four-point functions in the problem (namely, those defined geometrically, and hence for generic Q), also shedding light on the operator product expansion (OPE) algebra and the relevance of the partition functions determined in [43]. In particular, the set of operators—the so-called spectrum—required to describe the partition function [43] and correlation functions [20] in the Potts-model CFT was settled. While the picture remains incomplete, a complete solution of the problem now appears within reach.

An intriguing aspect of the spectrum proposed in [20, 43] is the appearance of fields with conformal weights given by the Kac formula $\Delta = h_{r,s}$, with $r, s \in \mathbb{N}^*$ (we call these "degenerate" weights). It is known that for some of these fields—such as the energy operator with weights $(h_{2,1}, h_{2,1})$—the null-state descendants are truly zero, and the corresponding four-point functions obey the Belavin–Polyakov–Zamolodchikov (BPZ) differential equations [5]. It is also expected that this does not hold for *all* fields with degenerate weights. In fact, it was suggested in [20, 21] that, in the Potts-model case, *only* fields with weights $(h_{r,1}, h_{r,1})$ give rise to null descendants. Since the spectrum of the model is expected to contain non-diagonal fields with weights $(h_{r,s}, h_{r,-s})$ and $(h_{r,-s}, h_{r,s})$ for $r, s \in \mathbb{N}^*$, this means that the theory should contain

fields with degenerate (left or right) weights whose null descendants are nonzero, even though their two-point function vanishes. It is well understood since the work of Gurarie [68] that in this case, "logarithmic partners" must be invoked to compensate for the corresponding divergences occurring in the OPEs. Such partners give rise to Jordan cells for L_0 or $\bar{L}_0$, and make the theory a logarithmic CFT—i.e., a theory where the action of the product of left and right Virasoro algebras $\mathrm{Vir} \otimes \overline{\mathrm{Vir}}$ is not fully reducible. This, in turn, is made possible by the theory not being unitary in the first place. (For further discussion on non-unitarity and logarithmicity, see Section 3.5 and e.g. [137].)

A great deal of our understanding of the fields with degenerate weights in the Potts model comes from indirect arguments, such as the solution of the bootstrap equations for correlation functions and the presence of an underlying "interchiral" algebra, responsible for relations between some of the conformal-block amplitudes [21]. In this chapter we explore this issue much more directly using the Koo-Saleur generators.

The chapter is organized as follows. In Section 7.1 we start by recalling some relevant facts about the two-dimensional Potts model and its CFT. In Section 7.3 we recall the general strategy to study the action of $\mathrm{Vir} \otimes \overline{\mathrm{Vir}}$ starting from the lattice model. New results then appear in Section 7.4 where we argue, based on several lattice arguments, for the existence of indecomposable modules of $\mathrm{Vir} \otimes \overline{\mathrm{Vir}}$ in the continuum limit of the Potts model for Q generic. Our main results are given in equations (7.4.3), (7.4.12), and (7.4.11). In Section 7.5 we present a CFT argument in which we analyze the OPE of two copies of a generic field Φ_Δ, which we suppose to produce a field X_ϵ that tends to $\phi_{1,2}$ when $\epsilon \to 0$. Regularizing the divergences of this OPE leads to the same indecomposable structure (7.4.11) as before and allows us to compute the corresponding indecomposability parameters. We note that some of these our results overlap with the recent work [6]. In Section 7.6 we consider the particular case where Φ_Δ is the Potts-model order parameter $\phi_{1/2,0}$. We first give two different CFT derivations of the corresponding logarithmic conformal block. Then we go back to the lattice Potts model and provide numerical evidence that the indecomposable structure (7.4.11) builds up when the continuum limit is approached, although in this case there is no indecomposability in finite size. To round off the paper, we briefly discuss in Section 7.7 the cognate "ordinary" loop model with $U(\mathfrak{m})$ symmetry and comment on the relation with recent results by Gorbenko and Zan [138] on the dilute $O(n)$ model. Two appendices provide details on our numerical work which is referred to throughout the article. Details on our numerical work are given in Appendices H and I.

7.1 The Q-state Potts model and its CFT

We consider the Q-state Potts model and its definition for Q non-integer using the Fortuin–Kasteleyn (FK) expansion, as reviewed in Chapter 2. A special point must be made in connection with the present chapter: there is sometimes a confusion related with the type of object one may wish to consider as part of "the" Potts model CFT. By such a CFT we shall mean here the field theory describing long-distance properties of observables which are built locally in terms of Potts spins for Q integer, then continued to Q real using the FK expansion. Examples include the spins themselves but also the energy and, of course, many more observables as discussed, for instance, in [139–141]. Other objects have been defined and studied in the literature, in particular those describing the properties of domain walls, boundaries of domains where the Potts spins take identical values [142, 143]. These are not local with respect to the

Potts spin variables, and we will not consider them further in this chapter.[1]

To have a better idea of the observables pertaining to the Potts model CFT for Q generic, one can start with the torus partition function, which was determined in the continuum limit in [43] and [63, 145]. Parametrizing[2]

$$\sqrt{Q} = 2\cos\left(\frac{\pi}{x+1}\right), \quad \text{with } x \in (0,\infty], \tag{7.1.1}$$

we recall the central charge (3.5.4) and the Kac table parametrization of the conformal weights (3.5.3). The continuum-limit partition function is then given by

$$\mathscr{Z}_Q = F_{0,\mathfrak{q}^{\pm 2}} + \frac{Q-1}{2}F_{0,-1} + \sum_{j>0}\hat{D}'_{j,0}F_{j,1} + \sum_{\substack{j>0, M>1\\ M|j}}\sum_{\substack{0<p<M\\ p\wedge M=1}}\hat{D}'_{j,\pi p/M}F_{j,\mathrm{e}^{2\pi i p/M}}\,. \tag{7.1.2}$$

As mentioned in Chapter 3, the coefficients $\hat{D}'_{j,K}$ can be thought of as "multiplicities," although of course, for Q generic, they are not integers. Their interpretation in terms of symmetries will play an important role in Chapter 8, see also [58]. They are given by

$$\hat{D}'_{j,K} = \frac{1}{j}\sum_{r=0}^{j-1}\mathrm{e}^{2\imath K r}w(j, j\wedge r)\,, \tag{7.1.3}$$

where $j\wedge r$ is the greatest common divisor of j and r (with $j\wedge 0 = j$ by definition), and

$$w(j,d) = \mathfrak{q}^{2d} + \mathfrak{q}^{-2d} + \frac{Q-1}{2}(i^{2d}+i^{-2d}) = \mathfrak{q}^{2d} + \mathfrak{q}^{-2d} + (Q-1)(-1)^d\,, \tag{7.1.4}$$

where the quantum group parameter $\mathfrak{q}$ (see Section 3.4) is defined via

$$\sqrt{Q} = \mathfrak{q} + \mathfrak{q}^{-1}\,. \tag{7.1.5}$$

The $F_{j,\mathrm{e}^{i\phi}}$ are defined in (6.1.8), and we recall them here for convenience:

$$F_{j,\mathrm{e}^{i\phi}} = \frac{q^{-c/24}\bar{q}^{-c/24}}{P(q)P(\bar{q})}\sum_{e\in\mathbb{Z}} q^{h_{e-e_\phi,-j}}\bar{q}^{h_{e-e_\phi,j}}\,. \tag{7.1.6}$$

As usual, $q, \bar{q}$ are the modular parameters of the torus.

Expressions (7.1.2) and (7.1.6) encode the operator content of the Q-state Potts model CFT as defined earlier. The conformal weights arising from the last term in (7.1.2) are of the form

$$(h_{e-p/M,j}, h_{e-p/M,-j}), \quad \text{with } e\in\mathbb{Z}\,. \tag{7.1.7}$$

The first two terms must be handled slightly differently. Using the identity

$$F_{0,\mathfrak{q}^{\pm 2}} - F_{1,1} = \sum_{n=1}^{\infty} K_{n,1}\bar{K}_{n,1} \equiv \bar{F}_{0,\mathfrak{q}^{\pm 2}} \tag{7.1.8}$$

[1] Whether there is a "bigger" CFT containing *all* these observables at once remains an open question—see [144] for an attempt in this direction.

[2] The values $x \in (0,1)$ correspond to the so-called unphysical self-dual case discussed in [146]. Note the negative determination of the square root $\sqrt{Q}$ in this case. There is no change of analytic behavior of the results for generic values $x \in (0,\infty]$.

with the Kac character

$$K_{r,s} = q^{h_{r,s}-c/24}\,\frac{1-q^{rs}}{P(q)}\,, \tag{7.1.9}$$

we see that we get the set of diagonal fields

$$(h_{n,1}, h_{n,1})\,, \quad \text{with } n \in \mathbb{N}^*\,. \tag{7.1.10}$$

The partition function can then be rewritten as

$$\mathcal{Z}_Q = \bar{F}_{0,\mathfrak{q}^{\pm 2}} + \frac{Q-1}{2}F_{0,-1} + F_{1,1} + \sum_{j>0}\hat{D}'_{j,0}F_{j,1} + \sum_{\substack{j>0, M>1\\ M|j}}\sum_{\substack{0<p<M\\ p\wedge M=1}}\hat{D}'_{j,\pi p/M}F_{j,\mathrm{e}^{2\pi i p/M}}\,. \tag{7.1.11}$$

We notice now that $\hat{D}'_{1,0} = \mathfrak{q}^2 + \mathfrak{q}^{-2} - (Q-1) = Q - 2 - (Q-1) = -1$. Hence $F_{1,1}$ disappears, in fact, from the partition function. Note that $F_{1,1}$ corresponds geometrically to the so-called hull operator [147]—related to the indicator function that a point is at the boundary of an FK cluster—with corresponding conformal weights $(h_{0,1}, h_{0,1})$. It should probably not come as a surprise that this operator is absent from the partition function, since the definition of the hull is not local with respect to the Potts spins. We will, nevertheless, consider $\mathscr{W}_{1,1}$ throughout this chapter, since this module *does* appear in related models, such as the "ordinary" loop model or the "$U(\mathfrak{m})$" model, to be discussed in Section 7.7 below. We note meanwhile that the higher hull operators—related to the indicator function that $j > 1$ distinct hulls come close together at the scale of the lattice spacing—with conformal weights $(h_{0,j}, h_{0,j})$ in $F_{j,1}$ do appear in the partition function, also in the Potts case.

The decomposition (7.1.2) of the Potts-model partition function for generic Q is in fact in one-to-one correspondence with an algebraic decomposition of the Hilbert space $\mathscr{H}_Q$ in terms of modules of the affine Temperley–Lieb algebra which is exact in finite size [148]. This decomposition formally reads

$$\mathscr{H}_Q = \overline{\mathscr{W}}_{0,\mathfrak{q}^{\pm 2}} \oplus \frac{Q-1}{2}\mathscr{W}_{0,-1} \oplus \mathscr{W}_{1,1} \oplus \bigoplus_{j>0}\hat{D}'_{j,0}\mathscr{W}_{j,1} \oplus \bigoplus_{\substack{j>0, M>1\\ M|j}}\bigoplus_{\substack{0<p<M\\ p\wedge M=1}}\hat{D}'_{j,\pi p/M}\mathscr{W}_{j,\mathrm{e}^{2\pi i p/M}}\,. \tag{7.1.12}$$

Equation (7.1.12) is only formal in the sense that, for Q generic, the multiplicities are not integers, and $\mathscr{H}_Q$ cannot be interpreted as a proper vector space. In contrast, the $\mathscr{W}_{j,\mathrm{e}^{i\phi}}$ are well-defined spaces with integer dimension *independent of* Q, as discussed in Chapter 3. Also, in (7.1.12) we have not taken into account the fact that, for a finite lattice system, the sums must be properly truncated.

The torus partition function (7.1.2) is obtained by the trace over $\mathscr{H}_Q$,

$$\mathrm{Tr}_{\mathscr{H}_Q}\,\mathrm{e}^{-\beta_R\mathscr{H}}\,\mathrm{e}^{-i\beta_I\mathscr{P}}\,, \tag{7.1.13}$$

where the real parameters $\beta_R > 0$ and β_I determine the size of the torus, while $\mathscr{H}$ and $\mathscr{P}$ denote respectively the lattice Hamiltonian and momentum operators. Recalling the (modular) parameters

$$q = \exp\left[-\frac{2\pi}{N}(\beta_R + i\beta_I)\right]\,, \tag{7.1.14a}$$

$$\bar{q} = \exp\left[-\frac{2\pi}{N}(\beta_R - i\beta_I)\right] \tag{7.1.14b}$$

we have, in the limit where the size of the system $N \to \infty$, with $\beta_R, \beta_I \to \infty$ so that q and $\bar{q}$ remain finite,

$$\mathrm{Tr}_{\mathscr{W}_{j,\mathrm{e}^{i\phi}}} \mathrm{e}^{-\beta_R \mathscr{H}} \mathrm{e}^{-i\beta_I \mathscr{P}} \overset{N\to\infty}{\longmapsto} F_{j,\mathrm{e}^{i\phi}} \,. \tag{7.1.15}$$

In order to understand better how $\mathrm{Vir} \otimes \overline{\mathrm{Vir}}$ acts in the Q-state Potts model CFT, we will consider the action of the Koo-Saleur generators introduced in Section 3.7 on the spaces $\mathscr{W}_{j,\mathrm{e}^{i\phi}}$.

7.2 Notes on loops and clusters

Recall that the Q-state Potts model can be formulated in terms of clusters through the Fortuin-Kasteleyn expansion, and furthermore reformulated in terms of loops on the medial lattice using the Euler relation. The critical point on the square lattice is $v_\mathrm{c} = \sqrt{Q}$, implying a simplification in the partition function (2.1.17):

$$Z = Q^{|V|/2} \sum_{A \subseteq E} Q^{\ell(A)/2} \,. \tag{7.2.1}$$

Note that the equivalence between loop and cluster formulations must be handled with care on the torus: there are subtle differences between the two, which are manifest in the decompositions (7.1.12) and (7.7.4) below.

The loop/cluster formulation gives rise to a representation—in the technical sense of a representation of an associative algebra—of T_N^a, as we now explain. In practice, states in the transfer matrix must be defined so as to allow the book-keeping of the non-local quantities $k(A)$ or $\ell(A)$. In the cluster picture, a state is a set partition of the L sites in a row, with two vertices belonging to the same block in the partition if and only if they are connected via the part of the FK clusters seen below that row. Equivalently, in the loop picture, a state is a pairwise matching of $N = 2L$ medial sites in a row, with each site seeing either a vertex of V on its left and a dual vertex on its right, or conversely. The above bijection between cluster and loop configurations provides as well a bijection between the corresponding cluster and loop states. The transfer matrix evolves the loop states by the relations (3.1.1)–(3.1.2) of the affine Temperley–Lieb algebra T_N^a, and to match the loop weights between (2.1.17) and (3.1.1a) we must identify

$$\mathfrak{m} = \sqrt{Q} \,. \tag{7.2.2}$$

To account also for the computation of correlation functions, a few modifications must be made. The case of four-point functions has been expounded in [20], but in the present chapter it is enough to consider the simpler case of two-point functions. These can be computed in the cylinder geometry by placing one point at each extremity of the cylinder. The issue is then ensuring the propagation of j distinct clusters between the two extremities in a setup compatible with the transfer matrix formalism. This can be done, on one hand, in the cluster picture by letting the states be L-site set partitions including j marked blocks, and on the other hand, in the loop picture by letting the states be N-site pairwise matchings including $2j$ defect lines—which are precisely the through-lines already encountered in the discussion of $\mathsf{T}_N^a(\mathfrak{m})$. The sum over states must then be restricted so as to ensure that the marked clusters or defect loop-lines propagate all along the cylinder. Moreover, it turns out to be necessary to keep track of the windings of either type of marked object around the periodic direction of the cylinder. Fortunately, in the loop picture, these considerations lead directly to the definition of the Temperley-Lieb standard modules that were described in Chapter 3.

7.3 Lattice Virasoro in the Potts model and the non-degenerate case

7.3.1 Hamiltonian and representations

The Hamiltonian describing the Q-state Potts model in the anisotropic limit can be expressed in terms of the Temperley-Lieb generators for N even [12]. We recall the Temperley-Lieb Hamiltonian (3.2.2),

$$\mathscr{H} = -\frac{\gamma}{\pi \sin\gamma} \sum_{j=1}^{N} (e_j - e_\infty)\,. \tag{7.3.1}$$

Here, the e_j can be taken to act in different representations of the $\mathsf{T}_N^a(\mathfrak{m})$ algebra. The original representation, used for Q integer, uses matrices $Q^L \times Q^L$, corresponding to a chain of $L = N/2$ Potts spins. The Fortuin–Kasteleyn formulation of the Potts model for Q real can be obtained by using instead the loop formulation discussed in Chapter 2 and further in the section above. We shall in the following use the loop representation as the basis for our construction of the Koo-Saleur generators. Recall that when taking one of the standard modules $\mathscr{W}_{j,\mathrm{e}^{i\phi}}$ as the representation of choice, the value of the energy density e_∞ is independent of ϕ.

7.3.2 Vir$\otimes\overline{\text{Vir}}$ modules in the Potts model CFT: the non-degenerate case

We recall once more that throughout this chapter $\mathfrak{q}$ is assumed to take generic values (not a root of unity). Whenever ϕ is such that the resonance criterion (3.1.4) is not met we say that ϕ is *generic*; and when (3.1.4) is satisfied ϕ is referred to as *non-generic*.

Since $\mathfrak{q}$ is generic throughout, both c and its parametrization x from (3.5.4) take generic, irrational values. The conformal weights may be degenerate or not, depending on the lattice parameters. In the non-degenerate case, which corresponds to generic lattice parameters (the opposite does not always hold) it is natural to expect that the Temperley–Lieb module decomposes accordingly into a direct sum of Verma modules,

$$\mathscr{W}_{j,\mathrm{e}^{i\phi}} \mapsto \bigoplus_{e\in\mathbb{Z}} \mathsf{V}_{e-e_\phi,-j} \otimes \overline{\mathsf{V}}_{e-e_\phi,j}\,. \tag{7.3.2}$$

The symbol $\mapsto$ means that action of the lattice Virasoro generators *restricted to scaling states* on $\mathscr{W}_{j,\mathrm{e}^{i\phi}}$ corresponds to the decomposition on the right-hand side when $N \to \infty$. This statement is discussed in considerable detail in Chapter 6. Throughout this chapter we systematically place a bar above the right tensorand in expressions of the form $\mathsf{V}\otimes\bar{\mathsf{V}}$, as a reminder that this refers to the $\overline{\text{Vir}}$ algebra.

Recall that a Verma module is a highest-weight representation of the Virasoro algebra (1.0.1) generated by a highest-weight vector $|h\rangle$ satisfying $L_n|h\rangle = 0, n > 0$, and for which all the descendants

$$L_{-n_1}\dots L_{-n_k}|h\rangle\,,\ \text{with } 0 < n_1 \le n_2 \le \dots \le n_k \text{ and } k > 0 \tag{7.3.3}$$

are considered as independent, subject only to the commutation relations (1.0.1). In the non-degenerate case where the Verma module is irreducible, it is the only kind of module that can occur, motivating the identification in (7.3.2). We note that this identification is independent of whether we consider the loop model or the XXZ spin chain.

7.3.3 The choices of metric. Duality

It is observed in Chapter 6 how the XXZ chain can be considered in a precise way as a lattice analogue of the twisted free boson theory. It is well known in the latter case that two natural scalar products can be defined. The first one—which is positive definite—corresponds to the continuum limit of the "native" positive-definite scalar product for the spin chain, and, in terms of the free boson current modes, corresponds to choosing $a_n^\dagger = a_{-n}$. A crucial observation is that for this scalar product $L_n^\dagger \neq L_{-n}$. This means that norm squares of descendants cannot be obtained using Virasoro algebra commutation relations.

The second scalar product corresponds to the conjugation $\ddagger$ with $L_n^\ddagger$ simply given by $L_n^\ddagger = L_{-n}$. This "conformal scalar product" is known to correspond [9, 10, 116], on the lattice, to a modified scalar product in the XXZ spin chain where $\mathfrak{q}$ is treated as a formal, self-conjugate parameter [117].

The loop model can be naturally equipped with two scalar products as well. Choosing basic loop states to be mutually orthogonal and of unit norm-square defines a "native" positive-definite scalar product for which the Temperley–Lieb generators, the transfer matrix and the Hamiltonian are not self-adjoint, while for the lattice Virasoro generators $\mathscr{L}_n^\dagger \neq \mathscr{L}_{-n}$: we will denote this scalar product by $\langle -, - \rangle$ (whenever necessary, will use the same notation for lattice and continuum quantities).

Meanwhile, we can also introduce the "loop scalar product" $(-,-)$, obtained by gluing the mirror image of one link state on top of the other and evaluating the result according to certain rules that we now describe. First, unless all through-lines connect through from bottom to top the result is zero. Considering a smeared-out phase we also take into account the weight of straightening the connected through-lines: a through-line that has moved to the right (left) is assigned the weight $\mathrm{e}^{i\phi/2N}$ ($\mathrm{e}^{-i\phi/2N}$) for each step. Each contractible loop carries the weight $\mathfrak{m} = \mathfrak{q} + \mathfrak{q}^{-1}$, while each non-contractible loop carries the weight $\mathrm{e}^{i\phi/2} + \mathrm{e}^{-i\phi/2}$. To illustrate this scalar product we take the following examples, where the solid lines around the rightmost diagrams signify that we assign them a value according to the aforementioned rules:

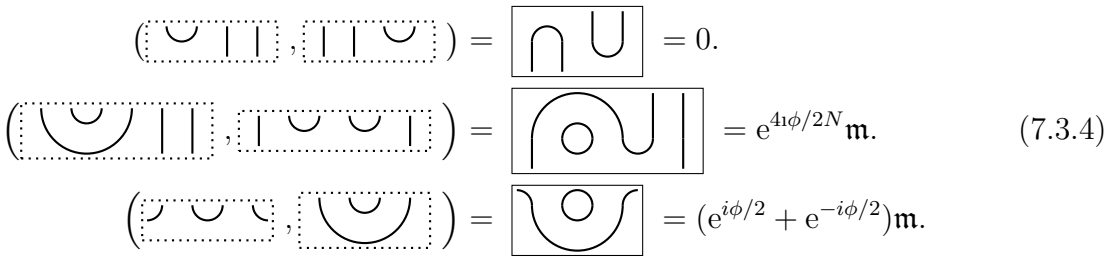

(7.3.4)

This "loop scalar product" is then extended by sesquilinearity to the whole space of loop states. The adjoint $U^\ddagger$ of a word U in the Temperley–Lieb algebra can be defined similarly by flipping the diagram representing it about a horizontal line, as in the following example:

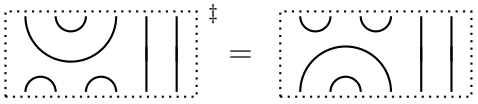

(7.3.5)

From this definition it is clear that the generators e_i themselves are self-adjoint, and consequently $L_n^\ddagger = L_{-n}$. It is well known that the loop scalar product is invariant with respect to the Temperley–Lieb action: $(x, Uy) = (U^\ddagger x, y)$. The loop scalar product is of course not positive definite. It is however not degenerate (provided $\mathfrak{m} \neq 0$). Moreover, it is known to go over to the conformal scalar product in the continuum limit [9].

For a given module $\mathscr{W}$, we can define the dual (conjugate) module $\widetilde{\mathscr{W}}$ by the map $u \to (u, -)$, i.e., by taking mirror images. In general, we have an isomorphism $\widetilde{\mathscr{W}}_{j,\mathrm{e}^{i\phi}} \approx \mathscr{W}_{j,\mathrm{e}^{-i\phi}}$. When $\mathscr{W}_{j,\mathrm{e}^{i\phi}}$

is reducible but indecomposable, the corresponding Loewy diagram has its arrows reversed, as illustrated in Section 3.3. The modules $\mathscr{W}_{j,1}$ are self-dual.

An important point is that, if a Temperley–Lieb module is self-dual, then since the Hamiltonian itself is, as well as the definition of scaling states, the action of the continuum limit of the Koo–Saleur generators should define an action on the scaling limit of the module that is also invariant under duality in the CFT. If both the Temperley–Lieb module and the $\mathrm{Vir}\otimes\overline{\mathrm{Vir}}$ module are irreducible, this has no useful consequences. We shall soon see however that the $\mathscr{W}_{j,1}$ modules, while irreducible, have a continuum limit which is not so. Self-duality of the $\mathscr{W}_{j,1}$ implies invariance of the Loewy diagrams for the continuum limit with respect to reversal of the $\mathrm{Vir}\otimes\overline{\mathrm{Vir}}$ arrows, with very interesting consequences.

7.4 Modules in the degenerate case: evidence from the lattice

In the degenerate cases the conformal weights may take degenerate values $h = h_{r,s}$ with $r, s \in \mathbb{N}^*$, in which case a singular vector appears in the Verma module. We recall the example of $|h_{1,1} = 0\rangle$, see (6.1.12) and the discussion below. In particular, recall the structure

$$\mathsf{V}^{(\mathrm{d})}_{1,1}: \quad \begin{array}{c} \mathsf{X}_{1,1} \\ \circ \\ \downarrow \\ \bullet \\ \mathsf{V}_{1,-1} \end{array} \quad . \tag{7.4.1}$$

We also recall that in cases of degenerate conformal weights, there is more than one possible module that could appear, and the identification in (7.3.2) may no longer hold. The identification now depends on the choice of representation of $\mathsf{T}^a_N(\mathfrak{m})$, such as the XXZ representation in Chapter 6 and the loop/cluster representation in the present chapter.

7.4.1 The loop-model case: without through-lines

For the modules $\mathscr{W}_{0,\mathfrak{q}^{\pm 2}}$, this Verma structure is seen even at finite size—see equation (3.3.2).[3] Using the numerical methods described in Appendix H we find that the corresponding loop states are never annihilated by the $A_{n,1}$ or $\bar{A}_{n,1}$ combinations of Virasoro generators.

We recall now from Section 3.1.2 that the module $\mathscr{W}_{0,\mathfrak{q}^{\pm 2}}$ appears in the loop model by keeping track of how points are connected across the periodic boundary condition. However, the Potts model where non-contractible loops have the same weight $\mathfrak{m}$ as contractible ones naturally involves the quotient $\overline{\mathscr{W}}_{0,\mathfrak{q}^{\pm 2}}$ for which there are no degenerate states on the lattice. The spectrum generating function for this module in the continuum limit is then

$$\bar{F}_{0,\mathfrak{q}^{\pm 2}} = F_{0,\mathfrak{q}^{\pm 2}} - F_{1,1} = \sum_{n=1}^{\infty} K_{n,1}\bar{K}_{n,1}\,, \tag{7.4.2}$$

[3] Recall that in the loop representation, the loop weight is $\mathfrak{m} = \mathfrak{q} + \mathfrak{q}^{-1}$, with $\mathfrak{q}^2 = \mathrm{e}^{i\phi}$ adjusting the weight of non-contractible loops, so the sign of the twist ϕ is immaterial. In contrast, in the XXZ case, one finds (see Chapter 6) that only one sign $\mathfrak{q}^{-2}$ corresponds to a standard module, while the other $\mathfrak{q}^2$ is a co-standard module.

where $K_{r,s}$ was defined in (6.1.14). It involves only Kac modules, so we have:

Quotient loop-model module without through-lines: *We have the scaling limit*

$$\overline{\mathscr{W}}_{0,\mathfrak{q}^{\pm 2}} \mapsto \bigoplus_{n=1}^{\infty} \mathsf{X}_{n,1} \otimes \overline{\mathsf{X}}_{n,1}\,. \tag{7.4.3}$$

Note that this implies that the corresponding highest-weight states $|h, \bar{h}\rangle$ are now annihilated:

$$A_{n,1}|h_{n,1}, h_{n,1}\rangle = \bar{A}_{n,1}|h_{n,1}, h_{n,1}\rangle = 0\,. \tag{7.4.4}$$

In particular, the ground state at central charge (3.5.4) is indeed annihilated by L_{-1} and $\bar{L}_{-1}$, a satisfactory situation physically. Results for $\overline{\mathscr{W}}_{0,\mathfrak{q}^{\pm 2}}$ are shown in Appendix H.2.

7.4.2 The loop model case: $j > 0$

For the modules $\mathscr{W}_{j,1}$ with $j > 0$, the numerical results in Appendix H.3 indicate that the highest-weight states with conformal weight $h_{e,j}$ and $e > 0$ are *never* annihilated by the corresponding $A_{e,j}$ operators, whether in the chiral or antichiral sector. It would be tempting to conclude that the modules are now systematically of Verma type, but this is not possible. Indeed, recall that for $\mathfrak{q}$ generic, the ATL (affine Temperley–Lieb) modules $\mathscr{W}_{j,1}$ are irreducible and thus self-dual. The Virasoro generators being obtained as continuum limits of ATL generators should also obey this self-duality (see the discussion in Section 4.3 of [58]).[4] Verma modules clearly do not, as their structure is not invariant under reversal of the $\mathrm{Vir} \otimes \overline{\mathrm{Vir}}$ action. To understand what might happen, let us discuss in more detail, as an example, the case $j = 2$. The generating function of levels shows a pair of primary fields

$$\Phi_{1,2} \equiv \phi_{1,2} \otimes \bar{\phi}_{1,-2}\,, \tag{7.4.5a}$$
$$\bar{\Phi}_{1,2} \equiv \phi_{1,-2} \otimes \bar{\phi}_{1,2} \tag{7.4.5b}$$

with conformal weights $(h_{1,2}, h_{1,-2})$ and $(h_{1,-2}, h_{1,2})$. Note that here by $\phi_{r,s}$ we simply mean a chiral primary field with conformal weight $h_{r,s}$: the structure of the associated Virasoro module will be discussed below. This means in particular that $\phi_{r,s} = \phi_{-r,-s}$.

By expanding the factor $1/P(q)P(\bar{q})$ in the spectrum generating functions, we see that model also has four descendants at level two, that is with conformal weights $(h_{1,-2}, h_{1,-2})$, where we have used that $h_{1,-2} = h_{1,2} + 2$. Now, if the modules generated by $\Phi_{1,2}$ and $\bar{\Phi}_{1,2}$ in the continuum limit were a product of two Verma modules, these four descendants would be the two independent fields, $L_{-2}\Phi_{1,2}$ and $L_{-1}^2\Phi_{1,2}$, as well as the two fields obtained by swapping chiral and antichiral components, $\bar{L}_{-2}\bar{\Phi}_{1,2}$ and $\bar{L}_{-1}^2\bar{\Phi}_{1,2}$. The chiral/antichiral symmetry corresponds to exchanging right and left (i.e., exchanging momentum p for momentum $-p$) and is present on the lattice as well, by reflecting the site index $i \to N + 1 - i$ (see Chapter 6). Whether or not we have two such independent states and their conjugates can be deduced based on the parity of the lattice states, as described in Appendix I. There, we find that the module in the continuum limit and at level two does *not* have, as a basis, a pair of independent states and their chiral/antichiral conjugates.

[4] This is a point well known in axiomatic CFT as well. Quoting [149]: "It is also worth mentioning that a non-degenerate bulk two-point function requires that $\mathscr{H}_{\mathrm{bulk}}$ is isomorphic to its conjugate representation $\mathscr{H}^*_{\mathrm{bulk}}$. A necessary condition for this is that the composition series does not change when reversing all arrows [...]."

Introducing

$$A_{1,2} = L_{-2} - \frac{3}{2+4h_{1,2}} L_{-1}^2 \,, \tag{7.4.6a}$$

$$\bar{A}_{1,2} = \bar{L}_{-2} - \frac{3}{2+4h_{1,2}} \bar{L}_{-1}^2 \tag{7.4.6b}$$

we now claim that, in the continuum limit, the identity

$$A_{1,2}\Phi_{1,2} = \bar{A}_{1,2}\bar{\Phi}_{1,2} \tag{7.4.7}$$

is satisfied. Note that both sides of the equation are primary fields—i.e., they are annihilated by $\mathrm{Vir}\otimes\overline{\mathrm{Vir}}$ generators $L_n, \bar{L}_n$ with $n > 0$. They are also of vanishing norm $(-,-)$. Corresponding numerical results are given in Appendix H.3.

We have therefore identified part of the module as a quotient of $(\mathsf{V}_{1,2}^{(\mathrm{d})}\otimes\overline{\mathsf{V}}_{1,-2})\oplus(\mathsf{V}_{1,-2}\otimes\overline{\mathsf{V}}_{1,2}^{(\mathrm{d})})$, corresponding to the following diagram for the degenerate fields:

$$\begin{array}{ccc} \Phi_{1,2} = \phi_{1,2}\otimes\bar{\phi}_{1,-2} & & \bar{\Phi}_{1,2} = \phi_{1,-2}\otimes\bar{\phi}_{1,2} \\ & \searrow^{A} \quad \swarrow_{\bar{A}} & \\ & A_{1,2}\Phi_{1,2} = \bar{A}_{1,2}\bar{\Phi}_{1,2} & \end{array} \tag{7.4.8}$$

Note we have the quotient modules (obtained by quotienting by the submodule generated by the bottom field), $\mathsf{X}_{1,2}\otimes\overline{\mathsf{V}}_{1,-2}$ and $\mathsf{V}_{1,-2}\otimes\overline{\mathsf{X}}_{1,2}$ and with generating functions $(q^{h_{1,-2}-c/24}/P(q))\times \bar{K}_{1,2}$ and $K_{1,2}\times(\bar{q}^{h_{1,-2}-c/24}/P(\bar{q}))$. The bottom field generates a product of Verma modules $\mathsf{V}_{1,-2}\otimes\overline{\mathsf{V}}_{1,-2}$ with generating function $(q^{h_{1,-2}-c/24}/P(q))\times(\bar{q}^{h_{1,-2}-c/24}/P(\bar{q}))$.

This cannot, however, be the end of the story, since the quotient identified so far is not self-dual—nor does it account for the proper multiplicity of fields. Invariance of the diagram under reversal of the arrow demands that there exists a field "on top," with a quotient which is also a product of Verma modules $\mathsf{V}_{1,-2}\otimes\overline{\mathsf{V}}_{1,-2}$. This should give rise, in terms of fields, to the diagram

$$\begin{array}{ccccc} & & \Psi_{1,2} & & \\ & \swarrow^{A^\dagger} & \downarrow{\scriptstyle (L_0-h_{-1,2})} & \searrow^{\bar{A}^\dagger} & \\ \Phi_{1,2} = \phi_{1,2}\otimes\bar{\phi}_{1,-2} & & & & \bar{\Phi}_{1,2} = \phi_{1,-2}\otimes\bar{\phi}_{1,2} \\ & \searrow_{A} & & \swarrow_{\bar{A}} & \\ & & A_{1,2}\Phi_{1,2} = \bar{A}_{1,2}\bar{\Phi}_{1,2} & & \end{array} \tag{7.4.9}$$

with $\Psi_{1,2}$ a field to be determined—see below.

The same construction seems to apply to all cases in the $F_{j,1}$ characters. The simplest example occurs, in fact, in $\mathscr{W}_{1,1}$—even though this module does not appear in the Potts model, as discussed around (7.1.11)—with $\Phi_{1,1}\equiv\phi_{1,1}\otimes\bar{\phi}_{1,-1}$ and $\bar{\Phi}_{1,1}\equiv\phi_{1,-1}\otimes\bar{\phi}_{1,1}$. In this case, the quotient is simply given by $L_{-1}\Phi_{1,1} = \bar{L}_{-1}\bar{\Phi}_{1,1}$.

The indecomposable structure for arbitrary positive integer values of e, j can then be con-

jectured to be

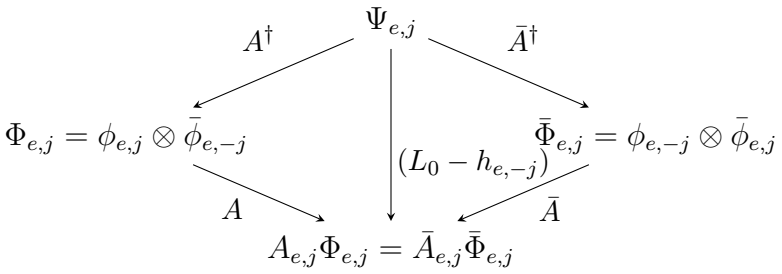

(7.4.10)

The validity of (7.4.10) in general comes from strong numerical evidence for small values of e, j. It is also the simplest structure we can imagine solving the problems of poles in the OPEs, based on our independent knowledge of the spectrum of the theory. More complete evidence comes from the construction of four-point functions using the corresponding regularized conformal blocks. (See [6], [150] and Chapter 8).

It is interesting to draw the corresponding structure of Virasoro modules defining the quotient modules $\mathscr{L}_{e,j}$:

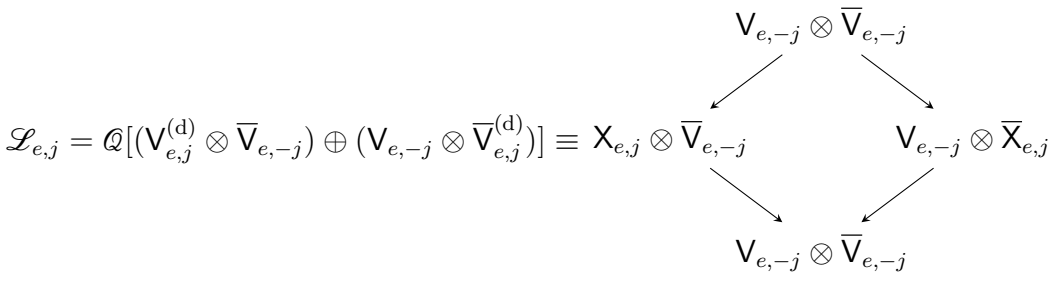

(7.4.11)

Accordingly we have the result:

Loop-model modules with through-lines: *For $j > 0$ and $2j$ through-lines we have the scaling limit*

$$\mathscr{W}_{j,1} \mapsto \left(\mathsf{V}_{0,-j} \otimes \overline{\mathsf{V}}_{0,j}\right) \oplus \bigoplus_{e>0} \mathscr{L}_{e,j}\,. \tag{7.4.12}$$

7.5 Modules in the degenerate case: the OPE point of view

As in the early works on logarithmic CFTs [10,151], it is possible to understand the appearance of indecomposable modules in the continuum limit of $\mathscr{W}_{j,1}$ by carefully examining the OPEs and their potential divergences when one of the fields in the s-channel has a degenerate conformal weight.

To start, imagine that we have some OPE of a field of dimension Δ with itself where a field with conformal weights $(h_{1,2}, h_{1,2})$ appears. In ordinary CFT, the descendants of this field at level two in the chiral and in the antichiral sector would not be independent: this fact is crucial to cancel the divergence arising in the OPE coefficients from to the fact that $h_{1,2}$ is in the Kac table, resulting in a finite OPE such as the ones arising in the minimal-model CFTs [5]. Let

us now see what happens if the null descendants are not zero, and the divergences potentially remain. To proceed, we factor out the $(z\bar{z})^{-2\Delta}$, with $\Delta = \bar{\Delta}$ denoting the conformal weight of the fields being fused, and analyze the potential divergences by slightly shifting the conformal weights of the field on the right-hand side of the OPE:

$$C(\epsilon)\Big\{(z\bar{z})^{h_{1+\epsilon,2}}\Big[\Big(X_\epsilon + \frac{z}{2}\partial X_\epsilon + \alpha^{(-2)}(\Delta, h_{1+\epsilon,2})z^2 L_{-2}X_\epsilon \\ + \alpha^{(-1,-1)}(\Delta, h_{1+\epsilon,2})z^2 L_{-1}^2 X_\epsilon\Big) \times \text{h.c.}\Big] + \dots\Big\} \quad (7.5.1)$$

where $C(\epsilon)$ is a number to be determined, the dots stand for other fields, and we have used the short-hand notations

$$X_\epsilon = \phi_{1+\epsilon,2}(z)\,, \quad (7.5.2a)$$
$$\bar{X}_\epsilon = \bar{\phi}_{1+\epsilon,2}(\bar{z})\,. \quad (7.5.2b)$$

The coefficients α in (7.5.1) are fully determined by conformal invariance

$$\alpha^{(-2)}(\Delta, h) = \frac{(h-1)h + 2\Delta(1+2h)}{16(h-h_{1,2})(h-h_{2,1})}\,, \quad (7.5.3a)$$
$$\alpha^{(-1,-1)}(\Delta, h) = \frac{(1+h)(c+8h) - 12(\Delta+h)}{64(h-h_{1,2})(h-h_{2,1})}\,, \quad (7.5.3b)$$

and note that we have

$$\alpha^{(-1,-1)}(\Delta, h)L_{-1}^2 + \alpha^{(-2)}(\Delta, h)L_{-2} = \alpha^{(-2)}(\Delta, h)A(h) + \alpha_0^{(-1,-1)}(h)L_{-1}^2, \quad (7.5.4)$$

where

$$A(h) \equiv L_{-2} - \frac{3}{2+4h}L_{-1}^2, \;\; \alpha_0^{(-1,-1)}(h) \equiv \frac{1+h}{4(1+2h)}. \quad (7.5.5)$$

It is important to notice that in writing (7.5.4), the dependence on the external field Δ only appears in the coefficient $\alpha^{(-2)}$, i.e., the operator A which will turn out to give rise to the Jordan cell structure is independent of the external field. This point will become more clear below.

Going back to $h = h_{1+\epsilon,2}$ with $\epsilon \to 0$, and writing $A_\epsilon \equiv A(h_{1+\epsilon,2})$, it is convenient to define

$$\gamma(\epsilon) \equiv \langle X_\epsilon | A_\epsilon^\dagger A_\epsilon | X_\epsilon \rangle = \frac{8(h-h_{1,2})(h-h_{2,1})}{(1+2h)} = \nu\epsilon\,, \quad (7.5.6)$$

with

$$\nu = -\frac{2(1-2\beta^2-\beta^4+2\beta^6)}{\beta^6}\,, \quad (7.5.7)$$

where we have used the parametrization $\beta^2 = x/(x+1)$. On the other hand, notice that as $\epsilon \to 0$, the coefficient $\alpha^{(-2)}(\Delta, h_{1+\epsilon,2})$ has a simple pole, since the denominator is proportional to the Kac determinant, as is obvious from equation (7.5.3a). This means that the OPE potentially presents singularities, which must be properly canceled by the contribution of other fields with the proper dimensions—a point well understood since the works [9, 10, 116, 151]. Obviously, the leading singularity in the OPE is a second-order pole coming from the descendants at level two of $X_\epsilon \bar{X}_\epsilon$. Keeping in mind that $h_{1,2} + 2 = h_{-1,2}$, and of course $h_{r,s} = h_{-r,-s}$, we therefore introduce the other fields

$$Y_\epsilon = \phi_{-1+\epsilon,2}(z)\,, \quad (7.5.8a)$$
$$\bar{Y}_\epsilon = \bar{\phi}_{-1+\epsilon,2}(\bar{z}) \quad (7.5.8b)$$

in order to cancel such singularities, and we complete the OPE as follows:

$$C(\epsilon)\Big\{(z\bar{z})^{h_{1+\epsilon,2}}\left[\left(X_\epsilon+\frac{z}{2}\partial X_\epsilon+\alpha_0^{(-1,-1)}(\epsilon)z^2L_{-1}^2X_\epsilon+\alpha^{(-2)}(\epsilon)z^2A_\epsilon X_\epsilon\right)\otimes\text{h.c.}\right] \\ +(z\bar{z})^{h_{-1+\epsilon,2}}a(\epsilon)Y_\epsilon\otimes\bar{Y}_\epsilon\Big\}\,, \tag{7.5.9}$$

where we have adopted the short-hand notations $\alpha_0^{(-1,-1)}(\epsilon)$, $\alpha^{(-2)}(\epsilon)$, and the new coefficient $a(\epsilon)$ is yet to be determined.

To study the necessary cancellation of singularities, we focus on the most divergent term at level 2:

$$\begin{aligned}&C(\epsilon)\Big\{(z\bar{z})^{h_{1+\epsilon,2}+2}[\alpha^{(-2)}(\epsilon)]^2A_\epsilon X_\epsilon\otimes\bar{A}_\epsilon\bar{X}_\epsilon+a(\epsilon)(z\bar{z})^{h_{-1+\epsilon,2}}Y_\epsilon\otimes\bar{Y}_\epsilon\Big\}\\&\quad=C(\epsilon)\Big\{\epsilon\kappa\ln(z\bar{z})(z\bar{z})^{h_{-1,2}}[\alpha^{(-2)}(\epsilon)]^2A_\epsilon X_\epsilon\otimes\bar{A}_\epsilon\bar{X}_\epsilon+\frac{1}{\sqrt{\epsilon}}(z\bar{z})^{h_{-1+\epsilon,2}}\Phi_\epsilon\Big\}\,,\end{aligned} \tag{7.5.10}$$

where we have defined

$$\kappa\equiv\frac{h_{1+\epsilon,2}+2-h_{-1+\epsilon,2}}{\epsilon}=\frac{1}{\beta^2} \tag{7.5.11}$$

and introduced the new field

$$\Phi_\epsilon\equiv\sqrt{\epsilon}\left([\alpha^{(-2)}(\epsilon)]^2A_\epsilon X_\epsilon\otimes\bar{A}_\epsilon\bar{X}_\epsilon+a(\epsilon)Y_\epsilon\otimes\overline{Y}_\epsilon\right). \tag{7.5.12}$$

The two-point function of this field is given by

$$\langle\Phi(w,\bar{w})\Phi(0,0)\rangle=\epsilon\left\{[\alpha^{(-2)}(\epsilon)]^4\gamma(\epsilon)^2(w\bar{w})^{-2h_{1+\epsilon,2}-4}+a^2(\epsilon)(w\bar{w})^{-2h_{-1+\epsilon,2}}\right\}. \tag{7.5.13}$$

Recall equation (7.5.6) and that $\alpha^{(-2)}(\epsilon)$ has a simple pole in ϵ. One can write

$$[\alpha^{(-2)}(\Delta,h_{1+\epsilon,2})]^2\gamma\equiv\frac{r}{\epsilon}+s+O(\epsilon)\,. \tag{7.5.14}$$

It is then clear that the coefficient of the first term in (7.5.13) has a double pole which must be canceled by the divergence from the second term. This requires $a^2(\epsilon)$ to be of the form

$$a^2(\epsilon)=\frac{\lambda}{\epsilon^2}+\frac{\mu}{\epsilon}+O(1)\,. \tag{7.5.15}$$

Such behavior can in fact be established using that $\phi_{2,1}$ is degenerate in the theory, as we will see in more detail in Section 7.6 below. The singularity cancellation condition then reads

$$\lambda=-r^2\,, \tag{7.5.16}$$

and the two point function (7.5.13) becomes

$$\langle\Phi(w,\bar{w})\Phi(0,0)\rangle=\frac{-2\kappa r^2\ln(w\bar{w})+2rs+\mu}{(w\bar{w})^{2h_{-1,2}}}\,. \tag{7.5.17}$$

Taking into account the $1/\sqrt{\epsilon}$ factor in (7.5.10), we must therefore take $C(\epsilon)=\sqrt{\epsilon}$, such that the contribution of Φ_ϵ in the OPE is of $O(1)$.

At this point, it is natural to introduce the normalized field

$$\hat{X}_\epsilon\equiv\frac{1}{\sqrt{\gamma}}A_\epsilon X_\epsilon\,, \tag{7.5.18}$$

and identify it as another copy of Y_ϵ in the limit $\epsilon \to 0$, since both have dimension $h_{-1,2}$ and are annihilated by L_1 and L_2. The first term in second line of (7.5.10) is then given by:

$$\frac{\kappa r}{2\sqrt{\nu}}(z\bar{z})^{h_{-1,2}} \ln(z\bar{z})(AX \otimes \bar{Y} + Y \otimes \bar{A}\bar{X}). \tag{7.5.19}$$

Combining with the remaining terms in the OPE (7.5.9), i.e.,

$$\sqrt{\epsilon}(z\bar{z})^{h_{1+\epsilon,2}} \left[\left(X_\epsilon + \frac{z}{2}\partial X_\epsilon + \alpha_0^{(-1,-1)}(\epsilon) z^2 L_{-1}^2 X_\epsilon \right) \otimes \alpha^{(-2)}(\epsilon)\sqrt{\gamma}\bar{z}^2 \bar{\hat{X}}_\epsilon + \text{h.c.} \right], \tag{7.5.20}$$

and recalling (7.5.14), we have then the full OPE as $\epsilon \to 0$:[5]

$$\begin{aligned} & z^{h_{1,2}}\bar{z}^{h_{-1,2}} \left[\left(X + \frac{z}{2}\partial X + \alpha_0^{(-1,-1)}(\epsilon) z^2 L_{-1}^2 X \right) \otimes \bar{Y} \right] + \text{h.c.} \\ & \quad + (z\bar{z})^{h_{-1,2}} \frac{\kappa\sqrt{r}}{\sqrt{\nu}} \left(\frac{1}{2}\ln(z\bar{z})(AX \otimes \bar{Y} + \text{h.c.}) + \frac{\sqrt{\nu}}{\kappa r}\Phi \right) \\ & = z^{h_{1,2}}\bar{z}^{h_{-1,2}} \left[\left(X + \frac{z}{2}\partial X + \alpha_0^{(-1,-1)}(\epsilon) z^2 L_{-1}^2 X \right) \otimes \bar{Y} \right] + \text{h.c.} \\ & \quad + (z\bar{z})^{h_{-1,2}} \frac{\kappa\sqrt{r}}{\sqrt{\nu}} \left(\ln(z\bar{z})(AX \otimes \bar{Y}) + \frac{\sqrt{\nu}}{\kappa r}\Phi \right). \end{aligned} \tag{7.5.21}$$

In the last line of (7.5.21) we have set

$$AX \otimes \bar{Y} = \sqrt{\gamma}\hat{X} \otimes \bar{Y} = \sqrt{\gamma} Y \otimes \bar{\hat{X}} = Y \otimes \bar{A}\bar{X}\,, \tag{7.5.22}$$

using the identification of $\hat{X}, \bar{\hat{X}}$ with $Y, \bar{Y}$ in the $\epsilon \to 0$ limit. As will become obvious below, this has the interpretation that $L_0 - \bar{L}_0$ is diagonalizable.

We are interested in the logarithmic mixing at level 2, i.e., the last line of (7.5.21). Inspecting the terms, it is natural to redefine the field

$$\Psi \equiv \frac{\sqrt{\nu}}{\kappa r}\Phi \tag{7.5.23}$$

which, as we shall see, becomes the logarithmic partner of $AX \otimes \bar{Y} = Y \otimes \bar{A}\bar{X}$. It is a simple exercise to calculate their two-point functions[6] and one arrives at

$$\langle (AX \otimes \bar{Y})(w,\bar{w})(AX \otimes \bar{Y})(0,0)\rangle = 0, \tag{7.5.24a}$$

$$\langle \Psi(w,\bar{w})(AX \otimes \bar{Y})(0,0)\rangle = \frac{\kappa^{-1}\nu}{(w\bar{w})^{2h_{-1,2}}}, \tag{7.5.24b}$$

$$\langle \Psi(w,\bar{w})\Psi(0,0)\rangle = \frac{-2\kappa^{-1}\nu\ln(w\bar{w}) + \frac{\nu}{\kappa^2 r^2}(2rs+\mu)}{(w\bar{w})^{2h_{-1,2}}}. \tag{7.5.24c}$$

We recognize the usual logarithmic structure of a rank-2 Jordan cell [68].

As a final step, we compute the action of Virasoro algebra on the pair $(AX \otimes \bar{Y}, \Psi)$:

$$L_0(AX \otimes \bar{Y}) = h_{-1,2}(AX \otimes \bar{Y}), \tag{7.5.25a}$$

$$\begin{aligned} L_0\Psi &= h_{-1,2}\Psi + \frac{\sqrt{\nu\epsilon}}{\kappa r}[\alpha^{(-2)}(\epsilon)]^2(h_{1+\epsilon,2} + 2 - h_{-1+\epsilon,2}) A_\epsilon X_\epsilon \otimes \bar{A}_\epsilon \bar{X}_\epsilon \\ &= h_{-1,2}\Psi + AX \otimes \bar{Y}, \end{aligned} \tag{7.5.25b}$$

[5] After factoring out a global factor of $\sqrt{r}$.

[6] In computing the two-point functions, one must keep in mind the distinction between $\hat{X}$ and Y when $\epsilon \neq 0$, and take the definition (7.5.23) at $\epsilon \neq 0$, i.e., $\Psi_\epsilon \equiv (\sqrt{\nu}/\kappa r)\Phi_\epsilon$.

and similarly for $\bar{L}_0$. Therefore we see that in the basis $(AX \otimes \bar{Y}, \Psi) = (Y \otimes \bar{A}\bar{X}, \Psi)$ we have

$$L_0 = \begin{pmatrix} h_{-1,2} & 1 \\ 0 & h_{-1,2} \end{pmatrix} = \bar{L}_0 \tag{7.5.26}$$

forming a rank-2 Jordan cell. In addition we find

$$A^\dagger \Psi = \frac{\sqrt{\nu\epsilon}}{\kappa r}[\alpha^{(-2)}]^2 \gamma X \otimes \bar{A}\bar{X} = \kappa^{-1}\nu X \otimes \bar{Y}\,, \tag{7.5.27}$$

where we have used (7.5.14), (7.5.6) and (7.5.18). Note also that $L_1\Psi = 0$. Hence, the module is depicted as

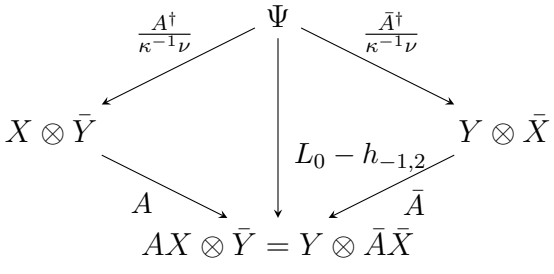

(7.5.28)

a structure that coincides with (7.4.9).

As we have briefly commented before, the logarithmic coupling $\kappa^{-1}\nu$ in (7.5.24c) which characterizes the Jordan-cell structure does not depend on the dimension Δ of the external fields. More explicitly, from (7.5.7) and (7.5.11), we have

$$\kappa^{-1}\nu = -\frac{2(1 - 2\beta^2 - \beta^4 + 2\beta^6)}{\beta^4}\,, \tag{7.5.29}$$

which is entirely determined by the Kac formula and the Kac determinant. In contrast, the coefficient $\kappa\sqrt{r}/\sqrt{\nu}$ in the OPE (7.5.21) does depend on Δ through r, due to (7.5.14). Similarly, the constant in the two-point function (7.5.24c) also depends on Δ. This is however compatible with the Jordan cell structure, since the field Ψ always admits a shift by a multiple of the null field [68],

$$\Psi \to \Psi + \text{const.} \times AX \otimes \bar{Y} = \Psi + \text{const.} \times Y \otimes \bar{A}\bar{X}\,, \tag{7.5.30}$$

which does not change (7.5.26).

The construction also generalizes to the case of operators $\phi_{r,s}$ and $\phi_{r,-s}$. In general, the module has the structure in (7.5.35) with $X = \phi_{r,s}$, $Y = \phi_{r,-s}$, and A replaced by the proper combination of Virasoro generators. Setting

$$\langle \phi_{r+\epsilon,s} | A^\dagger_{r,s} A_{r,s} | \phi_{r+\epsilon,s} \rangle = \nu_{r,s}\epsilon \tag{7.5.31}$$

and observing that

$$h_{r+\epsilon,s} + rs - h_{-r+\epsilon,s} = \kappa_{r,s}\epsilon\,, \quad \text{with } \kappa_{r,s} = \frac{r}{\beta^2}\,, \tag{7.5.32}$$

we find that the free parameter of the module (the so-called logarithmic coupling, or indecomposability parameter) is

$$b_{r,s} = \kappa^{-1}_{r,s}\nu_{r,s}\,, \tag{7.5.33}$$

so that

$$(L_0 - h_{-r,s})\Psi_{r,s} = (\bar{L}_0 - h_{r,-s})\Psi_{r,s} = A_{r,s}\phi_{r,s}\otimes\bar{\phi}_{r,-s} = \phi_{r,-s}\otimes\bar{A}_{r,s}\bar{\phi}_{r,s}\,, \quad (7.5.34a)$$

$$A^\dagger_{r,s}\Psi_{r,s} = b_{r,s}\phi_{r,s}\otimes\bar{\phi}_{r,-s}\,, \quad (7.5.34b)$$

$$\bar{A}^\dagger_{r,s}\Psi_{r,s} = b_{r,s}\phi_{r,-s}\otimes\bar{\phi}_{r,s} \quad (7.5.34c)$$

with the structure:

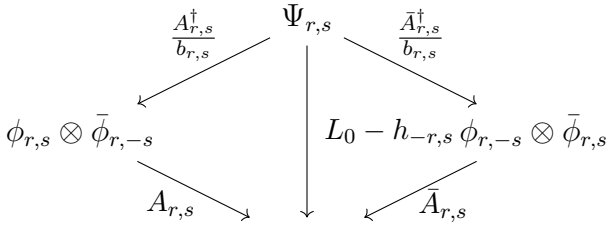

(7.5.35)

in agreement with (7.4.10).

For the special case $r = s = 1$, for instance, we find that $\nu_{1,1} = -1 + 1/\beta^2$ and therefore

$$b_{1,1} = 1 - \beta^2\,. \quad (7.5.36)$$

7.6 The particular case of the order operator and conformal blocks

In the case where the external field is given by the order operator $\Delta = h_{1/2,0}$, we can construct the s-channel expansion of conformal blocks by combining the OPEs of two pairs of external fields, and compare with the results obtained in [21].

7.6.1 Constructing logarithmic conformal blocks from OPEs

Our basic ingredients are the OPE (7.5.21) and the two-point functions (7.5.24). Take the OPE of two order operators $\Delta = h_{1/2,0}$ and focus on the contributions involving the module (7.5.28):

$$\Phi_\Delta(w,\bar{w})\Phi_\Delta(0,0) = (w\bar{w})^{-2\Delta}\Big\{ w^{h_{1,2}}\bar{w}^{h_{-1,2}}\left[\left(X + \frac{w}{2}\partial X + \alpha_0^{(-1,-1)}(\epsilon)w^2L_{-1}^2X\right)\otimes\bar{Y}\right] + \text{h.c.} \\ + (w\bar{w})^{h_{-1,2}}\frac{\kappa\sqrt{r}}{\sqrt{\nu}}[\ln(w\bar{w})(AX\otimes\bar{Y}) + \Psi] + \dots\Big\}\,, \quad (7.6.1)$$

where $\dots$ stands for other fields appearing in the OPE. The corresponding logarithmic conformal block can be constructed by combining two pair of fields $\Phi_\Delta(z_1,\bar{z}_1)\Phi_\Delta(z_2,\bar{z}_2)$ and $\Phi_\Delta(z_3,\bar{z}_3)\Phi_\Delta(z_4,\bar{z}_4)$ with cross-ratio $z = z_{12}z_{34}/z_{13}z_{24}$, and similarly for $\bar{z}$.

First, the usual calculations give the first few terms of the blocks

$$(z\bar{z})^{-2\Delta}\left[z^{h_{1,2}}\bar{z}^{h_{1,-2}} + z^{h_{1,-2}}\bar{z}^{h_{1,2}} + \frac{h_{1,2}}{2}\left(z^{h_{1,2}+1}\bar{z}^{h_{1,-2}} + z^{h_{1,-2}}\bar{z}^{h_{1,2}+1}\right)\right]. \quad (7.6.2)$$

Now, focus on the terms at level 2. The two-point function of $\alpha_0^{(-1,-1)}L_{-1}^2X\otimes\bar{Y} + \text{h.c.}$ in the first line of (7.6.1) gives contribution to the blocks with

$$4h(1+2h)[\alpha_0^{(-1,-1)}]^2(z\bar{z})^{-2\Delta}\left(z^{h_{1,2}+2}\bar{z}^{h_{1,-2}} + z^{h_{1,-2}}\bar{z}^{h_{1,2}+2}\right)\,, \quad (7.6.3)$$

where we have used

$$L_1^2 L_{-1}^2 |h\rangle = 4h(1+2h)|h\rangle\,. \tag{7.6.4}$$

The last line of (7.6.1) then contributes to the conformal block as (factoring out $(z\bar{z})^{-2\Delta}$)

$$\begin{aligned}(z_{12}\bar{z}_{12})^{h_{-1,2}}(z_{34}\bar{z}_{34})^{h_{-1,2}}\frac{\kappa^2 r}{\nu}\Big\{\big(\ln(z_{12}\bar{z}_{12})+\ln(z_{34}\bar{z}_{34})\big)\langle(AX\otimes\bar{Y})\Psi\rangle+\langle\Psi\Psi\rangle\Big\}\\ =\Big[\Big(\frac{z_{12}z_{34}}{z_{13}z_{24}}\Big)^{h_{-1,2}}\times\text{h.c.}\Big]\frac{\kappa^2 r}{\nu}\Big\{\kappa^{-1}\nu\big[\ln(z_{12}\bar{z}_{12})+\ln(z_{34}\bar{z}_{34})\big]\\ -2\kappa^{-1}\nu\ln(z_{13}\bar{z}_{13})+\frac{\nu}{\kappa^2 r^2}(2rs+\mu)\Big\}\,,\end{aligned} \tag{7.6.5}$$

where we have used the two-point functions (7.5.24). Simplifying expressions, we have the following term in the conformal block:

$$(z\bar{z})^{-2\Delta}(z\bar{z})^{h_{-1,2}}\Big(\kappa r\ln(z\bar{z})+2s+\frac{\mu}{r}\Big). \tag{7.6.6}$$

To summarize, (7.6.2), (7.6.3) and (7.6.6) assemble to the following logarithmic conformal block:

$$\begin{aligned}\mathscr{F}^{\log}(z,\bar{z}) =&(z\bar{z})^{-2\Delta}\Big\{z^{h_{1,2}}\bar{z}^{h_{1,-2}}+z^{h_{1,-2}}\bar{z}^{h_{1,2}}+\frac{h_{1,2}}{2}\left(z^{h_{1,2}+1}\bar{z}^{h_{1,-2}}+z^{h_{1,-2}}\bar{z}^{h_{1,2}+1}\right)\\ &+\Big[\frac{\kappa r}{2}\ln(z\bar{z})+s+\frac{\mu}{2r}+\frac{h_{1,2}(1+h_{1,2})^2}{4(1+2h_{1,2})}\Big]\left(z^{h_{1,2}+2}\bar{z}^{h_{1,-2}}+z^{h_{1,-2}}\bar{z}^{h_{1,2}+2}\right)+\dots\Big\}\,.\end{aligned} \tag{7.6.7}$$

Note that by construction $[L_{-1},A]=0$, so the correlations between Ψ and the terms in the first part of the OPE vanish. Note also that by construction we have $L_1 AX=0$, and since $A^\dagger AX=0$, $L_2 AX=0$ as well, so $X\otimes\bar{Y}$ is a primary field.

7.6.2 Input from ordinary conformal blocks

In this section, we obtain the logarithmic block (7.6.7) using input from the ordinary conformal blocks as a consistency check.

Recall the ordinary s-channel expansion of the ordinary conformal blocks

$$\begin{aligned}\mathscr{F}_h = z^{h-2\Delta}\Big[1+\frac{h}{2}z+\frac{z^2}{16(h-h_{1,2})(h-h_{2,1})}\begin{pmatrix}h(h+1) & h+\Delta\end{pmatrix}\begin{pmatrix}2+\frac{c}{4h} & -3\\ -3 & 4h+2\end{pmatrix}\begin{pmatrix}h(h+1)\\ h+\Delta\end{pmatrix}\\ +\dots\Big]\end{aligned} \tag{7.6.8}$$

and similarly for $\bar{z}$. We focus on the four-point function of the fields with conformal weight $\Delta=h_{1/2,0}$ (the Potts-model order operator) and consider the conformal block in the case of $\Phi_{1,2}$. As discussed in depth in [21], the amplitudes associated with the fields with weight $h_{1+\epsilon,2}$ and $h_{-1+\epsilon,2}$ are related by recursions resulting from the degeneracy of $\phi_{2,1}$. We then consider the combinations (first mentioned in [152])

$$\tilde{C}(\epsilon)\Big\{\mathscr{F}_{h_{1+\epsilon,2}}(z)\mathscr{F}_{h_{1+\epsilon,2}}(\bar{z})+\frac{A_{-1+\epsilon,2}}{A_{1+\epsilon,2}}\mathscr{F}_{h_{-1+\epsilon,2}}(z)\mathscr{F}_{h_{-1+\epsilon,2}}(\bar{z})\Big\}\,, \tag{7.6.9}$$

where $A_{-1+\epsilon,2}/A_{1+\epsilon,2}$ is a known function; see [21] for more details. To make connections with the OPE discussed in Section 7.5, we recognize that this ratio should be identified with $a^2(\epsilon)$ in (7.5.15) and thus has the expansion

$$\frac{A_{-1+\epsilon,2}}{A_{1+\epsilon,2}} = \frac{\lambda}{\epsilon^2} + \frac{\mu}{\epsilon} + O(1)\,. \tag{7.6.10}$$

More explicitly, taking $\Delta = h_{1/2,0}$, one finds

$$\lambda = -\left(\frac{1-\beta^4}{512}\frac{\beta^2}{2\beta^2-1}\right)^2. \tag{7.6.11}$$

This results in the following contribution from the second term of (7.6.9):

$$\begin{aligned}&\tilde{C}(\epsilon)(z\bar{z})^{-2\Delta}(z\bar{z})^{h_{-1+\epsilon,2}}\Big[\Big(\frac{\lambda}{\epsilon^2}+\frac{\mu}{\epsilon}\Big)+\dots\Big],\\ &\quad=\tilde{C}(\epsilon)(z\bar{z})^{-2\Delta}(z\bar{z})^{h_{-1,2}}\Big[\Big(\frac{\lambda}{\epsilon^2}+\frac{\mu}{\epsilon}-\frac{\lambda}{\epsilon}\frac{(2\beta^2+1)}{2\beta^2}\ln(z\bar{z})\Big)+\dots\Big]\,,\end{aligned} \tag{7.6.12}$$

where $\dots$ stands for higher powers in $z, \bar{z}$ and $O(1)$ terms.

Now focus on the first term in (7.6.9). As $\epsilon \to 0$, (7.6.8) has a simple pole for $h = h_{1,2}$. Explicit calculations then give

$$\frac{1}{16(h-h_{1,2})(h-h_{2,1})}\begin{pmatrix}h(h+1) & h+\Delta\end{pmatrix}\begin{pmatrix}2+\frac{c}{4h} & -3\\ -3 & 4h+2\end{pmatrix}\begin{pmatrix}h(h+1)\\ h+\Delta\end{pmatrix} = \frac{\rho}{\epsilon}+\sigma+O(\epsilon) \tag{7.6.13}$$

with

$$\rho = \frac{\beta^2(1-\beta^4)}{512(2\beta^2-1)}\,, \tag{7.6.14a}$$

$$\sigma = \frac{-12+16\beta^2+121\beta^4-216\beta^6-129\beta^8+288\beta^{10}}{1024\beta^2(-1+2\beta^2)^2}\,. \tag{7.6.14b}$$

The first term in (7.6.9) then gives the contribution

$$\begin{aligned}&\tilde{C}(\epsilon)(z\bar{z})^{-2\Delta}(z\bar{z})^{h_{1+\epsilon,2}}\Big|\Big(1+\frac{h_{1+\epsilon,2}}{2}z+z^2\big(\frac{\rho}{\epsilon}+\sigma\big)+\dots\Big)\Big|^2\\ &=\tilde{C}(\epsilon)(z\bar{z})^{-2\Delta}(z\bar{z})^{h_{1,2}}\Big\{\frac{\rho^2}{\epsilon^2}(z\bar{z})^2+\frac{\rho}{\epsilon}(z^2+\bar{z}^2)+\frac{\rho}{\epsilon}\frac{h_{1,2}}{2}(z\bar{z}^2+z^2\bar{z})\\ &\qquad\qquad+\frac{\rho}{\epsilon}\Big(2\sigma+\frac{\rho(1-2\beta^2)}{2\beta^2}\ln(z\bar{z})\Big)(z\bar{z})^2+\dots\Big\}\,,\end{aligned} \tag{7.6.15}$$

where again $\dots$ stands for higher powers in $z, \bar{z}$ and $O(1)$ terms.

Combining (7.6.12) and (7.6.15), we see first that the double poles cancel due to

$$\lambda + \rho^2 = 0\,, \tag{7.6.16}$$

as is evident from (7.6.11) and (7.6.14a). On the other hand, it is natural to take $\tilde{C}(\epsilon) = \frac{\epsilon}{\rho}$. Therefore the combination (7.6.9) reduces to

$$\begin{aligned}(z\bar{z})^{-2\Delta}\Big\{&z^{h_{1,2}}\bar{z}^{h_{1,-2}}+z^{h_{1,-2}}\bar{z}^{h_{1,2}}+\frac{h_{1,2}}{2}\left(z^{h_{1,2}+1}\bar{z}^{h_{1,-2}}+z^{h_{1,-2}}\bar{z}^{h_{1,2}+1}\right)\\ &+\Big(\sigma+\frac{\mu}{2\rho}+\frac{\rho}{2\beta^2}\ln(z\bar{z})\Big)\left(z^{h_{1,2}+2}\bar{z}^{h_{1,-2}}+z^{h_{1,-2}}\bar{z}^{h_{1,2}+2}\right)+\dots\Big\}\,,\end{aligned} \tag{7.6.17}$$

where we have used $h_{1,2} + 2 = h_{-1,2}$ and (7.6.16).

We now compare (7.6.17) with the logarithmic block (7.6.7) that we obtained previously.

First, it is obvious that the first lines of (7.6.17) and (7.6.7) agree. To compare the level-2 coefficients, we need r, s as defined in (7.5.14). As discussed above, these quantities depend on the external fields and in this case we take $\Delta = h_{1/2,0}$ in (7.5.14). First we find

$$r = \frac{\beta^2(1-\beta^4)}{512(2\beta^2-1)} = \rho\,. \tag{7.6.18}$$

Recall that in the OPE study in Section 7.5, we have obtained the singularity cancellation condition (7.5.16). Now we see that for the four-point function of the order operator we focus on here, this is the same as (7.6.16). On the other hand, it is a simple exercise to check that the following identity holds:

$$\sigma = s + \frac{h_{1,2}(1+h_{1,2})^2}{4(1+2h_{1,2})}\,, \tag{7.6.19}$$

using (7.5.14) and (7.6.14b). Therefore we have seen that the constant terms in the second lines of (7.6.17) and (7.6.7) agree. Finally, the coefficients for the $\ln(z\bar{z})$ terms are easily matched using (7.5.11) and (7.6.18).

7.6.3 Numerical amplitudes and Jordan cells

The investigation of the parity of lattice states in Appendix I indicates the existence of the indecomposable structure (7.4.10). To go further and find numerical evidence for the existence of the expected Jordan cell for $L_0, \bar{L}_0$ (or the conjectured values of the logarithmic couplings) is more difficult, since it turns out that the Hamiltonian and transfer matrices of the Potts model for Q generic remain, for the levels we are interested in, completely diagonalizable in finite size. In other words, *the $(L_0, \bar{L}_0)$ Jordan cells appear only in the continuum limit.* While this possibility was foreseen in [58], it makes the problem quite different from the one studied in [9, 10], where Jordan cells were present for finite systems as a result of Temperley–Lieb representation theory, with the indecomposable structures in the continuum limit being identical to those observed in the lattice model. Luckily, we shall see that it is nonetheless possible for the case at hand to observe the "build-up" of Jordan cells in the lattice model.

To that end, we now go back to the four-point functions of the order operator in the Potts model. In lattice terms, they are of the form $P_{a_1a_2a_3a_4}$, where a label a_i is associated with each of the four insertion points z_i (with $i = 1, 2, 3, 4$), the convention being that points are required to belong to the same FK cluster if and only if their corresponding labels are identical. For instance, P_{abab} denotes the four-point function in which z_1 and z_3 belong to the same cluster, while z_2 and z_4 belong to a different cluster (compare to the diagram D_{abab} in Figure 4.4). To study such correlation functions on the lattice by the transfer matrix technique, it is convenient to place points z_1, z_2 on the same time slice (i.e., lattice row) and points z_3, z_4 on a different, distant slice (see Figure 4.7). This geometric arrangement amounts to performing the s-channel expansion of the correlation function (see [20, 21] and Chapter 4). The simplest example of the structure (7.4.10) involves the fields $(\Phi_{e,j}, \bar{\Phi}_{e,j})$ from the standard module $\mathscr{W}_{j,z^2}$ with $j = 1$, but we have seen in (7.1.2) that these fields decouple from the Potts-model partition function, and the results of [20] show that they also decouple from the correlation functions of the order parameter.

It is therefore natural to turn to the next available case, $j = 2$, and thus the representation $\mathscr{W}_{2,z^2}$. The results of [20] show that P_{abab} and P_{abba} both have the property of coupling to $\mathscr{W}_{2,1}$

and $\mathscr{W}_{2,-1}$ in their s-channel expansion, and they are the only four-point functions that contain these two representations as their *leading* contributions (other correlation functions couple to $\overline{\mathscr{W}}_{0,\mathfrak{q}^{\pm 2}}$ and/or $\mathscr{W}_{0,-1}$ as well). Moreover, the symmetric combination

$$P_{\rm S} = P_{abab} + P_{abba} \tag{7.6.20}$$

decouples from $\mathscr{W}_{2,-1}$ for symmetry reasons, and since $\mathscr{W}_{2,1}$ contains the fields $(\Phi_{e,2}, \bar{\Phi}_{e,2})$ with integer $e \geq 0$, it transpires that $P_{\rm S}$ is the most convenient correlation function to investigate in the present context. Finally, the lowest-lying levels that can give rise to the structure (7.4.10) correspond to the case $e = 1$. For all these reasons we henceforth focus on the case $(e, j) = (1, 2)$.

Denoting the separation between the two groups of points z_1, z_2 and z_3, z_4 along the imaginary time direction[7] by ℓ, the correlation function in the cylinder geometry generically takes the form

$$P_{\rm S} = \sum_i A_i \left(\frac{\Lambda_i}{\Lambda_0}\right)^{\ell}, \tag{7.6.21}$$

where the sum is over the contributing eigenvalues Λ_i (with Λ_0 referring to the ground state), and A_i are the corresponding amplitudes. A rank-2 Jordan cell for the transfer matrix on the lattice manifests itself by a "generalized amplitude," with A_i of the form $a_i + \ell b_i$. This structure can be observed in many cases when $\mathfrak{q}$ is a root of unity [59]. In our problem, however, the Jordan cells *are not present* for L finite, and only expected to appear in the limit $L \to \infty$. A natural scenario for how this might happen is as follows: we should have two eigenvalues which become close as $L \to \infty$, with divergent and opposite amplitudes. Assuming that $\Lambda_1 = \Lambda(1+a\epsilon)$ and $\Lambda_2 = \Lambda(1 - a\epsilon)$ appear with respective amplitudes $A_1 = A + b/\epsilon$ and $A_2 = A - b/\epsilon$, where the small parameter $\epsilon \to 0$ when $L \to \infty$, we have then

$$\begin{aligned} A_1 \left(\frac{\Lambda_1}{\Lambda_0}\right)^{\ell} + A_2 \left(\frac{\Lambda_2}{\Lambda_0}\right)^{\ell} &\approx \left(A + \frac{b}{\epsilon}\right)\left(\frac{\Lambda}{\Lambda_0}\right)^{\ell}(1 + a\ell\epsilon) + \left(A - \frac{b}{\epsilon}\right)\left(\frac{\Lambda}{\Lambda_0}\right)^{\ell}(1 - a\ell\epsilon) \\ &= 2A\left(\frac{\Lambda}{\Lambda_0}\right)^{\ell} + 2ab\ell\left(\frac{\Lambda}{\Lambda_0}\right)^{\ell} \end{aligned} \tag{7.6.22}$$

reproducing as $L \to \infty$ the behavior expected from the presence of a Jordan cell for the continuum-limit Hamiltonian.

The method best adapted to identifying the scenario in (7.6.22) is based on scalar products, as discussed in Section 4.3.2 of [20]. Notice that although this method measures the amplitudes A_i directly in the $\ell \to \infty$ limit, the hypotheses leading to the scaling form can still be tested, and in particular the scaling of the amplitudes under the approach to the thermodynamic limit $L \to \infty$.

We now investigate this issue in the context of the $(\Phi_{1,2}, \bar{\Phi}_{1,2})$ structure, which is numerically the most accessible case for the reasons given above.

The finite-size level corresponding to the pair of fields $(\Phi_{1,2}, \bar{\Phi}_{1,2})$ has been identified in Appendix B (Table 14) of [17] as the line with $i_{13} = 3$. This is a twice degenerate level (doublet) in the transfer matrix spectrum, because the fields $\Phi_{1,2}$ and $\bar{\Phi}_{1,2}$ are related by the exchange of chiral and antichiral components. The corresponding combined amplitude (i.e., summed over the doublet) for the contribution of this level to $P_{\rm S}$ is shown in the first line of Table 7.1. The amplitudes are normalized by that of the leading contribution to $P_{\rm S}$, namely

[7] A shift between the two groups of points along the space-like direction was shown in [20] to be irrelevant. In the notations of Figure 1 in [20] one can therefore consider the two groups to be aligned, i.e., with a shift $x = 0$. This yields Figure 4.7.

Line	L						
i_{13}	5	6	7	8	9	10	11
3	0.51584673	0.53739515	0.51435306	0.53469774	0.52426708	0.53949703	0.53338217
24	−0.0041836648	−0.012473807	−0.018607995	−0.032601923	−0.041773974	−0.059633592	
25	−0.011807194	−0.025268048	−0.024113896	−0.034228263	−0.033153298	−0.040478536	
35	0.023005683	0.053207857	0.061027619	0.093065936	0.10297778	0.13439104	

Table 7.1: Amplitudes A_i of the correlation function P_{S} corresponding to selected fields within $\mathscr{W}_{2,1}$, in finite size L. The distance between the two points within each group is taken as $d = \lfloor L/2 \rfloor$. The lines of the table are labeled by the index i_{13}. For further details, see Appendix B of [17]

Line	L					
i_{13}	5	6	7	8	9	10
3	0.29631794	0.23327610	0.19042437	0.15916824	0.13539463	0.11679002
24	−0.000002260380	−0.000005746649	−0.000008815612	−0.000010766671	−0.000011635877	−0.000011709765
25	−0.0019402603	−0.0026491875	−0.0029769838	−0.0030550303	−0.0029897585	−0.0028501860
35	0.000038085542	0.000050876586	0.000053221816	0.000049738327	0.000043951008	0.000037766542

Table 7.2: Amplitudes A_i of the correlation function P_{S} corresponding to selected fields within $\mathscr{W}_{2,1}$, in finite size L. The distance between the two points within each group is now chosen the smallest possible, $d = 1$.

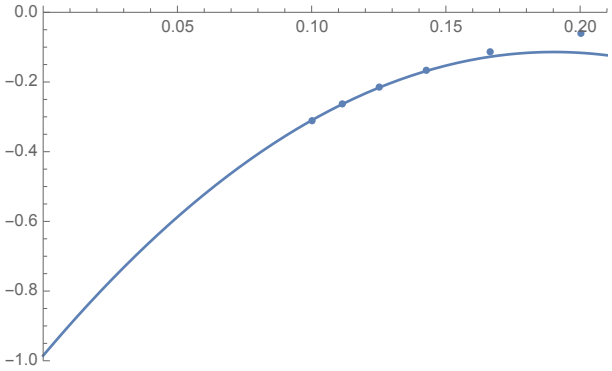

Figure 7.1: Ratio A_1/A_2 between the amplitudes of the two singlet fields (see Table 7.2), corresponding to the lines with $i_{13} = 24$ and $i_{13} = 35$ (see Table 14 of [17]), plotted against $1/L$. The curve is a second-order polynomial fit to the last three data points.

the amplitude of the line with $i_{13} = 1$ in Table Table 14 of [17]. To be precise, the table shows the amplitudes for cylinders of circumference $L = 5, 6, \ldots, 11$, and in all cases the distance d between the two points in each group (z_1, z_2 and z_3, z_4) is taken the largest possible: $d = L/2$ for L even, and $d = (L-1)/2$ for L odd. This choice (which was also used in the numerical work in [20,21]) corresponds to a fixed, finite distance between the two points in the continuum limit. Unfortunately, it also leads to parity effects in L, which are clearly visible from Table 7.1. It is nevertheless clear that the amplitude of the line with $i_{13} = 3$ converges to a finite constant, as expected for this non-logarithmic pair of fields, and this can be confirmed by independent fits of even and odd sizes. Regrettably, the situation for the remaining lines of Table 7.1 is less clear. Naively the amplitude for each one of the last three lines appears to grow with L, but our attempts to quantify this have not been very compelling, due to fact that we only have three sizes of each parity at our disposal.

We therefore turn to another strategy, in which the same amplitudes are measured with the smallest possible distance $d = 1$ between the two points in each group. This will eliminate the parity effects, so that more reliable fits can be studied. Note that the choice $d = 1$ corresponds to a vanishing distance in the continuum limit, so one might expect the finite-size amplitudes to pick up an extra factor of $1/L$. In particular, the amplitude of a generic, non-logarithmic field contributing to P_{S} is then expected to vanish as L^{-1} in the $L \to \infty$ limit. Indeed, the amplitude of the line with $i_{13} = 3$ in Table 7.2 fits very nicely to $c_0 + c_1 L^{-1} + c_2 L^{-2} + \cdots$, and the absolute value of the constant term c_0 can be determined to be at least 80 times smaller than the data point with $L = 10$. We therefore conjecture that, in this case, $c_0 = 0$ indeed.

For the line with $i_{13} = 24$ (a singlet level) we attempt a fit of the form $c_0 + c_1 L^{-\delta} + c_2 L^{-2\delta} + c_3 L^{-3\delta}$. This matches the data nicely with $\delta \simeq 1.005$, indicating that $\delta = 1$ might be the exact value of the exponent. But we find now that the absolute value of the constant term c_0 is about 3 times *larger* than the data point with $L = 10$, which is strongly indicative of c_0 being nonzero in this case. We therefore conjecture that this line should be identified with one of the two fields in the Jordan cell (7.5.24).

The same type of fit for the line with $i_{13} = 35$ (the other singlet level) yields $\delta \simeq 2.05$ and a constant term c_0 which is about 4 times *smaller* than the $L = 10$ data point. Finally, the line with $i_{13} = 25$ (a doublet) matches the fit with $\delta \simeq 1.3$ and c_0 about 3 times smaller than the data point with $L = 10$. Seen in isolation, these fits do not permit us to convincingly conclude whether the value of c_0 is finite or zero for those two lines. However, structural considerations provide more compelling evidence. According to the argument given in (7.6.22), the logarithmic

singlet with $i_{13} = 24$ needs to be accompanied by another singlet field with an opposite and diverging (for finite conformal distance) amplitude. Being a singlet, the line with $i_{13} = 35$ is the only possible candidate for such a logarithmic partner.

As a decisive test, we therefore plot in Figure 7.1 the ratio between the amplitudes of the two singlets. A second-order polynomial in $1/L$ fits the data nicely and gives an extrapolated value of the ratio of -0.985, very close to the exact ratio of -1 expected from (7.6.22). We believe that this settles the issue, showing that the two singlets correspond to the conformal fields $A_{1,2}\Phi_{1,2} + \bar{A}_{1,2}\bar{\Phi}_{1,2}$ and Ψ, and that the indecomposable structure (7.4.9) builds up only in the $L \to \infty$ limit. On the other hand, Figure 7.1 vividly illustrates that a maximum size of $L = 10$ is still quite far from the thermodynamic limit, and with hindsight it is therefore hardly surprising that only a combination of arguments can reveal the true nature (logarithmic or non-logarithmic) of the four fields from Table 14 of [17] having conformal weights $(h_{1,2}+2, h_{1,2}+2)$.

7.7 Currents and the "ordinary" loop model

The "ordinary" dense loop model is defined simply as a model of dense loops with fugacity $\mathfrak{m}$ for *all* loops. It can be considered as a continuation to all values of $\mathfrak{m}$ of a $U(\mathfrak{m})$ model defined initially for $\mathfrak{m}$ integer by introducing alternating fundamental and conjugate fundamental representations of $U(\mathfrak{m})$ on the edges of a square lattice, with a simple nearest neighbor spin-spin coupling [63]. The continuum limit partition function is similar to the one of the Potts model, with subtle differences:

$$\mathcal{Z}_{\mathfrak{m}} = F_{0,\mathfrak{q}^{\pm 2}} + \sum_{j>0} \hat{D}_{j,0} F_{j,1} + \sum_{\substack{j>0, M>1 \\ M|j}} \sum_{\substack{0<p<M \\ p\wedge M=1}} \hat{D}_{j,\pi p/M} F_{j,\mathrm{e}^{2\pi \mathrm{i} p/M}}\,, \tag{7.7.1}$$

where again

$$\hat{D}_{j,K} = \frac{1}{j} \sum_{r=0}^{j-1} \mathrm{e}^{2\imath K r} w(j, j\wedge r)\,, \tag{7.7.2}$$

but w takes the form

$$w(j,d) = \mathfrak{q}^{2d} + \mathfrak{q}^{-2d}\,, \tag{7.7.3}$$

to be compared with (7.1.4). This decomposition of the torus partition function corresponds to the exact decomposition of the Hilbert space over modules of T^a in finite size:

$$\mathscr{H}_{\mathfrak{m}} = \overline{\mathscr{W}}_{0,\mathfrak{q}^{\pm 2}} \oplus \mathscr{W}_{1,1} \oplus \bigoplus_{j>0} \hat{D}_{j,0} \mathscr{W}_{j,1} \oplus \bigoplus_{\substack{j>0, M>1 \\ M|j}} \bigoplus_{\substack{0<p<M \\ p\wedge M=1}} \hat{D}_{j,\pi p/M} \mathscr{W}_{j,\mathrm{e}^{2\pi \mathrm{i} p/M}}, \tag{7.7.4}$$

to be compared with (7.1.12). An interesting difference with the Potts model is the module $\mathscr{W}_{1,1}$ which now occurs with multiplicity $\hat{D}'_{1,1} + 1 = \mathfrak{m}^2 - 1$. A remarkable thing about this module is that it contains fields with conformal weight $(h_{1,-1}, h_{1,1})$ and $(h_{1,1}, h_{1,-1})$ with $\mathfrak{m}$-independent values $(1,0)$ and $(0,1)$, like for chiral *currents*. Of course, we do not expect to have currents in the Potts model, since the symmetry of the latter is only discrete: this is compatible with the fact that $\mathscr{W}_{1,1}$ disappears in this case, as observed earlier. In contrast, for the $U(\mathfrak{m})$ model, we find a multiplicity $D_{\mathrm{adj}} = \mathfrak{m}^2 - 1$ which is precisely the dimension of the adjoint representation, as expected for models with continuous symmetries. As discussed in [63], D_{adj} is half the multiplicity of the fields with weight $(1,1)$: the number $2D_{\mathrm{adj}}$ simply counts the two fields with weights $(h_{1,-1}, h_{1,-1})$ in the L_0 or $\bar{L}_0$ Jordan cell, and there are D_{adj} such cells.

It is then interesting to compare our results with those obtained by Gorbenko and Zan [138] in their study of the related $O(n)$ model. Their model describes "dilute loops" instead of the "dense loops" described by the $U(\mathfrak{m})$ model discussed here.[8] On top of this, it also differs from the $U(\mathfrak{m})$ model in that the number of non-contractible loops can be odd or even, while for $U(\mathfrak{m})$ it is necessarily even. It is nonetheless instructive to compare the Jordan-cell structure for the currents with the one obtained in [138]. To match their normalizations, we set

$$A \equiv \frac{\Psi_{1,1}}{\sqrt{-2\kappa_{1,1}^{-1}\nu_{1,1}}} = \frac{\Psi_{1,1}}{\sqrt{-2b_{1,1}}} \tag{7.7.5}$$

(this A from [138] should not be confused with the combination of Virasoro generators $A_{1,1}$ used earlier), so that

$$\langle A(w,\bar{w})A(0)\rangle = \frac{\ln(w\bar{w})}{(w\bar{w})^2}\,. \tag{7.7.6}$$

To match their current two-point function, reading in the notations of [138]

$$\langle J(w,\bar{w})J(0)\rangle = -\frac{1}{w^2}\,, \tag{7.7.7}$$

we set $X \otimes \bar{Y} = iJ$. We have then

$$L_1 A = \frac{L_1\Psi_{1,1}}{\sqrt{-2b_{1,1}}} = \sqrt{\frac{-b_{1,1}}{2}}X\otimes\bar{Y} = \sqrt{\frac{b_{1,1}}{2}}J = \sqrt{\frac{1-\beta^2}{2}}J\,. \tag{7.7.8}$$

Since $\beta^2 = x/(x+1)$, we find finally

$$L_1 A = \sqrt{\frac{1}{2(x+1)}}J\,, \tag{7.7.9}$$

where we recall that $\mathfrak{m} = 2\cos(\pi/(x+1))$. This must be compared with equations (5.24) and (5.31) from [138], where a similar but different result $L_1 A = J/\sqrt{2x}$ is found, with $n = 2\cos(\pi/x)$ and the usual central charge (3.5.4). The shift $x \to x+1$ is familiar in the context of the dilute/dense phases relationship. We believe that a lattice analysis similar to the one we have presented here—but carried out instead for the dilute critical loop model and the dilute Temperley–Lieb algebra—would fully reproduce the results in [138]. Conversely, their analysis could be extended to reproduce our result for the currents in the $U(\mathfrak{m})$ model.

This section concludes Chapter 7, in which we have explored Virasoro representations in the Potts and loop models. The logarithmic modules we have found are relevant in the $O(n)$ model as well, as was also seen in [6]. In the next chapter, we use the corresponding logarithmic conformal blocks to bootstrap the $O(n)$ model.

[8] These "dense loops" are sometimes referred to more correctly as "completely packed loops," because the cover all the edges of the medial lattice (see Section 7.2).

CHAPTER

8

BOOTSTRAPPING THE $O(N)$ MODEL

In this chapter we initiate the application of the bootstrap approach to the two-dimensional $O(n)$ conformal field theory, with the specific goals of understanding how the $O(n)$ symmetry acts on the spectrum, and how it manifests itself in crossing symmetry equations. It is in principle enough to define the theory as a set of CFT data, namely a space of states and the corresponding structure constants. However, this raises the issue of making contact with the continuum limit of the $O(n)$ lattice model [37].

In Chapter 2 we gave a quick introduction to the lattice model. Let us here add a few more details and comments, before defining the $O(n)$ conformal field theory.

The two-dimensional $O(n)$ model and its lattice description

The $O(n)$ model can be defined either on a lattice, or directly as a field theory on a continuous space via a Lagrangian. The lattice description has the advantages of allowing the torus partition function to be computed, and of allowing the model to be defined for non-integer values of n. These features are crucial to the bootstrap investigation that we undertake here, which starts with the torus partition function [43], and numerically solves crossing symmetry equations at complex values of n. The analyticity in n is less clear in the Lagrangian description, as we will discuss in Section 8.4.3.

Consider as in Chapter 2 the model on the honeycomb lattice, with the weight of a configuration given by $w(\{\phi(x)\}) = \prod_{<x,y>} (1 + K\phi(x) \cdot \phi(y))$ where $< x, y >$ denote nearest neighbour vertex pairs. We recall that for any $-2 \leq n \leq 2$, there is a critical value [37]

$$K_c(n) = \frac{1}{\sqrt{2 + \sqrt{2 - n}}} \ . \tag{8.0.1}$$

The model has four phases:

- For $0 < K < K_c(n)$, a high-temperature massive phase.

- At $K = K_c(n)$, the continuum limit of the critical point is a CFT, which we call the **critical dilute $O(n)$ model**.

- For $K_c(n) < K < \infty$ and $-2 < n < 2$, there is also a critical phase, called the dense loop gas. Its properties do not depend on the value of K. The continuum limit of that phase is called the **critical dense $O(n)$ model** [2].

- For $K = \infty$ and $-2 < n \leq 2$ the model exhibits a distinct critical phase, the fully-packed loop (FPL) gas in which the loops jointly cover all the lattice vertices [153]. This phase and its corresponding CFT are specific to the honeycomb lattice [154] and we shall not consider them further.

The cases $n = \pm 2$ are a bit special. For $n = -2$ and $K > K_c(n)$ the lattice model experiences a first-order phase transition. For $n = 2$ the continuum limits of the dilute and dense phases coincide. Other versions of the lattice model exist:

- The same model can be put on a square lattice. There is ample analytic and numerical evidence that this does not change the critical phases and their CFT description [155]. However, the square-lattice model also allows for a richer choice of multicritical interactions, which lead to extra critical phases [156–158].

- On the honeycomb lattice, we can use the alternative configuration weight $w(\{\phi(x)\}) = \prod_{<x,y>} \exp\left(K\phi(x)\cdot\phi(y)\right)$. It is widely believed that this does not change the phase diagram, and leads to the same critical dilute $O(n)$ model at $K = K_c(n)$ [38,155]. However, the limit $K \to \infty$ becomes ill-defined, and the continuum limit of the critical phase at $K > K_c(n)$ can change. This same change also occurs on the square lattice, where it is due to four-leg crossings becoming relevant [38].

In the loop gas description of the lattice model, n needs no longer be integer, and appears as a continuous parameter. On a finite lattice, correlation functions (including the partition function) are sums over finite numbers of graphs with polynomial n-dependent coefficients. After taking the continuum limit, n is still a continuous parameter of the resulting CFT. This is supposed to hold not only for the dilute loop gas, but also for the dense loop gas, at least if $n \neq 0$. There are however subtleties: in the dense loop gas, it is known that the limit $n \to 0$ does not commute with the continuum limit [159].

The $O(n)$ conformal field theory

As two-dimensional CFTs, the critical dilute and dense $O(n)$ models are characterized by their central charges, which are functions of n. These functions are better expressed via a parameter β^2:

$$c = 13 - 6\beta^2 - 6\beta^{-2} \quad , \quad n = -2\cos\left(\pi\beta^2\right) . \tag{8.0.2}$$

Then the difference between the dense and dilute models is the range of values of β^2:

Critical model	n	β^2	c
Dilute	$[-2,2]$	$[1,2]$	$[-2,1]$
Dense	$(-2,2)$	$(0,1)$	$(-\infty,1)$

(8.0.3)

In particular, for any $c \in [-2, 1)$, the dilute and dense models are two distinct CFTs with the same central charge. Remarkably, as functions of β^2, the correlation functions of these two CFTs are given by the same expressions. In principle, this can be understood by reformulating the honeycomb-lattice loop model as a square-lattice loop model in one particular regime, which comprises both the dense and dilute $O(n)$ models in their entire critical ranges $-2 < n \leq 2$ [155]. In practice, this is confirmed by numerical studies [155], including for the three-point functions [102].

We define the $O(n)$ **conformal field theory** as a family of CFTs parametrized by β^2, which includes the critical dilute and dense $O(n)$ models as special cases. Actually, just like the critical Q-state Potts model, the $O(n)$ CFT makes sense way beyond the interval $\beta^2 \in (0, 2]$ that covers these two models: the allowed range of β^2 is the complex half-plane [74]

$$\operatorname{Re} \beta^2 > 0 \quad \Longrightarrow \quad \operatorname{Re} c < 13 \ . \tag{8.0.4}$$

The $O(n)$ CFT therefore lives on a β^2-half-plane, or equivalently on a double cover of a c-half-plane, or equivalently on a covering of the n-complex plane with infinitely many sheets. Let us draw the β^2-complex plane, where the allowed range is divided into strips of width one. We call the first two strips dense and dilute, by extension of that terminology to complex values of the parameters:

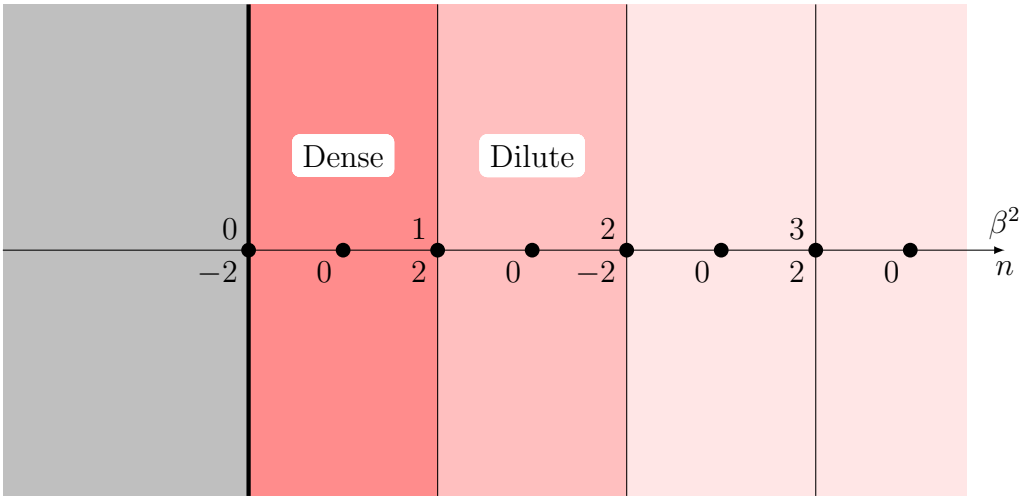

(8.0.5)

For some integer values of n, the $O(n)$ CFT describes models of particular physical interest:

n	c_{dilute}	Dilute model	c_{dense}	Dense model
-2	-2	Symplectic fermion (LERW)	$-\infty$	Not defined
-1	$-\frac{3}{5}$	Related to spanning forests?	-7	Related to spanning forests?
0	0	Dilute polymers (SAW)	-2	Dense polymers
1	$\frac{1}{2}$	Ising model	0	Percolation hulls ($T = \infty$ Ising)
2	1	Free boson	1	Free boson

(8.0.6)

Some comments and references:

- $n = 2$: The relation with the free boson follows directly from the Coulomb gas mapping [37, 43].

- $n = 1$ (dilute): The equivalence with the Ising model on a triangular lattice is a standard result of low-temperature expansion of the latter in terms of domain walls on the dual (honeycomb) lattice. Actually, the critical coupling $K_c(1) = \frac{1}{\sqrt{3}}$ matches the known critical coupling of the triangular-lattice Q-state Potts model at $Q = 2$ [160].

- $n = 1$ (dense): The infinite-temperature limit of the Ising model on the triangular lattice resides in the dense phase ($O(n)$ loops are the domain walls). It corresponds to the trivial value $K = 1$, which identifies the corresponding loops with the hulls of site-percolation clusters on the triangular lattice.

- $n = 0$: The polymer limits are extensively discussed in [2]. Dilute polymers are also known as self-avoiding walks (SAW) and provide arguably the single most important motivation for studying the $O(n)$ model.

- $n = -1$: The subtle relation between spanning forests and a non-linear sigma model with $n = -1$ components is treated in [161], but the relation to the $O(-1)$ models remains speculative [162].

- $n = -2$: The link to symplectic fermions and the loop-erased random walks (LERW) is covered by [163, 164].

Solving the $O(n)$ CFT: a brief history

In dimensions between two and four, the critical $O(n)$ model was the subject of early works by Lang and Rühl, who found quite a few nontrivial results on the spectrum and fusion rules [165].

The study of the two-dimensional $O(n)$ CFT has been closely intertwined with the study of the critical Q-state Potts model, which is technically very similar. While the central charge and the spectrum of conformal dimensions have been known for a long time [37, 43, 44], the determination of four-point functions and operator product expansions has long remained inaccessible, due to the absence of BPZ differential equations for most correlation functions of the theory. Progress came from work on lattice models and their algebraic aspects (see [63, 79, 141] and Chapter 7), from considerations of symmetry [138], and from the bootstrap approach (see [6, 19–21, 74] and Chapter 4).

However, the bootstrap approach was previously only applied to the Potts model, and then only in the case of four-point connectivities, which are the simplest nontrivial four-point correlation functions (but see [150] for more recent results for the Potts model, extending the work in the present chapter). In this chapter we will apply the bootstrap approach to the $O(n)$ CFT, and start a systematic scan of the model's four-point functions. To do this, we have developed and adapted numerical bootstrap code that was originally written for Liouville theory, the Q-state Potts model, and related CFTs [166].

One crucial aspect of our approach is to label primary fields $V^{\lambda}_{(r,s)}$ by both their conformal dimensions, in the form of Kac indices (r, s), and irreducible representations of $O(n)$, in the form of Young tableaux λ. We consider only generic parameter values $\beta^2 \notin \mathbb{Q}$, in order to keep the structures of indecomposable representations under control.

Highlights of this chapter

Let us point out a few ideas and results that we consider particularly worthy of attention:

- The definition of the $O(n)$ CFT over the complex β^2-plane, earlier in this introduction.

- The conjectured decomposition of the spectrum into irreducible representations of $O(n)$, Eqs. (8.1.20) and (8.1.26).
- The principles of the conformal bootstrap method in the presence of a global symmetry in Section 8.2.2, in particular the inequality (8.2.29) between numbers of bootstrap solutions and $O(n)$ invariants.
- The fusion rules of the fields $V^{[1]}_{(\frac{1}{2},0)}$, $V^{[2]}_{(1,0)}$ and $V^{[11]}_{(1,1)}$, in Sections 8.3.1 and 8.3.2.

8.1 The group $O(n)$ and its action on the spectrum

In order to solve the model, we need to determine its spectrum, i.e., its space of states. The known symmetries of the model are conformal symmetry, which is described by a product $\mathfrak{C}$ of two Virasoro algebras (left-moving and right-moving), and the global $O(n)$ symmetry. The spectrum should therefore decompose into representations of $O(n) \times \mathfrak{C}$.

In the $O(n)$ Wess–Zumino–Witten model, we would have the symmetry $O(n) \times \mathfrak{C}$, which would however be part of a larger symmetry, due to the presence of two conserved $O(n)$ currents: primary fields with conformal dimensions $(\Delta, \bar{\Delta}) = (1, 0)$ and $(0, 1)$, which belong to the adjoint representation of $O(n)$. In the $O(n)$ CFT, we also have two $O(n)$ currents, but they are not independently conserved, have logarithmic OPEs, and do not give rise to a Kac–Moody symmetry algebra.

8.1.1 Partition function and action of the conformal algebra

Our main source of information on the spectrum is the torus partition function. By definition, the partition function counts the generalized eigenvectors of the zero-mode generators $L_0, \bar{L}_0$ of the two Virasoro algebras. This is in principle not enough for decomposing the spectrum into representations of $\mathfrak{C}$, let alone $O(n)$. Nevertheless, that goal can be reached with the help of other sources of information, and of some guesswork.

Partition function

The conformal dimensions of the primary states in the $O(n)$ CFT are of the type

$$\Delta_{(r,s)} = P^2_{(r,s)} - P^2_{(1,1)} \quad \text{with} \quad P_{(r,s)} = \frac{1}{2}\left(\beta r - \beta^{-1} s\right) \ , \tag{8.1.1}$$

where the Kac table indices r, s take values in $\mathbb{Q}$. The relevant characters of the conformal algebra are the diagonal degenerate characters

$$\chi_{\langle r,s\rangle}(q) = \left| \frac{q^{P^2_{(r,s)}} - q^{P^2_{(r,-s)}}}{\eta(q)} \right|^2 \ , \tag{8.1.2}$$

as well as the non-diagonal characters

$$\chi^N_{(r,s)}(q) = \frac{q^{P^2_{(r,s)}} \bar{q}^{P^2_{(r,-s)}}}{|\eta(q)|^2} \ . \tag{8.1.3}$$

In these expressions, $q = e^{2\pi i \tau}$ is the exponentiated modulus of the torus, and $\eta(q)$ is the Dedekind eta function.

The partition function was obtained as early as 1987 by calculating the continuum limit of the lattice partition function on the torus [43]. The lattice partition function is a sum over all loop configurations on a doubly periodic system. By construction, the lattice partition function is already modular invariant. Its continuum limit is

$$\boxed{Z^{O(n)}(q) = \sum_{s\in 2\mathbb{N}+1} \chi_{\langle 1,s\rangle}(q) + \sum_{r\in\frac{1}{2}\mathbb{N}^*} \sum_{s\in\frac{1}{r}\mathbb{Z}} L_{(r,s)}(n)\chi^N_{(r,s)}(q)} \,, \tag{8.1.4}$$

where $L_{(r,s)}(n)$ is a polynomial function of n that we will write in Eq. (8.1.15). For the moment, we will focus on the dependence on q, and what it reveals on the representations of the conformal algebra that appear in the spectrum.

The partition function is a sum over Kac indices r, s. In a minimal model, these indices would take finitely many integer values. In the $O(n)$ CFT, the spectrum is much richer. Both indices can take infinitely many values, and the second index can take fractional values with arbitrarily high denominators, provided the conformal spin rs remains integer. Faced with such a rich spectrum, we may be tempted to look for a larger symmetry algebra that would help organize it. However, the presence of arbitrarily high denominators dooms such ideas, and indeed it is known that (except for $n = 1, 2$) there exists no chiral algebra that would organize the spectrum into finitely many representations, in other words that would make the CFT rational [63]. Actually, the CFT is not even quasi-rational, i.e. the fusion product of two representations may include infinitely many indecomposable representations.

The integer values of the indices that do appear in the $O(n)$ CFT lead to algebraic complications. For $r, s \in \mathbb{N}^*$, a primary field of dimension $\Delta_{(r,s)}$ has a null vector. In a unitary CFT, null vectors would have to vanish. In the $O(n)$ CFT, null vectors do not necessarily vanish, and they lead to the existence of logarithmic representations. Before reviewing these representations for generic values of β^2, let us point out that the situation is even more complicated if $\beta^2 \in \mathbb{Q}$: in this case, more null vectors appear, leading to more intricate algebraic structures that are just beginning to be understood [167].

Logarithmic representations of the conformal algebra

Let us briefly review the action of the conformal algebra on the spectrum of the $O(n)$ CFT, as determined in [6] and in Chapter 7. (For earlier partial results, see [79, 138].)

The appearance of degenerate characters in the partition function strongly suggests that the corresponding degenerate representations $\mathscr{R}_{\langle 1,s\rangle}$ appear in the spectrum, and we will work under that assumption. To be precise, $\mathscr{R}_{\langle 1,s\rangle}$ is the tensor product of the degenerate representation of the left-moving Virasoro algebra with a vanishing null vector at level s, with the same degenerate representation of the right-moving Virasoro algebra.

In the non-diagonal sector, the character $\chi^N_{(r,s)}(q)$ can only describe a Verma module unless $r, s \in \mathbb{Z}^*$. In that case, due to the existence of null vectors in the Verma module, there exist other representations with the same character, including an infinite family of logarithmic representations. To lift this ambiguity, one approach is to relate the ambiguous case $(r, s) \in \mathbb{Z}^*$ to the unambiguous case $(r, 0)$ via fusion with degenerate fields [6, 79, 138]. Another approach is to take the conformal limit of the lattice model as in Chapter 7. Both approaches converge on the same results, i.e., on an indecomposable logarithmic representation whose character is

$\chi^N_{(r,s)}(q) + \chi^N_{(r,-s)}(q)$. We introduce the notations

$$\mathscr{W}_{(r,s)} \underset{r,s\in\mathbb{N}^*}{=} \text{ indecomposable representation with character } \chi^N_{(r,s)}(q) + \chi^N_{(r,-s)}(q) \ , \tag{8.1.5a}$$

$$\mathscr{W}_{(r,s)} \underset{r,-s\in\mathbb{N}^*}{=} 0 \ , \tag{8.1.5b}$$

$$\mathscr{W}_{(r,s)} \underset{r\notin\mathbb{Z}^* \text{ or } s\notin\mathbb{Z}^*}{=} \text{ Verma module with character } \chi^N_{(r,s)}(q) \ . \tag{8.1.5c}$$

The convention of setting some representations to zero is meant to avoid overcounting in the spectrum (8.1.20), where we will have combinations of the type $\mathscr{W}_{(r,s)} \oplus \mathscr{W}_{(r,-s)}$ whenever $rs \neq 0$.

We refrain from recalling the structures of the logarithmic representations in more detail in this chapter, as we will not need them. What we do need are the corresponding conformal blocks, which we will discuss in Section 8.2.1.

8.1.2 Representations of $O(n)$ and their tensor products

Much is known about finite-dimensional representations of $O(n)$, whether n is integer or generic, but it is not always easy to find the relevant results in the mathematical literature. We will briefly review the results that we need. For more information and references, see the Wikipedia article on Representations of classical Lie groups.

$O(n)$ symmetry with non-integer n

Consider the n-dimensional vector representation of $O(n)$. A state in that representation shows up in the model's torus partition function (8.1.4) as a term $Z^{O(n)}(q) = n\chi^N_{(\frac{1}{2},0)}(q) + \cdots$. How do we deal with the corresponding fields? At first sight, it seems we must introduce a vector index $i \in \{1, 2, \dots, n\}$ and write a vector field as $V^{[1]}_i$, where [1] denotes the vector representation. (We omit other parameters such as the conformal dimension.) Then the fusion of this field with itself reads

$$V^{[1]}_{i_1} V^{[1]}_{i_2} \sim \delta_{i_1,i_2} V^{[]} + V^{[2]}_{(i_1,i_2)} + V^{[11]}_{[i_1,i_2]} \ , \tag{8.1.6}$$

i.e., the $O(n)$ symmetry allows three representations: the singlet representation [], the symmetric traceless tensor [2] and the antisymmetric tensor [11]. However, we can make sense of $O(n)$ symmetry with n generic by simply omitting the vector indices, and writing the fusion rule

$$V^{[1]} V^{[1]} \sim V^{[]} + V^{[2]} + V^{[11]} \ . \tag{8.1.7}$$

Now fields are no longer labelled by states in $O(n)$ representations, but only by the representations themselves. It no longer matters whether these representations have integer dimensions or not. Mathematically, this can be interpreted in terms of tensor categories of representations [168]. In this chapter, we will sometimes use $O(n)$ vector indices for explanatory purposes, or in order to relate our results to other approaches. However, our results themselves will always hold for generic values of n.

It turns out that the generic n case can be obtained formally from the integer n case by taking the limit $n \to \infty$. In our example, the fusion rule is only true if $n \geq 2$, as for $n = 1$ the representations [2] and [11] are actually zero. The fusion rule stabilizes at $n = 2$ and no longer changes as n increases. This stabilization at finite n is a general feature of the tensor products of $O(n)$ representations.

Irreducible representations and their dimensions

The finite-dimensional irreducible representations of $O(n)$ are parametrized by Young diagrams, which we write as decreasing sequences of natural integers, such as $[53321111] = [53^2 21^4]$. For example, $[k]$ is the fully symmetric representation with k indices, and $[1^k]$ is the fully antisymmetric representation with k indices.

For λ a Young diagram, let λ_i be the length of the i-th row, in other words $\lambda = [\lambda_1 \lambda_2 \cdots \lambda_r]$. Let $\tilde{\lambda}_i$ be the length of the i-th column. Let $h_\lambda(i,j) = \lambda_i + \tilde{\lambda}_j - i - j + 1$ be the hook length of the box (i,j) in the diagram λ.

$\lambda = [85542]$:

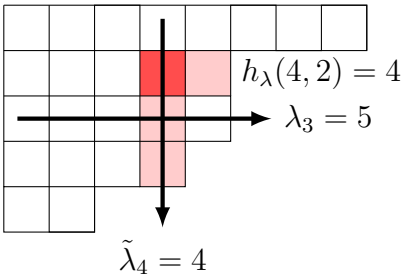

(8.1.8)

Then the dimension of the corresponding $O(n)$ representation is [169]

$$\dim_{O(n)} \lambda = \prod_{\substack{(i,j)\in\lambda \\ i\geq j}} \frac{n + \lambda_i + \lambda_j - i - j}{h_\lambda(i,j)} \prod_{\substack{(i,j)\in\lambda \\ i<j}} \frac{n - \tilde{\lambda}_i - \tilde{\lambda}_j + i + j - 2}{h_\lambda(i,j)} \ . \tag{8.1.9}$$

For example, the dimensions of the fully symmetric representations $[], [1], [2], [3], [4], \cdots$ are

$$\dim_{O(n)}[k] = 1, n, \tfrac{1}{2}(n+2)(n-1), \tfrac{1}{6}(n+4)n(n-1), \tfrac{1}{24}(n+6)(n+1)n(n-1), \cdots \tag{8.1.10}$$

The dimensions of the fully antisymmetric representations are

$$\dim_{O(n)}[1^k] = \binom{n}{k} \ , \tag{8.1.11}$$

which vanishes for $k > n$. More generally, for integer n, irreducible representations are actually parametrized by diagrams such that $\tilde{\lambda}_1 + \tilde{\lambda}_2 \leq n$. There is no such restriction for generic n. In this case, the dimensions of representations should be considered as formal polynomial functions of n. The degree of a polynomial is the size of the corresponding Young diagram, i.e., the number of boxes.

Tensor products and Newell–Littlewood numbers

Tensor products of $O(n)$ representations with n generic can be written as

$$\lambda \otimes \mu = \sum_\nu N_{\lambda,\mu,\nu} \nu \ , \tag{8.1.12}$$

where the tensor product coefficients $N_{\lambda,\mu,\nu}$ are called Newell–Littlewood numbers [170]. These numbers are n-independent natural integers. They can in principle be obtained as large n limits of their integer-n counterparts, although the integer-n coefficients are actually more complicated. For example,

$$[1] \otimes [1] = [2] + [11] + [] \ , \tag{8.1.13a}$$

$$[1]\otimes[2]=[21]+[3]+[1]\ , \tag{8.1.13b}$$
$$[1]\otimes[11]=[111]+[21]+[1]\ , \tag{8.1.13c}$$
$$[1]\otimes[21]=[31]+[22]+[211]+[2]+[11]\ , \tag{8.1.13d}$$
$$[1]\otimes[3]=[4]+[31]+[2]\ , \tag{8.1.13e}$$
$$[2]\otimes[2]=[4]+[31]+[22]+[2]+[11]+[]\ , \tag{8.1.13f}$$
$$[2]\otimes[11]=[31]+[211]+[2]+[11]\ , \tag{8.1.13g}$$
$$[11]\otimes[11]=[1111]+[211]+[22]+[2]+[11]+[]\ , \tag{8.1.13h}$$
$$[21]\otimes[3]=[321]+[411]+[42]+[51]+[211]+[22]+2[31]+[4]+[11]+[2]\ . \tag{8.1.13i}$$

The tensor product is commutative and associative, and $N_{\lambda,\mu,\nu}$ is symmetric under permutations of the three Young diagrams. The size $|\lambda|=\sum_i\lambda_i$ is conserved modulo 2 and obeys the inequalities

$$||\lambda|-|\mu||\leq|\nu|\leq|\lambda|+|\mu|\ . \tag{8.1.14}$$

In practice, all tensor products can be computed using associativity, together with the Pieri-type rule that determines the products of the type $[k]\otimes\mu$. The rule says that $[k]\otimes\mu$ is the sum of all possible Young diagrams that are obtained by, for each successive $i\in\{0,\dots,k\}$, first removing i boxes from μ in different columns, and then adding $k-i$ boxes in different columns.

8.1.3 Action of $O(n)$ on the spectrum

Dimensions of representations

In the partition function (8.1.4), the non-diagonal Virasoro characters come with the coefficients [63]

$$\boxed{L_{(r,s)}(n)=\delta_{r,1}\delta_{s\in2\mathbb{Z}+1}+\frac{1}{2r}\sum_{r'=0}^{2r-1}e^{\pi ir's}x_{(2r)\wedge r'}(n)}\ , \tag{8.1.15}$$

where we recall the condition $2r\in\mathbb{N}^*$, and introduce the polynomials $x_d(n)$ such that

$$x_0(n)=2\quad,\quad x_1(n)=n\quad,\quad nx_d(n)=x_{d-1}(n)+x_{d+1}(n)\ . \tag{8.1.16}$$

If we had set $x_0(n)=1$, we would have obtained the Chebyshev polynomials of the second kind. Instead, we obtain the polynomials

$$x_2(n)=n^2-2\ , \tag{8.1.17a}$$
$$x_3(n)=n(n^2-3)\ , \tag{8.1.17b}$$
$$x_4(n)=n^4-4n^2+2\ , \tag{8.1.17c}$$
$$x_5(n)=n(n^4-5n^2+5)\ , \tag{8.1.17d}$$
$$x_6(n)=(n^2-2)(n^4-4n^2+1)\ . \tag{8.1.17e}$$

This leads to the coefficients

$$L_{(\frac{1}{2},0)}(n) = n \ , \tag{8.1.18a}$$
$$L_{(1,0)}(n) = \tfrac{1}{2}(n+2)(n-1) \ , \tag{8.1.18b}$$
$$L_{(1,1)}(n) = \tfrac{1}{2}n(n-1) \ , \tag{8.1.18c}$$
$$L_{(\frac{3}{2},0)}(n) = \tfrac{1}{3}n(n^2-1) \ , \tag{8.1.18d}$$
$$L_{(\frac{3}{2},\frac{2}{3})}(n) = \tfrac{1}{3}n(n^2-4) \ . \tag{8.1.18e}$$

By construction, the coefficients obey

$$L_{(r,s)}(n) = L_{(r,-s)}(n) = L_{(r,s+2)}(n) \ . \tag{8.1.19}$$

These equations are rather easy to interpret. The first equation expresses the invariance of the theory under the exchange of left-moving and right-moving variables. The second equation follows from the existence of a degenerate field with Kac indices $(1,3)$. We will discuss similar equations for conformal blocks and correlation functions in Section 8.2.1.

We would now like to write the spectrum of the $O(n)$ CFT as a representation of $O(n) \times \mathfrak{C}$ of the type

$$\boxed{\mathcal{S}^{O(n)} = \bigoplus_{s \in 2\mathbb{N}+1} [] \otimes \mathscr{R}_{\langle 1,s \rangle} \oplus \bigoplus_{r \in \frac{1}{2}\mathbb{N}^*} \bigoplus_{s \in \frac{1}{r}\mathbb{Z}} \Lambda_{(r,s)} \otimes \mathscr{W}_{(r,s)}} \ . \tag{8.1.20}$$

Here, $\mathscr{R}_{\langle 1,s \rangle}$ and $\mathscr{W}_{(r,s)}$ are the representations of the conformal algebra $\mathfrak{C}$ that we introduced in Section 8.1.1. The unknown representation $\Lambda_{(r,s)}$ of $O(n)$ is a linear combination of irreducible finite-dimensional representations, with positive integer coefficients [168, 171]. By definition of the partition function (8.1.4), this implies

$$\boxed{\dim_{O(n)} \Lambda_{(r,s)} = L_{(r,s)}(n)} \ . \tag{8.1.21}$$

Given the dimensions (8.1.9) of $O(n)$ representations, the first three equations of this type have unique solutions,

$$\Lambda_{(\frac{1}{2},0)} = [1] \ , \tag{8.1.22a}$$
$$\Lambda_{(1,0)} = [2] \ , \tag{8.1.22b}$$
$$\Lambda_{(1,1)} = [11] \ . \tag{8.1.22c}$$

However, the next equation has two solutions, $\Lambda_{(\frac{3}{2},0)} \in \{[3]+[111], [21]+[1]\}$, and the number of solutions increases quickly with r. Some extra constraints can be obtained by considering the case $n = 2$ [138], but they are not enough for making the solution unique in general.

Structures of representations

In order to write the representations $\Lambda_{(r,s)}$, our basic idea is to use the formula (8.1.15) for its dimension, where we replace each occurrence of n with an n-dimensional formal representation, i.e., a combination of irreducible representations with coefficients in $\mathbb{Z}$. The sizes of the needed Young diagrams are constrained by the requirement that $\Lambda_{(r,s)}$ be a combination of diagrams of size $2r$ or less, since its dimension is a polynomial of degree $2r$. Therefore, for any $t \in \mathbb{N}^*$, we need to find at least one combination of irreducible representations of size t or less, whose dimension is n.

We propose the following alternating hook representations,

$$\boxed{\Lambda_t = \delta_{t\equiv 0 \bmod 2}[] + \sum_{k=0}^{t-1}(-1)^k[t-k,1^k]} \ . \tag{8.1.23}$$

The first few examples are

$$\Lambda_1 = [1] \ , \tag{8.1.24a}$$
$$\Lambda_2 = [2] - [11] + [] \ , \tag{8.1.24b}$$
$$\Lambda_3 = [3] - [21] + [111] \ , \tag{8.1.24c}$$
$$\Lambda_4 = [4] - [31] + [211] - [1111] + [] \ . \tag{8.1.24d}$$

Automated calculations for many values of t convince us that

$$\dim_{O(n)} \Lambda_t = n \ . \tag{8.1.25}$$

This leads us to the conjecture

$$\boxed{\Lambda_{(r,s)} = \delta_{r,1}\delta_{s\in 2\mathbb{Z}+1}[] + \frac{1}{2r}\sum_{r'=0}^{2r-1} e^{\pi i r' s} x_{(2r)\wedge r'}\left(\Lambda_{\frac{2r}{(2r)\wedge r'}}\right)} \ . \tag{8.1.26}$$

In each polynomial $x_d(n)$ that appears in the formula (8.1.15) for $L_{(r,s)}(n)$, we have replaced n with a representation Λ_t such that $d \times t = 2r$. Replacing powers of n with tensor products of Λ_t, we obtain the formal representation $x_d(\Lambda_t)$, which is a combination of diagrams of size $2r$ or less. According to the conjecture, the fully symmetric tensor $[2r]$ appears in $\Lambda_{(r,s)}$ with multiplicity $\delta_{s,0}$.

By construction, our representation $\Lambda_{(r,s)}$ has the correct dimension, i.e., Eq. (8.1.21) is satisfied. However, each term in $\Lambda_{(r,s)}$ is a formal representation, and involves irreducible $O(n)$ representations with coefficients that are neither positive nor even integer. Automated calculations in many examples show that $\Lambda_{(r,s)}$ itself is actually a representation, i.e., a combination with positive integer coefficients. Let us display the first few examples, beyond the cases already given in (8.1.22a)-(8.1.22c):

$$\Lambda_{(\frac{3}{2},0)} = [3] + [111] \ , \tag{8.1.27a}$$
$$\Lambda_{(\frac{3}{2},\frac{2}{3})} = [21] \ , \tag{8.1.27b}$$
$$\Lambda_{(2,0)} = [4] + [22] + [211] + [2] + [] \ , \tag{8.1.27c}$$
$$\Lambda_{(2,\frac{1}{2})} = [31] + [211] + [11] \ , \tag{8.1.27d}$$
$$\Lambda_{(2,1)} = [31] + [22] + [1111] + [2] \ , \tag{8.1.27e}$$
$$\Lambda_{(\frac{5}{2},0)} = [5] + [32] + 2[311] + [221] + [11111] + [3] + 2[21] + [111] + [1] \ , \tag{8.1.27f}$$
$$\Lambda_{(\frac{5}{2},\frac{2}{5})} = [41] + [32] + [311] + [221] + [2111] + [3] + 2[21] + [111] + [1] \ , \tag{8.1.27g}$$
$$\begin{aligned}\Lambda_{(3,0)} = {} & [6] + 2[42] + 2[411] + [33] + 2[321] + 2[3111] + 2[222] + [2211] + [21111] \\ & + 2[4] + 4[31] + 4[22] + 4[211] + 2[1111] + 4[2] + 2[11] + 2[] \ ,\end{aligned} \tag{8.1.27h}$$
$$\begin{aligned}\Lambda_{(3,\frac{1}{3})} = {} & [51] + [42] + 2[411] + [33] + 3[321] + [3111] + 2[2211] + [21111] \\ & + [4] + 5[31] + 2[22] + 5[211] + [1111] + 2[2] + 4[11] \ ,\end{aligned} \tag{8.1.27i}$$
$$\Lambda_{(3,\frac{2}{3})} = [51] + 2[42] + [411] + 3[321] + 2[3111] + [222] + [2211] + [21111]$$

$$+ 2[4] + 4[31] + 4[22] + 4[211] + 2[1111] + 4[2] + 2[11] + [] \ , \tag{8.1.27j}$$

$$\Lambda_{(3,1)} = [51] + [42] + 2[411] + 2[33] + 2[321] + 2[3111] + [222] + 2[2211] + [111111] + [4] + 5[31] + 2[22] + 5[211] + [1111] + 2[2] + 4[11] \ . \tag{8.1.27k}$$

In the case of $\Lambda_{(2,0)}$, our conjecture agrees with already known results [138]. More evidence will come from our bootstrap calculations, since the structure of $\Lambda_{(r,s)}$ leads to predictions on the numbers of solutions of crossing symmetry equations, as we will explain in Section 8.2.2. Future work [49] will consider the conjecture in more detail, as well as a similar conjecture for the Q-state Potts model; this is outside the scope of this thesis.

8.2 Conformal bootstrap

Since we know the representations of the conformal algebra that appear in the $O(n)$ CFT, we can in principle use the semi-analytic bootstrap method of [19], and write crossing symmetry as a system of linear equations for four-point structure constants. However, the $O(n)$ CFT gives rise to new technical and conceptual issues. In particular, the presence of a global $O(n)$ symmetry leads to the existence of large numbers of solutions of crossing symmetry, which we will have to count and to interpret. This is a priori not easy, because crossing symmetry equations know only about the conformal symmetry, and do not directly encode any information about the global symmetry.

Let us introduce notations for primary fields in the $O(n)$ CFT, which correspond to the representations in the spectrum (8.1.20):

- Let $V^D_{\langle 1,s\rangle}$ be a diagonal degenerate primary field: such fields always transform in the singlet representation [] of $O(n)$.
- Let $V_{(r,s)}$ be a non-diagonal primary field with the left and right conformal dimensions $(\Delta, \bar{\Delta}) = (\Delta_{(r,s)}, \Delta_{(r,-s)})$ (8.1.1).
- Let V^λ be a field that belongs to the irreducible representation λ of $O(n)$.
- Let $V^\lambda_{(r,s)}$ be a non-diagonal primary field that also belongs to the irreducible representation λ of $O(n)$. For example, the representation $\Lambda_{(\frac{3}{2},0)}$ (8.1.27a) gives rise to the two fields $V^{[3]}_{(\frac{3}{2},0)}$ and $V^{[111]}_{(\frac{3}{2},0)}$.

Unless $r, s \in \mathbb{Z}^*$, the primary field $V_{(r,s)}$ generates the Verma module $\mathscr{W}_{(r,s)}$ of the conformal algebra. If $r, s \in \mathbb{N}^*$, the logarithmic module $\mathscr{W}_{(r,s)}$ contains two primary fields $V_{(r,s)}, V_{(r,-s)}$, which however do not generate it [6]. Our notation is ambiguous whenever $\Lambda_{(r,s)}$ has nontrivial multiplicities. For example, $\Lambda_{(\frac{5}{2},0)}$ (8.1.27f) gives rise to two independent fields of the type $V^{[21]}_{(\frac{5}{2},0)}$.

8.2.1 Singularities of conformal blocks

In the $O(n)$ CFT, the existence of degenerate fields $V^D_{\langle 1,s\rangle}$ leads to shift equations for structure constants [72,79]. These equations allow us to combine linear sums of infinitely many conformal blocks into interchiral blocks [21, 172], and therefore to reduce the number of unknowns in crossing symmetry equations. Moreover, these equations allow us to determine logarithmic conformal blocks [6]. We will now study the singularities that can appear in these equations, and therefore also in conformal blocks.

Before that, let us comment on a small subtlety. The shift equations are usually derived from the existence of the degenerate field $V^D_{\langle 1,2\rangle}$, whereas the spectrum of the $O(n)$ CFT only contains $V^D_{\langle 1,3\rangle}$. Given the fusion rule $V^D_{\langle 1,2\rangle} \times V^D_{\langle 1,2\rangle} \sim V^D_{\langle 1,3\rangle} + V^D_{\langle 1,1\rangle}$, the $V^D_{\langle 1,3\rangle}$ shift equations must follow from the $V^D_{\langle 1,2\rangle}$ shift equations, but they could conceivably be weaker. However, a closer look shows that they are in fact equivalent: monodromies of third-order BPZ equations, while harder to compute, are in principle no less constraining than those of second-order BPZ equations.

Regularizing singularities in shift equations

Let us quickly review the shift equations for non-diagonal fields. (The argument would be the same in the presence of diagonal fields.) We assume that there exists a diagonal degenerate field $V^D_{\langle 1,2\rangle}$, whose fusion rule with the non-diagonal field $V_{(r,s)}$ is

$$V^D_{\langle 1,2\rangle} \times V_{(r,s)} \sim V_{(r,s+1)} + V_{(r,s-1)} \ . \tag{8.2.1}$$

Crossing symmetry and single-valuedness of the four-point function $\langle V^D_{\langle 1,2\rangle} \prod_{i=1}^3 V_{(r_i,s_i)}\rangle$ imply the conditions [72]

$$r_i s_i \in \mathbb{Z} \ , \tag{8.2.2a}$$

$$r_i \in \frac{1}{2}\mathbb{Z} \ , \tag{8.2.2b}$$

$$r_1 + r_2 + r_3 \in \mathbb{Z} \ . \tag{8.2.2c}$$

The first two conditions are obeyed by the spectrum (8.1.20) of the $O(n)$ CFT. The third condition is a basic constraint on fusion: the first index is conserved modulo integers. This constraint is equivalent to the conservation of $|\lambda|$ modulo 2 in tensor products of $O(n)$ representation, since the model only contains fields $V^\lambda_{(r,s)}$ such that $|\lambda| \equiv 2r \bmod 2$.

However, when it comes to the linear system [72](3.16) that leads to shift equations, only the last two conditions are necessary for a solution to exist. When we encounter singularities in shift equations, we can therefore regularize them by relaxing the integer spin condition (8.2.2a), i.e., by analytically continuing fields in their second index s_i while keeping r_i fixed.

To be concrete, our shift equations (8.2.5) and (8.2.6) will involve ratios of Gamma functions, which may include factors of the type $\rho = \frac{\Gamma(\frac{1}{2}r+\frac{1}{2}\beta^{-2}s)}{\Gamma(\frac{1}{2}r-\frac{1}{2}\beta^{-2}s)}$. In the $O(n)$ CFT, we may need the value of this ratio for $r = s = 0$. This value depends on the way we take the limit, in particular $\lim_{r\to 0}\lim_{s\to 0}\rho = 1$ while $\lim_{s\to 0}\lim_{r\to 0}\rho = -1$. From the analysis of the shift equations' derivation, we have just deduced that the correct limit is the second one.

Interchiral blocks

Let us consider a four-point function of non-diagonal primary fields, and its s-channel decomposition into conformal blocks:

$$\left\langle \prod_{i=1}^4 V_{(r_i,s_i)} \right\rangle = \sum_{s\in 2\mathbb{N}+1} D_s \mathcal{G}^D_{\langle 1,s\rangle} + \sum_{r\in\frac{1}{2}\mathbb{N}^*} \sum_{s\in\frac{1}{r}\mathbb{Z}} D_{(r,s)} \mathcal{G}_{(r,s)} \ . \tag{8.2.3}$$

Here we have summed over the whole spectrum of possible representations (8.1.20), and introduced the corresponding conformal blocks $\mathcal{G}^D_{\langle 1,s\rangle}$ and $\mathcal{G}_{(r,s)}$ for the channel representations $\mathscr{R}_{\langle 1,s\rangle}$

and $\mathscr{W}_{(r,s)}$ respectively. The coefficients D_s and $D_{(r,s)}$, which unlike the blocks do not depend on the fields' positions, are called four-point structure constants.

Actually, we already know that the sum is not over the whole spectrum. To begin with, r is conserved modulo integers, which implies $\sum_{i=1}^4 r_i \in \mathbb{Z}$, and eliminates half the terms in our decomposition. Furthermore, degenerate representations obey the fusion rule

$$V^D_{\langle 1,s\rangle} \times V_{(r_1,s_1)} \sim \sum_{j \overset{2}{=} 1-s}^{1+s} V_{(r_1,s_1+j)} \ , \tag{8.2.4}$$

where the sum runs by increments of two. This severely restricts the degenerate representations that can appear in the decomposition, and actually eliminates them completely unless $(r_1, r_3) = (r_2, r_4)$ and $(s_1, s_3) \equiv (s_2, s_4) \bmod (2,2)$.

Let us now discuss the influence of shift equations on the decomposition into conformal blocks. Shift equations determine how four-point structure constants behave under $s \to s+2$, namely [72]

$$\frac{D_{(r,s+1)}}{D_{(r,s-1)}} = (-)^{2r_2+2r_4+1} \prod_{\epsilon,\eta=\pm} \Gamma\left(\epsilon s\beta^{-2} + \eta r\right)^{-\epsilon} \Gamma\left(\tfrac{1-\eta}{2} + (\epsilon s+\eta)\beta^{-2} - r\right)^{-\epsilon} \\ \times \frac{M(P_{(r,s)}, P_1, P_2)}{M(P_{(r,-s)}, \bar{P}_1, \bar{P}_2)} \frac{M(P_{(r,s)}, P_3, P_4)}{M(P_{(r,-s)}, \bar{P}_3, \bar{P}_4)} \ , \tag{8.2.5}$$

$$\frac{D_{s+1}}{D_{s-1}} = (-)^{2r_2+2r_4+1} \prod_{\epsilon,\eta=\pm} \Gamma\left(\epsilon s\beta^{-2} - \epsilon\right)^{-\epsilon} \Gamma\left(\tfrac{1-\eta}{2} + (\epsilon s+\eta)\beta^{-2} - \epsilon\right)^{-\epsilon} \\ \times \frac{M(P_{(1,s)}, P_1, P_2)}{M(-P_{(1,s)}, \bar{P}_1, \bar{P}_2)} \frac{M(P_{(1,s)}, P_3, P_4)}{M(-P_{(1,s)}, \bar{P}_3, \bar{P}_4)} \ , \tag{8.2.6}$$

where we introduced the notations

$$\begin{cases} P_i = P_{(r_i,s_i)} \\ \bar{P}_i = P_{(r_i,-s_i)} \end{cases} \quad , \quad M(P_1,P_2,P_3) = \prod_{\pm,\pm} \Gamma\left(\tfrac{1}{2} - \beta^{-1}P_1 \pm \beta^{-1}P_2 \pm \beta^{-1}P_3\right) \ . \tag{8.2.7}$$

In the s-channel decomposition, it is therefore enough to reduce the second index to an interval of length 2,

$$\left\langle \prod_{i=1}^4 V_{(r_i,s_i)} \right\rangle = D_{s_0}\mathscr{H}_{s_0} + \sum_{r\in\frac{1}{2}\mathbb{N}^*} \sum_{s\in\frac{1}{r}\mathbb{Z}\cap(-1,1]} D_{(r,s)}\mathscr{H}_{(r,s)} \ , \tag{8.2.8}$$

provided we introduce the interchiral blocks

$$\mathscr{H}_{s_0} = \sum_{s\in s_0+2\mathbb{N}} \frac{D_s}{D_{s_0}} \mathscr{G}^D_{\langle 1,s\rangle} \quad , \quad \mathscr{H}_{(r,s)} = \sum_{j\in 2\mathbb{N}} \frac{D_{(r,s+j)}}{D_{(r,s)}} \mathscr{G}_{(r,s+j)} \ , \tag{8.2.9}$$

where s_0 is the smallest index that is allowed by the degenerate fusion rules (8.2.4), namely

$$s_0 = 1 + \min(|s_1-s_2|, |s_3-s_4|) \quad \text{if} \quad \begin{cases} (r_1,r_3) = (r_2,r_4) \ , \\ (s_1,s_3) \equiv (s_2,s_4) \bmod (2,2) \ . \end{cases} \tag{8.2.10}$$

In the interchiral blocks, the ratios of structure constants are determined by the shift equations. Therefore, just like the conformal blocks themselves, interchiral blocks are universal quantities. Working with interchiral blocks rather than conformal blocks reduces the number of unknown four-point structure constants to be determined in the conformal bootstrap.

Accidentally non-logarithmic blocks

Let us discuss the conformal blocks that appear in the decomposition (8.2.3) of the four-point function $\left\langle \prod_{i=1}^4 V_{(r_i,s_i)} \right\rangle$. Conformal blocks are functions of the channel representation, which can be a Verma module, a degenerate representation, or a logarithmic representation. In all cases, the blocks can be assembled from the well-known Virasoro conformal blocks $\mathcal{F}_\Delta$, which correspond to Verma modules of the left-moving Virasoro algebra, together with their counterparts $\bar{\mathcal{F}}_\Delta$, which correspond to Verma modules of the right-moving Virasoro algebra.

In the cases of Verma modules and degenerate representations, our conformal blocks factorize, and have the simple expressions

$$\mathcal{G}_{(r,s)} \underset{r\notin\mathbb{Z}^* \text{ or } s\notin\mathbb{Z}^*}{=} \mathcal{F}_{\Delta_{(r,s)}} \bar{\mathcal{F}}_{\Delta_{(r,-s)}} \ , \tag{8.2.11}$$

$$\mathcal{G}^D_{\langle 1,s\rangle} = \mathcal{F}_{\Delta_{(1,s)}} \bar{\mathcal{F}}_{\Delta_{(1,s)}} \ . \tag{8.2.12}$$

For $r,s \in \mathbb{N}^*$, the logarithmic representation $\mathcal{W}_{(r,s)}$ generically gives rise to a logarithmic block. To write this block, let us introduce the behaviour of $\mathcal{F}_\Delta$ near one of its poles,

$$\mathcal{F}_{\Delta_{(r,s)}+\epsilon} = \frac{R_{r,s}}{\epsilon} \mathcal{F}_{\Delta_{(r,-s)}} + \mathcal{F}^{\text{reg}}_{\Delta_{(r,s)}} + O(\epsilon) \ . \tag{8.2.13}$$

Here $R_{r,s}$ is called a conformal block residue, and the regularized block $\mathcal{F}^{\text{reg}}_{\Delta_{(r,s)}}$ is generically logarithmic. Reproducing the formula [6](3.43) while slightly changing the notations and the overall normalization, we have

$$\begin{aligned}\mathcal{G}_{(r,s)} \underset{r,s\in\mathbb{N}^*}{=} \mathcal{F}^{\text{reg}}_{\Delta_{(r,s)}} \bar{\mathcal{F}}_{\Delta_{(r,-s)}} + \frac{R_{r,s}}{\bar{R}_{r,s}} \mathcal{F}_{\Delta_{(r,-s)}} \bar{\mathcal{F}}^{\text{reg}}_{\Delta_{(r,s)}} \\ - R_{r,s} \frac{P_{(r,-s)}}{P_{(r,s)}} \left(\mathcal{F}_{\Delta_{(r,-s)}} \bar{\mathcal{F}}_{\Delta_{(r,-s)}} \right)' - R_{r,s} \frac{\ell_{(r,s)}}{2P_{(r,s)}} \mathcal{F}_{\Delta_{(r,-s)}} \bar{\mathcal{F}}_{\Delta_{(r,-s)}} \ ,\end{aligned} \tag{8.2.14}$$

where the prime is a derivative with respect to the conformal dimension.

Our formula for logarithmic conformal blocks becomes singular in special cases where $R_{r,s} = 0$, which is equivalent to $\bar{R}_{r,s} = 0$. Remembering that the formula was deduced from shift equations, we know that the singularity should be regularized by continuing the blocks in the second indices s_i, while keeping r_i fixed: this allows us to compute the ratio of residues $\frac{R_{r,s}}{\bar{R}_{r,s}}$. Moreover, simplifications occur in the formula (8.2.14): the regularized block (8.2.13) is no longer logarithmic or even regularized, i.e., $\mathcal{F}^{\text{reg}}_{\Delta_{(r,s)}} = \mathcal{F}_{\Delta_{(r,s)}}$, and the whole second line vanishes. (The coefficient $\ell_{(r,s)}$ has a finite limit.) We are left with

$$\boxed{\mathcal{G}_{(r,s)} \underset{\substack{r,s\in\mathbb{N}^* \\ R_{r,s}=0}}{=} \mathcal{F}_{\Delta_{(r,s)}} \bar{\mathcal{F}}_{\Delta_{(r,-s)}} + \frac{R_{r,s}}{\bar{R}_{r,s}} \mathcal{F}_{\Delta_{(r,-s)}} \bar{\mathcal{F}}_{\Delta_{(r,s)}}} \ . \tag{8.2.15}$$

Of course, the representation $\mathcal{W}_{(r,s)}$ itself is still logarithmic in this case, as its structure does not depend on the four-point function we are considering. The disappearance of logarithmic terms in the conformal block is because the logarithmic fields in the representation happen to give vanishing contributions to this particular block. The block is now a linear combination of two Verma module blocks (8.2.11), with a relative coefficient that is still determined by the structure of $\mathcal{W}_{(r,s)}$.

8.2.2 Global symmetry and crossing symmetry

The four-point functions of the $O(n)$ conformal field theory are subject to two apparently independent types of constraints: conformal symmetry leads to crossing symmetry equations, while $O(n)$ symmetry leads to other constraints. Since the two types of constraints apply to the same four-point functions, they should lead to compatible results, and this will allow us to test our conjecture (8.1.26) for the action of the $O(n)$ symmetry on the theory's spectrum. This reasoning should apply not only to the $O(n)$ CFT, but also to any CFT with global symmetries.

Crossing symmetry

Crossing symmetry is the equality between three decompositions of the same four-point function $\left\langle \prod_{i=1}^4 V_{(r_i,s_i)} \right\rangle$:

$$\sum_{V\in\mathcal{S}^{(s)}} D_V^{(s)} \quad \begin{matrix} 2 & & 3 \\ & V & \\ 1 & & 4 \end{matrix} \quad = \sum_{V\in\mathcal{S}^{(t)}} D_V^{(t)} \quad \begin{matrix} 2 & & 3 \\ & V & \\ 1 & & 4 \end{matrix} \quad = \sum_{V\in\mathcal{S}^{(u)}} D_V^{(u)} \quad \begin{matrix} 2 & & 3 \\ & V & \\ 1 & & 4 \end{matrix} \tag{8.2.16}$$

s-channel $\qquad$ t-channel $\qquad$ u-channel

In these equations, the known quantities are the spectra $\mathcal{S}^{(s)}, \mathcal{S}^{(t)}, \mathcal{S}^{(u)}$, and the diagramatically represented interchiral blocks. The s-channel decomposition is just another notation for the decomposition (8.2.8). We do not use the condition that four-point structure constants are products of three-point structure constants, and we view crossing symmetry as a system of linear equations whose unknowns are the four-point structure constants $D_V^{(s)}, D_V^{(t)}, D_V^{(u)}$.

In practice, the spectra $\mathcal{S}^{(s)}, \mathcal{S}^{(t)}, \mathcal{S}^{(u)}$ are subsets of the full spectrum of the $O(n)$ CFT. These subsets are determined by the constraints (8.2.2c) and (8.2.4), which we now express as conformal fusion rules for our non-diagonal fields:

$$V_{(r_1,s_1)} \times V_{(r_2,s_2)} \sim \delta_{r_1,r_2}\delta_{s_1-s_2\in 2\mathbb{Z}} \sum_{s\in|s_1-s_2|+1+2\mathbb{N}} V^D_{\langle 1,s\rangle} + \sum_{r\in\frac{1}{2}\mathbb{N}^*\cap(\mathbb{Z}+r_1+r_2)} \sum_{s\in\frac{\mathbb{Z}}{r}} V_{(r,s)} \ . \tag{8.2.17}$$

For example,

$$V_{\left(\frac{1}{2},0\right)} \times V_{\left(\frac{1}{2},0\right)} \sim \sum_{s\in 1+2\mathbb{N}} V^D_{\langle 1,s\rangle} + \sum_{r\in\mathbb{N}^*} \sum_{s\in\frac{\mathbb{Z}}{r}} V_{(r,s)} \ . \tag{8.2.18}$$

In these fusion rules, we only write primary fields on the right-hand side. In the corresponding OPEs, $V_{(r,s)}$ comes with all its descendant fields. Moreover, if $r, s \in \mathbb{Z}^*$, there also appear other fields from the indecomposable representation $\mathscr{W}_{(r,s)}$, which are not descendants of $V_{(r,s)}$.

According to the fusion rules, our four-point function is non-vanishing provided $\sum_{i=1}^4 r_i \in \mathbb{Z}$. This is the condition for the spectra $\mathcal{S}^{(s)}, \mathcal{S}^{(t)}, \mathcal{S}^{(u)}$ to be non-empty, in which case they are actually infinite. We therefore have infinitely many unknown four-point structure constants. We also have infinitely many equations, since interchiral blocks are functions of one complex variable (the cross-ratio of the four fields' positions). Let us write the number of independent solutions as

$$\boxed{\mathcal{N}_{\left\langle \prod_{i=1}^4 V_{(r_i,s_i)} \right\rangle} = \dim\{\text{solutions of (8.2.16)}\}} \ . \tag{8.2.19}$$

Based on results for the Q-state Potts model, we expect that this number is finite [6, 21]. In the case of cluster connectivities in the Q-state Potts model, the number of solutions is 4. Notice however that crossing symmetry equations that involve only 2 channels out of 3 can have infinitely many solutions. Leaving the third channel unconstrained can lead to spurious solutions and/or to solutions that belong to other CFTs.

Four-point $O(n)$ invariants

Let us now consider a four-point function $\left\langle \prod_{i=1}^4 V^{\lambda_i} \right\rangle$ from the point of view of $O(n)$ symmetry. The values of that four-point function are by definition invariant under $O(n)$, so the four-point function may be viewed as a morphism of $O(n)$ representations,

$$\left\langle \prod_{i=1}^4 V^{\lambda_i} \right\rangle \in \mathrm{Hom}\left(\bigotimes_{i=1}^4 \lambda_i, [] \right) \ . \tag{8.2.20}$$

The dimension of this space, which is also the number of linearly independent $O(n)$ invariants in the representation $\otimes_{i=1}^4 \lambda_i$, will be denoted as

$$\boxed{\mathcal{I}_{\left\langle \prod_{i=1}^4 V^{\lambda_i} \right\rangle} = \dim \mathrm{Hom}\left(\bigotimes_{i=1}^4 \lambda_i, [] \right)} \ . \tag{8.2.21}$$

Each channel s, t or u gives rise to a different basis of invariants, and to a different calculation of this dimension. Consider for example the s-channel, and consider the following decompositions into irreducible $O(n)$ representations ν:

$$\lambda_1 \otimes \lambda_2 = \bigoplus_i N_{\lambda_1,\lambda_2,\nu} \nu \quad , \quad \lambda_3 \otimes \lambda_4 = \bigoplus_i N_{\lambda_3,\lambda_4,\nu} \nu \ . \tag{8.2.22}$$

For each irreducible representation ν that appears in both $\lambda_1 \otimes \lambda_2$ and $\lambda_3 \otimes \lambda_4$, we can build $N_{\lambda_1,\lambda_2,\nu} N_{\lambda_3,\lambda_4,\nu}$ invariants such that ν propagates in the s-channel, using the intertwiners that underlie our decompositions of $\lambda_1 \otimes \lambda_2$ and $\lambda_3 \otimes \lambda_4$:

$$\mathrm{Hom}\left(\bigotimes_{i=1}^4 \lambda_i, [] \right) \simeq \mathrm{Hom}\left(\lambda_1 \otimes \lambda_2, \lambda_3 \otimes \lambda_4 \right) \tag{8.2.23}$$

$$\simeq \bigoplus_\nu \mathrm{Hom}\left(\lambda_1 \otimes \lambda_2, \nu \right) \otimes \mathrm{Hom}\left(\nu, \lambda_3 \otimes \lambda_4 \right) \ . \tag{8.2.24}$$

At the level of dimensions, these isomorphisms lead to the expression

$$\mathcal{I}_{\left\langle \prod_{i=1}^4 V^{\lambda_i} \right\rangle} = \sum_\nu N_{\lambda_1,\lambda_2,\nu} N_{\lambda_3,\lambda_4,\nu} \ . \tag{8.2.25}$$

Whenever $N_{\lambda_1,\lambda_2,\nu} N_{\lambda_3,\lambda_4,\nu} = 1$, we call $T_\nu^{(s)}$ the unique (up to rescaling) four-point invariant such that ν propagates in the s-channel. If all relevant fusion multiplicities $N_{\lambda_i,\lambda_j,\nu}$ are one, the three bases of invariants can be written as

$$\mathrm{Hom}\left(\bigotimes_{i=1}^4 \lambda_i, [] \right) = \mathrm{Span}\left\{ T_\nu^{(s)} \right\}_\nu = \mathrm{Span}\left\{ T_\nu^{(t)} \right\}_\nu = \mathrm{Span}\left\{ T_\nu^{(u)} \right\}_\nu \ . \tag{8.2.26}$$

Let us give two examples, one with trivial multiplicities, the other one with nontrivial multiplicities:

- Case of $\left\langle V^{[1]}V^{[1]}V^{[1]}V^{[1]}\right\rangle$: the s-channel basis is made of the three invariants $T^{(s)}_{[]}$, $T^{(s)}_{[2]}$, $T^{(s)}_{[11]}$. If n is integer, we can restore the indices $i \in \{1, 2, \dots, n\}$ in our four-point function $\left\langle \prod_{j=1}^4 V^{[1]}_{i_j} \right\rangle$. Using the fusion rule (8.1.6), we then write the invariants as explicit tensors such as $T^{(s)}_{[]} = \delta_{i_1,i_2}\delta_{i_3,i_4}$.
- Case of $\left\langle V^{[21]}V^{[21]}V^{[1]}V^{[1]}\right\rangle$: in the t-channel, $[1] \otimes [21]$ (8.1.13d) is a sum of 5 irreducible representations with trivial multiplicities, therefore $\mathscr{I}_{\left\langle V^{[21]}V^{[21]}V^{[1]}V^{[1]}\right\rangle} = 5$. In the s-channel, the same result follows from $[1] \otimes [1]$ (8.1.13a) together with

$$[21] \otimes [21] = \Big(\text{Representations with 6 or 4 boxes}\Big) + 2[2] + 2[11] + [] \ . \tag{8.2.27}$$

Four-point functions

Let us decompose a four-point function in the $O(n)$ conformal field theory over a basis $\{T_k\}_k$ of four-point invariants:

$$\left\langle \prod_{i=1}^4 V^{\lambda_i}_{(r_i,s_i)} \right\rangle = \sum_k T_k F_k \ . \tag{8.2.28}$$

The coefficients F_k are still solutions of crossing symmetry, and we conjecture that they generate the space of solutions. In other words, we conjecture that all solutions of the crossing symmetry equations belong to the $O(n)$ CFT. This conjecture is natural, because the nontrivial input in the crossing symmetry equations is the spectrum of the model. It would be interesting to test this conjecture in simpler cases, such as minimal models: in this case, the conjecture says that we would not find more solutions by allowing channel fields to violate fusion rules, while still belonging to the spectrum.

The conjecture would be wrong if we were only considering two-channel crossing symmetry equations: we could then find solutions that have nothing to do with the $O(n)$ CFT, as is known to happen in the Q-state Potts model [6, 21]. But the three-channel equations (8.2.16) are more constraining. All our numerical results will support the conjecture.

From the conjecture, it follows that the number of invariants provides an upper bound on the number of solutions of crossing symmetry,

$$\boxed{\mathscr{N}_{\left\langle \prod_{i=1}^4 V_{(r_i,s_i)}\right\rangle} \leq \mathscr{I}_{\left\langle \prod_{i=1}^4 V^{\Lambda_{(r_i,s_i)}}\right\rangle}} \ . \tag{8.2.29}$$

We expect an inequality, but not necessarily an equality, because two solutions can coincide by a dynamical accident. In numerical results, we will indeed find many cases where the inequality is strict.

Fusion rules

In order to explicitly determine a particular solution F_k of crossing symmetry, we should use the existence of fusion rules in our CFT,

$$V^{\lambda_1}_{(r_1,s_1)} \times V^{\lambda_2}_{(r_2,s_2)} \sim \delta_{r_1,r_2}\delta_{s_1-s_2\in 2\mathbb{Z}}\delta_{[]\subset\lambda_1\otimes\lambda_2} \sum_{s\in|s_1-s_2|+1+2\mathbb{N}} V^D_{\langle 1,s\rangle} + \sum_{r\in\frac{1}{2}\mathbb{N}^*\cap(\mathbb{Z}+r_1+r_2)} \sum_{s\in\frac{\mathbb{Z}}{r}} \sum_{\nu\subset\Lambda_{(r,s)}\cap(\lambda_1\otimes\lambda_2)} V^\nu_{(r,s)} \ . \tag{8.2.30}$$

These fusion rules take into account the conformal fusion rules (8.2.17), plus the constraints of $O(n)$ symmetry, and the condition $\nu \subset \Lambda_{(r,s)}$ from the structure of the spectrum (8.1.20). In the case of the four-point function $\left\langle \prod_{i=1}^4 V_{(\frac{1}{2},0)} \right\rangle$, the solution $F_{[]}^{(s)}$, which corresponds to the invariant tensor $T_{[]}^{(s)}$, may involve the s-channel Virasoro representation $\mathscr{W}_{(2,0)}$ since $[] \subset \Lambda_{(2,0)}$ (8.1.27c), but not the representations $\mathscr{W}_{(1,0)}$, $\mathscr{W}_{(1,1)}$, $\mathscr{W}_{(2,\frac{1}{2})}$ and $\mathscr{W}_{(2,1)}$. Removing these representations from the spectrum $\mathcal{S}^{(s)}$ in the crossing symmetry equations (8.2.16) reduces the dimension of the space of solutions from 3 to 1, singling out the desired solution.

This type of reasoning typically determines a solution $F_\nu^{(x)}$ (with $x \in \{s,t,u\}$) up to an overall normalization. To fix this normalization, we can use the relations between the three bases of solutions. For example, the bases of invariants $\left\{T_\nu^{(s)}\right\}_\nu$ and $\left\{T_\nu^{(t)}\right\}_\nu$ obey a linear relation of the type $T_\nu^{(s)} = \sum_\lambda M_{\nu\lambda} T_\lambda^{(t)}$, whose coefficients are rational functions of n [168]. Therefore, the corresponding bases of solutions $\left\{F_\nu^{(s)}\right\}_\nu$ and $\left\{F_\nu^{(t)}\right\}_\nu$ must obey a similar linear relation, whose matrix is M^{-1T}. We expect that this linear relation fixes the relative normalizations of the solutions, which determines the four-point function (8.2.28) up to one overall constant coefficient. We will sketch this fixing of normalizations in an example in Section 8.3.1.

OPE commutativity and parity of spins

The fusion rule of two identical fields $V_{(r_1,s_1)}^{\lambda_1} \times V_{(r_1,s_1)}^{\lambda_1}$ obeys an extra constraint, because of OPE commutativity. Exchanging the two fields, the term of $V_{(r,s)}^{\nu}$ in the OPE picks a factor $(-1)^{rs}$ from the dependence on field positions, and a factor $\epsilon_{\lambda_1}(\nu) \in \{-1,1\}$ from the Clebsch-Gordan coefficient. For example, since the map

$$\Big(v_i \otimes v_j \mapsto v_i \otimes v_j - v_j \otimes v_i\Big) \in \mathrm{Hom}([1]\otimes[1],[11]) \tag{8.2.31}$$

is antisymmetric under $i \leftrightarrow j$, we have $\epsilon_{[1]}([11]) = -1$. OPE commutativity then implies

$$V_{(r,s)}^{\nu} \in V_{(r_1,s_1)}^{\lambda_1} \times V_{(r_1,s_1)}^{\lambda_1} \implies (-1)^{rs} \epsilon_{\lambda_1}(\nu) = 1 \ . \tag{8.2.32}$$

This means that a given representation ν can only be associated to fields with conformal spins that are either odd, or even.

But how do we determine $\epsilon_{\lambda_1}(\nu)$? This quantity may actually be ambiguous if ν appears several times in $\lambda_1 \otimes \lambda_1$. We did not find general results on this subject. In Section 8.3.3, we will find that the constraint (8.2.32) is obeyed in numerical bootstrap results. For $\lambda_1 \in \{[1],[11],[2]\}$, we found that $\epsilon_{\lambda_1}(\nu)$ actually does not depend on λ_1, and

$$\lambda_1 \in \big\{[1],[11],[2]\big\} \implies \begin{cases} \epsilon_{\lambda_1}([]) = \epsilon_{\lambda_1}([2]) = \epsilon_{\lambda_1}([4]) = \epsilon_{\lambda_1}([22]) = \epsilon_{\lambda_1}([1111]) = 1 \ , \\ \epsilon_{\lambda_1}([11]) = \epsilon_{\lambda_1}([211]) = \epsilon_{\lambda_1}([31]) = -1 \ . \end{cases} \tag{8.2.33}$$

8.2.3 Numerical implementation

Our numerical treatment of crossing symmetry equations follows the method of [19], which is applicable when the spectrum of conformal dimensions is known exactly. The basic idea is to truncate the equations to a finite system, and to deduce the existence of exact solutions from the behaviour of the truncated system's solutions as the cutoff increases. In order to reduce

the size of the system, we follow [21] and use interchiral blocks rather than conformal blocks. We further reduce computing time by drawing only one set of random positions rather than several.

Truncated crossing symmetry equations

We are interested in solving the crossing equation (8.2.16) for the structure constants at generic central charge. Since Virasoro conformal blocks have poles at rational values of the central charge, we choose values $c \in \mathbb{C} - \mathbb{R}$.

We group the fields in the spectrum into infinite families, whose relative structure constants are fixed by shift equations from degenerate fields. At the level of conformal blocks, this amounts to replacing conformal blocks with interchiral blocks. The number of families is still infinite, so we need to truncate the spectrum using a cutoff on the total conformal dimension

$$\mathrm{Re}(\Delta + \bar{\Delta}) \leq \Delta_{\max} \ . \tag{8.2.34}$$

Given the structure of the spectrum (8.1.20), and the assumption (8.0.4) on the parameter β^2, this truncation leaves us with a finite number N_{unknowns} of "interchiral primary" fields. The truncation can also be applied to descendant fields when computing a conformal block, reducing this computation to summing a finite series.

Having made the number of unknowns N_{unknowns} finite, we can now afford to make the number of equations finite as well. In the three-channel bootstrap, there are in principle two equations for each value of the cross-ratio $z \in \mathbb{C}$ of the four fields' positions. Choosing $2N_{\text{cross-ratios}} = N_{\text{unknowns}} - 1$ would give us a unique solution up to an overall factor. But we still need to test whether this solves crossing symmetry at other values of z. In [19] this was done by looking at how the solution depends on the random draw of positions $\{z_k\}_{k=1,2,\ldots,N_{\text{cross-ratios}}}$. However, it is computationally wasteful to generate the system again with completely different positions.

Instead, we propose to add only a few more positions than necessary, i.e. to choose $2N_{\text{cross-ratios}} = N_{\text{unknowns}} + O(1)$. We can then compare the solution of the first $N_{\text{unknowns}} - 1$ equations, with the solution of the last $N_{\text{unknowns}} - 1$ equations. The relative difference of these two solutions is called the **deviation**. We have a good determination of a non-vanishing structure constant if its deviation goes to zero as $\Delta_{\max} \to \infty$. We have a solution of crossing symmetry if the deviation of any given non-vanishing structure constant goes to zero. In practice, a deviation that is much smaller than 1 usually indicates that the corresponding structure constant is nonzero, and that we know its value with a relative error of the order of the deviation.

Let us give more detail on the structure of our linear system of crossing symmetry equations. We write the truncated vector of unknowns as

$$\vec{d} = \begin{pmatrix} d^{(s)} \\ d^{(t)} \\ d^{(u)} \end{pmatrix} \ , \tag{8.2.35}$$

where $d^{(s)}, d^{(t)}$ and $d^{(u)}$ are themselves truncated vectors made of the four-point structures constants $D^{(s)}, D^{(t)}, D^{(u)}$ that appear in the crossing symmetry equations (8.2.16). In total, the vector $\vec{d}$ has N_{unknowns} components, split in some way between the three channels. We then write the crossing symmetry equations as

$$B\vec{d} = 0 \tag{8.2.36}$$

where we introduce the crossing matrix in block form

$$B = \begin{pmatrix} b^{(s)} & -b^{(t)} & 0 \\ 0 & b^{(t)} & -b^{(u)} \end{pmatrix} . \tag{8.2.37}$$

The same equation could equivalently be written using the alternative crossing matrices

$$B = \begin{pmatrix} b^{(s)} & -b^{(t)} & 0 \\ b^{(s)} & 0 & -b^{(u)} \end{pmatrix} \quad \text{or} \quad B = \begin{pmatrix} 0 & b^{(t)} & -b^{(u)} \\ b^{(s)} & 0 & -b^{(u)} \end{pmatrix} . \tag{8.2.38}$$

What matters is the structure of the submatrices $b^{(s)}, b^{(t)}, b^{(u)}$ themselves. These submatrices are made of values of interchiral conformal blocks:

$$d^{(s)} = \begin{bmatrix} D^{(s)}_{V_1} \\ D^{(s)}_{V_2} \\ D^{(s)}_{V_3} \\ \vdots \end{bmatrix} \quad \text{and} \quad b^{(s)} = \begin{bmatrix} \mathscr{H}^{(s)}_{V_1}(z_1) & \mathscr{H}^{(s)}_{V_2}(z_1) & \mathscr{H}^{(s)}_{V_3}(z_1) & \dots \\ \mathscr{H}^{(s)}_{V_1}(z_2) & \mathscr{H}^{(s)}_{V_2}(z_2) & \mathscr{H}^{(s)}_{V_3}(z_2) & \dots \\ \vdots & \vdots & \vdots & \end{bmatrix} , \tag{8.2.39}$$

where V_k are elements of the s-channel spectrum, after grouping the fields and truncating.

Singular values

In principle, the number $\mathscr{N}_{\langle \prod_{i=1}^4 V_{(r_i,s_i)} \rangle}$ of solutions of the crossing-symmetry equations is the number of vanishing singular values of the untruncated crossing matrix, i.e., of the analogue of B before truncation. However, after truncating the system, no singular value is exactly zero. We should therefore count singular values that are very small and/or that go to zero as $\Delta_{\max} \to \infty$. This is not necessarily straightforward, because large matrices tend to have small singular values, even if they are not degenerate.

We do not have a mathematically well-founded criterion for determining which singular values indicate the existence of bootstrap solutions. However, our experience with numerical data suggests that it is possible to deduce the number of solutions from the singular values of the crossing matrix B (8.2.37), provided the cutoff is large enough.

Let us demonstrate this in two examples, by plotting the few lowest singular values as functions of $\Delta_{\max}$. Here and in other numerical examples, we choose $\beta^{-1} = 0.8 + 0.1i$: a generic complex value of β, far enough from the singularities of the conformal blocks at $\beta^2 \in \mathbb{Q}$. In each case we draw in red the singular values that correspond to bootstrap solutions, as we see from the large and increasing gap that separates them from the other singular values. The first plot is for the simplest nontrivial four-point function $\left\langle V_{(\frac{1}{2},0)} V_{(\frac{1}{2},0)} V_{(\frac{1}{2},0)} V_{(\frac{1}{2},0)} \right\rangle$, where we have 3

solutions:

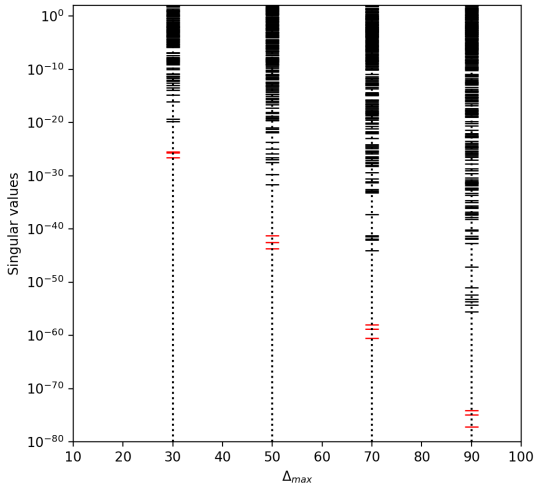

(8.2.40)

In the case of the four-point function $\left\langle V_{(\frac{3}{2},0)}V_{(\frac{3}{2},0)}V_{(\frac{1}{2},0)}V_{(\frac{1}{2},0)}\right\rangle$, the separation between the 5 lowest singular values and the rest is not large for low values of $\Delta_{\max}$, but increases as $\Delta_{\max} \to \infty$:

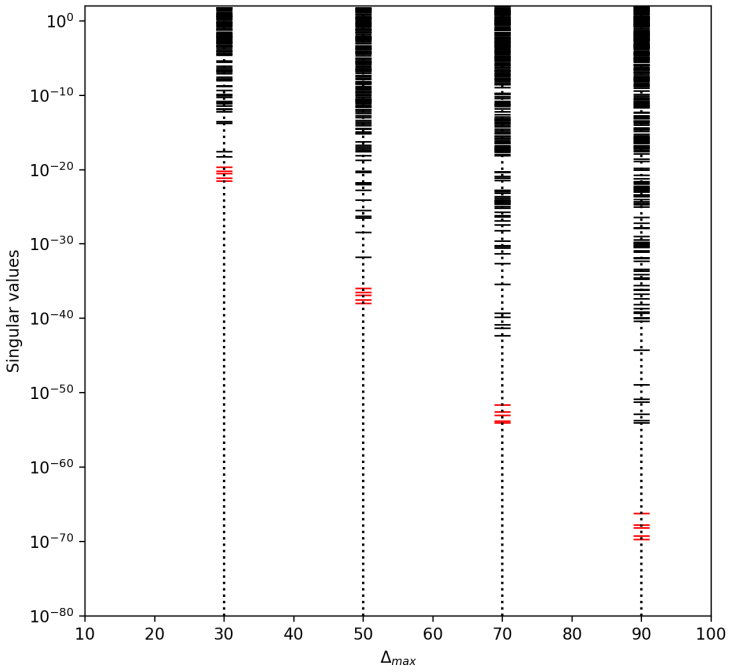

(8.2.41)

Counting solutions by examining singular values is therefore possible, but can take considerable amounts of resources because we need to compute the crossing matrix B at high precision. For instance, the crossing matrix for Figure (8.2.40) at $\Delta_{\max} = 90$ has a precision of around 70 digits. The computation took a standard desktop computer two days. And the needed precision increases with the number of solutions. To evade this issue, we will now introduce another method for counting solutions, which requires less computing power—but more human craftsmanship.

Method of excluding fields

In our bootstrap method, it is easy to detect whether the solution of the crossing symmetry equations is unique: when this happens, the deviations of non-vanishing structure constants go to zero. We can therefore single out a particular solution by adding constraints until a unique solution is found. The number of independent solutions is the number of constraints. In practice, the constraints that we use consist in setting structure constants to zero, i.e., excluding fields from the spectrum. (We also set one structure constant to one as a normalization condition.)

This method is however more an art than a science, due to the nontrivial structure of the bootstrap solutions. It can indeed happen that a structure constant (or a linear combination of structure constants) vanishes in all solutions of a given system of crossing symmetry equations. When this happens, setting that structure constant to zero does not reduce the number of solutions, and could therefore lead to miscounting.

In practice, it is rather easy to count solutions in any given example by this method, but we do not know how to automate the process. Excluding fields has the added advantage of singling out specific solutions of crossing symmetry.

Let us illustrate this method in the case of $\left\langle V^4_{(\frac{1}{2},0)} \right\rangle$ at $\Delta_{\max} = 40$ and $\beta^{-1} = 0.8 + 0.1i$. We will display the first few s-channel structure constants and their deviations, omitting the t- and u-channel structure constants for brevity. For brevity again, we only display real parts of structure constants, giving only one or two significant digits. We adopt the normalization condition $D^{(s)}_1 = 1$, i.e., we normalize the structure constant of the identity field in the s-channel. We display the data before and after excluding the fields $V_{(1,0)}$ and $V_{(1,1)}$:

	Before		After	
(r,s)	$\operatorname{Re} D^{(s)}_{(r,s)}$	Deviation	$\operatorname{Re} D^{(s)}_{(r,s)}$	Deviation
$\langle 1,1\rangle$	1	0	1	0
$(1,0)$	1.24	0.16	–	–
$(1,1)$	−0.029	0.15	–	–
$(2,0)$	-8.9×10^{-4}	0.14	-1.5×10^{-3}	1.5×10^{-19}
$(2,\pm\frac{1}{2})$	0.3×10^{-3}	0.15	-1.1×10^{-21}	0.21
$(2,1)$	-2×10^{-3}	0.16	-2.9×10^{-22}	0.24
$(3,0)$	2.8×10^{-7}	0.15	1.3×10^{-7}	6.7×10^{-11}
$(3,\pm\frac{1}{3})$	-8.0×10^{-8}	0.15	-1.7×10^{-18}	2.6
$(3,\pm\frac{2}{3})$	2.8×10^{-7}	0.15	8.3×10^{-8}	7.4×10^{-11}

(8.2.42)

Before excluding two fields, all deviations are large: we have not singled out a solution. After excluding the first two fields, the fields $V_{(2,0)}, V_{(3,0)}$ and $V_{(3,\pm\frac{2}{3})}$ have small deviations, while $V_{(2,\pm\frac{1}{2})}, V_{(2,1)}$ and $V_{(3,\pm\frac{1}{3})}$ have small values and large deviations. This signals the existence of a crossing symmetry solution with $D^{(s)}_{(2,\pm\frac{1}{2})} = D^{(s)}_{(2,1)} = D^{(s)}_{(3,\pm\frac{1}{3})} = 0$, whereas $D^{(s)}_{(2,0)}, D^{(s)}_{(3,0)}$ and $D^{(s)}_{(3,\pm\frac{2}{3})}$ have non-vanishing values that are well approximated by our numerical results, with relative errors of the order of their respective deviations. For example, we know $D^{(s)}_{(3,0)}$ with about 10 significant digits, i.e. with an absolute error $O(10^{-17})$. This solution is called $F^{(s)}_{\square}$.

Precision of the results

Finally, given a solution of crossing symmetry as a list of structure constants, we can compute the corresponding four-point function in all three channels. After all, the four-point function is the physical observable: in the Q-state Potts model, some four-point functions can be compared to results from Monte-Carlo simulations [74], and this should be doable in the $O(n)$ CFT too. Moreover, we can compare the results from the three channels, and directly check that crossing symmetry is obeyed at arbitrary values of the cross-ratio.

For example, here are the relative differences between the s, t and u-channel calculations of $F_{[]}^{(s)}$ at $\beta^{-1} = 0.8 + 0.1i$ and $z = 0.3 + 0.1i$, depending on $\Delta_{\max}$:

$\Delta_{\max}$	s versus t	t versus u
30	2.7×10^{-23}	3.6×10^{-22}
50	2.7×10^{-39}	4.3×10^{-37}
70	1×10^{-53}	2.2×10^{-51}
90	1×10^{-66}	3.7×10^{-64}

(8.2.43)

The relative differences decrease exponentially with $\Delta_{\max}$, which confirms that the results are converging towards an exact solution.

8.3 Solutions of crossing symmetry equations

The numerical results in this section were obtained using Python code that we have made publicly available [166]. In particular, relatively low-precision results for all considered solutions are found in the notebook `On4pt.ipynb`.

Let us introduce notations for writing which fields appear in a given correlation function or fusion rule. These fields must belong to the spectrum $\mathcal{S}^{O(n)}$ (8.1.20). However, due to the conservation of r modulo integers, it is convenient to introduce subspectra with values of r that differ by integers. For any $\ell \in \frac{1}{2}\mathbb{N}^*$, we introduce

$$\mathcal{S}_\ell = \left\{ (r,s) \in (\mathbb{N}+\ell) \times (-1,1] \middle| rs \in \mathbb{Z} \right\} . \tag{8.3.1}$$

Moreover, let $\mathcal{S}_0$ be $\mathcal{S}_1$ plus degenerate fields. While $\mathcal{S}^{O(n)}$ was initially defined as a vector space, we now identify it with a set of Kac indices for the corresponding indecomposable representations of the interchiral algebra, hence $s \in (-1,1]$. Furthermore, the commutativity of OPEs of identical fields (8.2.32) suggests the further split $\mathcal{S}_1 = \mathcal{S}_{\text{even}} \sqcup \mathcal{S}_{\text{odd}}$ according to the parity of the conformal spin, with

$$\mathcal{S}_{\text{even}} = \{(r,s) \in \mathbb{N} \times (-1,1] | rs \in 2\mathbb{Z}\} , \tag{8.3.2}$$

$$\mathcal{S}_{\text{odd}} = \{(r,s) \in \mathbb{N}^* \times (-1,1] | rs \in 2\mathbb{Z}+1\} . \tag{8.3.3}$$

It is also useful to list which indices are relevant to a given $O(n)$ representation,

$$\mathcal{S}^\lambda = \left\{ (r,s) \in \mathcal{S}^{O(n)} \middle| \lambda \subset \Lambda_{(r,s)} \right\} . \tag{8.3.4}$$

Based on our conjecture (8.1.26) for $\Lambda_{(r,s)}$, we further conjecture $\mathcal{S}^\lambda = \mathcal{S}_{\frac{1}{2}|\lambda|} - F_\lambda$, where F_λ is finite. For example,

$$\mathcal{S}^{[]} = \mathcal{S}_0 - \left\{ (1,0), (1,1), (2,\pm\tfrac{1}{2}), (2,1) \right\} , \tag{8.3.5a}$$

$$\mathcal{S}^{[1]} = \mathcal{S}_{\frac{1}{2}} - \left\{(\tfrac{3}{2},0),(\tfrac{3}{2},\pm\tfrac{2}{3})\right\} \ , \tag{8.3.5b}$$
$$\mathcal{S}^{[2]} = \mathcal{S}_{1} - \left\{(1,1),(2,\pm\tfrac{1}{2})\right\} \ , \tag{8.3.5c}$$
$$\mathcal{S}^{[11]} = \mathcal{S}_{1} - \left\{(1,0),(2,0),(2,1)\right\} \ , \tag{8.3.5d}$$
$$\mathcal{S}^{[3]} = \mathcal{S}_{\frac{3}{2}} - \left\{(\tfrac{3}{2},\pm\tfrac{2}{3})\right\} \ , \tag{8.3.5e}$$
$$\mathcal{S}^{[21]} = \mathcal{S}_{\frac{3}{2}} - \left\{(\tfrac{3}{2},0)\right\} \ , \tag{8.3.5f}$$
$$\mathcal{S}^{[111]} = \mathcal{S}_{\frac{3}{2}} - \left\{(\tfrac{3}{2},\pm\tfrac{2}{3})\right\} \ , \tag{8.3.5g}$$
$$\mathcal{S}^{[4]} = \mathcal{S}_{2} - \left\{(2,\pm\tfrac{1}{2}),(2,1)\right\} \ , \tag{8.3.5h}$$
$$\mathcal{S}^{[31]} = \mathcal{S}_{2} - \left\{(2,0)\right\} \ , \tag{8.3.5i}$$
$$\mathcal{S}^{[22]} = \mathcal{S}_{2} - \left\{(2,\pm\tfrac{1}{2})\right\} \ , \tag{8.3.5j}$$
$$\mathcal{S}^{[211]} = \mathcal{S}_{2} - \left\{(2,1)\right\} \ , \tag{8.3.5k}$$
$$\mathcal{S}^{[1111]} = \mathcal{S}_{2} - \left\{(2,0),(2,\pm\tfrac{1}{2})\right\} \ . \tag{8.3.5l}$$

Notice the equality $\mathcal{S}^{[3]} = \mathcal{S}^{[111]}$.

8.3.1 The simplest four-point function $\left\langle V^4_{(\frac{1}{2},0)} \right\rangle$

Invariants and bases

From the point of view of $O(n)$ representations, and with $O(n)$ vector indices explicit, our four-point function reads $\left\langle V^{[1]}_{i_1} V^{[1]}_{i_2} V^{[1]}_{i_3} V^{[1]}_{i_4} \right\rangle$. The s-channel invariants read

$$T^{(s)}_{[]} = \delta_{i_1 i_2}\delta_{i_3 i_4} \ , \tag{8.3.6a}$$
$$T^{(s)}_{[11]} = \delta_{i_1 i_4}\delta_{i_2 i_3} - \delta_{i_1 i_3}\delta_{i_2 i_4} \ , \tag{8.3.6b}$$
$$T^{(s)}_{[2]} = \delta_{i_1 i_3}\delta_{i_2 i_4} + \delta_{i_1 i_4}\delta_{i_2 i_3} - \frac{2}{n}\delta_{i_1 i_2}\delta_{i_3 i_4} \ . \tag{8.3.6c}$$

The decomposition (8.2.28) of our four-point function over this basis predicts three solutions of crossing symmetry $F^{(s)}_{[]}, F^{(s)}_{[2]}, F^{(s)}_{[11]}$. Consider the other basis of invariants,

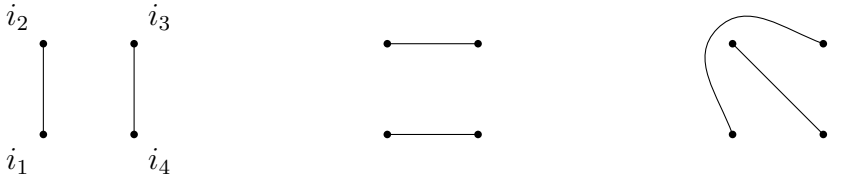

$$T^{(s)}_{[]} = \delta_{i_1 i_2}\delta_{i_3 i_4} \qquad T^{(t)}_{[]} = \delta_{i_2 i_3}\delta_{i_1 i_4} \qquad T^{(u)}_{[]} = \delta_{i_1 i_3}\delta_{i_2 i_4} \tag{8.3.7}$$

and let $F^{(s)}_0, F^{(t)}_0, F^{(u)}_0$ be the corresponding solutions of crossing symmetry. From the linear relations between the invariants, we deduce

$$F^{(s)}_0 = F^{(s)}_{[]} - \frac{2}{n}F^{(s)}_{[2]} \quad , \quad F^{(t)}_0 = F^{(s)}_{[2]} + F^{(s)}_{[11]} \quad , \quad F^{(u)}_0 = F^{(s)}_{[2]} - F^{(s)}_{[11]} \ . \tag{8.3.8}$$

From the definition (8.2.28), our four-point function is

$$\left\langle V^{[1]}_{i_1} V^{[1]}_{i_2} V^{[1]}_{i_3} V^{[1]}_{i_4} \right\rangle = \sum_{x\in\{s,t,u\}} T^{(x)}_{[]} F^{(x)}_0 \ . \tag{8.3.9}$$

The four-point function must be covariant under permutations of the four fields, and therefore also under permutations of the three channels. This implies that the three solutions $F_0^{(x)}$ are related by permutations, just like the three invariants $T_{[]}^{(x)}$. In particular, $D_{(r,s)}^{(t)}(F_0^{(t)}) = D_{(r,s)}^{(s)}(F_0^{(s)})$. Using Eq. (8.3.8), this allows us to fix the relative normalizations of the three solutions $F_{[]}^{(s)}, F_{[2]}^{(s)}, F_{[11]}^{(s)}$. For example, we know that $D_{\text{odd spin}}^{(s)}(F_0^{(s)}) = 0$, which implies $D_{\text{odd spin}}^{(t)}(F_{[2]}^{(s)} + F_{[11]}^{(s)}) = 0$, and therefore fixes the relative normalizations of $F_{[2]}^{(s)}$ and $F_{[11]}^{(s)}$. This determines the four-point function $\left\langle V_{i_1}^{[1]} V_{i_2}^{[1]} V_{i_3}^{[1]} V_{i_4}^{[1]} \right\rangle$ up to an overall constant prefactor.

Numerical results

From the rules (8.2.17) and (8.2.32), the representations that may appear in the s-channel decompositions of the solutions $F_{[]}^{(s)}, F_{[2]}^{(s)}, F_{[11]}^{(s)}$ are

$$\mathcal{S}^{(s)}\left(F_{[]}^{(s)}\right) = \mathcal{S}_{\text{even}}^{[]} \quad , \quad \mathcal{S}^{(s)}\left(F_{[2]}^{(s)}\right) = \mathcal{S}_{\text{even}}^{[2]} \quad , \quad \mathcal{S}^{(s)}\left(F_{[11]}^{(s)}\right) = \mathcal{S}_{\text{odd}}^{[11]} \ . \tag{8.3.10}$$

And indeed, for each one of these three s-channel spectra, we find a unique solution of crossing symmetry. We are able to single out these solutions in the 3-dimensional space of solutions because each spectrum involves setting two of the three structure constants $D_1^{(s)}, D_{(1,0)}^{(s)}, D_{(1,1)}^{(s)}$ to zero. In the t- and u-channels, these solutions have the largest possible spectra,

$$\mathcal{S}^{(t,u)}\left(F_{\lambda}^{(s)}\right) = \mathcal{S}_0 \ , \tag{8.3.11}$$

i.e. anything that is allowed by the conservation of r mod $\mathbb{Z}$. Let us display numerical data that underlie these results. We list all s-channel fields with small deviations < 0.1, together with the first field with a large deviation for comparison. For each field with a small deviation, we display the real part of the four-point structure constant with as many digits as the deviation suggests are significant. For example, in the case of $F_{[]}^{(s)}$, although $D_{(3,0)}^{(s)} = O(10^{-15})$ is rather small, we do know its value with about 15 significant digits, i.e., the absolute error is $O(10^{-30})$.

$F_{[]}^{(s)}$ at $\Delta_{\max} = 40$ and $\beta^{-1} = 0.8 + 0.1i$

(r,s)	$\operatorname{Re} D_{(r,s)}^{(s)}$	Deviation
$\langle 1,1\rangle$	1	0
$(2,0)$	$-1.515508647813802768 \times 10^{-3}$	2.2×10^{-19}
$(3,0)$	$1.39468476197762 \times 10^{-15}$	6.6×10^{-15}
$(3,\pm\frac{2}{3})$	$8.3751227046841 \times 10^{-8}$	1.2×10^{-14}
$(4,0)$	3.7×10^{-13}	0.87

(8.3.12)

$F^{(s)}_{[11]}$ at $\Delta_{\max} = 40$ and $\beta^{-1} = 0.8 + 0.1i$

(r,s)	$\operatorname{Re} D^{(s)}_{(r,s)}$	Deviation
$(1,1)$	1	0
$(2,\pm\frac{1}{2})$	$-1.136421079784788769 \times 10^{-3}$	4.7×10^{-20}
$(3,\pm\frac{1}{3})$	$4.60859597460550 \times 10^{-7}$	4.1×10^{-15}
$(3,1)$	$2.43369637600654 \times 10^{-7}$	3.1×10^{-15}
$(4,\pm\frac{1}{4})$	5.8×10^{-13}	0.48

(8.3.13)

$F^{(s)}_{[2]}$ at $\Delta_{\max} = 40$ and $\beta^{-1} = 0.8 + 0.1i$

(r,s)	$\operatorname{Re} D^{(s)}_{(r,s)}$	Deviation
$(1,0)$	1	0
$(2,0)$	$-6.249142617756265636 \times 10^{-3}$	2.1×10^{-19}
$(2,1)$	$-1.4658809155406988148 \times 10^{-3}$	7.9×10^{-20}
$(3,0)$	$2.06056149998946 \times 10^{-7}$	7.1×10^{-15}
$(3,\pm\frac{2}{3})$	$2.15149154275906 \times 10^{-8}$	3.9×10^{-15}
$(4,0)$	6.1×10^{-13}	0.57

(8.3.14)

Fusion rule interpretation

From the solutions of crossing symmetry in the s-channel basis, we deduce the fusion rule

$$\boxed{V^{[1]}_{(\frac{1}{2},0)} \times V^{[1]}_{(\frac{1}{2},0)} \sim \sum_{k \in \mathcal{S}^{[]}_{\text{even}}} V^{[]}_k + \sum_{k \in \mathcal{S}^{[2]}_{\text{even}}} V^{[2]}_k + \sum_{k \in \mathcal{S}^{[11]}_{\text{odd}}} V^{[11]}_k} \,. \tag{8.3.15}$$

In this case, the fusion rules coincide with what we would expect from the spectrum, after splitting it according to odd or even spins. In other words, all fields that are allowed by symmetry to appear, do in fact appear, i.e. they come with nonzero structure constants in the solutions $F^{(s)}_\lambda$. For instance, from (8.3.12), the field $V_{(2,1)}$ vanishes in the singlet-channel because it cannot be decomposed on to the singlet. In other fusion rules, we will however find examples of fields that could appear, but do not.

This provides a test of the conjectured spectrum. In particular, the conjecture predicts that the field $V^{[]}_{(2,1)}$ does not exist, see the expression (8.3.5a) for $\mathcal{S}^{[]}$. Finding such a field would have killed the conjecture. The power of this test is limited because $\mathcal{S}^{[]}$ contains all possible pairs (r,s) with $r \in \mathbb{N}_{\geq 3}$.

8.3.2 Four-point functions and fusion rules of $V_{(\frac{1}{2},0)}$, $V_{(1,0)}$ and $V_{(1,1)}$

The simplest non-degenerate fields in the $O(n)$ CFT are $V_{(\frac{1}{2},0)}$, $V_{(1,0)}$ and $V_{(1,1)}$. Each one of these fields correspond to a single irreducible representation of $O(n)$. The fields should therefore be written as $V^{[1]}_{(\frac{1}{2},0)}$, $V^{[2]}_{(1,0)}$ and $V^{[11]}_{(1,1)}$, but we can omit the $O(n)$ representation labels without introducing ambiguities.

The four-point functions $\left\langle V^2_{(1,0)} V^2_{(\frac{1}{2},0)} \right\rangle$ and $\left\langle V^2_{(1,1)} V^2_{(\frac{1}{2},0)} \right\rangle$

For each one of these four-point functions, there exist three independent $O(n)$ invariants, and we numerically find three independent solutions of crossing symmetry. Let us write the s- and t-channel bases of solutions:

4-point function	s-channel solutions	t-channel solutions
$\left\langle V^2_{(1,0)} V^2_{(\frac{1}{2},0)} \right\rangle$	$F^{(s)}_{[]}, F^{(s)}_{[2]}, F^{(s)}_{[11]}$	$F^{(t)}_{[1]}, F^{(t)}_{[21]}, F^{(t)}_{[3]}$
$\left\langle V^2_{(1,1)} V^2_{(\frac{1}{2},0)} \right\rangle$	$G^{(s)}_{[]}, G^{(s)}_{[2]}, G^{(s)}_{[11]}$	$G^{(t)}_{[1]}, G^{(t)}_{[21]}, G^{(t)}_{[111]}$

(8.3.16)

In the s-channel, each solution can be singled out by requiring the vanishing of two structure constants among $D^{(s)}_1$, $D^{(s)}_{(1,0)}$, $D^{(s)}_{(1,1)}$, see Eqs. (8.3.5a)-(8.3.5d). The situation is similar in the t-channel with $D^{(t)}_{(\frac{1}{2},0)}$, $D^{(t)}_{(\frac{3}{2},0)}$ and $D^{(t)}_{(\frac{3}{2},\frac{2}{3})}$.

We can therefore easily determine each solution numerically, and we find a nontrivial pattern of vanishing structure constants: all solutions obey $D^{(s)}_{(r,1)} = 0$ for $r \in \mathbb{N} + 2$. (Numerically, we are however limited to $r \leq 8$.) Let us display some of the structure constants in the singlet solution $F^{(s)}_{[]}$, computed at $\beta^{-1} = 0.8 + 0.1i$, to support our argument.

	$\Delta_{\max} = 40$		$\Delta_{\max} = 120$	
(r,s)	$\mathrm{Re}\, D^{(s)}_{(r,s)}$	Deviation	$\mathrm{Re}\, D^{(s)}_{(r,s)}$	Deviation
$\langle 1,1 \rangle$	1	0	1	0
$(2,0)$	$1.3371893\ldots \times 10^{-3}$	4.5×10^{-25}	$1.3371893\ldots \times 10^{-3}$	6.6×10^{-91}
$(2,1)$	3.0×10^{-28}	1.4	7.5×10^{-93}	0.91
$(4,0)$	$-2.7870591\ldots \times 10^{-13}$	3.0×10^{-13}	$-2.7870591\ldots \times 10^{-13}$	2.2×10^{-78}
$(4,1)$	-4.9×10^{-27}	0.92	-5.0×10^{-92}	4.0
$(6,0)$	-6.5×10^{-22}	1.8	$-7.9541852\ldots \times 10^{-31}$	2.5×10^{-57}
$(6,1)$	7.2×10^{-24}	1.9	2.5×10^{-87}	0.78
$(8,0)$	$-$	$-$	$2.864293\ldots \times 10^{-55}$	1.7×10^{-24}
$(8,1)$	$-$	$-$	6.1×10^{-80}	1.8

(8.3.17)

Moreover, the solutions $G^{(s)}_{[11]}$ and $G^{(t)}_{[1]}$ obey $D^{(t,u)}_{(\frac{5}{2},0)}=0$. These results may be written as

Solutions	s-channel	t-channel	u-channel
$F^{(s)}_{[]}$	$\mathcal{S}^{[]}_{\text{even}}-(2\mathbb{N}+2,1)$	$\mathcal{S}_{\frac{1}{2}}$	$\mathcal{S}_{\frac{1}{2}}$
$F^{(s)}_{[2]}$	$\mathcal{S}^{[2]}_{\text{even}}-(2\mathbb{N}+2,1)$	$\mathcal{S}_{\frac{1}{2}}$	$\mathcal{S}_{\frac{1}{2}}$
$F^{(s)}_{[11]}$	$\mathcal{S}^{[11]}_{\text{odd}}-(2\mathbb{N}+3,1)$	$\mathcal{S}_{\frac{1}{2}}$	$\mathcal{S}_{\frac{1}{2}}$
$F^{(t)}_{\lambda}$	$\mathcal{S}_0-(\mathbb{N}+2,1)$	$\mathcal{S}^{\lambda}$	$\mathcal{S}_{\frac{1}{2}}$
$G^{(s)}_{[]}$	$\mathcal{S}^{[]}_{\text{even}}-(2\mathbb{N}+2,1)$	$\mathcal{S}_{\frac{1}{2}}$	$\mathcal{S}_{\frac{1}{2}}$
$G^{(s)}_{[2]}$	$\mathcal{S}^{[2]}_{\text{even}}-(2\mathbb{N}+2,1)$	$\mathcal{S}_{\frac{1}{2}}$	$\mathcal{S}_{\frac{1}{2}}$
$G^{(s)}_{[11]}$	$\mathcal{S}^{[11]}_{\text{odd}}-(2\mathbb{N}+3,1)$	$\mathcal{S}_{\frac{1}{2}}-\{(\frac{5}{2},0)\}$	$\mathcal{S}_{\frac{1}{2}}-\{(\frac{5}{2},0)\}$
$G^{(t)}_{[1]}$	$\mathcal{S}_0-(\mathbb{N}+2,1)$	$\mathcal{S}^{[1]}-\{(\frac{5}{2},0)\}$	$\mathcal{S}_{\frac{1}{2}}-\{(\frac{5}{2},0)\}$
$G^{(t)}_{[21]}, G^{(t)}_{[111]}$	$\mathcal{S}_0-(\mathbb{N}+2,1)$	$\mathcal{S}^{\lambda}$	$\mathcal{S}_{\frac{1}{2}}$

(8.3.18)

We deduce the fusion rules

$$\boxed{V^{[2]}_{(1,0)}\times V^{[1]}_{(\frac{1}{2},0)}\sim\sum_{k\in\mathcal{S}^{[1]}}V^{[1]}_k+\sum_{k\in\mathcal{S}^{[3]}}V^{[3]}_k+\sum_{k\in\mathcal{S}^{[21]}}V^{[21]}_k}\,, \tag{8.3.19}$$

$$\boxed{V^{[11]}_{(1,1)}\times V^{[1]}_{(\frac{1}{2},0)}\sim\sum_{k\in\mathcal{S}^{[1]}-\{(\frac{5}{2},0)\}}V^{[1]}_k+\sum_{k\in\mathcal{S}^{[111]}}V^{[111]}_k+\sum_{k\in\mathcal{S}^{[21]}}V^{[21]}_k}\,. \tag{8.3.20}$$

These are the only fusion rules that we can deduce from $\left\langle V^2_{(1,0)}V^2_{(\frac{1}{2},0)}\right\rangle$ and $\left\langle V^2_{(1,1)}V^2_{(\frac{1}{2},0)}\right\rangle$. Our four-point function are indeed of the type $\langle V_1V_1V_2V_2\rangle$, which gives us access to $V_1\times V_2$ and to $(V_1\times V_1)\cap(V_2\times V_2)$, from which we however cannot deduce $V_1\times V_1$ or $V_2\times V_2$.

The four-point function $\left\langle V^2_{(1,0)}V^2_{(1,1)}\right\rangle$

There exist four independent $O(n)$ invariants, and we numerically find four independent solutions of crossing symmetry. According to the tensor products (8.1.13f)-(8.1.13h) of the representations [2] and [11], the s- and t-channel bases of solutions are

4-point function	s-channel solutions	t-channel solutions
$\left\langle V^{[2]}_{(1,0)}V^{[2]}_{(1,0)}V^{[11]}_{(1,1)}V^{[11]}_{(1,1)}\right\rangle$	$F^{(s)}_{[]}, F^{(s)}_{[2]}, F^{(s)}_{[11]}, F^{(s)}_{[22]}$	$F^{(t)}_{[2]}, F^{(t)}_{[11]}, F^{(t)}_{[31]}, F^{(t)}_{[211]}$

(8.3.21)

It is easy to single out the solutions $F^{(t)}_{[11]}$, $F^{(t)}_{[31]}$ and $F^{(t)}_{[211]}$ by requiring the vanishing of three structure constants in each case among $\left\{D^{(t)}_{(1,0)}, D^{(t)}_{(1,1)}, D^{(t)}_{(2,0)}, D^{(t)}_{(2,1)}\right\}$, see Eqs. (8.3.5d), (8.3.5i), (8.3.5k). However, this does not work for $F^{(t)}_{[2]}$: while $\mathcal{S}^{[2]}$ (8.3.5c) implies that $F^{(t)}_{[2]}$ obeys the

three equations $D^{(t)}_{(1,1)} = D^{(t)}_{(2,\frac{1}{2})} = D^{(t)}_{(2,-\frac{1}{2})} = 0$, these equations are not all independent, because all solutions happen to obey $D^{(t)}_{(2,\frac{1}{2})} = D^{(t)}_{(2,-\frac{1}{2})}$.

To determine $F^{(t)}_{[2]}$, we have to think about the fusion rule $V_{(1,0)} \times V_{(1,1)}$, and to remember that this fusion rule also appears in the four-point function $\left\langle V_{(1,0)} V_{(1,1)} V^2_{(\frac{1}{2},0)} \right\rangle$. The numerical study of that four-point function shows that $V^{[2]}_{(2,0)}$ does not appear in the s-channel. However, $V^{[2]}_{(2,0)}$ does appear in the fusion rule $V_{(\frac{1}{2},0)} \times V_{(\frac{1}{2},0)}$ (8.3.15). Since there is a unique field of this type, it must be absent from the fusion rule $V_{(1,0)} \times V_{(1,1)}$, and therefore also from $F^{(t)}_{[2]}$. This provides the third constraint that we need for singling out the solution $F^{(t)}_{[2]}$. From the solutions $F^{(t)}_{\lambda}$, we then deduce the fusion rule

$$\boxed{V^{[2]}_{(1,0)} \times V^{[11]}_{(1,1)} \sim \sum_{k \in \mathcal{S}^{[2]} - \{(2,0),(3,0)\}} V^{[2]}_k + \sum_{k \in \mathcal{S}^{[11]}} V^{[11]}_k + \sum_{k \in \mathcal{S}^{[31]}} V^{[31]}_k + \sum_{k \in \mathcal{S}^{[211]}} V^{[211]}_k} \,. \tag{8.3.22}$$

The fusion rules $V_{(1,0)} \times V_{(1,0)}$ and $V_{(1,1)} \times V_{(1,1)}$

To determine these fusion rules, it would be enough to find the crossing symmetry solutions associated to the the four-point functions $\left\langle V^4_{(1,0)} \right\rangle$ and $\left\langle V^4_{(1,1)} \right\rangle$. In these cases, there exist six independent $O(n)$ invariants, and we numerically find six independent solutions of crossing symmetry. Let us write the s-channel bases of solutions:

4-point function	s-channel solutions
$\left\langle V^4_{(1,0)} \right\rangle$	$F^{(s)}_{[]}, F^{(s)}_{[2]}, F^{(s)}_{[11]}, F^{(s)}_{[22]}, F^{(s)}_{[31]}, F^{(s)}_{[4]}$
$\left\langle V^4_{(1,1)} \right\rangle$	$G^{(s)}_{[]}, G^{(s)}_{[2]}, G^{(s)}_{[11]}, G^{(s)}_{[22]}, G^{(s)}_{[211]}, G^{(s)}_{[1111]}$

(8.3.23)

We can single out the solution $F^{(s)}_{[4]}$ by using the five independent constraints $D^{(s)}_1 = D^{(s)}_{(1,0)} = D^{(s)}_{(1,1)} = D^{(s)}_{(2,\frac{1}{2})} = D^{(s)}_{(2,1)} = 0$, see $\mathcal{S}^{[4]}$ (8.3.5h). In the case of the solution $F^{(s)}_{[31]}$, we have only four constraints, see $\mathcal{S}^{[31]}$ (8.3.5i), but we can add $D^{(s)}_{(2,1)} = 0$ thanks to the OPE commutativity rule (8.2.32) with $\epsilon_{[2]}([31]) = -1$. We are however unable to single out the remaining four solutions. To complete the determination of $V_{(1,0)} \times V_{(1,0)}$, we need to consider other correlation functions where this fusion rule appears.

Let us start with $\left\langle V^2_{(1,0)} V^2_{(\frac{1}{2},0)} \right\rangle$. We cannot deduce much from the nontrivial structures of the s-channel solutions (8.3.18): for example, since the field $V^{[2]}_{(4,1)}$ has nontrivial multiplicity in the spectrum, it could be absent from the s-channel solutions while being present in both fusion rules $V_{(1,0)} \times V_{(1,0)}$ and $V_{(\frac{1}{2},0)} \times V_{(\frac{1}{2},0)}$. The exception is $V^{[2]}_{(2,1)}$, which has multiplicity one. Since it appears in $V_{(\frac{1}{2},0)} \times V_{(\frac{1}{2},0)}$ but not in the s-channel of $\left\langle V^2_{(1,0)} V^2_{(\frac{1}{2},0)} \right\rangle$, it must be absent from $V_{(1,0)} \times V_{(1,0)}$.

This is just what we need for determining the s-channel solutions of $\left\langle V^2_{(1,0)} V^2_{(1,1)} \right\rangle$ (8.3.21). The solution that corresponds to [2] is a priori problematic: imposing $D^{(s)}_{(1,1)} = 0$ brings us to the three-dimensional subspace of even-spin solutions, where $D^{(s)}_1 = 0$ is not enough for singling

out our solution. The problem is solved by imposing $D^{(s)}_{(2,1)} = 0$. We then find that any field that is authorized by $O(n)$ symmetry and OPE commutativity does appear in the s-channel of $\left\langle V^2_{(1,0)} V^2_{(1,1)} \right\rangle$, except for $V^{[2]}_{(2,1)}$. All these fields must therefore appear in the fusion rule

$$\boxed{V^{[2]}_{(1,0)} \times V^{[2]}_{(1,0)} \sim \sum_{k \in \mathcal{S}^{[]}_{\text{even}}} V^{[]}_k + \sum_{k \in \mathcal{S}^{[2]}_{\text{even}} - \{(2,1)\}} V^{[2]}_k + \sum_{k \in \mathcal{S}^{[11]}_{\text{odd}}} V^{[11]}_k + \sum_{k \in \mathcal{S}^{[4]}_{\text{even}}} V^{[4]}_k + \sum_{k \in \mathcal{S}^{[31]}_{\text{odd}}} V^{[31]}_k + \sum_{k \in \mathcal{S}^{[22]}_{\text{even}}} V^{[22]}_k} \tag{8.3.24}$$

A similar reasoning allows us to determine

$$\boxed{V^{[11]}_{(1,1)} \times V^{[11]}_{(1,1)} \sim \sum_{k \in \mathcal{S}^{[]}_{\text{even}}} V^{[]}_k + \sum_{k \in \mathcal{S}^{[2]}_{\text{even}} - \{(2,1)\}} V^{[2]}_k + \sum_{k \in \mathcal{S}^{[11]}_{\text{odd}}} V^{[11]}_k + \sum_{k \in \mathcal{S}^{[1111]}_{\text{even}}} V^{[1111]}_k + \sum_{k \in \mathcal{S}^{[211]}_{\text{odd}}} V^{[211]}_k + \sum_{k \in \mathcal{S}^{[22]}_{\text{even}}} V^{[22]}_k} \tag{8.3.25}$$

8.3.3 More examples

In the examples that we studied so far, the number of bootstrap solutions always matched the number of four-point invariants, i.e., the inequality (8.2.29) was saturated. We will now start a more systematic scan of four-point functions, and find examples where the inequality is strict.

The 30 simplest four-point functions

We organize correlators by increasing level $L = \sum_{i=1}^4 r_i$. There are 30 inequivalent four-point functions with $L = 2, 3, 4$. By inequivalent we mean not related by permutations, or by flipping the signs of all second indices s_i.

In each case, we indicate the number $\mathscr{N}$ of solutions of crossing symmetry, and the number $\mathscr{I}$ of $O(n)$ invariant tensors. We find that the inequality $\mathscr{N} \leq \mathscr{I}$ (8.2.29) is saturated in 21 out of 30 cases.

Level-2 correlators	Bootstrap $\mathscr{N}$	Invariants $\mathscr{I}$
$\left(\frac{1}{2}, 0\right)^4$	3	3

Level-3 correlators	Bootstrap $\mathscr{N}$	Invariants $\mathscr{I}$
$(1,0)^2 \left(\frac{1}{2}, 0\right)^2$	3	3
$(1,1)^2 \left(\frac{1}{2}, 0\right)^2$	3	3
$(1,0)\,(1,1) \left(\frac{1}{2}, 0\right)^2$	2	2
$\left(\frac{3}{2}, 0\right) \left(\frac{1}{2}, 0\right)^3$	2	2
$\left(\frac{3}{2}, \frac{2}{3}\right) \left(\frac{1}{2}, 0\right)^3$	2	2

Level-4 correlators	Bootstrap $\mathscr{N}$	Invariants $\mathscr{I}$
$(1,0)^4$	6	6
$(1,0)^3(1,1)$	3	3
$(1,0)^2(1,1)^2$	4	4
$(1,0)(1,1)^3$	3	3
$(1,1)^4$	6	6
$\left(\frac{3}{2},0\right)(1,0)^2\left(\frac{1}{2},0\right)$	4	4
$\left(\frac{3}{2},0\right)(1,0)(1,1)\left(\frac{1}{2},0\right)$	4	4
$\left(\frac{3}{2},0\right)(1,1)^2\left(\frac{1}{2},0\right)$	4	4
$\left(\frac{3}{2},\frac{2}{3}\right)(1,0)^2\left(\frac{1}{2},0\right)$	4	4
$\left(\frac{3}{2},\frac{2}{3}\right)(1,0)(1,1)\left(\frac{1}{2},0\right)$	4	4
$\left(\frac{3}{2},\frac{2}{3}\right)(1,1)^2\left(\frac{1}{2},0\right)$	4	4
$\left(\frac{3}{2},0\right)^2\left(\frac{1}{2},0\right)^2$	5	6
$\left(\frac{3}{2},0\right)\left(\frac{3}{2},\frac{2}{3}\right)\left(\frac{1}{2},0\right)^2$	4	4
$\left(\frac{3}{2},\frac{2}{3}\right)^2\left(\frac{1}{2},0\right)^2$	5	5
$\left(\frac{3}{2},\frac{2}{3}\right)\left(\frac{3}{2},-\frac{2}{3}\right)\left(\frac{1}{2},0\right)^2$	4	5
$(2,0)(1,0)\left(\frac{1}{2},0\right)^2$	5	7
$(2,0)(1,1)\left(\frac{1}{2},0\right)^2$	5	6
$\left(2,\frac{1}{2}\right)(1,0)\left(\frac{1}{2},0\right)^2$	5	5
$\left(2,\frac{1}{2}\right)(1,1)\left(\frac{1}{2},0\right)^2$	5	6
$(2,1)(1,0)\left(\frac{1}{2},0\right)^2$	5	6
$(2,1)(1,1)\left(\frac{1}{2},0\right)^2$	5	5
$\left(\frac{5}{2},0\right)\left(\frac{1}{2},0\right)^3$	6	9
$\left(\frac{5}{2},\frac{2}{5}\right)\left(\frac{1}{2},0\right)^3$	6	9
$\left(\frac{5}{2},\frac{4}{5}\right)\left(\frac{1}{2},0\right)^3$	6	9

Reducible versus irreducible representations: $\left\langle V_{(\frac{3}{2},0)}V^3_{(\frac{1}{2},0)}\right\rangle$ versus $\left\langle V_{(\frac{3}{2},\frac{2}{3})}V^3_{(\frac{1}{2},0)}\right\rangle$

The structures of $\Lambda_{(\frac{3}{2},0)}$ (8.1.27a) and $\Lambda_{(\frac{3}{2},\frac{2}{3})}$ (8.1.27b) lead to the following predictions for the representations that may appear in the corresponding four-point functions with three $V_{(\frac{1}{2},0)}$ fields:

4-point function	s-channel	t-channel	u-channel
$\left\langle V^{[3]}_{(\frac{3}{2},0)}V^{[1]}_{(\frac{1}{2},0)}V^{[1]}_{(\frac{1}{2},0)}V^{[1]}_{(\frac{1}{2},0)}\right\rangle$	$[2]$	$[2]$	$[2]$
$\left\langle V^{[111]}_{(\frac{3}{2},0)}V^{[1]}_{(\frac{1}{2},0)}V^{[1]}_{(\frac{1}{2},0)}V^{[1]}_{(\frac{1}{2},0)}\right\rangle$	$[11]$	$[11]$	$[11]$
$\left\langle V^{[21]}_{(\frac{3}{2},\frac{2}{3})}V^{[1]}_{(\frac{1}{2},0)}V^{[1]}_{(\frac{1}{2},0)}V^{[1]}_{(\frac{1}{2},0)}\right\rangle$	$[2]+[11]$	$[2]+[11]$	$[2]+[11]$

(8.3.26)

And indeed, we numerically find that the bootstrap equations for $\left\langle V_{(\frac{3}{2},0)} V^3_{(\frac{1}{2},0)} \right\rangle$ have one solution with the irreducible representation [2] in all three channels, and another solution with [11] in all three channels. In the case of $\left\langle V_{(\frac{3}{2},\frac{2}{3})} V^3_{(\frac{1}{2},0)} \right\rangle$, we can still define a unique solution $F^{(s)}_{[2]}$ with the representation [2] in the s-channel, but that solution has both representations [2] and [11] appearing in the t and u channels. In other words, we have nontrivial fusion relations of the type $F^{(s)}_{[2]} = f_{[2],[2]} F^{(t)}_{[2]} + f_{[2],[11]} F^{(t)}_{[11]}$.

The results for $\left\langle V_{(\frac{3}{2},0)} V^3_{(\frac{1}{2},0)} \right\rangle$ are a strong confirmation that the determination $\Lambda_{(\frac{3}{2},0)} = [3] + [111]$ made in (8.1.27a) is correct. On the basis of the mere dimensions of representations, one might have proposed the determination $[21] + [1]$ instead, but this would have led us to expect five bootstrap solutions with very different properties.

When two solutions coincide: $\left\langle V^2_{(\frac{3}{2},0)} V^2_{(\frac{1}{2},0)} \right\rangle$

From $V^{[3]}_{(\frac{3}{2},0)}$ and $V^{[111]}_{(\frac{3}{2},0)}$, we can build 4 four-point functions of the type $\left\langle V^2_{(\frac{3}{2},0)} V^2_{(\frac{1}{2},0)} \right\rangle$. However, since $[3] \otimes [111] = [3111] + [411] + [31] + [211]$ and none of these representations appear in the tensor product $[1] \otimes [1]$ (8.1.13a), we have

$$\left\langle V^{[3]}_{(\frac{3}{2},0)} V^{[111]}_{(\frac{3}{2},0)} V^{[1]}_{(\frac{1}{2},0)} V^{[1]}_{(\frac{1}{2},0)} \right\rangle = \left\langle V^{[111]}_{(\frac{3}{2},0)} V^{[3]}_{(\frac{3}{2},0)} V^{[1]}_{(\frac{1}{2},0)} V^{[1]}_{(\frac{1}{2},0)} \right\rangle = 0 \ . \tag{8.3.27}$$

This leaves us with only two non-vanishing correlation functions, for which we introduce s-channel bases of solutions:

4-point function	s-channel solutions	t,u-channel representations
$\left\langle V^{[3]}_{(\frac{3}{2},0)} V^{[3]}_{(\frac{3}{2},0)} V^{[1]}_{(\frac{1}{2},0)} V^{[1]}_{(\frac{1}{2},0)} \right\rangle$	$F^{(s)}_{[]}, F^{(s)}_{[2]}, F^{(s)}_{[11]}$	$[4] + [31] + [2]$
$\left\langle V^{[111]}_{(\frac{3}{2},0)} V^{[111]}_{(\frac{3}{2},0)} V^{[1]}_{(\frac{1}{2},0)} V^{[1]}_{(\frac{1}{2},0)} \right\rangle$	$G^{(s)}_{[]}, G^{(s)}_{[2]}, G^{(s)}_{[11]}$	$[1111] + [211] + [11]$

(8.3.28)

We numerically find that the 6 solutions are not linearly independent: the space of solutions actually has dimension 5. Nevertheless, it is possible to single out each one of the 6 solutions numerically. The space of solutions for $\left\langle V^{[3]}_{(\frac{3}{2},0)} V^{[3]}_{(\frac{3}{2},0)} V^{[1]}_{(\frac{1}{2},0)} V^{[1]}_{(\frac{1}{2},0)} \right\rangle$ is defined by $D^{(t)}_{(1,1)} = D^{(u)}_{(1,1)} = 0$ (see Eqs. (8.3.5c), (8.3.5h) and (8.3.5i)), and each solution $F^{(s)}_{[]}, F^{(s)}_{[2]}, F^{(s)}_{[11]}$ is singled out by the additional vanishing of two structure constants among $D^{(s)}_1$, $D^{(s)}_{(1,0)}$, and $D^{(s)}_{(1,1)}$. There is a unique solution F_0 such that

$$\text{Span}(F_0) = \text{Span}\left(F^{(s)}_{[]}, F^{(s)}_{[2]}\right) \cap \text{Span}\left(G^{(s)}_{[]}, G^{(s)}_{[2]}\right) \ , \tag{8.3.29}$$

which is singled out by requiring $D^{(t)}_{(1,1)} = D^{(u)}_{(1,1)} = D^{(t)}_{(1,0)} = D^{(u)}_{(1,0)} = 0$. We can therefore attribute the existence of only 5 independent solutions to the coincidence of one solution for $\left\langle V^{[3]}_{(\frac{3}{2},0)} V^{[3]}_{(\frac{3}{2},0)} V^{[1]}_{(\frac{1}{2},0)} V^{[1]}_{(\frac{1}{2},0)} \right\rangle$ with one solution for $\left\langle V^{[111]}_{(\frac{3}{2},0)} V^{[111]}_{(\frac{3}{2},0)} V^{[1]}_{(\frac{1}{2},0)} V^{[1]}_{(\frac{1}{2},0)} \right\rangle$.

When $O(n)$ does not see the difference: $\left\langle V^2_{(\frac{3}{2},\frac{2}{3})} V^2_{(\frac{1}{2},0)} \right\rangle$ versus $\left\langle V_{(\frac{3}{2},\frac{2}{3})} V_{(\frac{3}{2},-\frac{2}{3})} V^2_{(\frac{1}{2},0)} \right\rangle$

The two fields $V^{[21]}_{(\frac{3}{2},\frac{2}{3})}$ and $V^{[21]}_{(\frac{3}{2},-\frac{2}{3})}$ differ by their behaviour with respect to conformal symmetry, but belong to the same $O(n)$ representation. We now study the simplest correlation functions that can see the difference.

We have $\dim \mathrm{Hom}\left([21]\otimes[21],[1]\otimes[1]\right)=5$, with s-channel invariants corresponding to the 5 irreducible representations in 2[2]+2[11]+[]. In the case of $\left\langle V^2_{(\frac{3}{2},\frac{2}{3})}V^2_{(\frac{1}{2},0)}\right\rangle$, we do find 5 solutions of crossing symmetry. But in the case of $\left\langle V_{(\frac{3}{2},\frac{2}{3})}V_{(\frac{3}{2},-\frac{2}{3})}V^2_{(\frac{1}{2},0)}\right\rangle$, we find only 4 solutions.

The difference between the two correlation functions can be attributed to the presence or absence of the identity field in the s-channel. In the second case, the identity field is forbidden by the fusion rule (8.2.4), because $V_{(\frac{3}{2},\frac{2}{3})}\neq V_{(\frac{3}{2},-\frac{2}{3})}$. This implies the constraint $D^{(s)}_1=0$, which is expected to reduce the dimension of the space of solutions by one.

This does not necessarily mean that the identity representation [] of $O(n)$ does not appear in the s-channel, though. We may try to define a solution $F^{(s)}_{[]}$ by setting $D^{(s)}_{(1,0)}=D^{(s)}_{(2,1)}=D^{(s)}_{\text{odd spin}}=0$, which would eliminate the s-channel representations [2] and [11]. However, it turns out that $D^{(s)}_{(2,1)}$ vanishes in all 5 solutions, so setting it to zero is actually not enough for eliminating [2]. The appearance of [] is therefore still an open question.

When solutions are linearly dependent: $\left\langle V_{(2,0)}V_{(1,0)}V^2_{(\frac{1}{2},0)}\right\rangle$

There are 7 four-point invariants, but only 5 solutions. The representation $\Lambda_{(2,0)}$ (8.1.27c) is made of 5 irreducible representations, so we have 5 fields of the type $V_{(2,0)}$. In the 4 cases $V^{[4]}_{(2,0)}$, $V^{[22]}_{(2,0)}$, $V^{[211]}_{(2,0)}$, $V^{[]}_{(2,0)}$, there exists a unique corresponding four-point function, which is easy to characterize by the representations that propagate in each channel:

4-point function	s-channel	t-channel	u-channel
$\left\langle V^{[4]}_{(2,0)}V^{[2]}_{(1,0)}V^{[1]}_{(\frac{1}{2},0)}V^{[1]}_{(\frac{1}{2},0)}\right\rangle$	[2]	[3]	[3]
$\left\langle V^{[22]}_{(2,0)}V^{[2]}_{(1,0)}V^{[1]}_{(\frac{1}{2},0)}V^{[1]}_{(\frac{1}{2},0)}\right\rangle$	[2]	[21]	[21]
$\left\langle V^{[211]}_{(2,0)}V^{[2]}_{(1,0)}V^{[1]}_{(\frac{1}{2},0)}V^{[1]}_{(\frac{1}{2},0)}\right\rangle$	[11]	[21]	[21]
$\left\langle V^{[2]}_{(2,0)}V^{[2]}_{(1,0)}V^{[1]}_{(\frac{1}{2},0)}V^{[1]}_{(\frac{1}{2},0)}\right\rangle$	[2] + [11] + []	[3] + [21] + [1]	[3] + [21] + [1]
$\left\langle V^{[]}_{(2,0)}V^{[2]}_{(1,0)}V^{[1]}_{(\frac{1}{2},0)}V^{[1]}_{(\frac{1}{2},0)}\right\rangle$	[2]	[1]	[1]

(8.3.30)

For example, to single out the solution $\left\langle V^{[22]}_{(2,0)}V^{[2]}_{(1,0)}V^{[1]}_{(\frac{1}{2},0)}V^{[1]}_{(\frac{1}{2},0)}\right\rangle$, we require the vanishing of $D^{(s)}_{(1,1)}$, $D^{(s)}_{(2,\frac{1}{2})}$, $D^{(t)}_{(\frac{1}{2},0)}$ and $D^{(t)}_{(\frac{3}{2},0)}$.

The four-point function $\left\langle V^{[2]}_{(2,0)}V^{[2]}_{(1,0)}V^{[1]}_{(\frac{1}{2},0)}V^{[1]}_{(\frac{1}{2},0)}\right\rangle$ a priori corresponds to 3 solutions: $F^{(s)}_{[]}$, $F^{(s)}_{[2]}$ and $F^{(s)}_{[11]}$. The solution $F^{(s)}_{[11]}$ can be determined modulo $\left\langle V^{[211]}_{(2,0)}V^{[2]}_{(1,0)}V^{[1]}_{(\frac{1}{2},0)}V^{[1]}_{(\frac{1}{2},0)}\right\rangle$, by requiring $D^{(s)}_{\text{even spin}}=0$. This leaves us with a 3-dimensional subspace of solutions such that $D^{(s)}_{\text{odd spin}}=0$. We already know 3 such solutions, corresponding to $V^{[4]}_{(2,0)}$, $V^{[22]}_{(2,0)}$, and $V^{[]}_{(2,0)}$. Therefore, the solutions $F^{(s)}_{[]}$ and $F^{(s)}_{[2]}$ are linear combinations of these already determined solutions.

Nontrivial multiplicity: $\left\langle V_{(\frac{5}{2},0)}V^3_{(\frac{1}{2},0)}\right\rangle$

The structure of $\Lambda_{(\frac{5}{2},0)}$ (8.1.27f) implies the existence of two distinct primary fields of the type $V^{[21]}_{(\frac{5}{2},0)}$. As the tensor product $[1]^{\otimes 3}$ can only reach representations λ with $|\lambda| \leq 3$, we therefore have 4 possible four-point functions, one of which comes with a nontrivial multiplicity:

4-point function	Multiplicity	s,t,u-channel representation
$\left\langle V^{[3]}_{(\frac{5}{2},0)}V^{[1]}_{(\frac{1}{2},0)}V^{[1]}_{(\frac{1}{2},0)}V^{[1]}_{(\frac{1}{2},0)}\right\rangle$	1	$[2]$
$\left\langle V^{[111]}_{(\frac{5}{2},0)}V^{[1]}_{(\frac{1}{2},0)}V^{[1]}_{(\frac{1}{2},0)}V^{[1]}_{(\frac{1}{2},0)}\right\rangle$	1	$[11]$
$\left\langle V^{[21]}_{(\frac{5}{2},0)}V^{[1]}_{(\frac{1}{2},0)}V^{[1]}_{(\frac{1}{2},0)}V^{[1]}_{(\frac{1}{2},0)}\right\rangle$	2	$[2]+[11]$
$\left\langle V^{[1]}_{(\frac{5}{2},0)}V^{[1]}_{(\frac{1}{2},0)}V^{[1]}_{(\frac{1}{2},0)}V^{[1]}_{(\frac{1}{2},0)}\right\rangle$	1	$[2]+[11]+[]$

(8.3.31)

The nontrivial multiplicity influences the counting of the 9 four-point invariants: each invariant associated to $\left\langle V^{[21]}V^{[1]}V^{[1]}V^{[1]}\right\rangle$ has to be counted twice, for a total of 4 invariants.

Numerically, we find 6 independent solutions of crossing symmetry equations. The solutions associated to $\left\langle V^{[3]}_{(\frac{5}{2},0)}V^{[1]}_{(\frac{1}{2},0)}V^{[1]}_{(\frac{1}{2},0)}V^{[1]}_{(\frac{1}{2},0)}\right\rangle$ and $\left\langle V^{[111]}_{(\frac{5}{2},0)}V^{[1]}_{(\frac{1}{2},0)}V^{[1]}_{(\frac{1}{2},0)}V^{[1]}_{(\frac{1}{2},0)}\right\rangle$ are easily singled out by allowing only one representation to propagate in each channel. The remaining 4 solutions are harder to disentangle, and we cannot say whether the two copies of $V^{[21]}_{(\frac{5}{2},0)}$ lead to linearly independent solutions.

8.4 Outlook

8.4.1 Solving the $O(n)$ CFT: achievements and challenges

We have completed the determination of the spectrum of the $O(n)$ CFT, and we now know the list of primary fields, together with their behaviour under the global $O(n)$ symmetry. In order to solve the $O(n)$ CFT, it remains to compute the correlation functions of these fields. We have done this numerically in a number of examples, and inferred some exact results about fusion rules and numbers of solutions of crossing symmetry equations. Let us discuss the interpretation of our results, and outline what remains to be done.

Coincidences of solutions of crossing symmetry

Given a four-point function, we have argued that the number $\mathscr{N}$ of independent solutions of crossing symmetry cannot exceed the number $\mathscr{I}$ of four-point $O(n)$ invariants. All four-point functions of the fields $V_{(\frac{1}{2},0)}$, $V_{(1,0)}$ and $V_{(1,1)}$ actually obey $\mathscr{N}=\mathscr{I}$. As the four-point functions become more complicated, we find examples where $\mathscr{N}<\mathscr{I}$, and it might well be that $\mathscr{N}=\mathscr{I}$ occurs only in a finite number of cases. There are two plausible interpretations for the existence of cases where $\mathscr{N}<\mathscr{I}$:

- *These may reflect the existence of a larger symmetry.* If conformal symmetry and $O(n)$ symmetry do not explain all relations between solutions of crossing symmetry, is there a larger symmetry at work? In the spectrum (8.1.20), the $O(n)$ representations $\Lambda_{(r,s)}$ are

not irreducible, but they are sums of (typically many) irreducible representations. There are indications that the representations $\Lambda_{(r,s)}$ follow from an algebra that is larger than $O(n)$ [148]. However, while it does act on the spectrum, this algebra is not a symmetry algebra of the model, because the representations $\Lambda_{(r,s)}$ do not close under tensor products.

More generally, the linear relations that lead to $\mathscr{N} < \mathscr{I}$ cannot be explained by grouping $O(n)$ representations into larger representations, be they $\Lambda_{(r,s)}$ or smaller representations: if there is a larger symmetry, it must work in a more subtle way.

- *These may be dynamical accidents.* Until we find an explanation from symmetry, we have to consider coincidences of solutions of crossing symmetry as dynamical accidents. For example, we saw that each one of the two four-point functions of Table (8.3.28) gives rise to three well-identified solutions of crossing symmetry. It just happens that these six solutions are linearly dependent, so that $5 = \mathscr{N} < \mathscr{I} = 6$ for the four-point function $\left\langle V^2_{(\frac{3}{2},0)} V^2_{(\frac{1}{2},0)} \right\rangle$.

  Coincidences of solutions of crossing symmetry are probably comparable to coincidences of dimensions of primary fields, starting with the two fields $V^{[3]}_{(\frac{3}{2},0)}$ and $V^{[111]}_{(\frac{3}{2},0)}$ which belong to different $O(n)$ representations but have the same conformal dimensions. These coincidences are probably specific to the two-dimensional $O(n)$ CFT: in higher dimensions, we would expect $\mathscr{N} = \mathscr{I}$ in all cases.

The number of invariants $\mathscr{I}$ is determined by the action of $O(n)$ on the spectrum, and therefore by our conjecture (8.1.26) for $\Lambda_{(r,s)}$. As we have seen in Section 8.3.3, numerical bootstrap results provide strong evidence for our conjecture.

Fusion rules and field multiplicities

In Sections 8.3.1 and 8.3.2, we have determined the fusion products of the fields $V_{(\frac{1}{2},0)}$, $V_{(1,0)}$ and $V_{(1,1)}$ with one another. Our results are given by Eqs. (8.3.15), (8.3.19)–(8.3.20), (8.3.22) and (8.3.24)–(8.3.25).

These products take into account $O(n)$ symmetry, and are thereby finer than the Virasoro-only fusion products that were recently conjectured by Ikhlef and Morin-Duchesne based on lattice arguments in related CFTs [173]. The Virasoro-only products obey the non-trivial rule $V_{(r,s)} \in V_{(r_1,s_1)} \times V_{(r_2,s_2)} \implies r \geq |r_1 - r_2|$. We found counter-examples to this rule, such as the field $V_{(1,1)}$ propagating in $\left\langle V_{(\frac{5}{2},0)} V^3_{(\frac{1}{2},0)} \right\rangle$. Maybe the rule's applicability depends on the behaviour of the involved fields under $O(n)$ transformations.

However, the fusion rules that we have established do not take into account field multiplicities, i.e., they do not distinguish two fields that transform similarly under the conformal and $O(n)$ symmetries. For example, according to $\Lambda_{(3,0)}$ (8.1.27h), there are four different fields of the type $V^{[22]}_{(3,0)}$. Taming field multiplicities will be needed for writing complete fusion rules, and therefore for solving the CFT. In the given example, knowing only that *some* fields of the type $V^{[22]}_{(3,0)}$ appear in two fusion rules $V_1 \times V_2$ and $V_3 \times V_4$, we cannot deduce that $V^{[22]}_{(3,0)}$ appears in the s-channel decomposition of the four-point function $\langle V_1 V_2 V_3 V_4 \rangle$. To deduce that, we would need to know precisely *which* fields of the type $V^{[22]}_{(3,0)}$ appear, and specifically that at least one of those fields is common to the two fusion rules.

Structure constants and nonlinear bootstrap

We have been treating crossing symmetry as a system of linear equations (8.2.16) for the four-point structure constants $D_{(r,s)}$. However, an essential axiom of the conformal bootstrap is that each four-point structure constant is the product of two three-point structure constants. In terms of three-point structure constants, crossing symmetry is a system of quadratic equations, and it is much more constraining, because there are much fewer three-point structure constants than four-point structure constants.

Our notations for four-point structure constants $D_{(r,s)}$ may be misleading, because they only indicate the dependence on conformal dimensions, and not on $O(n)$ representations. In fact, all structure constants of the CFT depend on $O(n)$ representations, just like the fields $V^{\lambda}_{(r,s)}$. For example, the s-channel four-point structure constants for the four-point function $\left\langle V^4_{(\frac{1}{2},0)} \right\rangle$ depend on $\lambda \in \big\{[], [2], [11]\big\}$, via their dependence on the choice of an s-channel solution $F^{(s)}_{\lambda}$.

Dealing with nonlinear bootstrap equations is surely the next technical step in the study of the $O(n)$ CFT and cognate CFTs. Of course, we could take the four-point structure constants as determined by our current method, and deduce three-point structure constants. This would provide strong tests of the consistency of our results, as the same three-point structure constant may appear in several different four-point structure constants. The question is whether we could do better, and simultaneously solve crossing symmetry equations for several four-point functions that share some three-point structure constants.

There is also the issue of finding analytic formulas for structure constants. In the critical Q-state Potts model, some structure constants are known analytically: to begin with, the simplest three-point structure constant is given by the Delfino–Viti conjecture [134], which has been numerically tested to high precision [6]. Moreover, some ratios between structure constants have been determined analytically (in the form of ratios of integer-coefficient polynomials in Q), both from the lattice model (see Chapter 4) and from the numerical bootstrap [6]. In the $O(n)$ CFT, we have been able to determine some ratios of structure constants analytically, but so far we have found no analogue of the Delfino–Viti conjecture.

8.4.2 Geometrical interpretation of the CFT

In the lattice description, the partition function of the $O(n)$ model is a sum over loops on a two-dimensional lattice. We will now discuss how this may lead to a geometrical interpretation of correlation functions in the $O(n)$ CFT. The ultimate aim is to determine fusion rules and numbers of crossing symmetry solutions, by counting two-dimensional topological graphs. We do not understand this systematically at the moment, so we will only sketch a few ideas.

$O(n)$ representations and watermelon operators

The basic spin observable $\phi(x)$ in the lattice model transforms in the vector representation of $O(n)$, and its continuum limit is the field $V_{(\frac{1}{2},0)}$ in the $O(n)$ CFT [20]. Using the high-temperature expansion, correlation functions of $\phi(x)$ can be represented as sums over lines and loops. For example, the two-point function $\big\langle \phi(x)\phi(y) \big\rangle$ is a sum over graphs where, in addition to the loops that already appear in the partition function, there is a line connecting x and y.

In the continuum limit, this suggests that the field $V_{(\frac{1}{2},0)}(z)$ inserts one line at point z. In a correlation function, this line has to end at the position of another field. For example, in the four-point function $\left\langle V^4_{(\frac{1}{2},0)} \right\rangle$, there are three ways to connect the four fields, see Figure (8.3.7).

The lines in that figure originally indicated contractions of $O(n)$ vector indices: this is an early hint that the model's geometrical and algebraic interpretations are closely related.

Similarly, the field $V_{(r,0)}^{[2r]}$ can be thought of as a $2r$-leg watermelon operator, i.e., an operator that inserts $2r$ lines:

$$\left\langle V_{(3,0)}^{[6]} V_{(3,0)}^{[6]} \right\rangle \longrightarrow \tag{8.4.1}$$

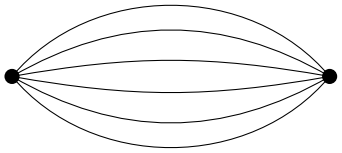

Such operators were introduced in Chapter 2, see also [2, 42]. In the lattice model, a $2r$-leg operator is built from $2r$ spin operators $\phi(x)$ inserted at neighboring sites, with their $O(n)$ labels projected onto the traceless symmetric tensor representation $[2r]$. In the continuum limit, the neighboring sites coincide. In correlation functions, due to the tracelessness of the representation $[2r]$, two legs of the same operator cannot be connected to one another, but have to be connected to legs of other operators.

More generally, the field $V_{(r,s)}(z)$ with $s \neq 0$ can be interpreted as an operator that inserts $2r$ lines, with the rule that a line that winds around its position z picks a phase $e^{i\pi s}$. (This means that the weight of a configuration with such a winding line is multiplied by $e^{i\pi s}$ [37, 42].) Actually, the notion of winding around an operator already makes sense on the lattice, even though the lattice operator is built from $2r$ distinct sites: since these sites are neighbors, a line cannot wind around only a subset of these sites. Since the conformal spin rs is integer, the phase factor is trivial if all $2r$ lines wind around z, and this allows watermelon operators to be mutually local. To see that the phase factors allow us to distinguish different values of s, consider the two-point functions of $V_{(1,0)}$ and $V_{(1,1)}$. In both cases, there are two inequivalent graphs:

$$\left\langle V_{(1,0)} V_{(1,0)} \right\rangle \text{ or } \left\langle V_{(1,1)} V_{(1,1)} \right\rangle \longrightarrow \tag{8.4.2}$$

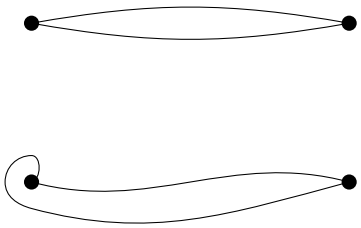

The bottom graph comes with a minus sign in the case of $\left\langle V_{(1,1)} V_{(1,1)} \right\rangle$, which therefore differs from $\left\langle V_{(1,0)} V_{(1,0)} \right\rangle$.

Young projectors and line crossings

Phase factors are enough for singling out fully symmetric or antisymmetric representations $[2r]$ or $[1^{2r}]$. However, in general they cannot distinguish the various fields $V_{(r,s)}^{\lambda}$ that have the same conformal dimensions, but belong to different $O(n)$ representations. To single out a representation λ, we should also apply a Young projector $P_{\lambda}^{2r} : [1]^{2r} \to \lambda$,

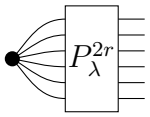

(8.4.3)

We do not know how to do this systematically, because lines are not allowed to cross in our graphs.

Young projectors are algebraic objects, which a priori know nothing about our two-dimensional model and the topology of our two-dimensional graphs. If we identified each line with a vector representation and applied Young projectors, we would sum over all permutations of lines, and obtain graphs with line crossings. In two dimensions, if we do not want lines to cross, only cyclic permutations are allowed.

A cyclic permutation of $2r$ lines has the signature $(-1)^{2r+1}$: it is odd for two lines, even for three lines, etc. As a consequence, the antisymmetrizer $P^3_{[111]}$ becomes trivial if we only sum over cyclic permutations. This explains why the representations [3] and [111] can both appear in $\Lambda_{(\frac{3}{2},0)}$ (8.1.27a), and lead to fields $V^{[3]}_{(\frac{3}{2},0)}$ and $V^{[111]}_{(\frac{3}{2},0)}$ with the same conformal dimensions and two-point functions.

This however does not imply that $V^{[3]}_{(\frac{3}{2},0)}$ and $V^{[111]}_{(\frac{3}{2},0)}$ coincide. This is because in higher correlation functions, the Young projectors associated to fields at different positions are expected to mix. For example, in the context of the four-point functions of Eq. (8.3.28), we do see a difference between these two fields.

Similarly, after projection on the representation [21], cyclic permutations of three lines have the eigenvalues $e^{\pm\frac{2\pi i}{3}}$, hence [21] appears in $\Lambda_{(\frac{3}{2},\frac{2}{3})}$.

Algebraic interpretation

The foregoing analysis should be greatly facilitated by turning to a more algebraic description, the principles of which we briefly sketch now. Graphs with crossings can be conveniently described using the formalism of diagram algebras—in this case, the Brauer algebra [174]. Technically, the Brauer algebra is the Schur–Weyl dual of $O(n)$ in the tensor product of vector representations: this implies that irreducible representations of the Brauer algebra are labelled by Young diagrams, just like irreducible representations of $O(n)$. The size $|\lambda|$ of a Young diagram corresponds to the number of legs of a site in the graph.

Forbidding crossings amounts to restricting to a subalgebra of the Brauer algebra: the Jones–Temperley–Lieb algebra (JTL) [63, 175]. Remarkably, we have found in preliminary investigations that when we decompose irreducible representations of the Brauer algebra into direct sums of irreducible JTL representations, the number of legs can increase from $|\lambda|$ to $|\lambda|+2n$ with $n \in \mathbb{N}$. This is at the root of the appearance of $O(n)$ representations with various sizes $|\lambda| \leq 2r$ in $\Lambda_{(r,s)}$ (8.1.26).

We also note that in the continuum limit, the JTL algebra becomes the interchiral algebra [172]: a symmetry algebra of the CFT that includes conformal symmetry.

8.4.3 Analytic continuation of the $O(n)$ model

As we have argued in the introduction, the $O(n)$ CFT is defined on infinitely many copies of the complex n-plane. Beyond $n \in [-2, 2]$, does the $O(n)$ CFT still describe the critical point of some $O(n)$ lattice model or field theory?

From a formal point of view, the critical coupling $K_c(n)$ (8.0.1) has two branch cuts $\pm(2, \infty)$, which correspond to vertical lines in the β^2-plane (8.0.5). It is tempting to conjecture that the model is critical for $n \in \mathbb{C} - ((2, \infty) \cup (-\infty, -2))$. If the situation is the same as in the CFT, we should still be able to analytically continue through the branch cuts, but the result would depend on whether we come from above or below.

In order to find out, we would need to carry out extensive numerical simulations of the lattice model with complex n and coupling constants. For the moment, let us collect some preliminary remarks on the question.

The real axis

The lattice $O(n)$ model that we have discussed in the introduction is naturally defined for $n \in [-2, 2]$. For $n > 2$, the lattice model (and all the refinements that have been studied so far) does not seem to have a phase transition at finite, real temperature, and cannot be related to the $O(n)$ CFT. This state of affairs is, for n integer at least, a consequence of the Mermin–Wagner theorem which precludes spontaneous breaking of continuous symmetries in two dimensions [176]—although this theorem leaves open the possibility of having Kosterlitz–Thouless phases like for $n = 2$ [177]. Note how the situation is different from the case of the Q-state Potts model, which retains a critical point for $Q > 4$, albeit a first-order critical point.

This can be made clearer using the Lagrangian description of the $O(n)$ model as a non-linear sigma model whose target space is the sphere S^{n-1}. In this model, the n-component vector ϕ subject to $\phi \cdot \phi = 1$ is no longer defined on a lattice, but on a continuous two-dimensional space. The Lagrangian density is

$$\mathscr{L} = \frac{1}{2g^2} \partial_\mu \phi \cdot \partial_\mu \phi \ . \tag{8.4.4}$$

The beta function for the coupling is

$$\beta(g^2) = (n-2)g^4 + O(g^6) \ . \tag{8.4.5}$$

For $n > 2$, the renormalization group flow is towards strong coupling at large length scales, and it is expected that the symmetry is restored and no transition occurs (that is the Mermin–Wagner theorem). For $n < 2$, on the other hand, zero coupling is an attractive fixed point, corresponding to a spontaneously broken symmetry phase. It is believed that for $n \geq -2$ there is a second-order phase transition separating this regime from the strong coupling regime, and that the dilute $O(n)$ CFT describes the corresponding critical point.

Strictly speaking, the only physical value of $n < 2$ is $n = 1$, which corresponds to the Ising universality class. To consider real values of $n < 2$ requires performing an analytic continuation of perturbative results at $n \in \mathbb{N}^*$. The case $n = 2$ is a bit special, as the beta function vanishes perturbatively to all orders. The model then exhibits a line of fixed points with continuously varying scaling dimensions. The corresponding critical phase terminates at the Kosterlitz–Thouless point, which is described by the free boson CFT.

The physics encompassed in the beta function (8.4.5) do not seem to be affected by the bound $n = -2$, and the critical coupling $K_c(n)$ admits a real determination for $n < -2$. This seems to suggest that the sigma model still exhibits a phase transition that may be described by the $O(n)$ CFT. In fact, there is evidence that the model for $n < -2$ does have a phase transition, albeit a first-order one, and that this transition is closely related with the first-order phase transition in the Potts model at $Q > 4$ [37].

Therefore, the sigma model picture confirms that the $O(n)$ CFT is not the critical limit of the $O(n)$ model for $n \in (-\infty, -2) \cup (2, \infty)$.

Complex values of n

For $\mathrm{Re}\, n < 2$, the behaviour of the perturbative beta function (8.4.5) is not qualitatively affected near the line $g^2 \in \mathbb{R}$ by allowing n to be complex. This suggests that the $O(n)$ CFT may be

related to the lattice model and the sigma model. This might even hold for $\operatorname{Re} n < -2$, as the first-order phase transition may morph into a second-order phase transition as n becomes complex.

For $\operatorname{Re} n > 2$, the small-coupling phase definitely seems unstable, just like for $n \in (2, \infty)$, where the model is expected not to have a phase transition. For the CFT to describe the critical behavior of the $O(n)$ lattice model, something has to happen: this might involve higher-order terms in the beta function, or the emergence of relevant operators not taken into account in the Lagrangian (8.4.4).

An example of the latter situation is well-known to occur in the case $n = 2$. The free boson CFT makes sense for all values $R \in \mathbb{C}^*$ of the compactification radius, but only describes the continuum limit of the lattice XY model in the Kosterlitz–Thouless (KT) phase, $0 < R < \sqrt{2}$. (In our convention, $R = 0$ is the low-temperature limit, $R = \frac{1}{\sqrt{2}}$ the self-dual point, and $R = \sqrt{2}$ the critical temperature or KT point.) This is because the lattice model is bound to contain local vortices, which are absent from the free boson action, since they can be described by perturbations that are irrelevant in the KT phase. However, for $R \geq \sqrt{2}$, these perturbations become relevant, and draw the XY model into a massive phase. This is not seen in the beta function (8.4.5), which vanishes to all orders for $n = 2$.

In our case, we would need terms such as vortices to render the system critical, instead of destroying criticality. This may be less unlikely than it seems, since we now allow complex couplings. There are indeed known examples where relevant perturbations with complex couplings give rise to flows towards other critical points [178].

Complex values of n are further discussed in [40], to which the interested reader is referred.

CHAPTER

9

CONCLUSION

In this thesis, we have seen how several different methods, both on the lattice and in the continuum, together have allowed us to gain insight into non-unitary CFTs that have resisted more "conventional" methods, such as BPZ differential equations, that rely on having semi-simple representations of the Virasoro algebra.

We have provided a graphical formulation of correlation functions in RSOS minimal models that involves quantities which are similar but different from those in the Potts model. This formulation has allowed us to analyse in detail how the complex spectrum conjectured in [20] for the Potts model does, indeed, reduce to the much simpler RSOS spectrum when probabilities are replaced by "pseudo-probabilities". This reduction involves a series of beautiful "facts" (and numbers), which we do not fully understand for the moment.

Using the geometrical formulation of correlation functions in RSOS minimal models, we have then been able to explain what the conjecture in [19] actually describes, why the "special combinations of probabilities" considered by these authors emerge, and to quantify how their results differ from the true Potts model result.

This analysis lays the groundwork for the solution of the Potts model itself. For recent work on the Potts model in the bootstrap approach, which builds on the work in this thesis, see [150]. Another future direction of this work is further investigation of the "facts" (exposed in sections 4.4.2–4.4.4), which hint at rich and largely unknown algebraic structures lurking beneath the problem of correlation functions on the lattice. It is hard not to speculate, in particular, that all the coefficients α_{j,z^2}, $\bar{\alpha}_{j,z^2}$, $\beta^{(k)}_{j,z^2}$ and $\gamma^{(\mathsf{a})}_{j,z^2}$ should have a natural algebraic meaning, and—especially since they can be expressed as relatively simple rational functions of Q—could be calculated from first principles, using maybe quantum-group [62] or S_Q representation theory [139, 141, 179]. This, however, remains to be seen.

We have also shown how the computation of correlation functions of the order parameter in A_n RSOS models corresponds to the evaluation of certain fusion diagrams of $su(2)_k$ anyons, with $k = n-1$, and how the anisotropic limit of these RSOS models corresponds to $su(2)_k$ anyon chains with a Temperley-Lieb Hamiltonian. Within this context we have shown the construction of topological defects, and that the lattice precursor of the $(1, s)$ defects commutes with the

Koo-Saleur generators. Future work will involve further studies of the topological defects, extending the work in [107] to other models than the Ising model and other topological defects than those of type $(1,2)$. In another direction, the mapping from $su(2)_3$ anyons to Fibonacci anyons through the process of "folding" deserves some further investigation to see whether there are any subtleties involved, or whether the relations to the A_4 RSOS model in Chapter 5 can be immediately extended to the Golden chain. The Fibonacci anyons, which are expected to emerge in the Read-Rezayi quantum Hall state, are of high interest in context of topological quantum computing, since they can be used for universal quantum computing [180].

We have presented considerable numerical evidence of the validity of the Koo-Saleur conjecture, namely that $\mathscr{L}_n \mapsto L_n$ as $N \to \infty$, in the scaling-weak sense. Thanks to the systematic use of form factors in the numerical computations, we have been able to increase significantly the size of the systems studied—and thus the accuracy of the checks—as compared with the pioneering paper [12].

The main mathematical question raised by these results—the exact nature of the convergence of the Koo-Saleur generators to their continuum limit, and the relation between limits of commutators and commutators of limits—certainly deserves further study. As a first step in this direction, we have conjectured that the limit of the commutators of the Koo-Saleur generators is correct *only up to the anomalous central charge term*, a result for which we have given qualitative and numerical evidence, but which we are not able to prove for now. Our results about the exchange of commutators and limits are encompassed in the conjectures (6.5.12),(6.5.22) and (6.5.23) and the result (6.5.21).

Usage of the Koo-Saleur generators has allowed us to analyse the structure of the Virasoro modules occurring in the continuum limit of the XXZ spin chain, as well as the structure of these modules for the loop model and the closely related Q-state Potts model.

In the degenerate case, where the conjectured conformal weights take values in the extended Kac table, one crucial result for the XXZ spin chain is that both Verma and co-Verma modules occur. The difference between Verma and co-Verma is related to the existence of two conjugate values of the Coulomb-gas charges giving rise to the same scaling dimension of the corresponding vertex operator. The notion of charge conjugation leads also to the identity of certain matrix elements, exact in finite size, as expressed in the result (6.2.20) about strong duality.

Meanwhile for the Q-state Potts model and the loop models (dense or dilute), one of our main finding is that Jordan cells for L_0 or $\bar{L}_0$ are expected to appear in the continuum limit of these models, even though there are no such Jordan cells in the finite-size lattice model. This possibility was already mentioned in [58] in the particular case $c = 0$, but occurs quite generically, whenever fields with degenerate conformal weights $h_{r,s}$, with $r, s \in \mathbb{N}^*$, appear in the spectrum. It is in fact a logical consequence of the self-duality of the modules $\mathscr{W}_{j,1}$, and thus can be argued on very general grounds.[1]

Our results for the nature of the modules arising in the continuum limit are given in equations (6.4.4) and (6.4.7) for the XXZ spin chain representation, and in equations (7.4.3) and (7.4.12)) for the loop model. The CFT for the XXZ spin chain seems well described by the somewhat mundane Dotsenko–Fateev twisted boson theory. In contrast, the Q-state Potts model or loop model CFTs appear to be new objects, related to but not identical with the $c < 1$ Liouville theory [102, 134, 135], and slowly getting under control thanks to this and other recent work.

A future direction is to extend the use of these techniques from $\mathfrak{q}$ generic and investigate the

[1] The absence of Jordan cells on the lattice makes measuring the logarithmic couplings $b_{r,s}$ appearing in the indecomposable modules (7.5.35) quite difficult, as there seems to be no simple way of normalizing the lattice version of the field $\Psi_{r,s}$.

structure of the Virasoro modules in the case where $\mathfrak{q}$ is a root of unity. This will be applied to the understanding of logarithmic CFTs, in particular the determination of the full "identity module" for $c = 0$ theories like the $sl(2|1)$ spin chain. For the Q-state Potts model and the loop models, more Jordan cells are expected to appear, with a rank higher than two [59].

Another interesting question deserving more work is the possible relation between the two scalar products we have introduced, and what they have to do with the natural positive definite scalar product in the RSOS case. We also hope to get back to this point in further work.

Finally we have applied the conformal bootstrap to the $O(n)$ model, using the information about the logarithmic modules in loop models found in Chapter 7 and independently in [6]. This has allowed us to numerically compute four-point functions at generic values of n, and the numerical computations have allowed us to infer exact results about the fusion rules, and also to compare the number of solutions with the predictions from $O(n)$ representation theory. The latter predictions rely on our conjectured decomposition of the spectrum into irreducible $O(n)$ representations.

In Section 8.4 we have outlined several of the future directions building on the results from the conformal bootstrap: to refine and extend the work on the $O(n)$ CFT, gaining better understanding of the number of independent solutions to the bootstrap as well as the fusion rules; to provide a geometrical interpretation of the solutions in terms of graphs; and to investigate the analytic continuation in n of the $O(n)$ model. Some of this work has been initiated in [40, 49].

Throughout this thesis, a leitmotif has been the interconnections between different frameworks, mathematical structures and physical models. Recalling only a few examples, we have seen: the map between the RSOS model and anyonic systems (in both the unitary and non-unitary case) which provides a link between CFTs and topological matter, the close relationship between the indecomposable modules of the Temperley-Lieb algebra and the Virasoro algebra, that the dual structure of Virasoro modules in the spin chain emerges as a consequence of the structure of the Bethe roots and relations in the Quantum Inverse Scattering Method, and that the conformal bootstrap solutions "knows about" and respects the $O(n)$ symmetry when given only information about the relevant conformal blocks as input.

It seems clear that future work will involve understanding and exploiting such interconnections even more, whether from a lattice approach or using other methods. Along the way there are plenty of concrete applications of the work, ranging from applying the Bootstrap methods developed in Chapter 8 to the $O(n)$ model in the $n \to 0$ limit (polymers) and to the Q-state Potts model in the $Q \to 1$ limit (percolation) in the short term, to gaining insights into critical points in different universality classes of topological insulators (like the plateau transition in the integer quantum Hall effect) through a deeper understanding of non-unitary CFTs in general in the long term.

In the introduction, we noted that in contrast to the representation theory of unitary CFTs, that of non-unitary CFTs is in a technical sense "wild". Yet when we venture into that wilderness we find it not devoid of order, but filled with intricate structure.

APPENDIX

A

THREE-POINT COUPLINGS C_{r_1,r_2,r_3} IN TYPE A_{p-1} AND TYPE $D_{1+\frac{p}{2}}$

In this appendix, we give the three-point couplings C_{r_1,r_2,r_3} for RSOS models of type A and D which we used in Chapter 4 for studying the cluster expansions of the RSOS four-point functions. Here we consider generic (p,q) with $p-q \geq 1$ and $p \wedge q = 1$ associated with a Dynkin diagram of type A or D with Coxeter number p as in Figure 4.3 and use the formula (5.2.11), where the special vector corresponding to identity field is $S_\sigma = S^\sigma_{(p-q)}$ and becomes $S^\sigma_{(1)}$ in the unitary case.

Type A

In A_{p-1}, the eigenvectors of the adjacency matrix $\mathscr{A}$ are

$$S^\sigma_{(r)} = \sqrt{\frac{2}{p}} \sin\left(\frac{r\pi}{p}\sigma\right),\ r = 1, \dots, p-1\,. \tag{A.0.1}$$

We thus obtain the following three-point couplings:

$$C^{A_{p-1}}_{r_1,r_2,r_3} = \begin{cases} (-1)^{\mathsf{b}_1+\mathsf{b}_2+\mathsf{b}_3}\frac{1-(-1)^{\mathsf{a}_1+\mathsf{a}_2+\mathsf{a}_3}}{2}, & |\mathsf{d}_1-\mathsf{d}_2|+1 \leq \mathsf{d}_3 \leq\ (\mathsf{d}_1+\mathsf{d}_2-1),\ \mathsf{d}_1+\mathsf{d}_2+\mathsf{d}_3 \leq 2p-1\,, \\ 0, & \text{otherwise}\,, \end{cases} \tag{A.0.2}$$

where a_i, b_i solve the Diophantine equation

$$r_i + \mathsf{b}_i p = \mathsf{a}_i(p-q) \tag{A.0.3}$$

and d_i is given by

$$\mathsf{d}_i = \frac{1+(-1)^{\mathsf{b}_i}}{2}\mathsf{a}_i + \frac{1-(-1)^{\mathsf{b}_i}}{2}(p-\mathsf{a}_i)\,. \tag{A.0.4}$$

Notice that in the unitary case, $\mathsf{d}_i = \mathsf{a}_i = r_i$ and $\mathsf{b}_i = 0$, and we recover the well-known unitary minimal models fusion rules.

Type D

In the case of $D_N = D_{1+\frac{p}{2}}$ with $p \equiv 2 \bmod 4$, the Dynkin diagram has a fork labeled by $N-1$ and $\overline{N-1}$, as shown in Figure 4.3. The eigenvectors of $\mathscr{A}$ read

$$S^{\sigma}_{(r)} = \frac{2}{\sqrt{p}} \cos \frac{(N-1-\sigma)r\pi}{p},\ \sigma \neq N-1, \overline{N-1} \tag{A.0.5}$$

$$S^{N-1}_{(r)} = S^{\overline{N-1}}_{(r)} = \frac{1}{\sqrt{p}},\ \text{for } r = 1, 3, \ldots, p-1,\ \text{odd} \tag{A.0.6}$$

and the last eigenvector corresponding to $r = \frac{\bar{p}}{2}$ is

$$S^{\sigma}_{(\bar{p}/2)} = (0, ..., 0, \frac{1}{\sqrt{2}}, -\frac{1}{\sqrt{2}})\,. \tag{A.0.7}$$

The three-point couplings are

$$C^{D_{1+\frac{p}{2}}}_{r_1,r_2,r_3} = \begin{cases} (-1)^{\frac{\mathsf{a}_1+\mathsf{a}_2+\mathsf{a}_3+1}{2}}, & |\mathsf{d}_1 - \mathsf{d}_2| + 1 \leq \mathsf{d}_3 \leq\ (\mathsf{d}_1 + \mathsf{d}_2 - 1),\ \mathsf{d}_1 + \mathsf{d}_2 + \mathsf{d}_3 \leq 2p-1\,, \\ 0, & \text{otherwise} \end{cases} \tag{A.0.8}$$

for $r \neq \bar{p}/2$ and the only non-vanishing C's involving $\bar{p}/2$ are $C^{D_{1+\frac{p}{2}}}_{\bar{p}/2,\bar{p}/2,r} = 1$, for $r = 1, \ldots, p/2, \ldots, p-1$.

APPENDIX

B

SOME REMARKS ON SCALAR PRODUCTS

It is interesting to discuss in more detail why the conformal scalar product in Chapter 6 (the one corresponding to the conjugation $L_n^\ddagger = L_{-n}$) is the one relevant for the calculation of correlation functions in the operator formalism, and, in our case, is the one obtained by "treating $\mathfrak{q}$ as a formal variable". Due to the exploratory nature of this Appendix, we shall use here the standard bra-ket notation $\langle -|-\rangle$, although the conformal scalar product will eventually be denoted by $(-,-)$ in Chapter 6.

We start by discussing a simple example. Consider a very simple system of two spins 1/2 coupled via the $U_\mathfrak{q} sl(2)$ invariant Hamiltonian, which reads (up to an irrelevant scalar factor)

$$\mathscr{H} = -e = -\begin{pmatrix} 0 & 0 & 0 & 0 \\ 0 & \mathfrak{q}^{-1} & -1 & 0 \\ 0 & -1 & \mathfrak{q} & 0 \\ 0 & 0 & 0 & 0 \end{pmatrix} \tag{B.0.1}$$

in the basis $\{++, +-, -+, --\}$. When $\mathfrak{q}$ is real, the normalized ground state is given by

$$|\Omega\rangle = \frac{1}{\sqrt{\mathfrak{q}+\mathfrak{q}^{-1}}}(\mathfrak{q}^{-1/2}|+-\rangle - \mathfrak{q}^{1/2}|-+\rangle)\,. \tag{B.0.2}$$

When $\mathfrak{q}$ is a complex number of modulus one—the case we are considering here—$\mathscr{H}$ *is not hermitian*. The ground state $|\Omega\rangle$ as we have written here is not normalized any more, since its norm square obtained with the usual scalar product is $\frac{2}{\mathfrak{q}+\mathfrak{q}^{-1}}$.

However, since the eigenvalues $(0, \mathfrak{q}+\mathfrak{q}^{-1})$ are real, we see that from

$$\mathscr{H}^\dagger |E_\mathrm{L}\rangle = E|E_\mathrm{L}\rangle \tag{B.0.3}$$

we get the left-eigenvalue problem

$$\langle E_\mathrm{L}|\mathscr{H} = E\langle E_\mathrm{L}| \tag{B.0.4}$$

to be compared with the right-eigenvalue problem initially considered

$$\mathscr{H}|E_\mathrm{R}\rangle = E|E_\mathrm{R}\rangle\,. \tag{B.0.5}$$

In our case we have (where the unprimed states correspond to the singlet, i.e., the ground state, while the primed states correspond to the triplet)

$$|E_{\mathrm{R}}\rangle = \frac{1}{\sqrt{\mathfrak{q}+\mathfrak{q}^{-1}}}\left(\mathfrak{q}^{-1/2}|+-\rangle - \mathfrak{q}^{1/2}|-+\rangle\right) , \tag{B.0.6a}$$

$$|E'_{\mathrm{R}}\rangle = \frac{1}{\sqrt{\mathfrak{q}+\mathfrak{q}^{-1}}}\left(\mathfrak{q}^{1/2}|+-\rangle + \mathfrak{q}^{-1/2}|-+\rangle\right) , \tag{B.0.6b}$$

and

$$|E_{\mathrm{L}}\rangle = \frac{1}{\sqrt{\mathfrak{q}+\mathfrak{q}^{-1}}}\left(\mathfrak{q}^{1/2}|+-\rangle - \mathfrak{q}^{-1/2}|-+\rangle\right) , \tag{B.0.7}$$

$$|E'_{\mathrm{L}}\rangle = \frac{1}{\sqrt{\mathfrak{q}+\mathfrak{q}^{-1}}}\left(\mathfrak{q}^{-1/2}|+-\rangle + \mathfrak{q}^{1/2}|-+\rangle\right) , \tag{B.0.8}$$

where we chose normalizations such that left and right eigenstates are orthonormal,

$$\langle E_{\mathrm{L}}|E_{\mathrm{R}}\rangle = \langle E'_{\mathrm{L}}|E'_{\mathrm{R}}\rangle = 1\,, \qquad \langle E_{\mathrm{L}}|E'_{\mathrm{R}}\rangle = \langle E'_{\mathrm{L}}|E_{\mathrm{R}}\rangle = 0\,, \tag{B.0.9}$$

and $\langle -|-\rangle$ stands for the ordinary scalar product. We see now that $|\Omega\rangle$ remains properly normalized with these conventions. Moreover, conjugating and switching L for R amounts to treating $\mathfrak{q}$ as a formal parameter, by which we mean that it does not undergo any complex conjugation in the process. We thus see that considering scalar products of the form $\langle E_L|E_R\rangle$ (with left and right eigenstates properly distinguished), instead of $\langle E_R|E_R\rangle$ (with no such distinction), amounts to treating $\mathscr{H}$ as self-conjugate, i.e., $\mathfrak{q}$ as a formal parameter indeed.

The second point is to establish what this has to do with physics. We start by demanding that calculations in our quantum (field theory or not) formalism describe well-defined objects in two-dimensional statistical physics. The mapping of the quantum system onto a statistical mechanics one proceeds via an imaginary-time representation, which can be depicted by taking the direction of imaginary time to be upwards. The density operator ρ introduces a horizontal cut in this time evolution, in the sense that its matrix elements ρ_{xy} are such that x (resp. y) refers to the degrees of freedom on the lower (resp. upper) lip of this cut. We now argue that one may write the density operator as $\rho = |0_{\mathrm{R}}\rangle\langle 0_{\mathrm{L}}|$, that is, in terms of the left and right ground states. Indeed, its matrix elements are of the form

$$\rho_{xy} \propto \langle +\infty|e^{-\tau H}|y\rangle\langle x|e^{-\tau H}|-\infty\rangle\,,$$

where $\langle +\infty|$ and $|-\infty\rangle$ denote "generic states" (initial conditions that are not orthogonal to the left and right ground states, respectively) introduced at imaginary times $\pm\infty$, that is, at the bottom and top of the time evolution. Taking τ large projects onto the lowest-energy eigenstates of $\mathscr{H}$ for the bottom part and $\mathscr{H}^\dagger$ for the top part, so

$$\rho_{xy} \propto \langle 0_L|y\rangle\langle x|0_R\rangle\,.$$

With proper normalizations it is therefore justified to write $\rho = |0_{\mathrm{R}}\rangle\langle 0_{\mathrm{L}}|$, as claimed. Correlation functions in the quantum theory are then obtained by tracing ρ with various insertions, and thus correspond to

$$\langle 0_{\mathrm{L}}|\cdots|0_{\mathrm{R}}\rangle\,, \tag{B.0.10}$$

with $\langle -|-\rangle$ denoting the ordinary scalar product.

In CFT, we demand that

$$\langle\phi| = |\phi\rangle^\dagger\,, \tag{B.0.11}$$

which leads to (on the surface where $\bar{z} = z^*$, the complex conjugate)

$$[\phi(z,\bar{z})]^\dagger \equiv \bar{z}^{-2h} z^{-2\bar{h}} \phi(1/\bar{z}, 1/z)\,, \tag{B.0.12}$$

so that

$$\begin{aligned} \langle\phi|\phi\rangle &= \lim_{z,\bar{z},w,\bar{w}\to 0} \langle 0|\phi(z,\bar{z})^\dagger \phi(w,\bar{w})|0\rangle \\ &= \lim_{\xi,\bar{\xi}\to\infty} \bar{\xi}^{2h} \xi^{2\bar{h}} \langle 0|\phi(\bar{\xi},\xi)\phi(0,0)|0\rangle \\ &= 1\,, \end{aligned} \tag{B.0.13}$$

where in the last step we would generally obtain the residue of the two-point function, if the latter were not normalized. Using this for $T(z)$ leads immediately to $L_n^\dagger = L_{-n}$. In general, we see that this dagger operation is the one that exchanges left and right eigenstates in the non-Hermitian case.

This conformal scalar product is the continuum limit of the loop scalar product, or the $sl(2|1)$-invariant scalar product as well. It is not, in general, positive definite. As already mentioned, it will be denoted $(-,-)$ in Chapter 6.

APPENDIX

C

MORE ON FORM FACTORS

For a general overview of transfer matrix formalism, Bethe ansatz and the Quantum Inverse Scattering Method (QISM), see [123].

C.1 General framework, notations, conventions

We shall follow the work in [181]. We first fix our notation. The XXZ R-matrix is written as

$$R(\lambda,\mu) = \begin{pmatrix} 1 & 0 & 0 & 0 \\ 0 & b(\lambda,\mu) & c(\lambda,\mu) & 0 \\ 0 & c(\lambda,\mu) & b(\lambda,\mu) & 0 \\ 0 & 0 & 0 & 1 \end{pmatrix}, \tag{C.1.1}$$

with

$$b(\lambda,\mu) = \frac{\sinh(\lambda-\mu)}{\sinh(\lambda-\mu+\eta)}, \tag{C.1.2a}$$

$$c(\lambda,\mu) = \frac{\sinh(\eta)}{\sinh(\lambda-\mu+\eta)} \tag{C.1.2b}$$

and $\eta = i\gamma$. Since R only depends on the difference $\lambda-\mu$, we shall sometimes write it in terms of only one variable, $R(u) \equiv R(\lambda,\mu)$ with $u = \lambda-\mu$. We write the corresponding monodromy matrix as $\mathbf{T}(u) = \left(\begin{smallmatrix} A(u) & B(u) \\ C(u) & D(u) \end{smallmatrix}\right)$, thereby defining the operators A, B, C, D that will be used below. Let $a(\lambda)$ and $d(\lambda)$ be the eigenvalues of $A(\lambda)$ and $D(\lambda)$ when acting on $|0\rangle$, where $|0\rangle$ denotes the pseudo-vacuum of all spins pointing up. The Bethe equations take the form

$$\frac{d(\lambda_j)}{a(\lambda_j)} \prod_{k\neq j} \frac{b(\lambda_k,\lambda_j)}{b(\lambda_j,\lambda_k)} = 1 \tag{C.1.3}$$

for $j = 1, 2, \ldots, \frac{N}{2} - S_z$, and an on-shell Bethe state is written as $\prod_j B(\lambda_j)|0\rangle$ with the Bethe roots λ_j solving (C.1.3). (If the roots do not solve the Bethe equations, the state is called off-shell.)

The above holds for periodic boundary conditions, but we also wish to consider boundary conditions parametrized by a twist ϕ. Let $\kappa \in GL_2(\mathbb{C})$. Then $\kappa\mathbf{T}$ gives us the monodromy matrix for the case of twisted boundary conditions on the form $\sigma^a_{N+1} = \kappa\sigma^a_1\kappa^{-1}$. For the boundary conditions that we wish to implement (namely $\sigma^z_{N+1} = \sigma^z_1$ and $\sigma^\pm_{N+1} = e^{\mp i\phi}\sigma^\pm_1$) the proper choice is the following diagonal twist matrix:

$$\kappa = \begin{pmatrix} 1 & 0 \\ 0 & e^{i\phi} \end{pmatrix}. \tag{C.1.4}$$

We obtain thus the twisted monodromy matrix

$$\kappa\mathbf{T}(u) = \begin{pmatrix} 1 & 0 \\ 0 & e^{i\phi} \end{pmatrix} \begin{pmatrix} A(u) & B(u) \\ C(u) & D(u) \end{pmatrix} = \begin{pmatrix} A(u) & B(u) \\ e^{i\phi}C(u) & e^{i\phi}D(u) \end{pmatrix}. \tag{C.1.5}$$

Twisting the monondromy matrix $\mathbf{T}(u) \to \kappa\mathbf{T}(u)$ in this fashion leads to a modified eigenvalue $d(u) \to e^{i\phi}d(u)$ that will enter into the Bethe equations, since the latter contain the ratios $\frac{d(\lambda_k)}{a(\lambda_k)}$.

With a diagonal twist κ as above, any general Bethe considerations for the untwisted case will also be valid for the twisted case. For instance, while (C.1.5) implies that $B^\dagger(\lambda^*) = C(\lambda)$ for the untwisted case (up to a phase), this same property will still hold after the twist (up to another phase).[1] Notice however that this does not carry over to the general case of non-diagonal κ, where the dual Bethe states (defined from C) might no longer be given by the conjugate of the Bethe states (defined from B).

C.2 Quantum Inverse Scattering Method

In the framework of the quantum inverse scattering method, we express local operators $\mathcal{O}$ in terms of the operators A, B, C, D. Let $t(\frac{\eta}{2}) = A(\frac{\eta}{2}) + D(\frac{\eta}{2})$ denote the transfer matrix, that is, the trace of $\mathbf{T}(u)$ in the homogeneous case $u = \eta/2 = i\gamma/2$ (which will sometimes have to be taken as a limit, as we shall see below). We recall that the XXZ Hamiltonian (2.1.8) is recovered from $T^{-1}(u)\frac{\partial T}{\partial u}\Big|_{u=\eta/2}$. (Note that we have here chosen different conventions than in Chapter 2, where the Hamiltonian limit corresponded to $u \to 0$.) Acting on a Bethe state, where n is the number of roots characterizing the state, the transfer matrix has eigenvalues

$$t\left(\frac{\eta}{2}\right)\prod_{k=1}^n B(\lambda_k)|0\rangle = \left[a\left(\frac{\eta}{2}\right)\prod_{k=1}^n b^{-1}\left(\lambda_k, \frac{\eta}{2}\right) + d\left(\frac{\eta}{2}\right)\prod_{k=1}^n b^{-1}\left(\frac{\eta}{2}, \lambda_k\right)\right]\prod_{k=1}^n B(\lambda_k)|0\rangle. \tag{C.2.1}$$

With the conventions used in [181], $a(\lambda) = 1$, $d(\lambda) = \prod_{m=1}^N b(\lambda, \xi_m)$, so that $d(\xi_m) = 0$ even before taking the homogeneous limit. We denote by $\phi_m\{\lambda\} = \prod_{k=1}^N \left(b^{-1}\left(\lambda_k, \frac{\eta}{2}\right)\right)^m$ the factor produced by the action of $t^m\left(\frac{\eta}{2}\right)$, which appears in the computation of form factors. We can then express the matrix elements of j neighbouring operators (acting on consecutive sites $m, m+1, \ldots, m+j-1$) in the form

$$\langle\{\mu\}|\prod_{i=1}^j (\mathcal{O}_i)_{m+i-1}|\{\lambda\}\rangle = \phi_{m-1}(\{\mu\})\phi^{-1}_{m+j-1}(\{\lambda\})F_{\mathcal{O}_1,\ldots,\mathcal{O}_j}, \tag{C.2.2}$$

where $F_{\mathcal{O}_1,\ldots,\mathcal{O}_j}$ depends on the combination of operators $\mathcal{O}$ whose matrix elements we wish to obtain, while the pre-factors $\phi_m\{\lambda\}$ only depend on how many operators we consider and at

[1] Note that the Bethe roots come in conjugate pairs (or are real, or self-conjugate), so that in total we do indeed get the expression for Bethe states as in eq (6.2.13).

which sites. The expression for $F_{\mathcal{O}_1,\ldots,\mathcal{O}_j}$ is site-independent: all dependence on the site m is in the phase coming from the ϕ pre-factors in (C.2.2). Below we use the shorthand notation $z \leftrightarrow \sigma^z$, $- \leftrightarrow \sigma^-$, $+ \leftrightarrow \sigma^+$ to denote the required operators $\mathcal{O}$, and we wish to compute expressions such as F_{-+}.

Because of this site-independence, in numerical applications it is most efficient to compute the relevant $F_{\mathcal{O}_1,\ldots,\mathcal{O}_j}$ only once for each size N, and then add up any site-dependent phases (see Section 6.2.3) in an independent step when using the form factors.[2] Combined with the parity and conjugation relations mentioned earlier, this significantly reduces the computational load. Furthermore most scalar products S_n (see below) are used in several form factors. This can be taken advantage of as well.

We wish to find $F_{\mathcal{O}_1,\ldots,\mathcal{O}_j}$ for the combinations of Pauli matrices shown in and below (6.2.11)–(6.2.12). To this end, we shall need to consider the following operators (given here with their shorthand abbreviation):

$$z \;:\; \sigma^z_m \leftrightarrow A(\xi_m) - D(\xi_m)\,,\ \text{or}\ 2A(\xi_m) - \mathbf{1}\,,\ \text{or}\ \mathbf{1} - 2D(\xi_m)\,, \tag{C.2.3a}$$

$$+ \;:\; \sigma^+_m \leftrightarrow C(\xi_m)\,, \tag{C.2.3b}$$

$$- \;:\; \sigma^-_m \leftrightarrow B(\xi_m) \tag{C.2.3c}$$

in the homogeneous limit $\xi_m \to \eta/2$. For instance, to get F_z we can compute $F_D = \langle C|D(\xi_m)|B\rangle$, where $\langle C| = \langle 0|\prod_j C(\mu_j)$ and $|B\rangle = \prod_k B(\lambda_k)$ are Bethe states. We shall always keep $\langle C|$ untouched (and thus still on-shell), commuting the operators above past the string of B-operators, so that the result will become expressed in terms of new, off-shell states $|\tilde{B}\rangle$. (See the commutation relations below, where some $B(\lambda_k)$ are swapped into $B\,(\xi_m)$ with $\xi_m = \frac{\eta}{2}$.) When computing the final scalar products $S_n = \langle C|\tilde{B}\rangle$, we can then still use relations that hold when one of the states is on-shell.

In order to commute all the operators past the B-operators we use the following commutation relations, where $\varphi(\lambda) = \sinh(\lambda)$:

$$\begin{aligned} A(\xi_m)\prod_{k=1}^n B(\lambda_k)|0\rangle \;=\; & \prod_{k=1}^n \frac{\varphi(\lambda_k - \xi_m + \eta)}{\varphi(\lambda_k - \xi_m)} \prod_{k=1}^n B(\lambda_k)|0\rangle \\ & - \sum_{a=1}^n \frac{\varphi(\eta)}{\varphi(\lambda_a - \xi_m)} \prod_{k=1,k\neq a}^n \frac{\varphi(\lambda_k - \lambda_a + \eta)}{\varphi(\lambda_k - \lambda_a)} B(\xi_m) \prod_{k=1,k\neq a}^n B(\lambda_k)|0\rangle\,, \end{aligned} \tag{C.2.4a}$$

$$C(\xi_m)\prod_{k=1}^n B(\lambda_k)|0\rangle \;=\; \sum_{a=1}^n M_a(\xi_m) \prod_{k=1,k\neq a}^n B(\lambda_k)|0\rangle + \sum_{a\neq b} M_{ab}(\xi_m) B(\xi_m) \prod_{k=1,k\neq a,b}^n B(\lambda_k)|0\rangle\,, \tag{C.2.4b}$$

$$D(\xi_m)\prod_{k=1}^n B(\lambda_k)|0\rangle \;=\; -\sum_{a=1}^n \frac{\varphi(\eta)}{\varphi(\xi_m - \lambda_a)} \prod_{k=1,k\neq a}^n \frac{\varphi(\lambda_a - \lambda_k + \eta)}{\varphi(\lambda_a - \lambda_k)} d(\lambda_a) B(\xi_m) \prod_{k=1,k\neq a}^n B(\lambda_k)|0\rangle\,, \tag{C.2.4c}$$

[2] For the specific purpose of computing the Koo-Saleur generators, keeping track of phases actually turns out to be unnecessary, because of the considerations about momentum conservation made in Section 6.3.1.

with

$$M_a(\xi_m) = \frac{\varphi(\eta)}{\varphi(\lambda_a-\xi_m)}\prod_{k\neq a}\frac{\varphi(\lambda_k-\xi_m+\eta)}{\varphi(\lambda_k-\xi_m)}\frac{\varphi(\lambda_k-\lambda_a+\eta)}{\varphi(\lambda_k-\lambda_a)}\,, \tag{C.2.5a}$$

$$M_{ab}(\xi_m) = \frac{\varphi(\eta)^2}{\varphi(\lambda_a-\xi_m)\varphi(\lambda_b-\xi_m)}\prod_{k\neq a}\frac{\varphi(\lambda_k-\lambda_a+\eta)}{\varphi(\lambda_k-\lambda_a)}\frac{\varphi(\lambda_k-\lambda_b+\eta)}{\varphi(\lambda_k-\lambda_b)}\,. \tag{C.2.5b}$$

We have written out factors of $b^{-1}(\mu,\lambda)$ explicitly to make it clearer later which terms will need to be combined in the homogeneous limit. Note that the B-operators commute among themselves.

Finally we need to divide through with the norms of the Bethe states after obtaining the required form factors, as the states we use are otherwise not normalized. For roots $\{\lambda\}$ solving the Bethe equations, the corresponding state has the norm squared (written using the conventions of [181])

$$N_n(\{\lambda\}) = \varphi^n(\eta)\prod_{\alpha\neq\beta}\frac{\varphi(\lambda_\alpha-\lambda_\beta+\eta)}{\varphi(\lambda_\alpha-\lambda_\beta)}\det(G(\{\lambda\})\,, \tag{C.2.6}$$

with

$$G_{ab}(\{\lambda\}) = -\frac{\partial}{\partial\lambda_b}\ln\left(r(\lambda_a)\prod_{k=1,k\neq a}^{n}\frac{b(\lambda_a,\lambda_k)}{b(\lambda_k,\lambda_a)}\right). \tag{C.2.7}$$

Here $r(\lambda)=a(\lambda)/d(\lambda)$.

C.3 The expressions for the necessary $F_{\mathcal{O}_1,\ldots,\mathcal{O}_j}$

In what follows we shall use the notation $\{\lambda\}$ to refer to the set of Bethe roots $\lambda_1,\ldots,\lambda_n$, while $\{\lambda\}_a$ denotes the set with the a'th root removed. We use $S_n(\{\mu\},\{\lambda\})$ to refer to scalar products $\langle\{\mu\}|\{\lambda\}\rangle$; these scalar products are given explicitly below.

Note: As when finding the Bethe roots, we must again keep in mind the modified eigenvalue $d(\lambda)\to e^{i\phi}d(\lambda)$. For the norm squared above any overall phase is ignored in the final normalization. Below, however, the phases $e^{i\phi}$ do matter. We obtain relative phases between the different terms, and also overall phases that we must keep in mind when we take conjugates as discussed in Section 6.2.3.

C.3.1 F_z, F_{zz}, F_{-+}

F_{-+} is taken directly from [181], up to minor changes in notation. For the other two we have chosen to write in terms of D, as it has somewhat nicer commutation relations. F_z, F_{zz} are given from F_D, F_{DD} in accordance with (C.2.3). We have:

$$F_D = -\sum_{a=1}^{n}\frac{\varphi(\eta)}{\varphi(\xi_m-\lambda_a)}\prod_{k=1,k\neq a}^{n}\frac{\varphi(\lambda_a-\lambda_k+\eta)}{\varphi(\lambda_a-\lambda_k)}e^{i\phi}d(\lambda_a)S_n(\{\mu\}|\xi_m,\{\lambda\}_a)\,, \tag{C.3.1a}$$

$$F_{DD} = \sum_{a,b=1,b\neq a}^{n}\frac{\varphi(\eta)^2}{\varphi(\xi_{m+1}-\lambda_a)\varphi(\xi_m-\lambda_b)}\prod_{k=1,k\neq a}^{n}\frac{\varphi(\lambda_a-\lambda_k+\eta)}{\varphi(\lambda_a-\lambda_k)}e^{i\phi}d(\lambda_a)\frac{\varphi(\lambda_b-\xi_{m+1}+\eta)}{\varphi(\lambda_b-\xi_{m+1})}$$
$$\times\prod_{k=1,k\neq a,b}^{n}\frac{\varphi(\lambda_b-\lambda_k+\eta)}{\varphi(\lambda_b-\lambda_k)}e^{i\phi}d(\lambda_b)S_n(\{\mu\}|\xi_m,\xi_{m+1},\{\lambda\}_{a,b})\,. \tag{C.3.1b}$$

For F_{-+} we need F_{BC}:

$$F_{BC} = \sum_{a=1}^{n} M_a(\xi_{m+1}) S_n(\{\mu\}|\xi_m, \{\lambda\}_a) + \sum_{b=1, b\neq a}^{n} M_{ab}(\xi_{m+1}) S_n(\{\mu\}|\xi_m, \xi_{m+1}, \{\lambda\}_{a,b}) \,. \quad \text{(C.3.2)}$$

For all these we can safely let $\xi_m, \xi_{m+1} \to \eta/2$, as long as we write the scalar products involving multiple $\eta/2$ as shown in Section C.3.3.

C.3.2 F_{z-+}, F_{-z+}

For F_{z-+} we will need F_{DBC}:

$$\begin{aligned} F_{DBC} = &-\sum_{a=1}^{n} M_a(\xi_{m+2}) \sum_{b=1, b\neq a}^{n} \frac{\varphi(\eta)}{\varphi(\xi_m - \lambda_b)} \frac{\varphi(\lambda_b - \xi_{m+1} + \eta)}{\varphi(\lambda_b - \xi_{m+1})} \\ &\times \prod_{k=1, k\neq a,b}^{n} \frac{\varphi(\lambda_b - \lambda_k + \eta)}{\varphi(\lambda_b - \lambda_k)} e^{i\phi} d(\lambda_b) S_n(\{\mu\}|\xi_m, \xi_{m+1}, \{\lambda\}_{a,b}) \\ &- \sum_{a\neq b} M_{ab}(\xi_{m+2}) \sum_{c=1, c\neq a,b}^{n} \frac{\varphi(\eta)}{\varphi(\xi_m - \lambda_c)} \frac{\varphi(\lambda_c - \xi_{m+1} + \eta)}{\varphi(\lambda_c - \xi_{m+1})} \frac{\varphi(\lambda_c - \xi_{m+2} + \eta)}{\varphi(\lambda_c - \xi_{m+2})} \\ &\times \prod_{k=1, k\neq a,b,c}^{n} \frac{\varphi(\lambda_c - \lambda_k + \eta)}{\varphi(\lambda_c - \lambda_k)} e^{i\phi} d(\lambda_c) S_n(\{\mu\}|\xi_m, \xi_{m+1}, \xi_{m+2}, \{\lambda\}_{a,b,c}), \end{aligned} \quad \text{(C.3.3)}$$

where we can again safely let $\xi_m, \xi_{m+1}, \xi_{m+2} \to \eta/2$.

For F_{-z+} we need both F_{BDC} and F_{BAC}:

$$\begin{aligned} F_{BDC} = &-\sum_{a=1}^{n} M_a(\xi_{m+2}) \sum_{b=1, b\neq a}^{n} \frac{\varphi(\eta)}{\varphi(\xi_{m+1} - \lambda_b)} \\ &\times \prod_{k=1, k\neq a,b}^{n} \frac{\varphi(\lambda_b - \lambda_k + \eta)}{\varphi(\lambda_b - \lambda_k)} e^{i\phi} d(\lambda_b) S_n(\{\mu\}|\xi_m, \xi_{m+1}, \{\lambda\}_{a,b}) \\ &- \sum_{a\neq b} M_{ab}(\xi_{m+2}) \sum_{c=1, c\neq a,b}^{n} \frac{\varphi(\eta)}{\varphi(\xi_{m+1} - \lambda_c)} \frac{\varphi(\lambda_c - \xi_{m+2} + \eta)}{\varphi(\lambda_c - \xi_{m+2})} \\ &\times \prod_{k=1, k\neq a,b,c}^{n} \frac{\varphi(\lambda_c - \lambda_k + \eta)}{\varphi(\lambda_c - \lambda_k)} e^{i\phi} d(\lambda_c) S_n(\{\mu\}|\xi_m, \xi_{m+1}, \xi_{m+2}, \{\lambda\}_{a,b,c}), \end{aligned} \quad \text{(C.3.4)}$$

$$
\begin{aligned}
F_{BAC} = &\sum_{a=1}^{n} M_a(\xi_{m+2}) \prod_{k=1,k\neq a}^{n} \frac{\varphi(\lambda_k - \xi_{m+1} + \eta)}{\varphi(\lambda_k - \xi_{m+1})} S_n(\{\mu\}|\xi_m, \{\lambda\}_a) \\
&- \sum_{a=1}^{n} M_a(\xi_{m+2}) \sum_{b=1,b\neq a}^{n} \frac{\varphi(\eta)}{\varphi(\lambda_b - \xi_{m+1})} \prod_{k=1,k\neq a,b}^{n} \frac{\varphi(\lambda_k - \lambda_b + \eta)}{\varphi(\lambda_k - \lambda_b)} S_n(\{\mu\}|\xi_m, \xi_{m+1}, \{\lambda\}_{a,b}) \\
&+ \sum_{a\neq b} M_{ab}(\xi_{m+2}) \frac{\varphi(\xi_{m+2} - \xi_{m+1} + \eta)}{\varphi(\xi_{m+2} - \xi_{m+1})} \prod_{k=1,k\neq a,b}^{n} \frac{\varphi(\lambda_k - \xi_{m+1} + \eta)}{\varphi(\lambda_k - \xi_{m+1})} S_n(\{\mu\}|\xi_m, \xi_{m+2}, \{\lambda\}_{a,b}) \\
&- \sum_{a\neq b} M_{ab}(\xi_{m+2}) \frac{\varphi(\eta)}{\varphi(\xi_{m+2} - \xi_{m+1})} \prod_{k=1,k\neq a,b}^{n} \frac{\varphi(\lambda_k - \xi_{m+2} + \eta)}{\varphi(\lambda_k - \xi_{m+2})} S_n(\{\mu\}|\xi_m, \xi_{m+1}, \{\lambda\}_{a,b}) \\
&- \sum_{a\neq b} M_{ab}(\xi_{m+2}) \sum_{c=1,c\neq a,b}^{n} \frac{\varphi(\eta)}{\varphi(\lambda_c - \xi_{m+1})} \frac{\varphi(\xi_{m+2} - \lambda_c + \eta)}{\varphi(\xi_{m+2} - \lambda_c)} \prod_{k=1,k\neq a,b,c}^{n} \frac{\varphi(\lambda_k - \lambda_c + \eta)}{\varphi(\lambda_k - \lambda_c)} \\
&\qquad \times S_n(\{\mu\}|\xi_m, \xi_{m+1}, \xi_{m+2}, \{\lambda\}_{a,b,c}).
\end{aligned}
\tag{C.3.5}
$$

In the latter expression, the third and fourth terms are divergent on their own if we take the homogeneous limit. They will, however, combine into a derivative. Let $\xi_{m+1} = \eta/2$, $\xi_{m+2} = \eta/2 + x$. We have a common factor $M_{ab}(\xi_{m+2})$ that causes no problem, and for the rest we can write

$$
\begin{aligned}
\frac{1}{\varphi(x)} [\text{third} - \text{fourth}] \xrightarrow[x\to 0]{} &\partial_x \Big(\varphi(\eta + x) S_n(\{\mu\}|\eta/2 + x, \eta/2, \{\lambda\}_{ab}) \Big) \Big|_{x=0} \prod \frac{\varphi(\lambda_k + \eta/2)}{\varphi(\lambda_k - \eta/2)} \\
&- \Big(\varphi(\eta) S_n(\{\mu\}|\eta/2, \eta/2, \{\lambda\}_{ab}) \Big) \partial_x \prod \frac{\varphi(\lambda_k - x + \eta/2)}{\varphi(\lambda_k - x - \eta/2)} \Big|_{x=0}.
\end{aligned}
\tag{C.3.6}
$$

C.3.3 Scalar products and the homogeneous limit

We give below the determinant representation for the scalar products S_n. Please note than when compared to [181] we have taken the factors of $r(\lambda) = a(\lambda)/d(\lambda)$ outside the matrix. This leads to an overall phase $e^{-in\phi}$ in front of the determinant from the modified eigenvalue $d(\lambda) \to e^{i\phi} d(\lambda)$.

$$
S_n(\{\mu\}, \{\lambda\}) \equiv \langle \{\mu\} | \{\lambda\} \rangle = \frac{e^{-in\phi} \det(H(\{\mu\}, \{\lambda\}))}{\prod_{j>k} \varphi(\mu_k - \mu_j) \prod_{\alpha<\beta} \varphi(\lambda_\beta - \lambda_\alpha)},
\tag{C.3.7}
$$

with

$$
H_{ab}(\{\mu\}, \{\lambda\}) = \frac{\varphi(\eta)}{\varphi(\mu_a - \lambda_b)} \Big(\prod_{k\neq a} \varphi(\mu_k - \lambda_b + \eta) - e^{i\phi} d(\lambda_b) \prod_{k\neq a} \varphi(\mu_k - \lambda_b - \eta) \Big).
\tag{C.3.8}
$$

We shall need the scalar products $S_n(\eta/2, \eta/2, \ldots)$, $S_n(\eta/2, \eta/2, \eta/2, \ldots)$, and the derivative $\partial_x S_n(\{\mu\}|\eta/2 + x, \eta/2, \{\lambda\}_{ab}) \Big) \Big|_{x=0}$ in the homogeneous limit, which must be taken carefully due to the denominator.

Subtracting the relevant columns of H from each other before taking the limit, and taking factors of the type $1/\varphi(\xi_m - \xi_{m+1})$ inside, we arrive at the replacement of the first columns

by their first and second derivatives. The second term in (C.3.8) disappears in these columns, thanks to $d(\xi_m) = 0$. Starting with $S_n(\eta/2, \eta/2, \ldots)$, we simply find the first column replaced by its derivative:

$$H'_{a1}(\{\mu\},\{\lambda\}) = -\partial_x \frac{\varphi(\eta)}{\varphi(\mu_a - \eta/2 - x)} \prod_{k\neq a} \varphi(\mu_k - x + \eta/2)\Big|_0 , \tag{C.3.9}$$

and the product in the denominator of S_n is now taken for $\beta > 2$. For $S_n(\eta/2, \eta/2, \eta/2, \ldots)$ we arrive at the following replacements for column 1 and 2:

$$H'_{a2}(\{\mu\},\{\lambda\}) = -\partial_x \frac{\varphi(\eta)}{\varphi(\mu_a - \eta/2 - x)} \prod_{k\neq a} \varphi(\mu_k - x + \eta/2)\Big|_0 , \tag{C.3.10a}$$

$$H''_{a1}(\{\mu\},\{\lambda\}) = \frac{1}{2}\partial_x^2 \frac{\varphi(\eta)}{\varphi(\mu_a - \eta/2 - x)} \prod_{k\neq a} \varphi(\mu_k - x + \eta/2)\Big|_0 . \tag{C.3.10b}$$

The product in the denominator of S_n is now taken for $\beta > 3$. Finally for $\partial_x S_n(\{\mu\}|\eta/2 + x, \eta/2, \{\lambda\})$ we can take the derivative inside $\det(H)$ and let it act on the relevant column. Taking the homogeneous limit then leads to further derivatives, so that in total we obtain

$$\begin{aligned}\partial_x S_n(\{\mu\}|\eta/2 + x, \eta/2, \{\lambda\})\Big|_0 &= -\frac{1}{2}\frac{e^{-in\phi}\det\Big(\tilde{H}''(\{\mu\}|\eta/2, \eta/2, \{\lambda\})\Big)}{\prod_{j>k}\varphi(\mu_k - \mu_j)\prod_{\alpha<\beta,\beta>2}\varphi(\lambda_\beta - \lambda_\alpha)} \\ &\quad + \sum_{2<\beta} \frac{\varphi'(\lambda_\beta - \eta/2)}{\varphi(\lambda_\beta - \eta/2)} S_n(\{\mu\}|\eta/2, \eta/2, \{\lambda\}) ,\end{aligned} \tag{C.3.11}$$

where $\tilde{H}''$ is obtained from H by differentiating the first column twice:

$$\tilde{H}''_{a0} = \partial_x^2 \frac{\varphi(\eta)}{\varphi(\mu_a - \eta/2 - x)} \prod_{k\neq a} \varphi(\mu_k - x + \eta/2)\Big|_{x=0} . \tag{C.3.12}$$

APPENDIX

D

NUMERICAL RESULTS FOR THE DEGENERATE CASE IN THE SIX-VERTEX MODEL

Within this Appendix we provide numerical evidence for the results (6.4.4) and (6.4.7) given in Chapter 6. Throughout this Appendix we take $x = \pi$, so that $\mathfrak{q}$ is not a root of unity. We consider states with degenerate conformal weights $h = h_{r,s}$ and/or $\bar{h} = h_{r,s}$. We shall use the same notation $|u\rangle, |v\rangle, |w\rangle$... for scaling states and the corresponding states in the continuum.

D.1 The case of $\mathscr{W}_{j,1}$

The main goal of this section is to provide numerical support for the conjecture (6.4.4) and the concept of strong duality (6.2.20). We start by showing explicitly in Table D.1 the duality for conjugate states for the first few sizes, giving an example of how matrix elements for raising operators will follow from those for the lowering operators. In this example we consider $S_z = 1$, $e = \pm 1$. We here also see the issue of mixing discussed in Section 6.2.1.

Call the $S_z = 1$, $e = -1$ primary state $|u_-\rangle$ and the $S_z = 1$, $e = 1$ primary state $|u_+\rangle$. The sector of relevant lattice momentum for the chiral level 1 state $|a_{-1}u_-\rangle$ is then the same as that of the anti-chiral level 1 state $|\bar{a}_{-1}u_+\rangle$. Within this sector, the two lowest-energy Bethe states have close but not identical energies. We call these two states $|v_1\rangle$ and $|v_2\rangle$. Since nothing in our theory favours chiral over anti-chiral, or vice versa, we must assume that we cannot identify one of $|v_1\rangle, |v_2\rangle$ to $|a_{-1}u_-\rangle$ and the other to $|\bar{a}_{-1}u_+\rangle$. Instead, to keep their energy on the lattice identical, we must consider them as linear combinations, containing equal parts of the two states. We identify $|\bar{a}_{-1}u_+\rangle = \frac{1}{\sqrt{2}}(|v_1\rangle + |v_2\rangle)$ and $|a_{-1}u_-\rangle = \frac{1}{\sqrt{2}}(|v_1\rangle - |v_2\rangle)$ (with the phases of the eigenvectors $|v_1\rangle, |v_2\rangle$ fixed to give the same phase for the relevant matrix elements.) We then obtain the results in Table D.2, which are in line with our conjectures.

	$\langle v_1\|\mathscr{L}_{-1}\|u_-\rangle$	$\langle v_2\|\mathscr{L}_{-1}\|u_-\rangle$	$\langle \bar{a}_{-1}u_-\|\bar{\mathscr{L}}_{-1}\|u_-\rangle$
N	$\langle u_+\|\bar{\mathscr{L}}_1\|v_1\rangle$	$\langle u_+\|\bar{\mathscr{L}}_1\|v_2\rangle$	$\langle u_+\|\mathscr{L}_1\|a_{-1}u_+\rangle$
8	0.0526552	0.08033931	0.71811371
10	0.04744019	0.07094947	0.87777283
12	0.04357369	0.06336333	0.9762023
14	0.04048884	0.0573236	1.03974472
16	0.03793402	0.05245015	1.08270653
18	0.03576776	0.04844714	1.11294418
20	0.03389957	0.04510245	1.13495942
22	0.03226707	0.04226491	1.15145137
p_7	0.00580449	0.00549332	1.23163297
conj	0	0	1.23170369

	$\langle v_1\|\bar{\mathscr{L}}_{-1}\|u_+\rangle$	$\langle v_2\|\bar{\mathscr{L}}_{-1}\|u_+\rangle$	$\langle a_{-1}u_+\|\mathscr{L}_{-1}\|u_+\rangle$
N	$\langle u_-\|\mathscr{L}_1\|v_1\rangle$	$\langle u_-\|\mathscr{L}_1\|v_2\rangle$	$\langle u_-\|\bar{\mathscr{L}}_1\|\bar{a}_{-1}u_-\rangle$
8	0.19977481	0.30480884	0.99943154
10	0.20854526	0.31189113	1.19506516
12	0.21572193	0.31369525	1.31480472
14	0.22148634	0.31357761	1.39180979
16	0.22616506	0.31271118	1.44376243
18	0.23002327	0.3115647	1.48028264
20	0.23325554	0.31034011	1.50685293
22	0.23600264	0.30912729	1.52674922
p_7	0.27168088	0.2829496	1.62371173
conj	0.27723073	0.27723073	1.62376715

Table D.1: Matrix elements of $\mathscr{L}_{\pm 1}$ and $\bar{\mathscr{L}}_{\pm 1}$ in the sector of $S_z = 1$, at $x = \pi$. We call $|u_-\rangle$ the primary state at $e = -1$ and $|u_+\rangle$ the primary state at $e = 1$ (both in the $N \to \infty$ limit), with charges given by (6.1.38). $|v_1\rangle$ and $|v_2\rangle$ are linear combinations of $|a_{-1}u_-\rangle$ and $|\bar{a}_{-1}u_+\rangle$ containing equal parts of both states, as discussed in Section 6.2.1. We here denote the corresponding scaling states on the lattice by the same labels as the states in the limits. The matrix elements are computed at increasing lattice size N, after which polynomial extrapolations $p_n(1/N)$ of degree $n = 7$ to all the data points is made in order to approximate the value at $N \to \infty$. The CFT value ("conj") $\langle a_{-1}u|L_{-1}u\rangle$ for a primary state u with charge α is $\sqrt{2}\alpha$, as described in Section 6.3.2. Due to $|v_1\rangle, |v_2\rangle$ being mixed states, the nonzero matrix elements involving these states are conjectured to come with a factor of $\frac{1}{\sqrt{2}}$: while the full value is 0.39206346 ($\alpha = 2\alpha_0$) we here instead conjecture a value of 0.27723073 each.

N	$\langle \bar{a}_{-1}u_+\|\mathscr{L}_{-1}\|u_-\rangle$	$\langle a_{-1}u_-\|\mathscr{L}_{-1}\|u_-\rangle$
8	0.09388641	0.02030561
10	0.08364162	0.01698464
12	0.07557809	0.01419611
14	0.06914237	0.01202808
16	0.0638982	0.01034544
18	0.05954055	0.00902118
20	0.05585724	0.00796118
22	0.05269816	0.00709863
p_7	0.00798875	-0.00022102
conj	0	0

N	$\langle \bar{a}_{-1}u_+\|\bar{\mathscr{L}}_{-1}\|u_+\rangle$	$\langle a_{-1}u_-\|\bar{\mathscr{L}}_{-1}\|u_+\rangle$
8	0.35679453	0.07427027
10	0.3680041	0.07307657
12	0.37435448	0.0692776
14	0.37834734	0.06511836
16	0.38104305	0.06119735
18	0.38296053	0.0576585
20	0.38438017	0.05450702
22	0.38546507	0.05170693
p_7	0.39218298	0.00796819
conj	0.39206346	0

N	$\langle u_+\|\bar{\mathscr{L}}_1\|\bar{a}_{-1}u_+\rangle$	$\langle u_+\|\bar{\mathscr{L}}_1\|a_{-1}u_-\rangle$
8	0.01957562	0.09404132
10	0.01662357	0.08371413
12	0.01399339	0.07561589
14	0.01190397	0.06916384
16	0.01026446	0.06391126
18	0.00896568	0.05954893
20	0.00792163	0.05586287
22	0.00706954	0.05270207
p_7	-0.00022003	0.00798876
conj	0	0

N	$\langle u_-\|\mathscr{L}_1\|\bar{a}_{-1}u_+\rangle$	$\langle u_-\|\mathscr{L}_1\|a_{-1}u_-\rangle$
8	0.07703985	0.35620678
10	0.07466382	0.36768535
12	0.07028121	0.37416736
14	0.06579726	0.37822987
16	0.06168015	0.38096519
18	0.0580154	0.38290662
20	0.05477911	0.38434149
22	0.05191965	0.38543648
p_7	0.00796872	0.39218313
conj	0	0.39206346

Table D.2: Matrix elements of $\mathscr{L}_{\pm 1}$ and $\bar{\mathscr{L}}_{\pm 1}$ in the sector of $S_z = 1$, at $x = \pi$, with the same conventions as in Table D.1. Having separated $|\bar{a}_{-1}u_+\rangle$ and $|a_{-1}u_-\rangle$ from each other we here obtain the full conjectured norm. We note that strong duality does not apply to this table, since we no longer deal with single Bethe states but rather linear combinations thereof.

With this result in mind we then restrict our attention to only considering lowering operators in tables D.4–D.7. In these four tables we look at the null states at level 1 and 2 for $\mathscr{W}_{1,1}$ and $\mathscr{W}_{2,1}$; the use of form factors here enables us to access higher sizes. For comparison we show in each table both the action of $A_{r,s}$ and $\bar{A}_{r,s}$, even though only one of the conformal weights of the primary state is degenerate.

We also restrict our attention to $|v_1\rangle$ in the case of mixing at level 1, having already seen in tables D.1–D.2 that we recover the full norm when taking both $|v_1\rangle$ and $|v_2\rangle$ into account. The reason for this restriction is technical: when using form factors instead of exact diagonalization, $|v_2\rangle$ corresponds to a singular Bethe state and would require regularization that in turn would perturb the numerical results. We note that when excluding singular states in this way in the cases of overlap, the results at both level 1 and 2 do not match the conjecture as well as in the cases of no overlap. Meanwhile we see in Table D.2 that the agreement when including all singular states and taking the proper linear combinations is comparable to the cases of no overlap.

D.1.1 Considerations at level 2

At level 2 we typically expect two orthogonal states, which we call $|w_1\rangle$ and $|w_2\rangle$. To get the total projection onto level 2 we consider

$$|\chi|_2 \equiv \sqrt{|\langle w_1|\chi\rangle|^2 + |\langle w_2|\chi\rangle|^2} \tag{D.1.1}$$

and same for the anti-chiral quantities. In the case of degenerate conformal weights we furthermore again have the issue of overlap, so that we once again must take into account twice as many states. However, the fourth state is a singular Bethe state, so we do not include it in our form-factor computations to avoid regularization. We label the norms with and without this fourth state as

$$|\chi|_2^* \equiv \sqrt{|\langle w_1|\chi\rangle|^2 + |\langle w_2|\chi\rangle|^2 + |\langle w_3|\chi\rangle|^2 + |\langle w_4|\chi\rangle|^2}\,, \tag{D.1.2a}$$

$$|\chi|_2^{**} \equiv \sqrt{|\langle w_1|\chi\rangle|^2 + |\langle w_2|\chi\rangle|^2 + |\langle w_3|\chi\rangle|^2}\,. \tag{D.1.2b}$$

We show the result for $|\chi|_2^*$ obtained from exact diagonalization in Table D.3 at $S_z = 2, e = 1$, before restricting to $|\chi|_2^{**}$ when going to higher sizes with form factors.

When using form factors, we need to know what conjecture to consider when we exclude the fourth, singular Bethe state. It turns out that the second and third Bethe states, which are found in a degenerate eigenspace of the Hamiltonian, have an almost zero contribution to the norm (or order $\mathcal{O}(10^{-3})$, respectively $\mathcal{O}(10^{-5})$, when extrapolating the form-factor results). Meanwhile the first and fourth states are at different energies, and so by the same argument as for level 1 (i.e., that we cannot favour chiral over anti-chiral, and so their energy must be the same) we expect that the two Bethe states contribute equally. Excluding the fourth state will thus roughly remove half the norm squared at $S_z = 2, e = 1$, up to the $\mathcal{O}(10^{-3})$ contribution from the second and third states. Meanwhile, when we consider the chiral side at $S_z = 2, e = -1$ the conjecture simply remains zero.

N	$\|\chi\|_2^*$	Full norm
10	0.45377412	0.45904775
12	0.47363006	0.47883132
14	0.48751301	0.49234698
16	0.4976002	0.50267043
18	0.50516327	0.51126303
20	0.51098601	0.51895827
22	0.51557136	0.52628211
p_5	0.54746072	0.84670007
p_6	0.54780548	1.02083064
conj	0.54675127	

Table D.3: Norm at level 2 in the case of overlap. Shown is projection onto the four relevant states. In the right column is the full norm for comparison. The presence of parasitic couplings in the latter case leads to a different result, which moreover cannot be reliably extrapolated. The conventions used for the extrapolations p_5 and p_6 are the same as in Table 6.1.

D.1.2 Form factor results for $\mathscr{W}_{j,1}$

For all form factor results we take the most extreme cutoff in any product of Koo-Saleur generators. (See further the discussion in Section 6.5.1.)

N	$\langle v_1\|\mathscr{L}_{-1}\|u_-\rangle$	$\langle\bar{a}_{-1}u_-\|\bar{\mathscr{L}}_{-1}\|u_-\rangle$
10	0.04744019	0.87777283
12	0.04357369	0.9762023
14	0.04048884	1.03974472
16	0.03793402	1.08270653
18	0.03576776	1.11294418
20	0.03389957	1.13495942
22	0.03226707	1.15145137
24	0.0308251	1.16410715
26	0.02953989	1.17402095
28	0.02838551	1.18192562
30	0.02734164	1.18832605
32	0.02639211	1.19357881
34	0.02552386	1.19794122
36	0.02472619	1.20160266
38	0.02399028	1.20470491
40	0.02330873	1.20735576
42	0.02267536	1.20963831
44	0.02208487	1.21161746
46	0.02153276	1.21334445
48	0.02101516	1.21486018
⋮	⋮	⋮

N	$\langle v_1\|\mathscr{L}_{-1}\|u_-\rangle$	$\langle\bar{a}_{-1}u_-\|\bar{\mathscr{L}}_{-1}\|u_-\rangle$
⋮	⋮	⋮
50	0.02052871	1.21619761
52	0.02007049	1.21738353
54	0.01963794	1.21843989
56	0.01922881	1.21938481
58	0.01884112	1.22023337
60	0.0184731	1.22099819
62	0.0181232	1.22168988
64	0.01779002	1.22231744
66	0.01747229	1.22288852
68	0.0171689	1.22340967
70	0.01687882	1.22388653
72	0.01660114	1.22432395
74	0.01633502	1.22472614
76	0.0160797	1.22509676
78	0.01583449	1.22543904
80	0.01559876	1.22575576
p_{25}	0.00214322	1.23169818
p_{30}	0.00218049	1.23169693
p_{35}	0.00208063	1.23170322
conj	0	1.23170369

Table D.4: Matrix elements of $\mathscr{L}_{\pm 1}$ and $\bar{\mathscr{L}}_{\pm 1}$ in the sector of $S_z = 1$, at $x = \pi$, with the same conventions as in Table D.1. In this table $e = -1$ is considered again. Polynomial extrapolations $p_n(1/N)$ of degrees $n = 25, 30, 35$ to all the data points are made in order to approximate the value at $N \to \infty$.

N	$\langle a_{-1}u_+\|\mathscr{L}_{-1}\|u_+\rangle$	$\langle v_1\|\bar{\mathscr{L}}_{-1}\|u_+\rangle$
10	1.19506516	0.20854526
12	1.31480472	0.21572193
14	1.39180979	0.22148634
16	1.44376243	0.22616506
18	1.48028264	0.23002327
20	1.50685293	0.23325554
22	1.52674922	0.23600264
24	1.5420146	0.23836731
26	1.55397203	0.24042566
28	1.56350664	0.24223501
30	1.57122775	0.24383928
32	1.57756543	0.2452726
34	1.58282995	0.2465619
36	1.58724958	0.24772868
38	1.59099515	0.24879034
40	1.59419657	0.24976108
42	1.59695398	0.25065264
44	1.59934555	0.25147477
46	1.60143303	0.25223568
48	1.60326571	0.25294229
⋮	⋮	⋮
50	1.60488329	0.25360052
52	1.60631806	0.25421543
54	1.60759648	0.25479138
56	1.60874039	0.25533217
58	1.60976797	0.25584109
60	1.61069443	0.25632105
62	1.61153256	0.25677457
64	1.61229323	0.25720392
66	1.61298565	0.25761109
68	1.61361774	0.25799785
70	1.61419627	0.25836579
72	1.61472713	0.25871633
74	1.61521538	0.25905076
76	1.61566545	0.25937022
78	1.61608122	0.25967576
80	1.61646607	0.25996833
p_{25}	1.6237699	0.27512229
p_{30}	1.62376682	0.27508581
p_{35}	1.62378719	0.27518577
conj	1.62376715	0.27723073

Table D.5: Matrix elements of $\mathscr{L}_{\pm 1}$ and $\bar{\mathscr{L}}_{\pm 1}$ in the sector of $S_z = 1$, at $x = \pi$, with the same conventions as in Table D.1. In this table $e = 1$ is considered again. Polynomial extrapolations $p_n(1/N)$ of degrees $n = 25, 30, 35$ to all the data points are made in order to approximate the value at $N \to \infty$. As discussed in Section D.1, the state $|v_2\rangle$ is not included here. The resulting additional factor of $\frac{1}{\sqrt{2}}$ has been taken into account in the conjecture.

N	$\lvert\chi\rvert_2^{**}$	$\lvert\bar{\chi}\rvert_2$
10	0.24726801	1.20983864
12	0.20066837	1.56533417
14	0.16972038	1.9115293
16	0.14727663	2.23720271
18	0.13029595	2.52679885
20	0.11707361	2.77534399
22	0.10653922	2.98500127
24	0.09798136	3.16074314
26	0.09090996	3.30802769
28	0.08497837	3.43184718
30	0.07993595	3.53644327
32	0.07559799	3.62530048
34	0.07182607	3.70123804
36	0.06851485	3.76652378
38	0.06558299	3.82298088
40	0.06296693	3.8720785
42	0.06061633	3.91500532
44	0.05849094	3.95272782
46	0.0565582	3.98603608
48	0.05479155	4.01557964
⋮	⋮	⋮
50	0.0531691	4.04189553
52	0.05167268	4.06543021
54	0.05028709	4.08655693
56	0.0489995	4.10558933
58	0.04779905	4.12279235
60	0.04667642	4.13839083
62	0.04562364	4.15257652
64	0.0446338	4.16551368
66	0.04370091	4.17734357
68	0.04281975	4.18818823
70	0.04198571	4.19815347
72	0.04119475	4.20733135
74	0.04044331	4.21580231
76	0.03972819	4.22363682
78	0.03904658	4.23089684
80	0.03839593	4.237637
p_{25}	0.00508552	4.37283102
p_{30}	0.0051748	4.37283425
p_{35}	0.00493341	4.37283415
conj	0	4.37266058

Table D.6: Values of $|\chi|_2, |\chi|_2^{**}$ as defined in (D.1.1),(D.1.2b), in the sector of $S_z = 2$ at $x = \pi$. The state χ in (D.1.2) is here taken to be the result of acting upon the primary state obtained for $S_z = 2, e = -1$ with the lowering operator $\mathscr{A}_{1,2}$ defined from $A_{1,2} = L_{-1}^2 - \frac{2(2h_{1,2}+1)}{3} L_{-2}$.The same conventions as Table D.1 are used for the extrapolation, and the CFT values ("conj") are computed using the general method described in Section 6.3.2. Note that on the chiral side we do not project on the fourth relevant state, as discussed in Section D.1.1.

N	$\lvert\chi\rvert_2$	$\lvert\bar{\chi}\rvert_2^{**}$
10	2.31045896	0.26408829
12	2.87163371	0.27340469
14	3.37941892	0.28280413
16	3.83197544	0.29119674
18	4.22184772	0.29847485
20	4.5502387	0.30475163
22	4.82397901	0.31017865
24	5.0515897	0.31489717
26	5.24122863	0.31902686
28	5.39994176	0.3226658
30	5.53353594	0.32589353
32	5.64669381	0.32877441
34	5.74315732	0.3313607
36	5.82591007	0.33369509
38	5.89733494	0.33581262
40	5.95934224	0.33774227
42	6.01347121	0.33950818
44	6.06096911	0.34113058
46	6.10285264	0.34262654
48	6.13995559	0.34401053
⋮	⋮	⋮
⋮	⋮	⋮
50	6.17296586	0.34529493
52	6.20245427	0.34649035
54	6.2288972	0.34760596
56	6.25269438	0.34864969
58	6.27418296	0.34962847
60	6.29364876	0.35054836
62	6.31133522	0.35141469
64	6.32745061	0.35223215
66	6.34217393	0.3530049
68	6.35565962	0.35373665
70	6.36804149	0.35443068
72	6.37943587	0.35508996
74	6.38994429	0.35571713
76	6.39965564	0.35631456
78	6.40864803	0.35688442
80	6.41699028	0.35742864
p_{25}	6.58058318	0.38348308
p_{30}	6.580578	0.38343063
p_{35}	6.58061875	0.38357299
conj	6.5805709	$0.387+\mathcal{O}(10^{-3})$

Table D.7: Values of $|\chi|_2, |\chi|_2^{**}$ as defined in (D.1.1),(D.1.2b), in the sector of $S_z = 2$ at $x = \pi$. The state χ in (D.1.2) is here taken to be the result of acting upon the primary state obtained for $S_z = 2, e = 1$ with the lowering operator $\mathscr{A}_{1,2}$ defined from $A_{1,2} = L_{-1}^2 - \frac{2(2h_{1,2}+1)}{3} L_{-2}$.The same conventions as Table D.1 are used for the extrapolation, and the CFT values ("conj") are computed using the general method described in Section 6.3.2. Note that on the anti-chiral side we do not project on the fourth relevant state. The effect of this on our conjecture is explained in Section D.1.1.

D.2 The case of $\mathscr{W}_{0,\mathfrak{q}^{\pm 2}}$

We here wish to provide, in particular, support for the conjecture (6.4.7). The results are shown in Table D.8. We here show how the indecomposability appears already at finite size in this particular case. We also again see the duality of conjugate states. While our focus here is on small system sizes and the indecomposability of the Temperley-Lieb modules, we still show the extrapolation as well—we see that already for these sizes it is quite close to the conjectured value.

	$\langle a_{-1}u_{\mathfrak{q}^2}\vert\mathscr{L}_{-1}\vert u_{\mathfrak{q}^2}\rangle$	$\langle \bar{a}_{-1}u_{\mathfrak{q}^2}\vert\bar{\mathscr{L}}_{-1}\vert u_{\mathfrak{q}^2}\rangle$
N	$\langle u_{\mathfrak{q}^{-2}}\vert\bar{\mathscr{L}}_1\vert\bar{a}_{-1}u_{\mathfrak{q}^{-2}}\rangle$	$\langle u_{\mathfrak{q}^{-2}}\vert\mathscr{L}_1\vert a_{-1}u_{\mathfrak{q}^{-2}}\rangle$
8-22	$\mathcal{O}(10^{-15})$	$\mathcal{O}(10^{-15})$
conj	0	0

	$\langle a_{-1}u_{\mathfrak{q}^{-2}}\vert\mathscr{L}_{-1}\vert u_{\mathfrak{q}^{-2}}\rangle$	$\langle \bar{a}_{-1}u_{\mathfrak{q}^{-2}}\vert\bar{\mathscr{L}}_{-1}\vert u_{\mathfrak{q}^{-2}}\rangle$
N	$\langle u_{\mathfrak{q}^2}\vert\bar{\mathscr{L}}_1\vert\bar{a}_{-1}u_{\mathfrak{q}^2}\rangle$	$\langle u_{\mathfrak{q}^2}\vert\mathscr{L}_1\vert a_{-1}u_{\mathfrak{q}^2}\rangle$
8	0.37384355	0.37384355
10	0.38058992	0.38058992
12	0.3842338	0.3842338
14	0.38641194	0.38641194
16	0.38781199	0.38781199
18	0.38876228	0.38876228
20	0.38943519	0.38943519
22	0.3899281	0.3899281
p_7	0.39204719	0.39204719
conj	0.39206346	0.39206346

Table D.8: Matrix elements of $\mathscr{L}_{\pm 1}$ and $\bar{\mathscr{L}}_{\pm 1}$ in the sector of $S_z = 0$, at $x = \pi$, $|e| = 1$ and twisted boundary conditions, with the same conventions as in Table D.1. We call $|u_{\mathfrak{q}^2}\rangle$ the primary state at twisted boundary conditions $e_\phi = \alpha_-/\alpha_+$, corresponding to the module $\mathscr{W}_{0,\mathfrak{q}^2}$, and $|u_{\mathfrak{q}^{-2}}\rangle$ the primary state at twisted boundary conditions $e_\phi = -\alpha_-/\alpha_+$, corresponding to the module $\mathscr{W}_{0,\mathfrak{q}^{-2}}$.

D.3 Relevant Bethe roots

In this section we list the Bethe roots used in the numerical results at $x = \pi, N = 10$ and with the twist ϕ as specified in each case. The roots for other values of x and the twist ϕ can be reached numerically by gradually modifying x, ϕ, using the previous roots as the starting guess of the numerical solver in each step. The roots at larger system sizes N are found in the same fashion. These roots can be inserted into the form factors listed in Appendix C in order to reproduce our numerical results. To find these sets of roots and integers we have used the values listed in [122] at $\Delta = 0.7$ as starting guesses. We remind the reader that as discussed in [122] it is expected that some Bethe integers may coincide.

We first show Bethe roots corresponding to the non-degenerate example in Section 6.3, in which $\phi = 1/10$, $S_z = 1$. The roots corresponding to the states in (6.3.4) are given by

$$\begin{aligned} |u_1\rangle &\leftrightarrow \{-0.26458064, -0.07736986, 0.0733926, 0.25830959\}, \\ |u_2\rangle &\leftrightarrow \{-0.6743697, -0.07413158, 0.07080173, 0.65194697\}, \\ |u_3\rangle &\leftrightarrow \{-0.66175052, -0.24704638, 0.24235079, 0.64024589\}, \end{aligned} \tag{D.3.1}$$

while the roots corresponding to the states in (6.3.5) are given by

$$\begin{aligned} |v_1\rangle &\leftrightarrow \{-0.65697428, -0.06400932, 0.08388252, 0.26957264\}, \\ |v_2\rangle &\leftrightarrow \{-0.6485393, -0.23998851, 0.07699763, 0.66517052\}, \\ |v_3\rangle &\leftrightarrow \{-0.29843157 + i\pi/2, -0.04047671, 0.0969293, 0.69411263\}. \end{aligned} \tag{D.3.2}$$

Meanwhile for the degenerate examples the roots used to produce the results in Appendix D.1.2 are given as follows.

At $S_z = 1, e = -1$, the Bethe roots necessary to reproduce Table D.4 are

$$\begin{aligned} |u_-\rangle &\leftrightarrow \{-0.59190986, -0.2125926, 0.10678414, -0.04262483\} \\ &\qquad \text{with integers } \left\{-\frac{5}{2}, -\frac{3}{2}, \frac{1}{2}, -\frac{1}{2}\right\}, \\ |\bar{a}_{-1}u_-\rangle &\leftrightarrow \{-0.60569326, -0.22013419, 0.28934619, -0.0495778\} \\ &\qquad \text{with integers } \left\{-\frac{5}{2}, -\frac{3}{2}, \frac{3}{2}, -\frac{1}{2}\right\}, \\ |v_1\rangle &\leftrightarrow \{-0.1439582, 0.1439582, i\pi/2, 0\} \\ &\qquad \text{with integers } \left\{-\frac{1}{2}, \frac{1}{2}, \frac{9}{2}, -\frac{1}{2}\right\}. \end{aligned} \tag{D.3.3}$$

The states $|u_+\rangle, |a_{-1}u_+\rangle$ relevant for Table D.5 are found by taking the opposite signs of the Bethe roots above. (State $|v_1\rangle$ remains the same under this action—recall that the root $i\pi/2$ is self-conjugate.)

At $S_z = 2, e = -1$ let us denote the primary state by $|u_-^{(2)}\rangle$. In the context of forming the norms (D.1.1) and (D.1.2b) we now distinguish descendants on the chiral resp. anti-chiral sides by superscripts: $|w_1^l\rangle, |w_2^l\rangle, |w_3^l\rangle$ resp. $|w_1^r\rangle, |w_2^r\rangle$. The Bethe roots necessary to reproduce Table

H.4 are

$$\begin{aligned}
|u_-^{(2)}\rangle &\leftrightarrow \{0.0199709, -0.12746759, -0.33759576\} \text{ with integers } \{0,-1,-2\} \\
|a_{-1}u_-^{(2)}\rangle &\leftrightarrow \{0.03251715, -0.10949347, -0.9283113\} \text{ with integers } \{0,-1,-3\} \\
|\bar{a}_{-1}u_-^{(2)}\rangle &\leftrightarrow \{0.16535175, -0.13383418, -0.34635301\} \text{ with integers } \{1,-1,-2\} \\
|w_1^l\rangle &\leftrightarrow \{-0.06631605, 0.06631605, i\pi/2\} \text{ with integers } \{0,0,-5\}, \\
|w_2^l\rangle &\leftrightarrow \{-0.03902337, 0.28513457, 0.88928688\} \text{ with integers } \{0,2,3\}, \\
|w_3^l\rangle &\leftrightarrow \{0.03902337, -0.28513457, -0.88928688\} \text{ with integers } \{0,-2,-3\}, \\
|w_1^r\rangle &\leftrightarrow \{0.15878868, 0.00783529, -0.35707322\} \text{ with integers } \{1,0,-2\}, \\
|w_2^r\rangle &\leftrightarrow \{0.37558835, -0.14134827, -0.35581938\} \text{ with integers } \{2,-1,-2\}.
\end{aligned} \tag{D.3.4}$$

Once more the states relevant for Table D.7 are found by taking the opposite signs of these Bethe roots. (The set of states $|w_1^l\rangle, |w_2^l\rangle, |w_3^l\rangle$ is invariant under this action—the first has real roots symmetric around zero and a self-conjugate imaginary root $i\pi/2$, while the other two have roots with opposite signs to one another.)

APPENDIX

E

PROOF OF (6.5.21)

We wish to prove (6.5.21b), from which (6.5.21a) then also follows thanks to the known result (6.5.20). Within this Appendix, we let $\langle \mathcal{O} \rangle$ refer to the ground-state expectation value of an operator $\mathcal{O}$ in the limit $N \to \infty$. Using the parity of the ground state we can restate (6.5.21b) as

$$\langle e_j e_{j+1} \rangle = \frac{3\sin^3\gamma\, I_1 - \sin\gamma\, I_0}{\cos\gamma}. \tag{E.0.1}$$

In [129] the following ground-state expectation values are given for spin operators $S^a = \sigma^a/2,\ a = x, y, z$:

$$\langle S^x_j S^x_{j+2} \rangle = -\frac{1}{2\pi \sin 2\gamma} I^{(0)} - \frac{3\cos 2\gamma \tan\gamma}{4\pi^3} I^{(2)} + \frac{\cos 2\gamma}{4\pi^2} I^{(1)} + \frac{\sin^2\gamma}{4\pi^4} I^{(3)}, \tag{E.0.2a}$$

$$\langle S^z_j S^z_{j+2} \rangle = \frac{1}{4} + \frac{\cot 2\gamma}{\pi} I^{(0)} + \frac{3\tan\gamma}{2\pi^3} I^{(2)} - \frac{1}{2\pi^2} I^{(1)} - \frac{\sin^2\gamma}{2\pi^4} I^{(3)}, \tag{E.0.2b}$$

$$\langle S^x_j S^x_{j+1} \rangle = -\frac{1}{4\pi \sin\gamma} I^{(0)} + \frac{\cos\gamma}{4\pi^2} I^{(1)}, \tag{E.0.2c}$$

$$\langle S^z_j S^z_{j+1} \rangle = \frac{1}{4} + \frac{\cot\gamma}{2\pi} I^{(0)} - \frac{1}{2\pi^2} I^{(1)}, \tag{E.0.2d}$$

where we have introduced the short-hand notations

$$I^{(0)} = \int_{-\infty}^{\infty} \frac{\sinh(1-\nu)t}{\cosh\nu t\, \sinh t}\, \mathrm{d}t, \tag{E.0.3a}$$

$$I^{(1)} = \int_{-\infty}^{\infty} t \frac{\cosh t}{\cosh^2\nu t\, \sinh t}\, \mathrm{d}t, \tag{E.0.3b}$$

$$I^{(2)} = \int_{-\infty}^{\infty} t^2 \frac{\sinh(1-\nu)t}{\cosh\nu t\, \sinh t}\, \mathrm{d}t, \tag{E.0.3c}$$

$$I^{(3)} = \int_{-\infty}^{\infty} t^3 \frac{\cosh t}{\cosh^2\nu t\, \sinh t}\, \mathrm{d}t, \tag{E.0.3d}$$

with $\gamma = \pi\nu$. By comparison with (3.2.4) and (6.5.13) we see that $I_0 = I^{(0)}/\pi$ and $I_1 = I^{(2)}/\pi^3$.

Using the expression (3.2.5) of the Temperley-Lieb generators in terms of Pauli matrices we now rewrite $\langle e_j e_{j+1}\rangle$ in terms of spin operators. We use $\sigma^a\sigma^b = \delta_{ab}\mathbf{1} + i\epsilon_{abc}\sigma^c$ to simplify the products, and by symmetry we may discard any resulting term that involves an odd number of any given spin operator. We obtain

$$\begin{aligned}
4\langle e_j e_{j+1}\rangle &= \Big\langle \Big(\sigma^x_j\sigma^x_{j+1} + \sigma^y_j\sigma^y_{j+1} + \cos\gamma\left(\sigma^z_j\sigma^z_{j+1} - \mathbf{1}\right) + i\sin\gamma\left(\sigma^z_j - \sigma^z_{j+1}\right)\Big) \\
&\qquad \Big(\sigma^x_{j+1}\sigma^x_{j+2} + \sigma^y_{j+1}\sigma^y_{j+2} + \cos\gamma\left(\sigma^z_{j+1}\sigma^z_{j+2} - \mathbf{1}\right) + i\sin\gamma\left(\sigma^z_{j+1} - \sigma^z_{j+2}\right)\Big)\Big\rangle \\
&= \langle\sigma^x_j\sigma^x_{j+2}\rangle + \langle\sigma^y_j\sigma^y_{j+2}\rangle + \cos^2\gamma\left(\langle\sigma^z_j\sigma^z_{j+2}\rangle + 1\right) \\
&\quad - \cos\gamma\left(\langle\sigma^x_j\sigma^x_{j+1}\rangle + \langle\sigma^x_{j+1}\sigma^x_{j+2}\rangle\right) - \cos\gamma\left(\langle\sigma^y_j\sigma^y_{j+1}\rangle + \langle\sigma^y_{j+1}\sigma^y_{j+2}\rangle\right) \\
&\quad - \cos^2\gamma\left(\langle\sigma^z_j\sigma^z_{j+1}\rangle + \langle\sigma^z_{j+1}\sigma^z_{j+2}\rangle\right) + \sin^2\gamma\left(\langle\sigma^z_j\sigma^z_{j+2}\rangle + 1\right) \\
&\quad - \sin^2\gamma\left(\langle\sigma^z_j\sigma^z_{j+1}\rangle + \langle\sigma^z_{j+1}\sigma^z_{j+2}\rangle\right).
\end{aligned} \tag{E.0.4}$$

Using translation invariance of the ground state and $U(1)$ symmetry we rewrite this as

$$\langle e_j e_{j+1}\rangle = 2\langle S^x_j S^x_{j+2}\rangle + \langle S^z_j S^z_{j+2}\rangle + \frac{1}{4} - 4\cos\gamma\langle S^x_j S^x_{j+1}\rangle - 2\langle S^z_j S^z_{j+1}\rangle. \tag{E.0.5}$$

Inserting the results from (E.0.2) we see immediately that the terms with $I^{(3)}$ cancel, as well as the terms involving no integrals at all, leaving

$$\begin{aligned}
\langle e_j e_{j+1}\rangle &= \left(-2\frac{1}{2\pi\sin 2\gamma} + \frac{\cot 2\gamma}{\pi} + 4\cos\gamma\frac{1}{4\pi\sin\gamma} - 2\frac{\cot\gamma}{2\pi}\right) I^{(0)} \\
&\quad + \left(2\frac{\cos 2\gamma}{4\pi^2} - \frac{1}{2\pi^2} - 4\cos\gamma\frac{\cos\gamma}{4\pi^2} + 2\frac{1}{2\pi^2}\right) I^{(1)} \\
&\quad + \left(-2\frac{3\cos 2\gamma\tan\gamma}{4\pi^3} + \frac{3\tan\gamma}{2\pi^3}\right) I^{(2)}.
\end{aligned} \tag{E.0.6}$$

By trigonometric identities we then see that the terms involving $I^{(1)}$ cancel as well, and that we finally obtain

$$\langle e_j e_{j+1}\rangle = \frac{\sin\gamma}{\pi\cos\gamma} I^{(0)} + \frac{3\sin^3\gamma}{\pi^3\cos\gamma} I^{(2)} = \frac{3\sin^3\gamma\, I_1 - \sin\gamma\, I_0}{\cos\gamma}, \tag{E.0.7}$$

proving (6.5.21).

E.1 The limit $\gamma \to 0$

In the limit $x \to \infty$, $\gamma \to 0$ we expect that the integrals in (6.5.21) can be expressed in terms of the polylogarithms $\mathrm{Li}_{2n+1}(-1)$, following the result for the XXX spin chain [130]

$$\langle S^z_j S^z_{j+1}\rangle = \frac{1}{12} - \frac{1}{3}\zeta_a(1), \tag{E.1.1a}$$

$$\langle S^z_j S^z_{j+2}\rangle = \frac{1}{12} - \frac{4}{3}\zeta_a(1) + \zeta_a(3), \tag{E.1.1b}$$

here written in terms of the alternating zeta function

$$\zeta_a(s) = \sum_{n>0}\frac{(-1)^{n-1}}{n^s} = -\mathrm{Li}_s(-1). \tag{E.1.2}$$

More precisely, as $\gamma \to 0$ (E.0.5) simplifies to

$$\langle e_j e_{j+1} \rangle = 3\langle S_j^z S_{j+2}^z \rangle + \frac{1}{4} - 6\langle S_j^z S_{j+1}^z \rangle \,, \tag{E.1.3}$$

such that by inserting (E.1.1) we expect that (6.5.21b) can be written as

$$\langle e_j e_{j+1} + e_{j+1} e_j \rangle = \frac{1}{2}\big(1 - 2 + 8\zeta_a(1) + 1 - 16\zeta_a(1) + 12\zeta_a(3)\big) = 6\zeta_a(3) - 4\zeta_a(1). \tag{E.1.4}$$

Comparing the rescaled integrals $\sin^{2n-1}\gamma\, I_n$ in the limit of $x \to \infty$ to the integral representation

$$-\operatorname{Li}_s(-1) = \frac{1}{\Gamma(s)} \int_0^\infty \frac{t^{s-1}}{e^t + 1}\, \mathrm{d}t \tag{E.1.5}$$

we find

$$\begin{aligned} \sin^{2n-1}\gamma\, I_n &= 2\frac{\sin^{n-1}(\gamma)}{\gamma^{n-1}} \int_0^\infty t^{2n} \frac{\sinh(xt)}{\sinh((x+1)t)\cosh(t)}\, \mathrm{d}t \\ &= 4\frac{\sin^{2n-1}(\gamma)}{\gamma^{2n-1}} \int_0^\infty \frac{t^{2n}}{e^{2t}+1} \left(\frac{1 - e^{-2xt}}{1 - e^{-2(x+1)t}}\, \mathrm{d}t \right) \\ &\xrightarrow[x\to\infty]{} \frac{4}{2^{2n+1}} \int_0^\infty \frac{t^{2n}}{e^t + 1}\, \mathrm{d}t = -\frac{4}{2^{2n+1}} \Gamma(2n+1) \mathrm{Li}_{2n+1}(-1)\,. \end{aligned} \tag{E.1.6}$$

In particular $\sin\gamma\, I_0 \to -2\mathrm{Li}_1(-1) = 2\zeta_\mathrm{a}(1)$ and $\sin^3\!\gamma\, I_1 \to -\mathrm{Li}_3(-1) = \zeta_\mathrm{a}(3)$, such that

$$\langle e_j e_{j+1} + e_{j+1} e_j \rangle = \frac{6\sin^3\!\gamma\, I_1 - 2\sin\gamma\, I_0}{\cos\gamma} \xrightarrow[\gamma\to 0]{} 6\zeta_a(3) - 4\zeta_a(1) \tag{E.1.7}$$

indeed.

APPENDIX

F

FURTHER NUMERICAL RESULTS FOR SECTION 6.5.2

Within this Appendix we collect figures providing further numerical evidence for the results (6.5.12) and (6.5.22) given in Section 6.5.2 regarding the limit of the commutator $[\mathscr{L}_{p+n} + \bar{\mathscr{L}}_{-p-n}, \mathscr{L}_{-p} - \bar{\mathscr{L}}_{p}]$. Throughout this Appendix we consider $x = \pi$, so that $\mathfrak{q}$ is not a root of unity. In Figures F.1 and F.2 we show results for $n = -2$, while in Figure F.3 we show results for $n = 0$ in the case where we do not project back on the original state, but rather on the first excited state corresponding to the same choices of lattice parameters. The figures indicate that the slope r obeys $r > 1$ for matrix elements of e_j, $e_j e_{j+1} + e_{j+1} e_j$ and $[e_j, [e_{j+1}, e_{j+2}]]$, while it obeys $r > 2$ for the remainder $\mathscr{R}$. We note that in some figures there are large finite size effects making it harder to discern the tendency of the curves, in particular those involving $[e_j, [e_{j+1}, e_{j+2}]]$ in which we have chosen to exclude the first data points entirely. These effects are larger for the states $|S_z = 1, e = 1\rangle$ and $|\not{p} = 1\rangle$, which have momenta $\not{p} \notin \{0, N/2\}$ making results involving these states more sensitive to finite size effects.

It is the case for all figures, including those in Section 6.5.2, that the estimated slope will vary slightly when data points for larger sizes are included. We note that if one follows and extrapolates the estimation of the slope as a function of the sizes used for the estimate, the bounds $r > 1$ and $r > 2$ are still expected to hold in the continuum limit, indicating that the finite size effects have not influenced the overall conclusions regarding convergence.

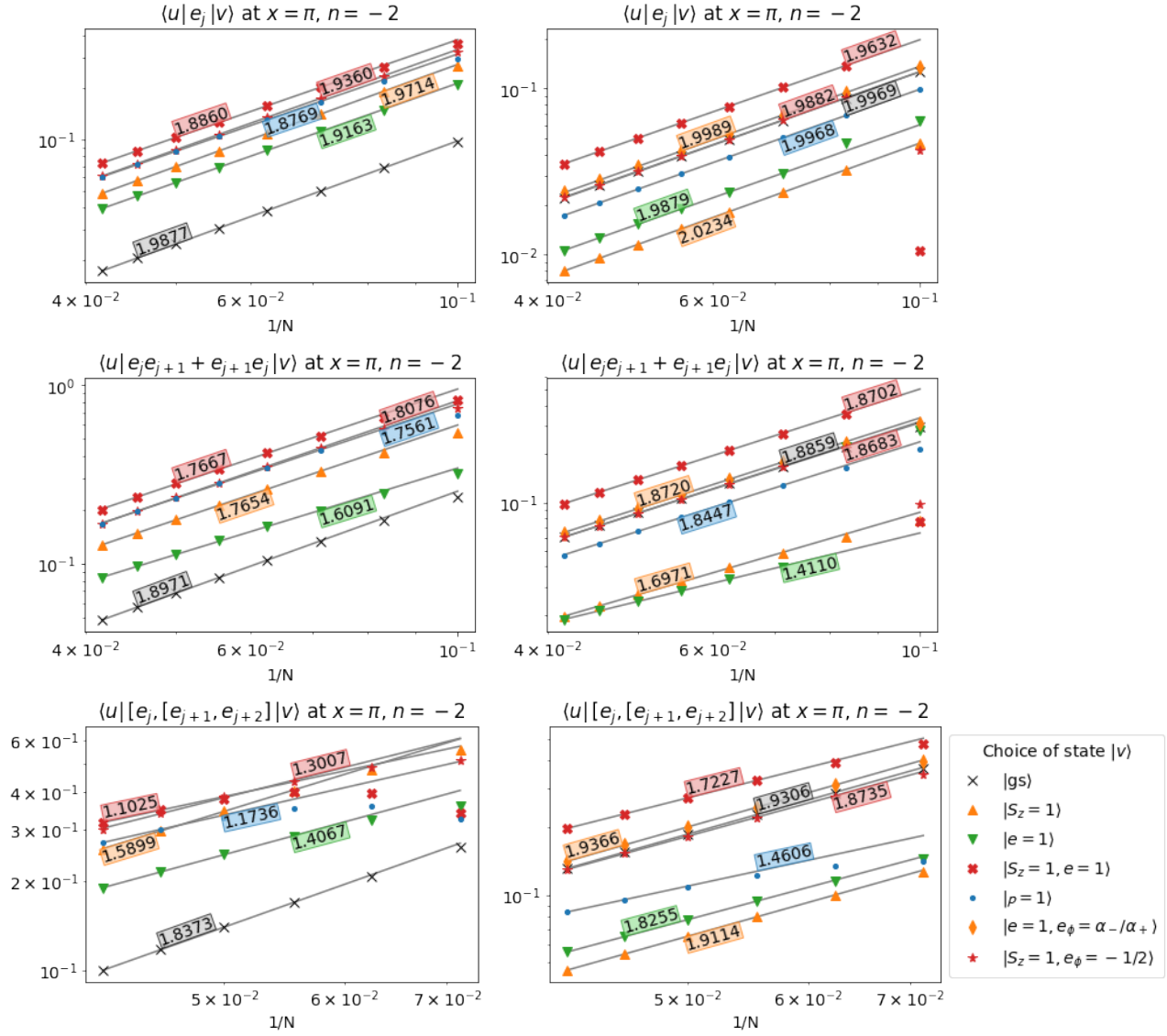

Figure F.1: Absolute value of matrix elements, plotted using the same conventions as in Figure 6.2 up to the choice of $|u\rangle$: For each state $|v\rangle$ the state $|u\rangle$ corresponds to the same choice of lattice parameters up to a change in momentum sector, $\mathcal{p} \to \mathcal{p} + 2$. To the left, the lowest energy state for each choice of lattice parameters is used for $|u\rangle$. To the right, the first excited energy state is used for $|u\rangle$ instead. In case of choices of $|v\rangle$ showing particularly strong finite size effects ($|S_z = 1, e = 1\rangle$ and $|\mathcal{p} = 1\rangle$ in the lower left plot, $|\mathcal{p} = 1\rangle$ in the lower right plot) the linear fit is performed using only the two leftmost points.

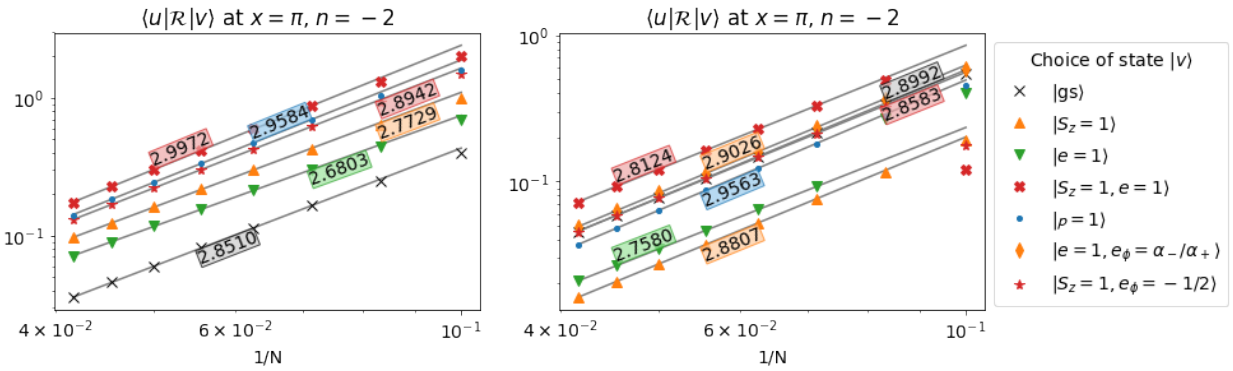

Figure F.2: Absolute value of matrix elements of $\mathscr{R}$ as defined in (6.5.11), plotted using the same conventions as in Figure 6.2 up to the choice of $|u\rangle$: For each state $|v\rangle$ the state $|u\rangle$ corresponds to the same choice of lattice parameters up to a change in momentum sector, $p \to p + 2$. To the left, the lowest energy state for each choice of lattice parameters is used for $|u\rangle$. To the right, the first excited energy state is used for $|u\rangle$ instead.

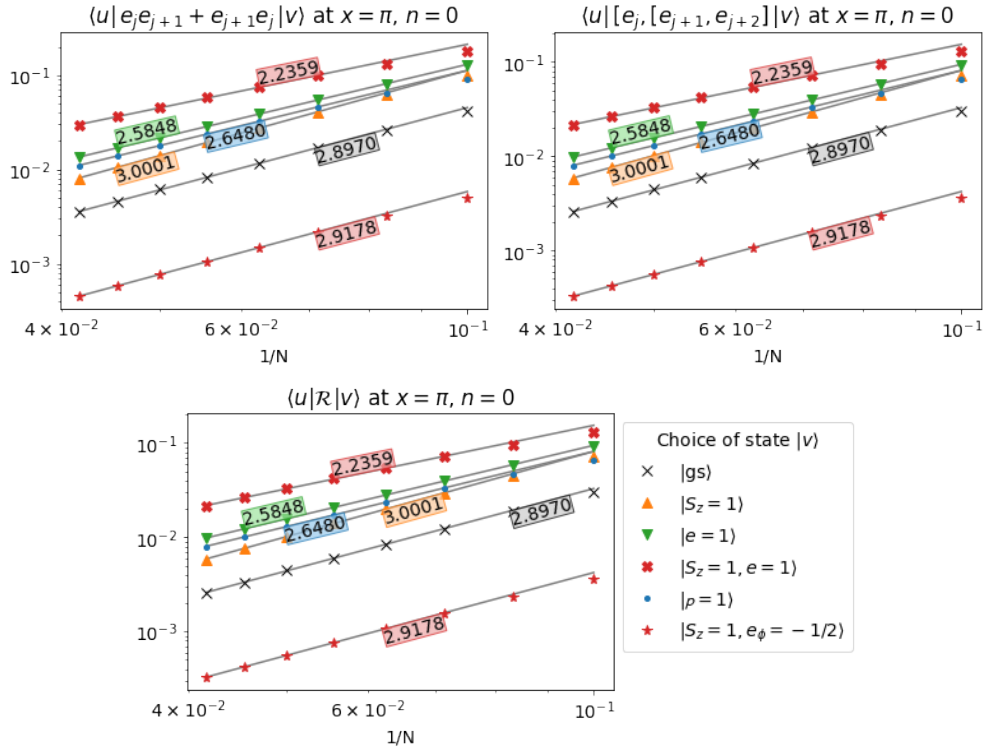

Figure F.3: Absolute value of matrix elements, plotted using the same conventions as in Figure 6.2 up to the choice of $|u\rangle$: For each state $|v\rangle$ the state $|u\rangle$ is taken to be the first excited energy state corresponding to the same choice of lattice parameters that were used for $|v\rangle$. (We recall that $|v\rangle$ is taken to be the lowest-energy state). In the lowest plot $\mathscr{R}$ is as defined in (6.5.11).

APPENDIX

G

THE CHIRAL-ANTICHIRAL COMMUTATOR

In [12] the limit of $[\mathscr{L}_{p+n} + \bar{\mathscr{L}}_{-p-n}, \mathscr{L}_{-p} + \bar{\mathscr{L}}_{p}]$ was checked, and was found to be correct. Meanwhile in Section 6.5 and Appendix F we found strong evidence for $[\mathscr{L}_{p+n} + \bar{\mathscr{L}}_{-p-n}, \mathscr{L}_{-p} - \bar{\mathscr{L}}_{p}]$ having the correct limit up to the central term. In order to isolate the chiral-antichiral commutator $[\mathscr{L}_{p+n}, \bar{\mathscr{L}}_{-p}]$ it remains to find the behaviour of $[\mathscr{L}_{p+n} - \bar{\mathscr{L}}_{-p-n}, \mathscr{L}_{-p} - \bar{\mathscr{L}}_{p}]$. We shall proceed in the same manner as in Section 6.5 and Appendix F. However, while we there showed figures for two different cases at $n = 0$, once case at $n = -1$ and two at $n = -2$, we shall here only reproduce the figures corresponding to one of the cases at $n = 0$ and the case at $n = -1$. This is partly to save space, and partly (for the $n = -2$ cases) due to increasingly disruptive finite size effects—as was already noted in Appendix F, such effects become generally more pronounced for products of several Temperley-Lieb generators.

Similarly to (6.5.4) we first expand the commutator under investigation. We obtain the expression

$$\begin{aligned}
&[\mathscr{L}_{p+n} - \bar{\mathscr{L}}_{-p-n}, \mathscr{L}_{-p} - \bar{\mathscr{L}}_{p}] \\
&\quad = -2i \left(\frac{N}{2\pi}\right)^2 \left(\frac{\gamma}{\pi \sin\gamma}\right)^4 \Bigg\{ \sin\left(\frac{4\pi p + 2\pi n}{N}\right) \sum_{j=1}^{N} e^{2i\pi n(j+3/2)/N} [[e_j, e_{j+1}], [e_{j+2}, e_{j+3}]] \\
&\quad + e^{-i\pi n/N} \sin\left(\frac{2\pi p + \pi n}{N}\right) \sum_{j=1}^{N} e^{2i\pi n(j+3/2)/N} \Big(- [e_j, e_{j+1}] - [e_{j+1}, e_{j+2}] \\
&\qquad\qquad + \sqrt{Q}(e_j e_{j+1} e_{j+2} - e_{j+2} e_{j+1} e_j) \Big) \Bigg\}.
\end{aligned} \tag{G.0.1}$$

Provided that the matrix elements of the combinations of Temperley-Lieb operators appearing above are of order $\mathcal{O}(1/N^r)$ with $r > 0$ for the first row and $r > 1$ for the second row, we

may restrict our attention to leading order terms the trigonometric functions as well as the exponential in the second row. To be concise, let us denote

$$\begin{aligned} r_1 &= [[e_j, e_{j+1}], [e_{j+2}, e_{j+3}]] \\ r_2 &= -[e_j, e_{j+1}] - [e_{j+1}, e_{j+2}] + \sqrt{Q}(e_j e_{j+1} e_{j+2} - e_{j+2} e_{j+1} e_j). \end{aligned} \tag{G.0.2}$$

We plot the matrix elements of r_1 and r_2 for $n = 0, -1$ in Figures G.1,G.2.We find that $r > 1$ in both cases. With this in mind we keep only leading terms in the expansion:

$$\begin{aligned} [\mathscr{L}_{p+n} - \bar{\mathscr{L}}_{-p-n}, \mathscr{L}_{-p} - \bar{\mathscr{L}}_p] = (2p+n)(-i)\frac{N}{2\pi}\left(\frac{\gamma}{\pi \sin\gamma}\right)^4 \sum_{j=1}^{N} e^{2i\pi n(j+3/2)/N}(2r_1 + r_2) \\ + \mathscr{O}\left(\frac{1}{N^{r-1}}\right). \end{aligned} \tag{G.0.3}$$

We now compare (G.0.3) to what is denoted $\hat{h}^{(4)}$ in [12], using this time the result KS (2.59)[1]

$$\begin{aligned} -i\,\frac{N}{2\pi}\left(\frac{\gamma}{\pi \sin\gamma}\right)^4 \sum_{j=1}^{N} e^{2i\pi n(j+3/2)/N} 6\,[[e_j, e_{j+1}], [e_{j+2}, e_{j+3}]] \\ + 6\sqrt{Q}[e_j(e_{j+1}e_{j+2} + e_{j+2}e_{j+1})] + (Q+2)[e_j, e_{j+1}] \mapsto \left(L_n - \bar{L}_{-n}\right). \end{aligned} \tag{G.0.4}$$

We note that as is the case for $\mathscr{P}$ in (3.7.1), also denoted by $\hat{h}^{(2)}$ in [12], the ground state expectation value of $\hat{h}^{(4)}$ is zero. For this reason we do not need to introduce normal ordering in (G.0.4). It turns out that the ground state expectation values of r_1, r_2 are also zero, as are some other matrix elements that are for this reason excluded from the figures below.

As before we define a remainder, here given by the difference between the summand in (G.0.3) and (G.0.4):

$$\begin{aligned} \mathscr{R}^{(4)} = -4\,[[e_j, e_{j+1}], [e_{j+2}, e_{j+3}]] - 6\sqrt{Q}[e_j(e_{j+1}e_{j+2} + e_{j+2}e_{j+1})] - (Q+2)[e_j, e_{j+1}] \\ - [e_j, e_{j+1}] - [e_{j+1}, e_{j+2}] + \sqrt{Q}(e_j e_{j+1} e_{j+2} - e_{j+2} e_{j+1} e_j). \end{aligned} \tag{G.0.5}$$

For the limit of (G.0.1) to be correct we need the remainder to decay as $\mathscr{O}(1/N^r)$ with $r > 2$. We see in Figures G.1,G.2 that the numerical results support this. Together with the previous results for $[\mathscr{L}_{p+n} + \bar{\mathscr{L}}_{-p-n}, \mathscr{L}_{-p} + \bar{\mathscr{L}}_p]$ and $[\mathscr{L}_{p+n} + \bar{\mathscr{L}}_{-p-n}, \mathscr{L}_{-p} - \bar{\mathscr{L}}_p]$ we can conclude that the numerical results strongly indicate that $[\mathscr{L}_{p+n}, \bar{\mathscr{L}}_{-p}] \mapsto 0$. Again we show the figures only for $n = 0, -1$ in the interest of saving space, but we note that at $n = -2$ the finite size effects are significantly smaller for $\mathscr{R}^{(4)}$ than they are for r_1 and r_2, and the numerical results for $\mathscr{R}^{(4)}$ show a clear $r > 2$ slope for $n = -2$ already at the sizes we can access.

[1] Generalized to $n \neq 0$ in the same way as in KS (3.33).

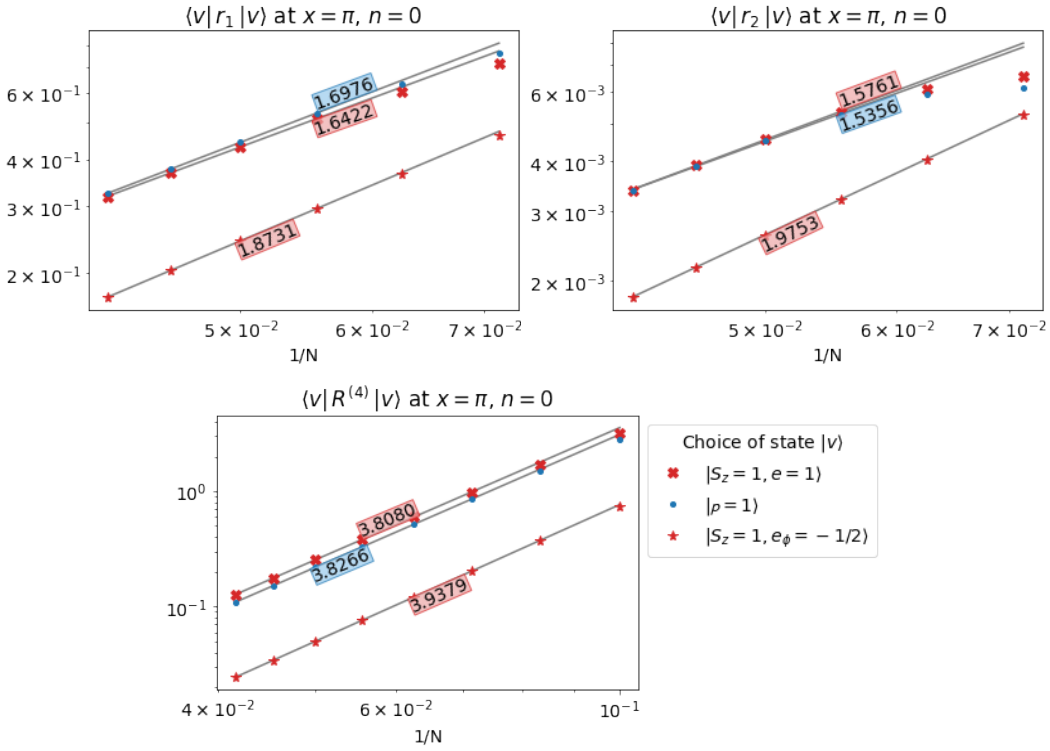

Figure G.1: Absolute value of matrix elements, plotted using the same conventions as in Figure 6.2 but with the choice of $|u\rangle = |v\rangle$.

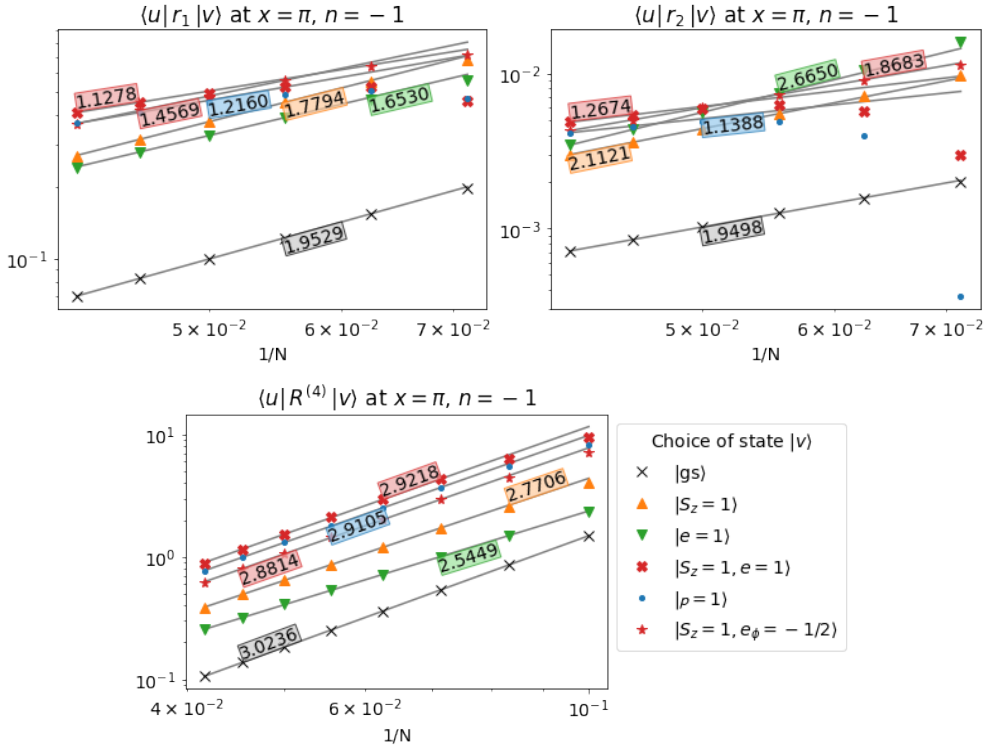

Figure G.2: Absolute value of matrix elements, plotted using the same conventions as in Figure 6.2. In case of choices of $|v\rangle$ showing particularly strong finite size effects ($|S_z = 1, e = 1\rangle$ and $|\not{p} = 1\rangle$ in upper two plots) the linear fit is performed using only the two leftmost points.

APPENDIX

H

NUMERICS FOR THE KOO–SALEUR GENERATORS IN POTTS AND LOOP MODELS

Within this appendix we provide partial evidence for the main results of Chapter 7, given in equations (7.4.3), (7.4.12) and (7.4.11), by acting directly with the Koo–Saleur generators (3.7.3) on eigenstates of the lattice Hamiltonian (3.2.2). As in the XXZ spin chain of Chapter 6, in these numerical studies we shall split our state space at each system size N into eigenspaces of the translation operator, with eigenvalues $\{e^{2\pi i p/N} | 0 \leq p \leq N-1\}$. As the Hamiltonian is manifestly invariant under translation we may diagonalize it independently within each such sector. Recall that the Koo–Saleur generators exactly reproduce the fact that the action of $\mathscr{L}_n[N]$ (resp. $\bar{\mathscr{L}}_n[N]$) on a state of momentum p produces a state of momentum $p-n$ (resp. $p+n$), at finite size. For a state of eigenvalue ϵ of the Hamiltonian at a given system size N, we consider lattice precursors to its conformal weights,[1] which we also denote $(h, \bar{h})$, defined as the solutions to

$$\begin{aligned} \epsilon &= \frac{2\pi}{N}\left(h + \bar{h} - \frac{c}{12}\right), \\ p &= h - \bar{h}. \end{aligned} \tag{H.0.1}$$

By "following" a state (say, the lowest-energy state within a given sector of lattice momentum) as N increases, and extrapolating the values of $h, \bar{h}$, we can identify the conformal weights in the continuum limit.To make the notation lighter, we shall in this appendix exclude the explicit dependence on system size, and write $\mathscr{L}_n, \mathscr{A}_{r,s}$ rather than $\mathscr{L}_n[N], \mathscr{A}_{r,s}[N]$ for Koo–Saleur generators and the combinations thereof. For the fields $\Phi_{r,s}$ the context will indicate

[1] Sometimes called "effective conformal weights." We will omit the qualifiers and simply refer to "conformal weights" when the context makes it clear that the term is being applied to lattice quantities. Similarly, we will frequently assign conformal weights $h_{r,s}$ given by the Kac formula to finite-size states—by this we mean that following a state for increasing N leads to an extrapolation $h = h_{r,s}$.

whether we are discussing the field in the continuum limit or the corresponding link state at finite size, since at finite size (resp. in the continuum limit) $\Phi_{r,s}$ is acted upon by calligraphic operators $\mathscr{L}_n$ and $\mathscr{A}_{r,s}$ (resp. Roman operators L_n and $A_{r,s}$). We will in practice only be able to access low values of r, s on the lattice, since larger system sizes are needed to accommodate a larger lattice momentum (which governs r) and a larger number of through-lines (which governs s).

Before discussing details of the numerics we must eliminate an ambiguity that may arise in the results due to phase degrees of freedom. In the following sections we will discuss quantities of the form $\|Z - Z'\|_2$,[2] where Z and Z' are (descendants of) eigenstates of the Hamiltonian (e.g. $Z = \mathscr{L}_{-1}\Phi_{1,1}$ and $Z' = \bar{\mathscr{L}}_{-1}\bar{\Phi}_{1,1}$). In quantum mechanics the overall phase of a vector or wave function has no observable consequences and $\mathrm{e}^{i\alpha}Z$ for any real α would serve just as well in computations of observables. Typically one chooses the phase of a state such that its components in some basis are entirely real, where possible. In the situation at hand, the eigenvectors of the Hamiltonian are generically complex[3] and there is no canonical way to fix the relative phase between eigenvectors. The measurement of $\|Z - \mathrm{e}^{i\alpha}Z'\|_2$ thus takes on a continuum of values. Where this ambiguity occurs, we fix the relative phase by choosing the value of α that minimizes this quantity:

$$\|Z - Z'\|_{\underline{2}} \equiv \inf_{\alpha} \|Z - \mathrm{e}^{i\alpha}Z'\|_2. \tag{H.0.2}$$

This optimization is succinctly denoted by the underlined 2 in the notation $\|Z - Z'\|_{\underline{2}}$.

Our main goal shall be to establish certain identities by observing whether deviations from these identities at finite size decay to zero. Let us give two examples. In order to provide evidence for (7.4.3) in the sector of $j = 0$ we wish to see if $\mathscr{L}_{-1}\mathbf{1} \to 0$ as $N \to \infty$, with $\mathbf{1} = |h_{1,1}, h_{1,1}\rangle$ being the identity state. Meanwhile, to provide evidence for (7.4.12) we would like to establish that $\mathscr{L}_{-1}\Phi_{1,1} \to \bar{\mathscr{L}}_{-1}\bar{\Phi}_{1,1}$, or equivalently that $\mathscr{L}_{-1}\Phi_{1,1} - \bar{\mathscr{L}}_{-1}\bar{\Phi}_{1,1} \to 0$ as $N \to \infty$. Using the positive-definite scalar product to define a norm $\|V\|_2^2 = \langle V|V\rangle$ we equivalently examine whether $\|\mathscr{L}_{-1}\mathbf{1}\|_2 \to 0$ and $\|\mathscr{L}_{-1}\Phi_{1,1} - \bar{\mathscr{L}}_{-1}\bar{\Phi}_{1,1}\|_{\underline{2}} \to 0$ as $N \to \infty$.

As shall be seen in the tables below, this simple measurement is insufficient for our purposes. Indeed, as N increases the values observed actually grow in magnitude in most cases. As discussed in Chapter 6, an interpretation of this observation is the fact that, since the finite-size Koo–Saleur generators do not yet furnish a representation of the Virasoro algebra, the action of $\bar{\mathscr{L}}_{-1}$ on $\Phi_{1,1}$, for instance, produces a state with nonzero components even in highly excited eigenstates of the Hamiltonian. While each such component would tend to zero on its own, the number of these so-called "parasitic couplings" grows rapidly, yielding a nonzero contribution in total.

To avoid the issue of this rapid growth, we choose to project on the d lowest-energy states within the relevant sector of lattice momentum, keeping d fixed as $N \to \infty$. This will be the subject of the following section.

H.1 Projectors $\Pi^{(d)}$ and scaling-weak convergence

For the following discussion we shall consider a concrete example, namely the fields $L_{-1}\Phi_{1,1}$ and $\bar{L}_{-1}\bar{\Phi}_{1,1}$ in the loop model. In the continuum limit, these fields have conformal weights $(1, 1)$. Their lattice analogues $\mathscr{L}_{-1}\Phi_{1,1}$ and $\bar{\mathscr{L}}_{-1}\bar{\Phi}_{1,1}$ both belong to the sector of lattice momentum

[2]The subscript 2 refers to the Euclidean norm or 2-norm.

[3]By this, we mean that no choice of phase can make all of the components real.

$\not{p} = N/2$. By following the energies ϵ of states within this sector for increasing lattice sizes N, we find that the two lowest-energy states will correspond to these conformal weights.

Let us write schematically

$$\mathscr{L}_{-1}\Phi_{1,1} = u + v, \tag{H.1.1}$$

where u is a linear combination of these two lowest states and v represents all other states in the sector of $\not{p} = N/2$. In order to exclude the consequences of the "parasitic couplings" described above, we wish to build a projection operator Π such that $\Pi\mathscr{L}_{-1}\Phi_{1,1} = u$.

In the basis of link states, and with respect to the scalar product $\langle\cdot|\cdot\rangle$ where distinct link states are declared to be orthogonal, the Hamiltonian is not Hermitian. We must therefore distinguish between left and right eigenstates: the usual right eigenstates $|i,R\rangle$ are determined by the familiar $\mathscr{H}\,|i,R\rangle = \epsilon_i\,|i,R\rangle$ and the left eigenstates $\langle i,L|$ are determined via $\mathscr{H}^\dagger\,|i,L\rangle = \epsilon_i\,|i,L\rangle \iff \langle i,L|\,\mathscr{H} = \epsilon_i\,\langle i,L|$. The projectors $|i\rangle\langle i|$ of Hermitian quantum mechanics are replaced by

$$\Pi_i = \frac{|i,R\rangle\langle i,L|}{\langle i,L|i,R\rangle} \tag{H.1.2}$$

which satisfy the expected properties of projectors, orthogonality and idempotency: $\Pi_i\Pi_j = \delta_{ij}\Pi_i$. For our purposes, Π_i picks out the ith component of a vector expressed in the basis of right eigenvectors:

$$\Pi_i \sum_j c_j\,|j,R\rangle = c_i\,|i,R\rangle\,. \tag{H.1.3}$$

Thus, letting $\Pi_{1,2}$ denote the projectors to the two lowest states of the $\not{p} = N/2$ sector, the projector $\Pi^{(2)} = \Pi_1 + \Pi_2$ accomplishes the desired goal of $\Pi^{(2)}\mathscr{L}_{-1}\Phi_{1,1} = u$. Since $\bar{L}_{-1}\bar{\Phi}_{1,1}$ has conformal weights $(1,1)$ as well, the projector $\Pi^{(2)}$ also truncates the lattice quantity $\bar{\mathscr{L}}_{-1}\bar{\Phi}_{1,1}$ to the same two states.

As discussed above it is not necessary to restrict to only the components in u (given by the projection to the lowest two states in the example at hand)—one could also include higher energy states. As long as the rank of the projection operator is kept fixed, we expect the influence of such parasitic couplings to vanish as $N \to \infty$. We call convergence of values in the context of this procedure "scaling-weak convergence." To illustrate this type of convergence, we will apply projectors of different rank d to $\mathscr{L}_{-1}\Phi_{1,1} - \bar{\mathscr{L}}_{-1}\bar{\Phi}_{1,1}$. We expect that for any fixed projector rank d independent of N, so long as $\Pi^{(d)}$ is composed of the lowest d states,[4]

$$\lim_{N\to\infty} \|\Pi^{(d)}(\mathscr{L}_{-1}\Phi_{1,1} - \bar{\mathscr{L}}_{-1}\bar{\Phi}_{1,1})\|_{\underline{2}} = 0\,, \quad \forall d \in \mathbb{N}\,; \tag{H.1.4}$$

i.e., scaling-weak convergence of the lattice values towards the identity $L_{-1}\Phi_{1,1} = \bar{L}_{-1}\bar{\Phi}_{1,1}$.

The notion of scaling-weak convergence is defined and discussed in greater detail in Chapter 6, where it is shown that a crucial difference compared to weak convergence is that limits of products of Koo–Saleur generators are in certain cases different than products of limits of Koo–Saleur generators, necessitating the insertion of projectors. This difference is found to affect the products with dual operators that are induced by the positive-definite inner product, as in $\|\mathscr{L}_{-1}\Phi_{1,1}\|_2 = \langle\Phi_{1,1}|\mathscr{L}_{-1}^\dagger\mathscr{L}_{-1}\Phi_{1,1}\rangle$, but not the product $\mathscr{L}_{-1}^2$ inside the operator $\mathscr{A}_{1,2}$ used below.

In general, for any of the fields Z relevant below, we say that its lattice analogue $\mathscr{Z}$ scaling-weakly converges to zero if

$$\lim_{N\to\infty} \|\Pi^{(d)}\mathscr{Z}[N]\| = 0\,, \quad \forall d \in \mathbb{N}\,, \tag{H.1.5}$$

[4]In fact, it is not strictly necessary to take the lowest d states, but it suffices to take d states with fixed conformal weights, so long as all of the lower states are eventually included as $d \to \infty$. In practice, however, convergence happens the most quickly at the lowest states.

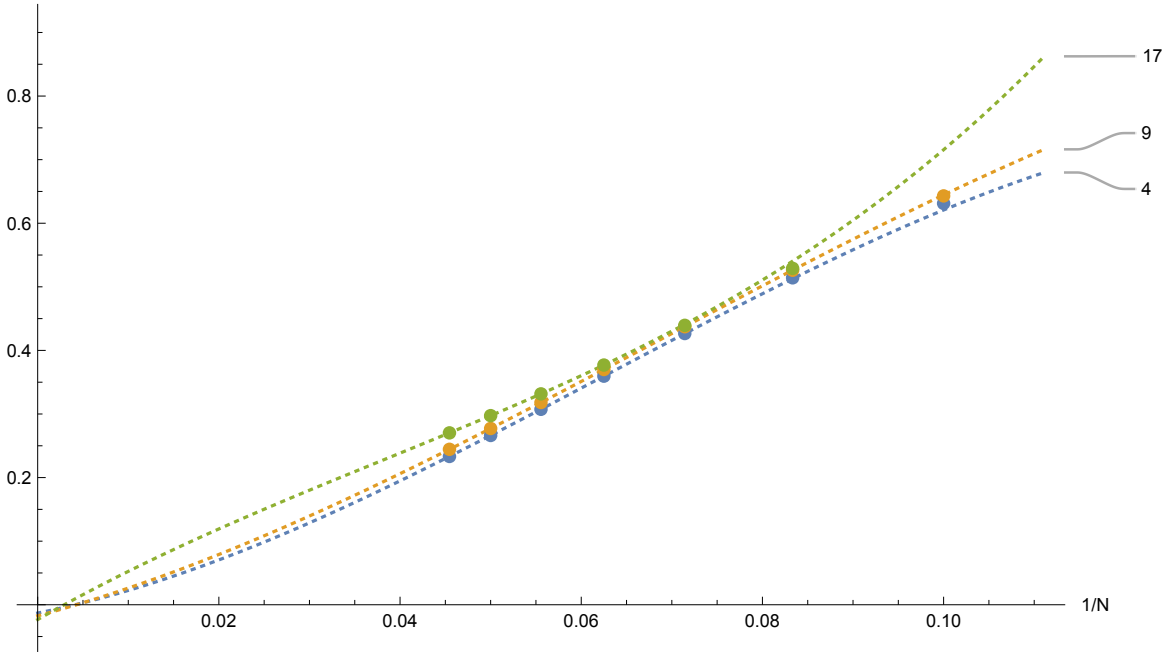

Figure H.1: Comparison of lattice results using projectors of different rank, illustrating the concept of scaling-weak convergence (H.1.4) at $j = 2$. The horizontal axis is $1/N$. The vertical axis is $\|\Pi^{(d)}(\mathscr{A}_{1,2}\Phi_{1,2} - \bar{\mathscr{A}}_{1,2}\bar{\Phi}_{1,2})\|_2 / \|\Pi^{(d)}\mathscr{A}_{1,2}\Phi_{1,2}\|_2$. The tags on the graphs indicate the rank d of the projector $\Pi^{(d)}$. The dotted lines are third-order polynomial fits (in $1/N$) to the last four data points.

with $\|\cdot\|$ some positive-definite norm. The meaning of $\Pi^{(d)}$ is context-dependent, but should be built in such a way that $\lim_{d\to\infty}\Pi^{(d)}$ effectively functions as the identity operator:[5]

$$\lim_{d\to\infty}\Pi^{(d)}\mathscr{Z}[N] = \mathscr{Z}[N]\,. \tag{H.1.6}$$

An analogous discussion applies to the demonstration of the identity $A_{1,2}\Phi_{1,2} = \bar{A}_{1,2}\bar{\Phi}_{1,2}$, mutatis mutandis. We present numerical evidence that $\mathscr{A}_{1,2}\Phi_{1,2} - \bar{\mathscr{A}}_{1,2}\bar{\Phi}_{1,2}$ scaling-weakly converges to zero.

We show in Figures H.1,H.2 that when applying projectors of different rank d, the numerical results extrapolate to almost the same value. We expect that the difference in the extrapolated values can be made arbitrarily small by including data points for large enough system sizes.

H.2 Numerical results for $\overline{\mathscr{W}}_{0,\mathfrak{q}^{\pm 2}}$

Within the module $\mathscr{W}_{0,\mathfrak{q}^{\pm 2}}$, the link states corresponding to primary fields with degenerate conformal weights are never annihilated by the $A_{n,1}$ or $\bar{A}_{n,1}$ combinations of Virasoro generators. However, the module of interest for the study of the loop model is rather the quotient module

[5] "Effectively," since $\lim_{d\to\infty}\Pi^{(d)}$ does not necessarily have to equal the identity operator. For instance, in the discussion of scaling-weak convergence of $\mathscr{L}_{-1}\Phi_{1,1} - \bar{\mathscr{L}}_{-1}\bar{\Phi}_{1,1}$ to zero, $\Pi^{(d)}$ is built from the lowest d states of lattice momentum $p = N/2$. Thus $\lim_{d\to\infty}\Pi^{(d)}$ is the identity operator in the subspace of momentum $N/2$ and zero elsewhere. However, $\mathscr{L}_{-1}\Phi_{1,1} - \bar{\mathscr{L}}_{-1}\bar{\Phi}_{1,1}$ is zero in all momentum sectors save for $p = N/2$. Thus $\lim_{d\to\infty}\Pi^{(d)}$ effectively functions as the identity in this measurement. It is also possible to construct $\Pi^{(d)}$ using the d lowest states of the entire Hamiltonian, regardless of momentum. This does not affect the limit (H.1.6), but merely the rate of convergence. In this case $\lim_{d\to\infty}\Pi^{(d)}$ becomes the identity operator.

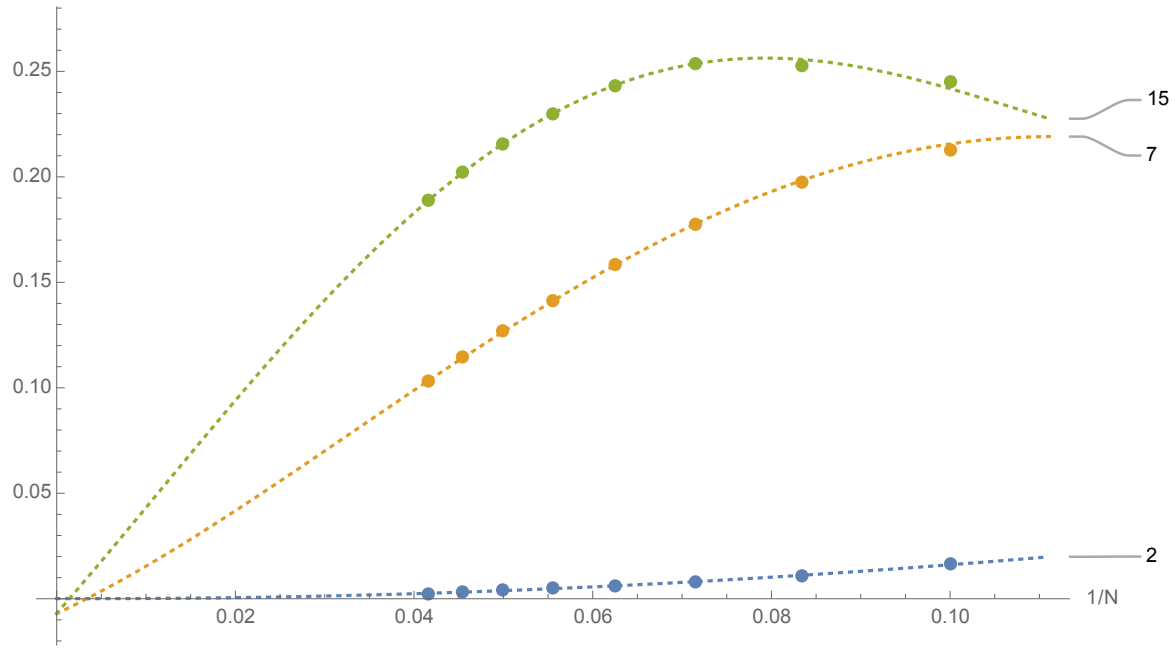

Figure H.2: Comparison of lattice results using projectors of different rank, illustrating the concept of scaling-weak convergence (H.1.4) at $j = 1$. The horizontal axis is $1/N$. The vertical axis is $\|\Pi^{(d)}(\mathscr{L}_{-1}\Phi_{1,1} - \bar{\mathscr{L}}_{-1}\bar{\Phi}_{1,1})\|_2 / \|\Pi^{(d)}\mathscr{L}_{-1}\Phi_{1,1}\|_2$. The tags on the graphs indicate the rank d of the projector $\Pi^{(d)}$. The dotted lines are fourth-order polynomial fits (in $1/N$) to the last five data points.

$\overline{\mathscr{W}}_{0,\mathfrak{q}^{\pm 2}}$. In this module we consider in particular the lowest-energy link state of lattice momentum $\not{p} = 0$, which in the continuum limit will correspond to the identity state $\mathbf{1}$ with conformal weights $(h, \bar{h}) = (0, 0)$. We act on this state with the Koo–Saleur generator $\mathscr{L}_{-1}$. The norm of the resulting state $\mathscr{L}_{-1}\mathbf{1}$ defined through the positive-definite scalar product is shown in Table H.1. (The norm of $\bar{\mathscr{L}}_{-1}\mathbf{1}$ yields the same values by symmetry.)

Within this module there is no state to project on that we expect to give a nonzero contribution in the limit $N \to \infty$, the only state with the proper conformal weights having been excluded by the quotient. Projecting on the lowest-energy state still remaining in the sector of the appropriate lattice momentum we therefore expect the result to approach zero at $N \to \infty$ (Table H.2).[6]

N	$x = \frac{\pi}{3}$	$\frac{\pi}{2}$	$\frac{\pi}{\sec^{-1}(2\sqrt{2})} - 1$	e	π
8	0.00105459	0.0134764	0.0140696	0.0319876	0.0360179
10	0.00151863	0.0183461	0.0191326	0.0430288	0.0484952
12	0.0018035	0.0212243	0.0221219	0.0495035	0.0558428
14	0.00200139	0.0231978	0.0241704	0.053899	0.0608373
16	0.00215397	0.0247167	0.0257464	0.0572352	0.0646218
18	0.00228117	0.0259884	0.0270657	0.0599884	0.0677341
20	0.00239306	0.0271153	0.0282345	0.0623992	0.0704482
22	0.00249505	0.0281508	0.0293087	0.0645961	0.0729122
24	0.00259016	0.0291244	0.0303188	0.0666511	0.0752099

Table H.1: The value of $\|\mathscr{L}_{-1}\mathbf{1}\|_2$ for a given length N and parameter x. $\mathbf{1}$ is the field in the $j = 0$ sector with conformal weights $(h_{1,1}, h_{1,1}) = (0, 0)$.

[6] In these tables, the peculiar value $x = \pi/\sec^{-1}(2\sqrt{2}) - 1$ corresponds to $Q = 1/2$, which is further studied in Appendix B of [17].

N	$x=\frac{\pi}{3}$	$\frac{\pi}{2}$	$\frac{\pi}{\sec^{-1}(2\sqrt{2})}-1$	e	π
8	0.00105459	0.0134764	0.0140696	0.0319876	0.0360179
10	0.00154453	0.0201482	0.0209567	0.0434477	0.0485887
12	0.00140952	0.0207429	0.0216739	0.0447805	0.0501347
14	0.00121929	0.0192739	0.0202699	0.0427614	0.0480059
16	0.00103467	0.0170396	0.0180351	0.0394988	0.044548
18	0.000875168	0.0147437	0.0156912	0.0359407	0.0407787
20	0.000742847	0.0126649	0.0135396	0.0325055	0.0371365
22	0.00063449	0.0108785	0.0116714	0.0293585	0.0337921
24	0.000545883	0.0093767	0.0100887	0.0265463	0.0307936
p_4	0.0000850643	0.00442133	0.00495163	0.000157526	−0.000258504

Table H.2: $\|\Pi^{(1)}\mathscr{L}_{-1}\mathbf{1}\|_2$ with the same conventions as in Table H.1. $\Pi^{(1)}$ is a projection to the state of lowest energy within the $j=0$, $\not{p}=1$ sector. This is the state within this sector that has conformal weights $(h_{1,-1},h_{1,1})=(1,0)$. The extrapolation p_4 is obtained by fitting the last five data points to a curve of the form $c_0+c_1/N+c_2/N^2+c_3/N^3+c_4/N^4$.

H.3 Numerical results for $\mathscr{W}_{j,1}$

In this section we numerically illustrate the equations $A_{1,2}\Phi_{1,2}=\bar{A}_{1,2}\bar{\Phi}_{1,2}$ and $L_{-1}\Phi_{1,1}=\bar{L}_{-1}\bar{\Phi}_{1,1}$ from Section 7.4.2. The general strategy is discussed above.

At $j=2$ we find $\Phi_{1,2},\bar{\Phi}_{1,2}$ in the sectors of $\not{p}=N/2-2$ and $\not{p}=N/2+2$, respectively. Thus, the descendant states $\mathscr{A}_{1,2}\Phi_{1,2}$ and $\bar{\mathscr{A}}_{1,2}\bar{\Phi}_{1,2}$ both belong to the sector of $\not{p}=N/2$. We show first in Table H.3 the norm $\|\mathscr{A}_{1,2}\Phi_{1,2}\|_2$ (which by symmetry equals $\|\bar{\mathscr{A}}_{1,2}\bar{\Phi}_{1,2}\|_2$). The ratio[7] $\|\mathscr{A}_{1,2}\Phi_{1,2}-\bar{\mathscr{A}}_{1,2}\bar{\Phi}_{1,2}\|_{\underline{2}}/\|\mathscr{A}_{1,2}\Phi_{1,2}\|_2$ is shown in Table H.4. We then repeat the same measurements using the projector $\Pi^{(4)}$ onto the four lowest-energy states in the sector of $\not{p}=N/2$, which we have identified as containing all fields up to conformal weights $(h_{1,2}+2,h_{1,-2})=(h_{1,-2},h_{1,-2})$. The results are shown in Table H.5 for $\|\Pi^{(4)}\mathscr{A}_{1,2}\Phi_{1,2}\|_2$ and in Table H.6 for the ratio $\|\Pi^{(4)}(\mathscr{A}_{1,2}\Phi_{1,2}-\bar{\mathscr{A}}_{1,2}\bar{\Phi}_{1,2})\|_{\underline{2}}/\|\Pi^{(4)}\mathscr{A}_{1,2}\Phi_{1,2}\|_2$.

Similarly, at $j=1$ we find $\Phi_{1,1},\bar{\Phi}_{1,1}$ in the sectors of $\not{p}=N/2-1$, $\not{p}=N/2+1$, and the descendants in the sector of $\not{p}=N/2$. The norm $\|\mathscr{L}_{-1}\Phi_{1,1}\|_2=\|\bar{\mathscr{L}}_{-1}\bar{\Phi}_{1,1}\|_2$ is given in Table H.7, and the ratio $\|\mathscr{L}_{-1}\Phi_{1,1}-\bar{\mathscr{L}}_{-1}\bar{\Phi}_{1,1}\|_{\underline{2}}/\|\mathscr{L}_{-1}\Phi_{1,1}\|_2$ is given in Table H.8. The same measurements are repeated with the projector $\Pi^{(2)}$ onto the two lowest-energy states in the sector of $\not{p}=N/2$, which we have identified as containing all fields up to conformal weights $(h_{1,1}+1,h_{1,-1})=(h_{1,-1},h_{1,-1})=(1,1)$. These results are shown in Table H.9 and Table H.10.

Both at $j=2$ (Table H.6) and $j=1$ (Table H.10) we find that the results support the equations $A_{1,2}\Phi_{1,2}=\bar{A}_{1,2}\bar{\Phi}_{1,2}$ and $L_{-1}\Phi_{1,1}=\bar{L}_{-1}\bar{\Phi}_{1,1}$ from Section 7.4.2 when we use projectors $\Pi^{(d)}$, with $d=4$ and $d=2$, respectively. Here we have used the lowest rank such that the states with the relevant conformal weights are included among the states we project on. As discussed earlier and illustrated in Figures H.1,H.2 we expect that the result in the limit $N\to\infty$ will remain the same for higher rank projectors. However, we do not expect the result to remain the same when no projector is applied. Indeed, the values in Tables H.4,H.8 do not tend to zero as N increases. The numerical proximity of $\|\mathscr{A}_{1,2}\Phi_{1,2}\|_2$ to $\|\Pi^{(4)}\mathscr{A}_{1,2}\Phi_{1,2}\|_2$ and of $\|\mathscr{L}_{-1}\Phi_{1,1}\|_2$ to $\|\Pi^{(2)}\mathscr{L}_{-1}\Phi_{1,1}\|_2$ strongly indicates that the lack of convergence can be attributed to parasitic

[7]While we numerically do observe scaling-weak convergence of $\mathscr{A}_{1,2}\Phi_{1,2}-\bar{\mathscr{A}}_{1,2}\bar{\Phi}_{1,2}$ to zero in the sense of definition (H.1.5), here we report the values of $\|\mathscr{A}_{1,2}\Phi_{1,2}-\bar{\mathscr{A}}_{1,2}\bar{\Phi}_{1,2}\|_{\underline{2}}/\|\mathscr{A}_{1,2}\Phi_{1,2}\|_2$ and $\|\Pi^{(4)}(\mathscr{A}_{1,2}\Phi_{1,2}-\bar{\mathscr{A}}_{1,2}\bar{\Phi}_{1,2})\|_{\underline{2}}/\|\Pi^{(4)}\mathscr{A}_{1,2}\Phi_{1,2}\|_2$ to give a measure of relative deviation from zero. The decay of the latter quantity to zero implies the scaling-weak convergence of $\mathscr{A}_{1,2}\Phi_{1,2}-\bar{\mathscr{A}}_{1,2}\bar{\Phi}_{1,2}$ so long as the norm $\|\Pi^{(4)}\mathscr{A}_{1,2}\Phi_{1,2}\|_2$ does not grow too quickly. That this is the case can be seen in Table H.5.

couplings to higher states, however small these couplings may be.

N	$x=\frac{\pi}{3}$	$\frac{\pi}{2}$	$\frac{\pi}{\sec^{-1}(2\sqrt{2})}-1$	e	π
10	0.724502	0.855299	0.859681	0.965547	0.985531
12	0.76937	0.879924	0.883733	0.977938	0.996234
14	0.794399	0.89486	0.898393	0.987034	1.00452
16	0.808303	0.903779	0.907193	0.993487	1.01062
18	0.81569	0.908984	0.912369	0.99819	1.01523
20	0.819132	0.91201	0.915425	1.00203	1.01916
22	0.820131	0.913885	0.917377	1.00577	1.02311

Table H.3: The value of $\|\mathscr{A}_{1,2}\Phi_{1,2}\|_2$ for a given length N and parameter x. $\Phi_{1,2}$ is the field in the $j=2$ sector with conformal weights $(h_{1,2},h_{1,-2})$.

N	$x=\frac{\pi}{3}$	$\frac{\pi}{2}$	$\frac{\pi}{\sec^{-1}(2\sqrt{2})}-1$	e	π
10	0.211762	0.451277	0.458346	0.621868	0.653152
12	0.151572	0.359414	0.365882	0.523169	0.555244
14	0.115725	0.304912	0.310899	0.459319	0.490658
16	0.09305	0.275545	0.281251	0.42097	0.450592
18	0.078301	0.264041	0.269673	0.402367	0.429735
20	0.0688143	0.265678	0.271421	0.399548	0.424477
22	0.0631192	0.277084	0.283096	0.409437	0.432035

Table H.4: $\|\mathscr{A}_{1,2}\Phi_{1,2}-\bar{\mathscr{A}}_{1,2}\bar{\Phi}_{1,2}\|_2/\|\mathscr{A}_{1,2}\Phi_{1,2}\|_2$ with the same conventions as in Table H.3. $\Phi_{1,2}$ and $\bar{\Phi}_{1,2}$ are fields in the $j=2$ sector with conformal weights $(h_{1,2},h_{1,-2})$ and $(h_{1,-2},h_{1,2})$.

N	$x=\frac{\pi}{3}$	$\frac{\pi}{2}$	$\frac{\pi}{\sec^{-1}(2\sqrt{2})}-1$	e	π
10	0.724473	0.853535	0.857809	0.959148	0.977917
12	0.769136	0.874667	0.87823	0.964825	0.981331
14	0.793913	0.886208	0.889353	0.967146	0.982324
16	0.807582	0.891969	0.894866	0.96719	0.981519
18	0.814765	0.894091	0.89683	0.965628	0.979399
20	0.81803	0.89391	0.896546	0.962969	0.976361
22	0.818871	0.892283	0.894845	0.959593	0.972719

Table H.5: $\|\Pi^{(4)}\mathscr{A}_{1,2}\Phi_{1,2}\|_2$ with the same conventions as in Table H.3. $\Pi^{(4)}$ is a projection to the four states of lowest energy within the $j=2$, $\not{p}=N/2$ sector. These are the states within this sector that have conformal weights up to $(h_{1,-2},h_{1,-2})$.

N	$x=\frac{\pi}{3}$	$\frac{\pi}{2}$	$\frac{\pi}{\sec^{-1}(2\sqrt{2})}-1$	e	π
10	0.210763	0.439128	0.445749	0.600649	0.63123
12	0.148284	0.332095	0.337881	0.482952	0.514155
14	0.110152	0.257777	0.26275	0.39576	0.426568
16	0.0852125	0.204972	0.209224	0.329727	0.359515
18	0.0679876	0.16651	0.170153	0.278915	0.307392
20	0.0555742	0.13779	0.14093	0.239167	0.26624
22	0.0463202	0.115847	0.118574	0.207563	0.233243
p_4	−0.0015914	−0.000137804	0.0000985782	−0.000155346	0.00040305

Table H.6: $\|\Pi^{(4)}(\mathscr{A}_{1,2}\Phi_{1,2}-\bar{\mathscr{A}}_{1,2}\bar{\Phi}_{1,2})\|_2/\|\Pi^{(4)}\mathscr{A}_{1,2}\Phi_{1,2}\|_2$ with the same conventions and the same projector as in Table H.5. $\Phi_{1,2}$ and $\bar{\Phi}_{1,2}$ are fields in the $j=2$ sector with conformal weights $(h_{1,2},h_{1,-2})$ and $(h_{1,-2},h_{1,2})$. Extrapolation p_4 as in Table H.2.

N	$x=\frac{\pi}{3}$	$\frac{\pi}{2}$	$\frac{\pi}{\sec^{-1}(2\sqrt{2})}-1$	e	π
8	0.325797	0.350787	0.351607	0.372103	0.376185
10	0.329276	0.352661	0.353516	0.376516	0.381388
12	0.328903	0.351523	0.35239	0.3768	0.382216
14	0.327108	0.349302	0.350173	0.375408	0.381203
16	0.324801	0.346738	0.347609	0.37335	0.379417
18	0.32236	0.34414	0.34501	0.371078	0.377346
20	0.319948	0.341637	0.342507	0.368803	0.375224
22	0.317637	0.339281	0.340151	0.366621	0.373165

Table H.7: The value of $\|\mathscr{L}_{-1}\Phi_{1,1}\|_2$ for a given length N and parameter x. $\Phi_{1,1}$ is the field in the $j=1$ sector with conformal weights $(h_{1,1},h_{1,-1})=(0,1)$.

N	$x=\frac{\pi}{3}$	$\frac{\pi}{2}$	$\frac{\pi}{\sec^{-1}(2\sqrt{2})}-1$	e	π
8	0.0106586	0.104747	0.108207	0.18703	0.199715
10	0.0114921	0.118893	0.12311	0.224566	0.241811
12	0.0117599	0.124101	0.128674	0.243359	0.263743
14	0.0119545	0.127043	0.131823	0.255388	0.278124
16	0.0121676	0.129476	0.134403	0.264557	0.289152
18	0.0124147	0.131931	0.136979	0.272425	0.298551
20	0.012693	0.134557	0.139716	0.279679	0.307105
22	0.012996	0.13737	0.142638	0.286636	0.315194

Table H.8: $\|(\mathscr{L}_{-1}\Phi_{1,1}-\bar{\mathscr{L}}_{-1}\bar{\Phi}_{1,1})\|_2/\|\mathscr{L}_{-1}\Phi_{1,1}\|_2$ with the same conventions as in Table H.7. $\Phi_{1,1}$ and $\bar{\Phi}_{1,1}$ are fields in the $j=1$ sector with conformal weights $(h_{1,1},h_{1,-1})=(0,1)$ and $(h_{1,-1},h_{1,1})=(1,0)$.

N	$x=\frac{\pi}{3}$	$\frac{\pi}{2}$	$\frac{\pi}{\sec^{-1}(2\sqrt{2})}-1$	e	π
8	0.325786	0.349822	0.350572	0.368581	0.37208
10	0.329244	0.350622	0.35134	0.36961	0.373372
12	0.328845	0.348905	0.349594	0.367684	0.371562
14	0.327027	0.34636	0.347031	0.364836	0.368753
16	0.324704	0.343605	0.344262	0.361773	0.365685
18	0.322251	0.340885	0.341533	0.358769	0.362653
20	0.319832	0.338301	0.338943	0.355932	0.359775
22	0.317515	0.335886	0.336524	0.353297	0.357092

Table H.9: $\|\Pi^{(2)}\mathscr{L}_{-1}\Phi_{1,1}\|_2$ with the same conventions as in Table H.7. $\Pi^{(2)}$ is a projection to the two states of lowest energy within the $j=1$, $\not{p}=N/2$ sector. These are the states within this sector that have conformal weights up to $(h_{1,-1},h_{1,-1})=(1,1)$.

N	$x = \frac{\pi}{3}$	$\frac{\pi}{2}$	$\frac{\pi}{\sec^{-1}(2\sqrt{2})} - 1$	e	π
8	0.0000527492	0.0058436	0.00627048	0.0215309	0.0251946
10	0.0000191654	0.00297587	0.00322369	0.0133976	0.0161156
12	8.26633×10^{-6}	0.00167699	0.00183148	0.00901364	0.0111168
14	4.03988×10^{-6}	0.00102009	0.00112185	0.00641199	0.00809058
16	2.16718×10^{-6}	0.0006584	0.000728471	0.00475643	0.00612835
18	1.25094×10^{-6}	0.000445437	0.000495467	0.00364534	0.004787994
20	7.62288×10^{-7}	0.000313082	0.000349894	0.00286778	0.00383424
22	4.87306×10^{-7}	0.000227096	0.000254879	0.0023049	0.00313292
extrapolation	4.38043×10^{-7}	−0.0000700002	−0.0000675678	0.000161454	0.0000896441

Table H.10: $\|\Pi^{(2)}(\mathscr{L}_{-1}\Phi_{1,1} - \bar{\mathscr{L}}_{-1}\bar{\Phi}_{1,1})\|_2 / \|\Pi^{(2)}\mathscr{L}_{-1}\Phi_{1,1}\|_2$ with the same conventions and the same projector as Table H.9. $\Phi_{1,1}$ and $\bar{\Phi}_{1,1}$ are fields in the $j = 1$ sector with conformal weights $(h_{1,1}, h_{1,-1}) = (0, 1)$ and $(h_{1,-1}, h_{1,1}) = (1, 0)$. The extrapolation is obtained by fitting the last six data points to a curve of the form $c_0 + c_1/N + c_2/N^2 + c_3/N^3 + c_4/N^4$.

APPENDIX H. NUMERICS FOR THE KOO–SALEUR GENERATORS IN POTTS AND LOOP MODELS

APPENDIX

I

PARITY AND THE STRUCTURE OF THE MODULES

In this appendix we correct the previous reasoning in Appendix B of [17], in which we had concluded that the number of singlets or doublets observed will directly yield insight into the structure of the continuum limit Virasoro modules. The error in this reasoning is clear when comparing the numerical results in Chapter 7 to those in Chapter 6, where we perform a similar investigation in the XXZ spin chain. We there have the same spectrum of the Hamiltonian and must thus have the same number of singlets and doublets, while the numerical results from using the Koo-Saleur generators indicate that the structures of the continuum limit Virasoro modules are not the same.

To distinguish between the two types of modules that appear for loop models and the XXZ spin chain, we must instead think more carefully about the symmetry under parity, under which chiral and anti-chiral are mapped to each other. On the lattice this corresponds to a mapping of site j to $-j$, which by (3.7.3) maps the Koo-Saleur generator $\mathscr{L}_n$ to $\bar{\mathscr{L}}_n$. The parity operation is idempotent, so we can distinguish the states by its eigenvalues, $P = \pm 1$. Let us consider the two states $\Phi_{1,2} = \phi_{1,2} \otimes \bar{\phi}_{1,-2}$ and $\bar{\Phi}_{1,2} = \phi_{1,-2} \otimes \bar{\phi}_{1,2}$, which are mapped to each other under parity. Different situations can occur for their descendants $L_{-1}^2\Phi_{1,2}$, $L_{-2}\Phi_{1,2}$, $\bar{L}_{-1}^2\bar{\Phi}_{1,2}$ and $\bar{L}_{-2}\bar{\Phi}_{1,2}$. On the lattice, the four scaling states that have the correct lattice momenta and energies to be identified with these descendants form two singlets and one doublet. The states v_1, v_2 in the doublet are mapped to each other by parity and can thus be combined into one $P = 1$ state $v_1 + v_2$ and one $P = -1$ state $v_1 - v_2$. We now wish to distinguish between the types of modules using the parity of the singlets.

If the four descendants are independent we can form four linear combinations that are eigenstates of the parity operator:

$$\begin{aligned} L_{-1}^2\Phi_{1,2} \pm \bar{L}_{-1}^2\bar{\Phi}_{1,2} \\ L_{-2}\Phi_{1,2} \pm \bar{L}_{-2}\bar{\Phi}_{1,2} \end{aligned} \tag{I.0.1}$$

Out of these two have parity $P = 1$ and two have $P = -1$.

Now consider instead the states depicted in the diagram of (7.4.9), reproduced here for convenience:

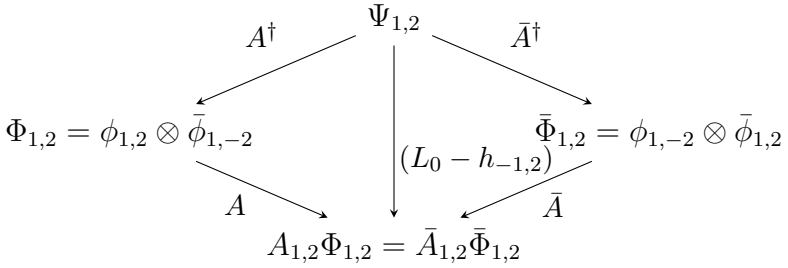

(I.0.2)

The four descendants are no longer independent. The bottom field $A_{1,2}\Phi_{1,2} = \bar{A}_{1,2}\bar{\Phi}_{1,2}$ is clearly invariant under parity. Meanwhile the top field satisfies $AA^\dagger\Psi = \bar{A}\bar{A}^\dagger\Psi$ and therefore also has $P = 1$. These two fields should both appear as singlets, while the doublet would correspond to the two linear combinations that can be formed with what remains (not shown in the diagram).

The above argument has been exposed for the continuum formulation. In order to validate our whole approach of inferring properties of the continuum theory from lattice discretizations, a similar scenario had better hold on the lattice as well. We therefore return to the finite-size numerics to seek the verdict. When acting with $P : j \to -j$ on the two singlets, we find that the results depend on the representation. In the loop model, both singlets have $P = 1$ corresponding to the situation in the diagram above, while in the XXZ spin chain we find that one has $P = 1$, one $P = -1$, so that we rather have the parities expected from four linearly independent descendants. The two lattice discretizations thus indeed confirm the general argument, and we find that only the loop model has the Jordan-cell structure (7.4.9) with the dependence $A_{1,2}\Phi_{1,2} = \bar{A}_{1,2}\bar{\Phi}_{1,2}$, which is one of the main points of Chapter 7.

Synthèse en Français

Les théories de champs conformes (CFTs) sont des théories de champs quantiques qui sont invariantes sous des transformations conformes (des transformations préservants les angles). Bien que les CFTs apparaissent dans de nombreux contextes, le contexte qui nous intéresse dans cette thèse est celui des modèles sur réseau bidimensionnels au point critique. L'exemple quintessentiel est le modèle d'Ising : au point critique, des amas de spin de toutes tailles sont présents – il y a invariance d'échelle. L'invariance d'échelle s'étend à l'invariance conforme, la longueur de corrélation diverge et la fonction de corrélation spin-spin décroît comme une loi de puissance. D'autres exemples incluent le modèle de Potts à Q états, qui dans la limite $Q \to 1$ décrit la percolation [1], et le modèle $O(n)$, qui dans la limite $n \to 0$ décrit les marches auto-évitantes (polymères) [2]. Une seule CFT peut décrire les propriétés à longue distance de plusieurs systèmes critiques tant qu'ils appartiennent à la même classe d'universalité, même si à l'échelle microscopique ils semblent très différents. Pour cette raison, les mêmes lois de puissances peuvent apparaître dans des domaines scientifiques apparemment sans rapport.

Cette thèse ne traitera que des CFTs bidimensionnelles. L'algèbre de symétrie d'une CFT bidimensionnelle est l'unique extension centrale de l'algèbre de Witt, l'*algèbre de Virasoro*, générée par $L_n, n \in \mathbf{Z}$ sous la relation suivante :

$$[L_m, L_n] \;=\; (m-n)L_{m+n} + \frac{c}{12} m(m^2-1)\delta_{m+n,0}$$

où c est la charge centrale.

L'étude des CFTs bidimensionnelles est donc basée sur l'étude des représentations de l'algèbre de Virasoro. Les CFTs qui correspondent à une somme directe d'un nombre fini de représentations irréductibles de Virasoro ont été entièrement classifiées et résolues (ce qui signifie que nous pouvons calculer leurs fonctions de corrélation). Ce sont les modèles minimaux, qui fournissent l'exemple le plus célèbre de CFTs rationnelles, définies comme des CFTs avec un nombre fini de champs primaires (champs annihilés par $L_n, n > 0$). Cependant, les CFTs avec une théorie de représentation plus compliquée sont beaucoup moins bien comprises. Celles-ci sont le thème principal de cette thèse.

Grâce à l'invariance conforme, les calculs des fonctions de corrélation se réduisent à déterminer certaines données conformes, telles que les valeurs propres de L_0, ainsi qu'à déterminer les représentations de Virasoro impliquées, ce qui fixe la forme des blocs conformes. Même en l'absence de certaines de ces données, la symétrie conforme impose des contraintes si fortes que les données manquantes peuvent généralement être déduites. L'objectif est donc de retrouver certaines de ces données et les structures des représentations de Virasoro. Pour cettes dernières, la situation est rendue plus compliquée dans les théories qui sont *non-unitaires*. Si l'unitarité est une caractéristique naturelle à exiger en physique des particules, de nombreux problèmes d'intérêt en physique de la matière condensée sont décrits par des CFTs non-unitaires à la criticité. Ceux-la incluent des problèmes géométriques tels que les polymères et la percolation, qui manquent de localité.

Les modèles sur réseau qui apparaissent dans cette thèse sont : le modèle à six sommets, le modèle RSOS, le modèle de Potts à Q états et le modèle $O(n)$. Ils sont tous liés à un modèle de boucle. Les modèles de boucle sont naturellement décrits par des CFTs non-unitaires, puisque la non-localité inhérente aux modèles peut être échangée contre la non-unitarité. Nous considérons les modèles sur réseau dans la limite anisotrope, avec des conditions aux limites périodiques. Leurs limites continues aux points critiques sont décrites par des CFTs du "bulk", dont la symétrie est décrite par deux copies de l'algèbre de Virasoro : $\mathrm{Vir} \otimes \overline{\mathrm{Vir}}$.

Les trois premiers de ces modèles sur réseau peuvent être décrits en termes de l'algèbre de Temperley-Lieb affine, qui joue un rôle important dans cette thèse. (Le dernier – le modèle $O(n)$ – est plutôt décrit par l'algèbre de Temperley-Lieb *diluée*). L'algèbre de Temperley-Lieb est générée par $e_j, j = 1, 2, ...N$ (avec N la largeur du réseau[1]), ainsi que l'identité, tels que [54] :

$$\begin{aligned} e_j^2 &= \mathfrak{m} e_j \,, \\ e_j e_{j\pm1} e_j &= e_j \,, \\ e_j e_k &= e_k e_j \qquad (\text{for } j \neq k,\ k \pm 1) \,. \end{aligned}$$

De plus, l'algèbre *affine* de Temperley-Lieb contient les éléments u et u^{-1} générants respectivement des translations d'un site vers la droite et vers la gauche. Ceux-ci obéissent à d'autres relations impliquant les e_j. Nous paramétrons $\mathfrak{m} = \mathfrak{q} + \mathfrak{q}^{-1}$, avec $\mathfrak{q} = e^{i\gamma}$ le paramètre de déformation du groupe quantique $U_\mathfrak{q} sl(2)$.

En termes d'algèbre de Temperley-Lieb affine, les hamiltoniens de la chaîne de spin prennent la forme suivante :

$$\mathscr{H} \propto \sum_{j=1}^{N} e_j \,,$$

où le choix d'une *représentation* de l'algèbre affine de Temperley-Lieb correspond au choix d'un modèle sur réseau. Par exemple, dans la représentation correspondant au modèle à six sommets, les générateurs e_j sont donnés par :

$$e_j = -\sigma_j^- \sigma_{j+1}^+ - \sigma_j^+ \sigma_{j+1}^- - \frac{\cos\gamma}{2}\sigma_j^z\sigma_{j+1}^z - \frac{i\sin\gamma}{2}(\sigma_j^z - \sigma_{j+1}^z) + \frac{\cos\gamma}{2} \,,$$

où les σ_j sont les matrices de Pauli, donc l'hamiltonien est l'hamiltonien familier de la chaîne de spin XXZ :

$$\mathscr{H} = \frac{\gamma}{2\pi\sin\gamma} \sum_{j=1}^{N} \left[\sigma_j^x\sigma_{j+1}^x + \sigma_j^y\sigma_{j+1}^y + \Delta(\sigma_j^z\sigma_{j+1}^z - 1)\right] \,,$$

avec un paramètre d'anisotropie $\Delta = \cos\gamma$. Les représentations de Temperley-Lieb affines qui apparaissent dans cette thèse sont paramétrées par j et z, et notées $\mathscr{W}_{j,z}$. L'interprétation physique de j et z dépend de la représentation : dans l'exemple de la représentation de la chaîne de spin XXZ, j paramétrise l'aimantation et z la torsion des conditions aux limites.

La première partie principale de la thèse concerne le calcul des fonctions à quatre points du modèle de Potts. En particulier, nous fournissons une interprétation géométrique des fonctions à quatre points construites dans un article de Picco et al. [19]. La détermination bootstrap des fonctions de corrélation géométriques proposées dans [19] s'est avérée ultérieurement incorrecte dans [20], le vrai spectre du modèle de Potts étant considérablement plus complexe qu'initialement conjecturé. Nous expliquons pourquoi les résultats obtenus par ces auteurs, bien qu'incorrects, semblaient si proches de ceux de leurs simulations numériques du modèle de Potts. Notre stratégie est basée sur une expansion en amas des fonctions de corrélation dans les modèles minimaux RSOS, puis sur une analyse numérique et algébrique du spectre du canal s.

Nous constatons que les fonctions de corrélation sur réseau de certains opérateurs dans les modèles RSOS ont des expansions en graphes très similaires à celles qui se produisent dans le modèle de Potts. La principale différence entre les deux modèles est les poids accordés aux amas

[1] ou, dans la limite anisotrope, la longueur de la chaîne de spins quantique correspondante

avec des topologies non-triviales. Nous découvrons des propriétés remarquables des amplitudes sur réseau, qui expliquent notamment la réduction du spectre de [20] au spectre beaucoup plus simple des modèles RSOS, et qui jettent les bases de la détermination des fonctions géométriques à quatre points du modèle de Potts lui-même.

Nous montrons également que le calcul des fonctions de corrélation des opérateurs d'ordre dans le modèle RSOS de type A_n correspond aux évaluations de certains diagrammes de fusion anyoniques $su(2)_k$, avec $k = n-1$ et que la limite anisotrope du modèle RSOS de type A_n donne la chaîne anyonique $su(2)_k$. Nous faisons le lien avec les défauts topologiques dans les CFTs.

Une grande partie du travail de cette thèse consiste à déduire la structure des représentations de Virasoro pertinentes dans deux modèles différents : le modèle à six sommets et le modèle de Potts (et le modèle de boucle associé). L'outil principal de ce travail est les générateurs *Koo-Saleur* : une discrétisation des générateurs de Virasoro en termes de générateurs de Temperley-Lieb :

$$\mathscr{L}_n[N] = \frac{N}{4\pi}\left[-\frac{\gamma}{\pi\sin\gamma}\sum_{j=1}^{N} e^{inj2\pi/N}\left(e_j - e_\infty + \frac{i\gamma}{\pi\sin\gamma}[e_j, e_{j+1}]\right)\right] + \frac{c}{24}\delta_{n,0}\,,$$
$$\bar{\mathscr{L}}_n[N] = \frac{N}{4\pi}\left[-\frac{\gamma}{\pi\sin\gamma}\sum_{j=1}^{N} e^{-inj2\pi/N}\left(e_j - e_\infty - \frac{i\gamma}{\pi\sin\gamma}[e_j, e_{j+1}]\right)\right] + \frac{c}{24}\delta_{n,0}\,.$$

L'ingrédient supplémentaire crucial dans ces formules est la charge centrale, donnée par $c = 1 - \frac{6}{x(x+1)}$ liée à γ par la paramétrisation $\gamma = \frac{\pi}{x+1}$.

Nous étudions d'abord l'action des générateurs de Koo-Saleur dans la chaîne de spin quantique XXZ critique. Nous explorons la structure des modules de Virasoro à la limite continue, avec une charge centrale générique, pour le modèle à six sommets. Nous trouvons des modules indécomposables, mais pas logarithmiques. La limite des modules de Temperley-Lieb $\mathscr{W}_{j,1}$ pour $j \neq 0$ contient des paires d'"états conjugués" avec des poids conformes $(h_{r,s}, h_{r,-s})$ et $(h_{r,-s}, h_{r,s})$ qui donnent lieu à des structures duales : modules de Verma ou co-Verma. La limite de $\mathscr{W}_{0,\mathfrak{q}^{\pm 2}}$ contient des champs diagonaux $(h_{r,1}, h_{r,1})$ et donne lieu soit uniquement à des modules de Verma, soit uniquement à des modules co-Verma, selon le signe de l'exposant dans $\mathfrak{q}^{\pm 2}$. Afin d'obtenir les éléments de matrice des générateurs de Koo-Saleur pour un système de grande taille N, nous utilisons l'ansatz de Bethe et les méthodes de diffusion inverse quantique, en calculant les facteurs de forme pour les combinaisons pertinentes de trois opérateurs de spin voisins. Les relations entre les facteurs de forme garantissent que la dualité ci-dessus existe déjà au niveau du réseau. Nous étudions également dans quel sens les générateurs de Koo-Saleur convergent vers les générateurs de Virasoro. Nous considérons la convergence au sens faible, en cherchant à savoir si le commutateur des limites est le même que la limite du commutateur. Nous constatons qu'il ne coïncide que jusqu'au terme central. Comme résultat secondaire, nous calculons la valeur attendue de l'état fondamental de deux générateurs de Temperley-Lieb voisins dans la chaîne de spin XXZ.

Plus précisément, les principaux résultats concernant la nature des modules qui apparaissent dans la limite continue du modèle à six sommets sont les suivants, pour $j = 0$:

$$\mathscr{W}_{0,\mathfrak{q}^2} \mapsto \left(\bigoplus_{n>0} \widetilde{\mathsf{V}}^{(\mathrm{d})}_{n,1} \otimes \widetilde{\mathsf{V}}^{(\mathrm{d})}_{n,1}\right) \oplus \left(\mathsf{V}_{0,1} \otimes \mathsf{V}_{0,1}\right),$$
$$\mathscr{W}_{0,\mathfrak{q}^{-2}} \mapsto \left(\bigoplus_{n>0} \mathsf{V}^{(\mathrm{d})}_{n,1} \otimes \mathsf{V}^{(\mathrm{d})}_{n,1}\right) \oplus \left(\mathsf{V}_{0,1} \otimes \mathsf{V}_{0,1}\right),$$

et pour $j > 0$:

$$S_z = j;\ \ \mathscr{W}_{j,1} \mapsto \left(\bigoplus_{e>0} \mathsf{V}_{e,-j} \otimes \mathsf{V}^{(\mathrm{d})}_{e,j}\right) \oplus \left(\mathsf{V}_{0,-j} \otimes \mathsf{V}_{0,j}\right) \oplus \left(\bigoplus_{e<0} \widetilde{\mathsf{V}}^{(\mathrm{d})}_{e,-j} \otimes \mathsf{V}_{e,j}\right),$$
$$S_z = -j;\ \ \mathscr{W}_{j,1} \mapsto \left(\bigoplus_{e>0} \mathsf{V}^{(\mathrm{d})}_{e,j} \otimes \mathsf{V}_{e,-j}\right) \oplus \left(\mathsf{V}_{0,j} \otimes \mathsf{V}_{0,-j}\right) \oplus \left(\bigoplus_{e<0} \mathsf{V}_{e,j} \otimes \widetilde{\mathsf{V}}^{(\mathrm{d})}_{e,-j}\right).$$

Ici, $\mathsf{V}_{r,s}$ fait référence à une structure de module de Verma, et $\widetilde{\mathsf{V}}_{r,s}$ fait référence à la structure duale ("co-Verma"). r et s sont des étiquettes de Kac.

Les principaux résultats concernant la nature de la convergence des générateurs de Koo-Saleur peuvent être résumés par une modification des relations de commutation de Virasoro sous la forme

$$[\mathscr{L}_m, \mathscr{L}_n] = (m-n)\mathscr{L}_{m+n} + \delta_{m+n,0}\frac{1}{12}(m^3 c^* - mc)\,,$$

avec

$$c^* = -\frac{24\gamma^3 I_0}{\pi^2 \sin^2\gamma} + \frac{48\gamma^3}{\pi^2} I_1$$

où $I_n = \int_{-\infty}^{\infty} t^{2n} \frac{\sinh(\pi-\gamma)t}{\sinh \pi t \, \cosh \gamma t}\,\mathrm{d}t$. Cette modification correspond à la relation obtenue en prenant uniquement la limite continue, et non la limite d'échelle qui est une double limit. En utilisant la limite d'échelle à la place de la limite continue, nous retrouvons la relation correcte.

Nous explorons ensuite la structure des modules de Virasoro à la limite continue, avec une charge centrale générique, pour le modèle de Potts et le modèle de boucle associé. Ceci est réalisé par un mélange de différentes techniques. Du côté numèrique : une étude minutieuse des générateurs de Koo-Saleur, combinée à des calculs d'amplitudes à quatre points. Du côté analytique : les OPEs et les amplitudes à quatre points récemment déterminées en utilisant le "bootstrap conformal interchiral" dans [21]. Nous trouvons que les descendants nuls des champs diagonaux ayant des poids $(h_{r,1}, h_{r,1})$ (avec $r \in \mathbb{N}^*$) sont vraiment nuls, donc ces champs viennent avec des modules Vir $\otimes$ $\overline{\text{Vir}}$ ("Kac") simples. Cependant, les champs avec des poids $(h_{r,s}, h_{r,-s})$ et $(h_{r,-s}, h_{r,s})$ (avec $r, s \in \mathbb{N}^*$) appartiennent à des représentations indécomposables mais pas complètement réductibles mélangeant quatre modules Vir $\otimes$ $\overline{\text{Vir}}$ simples avec une forme familière de "diamant". Les champs "en haut" et "en bas" de ces diamants ont des poids $(h_{r,-s}, h_{r,-s})$, et forment une cellule de Jordan de rang deux pour L_0 et $\bar{L}_0$. Ceci établit que la CFT du modèle de Potts est logarithmique pour Q générique. Contrairement au cas des valeurs non génériques de Q, ces structures indécomposables ne sont pas présentes en taille finie, mais nous pouvons néanmoins montrer à partir de l'étude numérique du modèle sur réseau comment les cellules de Jordan de rang deux s'accumulent dans la limite de la taille infinie.

Plus précisément, les principaux résultats concernant la nature des modules apparaissants dans la limite continue des modèles de Potts et de boucle sont, pour $j = 0$:

$$\overline{\mathscr{W}}_{0,\mathsf{q}^{\pm 2}} \mapsto \bigoplus_{n=1}^{\infty} \mathsf{X}_{n,1} \otimes \overline{\mathsf{X}}_{n,1}\,,$$

et pour $j > 0$:

$$\mathscr{W}_{j,1} \mapsto \left(\mathsf{V}_{0,-j} \otimes \overline{\mathsf{V}}_{0,j}\right) \oplus \bigoplus_{e>0} \mathscr{L}_{e,j}\,,$$

avec

$$\mathscr{L}_{e,j} = \mathscr{Q}[(\mathsf{V}^{(\mathrm{d})}_{e,j} \otimes \overline{\mathsf{V}}_{e,-j}) \oplus (\mathsf{V}_{e,-j} \otimes \overline{\mathsf{V}}^{(\mathrm{d})}_{e,j})] \equiv \begin{array}{ccc} & \mathsf{V}_{e,-j} \otimes \overline{\mathsf{V}}_{e,-j} & \\ \swarrow & & \searrow \\ \mathsf{X}_{e,j} \otimes \overline{\mathsf{V}}_{e,-j} & & \mathsf{V}_{e,-j} \otimes \overline{\mathsf{X}}_{e,j} \\ \searrow & & \swarrow \\ & \mathsf{V}_{e,-j} \otimes \overline{\mathsf{V}}_{e,-j} & \end{array}$$

Ici, $\mathsf{X}_{r,s}$ fait référence à un module de Kac. Les modules de Virasoro $\mathscr{L}_{e,j}$, qui ont une structure en diamant, sont *logarithmiques*. Ils correspondent aux cellules de Jordan de rang deux de L_0 et $\bar{L}_0$, et conduisent à des corrections logarithmiques des lois de puissance habituelles décrivant les fonctions de corrélation (d'où leur nom). De tels modules logarithmiques apparaissent également dans le modèle $O(n)$.

Dans la dernière partie de la thèse, nous définissons la théorie des champs conforme $O(n)$ à deux dimensions comme une théorie qui inclut les modèles $O(n)$ critiques dilués et denses comme cas particuliers, et qui dépend analytiquement de la charge centrale. Pour des valeurs génériques de $n \in \mathbb{C}$, nous écrivons une conjecture pour la décomposition du spectre en représentations irréductibles de $O(n)$. Nous expliquons ensuite comment bootstrap numériquement des fonctions à quatre points arbitraires de champs primaires en présence de la symétrie globale $O(n)$. Nous déterminons les blocs conformes nécessaires, y compris les blocs logarithmiques correspondants aux modules logarithmiques de Virasoro avec la structure en diamant vue ci-dessus, y compris dans les cas singuliers. Nous argumentons que la théorie des représentations d'$O(n)$ fournit des limites supérieures sur le nombre de solutions des équations de croisement pour toute fonction à quatre points donnée. Nous étudions en détail certaines des fonctions de corrélation les plus simples, et déterminons quelques règles de fusion. Nous comptons les solutions des équations de croisement pour les 30 fonctions à quatre points les plus simples, et trouvons que le nombre de solutions varie de 2 à 6, saturant la limite de la théorie des représentations d'$O(n)$ dans 21 des 30 cas.

Tout au long de cette thèse, un thème récurrent est l'interconnexion entre différentes structures mathématiques et modèles physiques. Il semble évident que les travaux futurs impliqueront la compréhension de ces interconnexions, que ce soit à partir d'une approche par le réseau ou en utilisant d'autres méthodes. Les applications concrètes de ces travaux sont nombreuses. À court terme : l'application des méthodes bootstrap non-unitaires au modèle $O(n)$ dans la limite $n \to 0$ (polymères) et au modèle Potts à Q états dans la limite $Q \to 1$ (percolation). À long terme : la compréhension des points critiques dans différentes classes d'universalité des isolants topologiques (comme la transition de plateau dans l'effet Hall quantique entier) par une compréhension plus approfondie des CFT non-unitaires.

BIBLIOGRAPHY

[1] P. W. Kasteleyn and C. M. Fortuin, "Phase Transitions in Lattice Systems with Random Local Properties," *J. Phys. Soc. Jpn.*, vol. 26, pp. 11–14, Supplement, 1969.

[2] B. Duplantier and H. Saleur, "Exact Critical Properties of Two-dimensional Dense Self-avoiding Walks," *Nucl. Phys. B*, vol. 290, pp. 291–326, 1987.

[3] G. E. Andrews, R. J. Baxter, and P. J. Forrester, "Eight vertex SOS model and generalized Rogers-Ramanujan type identities," *J. Stat. Phys.*, vol. 35, pp. 193–266, 1984.

[4] P. Di Francesco, P. Mathieu, and D. Sénéchal, *Conformal field theory*. Graduate texts in contemporary physics, New York, NY: Springer, 1997.

[5] A. A. Belavin, A. M. Polyakov, and A. B. Zamolodchikov, "Infinite Conformal Symmetry in Two-Dimensional Quantum Field Theory," *Nucl. Phys.*, vol. B241, pp. 333–380, 1984.

[6] R. Nivesvivat and S. Ribault, "Logarithmic CFT at generic central charge: from Liouville theory to the Q-state Potts model," *SciPost Phys.*, vol. 10, no. 1, p. 021, 2021.

[7] N. Read and H. Saleur, "Associative-algebraic approach to logarithmic conformal field theories," *Nucl. Phys. B*, vol. 777, pp. 316–351, 2007.

[8] A. Gainutdinov and R. Vasseur, "Lattice fusion rules and logarithmic operator product expansions," *Nucl. Phys. B*, vol. 868, no. 1, pp. 223–270, 2013.

[9] J. Dubail, J. L. Jacobsen, and H. Saleur, "Conformal field theory at central charge c = 0: A measure of the indecomposability (b) parameters," *Nucl. Phys. B*, vol. 834, pp. 399–422, 2010.

[10] R. Vasseur, J. L. Jacobsen, and H. Saleur, "Indecomposability parameters in chiral Logarithmic Conformal Field Theory," *Nucl. Phys. B*, vol. 851, pp. 314–345, 2011.

[11] Z. Maassarani and D. Serban, "Non-unitary conformal field theory and logarithmic operators for disordered systems," *Nucl. Phys. B*, vol. 489, no. 3, pp. 603–625, 1997.

[12] W. M. Koo and H. Saleur, "Representations of the Virasoro algebra from lattice models," *Nucl. Phys. B*, vol. 426, pp. 459–504, 1994.

[13] M. Ganahl and G. Vidal, "Continuous matrix product states for nonrelativistic quantum fields: A lattice algorithm for inhomogeneous systems," *Phys. Rev. B*, vol. 98, p. 195105, 2018.

[14] M. H. Freedman, "P/NP , and the quantum field computer," *PNAS*, vol. 95, no. 1, pp. 98–101, 1998.

[15] Y. He, L. Grans-Samuelsson, J. L. Jacobsen, and H. Saleur, "Four-point geometrical correlation functions in the two-dimensional Q-state Potts model: connections with the RSOS models," *JHEP*, vol. 05, p. 156, 2020.

[16] L. Grans-Samuelsson, J. L. Jacobsen, and H. Saleur, "The action of the Virasoro algebra in quantum spin chains. Part I. The non-rational case," *JHEP*, vol. 02, p. 130, 2021.

[17] L. Grans-Samuelsson, L. Liu, Y. He, J. L. Jacobsen, and H. Saleur, "The action of the Virasoro algebra in the two-dimensional Potts and loop models at generic Q," *JHEP*, vol. 10, p. 109, 2020.

[18] L. Grans-Samuelsson, R. Nivesvivat, J. L. Jacobsen, S. Ribault, and H. Saleur, "Global symmetry and conformal bootstrap in the two-dimensional $O(n)$ model," *SciPost Phys.*, vol. 12, p. 147, 2022.

[19] M. Picco, S. Ribault, and R. Santachiara, "A conformal bootstrap approach to critical percolation in two dimensions," *SciPost Phys.*, vol. 1, no. 1, p. 009, 2016.

[20] J. L. Jacobsen and H. Saleur, "Bootstrap approach to geometrical four-point functions in the two-dimensional critical Q-state Potts model: A study of the s-channel spectra," *JHEP*, vol. 01, p. 084, 2019.

[21] Y. He, J. L. Jacobsen, and H. Saleur, "Geometrical four-point functions in the two-dimensional critical Q-state Potts model: The interchiral conformal bootstrap," *JHEP*, vol. 12, p. 019, 2020.

[22] R. J. Baxter, *Exactly Solved Models in Statistical Mechanics*. World Scientific, 1985.

[23] R. Baxter, "q colourings of the triangular lattice," *J. Phys. A*, vol. 19, p. 2821, 1986.

[24] A. Milsted and G. Vidal, "Extraction of conformal data in critical quantum spin chains using the Koo-Saleur formula," *Phys. Rev. B*, vol. 96, no. 24, p. 245105, 2017.

[25] J. Dubail, J. Jacobsen, and H. Saleur, "Exact solution of the anisotropic special transition in the o(n) model in two dimensions," *Phys. Rev. Lett.*, vol. 103, p. 145701, 2009.

[26] E. H. Lieb, "Residual entropy of square ice," *Phys. Rev.*, vol. 162, pp. 162–172, 1967.

[27] R. J. Baxter, "Partition function of the eight-vertex lattice model," *Ann. Phys.*, vol. 70, pp. 193—228, 1972.

[28] J. L. Jacobsen, "Integrability in statistical physics and quantum spin chains," in *Integrability: From Statistical Systems to Gauge Theory: Lecture Notes of the Les Houches Summer School: Volume 106, June 2016*, Oxford Scholarship Online, 2019.

[29] V. Pasquier, "Two-dimensional critical systems labelled by Dynkin diagrams," *Nucl. Phys. B*, vol. 285, pp. 162–172, 1987.

[30] I. K. Kostov, "The ADE face models on a fluctuating planar lattice," *Nucl. Phys. B*, vol. 326, pp. 583–612, 1989.

[31] P. Roche, "On the construction of integrable dilute ADE models," *Phys. Lett. B*, vol. 285, no. 1, pp. 49–53, 1992.

[32] S. O. Warnaar, B. Nienhuis, and K. A. Seaton, "New construction of solvable lattice models including an Ising model in a field," *Phys. Rev. Lett.*, vol. 69, pp. 710–712, 1992.

[33] S. O. Warnaar and B. Nienhuis, "Solvable lattice models labelled by Dynkin diagrams," *J. Phys. A*, vol. 26, pp. 2301–2316, 1993.

[34] R. B. Potts, "Some generalized order-disorder transformations," *Math. Proc. Cambr. Phil. Soc.*, vol. 48, no. 1, p. 106–109, 1952.

[35] R. J. Baxter, "Potts model at the critical temperature," *J. Phys. C: Solid State Phys.*, vol. 6, no. 23, pp. L445–L448, 1973.

[36] E. Domany, D. Mukamel, B. Nienhuis, and A. Schwimmer, "Duality relations and equivalences for models with $O(N)$ and cubic symmetry," *Nucl. Phys. B*, vol. 190, pp. 279–287, 1981.

[37] B. Nienhuis, "Exact critical point and critical exponents of O(n) models in two dimensions," *Phys. Rev. Lett.*, vol. 49, pp. 1062–1065, 1982.

[38] J. L. Jacobsen, N. Read, and H. Saleur, "Dense Loops, Supersymmetry, and Goldstone Phases in Two Dimensions," *Phys. Rev. Lett.*, vol. 90, p. 090601, 2003.

[39] H. Duminil-Copin and S. Smirnov, "The connective constant of the honeycomb lattice equals $\sqrt{2+\sqrt{2}}$," *Annals Math.*, vol. 175, pp. 1653–1665, 2012.

[40] J. Böhm, J. L. Jacobsen, Y. Jiang, and Y. Zhang, "Geometric algebra and algebraic geometry of loop and Potts models," *JHEP*, vol. 05, p. 068, 2022.

[41] B. Nienhuis, "Loop models," in *Exact Methods in Low-dimensional Statistical Physics and Quantum Computing: Lecture Notes of the Les Houches Summer School: Volume 89, July 2008*, OUP Oxford, 2010.

[42] H. Saleur, "New exact critical exponents for 2d self avoiding walks," *J.Phys.A*, vol. 19, pp. L807–L810, 1986.

[43] P. Di Francesco, H. Saleur, and J.-B. Zuber, "Relations between the Coulomb gas picture and conformal invariance of two-dimensional critical models," *J. Stat. Phys.*, vol. 49, no. 1-2, pp. 57–79, 1987.

[44] V. Dotsenko and V. Fateev, "Conformal algebra and multipoint correlation functions in 2d statistical models," *Nucl. Phys. B*, vol. 240, no. 3, pp. 312–348, 1984.

[45] J. Kondev and C. L. Henley, "Four-coloring model on the square lattice: A critical ground state," *Phys. Rev. B*, vol. 52, pp. 6628–6639, 1995.

[46] J. Kondev, "Liouville field theory of fluctuating loops," *Phys. Rev. Lett.*, vol. 78, pp. 4320–4323, 1997.

[47] B. Nienhuis, "Critical behavior of two-dimensional spin models and charge asymmetry in the Coulomb gas," *J. Stat. Phys.*, vol. 34, pp. 731–761, 1984.

[48] J. L. Jacobsen and A. D. Sokal, "Mapping of a graph-homomorphism (RSOS) model onto a multi-variate Tutte polynomial (Potts model)," *unpublished*, 2008.

[49] J. Jacobsen, S. Ribault, and H. Saleur, "Spaces of states of the two-dimensional O(n) and Q-state Potts models," 2022. Article in preparation.

[50] J. Belletête and Y. Saint-Aubin, "The principal indecomposable modules of the dilute Temperley-Lieb algebra," *J. Math. Phys.*, vol. 55, p. 111706, 2014.

[51] P. A. Pearce, J. Rasmussen, and E. Tartaglia, "Logarithmic Superconformal Minimal Models," *J. Stat. Mech.*, vol. 1405, p. P05001, 2014.

[52] A. Lafay, A. M. Gainutdinov, and J. L. Jacobsen, "$u_q(\mathfrak{sl}_n)$ web models and $\mathbb{Z}_n$ spin interfaces," *J. Stat. Mech.*, vol. 2021, no. 5, p. 053104, 2021.

[53] A. M. Gainutdinov, H. Saleur, and I. Y. Tipunin, "Lattice W-algebras and logarithmic CFTs," *J. Phys. A*, vol. 47, no. 49, p. 495401, 2014.

[54] H. N. V. Temperley and E. H. Lieb, "Relation between the 'percolation' and 'colouring' problem and other graph-theoretical problems associated with planar lattices: some exact results for the 'percolation' problem," *Proc. Roy. Soc. London A*, vol. 322, p. 251, 1971.

[55] P. Martin and H. Saleur, "The Blob algebra and the periodic Temperley-Lieb algebra," *Lett. Math. Phys.*, vol. 30, p. 189, 1994.

[56] P. Martin and H. Saleur, "On an algebraic approach to non-planar statistical mechanics," *Comm. Math. Phys.*, vol. 158, pp. 155–190, 1993.

[57] J. Graham and G. Lehrer, "The representation theory of affine Temperley-Lieb algebras," *L'Ens. Math.*, vol. 44, p. 173, 1998.

[58] A. Gainutdinov, N. Read, H. Saleur, and R. Vasseur, "The periodic $sl(2|1)$ alternating spin chain and its continuum limit as a bulk Logarithmic Conformal Field Theory at c=0," *JHEP*, vol. 05, p. 114, 2015.

[59] L. Grans-Samuelsson, J. Jacobsen, L. Liu, and H. Saleur, "The action of the Virasoro algebra in quantum spin chains. II. The root of unity case," 2022. Article in preparation.

[60] V. G. Drinfeld, "Hopf algebras and the quantum Yang-Baxter equation," *Sov. Math. Dokl.*, vol. 32, pp. 254–258, 1985.

[61] M. Jimbo, "A q difference analog of U(g) and the Yang-Baxter equation," *Lett. Math. Phys.*, vol. 10, pp. 63–69, 1985.

[62] V. Pasquier and H. Saleur, "Common structures between finite systems and conformal field theories through quantum groups," *Nucl. Phys. B*, vol. 330, no. 2, pp. 523–556, 1990.

[63] N. Read and H. Saleur, "Exact spectra of conformal supersymmetric nonlinear sigma models in two-dimensions," *Nucl. Phys.*, vol. B613, p. 409, 2001.

[64] G. Keller, "Fusion Rules of $U_q(\mathrm{sl}(2,\mathbf{c})), \mathrm{q}^{\mathrm{m}} = 1$," *Lett. Math. Phys.*, vol. 21, pp. 273–286, 1991.

[65] H. Saleur and J. Zuber, "Integrable lattice models and quantum groups (CEA-CONF–10358)," 1990. Lecture notes.

[66] S. Ribault, "Minimal lectures on two-dimensional conformal field theory," 2016.

[67] V. Gurarie and A. W. W. Ludwig, "Conformal field theory at central charge c = 0 and two- dimensional critical systems with quenched disorder," 2004. arXiv preprint hep-th/0409105.

[68] V. Gurarie, "Logarithmic operators in conformal field theory," *Nucl. Phys. B*, vol. 410, no. 3, pp. 535–549, 1993.

[69] J. Cardy, "Logarithmic conformal field theories as limits of ordinary CFTs and some physical applications," *J. Phys.*, vol. A46, p. 494001, 2013.

[70] V. S. Dotsenko, "Four spins correlation function of the q states Potts model, for general values of q. Its percolation model limit $q \to 1$," 2019.

[71] S. Ribault, "On 2d CFTs that interpolate between minimal models," *SciPost Phys.*, vol. 6, p. 075, 2019.

[72] S. Migliaccio and S. Ribault, "The analytic bootstrap equations of non-diagonal two-dimensional CFT," *JHEP*, vol. 05, p. 169, 2018.

[73] S. Ribault, "The non-rational limit of D-series minimal models," *SciPost Phys. Core*, vol. 3, p. 002, 2020.

[74] M. Picco, S. Ribault, and R. Santachiara, "On four-point connectivities in the critical 2d Potts model," *SciPost Phys.*, vol. 7, no. 4, p. 044, 2019.

[75] V. Pasquier, "Operator content of the ADE lattice models," *J. Phys. A*, vol. 20, p. 5707, 1987.

[76] V. Pasquier, "Lattice derivation of modular invariant partition functions on the torus," *J. Phys. A*, vol. 20, no. 18, pp. L1229–L1237, 1987.

[77] G. Delfino and J. Viti, "Potts q-color field theory and scaling random cluster model," *Nucl. Phys. B*, vol. 852, pp. 149–173, 2011.

[78] M. den Nijs, "Extended scaling relations for the magnetic critical exponents of the Potts model," *Phys. Rev. B*, vol. 27, pp. 1674–1679, 1983.

[79] B. Estienne and Y. Ikhlef, "Correlation functions in loop models," 2015. arXiv preprint 1505.00585.

[80] A. B. Zamolodchikov and A. B. Zamolodchikov, "Structure constants and conformal bootstrap in Liouville field theory," *Nucl. Phys. B*, vol. 477, pp. 577–605, 1996.

[81] D. A. Huse, "Exact exponents for infinitely many new multicritical points," *Phys. Rev. B*, vol. 30, pp. 3908–3915, 1984.

[82] P. J. Forrester and R. J. Baxter, "Further exact solutions of the eight-vertex SOS model and generalizations of the Rogers-Ramanujan identities," *J. Stat. Phys.*, vol. 38, no. 3-4, pp. 435–472, 1985.

[83] H. Riggs, "Solvable lattice models with minimal and nonunitary critical behaviour in two dimensions," *Nucl. Phys. B*, vol. 326, no. 3, pp. 673–688, 1989.

[84] T. Nakanishi, "Nonunitary minimal models and RSOS models," *Nucl. Phys. B*, vol. 334, pp. 745–766, 1990.

[85] P. Di Francesco, H. Saleur, and J. B. Zuber, "Generalized Coulomb gas formalism for two-dimensional critical models based on $SU(2)$ coset construction," *Nucl. Phys. B*, vol. 300, pp. 393–432, 1988.

[86] P. Di Francesco, H. Saleur, and J. B. Zuber, "Modular invariance in nonminimal two-dimensional conformal theories," *Nucl. Phys. B*, vol. 285, p. 454, 1987.

[87] H. Saleur, "The antiferromagnetic Potts model in two dimensions: Berker-Kadanoff phase, antiferromagnetic transition, and the role of Beraha numbers," *Nucl. Phys. B*, vol. 360, pp. 219–263, 1991.

[88] V. S. Dotsenko, "Critical behavior and associated conformal algebra of the Z_3 Potts model," *J. Stat. Phys.*, vol. 34, no. 5, pp. 781–791, 1984.

[89] V. A. Fateev and A. B. Zamolodchikov, "Conformal quantum field theory models in two dimensions having Z_3 symmetry," *Nucl. Phys. B*, vol. 280, pp. 644–660, 1987.

[90] J. Belletête, A. M. Gainutdinov, J. L. Jacobsen, H. Saleur, and R. Vasseur, "On the correspondence between boundary and bulk lattice models and (logarithmic) conformal field theories," *J. Phys. A*, vol. 50, no. 48, p. 484002, 2017.

[91] J. L. Jacobsen and H. Saleur, "Exact valence bond entanglement entropy and probability distribution in the XXX spin chain and the Potts model," *Phys. Rev. Lett.*, vol. 100, p. 087205, 2008.

[92] F. Alcaraz, U. Grimm, and V. Rittenberg, "The XXZ Heisenberg chain, conformal invariance and the operator content of $c < 1$ systems," *Nucl. Phys. B*, vol. 316, no. 3, pp. 735–768, 1989.

[93] A. M. Gainutdinov, J. L. Jacobsen, and H. Saleur, "A fusion for the periodic Temperley-Lieb algebra and its continuum limit," *JHEP*, vol. 11, p. 117, 2018.

[94] A. Kitaev, "Fault-tolerant quantum computation by anyons," *Ann. Phys.*, vol. 303, no. 1, pp. 2–30, 2003.

[95] M. H. Freedman, A. Kitaev, M. J. Larsen, and Z. Wang, "Topological quantum computation," *Bull. Amer. Math. Soc.*, vol. 40, pp. 31–38, 2003.

[96] C. Nayak, S. H. Simon, A. Stern, M. Freedman, and S. Das Sarma, "Non-abelian anyons and topological quantum computation," *Rev. Mod. Phys.*, vol. 80, pp. 1083–1159, 2008.

[97] P. Bonderson, M. Freedman, and C. Nayak, "Measurement-only topological quantum computation," *Phys. Rev. Lett.*, vol. 101, p. 010501, 2008.

[98] V. Pasquier, "Etiology of IRF Models," *Commun. Math. Phys.*, vol. 118, p. 355, 1988.

[99] P. Bonderson, *Non-Abelian anyons and interferometry*. PhD thesis, California Institute of Technology, 2007.

[100] E. Ardonne, J. Gukelberger, A. W. W. Ludwig, S. Trebst, and M. Troyer, "Microscopic models of interacting yang-lee anyons," *New J. Phys.*, vol. 13, no. 4, p. 045006, 2011.

[101] S. MacLane, *Categories for the Working Mathematician*. New York: Springer-Verlag, 1971. Graduate Texts in Mathematics, Vol. 5.

[102] Y. Ikhlef, J. L. Jacobsen, and H. Saleur, "Three-point functions in $c \leq 1$ Liouville theory and conformal loop ensembles," *Phys. Rev. Lett.*, vol. 116, no. 13, p. 130601, 2016.

[103] W.-T. Xu and N. Schuch, "Characterization of topological phase transitions from a non-abelian topological state and its galois conjugate through condensation and confinement order parameters," *Phys. Rev. B*, vol. 104, p. 155119, 2021.

[104] S. Trebst, M. Troyer, Z. Wang, and A. Ludwig, "A short introduction to fibonacci anyon models," *Prog. Theor. Phys.*, vol. 176, p. Supplement, 2009.

[105] J. Belletête, A. M. Gainutdinov, J. L. Jacobsen, H. Saleur, and T. S. Tavares, "Topological defects in lattice models and affine Temperley-Lieb algebra," 2018. arXiv preprint 1811.02551.

[106] J. Belletête, A. M. Gainutdinov, J. L. Jacobsen, H. Saleur, and T. S. Tavares, "Topological defects in periodic RSOS models and anyonic chains," 2020. arXiv preprint 2003.11293.

[107] A. Roy and H. Saleur, "Entanglement Entropy in the Ising Model with Topological Defects," *Phys. Rev. Lett.*, vol. 128, no. 9, p. 090603, 2022.

[108] D. Rogerson, F. Pollmann, and A. Roy, "Entanglement entropy and negativity in the Ising model with defects," 2022. arXiv preprint 2204.03601.

[109] U. Grimm and V. Rittenberg, "The Modified XXZ Heisenberg Chain: Conformal Invariance, Surface Exponents Of $c < 1$ Systems And Hidden Symmetries Of Finite Chains," *Int. J. Mod. Phys. B*, vol. 04, no. 05, pp. 969–978, 1990.

[110] J. Jacobsen, *Conformal field theory applied to loop models, in A.J. Guttmann (ed) Polygons, Polyominoes and Polycubes*, vol. 775. Springer, Heidelberg, 2009.

[111] S. L. Lukyanov and V. Terras, "Long distance asymptotics of spin spin correlation functions for the XXZ spin chain," *Nucl. Phys. B*, vol. 654, pp. 323–356, 2003.

[112] B. L. Feigin and D. B. Fuchs, "Invariant skew symmetric differential operators on the line and Verma modules over the Virasoro algebra," *Funct. Anal. Appl.*, vol. 16, pp. 114–126, 1982.

[113] B. L. Feigin and D. B. Fuchs, "Verma modules over the Virasoro algebra," *Funct. Anal. Appl.*, vol. 17, pp. 241–241, 1983.

[114] S. L. Lukyanov, "Correlation amplitude for the XXZ spin chain in the disordered regime," *Phys. Rev. B*, vol. 59, pp. 11163–11164, 1999.

[115] T. Hikihara, A. Furusaki, and S. Lukyanov, "Dimer correlation amplitudes and dimer excitation gap in spin-1/2 XXZ and Heisenberg chains," *Phys. Rev. B*, vol. 96, no. 13, p. 134429, 2017.

[116] R. Vasseur, A. M. Gainutdinov, J. L. Jacobsen, and H. Saleur, "The Puzzle of bulk conformal field theories at central charge c=0," *Phys. Rev. Lett.*, vol. 108, p. 161602, 2012.

[117] R. Couvreur, J. L. Jacobsen, and H. Saleur, "Entanglement in nonunitary quantum critical spin chains," *Phys. Rev. Lett.*, vol. 119, no. 4, 2017.

[118] G. A. Kotousov and S. L. Lukyanov, "Bethe state norms for the Heisenberg spin chain in the scaling limit," *Nucl. Phys. B*, vol. 947, p. 114748, 2019.

[119] F. C. Alcaraz, M. N. Barber, and M. T. Batchelor, "Conformal invariance, the XXZ chain and the operator content of two-dimensional critical systems," *Ann. Phys.*, vol. 182, no. 2, pp. 280–343, 1988.

[120] E. Granet and J. L. Jacobsen, "On zero-remainder conditions in the Bethe ansatz," *JHEP*, vol. 03, p. 178, 2020.

[121] Z. Bajnok, E. Granet, J. L. Jacobsen, and R. I. Nepomechie, "On Generalized Q-systems," *JHEP*, vol. 03, p. 177, 2020.

[122] O. Shevchuk, "Classification of States in the XXZ model," 2012. Master's thesis published at the "Science in Progress" webpage of Universiteit van Amsterdam.

[123] N. A. Slavnov, "Algebraic Bethe ansatz," 2018. Lecture notes for a course given in the Scientific and Educational Center of Steklov Mathematical Institute in Moscow. arXiv preprint 1804.07350.

[124] R. Bondesan, J. Dubail, A. Faribault, and Y. Ikhlef, "Chiral $\mathrm{SU}(2)_k$ currents as local operators in vertex models and spin chains," *J. Phys. A*, vol. 48, no. 6, p. 065205, 2015.

[125] A. Doikou and R. I. Nepomechie, "Parity and charge conjugation symmetries and S matrix of the XXZ chain," 1998. arXiv preprint hep-th/9810034.

[126] V. Kac and A. Raina, *Bombay Lectures on Highest Weight Representations of Infinite Dimensional Lie Algebras*. World Scientific, 1988.

[127] K. Johnson, "Solution of the equations for the Green's functions of a two-dimensional relativistic field theory," *Nuovo Cim.*, vol. 20, pp. 773–790, 1961.

[128] A. Gainutdinov, N. Read, and H. Saleur, "Continuum limit and symmetries of the periodic spin chain," *Nucl. Phys. B*, vol. 871, no. 2, pp. 245–288, 2013.

[129] G. Kato, M. Shiroishi, M. Takahashi, and K. Sakai, "Next nearest neighbor correlation functions of the spin 1/2 XXZ chain at critical region," *J. Phys. A*, vol. 36, pp. L337–L344, 2003.

[130] M. Takahashi, "Half-filled hubbard model at low temperature," *J. Phys. C*, vol. 10, no. 8, pp. 1289–7301, 1977.

[131] M. S. Zini and Z. Wang, "Conformal Field Theories as Scaling Limit of Anyonic Chains," *Commun. Math. Phys.*, vol. 363, no. 3, pp. 877–953, 2018.

[132] H. Saleur, "Conformal invariance for polymers and percolation," *J. Phys. A*, vol. 20, no. 2, pp. 455–470, 1987.

[133] D. Friedan, Z.-a. Qiu, and S. H. Shenker, "Superconformal Invariance in Two-Dimensions and the Tricritical Ising Model," *Phys. Lett. B*, vol. 151, pp. 37–43, 1985.

[134] G. Delfino and J. Viti, "On three-point connectivity in two-dimensional percolation," *J. Phys. A*, vol. 44, p. 032001, 2011.

[135] M. Picco, R. Santachiara, J. Viti, and G. Delfino, "Connectivities of Potts Fortuin-Kasteleyn clusters and time-like Liouville correlator," *Nucl. Phys. B*, vol. 875, pp. 719–737, 2013.

[136] G. Gori and J. Viti, "Four-point boundary connectivities in critical two-dimensional percolation from conformal invariance," *JHEP*, vol. 12, p. 131, 2018.

[137] A. Gainutdinov, D. Ridout, and I. R. (eds.), "Special issue on logarithmic conformal field theory," *J. Phys. A*, vol. 49, 2013.

[138] V. Gorbenko and B. Zan, "Two-dimensional O(n) models and logarithmic CFTs," *JHEP*, vol. 2020, no. 10, 2020.

[139] R. Vasseur, J. L. Jacobsen, and H. Saleur, "Logarithmic observables in critical percolation," *J. Stat. Mech.: Theor. Exp.*, p. L07001, 2012.

[140] R. Vasseur and J. L. Jacobsen, "Operator content of the critical Potts model in d dimensions and logarithmic correlations," *Nucl. Phys. B*, vol. 880, pp. 435–475, 2014.

[141] R. Couvreur, J. L. Jacobsen, and R. Vasseur, "Non-scalar operators for the Potts model in arbitrary dimension," *J. Phys. A*, vol. 50, no. 47, p. 474001, 2017.

[142] J. Dubail, J. L. Jacobsen, and H. Saleur, "Critical exponents of domain walls in the two-dimensional Potts model," *J. Phys. A*, vol. 43, no. 48, p. 482002, 2010.

[143] J. Dubail, J. L. Jacobsen, and H. Saleur, "Bulk and boundary critical behaviour of thin and thick domain walls in the two-dimensional potts model," *J. Stat. Mech.*, vol. 2010, no. 12, p. P12026, 2010.

[144] R. Vasseur and J. Jacobsen, "Critical properties of joint spin and Fortuin-Kasteleyn observables in the two-dimensional Potts model," *J. Phys. A*, vol. 45, 2011.

[145] J.-F. Richard and J. Jacobsen, "Eigenvalue amplitudes of the Potts model on a torus," *Nucl. Phys. B*, vol. 769, 2006.

[146] J. L. Jacobsen and H. Saleur, "The Antiferromagnetic transition for the square-lattice Potts model," *Nucl. Phys. B*, vol. 743, pp. 207–248, 2006.

[147] H. Saleur and B. Duplantier, "Exact Determination of the Percolation Hull Exponent in Two Dimensions," *Phys. Rev. Lett.*, vol. 58, pp. 2325–2328, 1987.

[148] N. Read and H. Saleur, "Enlarged symmetry algebras of spin chains, loop models, and S-matrices," *Nucl. Phys. B*, vol. 777, pp. 263–315, 2007.

[149] M. R. Gaberdiel, I. Runkel, and S. Wood, "A Modular invariant bulk theory for the c=0 triplet model," *J. Phys. A*, vol. 44, p. 015204, 2011.

[150] R. Nivesvivat, "Global symmetry and conformal bootstrap in the two-dimensional Q-state Potts model," 2022.

[151] V. Gurarie and A. W. W. Ludwig, "Conformal algebras of 2-D disordered systems," *J. Phys. A*, vol. 35, pp. L377–L384, 2002.

[152] R. Santachiara and J. Viti, "Local logarithmic correlators as limits of Coulomb gas integrals," *Nucl. Phys. B*, vol. 882, pp. 229–262, 2014.

[153] J. Kondev, J. de Gier, and B. Nienhuis, "Operator spectrum and exact exponents of the fully packed loop model," *J. Phys. A*, vol. 29, no. 20, p. 6489–6504, 1996.

[154] J. L. Jacobsen and J. Kondev, "Field theory of compact polymers on the square lattice," *Nucl. Phys. B*, vol. 532, pp. 635–688, 1998.

[155] H. Blöte and B. Nienhuis, "Critical behaviour and conformal anomaly of the $O(n)$ model on the square lattice," *J. Phys. A*, vol. 22, p. 1415, 1989.

[156] E. Vernier, J. L. Jacobsen, and J. Salas, "Q-colourings of the triangular lattice: exact exponents and conformal field theory," *J. Phys. A*, vol. 49, no. 17, p. 174004, 2016.

[157] E. Vernier, J. L. Jacobsen, and H. Saleur, "Non compact conformal field theory and the $a_2^{(2)}$ (Izergin-Korepin) model in regime III," *J. Phys. A*, vol. 47, p. 285202, 2014.

[158] E. Vernier, J. L. Jacobsen, and H. Saleur, "A new look at the collapse of two-dimensional polymers," *J. Stat. Mech.: Theor. Exp.*, vol. 2015, p. P09001, 2015.

[159] H. Saleur, "Magnetic properties of the two-dimensional n=0 vector model," *Phys. Rev. B*, vol. 35, pp. 3657–3660, 1987.

[160] R. J. Baxter, H. N. V. Temperley, and S. E. Ashley, "Triangular Potts model at its transition temperature, and related models," *Proc. Roy. Soc. A*, vol. 358, pp. 535–559, 1978.

[161] S. Caracciolo, J. L. Jacobsen, H. Saleur, A. D. Sokal, and A. Sportiello, "Fermionic field theory for trees and forests," *Phys. Rev. Lett.*, vol. 93, p. 080601, 2004.

[162] J. L. Jacobsen and H. Saleur, "The arboreal gas and the supersphere sigma model," *Nucl. Phys. B*, vol. 716, pp. 439–461, 2005.

[163] G. Parisi and N. Sourlas, "Self avoiding walk and supersymmetry," *J. Physique Lettres*, vol. 41, pp. L403–L406, 1980.

[164] K. J. Wiese and A. A. Fedorenko, "Field theories for loop-erased random walks," *Nucl. Phys. B*, vol. 946, p. 114696, 2019.

[165] K. Lang and W. Rühl, "Critical O(N) vector nonlinear sigma models: A Resumé of their field structure," *Adv. Appl. Clifford Algebras*, vol. 4, no. S1, pp. 203–216, 1994.

[166] S. Ribault, R. Nivesvivat, L. Grans-Samuelsson et al, "Bootstrap_Virasoro 3.0: Bootstrapping two-dimensional CFTs with Virasoro symmetry," 2021. Code at `https://gitlab.com/s.g.ribault/Bootstrap_Virasoro/-/releases/v3.0`.

[167] Y. He and H. Saleur, "A note on the identity module in $c = 0$ CFTs," *SciPost Phys.*, vol. 12, p. 100, 2022.

[168] D. J. Binder and S. Rychkov, "Deligne Categories in Lattice Models and Quantum Field Theory, or Making Sense of $O(N)$ Symmetry with Non-integer N," *JHEP*, vol. 04, p. 117, 2020.

[169] N. El Samra and R. C. King, "Dimensions of irreducible representations of the classical Lie groups," *J. Phys. A*, vol. 12, no. 12, pp. 2317–2328, 1979.

[170] S. Gao, G. Orelowitz, and A. Yong, "Newell-Littlewood numbers," 2020. arXiv preprint 2005.09012.

[171] V. Gorbenko, S. Rychkov, and B. Zan, "Walking, Weak first-order transitions, and Complex CFTs II. Two-dimensional Potts model at $Q > 4$," *SciPost Phys.*, vol. 5, no. 5, p. 050, 2018.

[172] A. M. Gainutdinov, N. Read, and H. Saleur, "Associative algebraic approach to logarithmic CFT in the bulk: the continuum limit of the $\mathfrak{gl}(1|1)$ periodic spin chain, Howe duality and the interchiral algebra," *Commun. Math. Phys.*, vol. 341, no. 1, pp. 35–103, 2016.

[173] Y. Ikhlef and A. Morin-Duchesne, "Fusion in the periodic Temperley-Lieb algebra and connectivity operators of loop models," 2021. arXiv preprint 2105.10240.

[174] R. Brauer, "On algebras which are connected with the semi-simple continuous groups," *Annals of Mathematics*, vol. 38, pp. 857–872, 1937.

[175] V. Jones, "A quotient of the affine Hecke algebra in the Brauer algebra," *Enseign. Math.*, vol. 40, pp. 313–344, 1994.

[176] N. D. Mermin and H. Wagner, "Absence of Ferromagnetism or Antiferromagnetism in One- or Two-Dimensional Isotropic Heisenberg Models," *Phys. Rev. Lett.*, vol. 17, pp. 1133–1136, 1966.

[177] A. Patrascioiu and E. Seiler, "Universality class of $O(N)$ models," *Phys. Rev. B*, vol. 54, pp. 7177–7179, 1996.

[178] P. Fendley, H. Saleur, and A. B. Zamolodchikov, "Massless flows I: the sine-Gordon and $O(n)$ models," *Int. J. Mod. Phys. A*, vol. 08, no. 32, p. 5717–5750, 1993.

[179] R. Vasseur and J. L. Jacobsen, "Operator content of the critical Potts model in d dimensions and logarithmic correlations," *Nucl. Phys. B*, vol. 880, pp. 435–475, 2014.

[180] R. S. K. Mong, D. J. Clarke, J. Alicea, N. H. Lindner, P. Fendley, C. Nayak, Y. Oreg, A. Stern, E. Berg, K. Shtengel, and M. P. A. Fisher, "Universal Topological Quantum Computation from a Superconductor-Abelian Quantum Hall Heterostructure," *Phys. Rev. X*, vol. 4, p. 011036, 2014.

[181] N. Kitanine, J. M. Maillet, and V. Terras, "Form factors of the XXZ Heisenberg spin-$\frac{1}{2}$ finite chain," *Nucl. Phys. B*, vol. 554, pp. 647–678, 1999.